Lecture Notes in Physics

Edited by H. Araki, Kyoto, J. Ehlers, München, K. Hepp, Zürich
R. Kippenhahn, München, H.A. Weidenmüller, Heidelberg,
J. Wess, Karlsruhe and J. Zittartz, Köln
Managing Editor: W. Beiglböck

285

T. Paszkiewicz (Ed.)

Physics of Phonons

Proceedings of the XXIII Winter School of Theoretical Physics
Held in Karpacz, Poland, February 16–28, 1987

Springer-Verlag
Berlin Heidelberg New York London Paris Tokyo

Editors

Tadeusz Paszkiewicz
Institute of Theoretical Physics, Wroclaw University
ul. Cybulskiego 36, PL-50-205 Wroclaw, Poland

ISBN 3-540-18244-6 Springer-Verlag Berlin Heidelberg New York
ISBN 0-387-18244-6 Springer-Verlag New York Berlin Heidelberg

This work is subject to copyright. All rights are reserved, whether the whole or part of the material is concerned, specifically the rights of translation, reprinting, re-use of illustrations, recitation, broadcasting, reproduction on microfilms or in other ways, and storage in data banks. Duplication of this publication or parts thereof is only permitted under the provisions of the German Copyright Law of September 9, 1965, in its version of June 24, 1985, and a copyright fee must always be paid. Violations fall under the prosecution act of the German Copyright Law.

© Springer-Verlag Berlin Heidelberg 1987

Printed in Germany

Printing: Druckhaus Beltz, Hemsbach/Bergstr.;
Bookbinding: J. Schäffer GmbH & Co. KG., Grünstadt
2153/3140-543210

Participants of the first week

Participants of the second week

PREFACE

This volume contains the proceedings of the 1987 Karpacz Winter School on the Physics of Phonons.

The decisive role played by phonons in condensed matter is well known. They mediate interactions between various quasi-particles. Their presence changes almost every characteristic of condensed matter. Phonons carry the energy and quasi-momentum and interact with external fields.

Over the past few years a number of sophisticated theoretical and experimental methods of study and new subjects of research have emerged, which have considerably broadened the scope of phonon physics. One should mention in particular new methods of phonon spectroscopy, excitations in glasses, dynamics of surfaces and interfaces, and phonons in quasi-crystals.

Obviously it is impossible to present all these achievements during a two-week school and in one volume, therefore we have selected several topics, which correspond to the first three parts of the volume. Part I is devoted to the foundations of the dynamics of condensed media, including surface vibrations and localization of phonons. Problems of phonon kinetics with the emphasis on phonon spectroscopy are presented in the second part. The interaction of phonons with electrons is discussed in the third part. The fourth part contains selected contributed talks.

I am grateful to Professor A.A. Maradudin for a review paper on the current status of phonon physics.

I express my deep gratitude to the lecturers who came to Karpacz despite different obstacles and the usual lack of time, and discussed their and other work in the broad, instructive way required by the school format. I wish to thank them also for their efforts to produce work of the highest scientific and pedagogical quality even under pressure of time.

There are many people I want to acknowledge. Major credit goes to the Organizing Committee - Janusz Jedrzejewski (secretary), Jan Lorenc (treasurer), Zbigniew Strycharski (technical assistance), Jerzy Cisło, Tadeusz Hałaczek, Paweł Misiak, Paweł Morawiec, Czesław Oleksy, Zygmunt Petru, Aleksandra Podolska-Strycharska, Danuta Skrajna for their input and advice. It was a privilege to work with them.

I would like to express my indebtedness to colleagues from the Institute of Physics of the Polish Academy of Sciences in Warsaw, especially to Professor Andrzej Czachor, for taking care of our guests.

Finally, I am grateful to the authorities of Wrocław University, especially to the Rector, Professor Jan Mozrzymas, for their financial and moral support.

Wrocław, May 1987

Tadeusz Paszkiewicz
Director of the XXIII School

CONTENTS

A.A. Maradudin
Phonon Physics - a Survey 1

INVITED TALKS

I. FOUNDATIONS

G.K. Horton, E.R. Cowley
Lattice Dynamics at High Temperature 50

N.M. Plakida
A Comment on the Applicability of Thermodynamics Perturbation Theory 81

A.A. Maradudin
Surface Acoustic Waves on Real Surfaces 82

B. Djafari Rouhani
Acoustic Phonons in Infinite and Semi-Infinite Superlattices 148

J.M. Worlock
Phonons in Superlattices 159

N.M. Plakida
Nonergodic Behaviour and Phonon Localization at Structural Phase Transitions 168

A. Czachor
Spectrum of Local Frequencies for the Orderless Solids 177

H.R. Schober
Interaction of Phonons and Point Defects and Its Influence on Defect Mobility 188

A. Thellung
Equivalence of Eulerian and Lagrangian Phonons: Sound Pressure and Two-Fluid Equations 208

I. Białynicki-Birula
Squeezed States of Light and Sound 226

II. KINETICS OF PHONON SYSTEMS

W.E. Bron
Ultrashort Transient Dynamics of Phonons and Electrons in Semiconductors 236

L.J. Challis
Crossing Effects in Phonon Scattering 264

D.V. Kazakovtsev, Y.B. Levinson
Theory of Formation, Dynamics and Explosion of a Phonon Hot Spot 276

H. Kinder
Superconducting Tunnel Junctions, Very High Frequency Phonons and the Kapitza Resistance 289

K.S. Viswanathan
Phonon Focussing in Crystals 301

O. Weis
Phonon Scattering at Plane Interfaces and Surfaces 313

III. ELECTRON-PHONON INTERACTION

H. Eschrig, M.I. Kaganov
Quasi-Particle Interaction and Anomalies in the Excitation Spectra of Metals 334

L.J. Challis, G.A. Toombs and F.W. Sheard
Acoustic Phonon Interaction with a Two-Dimensional Electron Gas (2DEG) ... 348

R.H. Gurzhi, A.I. Kopeliovich, S.B. Rutkevich
Electron-Phonon Relaxation Mechanisms and Kinetic Effects in Two-Dimensional Conducting Systems 375

D.I. Khomskii
Electron-Phonon Interaction in Systems with Strong Electron Correlations . 390

CONTRIBUTED PAPERS

A.L. Efros
Density of States of a 2D Electron Gas in a Magnetic Field 402

T.I. Galkina
Generation and Propagation of Phonons in Crystalline and Amorphous Silicon Under Optical Excitation 410

A.M. Kosevich, Yu.S. Kivshar and O.A. Chubykalo
Bound Quasiparticles Scattering by Point Impurities in One-Dimensional Systems as a Soliton Problem 419

A.A. Levchenko, L.P. Mezhov-Deglin
Phonon Scattering on Dislocations and Recovery Processes in Plastically Deformed ^{4}He Crystals 438

Y.B. Levinson
Inelastic Phonon Scattering in an Amorphous Subsurface Layer and the Establishment of a Temperature Below 1K 444

A.A. Maksimov, U.U. Tartakovskii
Propagation and Relaxation in Nonequilibrium Phonons in Thin Monocrystal Plates 450

K. Parliński
Molecular Dynamics Study of a Model with Incommensurate Phases 457

Z.K. Petru
Anisotropy of Relaxation of Acoustic Phonons Scattered by Isotopic Impurities 467

M.A. Smondyrev
Selected Topics on Polaron 477

T.L. Hałaczek, B. Sujak
Phonon Detection by Means of TSEE 479

LIST OF PARTICIPANTS 481

TALKS NOT INCLUDED IN THIS VOLUME

V.B. Efimov, L.P. Mezhov-Deglin
Nonlinear Waves of Second Sound in He II

M. and Zs. Gulácsi
Spin-Density Waves in Heavy Fermion Systems

D. Ihle
Small Polaron Conductivity and Short-Range Order in Magnetite

M. Kurzyński
Protein Dynamics and Theory of Enzymatic Catalysis

J. Lefebvre
Two Examples of Coherent Neutron Scattering on Plastic Crystals: Admantane and Carbon Tetrabromide

L.P. Mezhov-Deglin
Hydrodynamic Effects in Heat Conductivity of Solids

L.P. Mezhov-Deglin
Heat Pulses Propagation in Superfluid He II

T. Paszkiewicz
Lorentz Gas - Crossover from Kinetic to Hydrodynamic Regime

J. Schreiber
Localization and Glass-Like Behaviour in the Lattice φ^4 Model of Structural Phase Transition

V.S. Tsoi
The Study of Electron-Phonon Interaction Using the Transversal Focussing of Electrons

W. Weller
Recursion Relation in Theory of Localization. Application to Electron-Phonon Interaction in a 1D Disordered Chain

Phonon Physics - a Survey

Alexei A. Maradudin
Department of Physics
University of California
Irvine, CA 92717, USA

1. Introduction

In these lectures I would like to survey some recent developments in the field of phonon physics, and to indicate, here and there, some possible directions for future work in this field. Because of limitations of space and time, this cannot be an exhaustive overview of the subject, either in the breadth of the subject matter covered or in the depth of the discussion of any given topic. I have therefore restricted myself to a selection of topics that represent areas of phonon physics that have emerged, or have taken some new turns, during the past half-dozen years or so. In the context of this School this is not as limiting as it might seem at first glance, because some of the topics I might otherwise have included for discussion will be covered in the lectures that follow, in more detail than would have been possible in this talk. Nevertheless, I apologize in advance to authors whose work is not mentioned here. In addition, since these lectures are being delivered at a School of Theoretical Physics, the emphasis in them will be on theoretical developments in phonon physics during the time period indicated. However, experimental work will be described where appropriate.

2. Ab Initio Calculations of Bulk Phonons

Since the pioneering work of Born and von Karman in 1912,(1) the majority of the theoretical work done on the vibrational properties of solids has been based on force constant models in which the values of the atomic force constants have been obtained by fitting theoretical dispersion curves to experimental data. In the early days of the subject, the dispersion curves of long wavelength acoustic phonons could be fitted to the predictions of elasticity theory, while the frequencies of long wavelength optical phonons could be fitted to the results of infrared absorption or Raman scattering studies. With the introduction of neutron spectroscopy as an experimental tool such fitting could be done to the experimental phonon dispersion curves along symmetry directions in the first Brillouin zone of a crystal.

Useful as such phenomenological approaches to lattice dynamics are, they suffer from two major deficiencies. The first is that they are not predictive: the values of the atomic force constants and of the resulting dispersion curves are inferred from experimental data rather than predicted by some more fundamental approach to their determination. The second is that they are not unique: often more than one model can reproduce the experimental dispersion curves equally well.

Consequently, beginning with the work of Toya in 1958(2), a steadily increasing effort has been devoted to the determination of atomic force constants and phonon dispersion curves from first principles. Surveys of the progress that has been achieved in such calculations up to a half a dozen years ago can be found in Refs. 3-6.

In the past few years particularly impressive strides in this field of phonon physics have been made in connection with the calculation of phonon dispersion curves, and other dynamical properties, of semiconductors, both elemental and compound, particularly by Martin and Kunc. This has been made possible by the combination of four theoretical ideas: (a) the local density functional approximation; (b) ab initio pseudopotentials; (c) the frozen-phonon method; and (d) the Hellmann-Feynman theorem(7,8). The local density functional method is based on the theorem(9-11) that the total ground state energy of an inhomogeneous system of interacting electrons is a unique and universal functional of the electronic charge density. Although the exact form of this functional is not known, approximating its exchange-correlation part by relatively simple local expressions, derived by many-body theories of homogeneous electron systems, provides a workable computational scheme that is capable of determining the small energy differences that result from the displacements of ions from their equilibrium positions with good accuracy. The calculations are significantly simplified if the core electrons on each ion are eliminated from the problem through the use of pseudopotentials. At the present time the pseudopotential is calculated from ab initio atomic calculations(12) and simulates the effects of the core with essentially arbitrary accuracy. In the frozen phonon approach the atoms in a crystal are displaced in a known fashion, viz. the two sublattices are displaced relative to each other by a known distance, and the increase in the ground state energy of the crystal (electronic plus ionic) gives the energy of the phonon corresponding to this displacement pattern(13). Since this displacement need not be small, it is possible to study anharmonic effects in this way. However, the frozen phonon method is applicable only to phonons at high symmetry points in the first Brillouin zone. To calculate an entire phonon dispersion curve $\omega(\vec{k})$ for $\vec{k}$ along a selected direction of propagation, entire planes of atoms are displaced by a known amount $\vec{u}$, and the self-consistent charge density in this distorted crystal calculated. The latter determine forces on individual atoms, according to the Hellmann-Feynmann theorem, and from these forces one can calculate the interplanar force constants k_n, which are defined as the negative of the force acting on an atom in plane 0 per unit displacement of plane n. The set of $\{k_n\}$ suffices for calculating the entire phonon dispersion curve $\omega(\vec{k})$ along the direction perpendicular to the planes. Ideally, one would like to calculate the interplanar force constants by displacing only one plane of atoms through a known distance, and calculating the forces acting on the remaining atoms of the crystal. However, the loss of periodicity that results from this kind of displacement pattern makes such calculations impractical at this time. Consequently, in practice the calculation is carried out by defining a supercell consisting of 8-12 atoms that generates the entire crystal by parallel displacements. One plane of like atoms in the supercell is given a known displacement, and the resulting force on every other atom in the cell is calculated (Fig. 1). Thus periodic structures always appear in the calculations, albeit with large unit cells. This procedure has to be modified for long wavelength longitudinal optical phonons in polar semiconductors such as GaAs. Longitudinal displacements of charged planes give rise to a macroscopic electric field, which leads to the Lyddane-Sachs-Teller splitting between the LO and TO branches of the phonon spectrum at $\vec{k} = 0$. In the large periodic cells the boundary conditions require this field to vanish, which is equivalent to adding a depolarizing electric field that is constant over the crystal. This field can be calculated from first principles. It exerts forces on the ions. If these forces are subtracted from those calculated by the Hellmann-Feynman theorem, one obtains the interplanar force constants that include the effects of the macroscopic field. This method has been used to obtain phonon

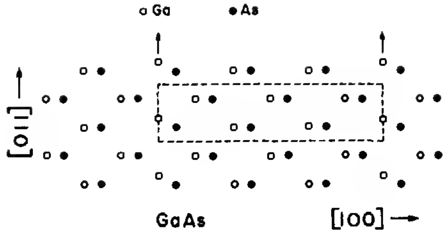

Fig. 1. Periodic supercells containing twelve atoms defined by the displacement of (100)Ga planes in GaAs in the [011] direction.

dispersion curves in GaAs,$^{(14)}$ Ge,$^{(15)}$ and Si$^{(17,18)}$, with errors that do not exceed a few per cent (Fig. 2). It has also been applied to the calculation of dynamic effective charges e_T^* and e_L^*, as well as the static dielectric constant, of GaAs$^{(14)}$.

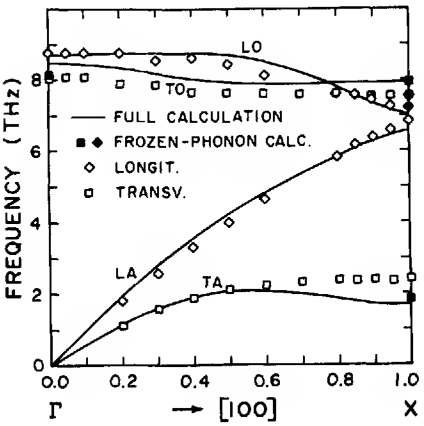

Fig. 2. Phonon dispersion curves along the [100] direction in GaAs obtained from the force constants calculated by the use of twelve atom supercells (solid lines) [Ref. 10]. Open symbols denote experimental points [Ref. 10a], and the solid symbols denote the results of "frozen phonon" calculations obtained using the same Hamiltonian [Ref. 13].

In a related development Falter et al.$^{(19)}$ have obtained a decomposition of the total charge density of a crystal into contributions that can be assigned uniquely to individual ions. These partial charge distributions are used to decompose the charge density variations caused by the displacements of ions into a part that moves rigidly with the ions and a part that distorts during the displacements. The dynamical matrix of the crystal can be expressed in terms of the contributions. It is found that in Si the distortion part of the partial charge distributions is small, and that calculations of the phonon dispersion curves along the [100] direction with their inclusion and with their omission do not differ significantly except perhaps at the zone boundary where the differences are of the order of 10-15%. These results suggest approximating the rigid part of the partial charge distributions by superpositions of Gaussians fitted to the results of exact *ab initio* calculations of these quantities. The phonon dispersion curves calculated in this way are in reasonable agreement with experimental data.

It should be noted that a similar decomposition of the atomic charge densities, in metals, together with pseudopotential theory, has been used very recently in calculations of phonon dispersion curves in a number of cubic metals by Wang and Overhauser.(20)

3. Anharmonic Properties of Solids

There have been several advances in the study of anharmonic properties of solids in the past few years, which we review in this section.

3.1. Perturbation Theory

A traditional way of calculating such properties of anharmonic crystals as thermodynamic functions, spectral densities or proper self-energies, and mean-square displacements of atoms from their equilibrium positions has been perturbation theory. In this approach the vibrational Hamiltonian for an anharmonic crystal is written as

$$H = H_o + H_A, \tag{3.1}$$

where H_o is the harmonic part of the Hamiltonian, while

$$H_A = \lambda V_3 + \lambda^2 V_4 + \lambda^3 V_5 + \dots \tag{3.2}$$

is the anharmonic part, with V_n the contribution to the potential energy that is of n^{th} order in the nuclear displacements. The constant λ is an ordering parameter that expresses the relative magnitudes of the various anharmonic terms in the Hamiltonian(21), and can be set equal to unity at the end of a calculation. Until recently, most calculations of anharmonic properties of solids were carried out to $O(\lambda^2)$, i.e. in an approximation in which the cubic anharmonic terms (V_3) were treated to second order in perturbation theory while the quartic terms (V_4) were treated in the first order(22-24). In addition, approximations were often made in evaluating the expressions provided by perturbation theory, e.g. the leading term approximation, in which only the highest-order radial derivative of the interatomic pair potential is retained in evaluating the Fourier transformed cubic and quartic force constants.

In the past several years Shukla and his coworkers have extended the perturbation theoretic expansion of the Helmholtz free energy for an anharmonic crystal to obtain all the terms of $O(\lambda^4)$.(25-28) They have evaluated the resulting expressions in the high temperature limit, for nearest neighbor, central force models of face centered crystals, for a variety of interatomic pair potentials, with(25) and without(26) the leading term approximation. The results have been compared with those obtained with the leading term approximation(26), with the improved self-consistent scheme(26,27,29) for calculating anharmonic properties, and with the results of Monte Carlo simulations for the same crystal models(27). The results suggest that (a) the use of the leading term approximation leads to significant inaccuracies in the calculation of anharmonic properties; (b) the improved self-consistent scheme of selecting the most important diagrams in higher orders of perturbation theory is probably as good as doing perturbation theory to $O(\lambda^4)$; and (c) the theory to $O(\lambda^4)$ converges well up to 40% of the melting temperature, in contrast with the theory to $O(\lambda^2)$, which is in error above one-quarter to one-third of the melting temperature.

Efforts to calculate the Helmholtz free energy to $O(\lambda^6)$ are now underway(30).

Similarly perturbative efforts to calculate the Debye-Waller factor, $\exp(-M_\ell) = \langle \exp i\vec{\kappa}\cdot\vec{u}(\ell)\rangle$, where the angular brackets denote an average over the canonical ensemble defined by the Hamiltonian (3.1) - (3.2), $\vec{\kappa}$ is the wave vector transfer in a scattering experiment, and $\vec{u}(\ell)$ is the displacement of the ℓ^{th} atom from its equilibrium position, have recently been carried out for bcc metals by Shukla and Mountain(31), following up and complementing earlier work by Maradudin and Flinn(24) and Wolfe and Goodman(32) for fcc metals. In this work all contributions to M_ℓ through $O(\lambda^2)$ have been calculated. The interatomic potential used by Shukla and Mountain is a long-range potential, (out to sixth nearest neighbors), in contrast with the nearest neighbor model for the anharmonic forces assumed by Maradudin and Flinn and by Wolfe and Goodman. The lattice dynamics results were compared with the results of a molecular dynamics calculation of the Debye-Waller factor(31), and it was found that the former are in good agreement with the latter for temperatures up to the melting temperatures of Li and Rb. The quasiharmonic contribution to M_ℓ, in which the normal mode frequencies entering the harmonic approximation expression for this quantity are determined at the volume of interest rather than for the OK equilibrium volume, gives about 90% of the result. The intrinsic anharmonic interactions provide the remaining 10%. A comparison of the molecular dynamics results with experimental data for M_ℓ (33) reveal some differences which could be due to the choice of interatomic potential used in the simulation (the same as in the lattice dynamics calculations).

3.2 Nonperturbative Treatments

Perturbation theoretic calculations of anharmonic properties of crystals, in those cases where perturbation theory is applicable (viz. for non-quantum crystals), have the advantage that they proceed systematically in powers of a well defined parameter (λ in Eq. (3.2)), so that it is clear which anharmonic contributions have been included and which have not. However, the number of terms contributing, e.g. to the Helmholtz free energy, in each order of λ grows rapidly with increasing order, and the expressions for these contributions become progressively more complex, involving multiple sums over wave vectors within the first Brillouin zone, with restrictions on them that are due to the periodicity of the crystal. Although it is almost certain that efforts will be made to push such calculations to higher orders in λ, it is also understandable that alternatives to perturbation theory have been, and continue to be, sought for the theoretical investigations of anharmonic properties of solids. In this section we consider two such approaches that do not involve expansions of the potential energy in powers of atomic displacements; the first is based on clusters and modified Einstein oscillator models of anharmonic crystals; the second is purely computational in nature. Other approaches to this problems will be described by Professors Horton and Plakida in their lectures.

3.2.1. Cluster Calculations of Anharmonic Properties of Crystals

Nearly thirty years ago , efforts were made to calculate the thermodynamic properties of anharmonic crystals by considering the energy levels of a single atom vibrating in the anharmonic potential well due to all the other atoms at rest in their equilibrium positions,(34,35) and classical versions of this model.(36-38) The simplicity of calculations based on this model is offset by the fact that it ignores completely the correlations between the motions of the various atoms in the crystal. Attempts to take these correlations into account have been made by several authors, and are still continuing.

Westera and Cowley(39) wrote the classical configuration integral for a crystal of N atoms in the form

$$Q = \int_{WS} d^3u_1 \ldots \int_{WS} d^3u_N e^{-\beta\Phi} , \tag{3.3}$$

where the subscript "WS" indicates that the integration over each displacement vector is carried out over the volume of the Wigner-Seitz cell associated with that atom. The total potential energy of the crystal

$$\Phi = \frac{1}{2} \sum_{i,j}{}' \phi(|\vec{R}_j+\vec{u}_j - \vec{R}_i-\vec{u}_i|) \tag{3.4}$$

is rewritten formally as the sum of a static term, a sum of one-particle terms, and a sum of two-particle terms:

$$\Phi = N\phi_o + \sum_i \phi_1(\vec{u}_i) + \frac{1}{2} \sum_{i,j}{}' \phi_2(\vec{u}_i,\vec{u}_j) , \tag{3.5}$$

where the primes in Eqs. (3.4)-(3.5) indicate that the terms with i=j are omitted from the corresponding sums. When Eq. (3.5) is substituted into Eq. (3.3) the result is then written in the form

$$Q = e^{-\beta N\phi_o} \int_{WS} d^3u_1 \ldots \int_{WS} d^3u_N \, e^{-\beta\sum_i \phi_1(\vec{u}_i)} \times$$

$$\times \left[1 + \sum_{i>j} f_{ij} + \frac{1}{2} \left(\sum_{i>j} \sum_{k>\ell} f_{ij} f_{k\ell} - \sum_{i>j} f_{ij}^2 \right) + \ldots \right] , \tag{3.6}$$

where $f_{ij} \equiv \exp(-\beta\phi(\vec{u}_i,\vec{u}_j))-1$. The first term gives Q in an anharmonic Einstein-type of approximation in which each atom vibrates independently of the others. All terms in the brackets beyond the first describe the correlations between the motions of different atoms. Westera and Cowley have evaluated Q to the order in the $\{f_{ij}\}$ shown, for a nearest neighbor model of an fcc crystal in which the atoms interact via a Lennard-Jones 6-12 potential. (In fact, these authors worked with a modified form of Eq. (3.6) which yields a Helmholtz free energy that is proportional to N.) The calculated results for such quantities as the temperature dependence of the nearest-neighbor distance, the volume thermal expansivity, the isothermal compressibility, and the specific heats at constant volume and at constant pressure, are in reasonable agreement with experimental data for the rare gas solids and with the results of a Monte Carlo simulation of such a crystal.

A somewhat different version of such calculations has been presented by Hardy and Jones$^{(40)}$. They assume a Hamiltonian of the form

$$H = H_o + \sum_p A_p, \tag{3.7}$$

where H_o is a harmonic Hamiltonian while A_p is the anharmonic part of the potential energy of interaction of the pair of atoms p, and the summation is over all pairs of atoms. The classical Helmholtz free energy is given exactly by

$$F = - k_B T \ln Z_o + \Delta F \tag{3.8}$$

where

$$\Delta F = - k_B T \ln \langle \prod_p e^{-\beta A_p} \rangle_o . \tag{3.9}$$

Z_o in Eq. (3.8) is the harmonic partition function, and the angular brackets $\langle\ldots\rangle_o$ denote an average over the canonical ensemble defined by the harmonic Hamiltonian H_o. Hardy and Jones approximate Eq. (3.9) by

$$\Delta F \cong -k_B T \ln \prod_p \langle e^{-\beta A_p} \rangle_o , \tag{3.10}$$

and call the result the uncorrelated pairs approximation. It neglects the contribution of the correlations between the motions of different pairs of atoms to the anharmonic part of F, but not to the harmonic part. Results based on Eq. (3.10) have been obtained for various thermodynamic properties of a nearest neighbor model of an fcc crystal in which the atoms interact through a Lennard-Jones 6-12 pair potential. These results are in quite good agreement with the results of Monte Carlo simulations of the same crystal(41).

A modified version of this theory has been presented recently by Hardy and Day(42). In that the harmonic part of the potential is taken to be a sum of Einstein oscillators whose parameters are determined self-consistently, this version has something in common with the cluster calculations of Westera and Cowley. Because of this form of the harmonic Hamiltonian it is easier to apply than the uncorrelated pairs approximation, but is found to be at least as accurate.

It seems likely that further work along the lines of these calculations will be forthcoming, in which the complete potential energy function, and not its expansion in powers of the atomic displacements, provides the starting point for the study of anharmonic properties of crystals.

3.2.2. Computer Simulations

Computer simulations pervade virtually every branch of contemporary theoretical physics. They provide a means for dealing with problems of such complexity as to be intractable by conventional analytic-cum-numerical approaches. At the same time, the results of such simulations can sometimes reveal features that then lead to successful analytic attacks on a problem. Two types of computer simulations have been applied to the study of the vibrational properties of anharmonic crystals, and we consider them in this section.

3.2.2.1. Molecular Dynamics Simulations

Molecular dynamics simulations have been used for several years for the determination of the anharmonic properties of solids in the classical regime of temperatures(43). In this method, a system of N classical particles have coordinates $\{\vec{r}_i\}$, velocities $\{\dot{r}_i\}$ and masses $\{m_i\}$ $(i = 1,2,\ldots,N)$. The particles interact through a potential that in most cases is assumed to be a sum of pair potentials

$$\Phi = \frac{1}{2}\sum_{i,j}{}' \phi(|\vec{r}_i-\vec{r}_j|), \qquad (3.11)$$

where the prime on the summation excludes the terms with i = j. The assumption of pair potentials is not an essential ingredient of the method. Newton's equations of motion are then

$$m_i\ddot{\vec{r}}_i = -\sum_{j(\neq i)} \phi'(r_{ij})\hat{r}_{ij}, \quad i = 1, 2,\ldots,N, \qquad (3.12)$$

where the prime here denotes differentiation with respect to argument, while $\hat{r}_{ij}$ is a unit vector in the direction of $(\vec{r}_i-\vec{r}_j)$. These equations are solved numerically to give $\vec{r}_i$ and $\dot{\vec{r}}_i$ (i = 1, 2,...N) as functions of time. As the system evolves, it eventually reaches thermal equilibrium conditions in its structural and dynamical properties. The statistical averages of interest are then calculated from $\{\vec{r}_i(t)\}$ and $\{\dot{\vec{r}}_i(t)\}$ as time averages over the trajectory of the system in phase space.

The number of particles N whose dynamics can be studied in this way is a few thousand at most, because of computer limitations. Periodic boundary conditions are generally used in simulations of bulk systems. These are obtained by periodically replicating a unit cell of volume Ω in which the N particles are situated by suitable translations.

Since the potential energy Φ is a function of the $\{\vec{r}_i\}$ only, the solutions of Eqs. (3.12) conserve the total energy E of the system, and the statistical ensemble generated in a conventional molecular dynamics simulation is an (Ω, E, N) ensemble, i.e. a microcanonical ensemble.

In conventional molecular dynamics simulations the molecular dynamics cell is restricted to have a constant volume Ω and a constant shape. This restriction severely limits the applicability of the method to problems involving structural phase transitions, in which changes in the shape of the cell play an essential role. In what is probably the most important innovation in the theory of molecular dynamics simulations in the past decade, Parrinello and Rahman(44) have modified an earlier method of Andersen(45) in a way that allows for changes in both the volume and shape of a molecular dynamics cell containing a system of particles under constant external hydrostatic pressure. (In Andersen's method changes in the volume of the molecular dynamics cell were possible, but not changes in its shape.) The theory has been extended further to systems under general external stresses(46-48) and to make it consistent with the theory of finite elasticity(49). The methods of Parrinello and Rahman have been used in a variety of studies, including the study of polymorphic phase transitions(50). Among the interesting results found in this way is that for a model of nickel in which the particles interact via pairwise additive potential of the Morse type, the fcc structure upon uniform uniaxial compression transforms into an hcp structure(46). These methods have also been applied to the determination of the elastic moduli of a crystal as functions of temperature and arbitrary external stress(51). This method is still comparatively new, but can be expected to yield additional interesting results concerning structural phase transtions in which phonons participate in the future.

3.2.2.2. Monte Carlo Simulations

A second numerical simulation technique that has been employed recently in the study of anharmonic properties of solids in the classical limit is the Monte Carlo method(52). It seems to have been used less frequently in studies of the anharmonic properties of solids than have molecular dynamics simulations, perhaps because it is a time-consuming method of calculation. However, the increased speed of present-day computers compared to that of the computers available nearly twenty years ago when the first Monte Carlo calculations of anharmonic properties were carried out(53), makes it certain that more such calculations using this method will be carried out in the future.

In the classical Monte Carlo method the independent variables are the temperature and the size and shape of the crystal. Once the potential energy is specified as a function of the positions of the atoms, the computer generates many different configurations of a model crystal by successive small random displacements of individual atoms in the vicinity of the initial one, tests each, and accepts or rejects it according to a prescription that ensures that averages over all configurations tend to averages over the canonical ensemble(52). Expressions for various thermodynamic and elastic properties in crystals in terms of such averages are now available in the literature.(53,54)

The Monte Carlo method is exact in principle in the classical limit. In practice, its accuracy is limited by the necessarily finite (small) number of atoms in the model crystal (usually a few hundred), and the statistical uncertainty of the averages, which depends on the number of configurations sampled (up to ~ 10^7). Recently Cowley(55) has shown how the accuracy of Monte Carlo simulations can be increased significantly even for model crystals consisting of a very small (32) number of atoms. The improvement is based on the idea that the thermodynamic functions such as the thermal energy and specific heat of a classical quasiharmonic crystal satisfying periodic boundary conditions are proportional to N-1 rather than to N, where N is the number of atoms. Such a proportionality is also approximately valid for the vibrational contributions to the pressure and bulk modulus. The static contributions to these quantities, however, are proportional to N. Thus Cowley calculated the vibrational contributions to these quantities and normalized them by N-1 before adding them to the static contributions. The errors in the calculation of the mean energy, specific heat, bulk modulus, and Gruneisen constant at a temperature close to the melting point of an fcc crystal of 108 atoms interacting through a Lennard-Jones potential were estimated to be no larger than 1%, when 2,160,000 configurations were averaged over (Fig. 3).

More recently, Day and Hardy(56) have carried out further Monte Carlo calculations of the thermodynamic properties of the same nearest neighbor, fcc, Lennard-Jones crystal studied earlier by Cowley(55). Instead of using the Metropolis algorithm(52) for generating and accepting or rejecting configurations of the model crystal, these authors used a Gaussian algorithm that is particularly convenient for dealing with solids.

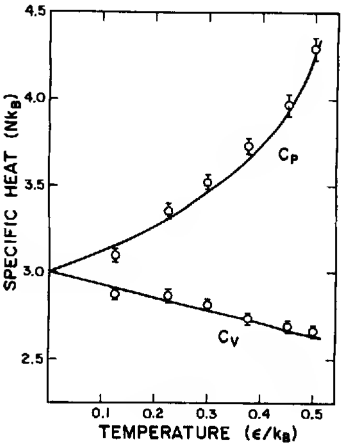

Fig. 3. Specific heats C_V and C_p. The circles are the results of Monte Carlo calculations. The solid curve is drawn through the cell-cluster results of Ref. 39. [Ref. 55].

With this algorithm new points in configuration space are chosen with a distribution that is characteristic of an Einstein-type harmonic approximation. The chosen points are then accepted or rejected on the basis of a criterion similar to that used in the Metropolis algorithm, which also ensures that averages over all configurations tend to averages over the canonical ensemble. The results of Day and Hardy for a 108 atom crystal have been have been combined with those of Cowley, and have halved the uncertainties in his results thereby. Monte Carlo molecular dynamics simulations are now approaching levels of accuracy in the calculation of anharmonic properties that are limited only by the accuracy of the interatomic potentials used in them.

Although both of these methods are valid only in the classical limit of high temperatures, there is now an expectation that used in conjunction with path-integral expressions for thermodynamic functions and dynamic correlation functions(57) they can yield results in the low temperature region where quantum effects are important. (There is some evidence that Monte Carlo methods are better suited for such calculations than molecular dynamics simulations(58).) This is an application that certainly deserves exploration in the near future.

4. Localization of Phonons

Theoretical investigations of phonons in disordered solids have been carried out for more than thirty years, and experimental studies of such systems, e.g. by neutron scattering and by infrared absorption and Raman scattering techniques, have been conducted for almost as long a time. Much of this work has been devoted to the determination of the phonon frequency distribution function, or related quantities, such as absorption or scattering spectra. However, very little is known about the actual nature of the phonon states. By analogy with what is known about electrons in disordered systems, it is expected that for strong disorder phonons will be localized excitations in the Anderson sense(59). Studies aimed at elucidating the nature of phonons in disordered two- and three-dimensional solids have been carried out by a number of different approaches recently, and we consider them here.

4.1. Computer Simulations

Recently, two types of numerical studies of phonon localization have appeared. One of them effectively involves the diagonalization of the dynamical matrix of a compositionally disordered crystal. The second is based on a molecular dynamics simulation of a structurally disordered medium.

As an example of the first type of study, Canisius and van Hemmen(60) have obtained the normal mode frequencies and the corresponding eigenvectors of an isotopically disordered d-dimensional (where $d = 2,3$) simple cubic lattice(54), in which the equations of motion of the d components of the displacement vector of each atom decouple. It was assumed that the mass at each lattice site is M with probability p and m with a probability $q = 1-p$, where $M > m$. The dynamical matrix was diagonalized numerically for crystals containing 27 × 27 and 10 × 10 × 10 atoms for $d = 2$ and 3, respectively. Each eigenvector $(y_1, y_2, \ldots, y_N)$ for a lattice of N sites was used in a calculation of the inverse participation ratio (IPR),

$$\mathrm{IPR}(\vec{y}) = \sum_{i=1}^{N} y_i^4 / \Big(\sum_{i=1}^{N} y_i^2 \Big)^2 . \tag{4.1}$$

For extended states y_i is of $O(N^{-1/2})$, so that the corresponding IPR is of $O(N^{-1})$. For a state localized about the j^{th} site $y_i \sim \delta_{ij}$, so that the corresponding IPR is of $O(1)$. These authors find that classical percolation theory gives a nearly complete description of the results they obtain (however, see the discussion in Section 4.2). The site percolation threshold p_c of a cubic lattice is 0.593 in two dimensions and 0.311 in three.(62) Thus, when $p > p_c > q$ the heavy masses percolate, the light masses do not, and all modes with squared frequencies in $[0, 4d/M]$ are expected to be associated with the infinite, percolating M-cluster. Since delocalized eigenstates are associated with an infinite cluster, these states are delocalized. The light masses, however, have squared frequencies in $[4d/M, 4d/m]$, cannot diffuse in to the infinite M cluster and should be localized on the m islands, which are finite since $q < p_c$. Thus, in this case there is a mobility edge. If $p > p_c$ and $q > 1 - p_c$, so that both the heavy and light masses percolate, only delocalized states are expected. Finally, when $p < p_c < q$, so that the lighter masses percolate while the heavier ones do not, the light atoms form an infinite cluster while the heavy atoms stay together on finite islands. For modes with squared frequencies greater than 4d/M extended states are still allowed as far as the light masses are concerned because they constitute an infinite cluster. The states with squared frequencies in the interval [0, 4d/M] will live on both the heavy and light atom clusters and will be extended. These predictions are largely borne out by the numerical results.

Direct diagonalization of the dynamical matrix becomes unfeasible if the number of atoms in the crystal becomes large. Williams and Maris(63) have devised a different numerical approach to obtaining the frequency distribution function and the eigenvectors of an isotopically disordered crystal. It is based on solving the equations of motion of the crystal in the presence of an external driving force. They have applied their method to a 40 × 40 square lattice of atoms whose masses M are randomly distributed in the range $1-q < M < 1+q$. Their results show that high frequency modes are localized, while below a critical frequency, which is lower the greater the disorder, i.e. the larger is q, the modes are delocalized or perhaps only weakly localized.

A different type of computer study of phonon localization has been carried out by Nagel *et al.*(64) These authors have carried out molecular dynamics simulations of phonons in several Lennard-Jones glasses at low temperatures. The glasses were made by first preparing a liquid above the equilibrium melting temperature T_M and then quenching the samples to a low temperature ($\sim 10^{-5}\ T_M$) where no diffusion could be observed. The normal modes of the resulting glass were studied numerically, and it was found that above a certain frequency the modes are localized.

4.2. Continuum Calculations

In contrast to the numerical studies of phonon localization just described are the recent field-theoretic investigations by John *et al.*(65) of the transition from extended to localized states in a disordered elastic medium that supports both longitudinal and transverse vibration modes. These authors have studied the average diffusivity of a system possessing a random mass density of the form $m(\vec{x}) = m_o + m'(\vec{x})$, where m_o is the average mass density, and $m'(\vec{x})$ is the fluctuating mass density characterized by the correlation function

$$\langle m'(\vec{x})m'(\vec{y})\rangle = \gamma^2\delta^d(\vec{x}-\vec{y}) \tag{4.2}$$

in a medium of d spatial dimensions, where the angular brackets denote an average over the ensemble of realizations of $m'(\vec{x})$, and γ is a parameter that measures the amount of disorder. The averaged diffusivity D of the medium is expressed in terms of frequency and coordinate moments of the averaged two-particle Green's function $\langle G_{ki}(\vec{x},\vec{0},\omega_+)G_{ki}(\vec{x},\vec{0},\omega_-)\rangle$ ($\omega_\pm = \omega \pm i\eta$), where $G_{ki}(\vec{x},\vec{y},\omega_+)$ is the Fourier transform of the retarded Green's function $G^+_{ki}(\vec{x},\vec{y},t)$ that satisfies the equations

$$m(\vec{x})\ddot{G}^+_{ki}(\vec{x},\vec{y},t) = (\lambda+\mu)\frac{\partial^2}{\partial x_k \partial x_\ell} G^+_{\ell i}(\vec{x},\vec{y},t) + \mu\nabla^2 G^+_{ki}(\vec{x},\vec{y},t), \tag{4.3}$$

$$G^+_{ki}(\vec{x},\vec{y},t) = 0 \qquad t < 0, \tag{4.4}$$

$$\dot{G}^+_{ki}(\vec{x},\vec{y},0) = \delta_{ki}\delta^d(\vec{x}-\vec{y}), \tag{4.5}$$

where λ and μ are the Lame constants of an isotropic elastic medium. Explicitly, we have that

$$D = \lim_{\eta\to 0} 2\eta \frac{\int_{-\infty}^{\infty} d\omega\, \omega^2 \int d^d x\; x^2 \langle G_{ki}(\vec{x},0,\omega_+)G_{ki}(\vec{x},0,\omega_-)\rangle}{\int_{-\infty}^{\infty} d\omega\, \omega^2 \int d^d x \langle G_{ki}(\vec{x},0,\omega_+)G_{ki}(\vec{x},0,\omega_-)\rangle} . \tag{4.6}$$

This equation is rewritten in the form

$$D = \frac{\int_{-\infty}^{\infty} d\omega\; E(\omega)D_0(\omega)}{\int_{-\infty}^{\infty} d\omega\; E(\omega)} , \tag{4.7}$$

where $E(\omega)$ is the spectral density of energy excited in the medium by the initially injected phonon packet. Equation (4.7) defines the frequency-dependent diffusivity $D_0(\omega)$. The behavior of $D_0(\omega)$ determines whether normal modes of frequency ω are extended or localized. If phonons of frequency ω are localized, $D_0(\omega)$ will renormalize to zero, whereas extended states of frequency ω give rise to a nonzero value of the diffusivity at that frequency. The results of a field-theoretic calculation shows that all finite frequency phonons in one and two dimensions are localized, with low frequency localization lengths diverging as ω^{-2} and $\exp(1/\omega^2)$, respectively. (The localization length is the characteristic distance defining the spatial decay of the displacement field of a vibrational mode with increasing distance from the point about which it is localized.) They have also shown that a mobility edge at a frequency ω^*, separating low frequency extended states from high frequency localized states, exists in greater than two dimensions. The former results indicate why it is difficult to demonstrate localization of low frequency phonons by numerical methods applied to lattices of finite size. The phonon localization length at $\omega = \omega^*$ diverges as $|\omega-\omega_*|^{-1}$ in three dimensions.

In subsequent work John and Stephen(66) have replaced the right hand side of Eq. (4.2) by $B(\vec{x}-\vec{y})$, where $B(\vec{x})$ decays to zero over a characteristic distance a, either exponentially or as some inverse power of $|\vec{x}|$. The results for the average diffusivity are qualitatively similar to those obtained by John et al.(65)

4.3. How Can Phonon Localization be Observed?

All of the calculations of phonon localization, whether numerical or analytic, described above were based on the harmonic approximation. The scattering of phonons from the mass defects is therefore elastic. In this approximation the mean free path for phonons in a perfect crystal is infinite. If one now includes phonon-phonon interactions due, say, to lattice anharmonicity, in the theory, a new length is introduced into the problem, viz. the inelastic mean free path. The latter must be longer than the phonon localization length due to disorder if localization of phonons in the harmonic approximation is to be important.(65) The inelastic mean free path for phonons due to anharmonic three-phonon processes becomes longer as the temperature of a crystal is lowered. However, at the same time the frequency of the phonons that contribute predominantly to transport properties of solids becomes lower, and the localization length of the phonons diverges with the lowering of the phonon frequencies. These competing effects of localization and inelastic scattering on phonon transport coefficients, in particular on the thermal diffusivity of phonons, have been discussed by Jackle(67). He has suggested that in solids that have a chain-like structure with weak inter-chain forces a minimum in the diffusivity vs. temperature curve is expected to exist at some intermediate temperature, in contrast to a monotonically decreasing dependence on temperature in the absence of localization effects. I am unaware of any experimental verification of this result as yet.

5. Phonons in Amorphous Materials

A good deal of the interest in amorphous materials, specifically amorphous semiconductors, arises from the fact that it is much more economical to prepare them than it is to prepare their single crystal counterparts. This makes such materials interesting for technological applications. These materials are also interesting because they display physical properties that are different from those of their crystalline modifications, and demand theoretical understanding.

One of the fundamental properties of an amorphous material is its structure, which so far has eluded direct experimental determination, apart from measurements of the pair distribution function (i.e. the probability of finding an atom at a distance r from a given atom) by neutron and x-ray scattering techniques. Indirect ways of obtaining information about the structure of amorphous materials can be obtained from the confrontation between experimental data and the predictions of theoretical calculations of various properties of such materials on the basis of different structural models for them. In particular, the vibrational properties of such models can be used to interpret the results of infrared absorption, Raman, and neutron scattering experiments to provide insight into the structure of amorphous materials.

Up to now, the dynamical properties of such materials have been studied on the basis of two rather different approaches. In the first of these a structural model is constructed from a finite number of atoms according to some specification of bond lengths and angles(68), and the normal mode frequencies and associated eigenvectors are calculated by a numerical diagonalization of the corresponding dynamical matrix. Quite recently, a relatively simple prescription for generating amorphous structures by the introduction of topological defects into crystalline materials has been developed by Wooten and Weaire(69). It has been used by de Leeuw, He and Thorpe(70), and by Thorpe and de Leeuw(71) in studies of the vibrational properties of such structures.

The second approach to the theoretical study of amorphous materials is to use simple structural models for which analytic solutions are possible. The most convenient of these, and the one most frequently used, is the Bethe lattice(72,73). A Bethe lattice is a nonperiodic branching structure that contains no rings of bonds. It preserves the tetrahedral local coordination characteristic of many elemental semiconductors, but it approximates the range order by eliminating all rings of bonds. Hybrid models have also been constructed in which a finite cluster of atoms has its local atomic arrangement considered precisely, but the effects of atoms outside the cluster are approximated by attaching a Bethe lattice to each of the atoms in the surface of the cluster(74,75). A survey of recent studies of dynamical properties of amorphous materials carried out on the basis of this second approach has been given recently by Elliott(76).

Amorphous materials show some characteristic differences in their low temperature thermal properties from those of crystalline materials.(77) For example, the specific heat follows a $c_1T + c_3T^3$ law at temperatures below 1 K, while the curve of C/T^3 vs T has a mild upturn with a maximum at a temperature between 1 and 10 K. The thermal conductivity κ varies roughly as T^2 at temperatures below 1 K, displays a "plateau" region of little temperature dependence at temperatures between 1 and 10 K, and increases again at higher temperatures. The behavior of these thermal properties at temperatures below 1 K can be explained in terms of the presence of two-level systems in amorphous materials, whose nature is as yet unknown(78-79) (see, however, Ref. 80). The thermal properties in the temperature range of 1-10 K, however, are not yet understood satisfactorily.

It has been suggested recently, that an explanation of this behavior might be found in the following picture of the structure of amorphous solids. Many random systems, e.g. percolation clusters, polymers, rubbers, gels, behave like homogeneous (translationally invariant) systems for length scales L large compared to some "correlation length" ξ, and exhibit a self-similar (fractal) geometry for $L < \xi$. [In the case of percolating networks near the percolation threshold p_c, ξ is the percolation correlation length ξ_p, which diverges as p_c is approached from above(81).] Alexander and Orbach(82) suggested that in such systems the vibrational modes whose wavelength λ is larger than ξ have the usual low frequency phonon dispersion relation $\omega_{ph}(\lambda^{-1}) \propto \lambda^{-1}$, while the vibrational modes whose wavelength is smaller than ξ have a modified dispersion relation $\omega_{fr}(\lambda^{-1}) \propto \lambda^{-\bar{d}/\tilde{d}}$. Here $\bar{d}$ is the Hausdorff (fractal) dimensionality of the system, which describes how the mass of the system depends on the length scale, while $\tilde{d}$ is the so-called fracton (fractal phonon) dimensionality that characterizes the low frequency behavior of the density of states of the system. In general, it is the case that $\tilde{d} < \bar{d}$.(83) There should be a sharp increase in the density of vibrational states at a crossover frequency ω_c, (84-86) which corresponds to excitations with wavelengths of the order of ξ. This increase is related to the excess specific heat of amorphous materials in the temperature range ~10 K. The excitations (fractons) whose wavelengths are smaller than ξ should be localized.(83)

The explanation of the observed temperature dependence of the lattice thermal conductivity of amorphous materials that emerges from these results is the following(87). The lowest temperature regime is associated with the scattering of phonons off two level systems, and is characterized by a thermal conductivity that increases with increasing temperature as the square of the temperature. For higher temperatures the thermally excited vibrational excitations cross over from phononlike to fractonlike at a temperature $T \approx \hbar\omega_c/k_B$. Because the fractons are spatially localized(83), they cannot contribute to the heat current. In this range of temperatures k_BT is larger than the phonon energies. But only the phonons can conduct heat. Thus one is in the Dulong-Petit regime for the heat-carrying phonons, and if the phonon mean free path is temperature independent, the thermal conductivity is a constant. Arguments have been presented to show how the phonon mean free path in this temperature region can have the required property(87). At higher temperatures phonon-assisted fracton hopping leads to a subsequent increase in the thermal conductivity with increasing temperature that is linear in the temperature(87).

The preceding is not the only explanation of the low temperature thermal properties of amorphous materials. Experimental evidence against it has been presented(88), as well as support for it(89-92), and alternative explanations have been advanced for the observed phenomena(80,93-96). It is not my intention here to argue for or against the fracton explanation of the low temperature thermal properties of amorphous materials. What I do want to emphasize is that the work of Orbach and his colleagues referred to above has stimulated a great many theoretical and experimental studies of phonons in fractal systems, and that such studies can be expected to continue.

Some recent theoretical work of this kind has dealt with phonons on specific fractal lattices, viz. d-dimensional Sierpinski gaskets(97-98) and on percolation clusters in a simple cubic crystal(99). The results of these numerical, real space renormalization group studies show a smooth crossover from a phonon to a fracton regime in the density of states, but with no apparent sharp increase in the density of sates at a crossover frequency. The density of states has many gaps that contain localized modes. The higher frequency part of the density of states consists of both extended and localized states.

Because fractals are intermediate between crystalline structures and disordered materials, they will undoubtedly be studied in the future for the light their properties can shed on the properties of the latter class of materials.

6. Phonons in Quasicrystals

One of the most striking experimental discoveries in the field of materials science in the past few years was the discovery(100) of a metallic solid, $A\ell_{0.14}\ Mn_{0.86}$, that has point group symmetry $m\bar{3}\ \bar{5}$ (icosahedral), which is incompatible with lattice translations(101). Since the initial discovery of such compounds several more have been found(102-104). Levine and Steinhardt(105) termed such solids quasicrystals. In general, quasicrystals are solids that possess the following properties(105): (1) the distance between any two lattice points is greater than some $r > 0$; every lattice point lies within some distance $R > 0$ of another lattice point; (2) the lattice is self-similar in the sense that one can eliminate a subset of the lattice points and obtain another quasicrystal lattice with nearest neighbor distances increased by a constant factor; (3) the lattice has perfect long-range bond orientational order; (4) the lattice has quasiperiodic translational order with $k(>1)$ linearly independent (incommensurate) lattice spacings along each lattice vector direction.

The construction of one-dimensional quasicrystals is described clearly by Lu *et al.*(106), who give several examples of such quasicrystals. The simplest of these is the Fibonacci sequence that is formed iteratively from two basic elements (bond lengths) A and B, by starting with the unit AB as stage zero of the construction and obtaining stage n+1 from state n by replacing each A by AB and each B by A:

$$AB \rightarrow ABA \rightarrow ABAAB \rightarrow ABAABABA \rightarrow ABAABABAABAAB \rightarrow \ldots \qquad (6.1)$$

Although the result of this procedure is a nonperiodic structure, it is deterministic and highly ordered. (Note that one-dimensional quasicrystals do not have any nontrivial long-range bond orientational order.)

An example of a two-dimensional quasicrystal is provided by the pattern of Penrose tilings(107,108) depicted in Fig. 4.(108) In any Penrose tiling two tiles, the so-called kite and the dart, fill two-dimensional space, only nonperiodically. Each tile consists of two long and two short edges, with the ratio of the lengths of the long and short edges being the golden ratio $\tau \equiv (\sqrt{5}+1)/2 = 1.61803...$ There is an infinite number of Penrose tilings, in each of which the ratio of kites to darts is τ:1.

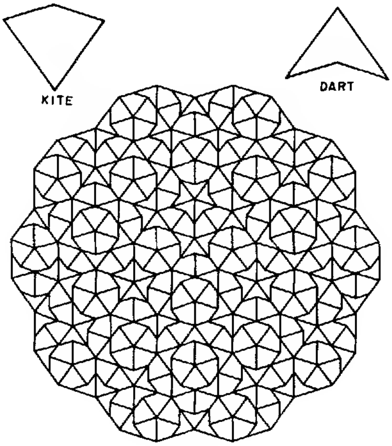

Fig. 4. A two-dimensional Penrose tiling [Ref. 108].

Quasicrystals in three dimensions have correspondingly more complex structures.(109)

The experimental discovery of such solids has prompted many investigations into such questions as to how such structures can give rise to sharp diffraction peaks(105), and why the icosahedral structure should be favored over the bcc structure in the quenching process by which such solids are formed(110-112). The elastic properties of quasicrystals have also been studied(113), as have certain electronic(114,115) and vibrational(106,115) properties. It is the latter that concern us here.

Lu *et al.* calculated the integrated density of states for a Fibonacci chain of 2000 atoms with fixed-end boundary conditions by a transfer matrix method(116) and found that it has a self-similar nature (Fig. 5).

Odagaki and Nguyen$^{(114)}$ have studied the vibrations of three, nearest-neighbor models of two-dimensional quasicrystals described by Penrose tilings consisting of ~ 400 atoms in which the atoms vibrate perpendicular to the plane of the lattice. Two of these crystals have a five-fold rotational symmetry axis, which indicates an absence of translational symmetry. The corresponding dynamical matrix was diagonalized numerically, and the density of states, the integrated density of states, and the participation ratio for each mode were calculated. The spectra for different Penrose tilings appear to be very similar. They show several gaps, and van Hove singularities seem to exist. Localized states seem to exist, and the number of localized states becomes significant when $k_L/k_S < 0.4$, where $k_L(k_S)$ is the force constant associated with the long (short) edge of a tile.

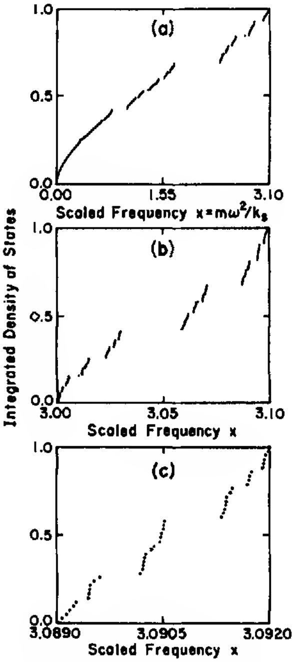

Fig. 5. (a) Integrated density of states for a Fibonacci chain of 2000 atoms with $k_L/k_S = (\sqrt{5}-1)/2$, where $k_L(k_S)$ is the force constant associated with a long (short) bond. (b) is the same as (a), enlarged around x = 3.10. (c) is the same as (b), further enlarged about x = 3.0905. Self-similarity is evident. [Ref. 106].

Although the vibrational properties of three-dimensional quasicrystals have yet to be studied, the electronic density of states has been calculated for a quasicrystal of the type discussed in Ref. 109, consisting of ~ 2000 atoms and terminated by Bethe lattices$^{(115)}$ It is almost featureless. The participation ratio indicates that the states are delocalized. Qualitatively similar results are expected for the vibrational properties of such solids.

The study of the dynamical properties of quasicrystals is just beginning. New computational methods for calculating the normal mode frequencies and the associated eigenvectors will have to be found, since the direct numerical diagonalization of the large dynamical matrices corresponding to crystals of large numbers of atoms will rapidly become unfeasible. In time, nonequilibrium properties, e.g. phonon transport properties, will be investigated, as well as anharmonic properties, in which the effects of the nonlinearity of the interatomic forces compete with those originating in the quasi-periodicity of the structure.

7. Phonons in Superlattices

Deliberately structured materials are materials that have been structured either during or after growth to have dimensions or properties that do not occur naturally. Deliberately structured materials can be ordered in their structures, as in the case of artificial periodic superlattices that consist of alternating layers of different metals, or semiconductors and metals. Alternatively, they can be ordered on a microscopic scale and yet be disordered overall, as in the case of systems composed of small particles of one material embedded in a matrix of a second. Such materials possess transport, elastic, and optical properties that can differ considerably from those of their constituents in the bulk state and, perhaps more significantly, these properties can be tuned in desirable ways by varying the constituents and thicknesses, in the case of superlattices, or by altering the constituents, their size distributions, and their relative concentrations, in the case of mixed media.

In this section I will be concerned with phonons in only one type of deliberately structured material, viz. superlattices. Such structures have been the objects of intense theoretical and experimental study in the past decade. They have already yielded interesting new physics through the discovery of the quantum Hall effect(117) and the fractional quantum Hall effect(118), and the ability to modify their physical properties in the manner described above makes them candidates for a variety of technological applications.

7.1. Phonons in Periodic Superlattices

The study of the propagation of acoustic waves through layered media goes back more than seventy years. The motivation for much of the earliest work was the desire for an accurate description of the propagation of seismic waves through the earth's crust, whose density and elastic properties vary with distance from the surface of the earth.

With the development of techniques (e.g. molecular beam epitaxy) for fabricating artificial semiconductor superlattices consisting of a periodic sequence of very thin layers of (say) two different materials such as GaAs and $Al_xGa_{1-x}As$ (compositional superlattices)$^{(119,120)}$, or of a periodic n- and p-doping structure in an otherwise homogeneous semiconductor crystal, perhaps with undoped regions in between (doping superlattices)$^{(121,122)}$, interest has begun to turn to the study of phonons in such periodically modulated structures from a lattice as opposed to a continuum point of view. This tendency has been accelerated recently by the development of techniques for the fabrication of metallic superlattices$^{(123)}$ and of superlattices consisting of alternating layers of magnetic and nonmagnetic metals$^{(124)}$.

In what follows, we consider phonons in periodic superlattices from a continuum and from a lattice point of view in turn.

7.1.1. Continuum Theories

In this subsection phonons in superlattices will be discussed on the basis of elasticity theory for several different kinds of situations that can arise in practice. Both infinitely extended and semi-infinite media will be considered.

7.1.1.1. Infinitely Extended Structures

The earliest modern investigations of elastic wave propagation in a medium that consists of alternating layers of two different materials focused largely on the determination of the effective elastic moduli of such laminated media which, in general are anisotropic, even if the lamina out of which they are fabricated are themselves isotropic$^{(125-131)}$. For example, a medium that consists of alternating layers of two different isotropic elastic media is hexagonal, with its axis of six-fold symmetry perpendicular to the lamina.

While such an approach to wave propagation in periodically layered systems, usually called an effective modulus theory, simplifies all subsequent calculations based on its results, it has the drawback that it predicts bulk and surface acoustic waves that are nondispersive, while calculations that take the laminations into account explicitly yield dispersive modes. Consequently, recent work dealing with such systems has avoided the use of effective modulus theories.(132-141)

To illustrate the kinds of results that can be obtained for the propagation of elastic waves through layered media, I consider a few simple examples.

A particularly simple case is presented by the propagation of a transverse wave through a laminated medium in which the layers are oriented perpendicular to the x_1-axis. The displacement vector $\vec{u}(\vec{x},t)$ has the form $\vec{u}(\vec{x},t) = (0,u(x_1x_3|\omega),0)\exp(-i\omega t)$. The boundary conditions in the problem are that the displacements and stresses be continuous across each interface. At the same time $u(x_1x_3|\omega)$ must satisfy the Bloch condition $u(x_1+L, x_3|\omega) = \exp ikL\, u(x_1x_3|\omega)$, where L is the period of the structure. It is now convenient to make the Ansatz $u(x_1x_3|\omega) = u(\kappa\omega|x_1)\cos\kappa x_3$. When this is substituted into the equations of motion and the several boundary conditions, we obtain as the dispersion relation for waves in this system

$$\cos kL = \cos\alpha d_1\cos\beta d_2 - \frac{1}{2}(F+F^{-1})\sin\alpha d_1\sin\beta d_2, \qquad (7.1)$$

with $\alpha(\kappa\omega) = ((\omega^2/c_t^2)-\kappa^2)^{1/2}$, $\beta(\kappa\omega) = ((\omega^2/c_t'^2 - \kappa^2)^{1/2}$, and $F = \rho c_t^2\alpha/\rho' c_t'^2\beta$. Here $\rho, c_t d_1 (\rho', c_t', d_2)$ are the density, speed of transverse waves, and thickness of the material in the range $nL < x_1 < nL + d_1$ $(nL + d_1 < x_1 < (n+1)L)$.

There are two interesting special cases to consider. The first is the case $\kappa=o$. With the wave vector k restricted to the first Brillouin zone $(-\pi < kL < \pi)$, the dispersion curve (Eq. 7.1) possesses an infinite number of branches with gaps at $k=o$ and at $k = \pm\pi/L$. Crudely speaking, the higher frequency branches are the result of folding back into the first Brillouin zone the portions of the dispersion curves corresponding to values of k outside the first zone. The presence of gaps in the dispersion curves, which correspond to stop bands for the waves considered here, is characteristic for wave propagation in layered media.

A second interesting case of Eq. (7.1) arises when we set $\kappa=(2n+1)\pi/2d$ with $n=0,1,2,\ldots$ In this case the surfaces $x_3 = \pm d$ become stress-free, and Eq. (7.1) is the dispersion curve for transverse waves propagating in a slab of thickness 2d made up of alternating sections of two different isotropic media, with stress-free surfaces. The dispersion curves are more complex in this case, as they are for a homogeneous slab of finite thickness, but the occurrence of gaps in these curves persists.

7.1.1.2. Semi-Infinite Structures

Not all layered media of interest in connection with elastic wave propagation in them are of infinite extent. Semi-infinite superlattices are of considerable interest as well, because they can support surface acoustic waves, and the latter are becoming increasingly interesting due to the possibility of their use in device applications.

An interesting example of effects that are made possible by the presence of a superlattice is the binding of shear horizontal surface acoustic waves to a surface when the medium supporting these waves is periodically laminated parallel to the stress-free surface $x_3=0$.(140) In shear horizontal waves the displacement is polarized normal to the sagittal plane. We can take the direction of propagation to be the x_1-direction, in which case the sagittal plane is the x_1x_3-plane. If the region $x_3 > 0$ is occupied by a homogeneous elastic medium, it is impossible to satisfy the stress-free boundary condition at the surface $x_3 = 0$ with a solution of the equation of motion of the medium that decays exponentially as $x_3 \to \infty$. However, when the semi-infinite medium is periodically layered, it becomes possible to bind a shear horizontal wave to the surface, provided that the outermost layer is made from the medium with the lower speed of bulk transverse waves.

Recently Kueny and Grimsditch(136) have calculated numerically the speeds of Rayleigh surface waves propagating along the stress-free surface of a semi-infinite medium made up of alternating layers of two different isotropic media of equal thickness parallel to the surface. In a Rayleigh wave the elastic displacement vector lies in the sagittal plane, i.e. the plane defined by the direction of the wave vector and the normal to the surface. In the numerical calculations a system of n layers of two isotropic media was assumed to be deposited on a substrate of the material with the larger speed of bulk transverse waves. Systems of up to 1000 layers were studied in this work. More recently, exact solutions for the speeds of Rayleigh waves, and for the dynamic elastic Green's tensor, of the semi-infinite version of this system were obtained by exploiting the periodicity of the infinite medium from which the semi-infinite system being studied can be assumed to be excised. This leads to working with only 4 x 4 matrices$^{(141)}$. The Rayleigh waves obtained in this structure are dispersive, in contrast with Rayleigh waves on the surface of a homogeneous medium, and the nature of the dispersion can be altered by varying the number of layers, the elastic properties of the two media, and the thickness of each layer.

The laminations in a semi-infinite superlattice need not be parallel to the surface of the medium as in the examples just described. If the laminations are perpendicular to the stress-free surface of the medium$^{(142)}$, a Rayleigh wave propagating normal to the lamination has properties similar to those of a Rayleigh wave propagating across the grooves of a grating ruled on the surface of a homogeneous, semi-infinite elastic medium$^{(143)}$. The dispersion curve possesses at most two branches in the nonradiative region of the (ω,k)-plane within the one-dimensional first Brillouin zone $-\pi/a < k \leq \pi/a$ defined by the period a of this structure, separated by a gap at the Brillouin zone boundaries $k = \pm \pi/a$. The existence of such a stop band in the dispersion curve of Rayleigh surface acoustic waves can be useful in the design of filters for the propagation of these waves.

Finally, we note that Camley and Mills$^{(144)}$ (see also Refs. 145-149) have studied electrostatic surface waves in a semi-infinite superlattice consisting of alternating layers of two different dielectric media, characterized by isotropic, frequency-dependent dielectric constants $\varepsilon_A(\omega)$ and $\varepsilon_B(\omega)$, and thicknesses d_1 and d_2, respectively. The laminations in this case are parallel to the interface of this semi-infinite superlattice with a semi-infinite half-space characterized by an isotropic, frequency-independent dielectric constant ε_c (e.g. vacuum). At first glance this work would appear to have nothing to do with phonons. However, if it is recalled that the dielectric constant of a diatomic polar semiconductor in the infrared range of the optical spectrum is vibrational in origin, and has the form

$$\varepsilon(\omega) = \varepsilon_\infty \frac{\omega_L^2-\omega^2}{\omega_T^2-\omega^2}, \tag{7.2}$$

where ε_∞ is the optical frequency dielectric constant and $\omega_L(\omega_T)$ is the frequency of the longitudinal (transverse) optical phonon of infinite wavelength, then the kinds of modes studied by Camley and Mills correspond to optical surface interface modes in semiconductor superlattices. The experimental observation of optical surface phonons at the vacuum-superlattice interface of $GaAs$-$A\ell_{0.3}Ga_{0.7}As$

superlattices by means of high resolution electron energy loss spectroscopy has been reported recently(150). In addition, the Rayleigh mode and several Sezawa modes have been observed in a metallic (Fe-Pd) superlattice by Brillouin scattering techniques(151).

7.1.2. Lattice Theories

Many dynamical properties of superlattices, regarded as consisting of alternating layers of crystal lattices can be understood qualitatively and even semi-quantitatively on the basis of linear chain models of crystals, in which the constituent atoms interact with short range forces(152). With one qualification, this model is valid in bulk cubic crystals for phonons propagating along the [100] direction, where planes of atoms move as a whole and the longitudinal and transverse vibrations are uncoupled. If the longitudinal modes are treated independently of the transverse modes in each layer, a single, nearest-neighbor force constant constitutes the only free parameter for the former modes, while two different nearest neighbor force constants provide the anisotropy required for describing the latter modes(152). If it is desired to fit both the longitudinal and transverse branches simultaneously in each layer, interactions between more distant neighbors must be included.(153)

The qualification that must be attached to the results obtained on the basis of such a model is that they do not reflect the presence of the long-range Coulomb interactions that are present in polar semiconductors. These effects can be taken into account for the long wavelength optical modes by the continuum approach described in the preceding subsection, but the inclusion of the effects of spatial dispersion in the dielectric constants will be required if the short wavelength modes are to be treated correctly.

The qualitative nature of the vibrational modes in a compositional superlattice can be understood on the basis of the following simple argument. Consider the linear chain model for (say) a GaAs-AℓAs bilayer superlattice depicted in Fig. 6. If we initially ignore the difference between the Ga and Aℓ atoms, the dispersion curves for the longitudinal acoustic and longitudinal optical branches of the phonon spectrum have the forms depicted schematically by the solid curves in Fig. 7. Here a is the thickness of the bilayer, and $k = \pm\pi/a$ define the boundaries of the first Brillouin zone for this diatomic crystal. If we neglect the difference in the spacing

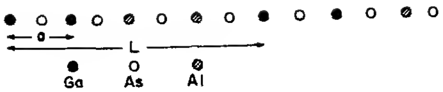

Fig. 6. Model used for linear chain calculations of the phonon dispersion curves of a GaAs-AℓAs bilayer superlattice.

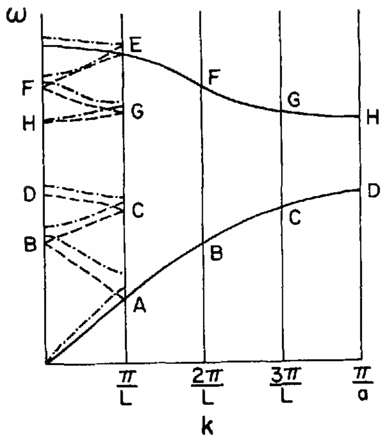

Fig. 7. Dispersion curves for a GaAs-AℓAs bilayer superlattice in the reduced zone scheme.

between the planes of Aℓ and As atoms compared to the difference in the spacing between planes of Ga and As atoms, the period of the superlattice will be $L = 4a$. We have thus superimposed the boundaries of the 1st, 2nd, and 3rd Brillouin zones of the superlattice onto the plot of the GaAs dispersion curves in Fig. 7. We now recall that the latter curves have mirror symmetry about the line $k = 0$, and are periodic in k with period $2\pi/a$. We can therefore translate the portions of these dispersion curves in the 2nd, 3rd, and 4th Brillouin zones of the superlattice into the first Brillouin zone by displacing them to the left or right by integer multipoles of $2\pi/L$, the period of the lattice reciprocal to that of the superlattice. The result is the dashed staircase shaped dispersion curves drawn in the interval $0 \leq k \leq \pi/L$. We now see that the points marked A-D and E-H are special. The frequencies of the GaAs chain are degenerate at these values of k $(\omega(-\pi/L) = \omega(\pi/L))$, and they are separated by translation vectors of the lattice reciprocal to the superlattice ($2\pi/L$, $4\pi/L$, ...). If we now "switch on" the superlattice by replacing Ga atoms by Aℓ atoms to achieve the structure depicted in Fig. 6, degenerate perturbation theory tells us that gaps should open up in the dispersion curves at these points, if the periodic perturbation on GaAs represented by the Aℓ atoms has nonzero Fourier coefficients at these reciprocal lattice vectors.

In addition, the dispersion curves are shifted somewhat from those of pure GaAs. The result is depicted schematically by the dash-dot curves in Fig. 7. This is the phenomenon of the zone folding of phonons in superlattices. One of the consequences of this is that phonons at points such as B, D, F, and H, which are now k = 0 phonons in the superlattice, can become infrared and/or Raman active, whereas they are inactive in the bulk because of the finiteness of the corresponding wave vectors.

Related to the zone-folding of bulk phonons in a superlattice is the notion of confined phonons. In frequency ranges where one component of a superlattice (e.g. GaAs) has a pass band, while the other (e.g. AℓAs) has a stop band, the atomic vibrations are more or less confined to the component for which the frequency range in question is a pass band. This notion applies more commonly to optical phonons than to acoustic phonons because the dispersion curves for the former in each constituent tend to be flatter than those for the latter, so that the likelihood of the overlap of the optical phonon dispersion curves of the two consituents is smaller than for the acoustic branches. Essentially this behavior is observed experimentally. Raman spectroscopic studies of semiconductor superlattices have revealed both the zone-folding of phonons (Fig. 8) and the confinement of optical phonons (Fig. 9).

Although much of the current theoretical analysis of phonons in periodic superlattices is based on linear chain models of such structures, a few papers have appeared in recent years that report calculations of phonon dispersion curves in periodic superlattices in which the true three-dimensional nature of the superlattice is taken into account.(156-157) They carry out for a three-dimensional crystal the kind of "gedanken" construction of a one-dimensional superlattice described above. An interesting recent calculation of this

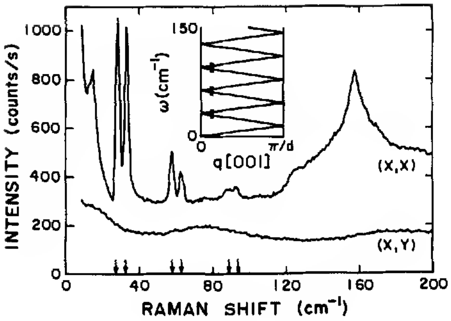

Fig. 8. Raman spectrum of a GaAs-$A\ell_{0.3}Ga_{0.7}As$ superlattice. The inset shows the results of a theoretical calculation showing the wave vectors of folded LA peaks. The arrows indicate predicted peak frequencies [Ref. 154].

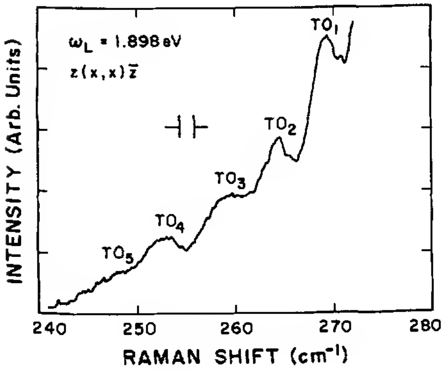

Fig. 9. Raman spectrum of TO-phonons confined in a (7,7)GaAs-AℓAs superlattice. [Ref. 155].

kind has been carried out by Kanellis(157). It is based on the observation that a given crystal structure can be described either in terms of a primitive unit cell or in terms of a supercell containing several primitive unit cells. In the latter case a larger dynamical matrix is required than in the former. These two dynamical matrices are related by a similarity transformation. One can then introduce the effects of a modulation of the structure of the original crystal by modifying appropriate elements of the larger dynamical matrix in a suitable fashion. This approach has been carried out for GaAs-AℓAs superlattices on the basis of a rigid ion model for bulk GaAs and AℓAs. These two crystals were assumed to differ only in the masses of the Ga and Aℓ atoms. However, the Coulomb interactions among the ions are incorporated into the calculations, albeit through the assumption of point ions. The results are in qualitative agreement with experimental results(155). The differences that exist may be attributable to the use of the rigid ion model and the assumption of the same force constants as in GaAs.

Phonons in doping superlattices have been studied by Ruden and Dohler(158). In their model a homogeneous semiconductor has introduced into it planes of donor atoms at x_3 = md and planes of acceptor atoms at $x_3 = (m + \frac{1}{2})d$, where $m = 0, \pm 1, \pm 2, \ldots$, with equal concentrations of both kinds of impurities, under conditions where all impurity atoms are ionized and there are no free charge carriers in the crystal in the ground state. It is found that the presence of the charged sheets of impurity ions has little effect on the phonon dispersion curves. However, since the zone folded acoustic phonons are now optical modes in the superlattice, they should be excitable by electromagnetic fields of very long wavelength. The absorption coefficient for the interaction of long wavelength transverse electromagnetic radiation propagating perpendicular to the doping layers with the transverse new "optical" branches has been calculated by Ruden and Dohler(158) for a realistic system, with the conclusion that this interaction should be observable. It should even be possible to couple an electromagnetic field polarized normal to the doping layers and propagating along the layers to the back-folded longitudinal "optical" phonons created by the superlattice.

Ren and Dow(159-160) have recently calculated the lattice thermal conductivity of an infinitely extended superlattice in which M atomic layers of one simple cubic lattice alternate with N layers of a second simple cubic lattice, that differs from the first only in the masses of the atoms. It is known that Umklapp processes determine the lattice thermal conductivity at intermediate to high temperatures(161). In such processes two phonons propagating normal to the layers with positive group velocities with frequencies of the order of half the Debye frequency for that direction of the propagation can combine to produce a third phonon with nearly the Debye frequency, with a wave vector and a group velocity directed oppositely to those of the initial pair: $k_3 = k_1 + k_2 - G < 0$, where G is a vector of the reciprocal lattice of the superlattice perpendicular to the laminations of the latter. Since G is typically smaller by a factor of M+N than the reciprocal lattice vectors of each of the constituents of the superlattice, the values of k_1 and k_2, and consequently the corresponding phonon frequencies, needed to activate Umklapp processes become important at a lower temperature, and as a result the height of the peak in the curve of the thermal conductivity as a function of temperature is lowered. Similar effects can be expected for other transport coefficients where phonons play a role.

7.2. Phonons in Nonperiodic Superlattices

We have mentioned in the preceding section that the simplest example of a one-dimensional quasicrystal is provided by a Fibonacci sequence of bond lengths in a two-component material. Very recently two groups have succeeded in preparing one-dimensional, quasiperiodic superlattices.

Merlin *et al.*(162) have grown by molecular beam epitaxy on a GaAs (001) substrate, a 13 stage Fibonacci superlattice in which the blocks A and B in the sequence (6.1) consist nominally of (17ÅAℓAs)-(42ÅGaAs), and (17ÅAℓAs)-(20ÅGaAs), respectively. The Raman spectrum of this superlattice showing scattering by LA phonons propagating along [001] is a continuous spectrum that is expected to be a phonon density of states weighted by certain scattering matrix elements. It shows dips that are attributed to gaps in the density of states of the LA modes in agreement with general results for densities of states of quasiperiodic structures(163).

Hu *et al.*(164) prepared metallic Nb-Cu quasiperiodic (Fibonacci) superlattices by magnetron sputtering. The blocks A and B in this case were (18ÅNb)-(41ÅCu) and (18ÅNb)-(19ÅCu), respectively. No measurements of any physical properties of this system have been reported up to now.

Thus the possibility now exists of producing one-dimensional quasicrystals in the form of quasiperiodic superlattices, and we can expect to see a growing number of investigations in the future of the unusual properties these systems are expected to possess.

A second type of nonperiodic superlattice is a disordered one. Consider a structure consisting of alternating layers of two different isotropic elastic media. The elastic properties of one medium are defined by its mass density ρ and the speed of transverse sound c_t; the mass density and speed of transverse sound in the second medium are ρ' and c_t', respectively. If the thicknesses of the successive layers in this structure do not alternate in a periodic fashion, but instead in each pair of $(\rho,c_t)-(\rho',c_t')$ layers the thicknesses d and d' are randomly different, Levine and Willemsen(165) have shown that the amplitudes of the waves in the N^{th} layer pair, computed in terms of the amplitudes at some initial boundary, always decay exponentially with increasing N. In computer experiments they show, moreover, that a cutoff frequency exists above which all realizations of the randomly layered system have wave reflection coefficients of unity. This suggests that a high degree of perfection is required in the fabrication of microstructures of the kind considered here if they are to transmit high frequency waves.

8. Surface Phonons

The theoretical and experimental study of surface phonons has fluorished in the past six years. From among the many developments that have occurred in this field during this time I have selected two, one theoretical, one experimental, that strike me as particularly exciting, to describe in this section.

During the past six years several reviews have appeared that deal with various aspects of the physics of surface phonons.(166-172) The reader is referred to them for a more detailed survey of the current state of this field.

8.1. Ab Initio Calculations of Surface Phonons

Certainly one of the most significant developments in the theory of surface phonons during the past six years has been the appearance of first principles calculations of the dispersion curves of surface phonons on low index surfaces of simple metals. The first such calculations, for Na(001) and subsequently for K(001), were carried out by Beatrice and Calandra,(173-175) who expanded the electronic ground state energy of 15 layer slabs of Na(001) and K(001) to second order in the pseudopoential describing the electron-ion interaction(176), and then re-expanded the result in powers of the displacements of the ion cores from their rest positions to obtain the electronic contribution to the atomic force constants. Combined with the ionic contribution the latter permit the dynamical matrix of the crystal slab, and hence the surface mode frequencies, to be obtained. The unperturbed electronic subsystem in this work consisted of non-interacting electrons confined to a finite region in the direction normal to the surfaces of the slab by infinite potential barriers. The effects of a multilayer relaxation of the spacings between the atomic layers(177) on the normal mode frequencies of the slab were also studied in this work.

In more recent work, Eguiluz _et al_(178,179) have used a very similar approach to calculate the frequencies of surface phonons on the (001) surfaces of Na and Aℓ, and on the (110) surface of Aℓ. The chief differences between their work and that of Beatrice and Calandra are that the wave functions of the unperturbed electronic subsystem were calculated self-consistently on the basis of the Kohn-Sham equations(10) of the local density functional theory, and the effects of exchange and correlation were built into the calculation of the density response function that appears in the electronic contribution to the dynamical matrix. The results of the self-consistent calculation of the surface phonon frequencies differ in some significant ways from those obtained on the basis of the infinite barrier model, particularly in the case of Aℓ. In the later calculations of Eguiluz _et al_.(179) surface relaxation was taken into account in a first principles fashion, and has some effect on the frequencies of surface phonons, particularly on those associated with the Aℓ(110) surface. A typical result of such calculations, for a 17 layer slab of Aℓ(100) is presented in Fig. 10. The relaxation of this surface is very small, so that the curves presented are for an unrelaxed surface. The surface phonons are clearly seen below the continuum of bulk modes along the $\bar{\Gamma}\ \bar{X}$ direction in the surface first Brillouin zone, and in the gaps in the continuum of bulk modes.

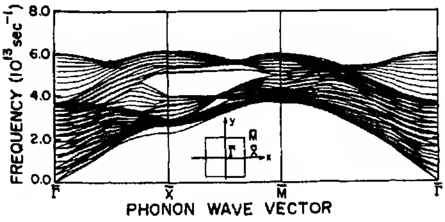

Fig. 10. Dispersion curves of phonons in a 17 layer Aℓ(100) slab. [Ref. 179].

A somewhat different approach to the first principles calculation of the dispersion curves of surface phonons on melted surfaces was taken by Ho and Bohnen(180), who studied Aℓ(110). In these calculations the atomic force constants were obtained from self-consistent total energy calculations in which surface relaxation was taken into account. The change in the total energy of an aluminum slab bounded by (110) surfaces associated with known relative displacements of the atomic layers constituting it was calculated sefl-consistently, and individual atomic force constants were obtained by fitting the results to a force constant model.

Such calculations are still in their infancy. The calculations cited indicate their feasibility at the same time that they reveal their difficulty. We stand at the threshold of an era in which parameter-free determinations of surface dynamical properties from first principles will become as commonplace as the determination of bulk electronic structures of solids are today, but we still have a long way to go before that goal is achieved.

8.2. Experimental Studies of Surface Phonons

At the beginning of the time period to which this review is devoted, the use of helium atom scattering for the determination of surface phonon dispersion curves was barely one year old. It had been used at that time only for the measurement of surface phonon dispersion curves on the surfaces of alkali-halide crystals. Since then the technique has been applied to the study of surface phonons on metal surfaces(181,182), and on layered compounds(168), to the study of surface phonons in layers of rare gas atoms adsorbed in an incommensurate fashion on silver substrates(183,184), and to the observation of surface optical phonons in NaF(185) and LiF.(186) The energy resolution of the method has been improved to the point that it is now in the range of 0.2 to 0.5 meV. One can begin to think about measurements of surface phonon lineshapes in the not too distant future.

During the same period a second experimental technique has been introduced for the determination of the dispersion curves of surface phonons on the clean surfaces of metals and on adsorbate covered surfaces, viz. electron energy loss spectroscopy(187). In this method a beam of electrons of energy E_i and wave vector $\vec{k}_i$ impinges on a crystal surface, excites or de-excites a phonon of frequency ω and wave vector $\vec{q}_\parallel$, and emerges with energy E_s and wave vector $\vec{k}_s$. If we take into account that $h\omega$ is always negligible compared to E_i and E_s, the surface phonon dispersion curve $\omega = \omega(\vec{q}_\parallel)$

is obtained from the pair of equations that express the conservation of energy and the components of the wave vectors parallel to the surface(187):

$$|E_i - E_s| = h\omega \qquad (8.1)$$

$$k(\sin\theta_i - \sin\theta_s) = q_{\parallel}, \qquad (8.2)$$

where $k = |\vec{k}_i| = |\vec{k}_s|$, and θ_i and θ_s are the polar angles of $\vec{k}_i$ and $\vec{k}_s$, respectively, measured from the normal to the surface. At each value of θ_i for a fixed θ_s (i.e. for each value of $q_{\parallel}$) the intensity of the outgoing beam is measured as a function of $E_i - E_s$, which yields the loss spectrum. A peak occurs in this spectrum when the conditions for exciting or de-exciting a surface phonon are satisfied. The energy resolution of this method is now about 7 meV for the large angle scattering required for mapping out surface phonon dispersion curves. Surface phonon dispersion curves have been obtained by this method for Ni(001),(188,189) TaC(001), (190), NbC(001)(191), Ni(001)-p(2×2)O (192) and Ni(001)-c(2×2)O.(193) This method is not limited by the energy of the surface phonon and is thus well suited to the study of high frequency surface phonons associated with adsorbed layers of atoms.

The existence of two experimental methods for measuring surface phonon dispersion curves provides us with a way of testing models used in calculating dynamical properties of surfaces, and of estimating the magnitude of surface relaxation if the variation of atomic force constants with interatomic separation is known from an independent calculation. In the case of adsorbate covered surfaces these methods can provide information about the symmetry of the adsorption site and, together with the results of quantum chemistry caculations, can give information about the adsorbate-substrate distance. Activity in this field should be intense for the forseeable future.

Acknowledgements

I am grateful to the Graduate Council of the University of California, Irvine, for travel funds that made my participation in this School possible. This work was supported in part by NSF Grant No. 85-17634.

References

1. M. Born and Th. von Karman, Phys. Z. 13, 297 (1912).
2. T. Toya, J. Res. Inst. Cat. Hokkaido Univ. 6, 161, 183 (1958).
3. H. Bilz, B. Gliss, and W. Hanke, in Dynamical Properties of Solids, vol. 1, eds. G. K. Horton and A. A. Maradudin (North-Holland, Amsterdam, 1974), p. 343.
4. E. G. Brovman and Yu. M. Kagan, in Dynamical Properties of Solids, vol. 1, eds. G. K. Horton and A. A. Maradudin (North-Holland, Amsterdam, 1974), p. 191.
5. S. K. Sinha, in Dynamical Properties of Solids, vol. 3, eds. G. K. Horton and A. A. Maradudin (North-Holland, Amsterdam, 1980), p. 1.
6. Ab Initio Calculations of Phonon Spectra, ed. J. T. de Vreese, V. E. van Doren, and P. E. van Camp, (Plenum, New York, 1983).
7. J. Ihm, A. Zunger, and M. L. Cohen, J. Phys. C12, 4409 (1979).
8. R. M. Martin and K. Kunc, Ref. 6, p. 65.
9. P. Hohenberg amd W. Kohn, Phys. Rev. 136, B864 (1964).
10 W. Kohn and L. J. Sham, Phys. Rev. 140, A1133 (1965).
11. L. J. Sham and W. Kohn, Phys. Rev. 145, B561 (1966).
12. D. R. Hamann, M. Schluter, and C. Chiang, Phys. Rev. Letters 43, 1494 (1979).
13. K. Kunc and R. M. Martin, Phys. Rev. B24, 2311 (1981).
14. K. Kunc and R. M. Martin, Phys. Rev. Letters 48, 406 (1982.
15. G. Dolling and J. L. T. Waugh, in Lattice Dynamics, ed. R. F. Wallis, (Pergamon, Oxford, 1965), p. 19.
16. K. Kunc and R. M. Martin, J. de Physique, Colloque C6, supplement au no^o 12, Tome 42, decembre 1981, p. C6-649.
17. M. T. Yin and M. L. Cohen, Phys. Rev. Letters 45, 1004 (1980).
18. J. Ihm, M. T. Yin, and M. L. Cohen, Solid State Commun. 37, 491 (1981).
19. C. Falter, M. Selmke, W. Ludwig, and K. Kunc, Phys. Rev. B32, 6518 (1985).
20. Y. R. Wang and A. W. Overhauser, Phys. Rev. B35, 497, 501 (1987).
21. L. van Hove, Quantum Theory of Many Particle Systems (W. A. Benjamin, New York, 1961).
22. A. A. Maradudin, P. A. Flinn, and R. A. Coldwell-Horsfall, Ann. Phys. (N.Y.) 15, 360 (1961).
23. A. A. Maradudin and A. E. Fein, Phys. Rev. 128, 2589 (1962).
24. A. A. Maradudin and P. A. Flinn, Phys. Rev. 129, 2529 (1963).

25. R. C. Shukla and E. R. Cowley, Phys. Rev. B3, 4055 (1971).

26. R. C. Shukla and L. Wilk, Phys. Rev. B10, 3660 (1974).

27. R. C. Shukla and E. R. Cowley, Phys. Rev. B31, 372 (1985).

28. R. C. Shukla and F. Shanes, Phys. Rev. B32, 2513 (1985).

29. V. V. Goldman, G. K. Horton, and M. L. Klein, Phys. Rev. Letters 21, 1527 (1968).

30. R. C. Shukla (private communication).

31. R. C. Shukla and R. D. Mountain, Phys. Rev. B25, 2649 (1982).

32. Gordon A. Wolfe and Bernard Goodman, Phys. Rev. 178, 1171 (1969).

33. C. M. McCarthy. C. W. Tomson, and S. A. Werner, Phys. Rev. B22, 574 (1980).

34. J. H. Henkel, J. Chem. Phys. 23, 681 (1955).

35. I. J. Zucker, Philos. Mag. 3, 987 (1958).

36. G. L. Morley, J. Chem. Phys. 51, 2336 (1969).

37. A. C. Holt, W. G. Hoover, S. G. Gray, and D. R. Shortle, Physica 49, 61 (1970).

38. F. H. Ree and A. C. Holt, Phys. Rev. B8, 826 (1973).

39. K. Westera and E. R. Cowley, Phys. Rev. B11, 4008 (1975).

40. Robert J. Hardy and Bruce W. Jones, in Lattice Dynamics, ed. M. Balkanski (Flammarion, Paris, 1978), p. 106.

41. E. L. Pollock, J. Phys. C9, 1129 (1976).

42. Robert J. Hardy and Michael A. Day, Phys. Rev. B29, 4108 (1984).

43. J. M. Dickey and A. Paskin, Phys. Rev. 188, 1407 (1969).

44. M. Parrinello and A. Rahman, Phys. Rev. Letters, 45, 1196 (1980).

45. H. C. Andersen, J. Chem. Phys. 72, 2384 (1980).

46. M. Parrinello and A. Rahman, J. Appl. Phys. 52, 7182 (1981).

47. M. Parrinello and A. Rahman, J. Chem. Phys. 76, 2662 (1982).

48. M. Parrinello and A. Rahman, in Melting, Localization and Chaos, eds. R. K. Kalia and P. Vashista (Elsevier, New York, 1982), p. 97.

49. John R. Ray and Aneesur Rahman, J. Chem. Phys. 80, 4423 (1984).

50. M. Parrinello and A. Rahman, J. de Physique, Colloque C6, supplement au n^{o} 12, Tome 42, decembre 1981, p. C6-511.

51. John R. Ray, Michael C. Moody, and Aneesur Rahman, Phys. Rev. B32, 733 (1985).

52. N. Metropolis, A. W. Rosenbluth, M. N. Rosenbluth, A. H. Teller, and E. Teller, J. Chem. Phys. 21, 1087 (1953).

53. D. R. Squire, A. C. Holt, and W. G. Hoover, Physica 42, 388 (1969).

54. W. W. Wood, in *Physics of Simple Fluids*, eds. H. N. V. Temperly, J. S. Rowlinson, and G. S. Rushbrooke (Wiley, New York, 1968).
55. E. R. Cowley, Phys. Rev. B**28**, 3160 (1983).
56. M. A. Day and R. J. Hardy, J. Phys. Chem. Solids **46**, 487 (1985).
57. V. Samathiyakanait, and H. R. Glyde, J. Phys. X**6**, 1166 (1973).
58. Randall W. Hall and Bruce J. Berne, J. Chem. Phys. **81**, 3641 (1984).
59. P. W. Anderson, Phys. Rev. **109**, 673 (1958).
60. J. Canisius and J. L. van Hemmen, J. Phys. C**18**, 4873 (1985).
61. E. W. Montroll, in *Proc. Third Berkeley Symposium on Mathematical Statistics and Probability*, ed. J. Neyman (U. of California Press, Berkeley, Calif., 1956), p. 209.
62. D. Stauffer, Physics Reports **54**, 1 (1979).
63. M. L. Williams and H. J. Maris, Phys. Rev. B**31**, 4508 (1985).
64. S. R. Nagel, G. S. Grest and A. Rahman, in *Phonon Physics*, eds. J. Kollar, N. Kroo, N. Menyhard, T. Siklos (World Scientific, Singapore, 1985), p. 354.
65. S. John, H. Sompolinsky, and M. J. Stephen, Phys. Rev. B**27**, 5592 (1983).
66. S. John and M. J. Stephen, Phys. Rev. B**28**, 6358 (1983).
67. J. Jackle, Solid State Commun. **39**, 1261 (1981).
68. P. Steinhardt, D. Weaire, and R. Alben, J. Non-Cryst. Solids **15**, 199 (1984).
69. F. Wooten and D. Weaire, J. Non-Cryst. Solids **64**, 325 (1984); F. Wooten, K. Winer, and D. Weaire, Phys. Rev. Letters, **54**, 1392 (1985).
70. S. W. deLeeuw, H. He, and M. F. Thorpe, Solid State Commun. **56**, 343 (1985).
71. M. F. Thorpe and S. W. deLeeuw, Phys. Rev. B**33**, 8490 (1986).
72. M. F. Thorpe, Phys. Rev. B**8**, 5352 (1973).
73. P. N. Sen and M. F. Thorpe, Phys. Rev. B**15**, 4030 (1977).
74. J. D. Joannopoulos and F. Yndurain, Phys. Rev. B**10**, 5164 (1974).
75. F. Yndurain and P. N. Sen, Phys. Rev. B**14**, 531 (1976).
76. R. J. Elliott, in *Phonon Physics*, eds. J. Kollar, N. Kroo, N. Menyhard, T. Siklos (World Scientific, Singapore, 1985), p. 15.
77. R. C. Zeller and R. O. Pohl, Phys. Rev. B**4**, 2029 (1971).
78. W. A. Phillips, J. Low Temp. Phys. **7**, 351 (1972).
79. P. W. Anderson, B. I. Halperin, and C. M. Varma, Philos. Mag. **25**, 1 (1972).
80. U. Buchenau, Solid State Commun. **56**, 889 (1985).

81. Y. Gefen, A. Aharoney, B. B. Mandelbrot, and S. Kirkpatrick, Phys. Rev. Letters 47, 1771 (1981).

82. S. Alexander and R. Orbach, J. Phys. (Paris) Letters 43, L625 (1982).

83. R. Rammal and G. Toulouse, J. Phys. (Paris) Letters 44, L13 (1983).

84. S. Alexander, C. Laermans, R. Orbach, and H. M. Rosenberg, Phys. Rev. B28, 4615 (1986).

85. B. Derrida, R. Orbach, and K.-Wah Yu, Phys. Rev. B29, 6645 (1984).

86. A. Aharony, S. Alexander, O. Entin-Wohlmann, and R. Orbach, Phys. Rev. B31, 2565 (1985).

87. S. Alexander, Ora Entin-Wohlman, and R. Orbach, Phys. Rev. B34, 2726 (1986).

88. U. Buchenau, in *Phonon Physics*, eds. J. Kollar, N. Kroo, N. Menyhard, T. Siklos (World Scientific, Singapore, 1985), p. 30.

89. H. M. Rosenberg, in *Phonon Physics*, eds. J. Kollar, N. Kroo, N. Menyhard, T. Siklos (World Scientific, Singapore, 1985), p. 26.

90. E. Courtens, J. Pelous, J. Phalippou, R. Vacher, and T. Woignier, Phys. Rev. Letters 58, 128 (1987).

91. A. Fontana, F. Rocca, and M. P. Fontana, Phys. Rev. Letters 58, 503 (1987).

92. A. J. Dianoux, J. N. Page, and H. M. Rosenberg, Phys. Rev. Letters 58, 886 (1987).

93. J. C. Phillips, Phys. Rev. B24, 1744 (1981).

94. V. G. Karpov and D. A. Parshin, Pisma v Zh. Eksper. i Teor. Fiz. 38, 536 (1983) [Soviet Physics - JETP Letters 38, 648 (1983)].

95. V. G. Karpov and D. A. Parshin, Zhur. Eksper. i Teor. Fiz. 88, 2212 (1985) [Soviet Physics - JETP 61, 1308 (1985)].

96. J. A. Krumhansl, Phys. Rev. Letters 56, 2696 (1986).

97. R. Rammal, Phys. Rev. B28, 4871 (1983).

98. B. W. Southern and A. R. Douchant, Phys. Rev. Letters 55, 966 (1985); 55, 1808(E) (1985).

99. G. S. Grest and I. Webman, J. Phys. (Paris) Letters 45, L1155 (1984).

100. D. Shechtman, I. Blech, D. Gratias, and J. W. Cahn, Phys. Rev. Letters 53, 1951 (1984).

101. See, for example, C. Kittel, *Introduction to Solid State Physics*, 5th Edition (John Wiley and Sons, New York, 1976), p. 9.

102. D. D. Kofalt, S. Sanao, T. Egami, K. M. Wong, andS. J. Poon, Phys. Rev. Letters 57, 114 (1986).

103. S. Nanao, W. Dmowski, T. Egami, J. W. Richardson, Jr., and J. D. Jorgensen, Phys. Rev. B35, 435 (1987).

104. P. Ramachandrarao and G. V. S. Sastry, Pramana 25, L225 (1985).

105. D. Levine and P. J. Steinhardt, Phys. Rev. Letters 53, 2477 (1984).

106. J. P. Lu, T. Odagaki, and J. L. Birman, Phys. Rev. B33, 4809 (1986).

107. R. Penrose, Bull. Inst. Maths. Its. Appl. 10, 266 (1974).

108. M. Gardner, Sci. Am. 236, 110 (1977).

109. V. Elser and C. L. Henley, Phys. Rev. Letters 55, 2883 (1985).

110. P. Bak, Phys. Rev. Letters 54, 1517 (1985).

111. N. D. Mermin and Sandra M. Troian, Phys. Rev. Letters 54, 1524 (1985).

112. M. V. Jaric, Phys. Rev. Letters 55, 607 (1985).

113. D. Levine, T. C. Lubensky, S. Ostlund, S. Ramaswamy, P. Steinhardt, and J. Toner, Phys. Rev. Letters 54, 1520 (1985).

114. T. Odagaki and D. Nguyen, Phys. Rev. B33, 2184 (1986).

115. M. A. Marcus, Phys. Rev. B34, 5981 (1986).

116. H. Matsuda, Progr. Theor. Phys. Suppl. 23, 23 (1962).

117. K. von Klitzing, G. Dorda, and M. Pepper, Phys. Rev. Letters 45, 494 (1980).

118. D. C. Tsui, H. L. Stormer, and A. C. Gossard, Phys. Rev. Letters 48, 1559 (1982).

119. L. Esaki and R. Tsu, IBM J. Res. Develop. 14, 61 (1970).

120. G. H. Dohler, Physica Scripta 24, 430 (1981).

121. G. H. Dohler, phys. stat. solidi (b) 52, 79 (1972).

122. G. H. Dohler, J. Vac. Sci. Technol. 16 (3), 851 (1979).

123. Z. H. Zheng, C. M. Falco, J. B. Ketterson, and I. K. Schuller, Appl. Phys. Letters, 38, 424 (1981).

124. B. Hillebrands, P. Baumgart, R. Mock, G. Guntherodt, A. Boufelfel, and C. M. Falco, Phys. Rev. B 34, 9000 (1986).

125. D. A. G. Bruggeman, Ann. Phys. (Leipzig) 29, 160 (1937).

126. Yu. V. Rizmichenko, Bull, Acad. Sci. USSR Geograph. Geophys. Ser. 13, 114 (1949); 13, 518 (1949).

127. G. W. Postma, Geophys. 20, 780 (1955).

128. J. E. White and F. A. Angona, J. Acoust. Soc. Am. 27, 310 (1955).

129. S. M. Rytov, Akust. Zh. 2, 71 (1956) [Soviet Physics - Acoustics 2, 68 (1956).

130. G. E. Backus, J. Geophys. Res. 67, 4427 (1962).

131. E. Behrens, J. Acoust. Soc. Am. 42, 378 (1967).

132. C.-T. Sun, J. D. Achenbach, and G. Herrmann, J. Appl. Mech. 35, 408, 467 (1968).

133. J. D. Achenbach, C.-T. Sun, and G. Herrmann, J. Appl. Mech. 35, 689 (1968).

134. C.-T. Sun, Bull. Seismol. Soc. Am. 60, 345 (1970).

135. V. G. Savin and N. A. Shul'ga, Akust. Zh. 21, 448 (1975) [Soviet Physics - Acoustics 21, 276 (1975)].

136. A. Keuny and M. Grimsditch, Phys. Rev. B26, 4699 (1982).

137. T. J. Delph, G. Herrmann, and R. K. Kaul, J. Appl. Mech. 45, 343 (1972).

138. B. A. Auld, G. S. Beaupre, and G. Herrmann, Electr. Letters 13, 525 (1977).

139. B. A. Auld, in Modern Problems in Elastic Wave Propagation, eds. J. Miklowitz and J. D. Achenbach (Wiley, New York, 1978), p. 459.

140. R. E. Camley, B. Djafari-Rouhani, L. Dobrzynski, and A. A. Maradudin, Phys. Rev. B27, 7318 (1983).

141. B. Djafari-Rouhani, L. Dobrzynski, O. Hardouin Duparc, R. E. Camley, and A. A. Maradudin, Phys. Rev. B28, 1711 (1983).

142. B. Djafari-Rouhani, A. A. Maradudin, and R. F. Wallis, Phys. Rev. B29, 6454 (1984).

143. N. E. Glass, R. Loudon, and A. A. Maradudin, Phys. Rev. B24, 6843 (1981).

144. R. E. Camley and D. L. Mills, Phys. Rev. B29, 1695 (1984).

145. A. K. Sood, J. Menendez, and M. Cardona, Phys. Rev. Letters 54, 2115 (1985).

146. E. P. Pokatilov and S. I. Beril, phys. stat. solidi (b) 110, K75 (1982); 118, 567 (1983).

147. F. Bechstedt and R. Enderlein, phys. stat. solidi (b) 131, 53 (1985).

148. R. Lassnig and W. Zawadzki, Surf. Sci. 142, 361 (1984).

149. N. Raj and D. R. Tilley, Solid State Commun. 55, 373 (1985).

150. Ph. Lambin, J. P. Vigneron, A. A. Lucas, P. A. Thiry, M. Liehr, J. J. Pireaux, R. Candano, and T. J. Knech, Phys. Rev. Letters 56, 1842 (1986).

151. P. Baumgart, B. Hillebrands, R. Mock, G. Guntherodt, A. Boufelfel, and C. M. Falco, Phys. Rev. B34, 9004 (1986).

152. A. S. Barker, Jr., J. L. Merz, and A. C. Gossard, Phys. Rev. B*17*, 3181 (1978).
153. K. Kunc and R. M. Martin, in *Proceedings of the 16th International Conference on the Physics of Semiconductors*, ed. M. Avernous (North-Holland, Amsterdam, 1983), p. 511.
154. C. Colvard, T. A. Grant, M. V. Klein, R. Merlin, R. Fischer, H. Morkoc, and A. C. Gossard, Phys. Rev. B*31*, 2080 (1985).
155. A. K. Sood, J. Menendez, M. Cardona, and K. Ploog, Phys. Rev. Letters, *54*, 2111 (1985).
156. Sung-kit Yip and Yia-Chung Chang, Phys. Rev. B*30*, 7037 (1984).
157. G. Kanellis, Phys. Rev. B*35*, 746. (1987).
158. P. Ruden and G. H. Dohler, Solid State Commun. *45*, 23 (1983).
159. S. Y. Ren and J. D. Dow, Phys. Rev. B*25*, 3750 (1982).
160. S. Y. Ren and J. D. Dow, Solid State Commun. *41*, 211 (1982).
161. See, for example, J. M. Ziman, *Electrons and Phonons* (Clarendon Press, Oxford, 1960), Ch. VIII.
162. R. Merlin, K. Bajema, R. Clarke, F.-Y. Juang and P. K. Bhattacharya, Phys. Rev. Letters *55*, 1768 (1985).
163. See, for example, S. Ostlund and R. Pandit, Phys. Rev. B*29*, 1394 (1984).
164. An Hu, Chiang Tien, Xiang-jin Li, Yuan-hang Wang, and Duan Feng, Phys. Lett A*119*, 313 (1986).
165. H. Levine and J. W. Willemsen, J. Acoust. Soc. Am. *73*, 32 (1983).
166. G. Benedek, Surf. Sci. *126*, 624 (1983).
167. F. W. deWette, Comments on Solid State Physics *11*, 89 (1984).
168. J. P. Toennies, J. Vac. Sci. Tech. A*2*, 1055 (1984).
169. G. Benedek, Physica *127B*, 59 (1984).
170. R. F. Wallis, J. Vac. Sci. Technol. A*3*, 1422 (1985).
171. J. Szeftel, Surf. Sci. *152/153*, 797 (1985).
172. J. E. Black, in Topics in Current Physics. Vol. 41: *Structure and Dynamics of Surface 1*, eds. W. Schommers and P. von Blanckenhagen (Springer-Verlag, Berlin, 1986), p. 153.
173. C. Beatrice and C. Calandra, Phys. Rev. B*28*, 6130 (1983).
174. C. Calandra, A. Catellani, and C. Beatrice, Surf. Sci. *148*, 90 (1984).
175. C. Calandra, A. Catellani, and C. Beatrice, Surf. Sci. *152/153*, 814 (1985).
176. E. G. Brovman and Yu. M. Kagan, in *Dynamical Properties of Solids*, vol. 1, eds. G. K. Horton and A. A. Maradudin (North-Holland, Amsterdam, 1974), p. 191.

177. R. N. Barnett, U. Landman, and C. L. Cleveland, Phys. Rev. B28, 1667 (1983).

178. A. G. Eguiluz, A. A. Maradudin, and R. F. Wallis, in Phonon Physics, eds. J. Kollar, N. Kroo, N. Menyhard, T. Siklos (World Scientific, Singapore, 1985), p. 604.

179. A. G. Eguiluz, R. F. Wallis, and A. A. Maradudin, Bull. Am. Phys. Soc. 32, 683 (1987).

180. K. M. Ho and K. P. Bohnen, Phys. Rev. Letters 56, 934 (1986).

181. U. Harten, J. P. Toennies, and Ch. Woll, Farad. Discuss. Chem. Soc. 80, 1 (1985).

182. U. Harten, J. P. Toennies, Ch. Woll, and G. Zhang, Phys. Rev. Letters 55, 2308 (1985).

183. B. F. Mason and B. R. Williams, Surf. Sci. 139, 173 (1984).

184. K. Gibson, S. J. Sibener, B. Hall, D. L. Mills, and J. E. Black, J. Chem. Phys. 83, 4256 (1985).

185. G. Brusdeylins, R. Rechsteiner, J. G. Skofronick, J. P. Toennies, G. Benedek, and L. Miglio, Phys. Rev. Letters 54, 466 (1985).

186. G. Bracco, R. Tatarek, S. Terreni, and F. Tommasini, Phys. Rev. B34, 9045 (1986).

187. See, for example, H. Ibach and D. L. Mills, Electron Energy Loss Spectroscopy and Surface Vibrations (Academic Press, New York, 1982).

188. S. Lehwald, J. M. Szeftel, H. Ibach, T. S. Rahman, and D. L. Mills, Phys. Rev. Letters 50, 518 (1983).

189. M. Rocca, S. Lehwald, H. Ibach, and T. S. Rahman, Surf. Sci. 138, L123 (1984).

190. C. Oshima, R. Souda, M. Aono, S. Otani, and Y. Ishizawa, Phys. Rev. B30, 5361 (1984); Solid State Commun. 57, 283 (1986).

191. C. Oshima, R. Souda, M. Aono, S. Otani, and Y. Ishizawa, Phys. Rev. Letters 56, 240 (1986).

192. H. Ibach an D. Bruchmann, Phys. Rev. Letters 44, 36 (1980).

193. J. M. Szeftel, S. Lehwald, H. Ibach, T. S. Rahman, J. E. Black, and D. L. Mills, Phys. Rev. Letters 51, 268 (1983).

Lattice Dynamics at High Temperature

G.K. Horton
Serin Physics Laboratory, Rutgers - The State University
Piscataway, NJ 08855-0849

and

E.R. Cowley
Department of Physics, Camden College of Arts and Sciences
Rutgers - The State University, Camden, NJ 08102

Lectures delivered by G.K.H. at the XXIII Winter School, Karpacz,
Poland, February 1987.

1. Introduction

The fact that, unlike the other contributions, this talk will be about phonons in ideal crystals, like rare gas solids (RGS) whose dynamical properties are surely well understood, deserves an explanation. This is particularly true since we are celebrating the 75th anniversary of the great paper by Born and von Kármán (1912) which, in a sense, represents the beginning of our subject. Yet, isn't it interesting that when Eckert and Youngblood (1986) published dispersion curves for ^{36}Ar near melting they analyzed these using Born-von Kármán theory. What is one to make of the quasiharmonic force constants they obtained? And when they turned to Glyde and Smoes (1980) for a most sophisticated self-consistent theory based on an excellent potential by Aziz and Chen (1977), the hoped for agreement between theory and experiment proved disappointingly elusive.

There is a story here that deserves telling. And we believe that our results may find a place in many modern applications of lattice dynamics.

2. Quasi-Harmonic Born-von Kármán Theory

Let us assume we know the crystal potential energy Φ as a function of the instantaneous positions of the atoms. For rare gas solids we have the widely used Mie-Lennard-Jones (MLJ) (12-6) potential or the model potentials such as the Aziz-Chen potential for Ar or the Beck (1968) potential for He. These are based primarily on gas data. For semi-conductors, metals or ionic crystals, Φ, whether from ab initio calculations or model potentials, is known much less precisely. So we'll refer mostly to RGS.

Our problems is to calculate the Helmholtz free energy F and the dynamical form factor $S(\underset{\sim}{Q},\omega)$ - i.e. formally, for F

$$F = -kT \ln Z, \qquad Z = \mathrm{tr}\, e^{-H/kT} \tag{1}$$

The solution of this problem was presented by Born and von Kármán in 1912. This paper is still alive and well and is actively being used in current research. The frequencies of vibration of a solid are obtained by expanding the crystal potential energy as a Taylor series in the displacement $\underset{\sim}{u}^i$ of the i-th atom from its equilibrium position $\underset{\sim}{R}_i$

$$\Phi = \phi_o + \frac{1}{2} \sum_{\substack{ij\\xy}} \phi^{ij}_{xy}\, u_x{}^i u_y{}^j$$

$$+ \frac{1}{6} \sum_{\substack{ijk\\xyz}} \phi^{ijk}_{xyz}\, u_x{}^i u_y{}^j u_z^k + \frac{1}{24} \sum_{\substack{ijkl\\wxyz}} \phi^{ijkl}_{wxyz}\, u^i_{wxyz}\, u^i_w u^j_x u^k_y u^l_z + \cdots \tag{2}$$

The first line is the harmonic and the second the anharmonic contribution. Born and von Kármán only considered the harmonic contribution. By allowing the equilibrium positions of the atoms to change, i.e. allowing the 2nd order force constants to depend on or change with volume, we obtain the quasi-harmonic theory (QH), (after making the familiar normal coordinate transformation to obtain the crystal excitations--the non-interacting phonons)

$$\omega^2(\underset{\sim}{q}j) = \Sigma\, e_\alpha(\underset{\sim}{q}j)\, D_{\alpha\beta}(\underset{\sim}{q})\, e_\beta(\underset{\sim}{q}j) \tag{3}$$

with $$D_{\alpha\beta}(\underset{\sim}{q}) = \frac{1}{M} \sum_\rho \left(1-\cos\,(\underset{\sim}{q} \cdot \underset{\sim}{R}_\rho)\right) \nabla_\alpha \nabla_\beta \phi\,(R_\rho) \tag{4}$$

$$F = \phi_o + \sum_{\underset{\sim}{q}j} \beta^{-1} \ln\,(2 \sinh \beta \hbar\, \omega/2) \tag{5}$$

$$S = k \sum_{qj} \left(\frac{1}{2}\beta \hbar \omega \coth \frac{1}{2} \beta \hbar \omega - \ln \left(2 \sinh \frac{1}{2} \beta \hbar \omega\right)\right) \tag{6}$$

etc. These expressions are single sums over normal modes.

This theory, expounded by Born and Huang (1954), was standard for forty years. It took a long time to figure out how to evaluate these sums, and, of course, there were no computers available then.

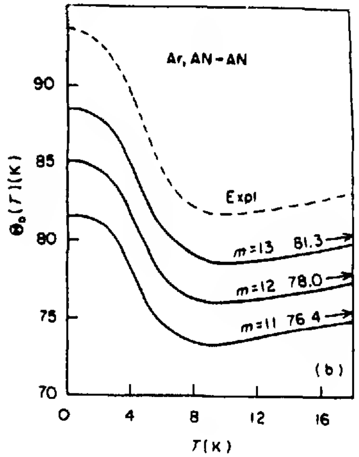

Fig. 1

The predictions of this theory can be illustrated by fig. 1, Horton and Leech (1963), only the MLJ potential was available then.

Next came the experimental implementation of neutron spectroscopy by Brockhouse (1961) and his collaborators--at last the dispersion of phonons could be measured directly. As an example look at fig. 2. The measurements are from the paper by J. Eckert and R.W. Youngblood, (1986) for ^{36}Ar at 81K. The force constants are fitted out to 3rd neighbors. They correspond to the broken line. We will show the other directions and discuss the solid curve due to Glyde and Smoes later. The force constants obtained from the Born-von Karman fit are listed in table 1. The Born-von Karman analysis of neutron scattering data has been a favorite tool of experimentalists. But table 1

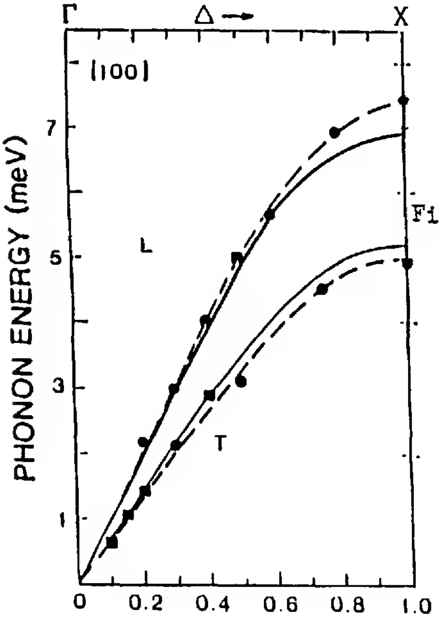

Fig. 2

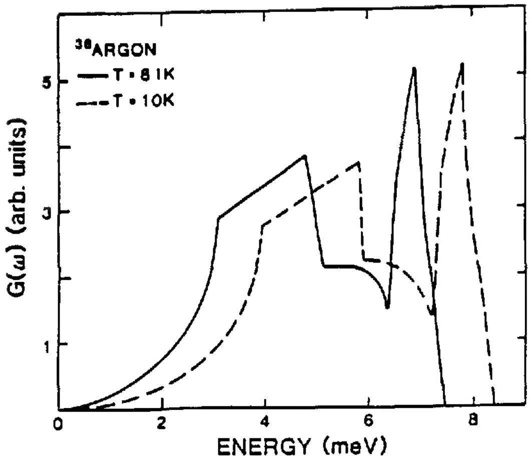

Fig. 3

illustrates the problem with this analysis. It leads to temperature dependent phonon spectra, fig. 3, for which there is no place in the quasiharmonic theory (volume expansion is not an adequate explanation).

Table 1. Interatomic force constants (in dyn cm^{-1}) of solid ^{36}Ar at 81K and at 10K. The values of 10K are for a three-neighbor, general force model, while the data at 81K were fitted with a three-neighbor axially symmetric model. In the latter case, one has the constraints 1XX-1ZZ = 1XY, 3XX-3YY = 3(3YZ) and 2(3XX) - 2(3YY) = 3(3XZ).

Force constant	10K	81K
1XX	605(10)	503(33)
1ZZ	5(14)	-16(16)
1XY	633(18)	520(44)
2XX	-24(22)	-14(21)
2YY	-3(8)	-6(22)
3XX	-5(8)	-31(11)
3YY	0(2)	-9(4)
3XZ	-2(4)	-7(3)
3YZ	0(4)	-15(6)

3. Anharmonic Perturbation Theory

To improve the Born-von Kármán theory the next step that was tried was to include the anharmonic terms of eqn. 2.

The potential energy contribution to the partition function can be written

$$Z = \langle e^{-\beta(\Phi_{\mathrm{harmonic}} + \Phi_{\mathrm{anharmonic}})} \rangle \qquad (7)$$

The harmonic part is handled exactly by the normal coordinate transformation. To calculate the anharmonic contribution to the thermodynamic properties we expand the Boltzmann factor

$$Z = Z_h \langle 1 - \beta\Phi_{\mathrm{anh}} + \frac{1}{2}\beta^2\Phi^2_{\mathrm{anh}} ----\rangle_o \qquad (8)$$

To evaluate this expression, we note that for harmonic basis functions

$$\langle u \rangle_o = \langle u\ u\ u \rangle_o = 0 \qquad \langle u^2 \rangle_o,\ \langle u\ u\ u\ u \rangle_o \neq 0$$

The second term in equation 8 contains $\phi^{ijkl}_{wxyz} \langle u\ u\ u\ u \rangle_o$. The third term contains $\phi^2_{xyz} \langle u\ u\ u,\ u\ u\ u \rangle_o$. Clearly, to get non-zero contributions, the u operators must be paired. So the lowest order, corrections to Born-von Kármán theory are a term containing a fourth derivative of the potential (and four u's) and one containing the product of two third order derivatives (and six u's).

For RGS, in fact, the fourth derivative term is larger than the cubic derivative squared term, but that depends on the interatomic potential. The conventional wisdom is to retain both terms.

Let's use a diagrammatic approach. The fourth derivative of the potential is represented by a blob with four lines coming from it, and the pairing requirement means that we complete the diagram by forming loops of all the line ends. For the cubic derivative squared the diagram has all three lines joining the two vertices. These are the only non-zero diagrams, fig. 4. For a number of years,

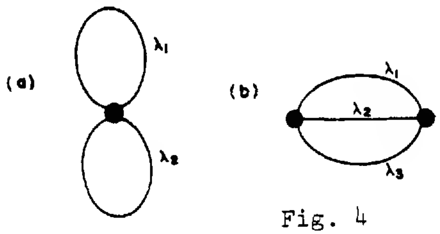

Fig. 4

these two diagrams represented the accepted theory of anharmonicity which was applied to a variety of substances.

About 20 years ago, Klein and Horton (1968) realized that if you make numerical calculations of these terms using a MLJ potential to model RGS, the contribution of these anharmonic terms became unacceptably large at quite low temperatures, about $T_m/3$, fig. 5a. The same thing happens in NaCl, fig. 5b. Clearly, if all the terms in anharmonic perturbation series are included the theory is exact. Indeed, all existing theories can probably be interpreted as corresponding to the selection of subsets of all the diagrams. Can we calculate all the diagrams? It seems reasonable to see how far such a comprehensive program can be pursued without being overwhelmed by unmanageable algebraic and numerical complexities.

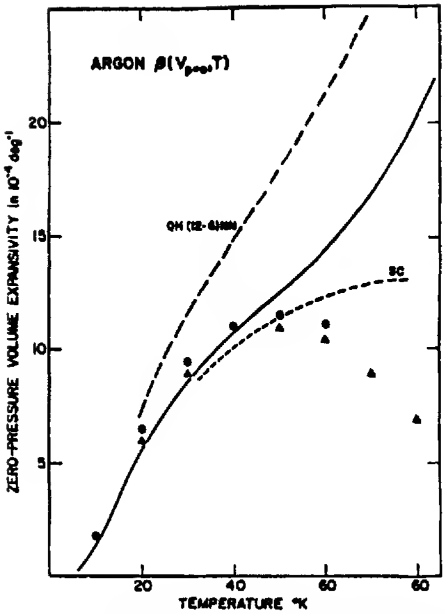

Fig. 5a

Expansivity of Ar. The circles and triangles correspond to perturbation theory results for (12-6) nn and (13-6) nn potentials, respectively. The curve labeled sc is for the (12-6) nn potential in the lowest-order self-consistent phonon approximation. The quasiharmonic curve QH (12-6) nn is included so that the explicit contribution of the anharmonicity can be seen.

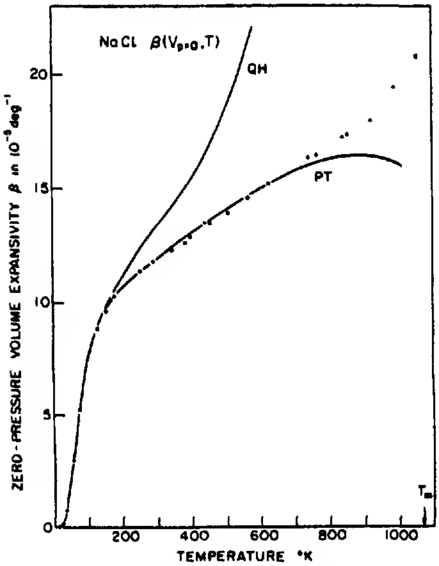

Fig. 5b

Volume expansivity of sodium chloride: QH is the quasi-harmonic approximation and PT are the perturbation theory results based on the leading anharmonic terms [Eq. (8)]. The experimental results are shown as points.

Together with our indefatigable colleague Ramesh Shukla, Shukla and Wilk (1971), Shukla and Cowley (1985), we have followed this path using for our analysis a scheme for ordering the diagrams introduced by van Hove. Each third derivative counts a factor λ of the ordering parameter, each fourth derivative λ^2 etc. The magnitude of λ equals a typical atomic displacement divided by the nearest neighbor distance.

Then the diagrams of fig 5 are of order λ^2. There are eight diagrams of order λ^4, 43 of order λ^6 etc; those of order λ^4 are shown in fig. 6.

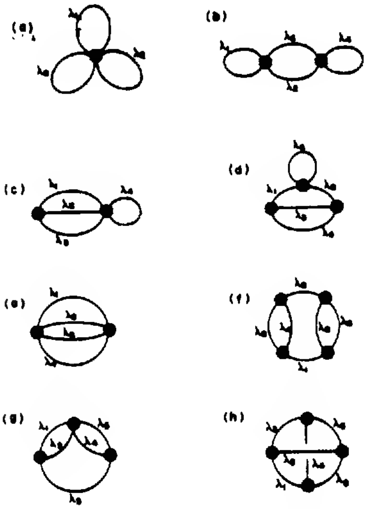

After working out the algebra for all these diagrams in figs. 4 and 6, they were evaluated for a MLJ potential in the high T limit. The contributions to the free energy of order λ^2 are in units of $N(kT)^3/\epsilon$, those of order λ^4 are in units of $N(kT)^4/\epsilon^2$. The results are listed in Table 2.

Fig. 6

Table 2 **Anharmonic contributions to the free energy.**

Diagram	Contribution	Partial total
$F(2(a))$	0.2049	
$F(2(b))$	−0.6627	$F(SC1) = -0.4578$
$F(2(c))$	−0.6012	
$F(2(d))$	(0.9146)	$F(ISC) = -0.1444$
$F(2(e))$	−0.2234	
$F(2(f))$	−0.3533	$F(SC2) = -0.7211$
$F(2(g))$	0.5814	
$F(2(h))$	−0.0912	$F(\lambda^4) = -0.2309$
$F(1(a))$	0.6910	
$F(1(b))$	−0.3424	$F(\lambda^2) = 0.3486$

Clearly, none of the contributions are negligible and there is much cancellation. In order to assess the convergence of the perturbation expansion we note that

$$F(\lambda^4)/F(\lambda^2) = -0.662\ (kT/\epsilon) \tag{9}$$

and for RGS, $\epsilon \sim 2kT_m$, so that

$$F(\lambda^4)/F(\lambda^2) = -0.331\ (T/T_m) \tag{10}$$

This suggests a convergence to $T \sim T_m/3$. And as figure 7 shows convergence is poor.

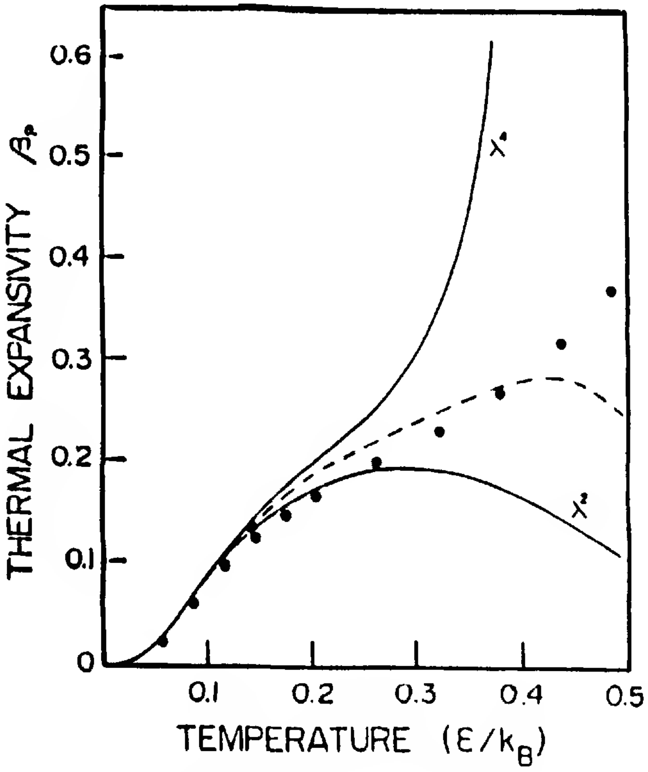

Fig. 7 Thermal expansivity β_p in reduced units of k/ϵ for NN LJ model of argon.

Points are the experimental data; solid lines are perturbation theory to $O(\lambda^2)$ and $O(\lambda^4)$; dashed line is the approximation to ISC.

Shukla has almost calculated all forty-three diagrams of $O(\lambda^6)$, but nothing has yet been published.

We feel that any scheme that stops after a finite number of terms in the Taylor-expansion, eqn 8, will turn out to be unsatisfactory for some cases. The strength of the self-consistent formalism is that it does sum selected infinite series of terms. However, we believe that the perturbation series approach is useful for some situations and in indicating the viability of different approximations.

4. Self Consistent Phonon Theory

We now turn to self-consistent theories. First order self-consistent theory, SC1, simply replaces the second derivative of the potential in eqn. 4 by its average over the harmonic pair correlation function. The self-consistency arises because the harmonic pair correlation function itself contains the harmonic frequencies. In practice, one starts with, say, quasi-harmonic force constants and iterates to achieve a self-consistent solution of the SC1 equations.

These are

$$\omega^2(\underset{\sim}{q}j) = \sum e_\alpha(\underset{\sim}{q}j)\, D_{\alpha\beta}(\underset{\sim}{q})\, e_\beta(\underset{\sim}{q}j) \qquad (11)$$

with $$D_{\alpha\beta}(\underset{\sim}{q}) = \frac{1}{M}\sum_\rho (1 - \cos(\underset{\sim}{q} \cdot \underset{\sim}{R}_\rho))< \nabla_\alpha\nabla_\beta\phi(\underset{\sim}{R}_\rho)> \qquad (12)$$

$\phi(r)$ is the interatomic potential, M = atomic mass, the sum over ρ is over neighbors, at $\underset{\sim}{R}_\rho$, of an atom at the origin. For RGS we will assume $\phi(r)$ is central and that the Axilrod-Teller-Muto triple dipole contributions, see Barker (1976), can be added later using quasiharmonic theory. The smeared force constants may be written as

$$\phi_{\alpha\beta}(\underset{\sim}{R}_\rho) = < \nabla_\alpha\nabla_\beta\phi\ (\underset{\sim}{R}_\rho) > = \int g_h(\underset{\sim}{R}_\rho, \underset{\sim}{r})\nabla_\alpha\nabla_\beta\phi(r)d^3r \qquad (13)$$

and, for later use,

$$\phi_{\alpha\beta\gamma}(\underset{\sim}{R}_\rho) = < \nabla_\alpha\nabla_\beta\nabla_\gamma\phi\ (\underset{\sim}{R}_\rho) > = \int g_h(\underset{\sim}{R}_\rho, \underset{\sim}{r})\nabla_\alpha\nabla_\beta\nabla_\gamma\phi(r)d^3r \qquad (14)$$

and so on.

The pair correlation function, normalized to unity, is given by

$$g_h(\underline{R}_\rho, \underline{r}) = [(2\pi)^3 \det\underline{\Delta}]^{-1/2} \exp[-\frac{1}{2}(\underline{r}-\underline{R}_\rho)\cdot\underline{\Delta}^{-1}\cdot(\underline{r}-\underline{R}_\rho)] \qquad (15)$$

The free energy and entropy in SC1 are given by

$$F = \frac{N}{2} \sum_\rho < \phi(\underline{R}_\rho) > + \sum_{\underline{q}j} [\beta^{-1} \ln 2\sinh x - (\omega(\underline{q}j)/4)\coth x] \qquad (16)$$

and $S = k \sum_{\underline{q}j} (x \coth x - \ln(2 \sinh x))$ (17)

with $x = \hbar\, \omega(\underline{q}j)\beta/2, \ \beta = (kT)^{-1}$ (18)

The displacement-displacement correlation function is

$$<((u_\alpha(\underset{\sim}{R}_\rho) - u_\alpha(0))\cdot(u_\beta(\underset{\sim}{R}_\rho) - u_\beta(0)) > = \Lambda_{\alpha\beta}(\underset{\sim}{R}_\rho) \text{ where}$$

$$\Lambda_{\alpha\beta}(\underline{R}_\rho) = \frac{2}{MN} \sum_{\underline{q}j} (1 - \cos \underline{q} \cdot \underline{R}_\rho) e_\alpha(\underline{q}j) e_\beta(\underline{q}j) \epsilon(\underline{q}j)/\omega^2(\underline{q}j) \qquad (19)$$

where $\epsilon(\underline{q}j) = (n(\underline{q}j) + 1/2))h\, \omega(\underline{q}j)$ is the average energy per mode. The average occupation number

$$n(\underline{q}j) = (\exp(\hbar\omega(\underline{q}j)/kT - 1)^{-1} \qquad (20)$$

The sum is over the 3N normal modes in the first Brillouin zone.

This set of equations is solved by a computer program that iterates them to the required accuracy, starting, say, with quasi-harmonic force constants. Eqns. 13 and 14 diverge near $r = 0$, especially for the MLJ potential, a problem that is usually handled by cutting off the integrals. We will return to this point later.

In the late sixties and early seventies, self-consistent phonon theory, which is a mean field or Hartree theory, appeared to be an important break-through in the development of lattice dynamics. It

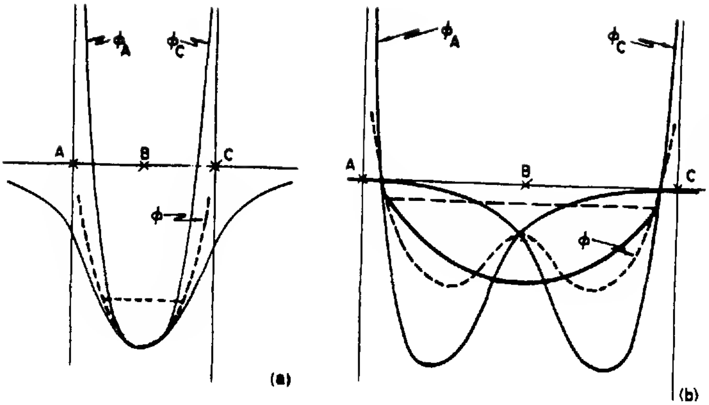

Fig. 8

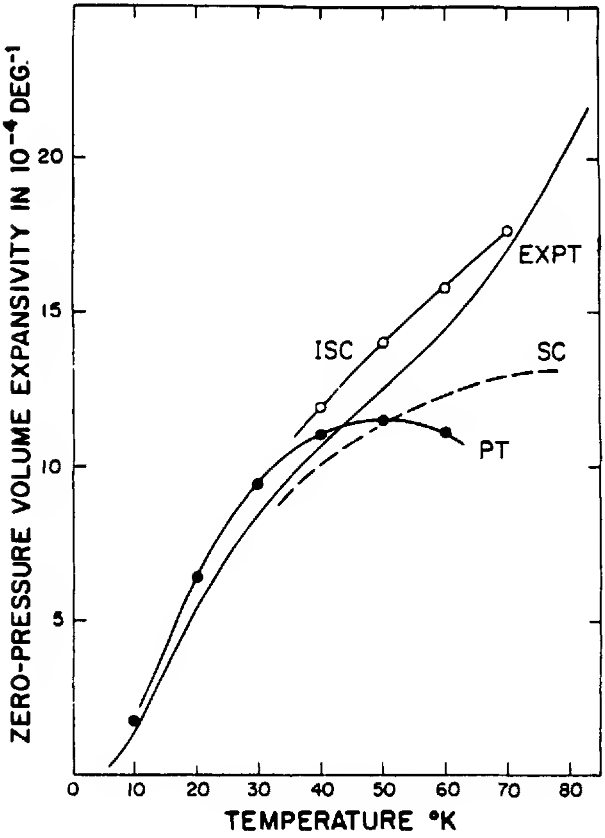

Fig. 9a Expansivity of Ar. ISC, improved self-consistent theory; SC, lowest-order self-consistent theory; PT, conventional perturbation theory; and EXPT, data from Choquard

was developed simultaneously by three or four groups and it was then found that Max Born (1951) had written it all down twenty years earlier to cope with the solid He problem. For this case Born-von Kármán theory does not exist because eqn. 3 turns out to be negative. The physics behind this situation is illustrated in fig. 8.

A helium atom moves in the *dynamic* field of its neighbors. So, the dashed line in fig. 8b, which corresponds to the Born-von Kármán approach, does not express the correct physics. Born's idea then is to solve the following problem. Knowing the He atom vibrates in an effective harmonic well, due to its neighbors, make an

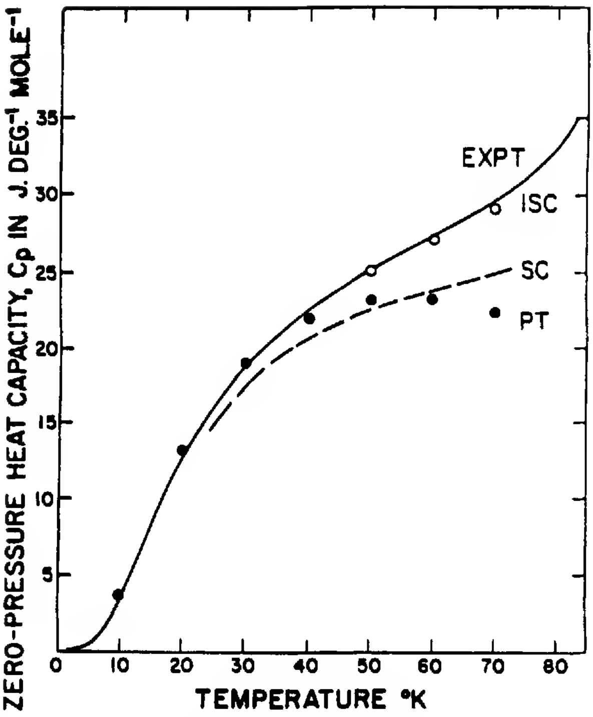

Fig. 9b **Heat capacity of Ar. ISC, SC, and PT**

assumption about the force constant and solve this problem. Then ask: what is the motion of the neighboring atoms in its potential? And so on back and forth, till the motions one obtains are self-consistent.

It was one of the triumphs of SC1 that the smeared second order force constants, eqn. 12, were positive. Thus the self-consistent theory was extensively applied, particularly to solid helium.

Unfortunately, it soon became clear that numerically SC1 was little better than anharmonic perturbation theory, see figs. 9a,b. The agreement with experiment was good at rather low temperatures only. For instance, C_p for Ar was 26 J deg^{-1} mole^{-1} at the triple point compared with the experimental value of 33.17 J deg^{-1}mole^{-1}.

It seems natural to try to extend the range of applicability of SC1 by including the cubic terms of fig. 4 as a perturbation of the free energy, evaluated using SC1 basis functions. In this way, one includes, in an approximate way, both diagrams of fig. 4 in the theory. In this theory, called the improved self consistent theory, or ISC, the phonons are shifted in frequency from their SC1 values and broadened due to their finite lifetime, see Goldman et al. (1968 and 1970). This shift and width are given by the imaginary part of the one-phonon Green's function

$$\mathrm{Im}\,(G(\underline{q}j,\Omega)) = A(\underline{q}j,\Omega)$$

$$= \frac{2\omega(\underline{q}j)\ \Gamma(\underline{q}j,\Omega)}{[\Omega^2 - \omega^2(\underline{q}j) - 2\omega(\underline{q}j)\Delta(\underline{q}j,\Omega]^2 + [2\omega(\underline{q}j)\ \Gamma(\underline{q}j,\Omega)]^2} \qquad (21)$$

If Δ and Γ depend little on Ω, then $A(\underline{q}j,\Omega)$ is a simple Lorentzian function peaking at

$$\Omega^2 = \omega^2(\underline{q}j) + 2\omega(\underline{q}j)\ \Delta(\underline{q}j,\Omega) \qquad (22)$$

with full width at half maximum of $W = 2\Gamma(\underline{q}j,\Omega)$. The position of this peak is usually identified as the SC1 plus cubic terms phonon frequency. Expressions for Δ and Γ can be found in the literature; both are proportional to the square of the Fourier transform of the third order smeared force constants.

The one phonon dynamic form factor describing the inelastic scattering of a neutron in which a single phonon is excited having a wave vector $\underline{q} = \underline{Q} + \underline{\tau}$ is given by

$$S_1(\underline{Q},\Omega) = [n(\Omega)+1]d^2(Q) \sum_{\underline{q}j} (\underline{Q} \cdot \underline{e}(\underline{q}j))^2 f^2(\underline{q}j) \quad A(\underline{q}j,\Omega)\Delta(\underline{Q} - \underline{q}) \quad (23)$$

where $d(Q)$ is the Debye-Waller factor, $f^2(\underline{q}j) = (\frac{\hbar}{2m\omega(\underline{q}j)})$ etc.

From fig. 9.a,b, we see that ISC represents a considerable improvement over SC1 to higher T.

Let us relate the diagrammatic perturbation expansion to the self-consistent phonon theory of lattice dynamics as illustrated in fig. 10. There are two basic building blocks we want to introduce. The averaging (or smearing) of a potential derivative over the harmonic (or Gaussian) probability distribution corresponds to adding any number of loops to the corresponding vertex. Thus, starting from the second diagram of $O(\lambda^2)$, fig. 4, we can generate a family of diagrams by adding any number of loops to one or both of the vertices. This coresponds to smearing the vertices in the improved self consistent approximation, or including all even derivatives of the potential, Choquard (1967), Horner (1974).

Second, the lines represent, in the first instance, a pairing of displacement operators. When we make the normal coordinate

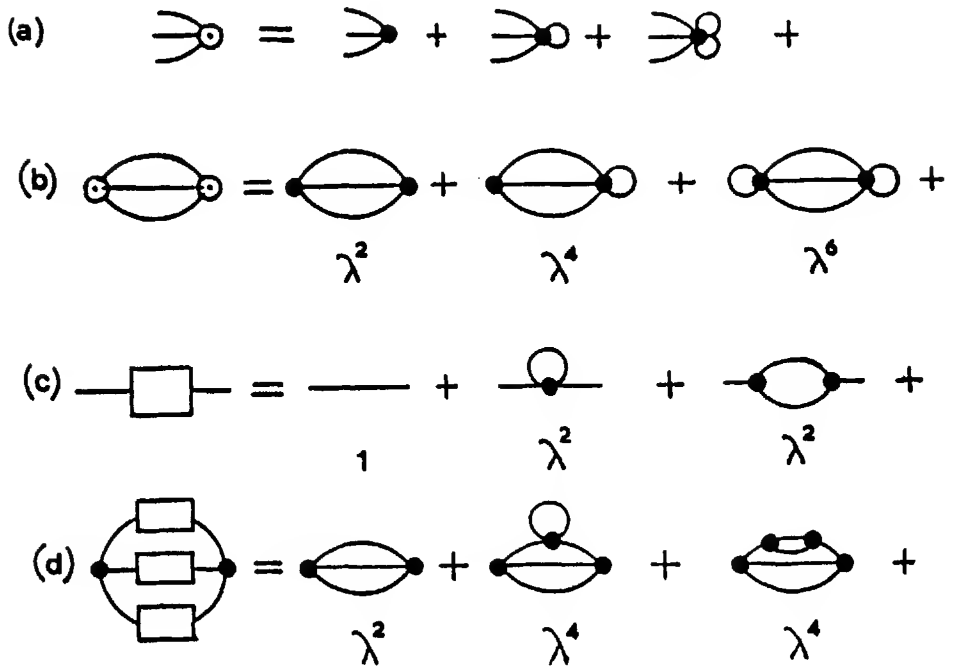

Fig. 10

transformation to a phonon picture, each line represents a phonon propagator. In self-consistent schemes, the normal mode frequencies are calculated using average force constants and this corresponds to adding anharmonic shifts, or self-energies, into the phonon lines. The SC theories are equivalent to only including the first type of insert from fig. 10. In this way, we see that of the 8 diagrams of order λ^4, fig. 6, only two are incorporated in the first order, SC1, scheme and two more are generated from diagrams with two cubic vertices (by dressing either vertex or a phonon line--in practice these theories also contain all the higher order diagrams). This correspond to ISC. Including the first six diagrams corresponds to the second order self-consistent theory, SC2. The remaining two diagrams cannot be regarded as belonging to either SC1 or SC2.

Looking at the numerical results, we see that the contributions of all the diagrams are roughly of the same order and of different signs. The total is much smaller than any of the individuals terms.

We can look at the subtotals for the free energy and find that the sum of the first two terms is way off the final total; the sum of the first four terms is closest to the final total; and the sum of the first six terms is far from the final answer. These results are consistent with the difficulties of SC1, the modest success of ISC and the failure of a version of SC2 which diverges at high T, something that SC1 never does, Kanney and Horton (1975).

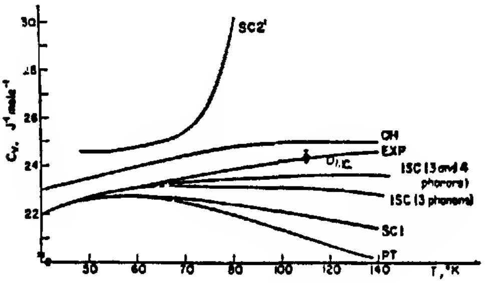

Fig. 11. A version of SC2, SC2', from Kanney and Horton.

Before leaving this work, we would like to comment on the last diagram of order λ^4 (fig. 6). We can redraw it to look like a ring diagram with a single insert consisting of a double cubic bubble with a single line across the middle.

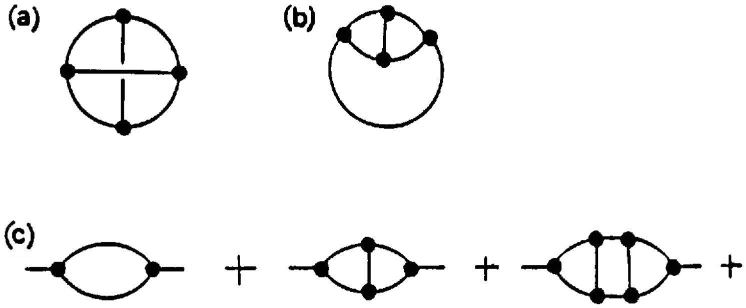

Fig. 12, Ladder diagrams

This is called a ladder diagram and, of course, it is only the first member of an infinite series with different numbers of rungs in the ladder.

Diagrams with this structure are amongst the most difficult to evaluate numerically and there is a temptation to sweep them under the table. However, there are indications here and in quite different contexts that they are often not negligible.

Some years ago we studied the two phonon Raman scattering of light in Ar and Xe. This is described by a scattering efficiency of which S_{11} and S_{44} correspond, respectively, to the polarized and depolarized scattering for single crystals of Ar. Our calculations did not agree particularly well with the experiment, see fig. 13. In the calculations, we included diagrams of type a) but ignored interactions between the phonons--diagrams of type b) in fig. 14. Our work left us with the distinct impression that the cause of some of the discrepancies between theory and experiment was the neglect of additional scattering processes between the two phonons giving contributions from these ladder diagrams, Leese, Horton and Cowley (1980).

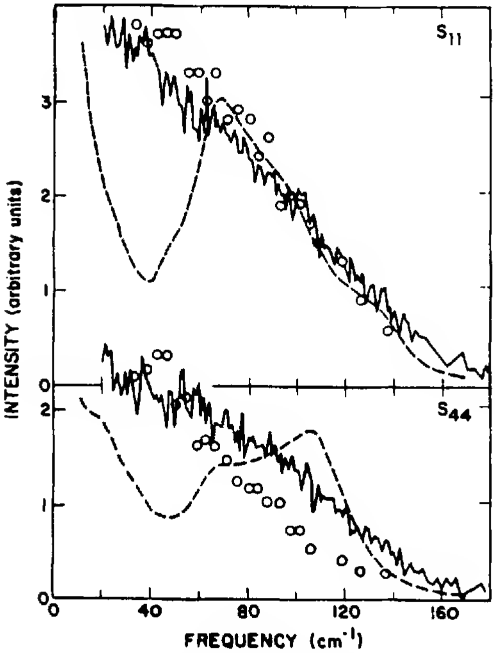

Fig. 13. Solid Ar spectra at 153.5K, 22.3cm^3/mole. Solid lines-experimental results. Dashed lines-smoothed spectra calculated by Leese, Horton and Cowley. Circles-molecular dynamics calculations of Adler et al. The latter are scaled in intensity but not in frequency.

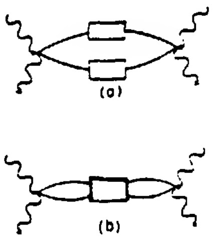

Fig. 14

We have seen that for $T < T_m/2$, or so, the various self-consistent theories are satisfactory (ISC more so), i.e. they lead to the T^3 law for C_v and yield broad agreement with experiment, where good model potentials are available, for RGS and other crystals. Between $T_m/2$ and T_m, the low order SC theories are far from satisfactory.

4. Horner Ansatz

To attack this problem let us pursue the idea of Heinz Horner (1974) who attributed the failure of SC theories at high T to the neglect of hard core effects. The importance of these effects for highly anharmonic solids, like He, was known ever since the work of Nosanow (1976) but their appearance in Ar is something of a surprise. Of course, we are concerned with anharmonic effects. But these are short range anharmonic effects as opposed to the long range effects incorporated in low order SC theories. Obviously, all these effects are included in a complete theory. But none of the standard formulations of the theory, such as that of Choquard (1967) or Werthamer (1970) readily accommodates hard core effects. The problem is that at every level the theory depends on effective harmonic frequencies so that the pair correlation function, eqn. 15, is always a Gaussian. This means that, in principle, there is a finite probability that an atom will penetrate close to a neighbor. As a result, the potential and the force constants, averaged with a Gaussian pair correlation function become very large or even infinite.

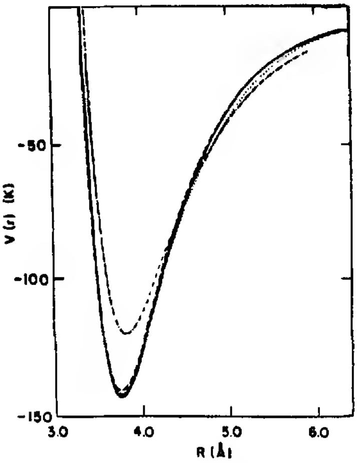

Fig. 15. Aziz-Chen potential for Ar. MLJ potential is broken line.

The integrands in eqns. 13 and 14 look like that in figure 17 and the question arises whether an unambiguous separation of the physical and unphysical contributions can be made by using a cutoff. This problem is

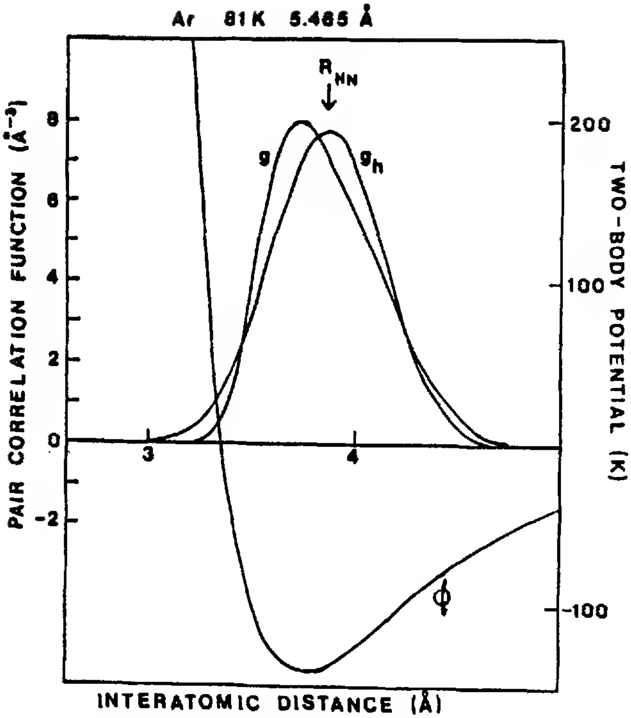

Fig. 16 : Gaussian g_h and Horner g pair correlation function with Aziz-Chen potential.

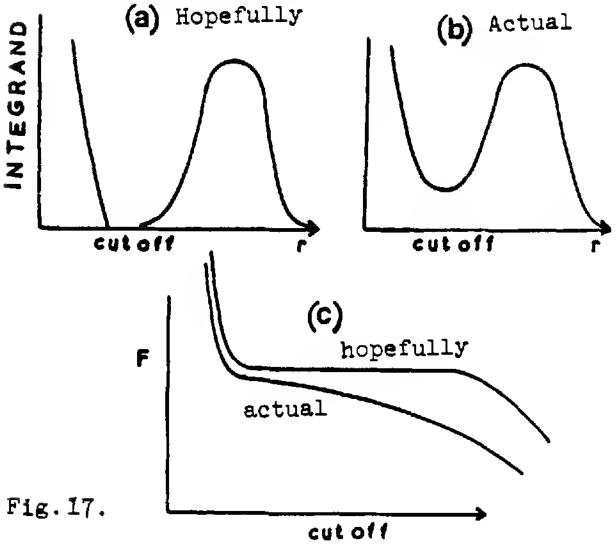

Fig. 17.

particularly acute for the MLJ potential which diverges at the origin. It has been customary to hide this problem by truncating the potential at small r and hoping that the numerical work is insensitive to the cut-off. Horner's solution to this problem was to modify the Gaussian pair correlation function empirically so as to reduce the probability of close approach of any two atoms. For an isolated pair of atoms this modification can be derived at low temperatures (He) and at high T, the region we are interested in. The modification involves the Boltzmann factor of the pair potential at high T. Horner's ansatz is

$$g(\underline{R}_\rho,\underline{r}) = g_h(\underline{R}_\rho,\underline{r})\gamma(r)(a_o+a_1(r-R_\rho)+a_2(r-R_\rho)^2) \qquad (24)$$

with $\gamma(r) = \exp\{-\beta\Phi(r)\}$ (25)

being the familiar Jastrow factor.

In order to determine the three coefficients a_o, a_1, a_2, Horner postulated that

1) $g(\underline{R}_\rho,\underline{r})$ be normalized

2) $g(\underline{R}_\rho,\underline{r})$ be peaked at $\underline{r} = \underline{R}_\rho$, just like the $g_h(\underline{R}_\rho,\underline{r})$, thus preserving the lattice structure

3) $g(\underline{R}_\rho,\underline{r})$ have the same second moment as $g_h(\underline{R}_\rho,\underline{r})$, i.e. that the $\Lambda_{\alpha\beta}$ of eqn 19 be unchanged.

It is not known what class of diagrams this ansatz corresponds to. It is surely an infinite set. So, overcounting is always a potential problem, especially for the thermodynamics. Originally, Horner introduced a polynomial in a non-spherically symmetrical form. This would enable us to adapt $g(\underline{R}_\rho,\underline{r})$ to the symmetry of the crystal, as is true for $g_h(\underline{R}_\rho,\underline{r})$. Here we can only satisfy condition 3 in the longitudinal direction but happily this is the principal direction for short range correlations. Goldman (1979) has reported that near T_m for moderate densities, Horner's g may become negative for some r. Goldman proposed an alternative ansatz

$$g(\underline{R}_\rho,\underline{r}) = A\gamma(r)\exp\{-\frac{1}{2}(\underline{r}-\underline{\xi})\cdot\underline{\gamma}\cdot(\underline{r}-\underline{\xi})\} \qquad (26)$$

which has the symmetry of the lattice, never becomes negative and in which the parameters A, $\underline{\xi}$ and $\underline{\gamma}$ are determined by the normalization, peak position of the Gaussian and its width. We use eqn. 24.

The three conditions can be written as

$$\int g(\underline{r})d^3r = 1 \qquad (27)$$

$$\int \mathbf{r}\, g(\mathbf{r}) d^3\mathbf{r} = \mathbf{R}_\rho \quad \text{or} \quad \int (\mathbf{r} - \mathbf{R}_\rho)\, g(\mathbf{r}) d^3 r = 0 \tag{28}$$

$$\int (\mathbf{r} - \mathbf{R}_\rho)_\alpha (\mathbf{r} - \mathbf{R}_\rho)_\beta\, g(\mathbf{r})\, d^3 r = \Lambda_{\alpha\beta} \tag{29}$$

As we pointed out, with three parameters these three conditions can only be satisfied in the longitudinal direction.

Let $\hat{\epsilon} = \mathbf{R}_\rho / |\mathbf{R}_\rho|$, a unit vector pointing in the nearest neighbor direction, and put $\mu_{ij} = \int (r-R_\rho)^i [(\mathbf{r}-\mathbf{R}_\rho)\cdot\hat{\epsilon}]^j \gamma\, (r) \quad g_h(\mathbf{R}_\rho,\mathbf{r})\, d^3 r$ (30)

With $\Lambda_L = \sum_{\alpha\beta} \hat{\epsilon}_\alpha \hat{\epsilon}_\beta \Lambda_{\alpha\beta}$, $R_{\rho L} = \mathbf{R}_\rho \cdot \hat{\epsilon}$ (31)

so that for a neighbor in the 110 direction

$$\Lambda_L = \Lambda_{xx} + \Lambda_{xy}. \tag{32}$$

We can write this set of three equations, eqns, 27, 28, 29, as

$$\sum_{i=0}^{2} a_i\, \mu_{ij} = I_j, \quad I_o = 1,\ I_1 = 0,\ I_2 = \Lambda_L \tag{33}$$

Let us briefly review the adiabatic approximation underlying the Horner Ansatz in which $g(\mathbf{R}_\rho,\mathbf{r})$ is allowed to change with $\mathbf{R}_\rho$, the interparticle distance. However, in this approximation the separation of one pair of atoms changes, while the spacing of the rest of the crystal remains unchanged. Hence the explicit value of R_ρ as it appears in the factor $\{a_o + a_1(r-R_\rho) + a_2(r-R_\rho)\}$ does not change since it describes the shape of the potential well formed by all the other atoms, except the pair in question. For the same reason Λ does not change with $\mathbf{R}_\rho$. The a_i change with $\mathbf{R}_\rho$ and Λ and they depend only on $R_{\rho L}$ and Λ_L. Now

$$\partial g_h / \partial R_{\rho L} = (\Lambda^{-1})_L (\mathbf{r} - \mathbf{R}_\rho)_L\, g_h \tag{34}$$

so that

$$\partial\mu_{ij}/\partial R_{\rho L} = - j\ \mu_{i,j-1} + \Lambda^{-1}\mu_{i,j+1} \tag{35}$$

$$\text{and } \partial g_h/\partial\Lambda_L = \frac{1}{2}\ (\underline{\mathbf{r}} - \underline{\mathbf{R}}_\rho)_L^2\ (\Lambda_L^{-2})\ (\underline{\mathbf{r}} - \underline{\mathbf{R}}_\rho)^2\ g_h - \frac{g_h}{2\Lambda_L} \tag{36}$$

so that

$$\partial\mu_{ij}/\partial\Lambda_L = \frac{1}{2}\ (\mu_{i,j+2}\ \Lambda_L^{-2} - \mu_{ij}\Lambda_L^{-1}) \tag{37}$$

We have assumed that $(\underset{\wedge}{\underline{\Delta}}^{-1})_L = (\Lambda_L)^{-1}$, i.e. that $\underline{\Delta}$ diagonalizes with one eigenvector along $\underline{\ell}$. This is true in our case. Putting these results together we obtain

$$\delta\mu_{ij} = (-j\mu_{i,j-1} + \Lambda_L^{-1}\ \mu_{i,j+1})\ \delta R_{\rho L} + \frac{1}{2}\ (\mu_{i,j+2}\Lambda_L^{-2} - \mu_{ij}\Lambda_L^{-1})\delta\Lambda_L \tag{38}$$

where, to make the connection with Horner's notation, $\underline{r} = \frac{1}{2}\ \Delta^{-1}$. It also follows from eqn 33 that

$$\sum_{i=0}^{2} \frac{\partial a_i}{\partial R_{\rho L}}\ \mu_{ij} = -\sum_{i=0}^{2} a_i\ \frac{\partial\mu_{ij}}{\partial R_{\rho L}} \tag{39}$$

$$\text{and } \sum_{i=0}^{2} \frac{\partial a_i}{\partial\Lambda_L}\ \mu_{ij} = \delta_{j3} - \sum_{i=0}^{2} a_i\ \frac{\partial\mu_{ij}}{\partial\Lambda_L} \tag{40}$$

We have derived eqn 38 explicity because in Horner's (1974) review article p, 493, eqn. 4.52 the second term in the coefficient of $\delta R_{\rho L}$ in eqn 38 is omitted. We also note, without detailed proof, that, in high symmetry situations and assuming that Δ does not depend on $\underline{\mathbf{R}}_\rho$, and using the fact that

$$\partial g_n/\partial R_{\rho\alpha} = - \partial g_h/\partial r_\alpha = -\nabla_\alpha g_h \tag{41}$$

$$\langle\partial g_h/\partial\Lambda_{\alpha\beta}\rangle = \frac{1}{2}\ \langle\partial^2 g_h/\partial r_\alpha\partial r_\beta\rangle = \frac{1}{2}\ \langle\partial^2 g_h/\partial R_{\rho\alpha}\partial R_{\rho\beta}\rangle. \tag{42}$$

The force on an atom due to its neighbor at $\underline{\mathbf{R}}_\rho$ has the value

$$K_\alpha = \int g(\mathbf{R}_\rho, \mathbf{r})\ \nabla_\alpha \phi(r) d^3r$$

$$= \sum_{i=0}^{2} a_i \int \gamma(r)\ (r - R_\rho)^i g_h\ (\mathbf{R}_\rho, \mathbf{r}) \nabla_\alpha\ \phi(r) d^3r \qquad (43)$$

Horner next introduces the W_i functions defined by

$$dW_i/dr = \gamma(r)(r - R_\rho)^i\ d\phi/dr \qquad (44)$$

with $W_i \to 0$ as $r \to \infty$

$$\text{Then } K_\alpha = \sum_{i=0}^{2} a_i \int g_h(\underset{\sim}{R}_\rho, \mathbf{r}) \nabla_\alpha W_i d^3r \qquad (45)$$

Integrating by parts gives

$$K_\alpha = - \sum_{i=0}^{2} a_i \int W_i\ \nabla_\alpha g_h d^3r \qquad (46)$$

Now $M_{\alpha\beta} = \partial K_\alpha / \partial R_{\rho\beta}$ and with $\dfrac{\partial g_h}{\partial R_{\rho\beta}} = -\nabla_\beta g_h$ we find

$$M_{\alpha\beta} = \sum_{i=0}^{2} \left(a_i \int W_i \nabla_\alpha \nabla_\beta g_h d^3r - \frac{\partial a_i}{\partial R_{\rho\beta}} \int W_i \nabla_\alpha g_h d^3r \right)$$

$$= \sum_{i=0}^{2} \left(a_i \int W_i \nabla_\alpha \nabla_\beta g_h d^3r - \frac{R_\alpha R_\beta}{R^2} \frac{\partial a_i}{\partial R_{\rho L}} \int W_i\ \hat{\underset{\sim}{\epsilon}} \cdot \underset{\sim}{\nabla} g_h d^3r \right) \qquad (47)$$

This is Horner's expression, except for the minus sign. The wrong sign also appears in the review by Henry Glyde, (1976) and Tom Koehler, (1975), pp 54-5, eqns. 4.49 and 4.51.

The cubic force constants are given by

$$M_{\alpha\beta\gamma} = \partial^2 K_\alpha / \partial R_{\rho\beta}\ \partial R_{\rho\gamma} = 2\ \partial K_\alpha / \partial \Lambda_{\beta\gamma} \qquad (48)$$

Using the second form and additional algebra gives the explicit expression

$$
\begin{aligned}
M_{\alpha\beta\gamma} = \sum_{i=1}^{2} a_i \int g_h \gamma(r)(r-R_\rho)^i [\; & \frac{r_\alpha r_\beta r_\gamma}{r^3} ((\phi'''/r - 3\phi''/r + 3\phi'/r^2) \\
& + \phi'(\gamma'' - \gamma'/r)\gamma + \phi'(i(i-1)(r-R_\rho)^{-2} - i(r-R_\rho)^{-1}/r) \\
& + 2(\gamma'/\gamma)(\phi'' - \phi'/r) + 2i\,(r-R_\rho)^{-1}(\phi'' - \phi'/r) + (2i\gamma'/\gamma)(r-R_\rho)^{-1}\phi') \\
& + (\delta_{\alpha\beta}\, r_\gamma/r + \delta_{\beta\gamma}\, r_\alpha/r + \delta_{\gamma\alpha} r_\beta/r)((\phi''/r - \phi'/r^2) + \gamma'\phi'/\gamma r \\
& + i(r - R_\rho)^{-1}\phi'/r)] d^3r \; + \\
2 \sum_{i=0}^{2} \frac{R_{\rho\alpha} R_{\rho\beta} R_{\rho\gamma}}{R^3} & \frac{\partial a_i}{\partial \Lambda_L} \int \gamma(r)(r-R_\rho)^i g_h \; \hat{\underline{e}} \cdot \underline{\nabla}\, \phi \; d^3r \qquad (49)
\end{aligned}
$$

To be able to evaluate these force constants, eqns. 47 and 49, we must know the W_i functions. Clearly, from eqn. 44, for

$i = 0$ $\qquad dW_o/dr = e^{-\beta\phi} d\phi/dr,$

so that $\qquad W_o = (1 - e^{-\beta\phi})/\beta,$

this obeys the correct boundary condition.

$i = 1$ $\qquad$ $$W_1 = (r-R_\rho)W_o - \int_\infty^r W_o dr \qquad (50)$$

$i = 2$ $\qquad$ $$W_2 = (r-R_\rho)W_1 - \int_\infty^r W_1\, dr$$

5. Implementing Horner Theory

A flow chart of our procedure goes as follows:

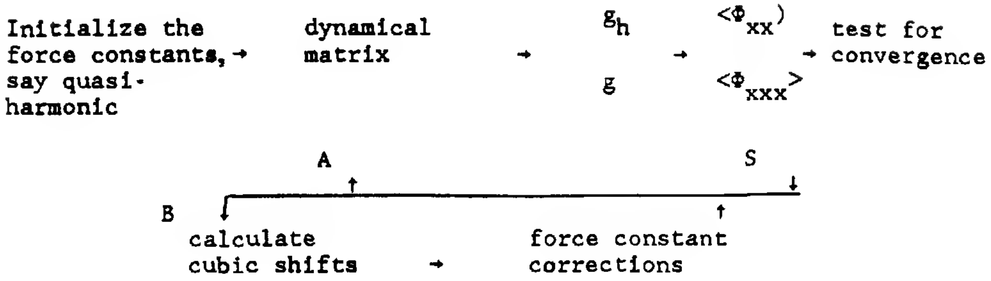

Loop A with g_h and only $<\phi_{xx}>$ gives SC1, needs about 20 iterations and takes about 1 hour on a minicomputer, Vax or HP. To work out ISC, you use the SC1 frequencies and eigenvectors to evaluate the cubic contribution to the free energy; that takes another hour on a mini, for a reasonable set of volumes and temperatures. The reciprocal lattice sums were done with 4000 points in the full Brillouin zone.

To implement the full Horner Ansatz, after obtaining SC1 by loop A, using g, one goes into loop B. In this loop, after obtaining the cubic frequency shifts at 27 points in the zone, these are fitted by a Born-von Kármán three neighbor model which gives us new ϕ_{xx} which are then fed into loop A. We then iterate loop A again to convergence and then redo loop B. The number of iterations needed for loop A decreases from 20 to about 8, loop B is typically run about three times. On a main frame computer (AS9000, IBM3070) the Horner calculation takes about five minutes.

The volume integrals are done using Gauss-Hermite integration with 20 points in all the three dimensions. Eight neighbors were included in our calculations and only the first three were treated self-consistently but only for nearest neighbors did we include the Horner Ansatz. Restricting HA to nearest neighbors is justified because it represents the major short range correlation effect. The triple dipole, ATM, forces were added on using quasiharmonic theory.

6. Results

a) The pair correlation function is changed at all r (fig. 16)

b) Force constants in Ar at 82K, $a_o = 5.4603Å$

	ϕ_{xx}(dyn/cm)	ϕ_{xxx}(10^8dyn/cm^2)
Quasi-harmonic	322.0	-1217
SC1	557.3	-1720
1st order, HA	496.4	-1023
2nd order, HA	505.0	- 959
SC1 + cubic corrections	419.0	---
2nd order, HA + cubic corrections	457.0	

line 2: the large increase in the force constants due to (SC1) smearing is typical.

line 3: the effect of HA without including the second order cubic shifts

line 4: the force constants using HA with the self-consistent 2nd order cubic shifts included

To illustrate the importance of the 2nd order shifts, in the last two lines we show the effect of modifying the 2nd order force constants by the corrections arising from the cubic shifts, line 5 without and line 6 with HA. In the latter case ϕ_{xx} is decreased by 10%. In the former, the large SC1 cubic force constants (line 2) give large corrections $(\sim\phi_{xxx}^2/\phi_{xx}^3)$ leading to unrealistically low frequencies. In fact, at this T and a_o, if the cubic shifts are included iteratively, omitting HA, the frequencies become imaginary (divergence of SC2). It is a major success of HA that it removes this divergence. The first iteration corresponds to the calculations of Glyde and Smoes, (1980).

c) Dispersion Relations

One of the stimuli for our work on HA was the recent paper on lattice dynamics and phonon lineshapes in ^{36}Ar at 81K by J. Eckert and

R.W. Youngblood (1986). We show their experimental results and our calculations in Fig. 18 from Cowley and Horton (1987). Three points require comment. The zone boundary

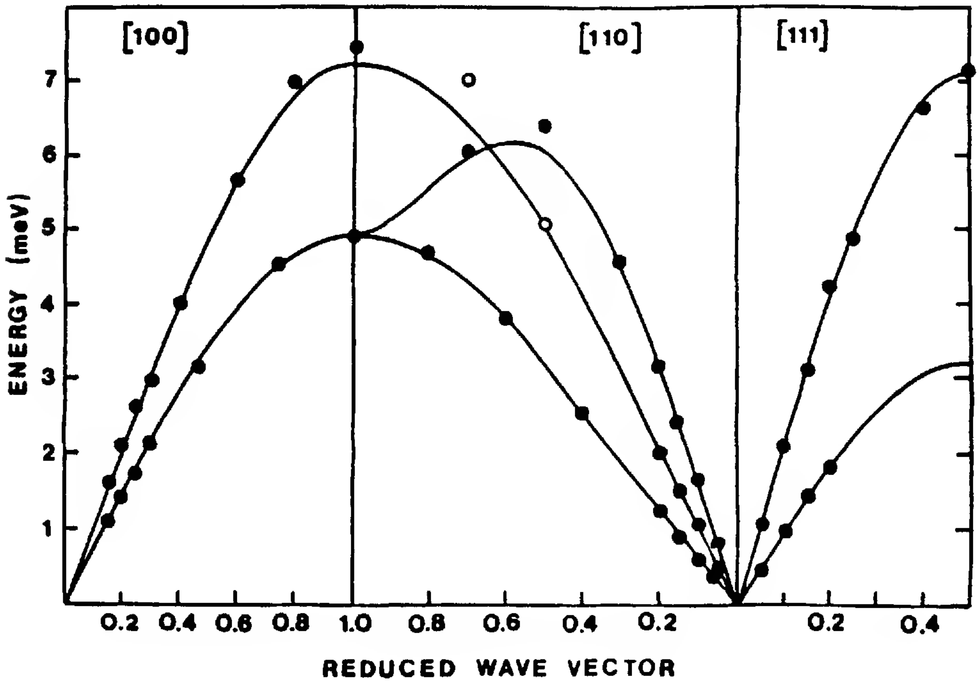

Fig. 18: Phonon dispersion relation in ^{36}Ar. Experimental circles from Eckert and Youngblood. Solid lines from Cowley and Horton.

longitudinal peak is extremely broad and the error estimate of Eckert and Youngblood encompasses our value. The discrepancy is probably due to the two phonon contribution to $S(Q,\omega)$, which Glyde and Smoes (1980) have shown to give rise to a high energy shoulder. The hollow circles were obtained serendipitously under conditions where they should normally be invisible and are more uncertain than the other values. The remaining discrepant point, in the (110) direction also seems to be slightly high in calculations at low T and may indicate a small shortcoming in the Aziz-Chen potential. The agreement with the experimental results of Eckert and Youngblood at 55K of our calculated HA dispersion curves is comparable to the agreement at 81K. Their lattice spacing should be 5.386Å instead of the reported 5.440Å. This suggests that the HA holds quantitatively to much lower temperatures than its original derivation suggested.

d) Elastic Constants

We have extracted values of the zero-sound elastic constants from the slopes of the dispersion curves at long wavelengths, using either curves measured by inelastic neutron scattering or the calculated spectral functions. Experimental measurements of the long-wavelength modes were performed by Y. Fujii et al. (1974) and their elastic constants and ours are listed in table 3. We also include the first-sound elastic constants, measured by Brillouin scattering, by Gewürtz and Stoicheff, (1974). We also include elastic constants calculated at 163.9K using a nearest neighbor MLJ potential corresponding to Xe because for this case we have the corresponding Monte Carlo results of E.R. Cowley, (1983). The discrepancy for c_{44} may reflect differences between zero and first sound values.

Table 3. Elastic constants in Argon, at 82K, and Xenon at 163.9K.

	Elastic constants (10^8 dyn/cm^2)		
	c_{11}	c_{12}	c_{44}
Ar, present theory	257 ± 3	156 ± 5	130 ± 2
Ar, neutron.	248 ± 6	153 ± 5	124 ± 4
Ar, Brillouin	238 ± 4	156 ± 3	112 ± 3
Xe, present theory	300 ± 4	150 ± 5	134 ± 2
Xe, Monte Carlo	290 ± 1.5	154 ± 1.5	117 ± 1

e) Specific Heat

An additional intriguing application of the frequencies calculated in the Horner formalism is in the evaluation of thermodynamic quantities. In theories such as ISC, or the Monte Carlo method, a thermodynamic variable such as the heat capacity is not directly expressible as a single sum over normal modes. However, the Horner formalism is designed to generate a set of frequencies which in some sense gives the "best" description of the lattice dynamics, and it is worth trying to use them to calculate thermodynamic functions. In particular, we assume that the entropy can be calculated using the formula corresponding to a set of harmonic normal modes, since this is known to work for the SCH and low-order perturbation theories. The most direct comparison with experiment is to calculate the heat capacity at constant pressure, C_p, by evaluating the entropy at a number of closely spaced temperatures, using for each temperature the equilibrium lattice spacing for that temperature. In this way we obtain a value for Ar at 80K of 32.06 J/mole-K. The experimental value is 33.175/mole-K, and the difference is well within the range of estimated values for a vacancy contribution.

To eliminate this uncertainty, we have again made a comparison using the MLJ model of Xe at 163.9K with the Monte Carlo results of Day and Hardy (1985). In this case we calculate a value for the heat capacity C_v of 2.60R, while the best Monte Carlo value is $(2.64 \pm 0.015)R$. While the differences seem to be outside the combined uncertainties of the two calculations, our result is an improvement over the ISC value of 2.57R. In any case we believe that the formulation of the thermodynamics of lattice dynamics using HA could do with further examination.

f) Thermal expansion

We have calculated $\partial S/\partial V = \partial p/\partial T = \beta B_T$ at 80K for Ar. Our result is 0.0255 kbars/K while the experimental result is $0.0244 \pm .001$ kbars/K. The largest part of the experimental error comes from the measurement of the bulk modulus. At any rate there is, again, agreement within the combined uncertainties.

g) Phonon lineshapes

Eckert and Youngblood made detailed measurements of the lineshapes of a number of phonons and compared them with the calculation of Glyde and Smoes which included multiphonon and interference terms. We have calculated only the one phonon term. We are able to reproduce the extreme broadening of the longitudinal mode at the (100) zone boundary. But our transverse mode (Fig. 18) is calculated to be rather sharper than is seen experimentally. Our calculated results were folded with a Gaussian of FWHM of 0.5 meV to simulate the neutron scattering instrumental resolution width. However, that is the value normally used when there is zero momentum transfer which is far from the conditions of the relevant experiment. There is also some difficulty in making comparison with the molecular dynamics work of Hansen and Klein (1976), whose results show a great deal of structure and were obtained for a different potential. We plan to pursue these discrepancies further.

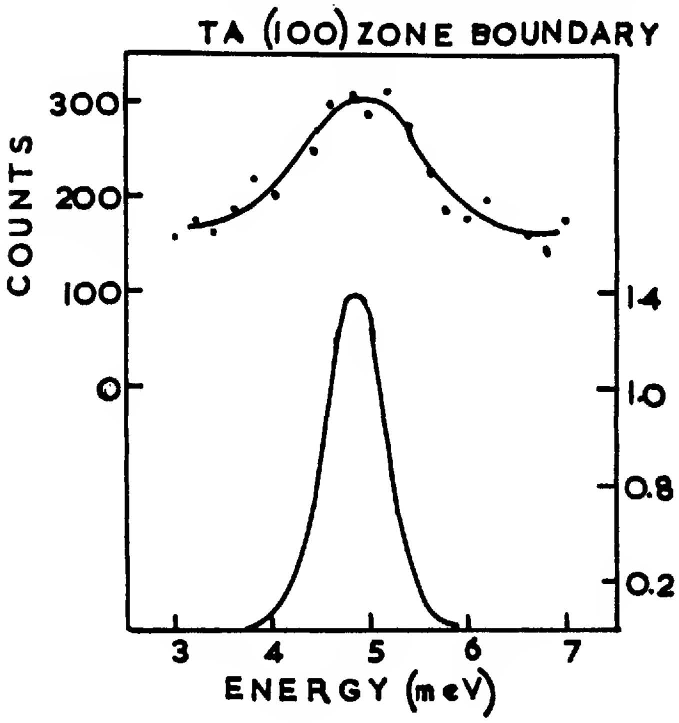

Fig. 18: Phonon Line Shapes in ^{36}Ar.

To summarize, the lattice dynamics of Max Born, a native son of Wroclaw, of whom Poland can be justly proud, is alive and well and can be quantitatively trusted close to melting-even when there are strong hard core effects leading to the interplay of both short and long range correlations.

References

Aziz, R.A. and Chen, H.H. (1977), J. Chem. Phys. 67, 5719.

Barker, J.A. (1976), in Rare Gas Solids (Academic, Landen, 1976), Vol. 1, Ch. 4, p. 212. Also note the article by R.J. Bell and I.J. Zucher in the same volume, Ch. 2.

Beck, D.E. (1968), Mol. Phys. 14, 311.

Born, M. and von Kármán, Th. (1912), Phys. Z. 13, 297.

Born, M. (1951), in Festschrift zur Feier des Zweihundertjährigen Bestehens der Akademie der Wissenschaften der Universtät Göttingen I. Mathematisch-Physikalische Klasse (Springer-Verlag, Berlin, 1951).

Born, M. and Huang, K. (1954), Dynamical Theory of Crystal Lattice, (Clarenden Press, Oxford, 1954).

Brockhouse, B.N. (1961), in Inelastic Scattering of Neutrons in Solids and Liquids (IAEA, Vienna), p113.

Choquard, P. (1967), The Anharmonic Crystal (Benjamin, New York, 1967).

Cowley, E.R. (1983), Phys. Rev. B28, 3160.

Cowley E.R. and G.K. Horton, Phys. Rev. Lett., 58, No. 8, 789, 1987.

Cowley, E.R., Horton, G.K. and Leese, J.G. in Proceedings of the Second International Conference on Phonon Physics, Budapest, Hungary, edited by J. Kollár et al., World Scientific, Singapore, p 165. 1985,

Day, M.A. and Hardy R.J. (1989), J. Phys. Chem. Solids, 46, 487.

Eckert, J. and Youngblood, R.W. (1986), Phys. Rev. B34, 2770.

Fujii, Y., Lurie, N.A., Pynn, R., and Shirane, G. (1974), Phys. Rev. B10, 3647.

Gewürtz S. and Stoicheff, B.P. (1974), Phys. REv. B10, 3487.

Glyde, H.R. (1976), in Rare Gas Solids (Academic, London), Vol. 1, Ch. 7.

Glyde, H.R. and Smoes M.G. (1980), Phys. Rev. B.22, 6391.

Goldman, V.V., Horton, G.K., and Klein, M.L. (1968), Phys. Rev. Lett. 21, 1527.

Goldman, V.V., Horton, G.K. and Klein, M.L. (1970), Phys. Rev. Lett. 24, 1424.

Goldman, V.V. (1979), Phys. Rev. B20, 4478.

Hansen, J.-P. and Klein, M.L. (1976), Phys. Rev. B13, 878.

Horner, H. (1974), in Dynamical Properties of Solids, edited by G.K. Horton and A.A. Maradudin (North-Holland, Amsterdam, 1974), Vol. 1.

Horton, G.K. and Leech, J.W. (1963), Proc. Phys. Soc. (London) 82, 816.

Kanney, L.B., and Horton, G.K. (1975), Sov. J. Low Temp. Phys. (Kiev) 1, 739.

Klein, M.L. and Horton, G.K. (1968), Proc. L.T. 11, St. Andrews, Scotland, 1, 553.

Koehler, T.R. (1975), in Dynamical Properties of Solids, edited by G.K. Horton and A.A. Maradudin (North-Holland, Amsterdam, 1975), Vol. 2, Ch. 1.

Leese, J.G., Horton, G.K., and Cowley, E.R. (1980), J. Low Temp. Phys 41, 543.

Nosanow, L.H. (1966), Phys. Rev. 146, 120.

Shukla, R.C. and Wilk, L. (1971), Phys. Rev. B3, 4055.

Shukla, R.C. and Cowley, E.R. (1985), Phys. REv. B31, 372.

Werthamer, N.R. (1970), Phys. REv. 31, 522.

A COMMENT ON THE APPLICABILITY OF THERMODYNAMIC PERTURBATION THEORY

N.M.Plakida
Joint Institute for Nuclear Research
Dubna,USSR

The effective parameter of the thermodynamic perturbation theory is $\varepsilon^2 = \gamma^2\lambda^2$. The small parameter λ^2 was introduced by van Hove

$$\lambda^2 = \frac{\langle u^2\rangle_T}{a^2} , \qquad (1)$$

a is the lattice spacing and $\langle u^2\rangle_T$ – the mean value of the square of the displacement of an atom from its rest position, T is the temperature. According to (1) this small parameter is multiplied by a large constant γ^2

$$\gamma^2 = a^2\Phi^{(n+n)}/\Phi^{(n)}, \quad (n \geq 2) \qquad (2)$$

where $\Phi^{(n)}$ is the n-th derivative of the potential Φ. One has $\Phi(a) \sim a^{-2}$, hence $\gamma \geq 10$. Thus, for temperatures close to the melting temperature T_m one has

$$\varepsilon^2 \sim 10^2 * 10^{-2} \sim 1, \quad (T \sim T_m) \qquad (3)$$

so the thermodynamic perturbation theory breaks down.

The parameter ε can be represented also as the ratio of $\sqrt{\langle u^2\rangle}$ and the difference $(a - \sigma)$, where σ is the hard core distance of the pair potential. According to the Lindenmann law of melting at $T \sim T_m$ this ratio is of the order of unity:

$$\varepsilon = \frac{\sqrt{\langle u^2\rangle_T}}{a - \sigma} \sim 1. \qquad (4)$$

Surface Acoustic Waves on Real Surfaces

Alexei A. Maradudin
Department of Physics
University of California
Irvine, California 92717, USA

1. Introduction - What Is a Real Surface?

The equations of motion of an elastic medium, within the linear theory of elasticity, are

$$\rho \ddot{u}_{\alpha} = \sum_{\beta} \frac{\partial T_{\alpha\beta}}{\partial x_{\beta}}, \quad \alpha = 1, 2, 3, \tag{1.1}$$

where ρ is the mass density of the medium, assumed to be constant, $u_{\alpha}(\vec{x};t)$ is the α Cartesian component of the displacement of the medium at the point $\vec{x}$ and time t, and $T_{\alpha\beta}$ is an element of the stress tensor. The latter is given by Hooke's law

$$T_{\alpha\beta} = \sum_{\mu\nu} C_{\alpha\beta\mu\nu} \frac{\partial u_{\mu}}{\partial x_{\nu}}, \quad \alpha,\beta = 1,2,3, \tag{1.2}$$

where the $\{C_{\alpha\beta\mu\nu}\}$ are the elements of a fourth rank tensor called the elastic modulus tensor. Although the elastic modulus tensor is a fourth rank tensor, the fact that it is symmetric in α and β, in μ and ν, and in $\alpha\beta$ and $\mu\nu$ makes it possible to express it equivalently in a two subscript notation, $C_{\alpha\beta\mu\nu} \rightarrow c_{ij}$, according to the scheme

11	22	33	23=32	31=13	12-21
1	2	3	4	5	6

The resulting 6 × 6 matrix representation of the elastic modulus tensor is referred to as the contracted, or Voigt, representation of this tensor. It should be emphasized, however, that the $\{c_{ij}\}$ are not the elements of a second rank tensor, since they lack the transformation properties of the latter under real, orthogonal transformations of the medium.

When we combine Eqs. (1.1) and (1.2) we obtain the equation of motion of the medium in the form

$$\rho\ddot{u}_\alpha = \sum_{\beta\mu\nu} C_{\alpha\beta\mu\nu} \frac{\partial^2 u_\mu}{\partial x_\beta \partial x_\nu}, \qquad \alpha = 1,\ 2,\ 3. \tag{1.3}$$

If the elastic medium occupies a volume V bounded by a surface S that is assumed to be stress-free, the boundary conditions on the displacement field that express this assumption can be expressed as

$$\sum_\beta T_{\alpha\beta}\hat{n}_\beta \Big|_S = 0 \qquad \alpha = 1,\ 2,\ 3, \tag{1.4}$$

where $\hat{n}$ is the unit vector normal to the surface S at each point, directed away from the volume V.

In 1885, Lord Rayleigh$^{(1)}$ applied the preceding equations to establish the existence of elastic waves that propagate along the stress-free surface $x_3 = 0$ of a semi-infinite, isotropic medium, occupying the half-space $x_3 > 0$, and are bound to the surface. As an introduction to the material that follows, and because some of the results will be used repeatedly there, it is useful to reproduce here Lord Rayleigh's derivation of the dispersion relation and displacement field of such a surface-localized elastic wave, albeit in a more contemporary form.

For the isotropic medium considered by Lord Rayleigh, the elastic modulus tensor $C_{\alpha\beta\mu\nu}$ is given by$^{(2)}$

$$C_{\alpha\beta\mu\nu} = \rho(c_\ell^2 - 2c_t^2)\delta_{\alpha\beta}\delta_{\mu\nu} + \rho c_t^2(\delta_{\alpha\mu}\delta_{\beta\nu} + \delta_{\alpha\nu}\delta_{\beta\mu}), \tag{1.5}$$

where c_ℓ and c_t are the speeds of longitudinal and transverse sound waves in the medium, respectively. Since all directions in the surface $x_3 = 0$ are equivalent in this case, with no loss of generality we can study a wave that propagates in the x_1-direction. If we assume that the wave is straight-crested, the displacement field is independent of the coordinate x_2 ($\partial/\partial x_2 \equiv 0$), and has the form

$$u_\alpha(\vec{x};t) = \hat{u}_\alpha(k\omega|x_3)\exp(ikx_1 - i\omega t), \qquad \alpha = 1,\ 2,\ 3. \tag{1.6}$$

The equations of motion (1.3) and the boundary conditions (1.4) then break up into the following two sets for the amplitude functions $\{\hat{u}_\alpha(k\omega|x_3)\}$:

$$-\omega^2\hat{u}_1 = \left(c_t^2 \frac{d^2}{dx_3^2} - c_\ell^2 k^2\right)\hat{u}_1 + i\left(c_\ell^2 - c_t^2\right) k \frac{d\hat{u}_3}{dx_3} \tag{1.7a}$$

$$-\omega^2\hat{u}_3 = i(c_\ell^2-c_t^2)\,k\,\frac{d\hat{u}_1}{dx_3} + \left(c_\ell^2\,\frac{d^2}{dx_3^2} - c_t^2k^2\right)\hat{u}_3 \tag{1.7b}$$

$$c_t^2\left(\frac{d\hat{u}_1}{dx_3} + ik\hat{u}_3\right)_{x_3=0} = 0 \tag{1.8a}$$

$$\left[i(c_\ell^2-2c_t^2)k\hat{u}_1 + c_\ell^2\,\frac{d\hat{u}_3}{dx_3}\right]_{x_3=0} = 0\ ; \tag{1.8b}$$

and

$$-\omega^2\hat{u}_2 = c_t^2\left(\frac{d^2}{dx_3^2} - k^2\right)\hat{u}_2 \tag{1.9}$$

$$\left.\frac{d\hat{u}_2}{dx_3}\right|_{x_3=0} = 0. \tag{1.10}$$

The solution of Eqs. (1.7)-(1.8) describes a wave polarized in the sagittal plane, i.e. the plane defined by the normal to the surface and the direction of propagation of the wave. The solution of Eqs. (1.9)-(1.10) describes a wave polarized perpendicular to the sagittal plane, a polarization that is often called shear horizontal.

We consider the case of sagittal polarization first. The solutions of Eqs. (1.7) that vanish as $x_3 \to \infty$, as befits a wave localized to the surface $x_3 = 0$, are

$$\hat{u}_1(k\omega|x_3) = A_\ell e^{-\alpha_\ell x_3} + A_t e^{-\alpha_t x_3} \tag{1.11a}$$

$$\hat{u}_3(k\omega|x_3) = i\left[\frac{\alpha_\ell}{k}\,A_\ell\,e^{-\alpha_\ell x_3} + \frac{k}{\alpha_t}\,A_t\,e^{-\alpha_t x_3}\right], \tag{1.11b}$$

where

$$\alpha_{\ell,t}(k\omega) = \left(k^2 - \frac{\omega^2}{c_{\ell,t}^2}\right)^{1/2}\ . \tag{1.12}$$

In order that Eqs. (1.11) describe a surface wave, α_ℓ and α_t must be real and positive. Assuming that k and ω are real, and keeping in mind that $c_\ell^2 > c_t^2$ in general$^{(3)}$, we see from Eqs. (1.12) that this requires that $k^2 > \omega^2/c_t^2$.

When Eqs. (1.11) are substituted into the boundary conditions (1.8) we obtain a pair of homogeneous equations for the amplitudes A_ℓ and A_t:

$$2\alpha_{\ell}(k\omega)A_{\ell} + \frac{k^2+\alpha_t^2(k\omega)}{\alpha_t(k\omega)} A_t = 0 \tag{1.13a}$$

$$\frac{k^2+\alpha_t^2(k\omega)}{k} A_{\ell} + 2kA_t = 0. \tag{1.13b}$$

The solvability condition for this system yields the dispersion relation

$$4k^2\alpha_{\ell}(k\omega)\alpha_t(k\omega) - (k^2+\alpha_t^2(k\omega))^2 = 0 \tag{1.14}$$

connecting the frequency ω of the wave (1.6) to its wave vector k. From the form of Eq.(1.14) and Eqs. (1.12) we see that ω must be a linear function of k, and we write the relation between these two variables as

$$\omega_S(k) = c_R k. \tag{1.15}$$

The fact that the surface wave studied here is dispersionless, i.e. the fact that the phase (and group) velocity c_R is independent of k, is due to the absence of any characteristic length in the physical system supporting this wave against which its wavelength can be compared.

To obtain the equation for the phase (and group) velocity c_R of these sagittally polarized surface waves, we move the second term on the left hand side of Eq. (1.14) to the right hand side and square both sides of the resulting equation. The equation for c_R then takes the form

$$\xi^6 - 8\xi^4 + 8(3-2\lambda^2)\xi^2 - 16(1-\lambda^2) = 0, \tag{1.16}$$

where we have introduced the definitions $\xi = c_R/c_t$ and $\lambda = c_t/c_{\ell}$. In view of the restriction that $k^2 > \omega^2/c_t^2$, only the real root of Eq. (1.16) for which $0 < \xi < 1$ yields the speed of a surface wave. The only solution of Eq. (1.16) that satisfies this condition is plotted as a function of λ in Fig. 1. [We note that the physically permissible values of λ range from 0, which corresponds to an incompressible solid, to $(3/4)^{1/2}$, which is the largest value consistent with the stability of the isotropic elastic medium, i.e., consistent with a positive-definite strain energy$^{(3)}$.]

From Eqs. (1.13) we see that the amplitudes A_{ℓ} and A_t are related by

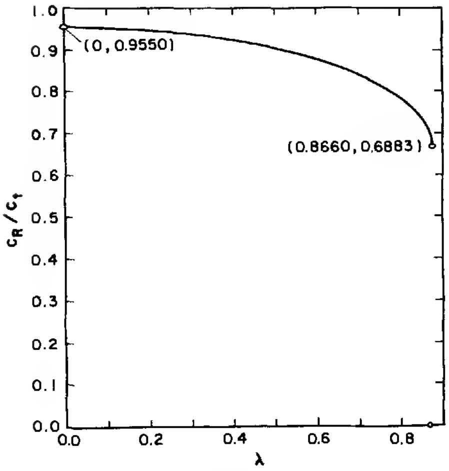

Fig. 1. A plot of c_R/c_t, the speed of Rayleigh waves on an istropic substrate, as a function of $\lambda = c_t/c_\ell$.

$$\frac{A_t}{A_\ell} = -\frac{2\beta_\ell\beta_t}{2-\xi^2} = -(\beta_\ell\beta_t)^{1/2} = -(1-\lambda^2\xi^2)^{1/4}(1-\xi^2)^{1/4} = -(1-\tfrac{1}{2}\xi^2), \qquad (1.17)$$

where

$$\beta_\ell = (1-\lambda^2\xi^2)^{1/2}, \quad \beta_t = (1-\xi^2)^{1/2}, \qquad (1.18)$$

and we have used Eq. (1.14) in obtaining the several alternative forms of this relation. In this way we find that the displacement field in this surface wave, obtained by combining Eqs. (1.6), (1.11), and (1.17), is given by

$$u_1(\vec{x};t) = A_\ell[e^{-k\beta_\ell x_3} - (1-\tfrac{1}{2}\xi^2)\, e^{-k\beta_t x_3}]\exp[ik(x_1-c_R t)] \qquad (1.19a)$$

$$u_3(\vec{x};t) = iA_\ell\beta_\ell[e^{-k\beta_\ell x_3} - \frac{1}{(1-\tfrac{1}{2}\xi^2)}\, e^{-k\beta_t x_3}]\exp[ik(x_1-c_R t)]. \qquad (1.19b)$$

On the assumption that A_ℓ is real, the physical displacement components, given by the real parts of Eqs. (1.19), are

$$u_1(\vec{x};t) = A_\ell[e^{-k\beta_\ell x_3} - (1-\tfrac{1}{2}\xi^2)e^{-k\beta_t x_3}]\cos k(x_1-c_R t) \qquad (1.20a)$$

$$u_3(\vec{x};t) = -A_\ell\beta_\ell\left[e^{-k\beta_\ell x_3} - \frac{e^{-k\beta_t x_3}}{(1-\frac{1}{2}\xi^2)}\right]\sin k(x_1-c_R t) \quad . \tag{1.20b}$$

From Eqs. (1.18) we find that the penetration depths of these sagitally polarized surface waves, $(k\beta_\ell)^{-1}$ and $(k\beta_t)^{-1}$, are of the order of the wavelength $\lambda = (2\pi/k)$ of the wave along the surface. For example, in the typical case in which $c_\ell^2 = 3c_t^2$ (the so-called Poisson case) we find that $\xi = [2 - \frac{2}{3}\sqrt{3}]^{1/2} = 0.9194$, whence it follows that

$$(k\beta_\ell)^{-1} = \frac{1.18}{2\pi}\lambda = 0.188\lambda, \quad (k\beta_t)^{-1} = \frac{2.54}{2\pi}\lambda = 0.404\lambda. \tag{1.21}$$

The result that the penetration depths are of the order of the wavelength of a surface acoustic wave along the surface over which it propagates is found for many other types of surface waves.

We also see, from Eqs. (1.20), that the particle displacements in this surface wave execute ellipses in the sagittal plane. Near the surface the wave motion is retrograde, and it reverses its sense at depths greater than approximately one-fifth of a wavelength. The major axes of the ellipses are normal to the surface, and the aspect ratio varies with depth.

Because the frequency of this sagitally polarized wave vanishes with vanishing wave vector k, it is termed an acoustic wave; because it is a wave localized to the surface of the medium, it is further termed a *surface acoustic wave*. Finally, in honor of its discoverer, the surface acoustic wave we have just discussed is called a *Rayleigh wave*.

Turning briefly to the case of shear horizontal polarization defined by Eqs. (1.9)-(1.10), we find that the solution of Eq. (1.9) that vanishes as $x_3 \to \infty$ is

$$\hat{u}_2(k\omega|x_3) = Ae^{-\alpha_t x_3} \quad . \tag{1.22}$$

When this solution is substituted into the boundary condition (1.10) we obtain the equation

$$\alpha_t(k\omega)\ A = 0. \tag{1.23}$$

If we are to have a wave at all, we must have $A \neq 0$. It follows then that $\alpha_t(k\omega) = 0$, so that from Eqs. (1.12) we see that the frequency of the resulting shear horizontal wave is

$$\omega_{SH}(k) = c_t k. \tag{1.24}$$

This wave is not a surface wave ($\alpha_t = 0$ in Eq. (1.22)). It is in fact a bulk wave that propagates parallel to the surface, and is therefore called a surface skimming bulk transverse wave.

This surface skimming bulk transverse wave has been called "unstable" by Viktorov$^{(4)}$, in the sense that a slight variation of the boundary conditions or properties of the medium convert it into a surface wave. In the remaining sections of these lectures we will see several examples of this conversion of surface skimming bulk transverse waves into true surface acoustic waves by perturbations of the usual stress-free boundary conditions.

The preceding results can be summarized by saying that the surface acoustic waves discovered by Lord Rayleigh in 1885, that now bear his name, are solutions of the equations of motion of a linear, semi-infinite, homogeneous, isotropic elastic medium that satisfy stress-free boundary conditions at the planar surface of the medium. They propagate in a wavelike fashion in directions parallel to the surface; their displacement vector lies in the sagittal plane; they decay in amplitude exponentially with increasing distance into the medium from the surface, with a decay length that is of the order of the wavelength of the wave along the surface; and they are dispersionless due to the lack of any characteristic length in the system supporting these waves. In addition, surface acoustic waves polarized perpendicular to the sagittal plane do not exist on such surfaces.

Real solids, however, are generally not elastically isotropic, but instead are anisotropic. In fact, they are often not purely elastic but are piezoelectric or magnetic. They can also be inhomogeneous in their material properties. Often the latter are functions of the distance into the medium from the surface. Real solids can have internal stresses, due to the manner in which they are prepared, for example. The surface bounding the medium can present transverse discontinuities, material and/or geometrical, to the propagation of surface acoustic waves across it. It may also not be planar, but curved or rough, deterministically but not periodically, periodically, or randomly. Real surfaces possess a surface tension that affects the dispersion relation for surface waves propagating across them. Because of the discreteness of a real crystal at the atomic level, the stress-strain relation in a medium is nonlocal in fact, and this modifies the surface acoustic waves discovered by Lord Rayleigh in interesting ways. Real elastic media are also nonlinear, rather than linear. Finally, real surfaces can have one-dimensional structures present either naturally or artificially on them, e.g. edges or topographic waveguides that can support acoustic waves that are spatially localized in the vicinity of the structure, viz. edge acoustic waves.

In these lectures I would like to describe briefly, and in somewhat didactic fashion, some results of recent investigations of the consequences of several of the properties of real surfaces listed above on surface acoustic waves. Much of this work has been carried out by my colleagues and myself at the University of California, Irvine. Discussions of the remaining properties not covered here can be found in Refs. 5-8.

2. Surface Acoustic Waves on Rough Surfaces

Why study surface acoustic waves on rough surfaces? A simple answer is that all real surfaces, even the most carefully prepared ones, possess some degree of roughness. It is therefore of interest to know how their properties are modified by that roughness. For example, a surface acoustic wave propagating across a rough surface can be scattered by the hills and valleys on the surface into other acoustic waves and into bulk waves. Energy is drawn from the wave and it is attenuated thereby, even if it is propagating on the surface of a lossless medium. It can be important for applications of surface acoustic waves to know what degree of such surface roughness is tolerable before the attenuation to which it gives rise reaches an unacceptable level. In the same vein, the propagation of surface acoustic waves across a rough surface gives rise to the phenomenon of wave slowing, viz. the reduction of its phase velocity below its value for a planar surface. If the surface is periodically corrugated a surface acoustic wave propagating across it displays pass bands and stop bands in its dispersion curve that can be useful in the design of filters for surface acoustic waves. The controlled conversion (transduction) of surface acoustic waves into bulk waves (and *vice versa*) can also be effected by such surfaces.

A second reason for studying surface acoustic waves on rough surfaces is that surface roughness gives rise to new types of surface acoustic waves that cannot exist in the absence of the roughness. This enriches the taxonomy of this field of surface science, and adds to the armamentarium of those interested in applications of surface acoustic waves.

When one speaks of rough surfaces one instinctively thinks of randomly rough surfaces. However, that is only one type of rough surface. In this section I will consider three types of rough surfaces, each of which would be planar in the absence of the roughness. They are all defined by an equation for the position of the surface of the form $x_3 = \zeta(x_1)$. [A discussion of surface acoustic waves on surfaces defined by an equation of the form $x_3 = \zeta(x_1,x_2)$ can be found in Ref. 6.] They differ in the nature of the surface profile function $\zeta(x_1)$. For the first type of rough surface $\zeta(x_1)$ is deterministic and is nonzero only for a finite range of values of x_1. It describes an isolated ridge or groove on an otherwise planar surface. For the second type of rough surface $\zeta(x_1)$ is again deterministic, but is a periodic function of x_1. It describes a classical grating on a material surface. For the third type of rough surface $\zeta(x_1)$ is a stochastic function of x_1 and describes a randomly rough surface.

2.1. A Deterministic, Nonperiodic, Rough Surface

Surface shape resonances are excitations that are spatially localized in the vicinity of an isolated protuberance or indentation on the otherwise planar surface of a solid. Because of the destruction of translational invariance in directions parallel to the nominal planar surface of the solid caused by the presence of the protuberance or indentation, the frequencies of surface shape resonances are discrete, and depend on the shape of the protuberance or indentation. Because these frequencies fall in the frequency range allowed the normal modes of the solid in the absence of the protuberance or indentation, the surface shape resonances can decay into the latter modes, and acquire a finite lifetime thereby.

All of the studies of surface shape resonances to date have dealt either with electrostatic(9) and electromagnetic(9) surface shape resonances, or with magnetostatic surface shape resonances(7). In this section I describe some first steps(10) in the study of acoustic surface shape resonances by considering what is perhaps the simplest system that can support such excitations. This is a rectangular ridge of height d and width 2ℓ, oriented parallel to the x_2-axis, on a semi-infinite substrate of the same or different material occupying the regions $x_3 < 0$ (Fig. 2). The displacement field is assumed to have only a single, nonvanishing component, along the x_2-axis, i.e. parallel to the ridge, that is a function only of x_1 and x_3.

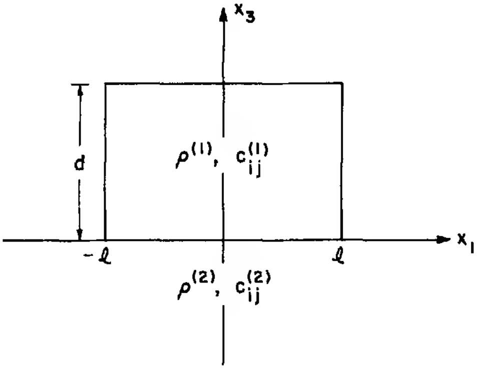

Fig. 2. A ridge of height d and width of 2ℓ of one material bonded to a semi-infinite substrate of a second material.

We assume that the ridge is fabricated from a material of mass density $\rho^{(1)}$ and elastic moduli $\{c_{ij}^{(1)}\}$. It is bonded to a semi-infinite substrate fabricated from a material of mass density $\rho^{(2)}$ and elastic moduli $\{c_{ij}^{(2)}\}$. Each of these materials is assumed to possess cubic symmetry, with the cube axes aligned parallel to the coordinate axes.

The displacement field in this system is assumed to have the form

$$\vec{u}(\vec{x};t) = (0,u_2(x_1x_3|\omega),0)\exp(-i\omega t), \tag{2.1}$$

where ω is the frequency of the modes we seek. The equation of motion satisfied by $u_2(x_1x_3|\omega)$ in the region occupied by the ridge is

$$-\rho^{(1)}\omega^2u_2^{(1)}(x_1x_3|\omega) = c_{44}^{(1)}\left(\frac{\partial^2}{\partial x_1^2} + \frac{\partial^2}{\partial x_3^2}\right)u_2^{(1)}(x_1x_3|\omega)$$
$$-\ell < x_1 < \ell,\ 0 < x_3 < d. \tag{2.2}$$

The equation satisfied by $u_2(x_1x_3|\omega)$ in the substrate is

$$-\rho^{(2)}\omega^2u_2^{(2)}(x_1x_3|\omega) = c_{44}^{(2)}\left(\frac{\partial^2}{\partial x_1^2} + \frac{\partial^2}{\partial x_3^2}\right)u_2^{(2)}(x_1x_3|\omega) \qquad (2.3)$$

$$-\infty < x_1 < \infty, \qquad x_3 < 0.$$

The condition that the surface of the ridge be stress-free reduces to the requirement that the normal derivative of $u_2^{(1)}(x_1x_3|\omega)$ vanish at every point of the boundary. Additional boundary conditions require that the surface $x_3 = 0$ be stress-free in the region $|x_1| > \ell$,

$$\frac{\partial}{\partial x_3}u_2^{(2)}(x_1x_3|\omega) = 0 \qquad |x_1| > \ell,\ x_3 = 0, \qquad (2.4)$$

and the displacement field and the stress acting on the interface $x_3 = 0$ be continuous across this interface in the region $|x_1| < \ell$,

$$u_2^{(1)}(x_1x_3|\omega) = u_2^{(2)}(x_1x_3|\omega) \qquad |x_1| < \ell,\ x_3 = 0 \qquad (2.5)$$

$$c_{44}^{(1)}\frac{\partial}{\partial x_3}u_2^{(1)}(x_1x_3|\omega) = c_{44}^{(2)}\frac{\partial}{\partial x_3}u_2^{(2)}(x_1x_3|\omega) \qquad |x_1| < \ell,\quad x_3 = 0. \qquad (2.6)$$

Finally, $u_2^{(2)}(x_1x_3|\omega)$ must vanish as $x_3 \to -\infty$.

The solution of Eq. (2.2) that satisfies the boundary conditions on the surface of the ridge can be written in the form

$$u_2^{(1)}(x_1x_3|\omega) = \sum_{n=0}^{\infty}\varepsilon_nB_n\cos\frac{n\pi}{2\ell}(x_1-\ell)\cos\beta_n(\omega)(x_3-d)$$

$$-\ell < x_1 < \ell, \quad 0 < x_3 < d, \qquad (2.7)$$

where $\varepsilon_n = \frac{1}{2}$ for $n = 0$ and 1 for $n > 1$, and

$$\beta_n(\omega) = \left(\frac{\omega^2}{c_1^2} - \left(\frac{n\pi}{2\ell}\right)^2\right)^{1/2} \qquad \frac{\omega}{c_1} > \frac{n\pi}{2\ell} \qquad (2.8a)$$

$$= i\left(\left(\frac{n\pi}{2\ell}\right)^2 - \frac{\omega^2}{c_1^2}\right)^{1/2} \qquad \frac{\omega}{c_1} < \frac{n\pi}{2\ell}, \qquad (2.8b)$$

with $c_1 = (c_{44}^{(1)}/\rho^{(1)})^{1/2}$. The solution of Eq. (2.3) that satisfies the boundary condition at infinity can be written as

$$u_2^{(2)}(x_1x_3|\omega) = \int\frac{dk}{2\pi}A(k\omega)e^{ikx_1+\alpha(k\omega)x_3} \qquad (2.9)$$

$$-\ell < x_1 < \ell, \quad x_3 < 0,$$

where

$$\alpha(k\omega) = \left(k^2 - \frac{\omega^2}{c_2^2}\right)^{1/2} \qquad k^2 > \frac{\omega^2}{c_2^2} \tag{2.10a}$$

$$= -i\left(\frac{\omega^2}{c_2^2} - k^2\right)^{1/2} \qquad k^2 < \frac{\omega^2}{c_2^2}\,, \tag{2.10b}$$

and $c_2 = \left(c_{44}^{(2)}/\rho^{(2)}\right)^{1/2}$.

The coefficients $\{B_n\}$ and $A(k\omega)$ are determined from the boundary conditions (2.4)-(2.6). The equation for the $\{B_n\}$ obtained in this way is

$$\cos(\beta_m(\omega)d)B_m = \frac{\ell}{d}\,\frac{c_{44}^{(1)}}{c_{44}^{(2)}} \sum_{n=0}^{\infty} M_{mn}(\omega)\varepsilon_n(\beta_n(\omega)d) \times$$

$$\times \sin(\beta_n(\omega)d)B_n \qquad m = 0,1,2\ldots \tag{2.11}$$

where

$$M_{mn}(\omega) = \int \frac{dk}{2\pi}\,\frac{S_m^*(k)\;S_n(k)}{\alpha(k\omega)} \tag{2.12a}$$

and

$$S_n(k) = \frac{1}{\ell}\int_{-\ell}^{\ell} dx_1\; e^{-ikx_1} \cos\frac{n\pi}{2\ell}(x_1-\ell)\,. \tag{2.12b}$$

Equating to zero the determinant of the coefficients in Eq. (2.11) yields the equation for the frequencies of the surface shape resonances associated with the structure in Fig. 2. In practice the infinite determinant defined by Eq. (2.11) is made into an NxN determinant by restricting m and n to the values 0,1,2,...,N-1. N is then increased until convergence of the frequencies is achieved. Because, according to Eq. (2.10), $\alpha(k\omega)$ is real for $|k| > \omega/c_2$ and imaginary for $|k| < \omega/c_2$, the matrix elements $\{M_{mn}(\omega)\}$ are complex even if ω is real. The physical reason for this is the decay of the surface shape resonances into the bulk vibrational modes of the substrate.

Rather than solving for the complex zeros of a complex determinant we can obtain the complex frequencies of the acoustic surface shape resonances in the following way. Let us denote the determinant of the coefficients in Eq. (2.11) by $D(\omega)$. The frequency of an acoustic surface shape resonance is written as

$$\omega = \omega_R - i\omega_I, \tag{2.13}$$

where both ω_R and ω_I are real and ω_I is positive for a mode that decays with increasing time. Let us expand $D(\omega)$ for ω in the vicinity of $\omega_R - i\omega_I$:

$$D(\omega) = (\omega-\omega_R + i\omega_I)D'(\omega_R-i\omega_I) + O((\omega-\omega_R+ i\omega_I)^2), \qquad (2.14)$$

where the constant term vanishes because $D(\omega_R-i\omega_I) = 0$ by hypothesis. It follows, therefore, that for ω real and in the vicinity of ω_R

$$\frac{1}{|D(\omega)|^2} = \frac{1}{|D'(\omega_R- i\omega_I)|^2}\,\frac{1}{(\omega-\omega_R)^2 + \omega_I^2}\,. \qquad (2.15)$$

Consequently, a plot of $|D(\omega)|^{-2}$ as a function of real ω will have a peak at $\omega = \omega_R$ and a full width at half-maximum of $2\omega_I$, for each acoustic surface shape resonance, from which circumstance both ω_R and ω_I can be obtained. The preceding discussion assumes that ω_I is small conmpared with ω_R in order that terms of $O((\omega-\omega_R+i\omega_I)^2)$ and higher can be neglected on the right hand side of Eq. (2.14).

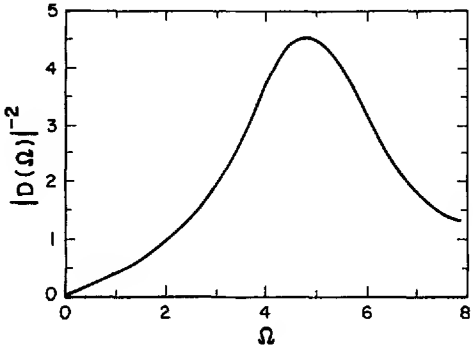

Fig. 3. A plot of $|D(\Omega)|^{-2}$ vs Ω, where Ω is the dimensionless frequency $\Omega = (\omega\ell/c_2)$. The peak at $\Omega \cong 4.85$ corresponds to the surface shape resonance associated with the structure in Fig. 2 when $d = 2\ell$, $\rho^{(1)} = \rho^{(2)}$, and $c_{ij}^{(1)} = c_{ij}^{(2)}$.

A plot of $|D(\Omega)|^{-2}$ vs. Ω is shown in Fig. 3 for the case in which $\rho^{(1)} = \rho^{(2)}$, $c_{ij}^{(1)} = c_{ij}^{(2)}$ and $d = 2\ell$, where Ω is the dimensionless frequency $\Omega = \omega\ell/c_2)$. In preparing this plot only the simplest approximation to $D(\Omega)$ was used, viz. the one obtained by setting $m = n = 0$ in Eq. (2.11). The peak corresponding to the lowest frequency acoustic surface shape resonances is shown. In the present case it is quite broad ($\omega_I \approx \omega_R$), so that this mode is strongly damped. This result is not expected to change when a fully converged result for $D(\Omega)$ is used.

Interest in such surface shape resonances derives from the fact that their resonant excitation by, e.g. surface acoustic waves impinging on the protuberance supporting these excitations, can lead to stress concentrations in the vicinity of the protuberance that in turn can affect physical processes occurring at a solid surface, such as chemical reactions. In addition, some rough surfaces, whether peiodically or randomly corrugated, can be regarded as an array of protuberances on an otherwise planar surface. A knowledge of the excitations associated with an isolated protuberance could be of value in understanding the excitations associated with such a rough surface.

2.2. A Deterministic, Periodic, Rough Surface

In contrast with the discussion in the preceding subsection, where a very specific surface profile function was assumed, we consider here the case of an isotropic elastic medium that occupies the region $x_3 > \zeta(x_1)$, where the surface profile function $\zeta(x_1)$ is arbitrary except for the assumption that it is a single-valued function of x_1 (Fig. 4). The unit vector normal to the surface at each point, and directed away from the solid, is given by

$$\hat{n} = [1 + (\zeta'(x_1))^2]^{-1/2} (\zeta'(x_1), 0, -1). \qquad (2.16)$$

It is convenient to study the propagation of surface acoustic waves of sagittal and shear horizontal polarization across such a surface separately, and we take up these cases in turn in the remainder of this section

2.2.1. Sagittal Polarization

The displacement field of a sagittally polarized surface acoustic wave propagating in the x_1-direction across the surface

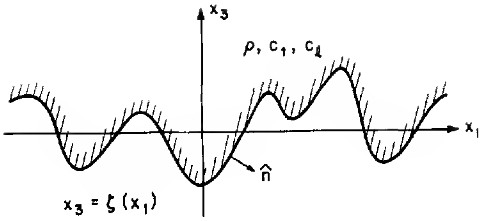

Fig. 4. A nonplanar, rough, surface profile on a semi-infinite, isotropic elastic medium.

depicted in Fig. 4. The displacement field in this case has the form

$$\vec{u}(\vec{x};t) = (u_1(x_1x_3|\omega), 0, u_3(x_1x_3|\omega))\exp(-i\omega t) \tag{2.17}$$

in the region $x_3 > \zeta(x_1)$. The amplitudes $u_{1,3}(x_1x_3|\omega)$ satisfy a pair of coupled equations of motion in this region:

$$-\omega^2 u_1 = \left(c_\ell^2 \frac{\partial^2}{\partial x_1^2} + c_t^2 \frac{\partial^2}{\partial x_3^2}\right)u_1 + (c_\ell^2 - c_t^2)\frac{\partial^2 u_3}{\partial x_1 \partial x_3} \tag{2.18a}$$

$$-\omega^2 u_3 = (c_\ell^2 - c_t^2)\frac{\partial^2 u_1}{\partial x_1 \partial x_3} + \left(c_t^2 \frac{\partial^2}{\partial x_1^2} + c_\ell^2 \frac{\partial^2}{\partial x_3^2}\right). \tag{2.18b}$$

The conditions (1.4), that ensure that the surface $x_3 = \zeta(x_1)$ is stress-free, take the forms

$$\Big\{\Big[-c_\ell^2\zeta'(x_1)\frac{\partial}{\partial x_1} + c_t^2\frac{\partial}{\partial x_3}\Big]u_1 + \Big[-(c_\ell^2-2c_t^2)\zeta'(x_1)\frac{\partial}{\partial x_3} + c_t^2\frac{\partial}{\partial x_1}\Big]u_3\Big\}_{x_3=\zeta(x_1)} = 0 \tag{2.19a}$$

$$\Big\{\Big[-c_t^2\zeta'(x_1)\frac{\partial}{\partial x_3} + (c_\ell^2 - 2c_t^2)\frac{\partial}{\partial x_1}\Big]u_1 + \Big[-c_t^2\zeta'(x_1)\frac{\partial}{\partial x_1} + c_\ell^2\frac{\partial}{\partial x_3}\Big]u_3\Big\}_{x_3=\zeta(x_1)} = 0. \tag{2.19b}$$

In addition, we require that $u_{1,3}(x_1x_3|\omega)$ vanish as $x_3 \to \infty$.

The solutions of Eqs. (2.18) in the region $x_3 > \zeta(x_1)_{\max}$ that satisfy the the boundary condition at infinity can be written as the Fourier integrals

$$u_1(x_1x_3|\omega) = \int \frac{dk}{2\pi} e^{ikx_1} \{A_\ell(k\omega) e^{-\alpha_\ell(k\omega)x_3} +$$

$$+ A_t(k\omega) e^{-\alpha_t(k\omega)x_3}\} \qquad (2.20a)$$

$$u_3(x_1x_3|\omega) = \int \frac{dk}{2\pi} e^{ikx_1} i\{\frac{\alpha_\ell(k\omega)}{k} A_\ell(k\omega) e^{-\alpha_\ell(k\omega)x_3} +$$

$$+ \frac{k}{\alpha_t(k\omega)} A_t(k\omega) e^{-\alpha_t(k\omega)x_3}\}, \qquad (2.20b)$$

where

$$\alpha_{\ell,t}(k\omega) = (k^2 - \frac{\omega^2}{c^2_{\ell,t}})^{1/2} \qquad k^2 > \frac{\omega^2}{c^2_{\ell,t}} \qquad (2.21a)$$

$$= -i(\frac{\omega^2}{c^2_{\ell,t}} - k^2)^{1/2} \qquad k^2 < \frac{\omega^2}{c^2_{\ell,t}} . \qquad (2.21b)$$

We now invoke the Rayleigh hypothesis$^{(11)}$ and use the solutions (2.20) in satisfying the boundary conditions (2.19) at the rough surface $x_3 = \zeta(x_1)$. When the k^{th} Fourier coefficient on the left hand side of each of the resulting homogeneous equations is equated to zero, we obtain a pair of coupled, homogeneous integral equations satisfied by the amplitudes $A_\ell(k\omega)$ and $A_t(k\omega)$:

$$\int \frac{dq}{2\pi} \{\frac{I(\alpha_\ell(q\omega)|k-q)}{q\alpha_\ell(q\omega)} [(k-q) \frac{\omega^2}{c_t^2} + 2k\alpha_\ell^2(q\omega)] A_\ell(q\omega) +$$

$$+ \frac{I(\alpha_t(q\omega)|k-q)}{\alpha_t(q\omega)} (2kq - \frac{\omega^2}{c_t^2}) A_t(q\omega)\} = 0 \qquad (2.22a)$$

$$\int \frac{dq}{2\pi} \{\frac{I(\alpha_\ell(q\omega)|k-q)}{q} (2kq - \frac{\omega^2}{c_t^2}) A_\ell(q\omega) +$$

$$+ \frac{I(\alpha_t(q\omega)|k-q)}{\alpha_t^2(q\omega)} [2kq^2 - (k+q) \frac{\omega^2}{c_t^2}] A_t(q\omega)\} = 0 . \qquad (2.22b)$$

In obtaining these equations we have used the representations

$$e^{-\alpha\zeta(x_1)} = \int \frac{dQ}{2\pi} e^{iQx_1} I(\alpha|Q) \qquad (2.23a)$$

$$\zeta'(x_1)e^{-\alpha\zeta(x_1)} = -\frac{i}{\alpha}\int\frac{dQ}{2\pi}\,e^{iQx_1}\,QI(\alpha|Q), \tag{2.23b}$$

where

$$I(\alpha|Q) = \int dx_1 e^{-iQx_1}\,e^{-\alpha\zeta(x_1)} . \tag{2.24}$$

Within the Rayleigh hypothesis Eqs. (2.22) and (2.24) are the exact equations for $A_\ell(k\omega)$ and $A_t(k\omega)$.

To apply the results to the case of a periodically corrugated surface, we assume that $\zeta(x_1)$ is a periodic function of x_1 with period a: $\zeta(x_1+a) = \zeta(x_1)$. We then substitute the expansions

$$A_{\ell,t}(k\omega) = 2\pi\sum_{n=-\infty}^{\infty} A_n^{(\ell,t)}(q\omega)\delta(k-q_n) , \tag{2.25}$$

where $q_n = q+(2\pi n/a)$, into Eqs. (2.20) and (2.22). From the former equations we obtain a displacement field that satisfies the Bloch theorem,

$$u_{1,3}(x_1+a,x_3|\omega) = \exp(iqa)u_{1,3}(x_1x_3|\omega), \tag{2.26}$$

as must be the case for the periodic system we are considering. From the latter equations we obtain a pair of coupled, homogeneous matrix equations of infinite order for the coefficients $\{A_n^{(\ell,t)}(k\omega)\}^{(12)}$:

$$\sum_{n=-\infty}^{\infty}\Big\{\frac{I_{m-n}(\alpha_\ell(k_n\omega))}{k_n\alpha_\ell(k_n\omega)}\Big[(k_m-k_n)\frac{\omega^2}{c_t^2} + 2k_m\alpha_\ell^2(k_n\omega)\Big]A_n^{(\ell)}(k\omega) + $$
$$+\frac{I_{m-n}(\alpha_t(k_n\omega))}{\alpha_t(k_n\omega)}\Big[2k_mk_n - \frac{\omega^2}{c_t^2}\Big]A_n^{(t)}(k\omega)\Big\} = 0 \tag{2.27a}$$

$$m = 0,\pm1,\pm2,\pm3 \ldots$$

$$\sum_{n=-\infty}^{\infty}\Big[\frac{I_{m-n}(\alpha_\ell(k_n\omega))}{k_n}\Big[2k_mk_n - \frac{\omega^2}{c_t^2}\Big]A_n^{(\ell)}(k\omega) + $$
$$+\frac{I_{m-n}(\alpha_t(k_n\omega))}{\alpha_t^2(k_n\omega)}\Big[2k_mk_n^2-(k_m+k_n)\frac{\omega^2}{c_t^2}\Big]A_n^{(t)}(k\omega)\Big\} = 0 \tag{2.27b}$$

$$m = 0,\pm1,\pm2,\pm3,\ldots$$

where

$$I_m(\alpha) = \frac{1}{a}\int_0^a dx_1 e^{-i\frac{2\pi m}{a}x_1} e^{-\alpha\zeta(x_1)} . \qquad (2.28)$$

In writing Eqs. (2.27) we have denoted by k the wave number of the Rayleigh wave. The dispersion relation for Rayleigh waves on a grating is obtained by equating to zero the determinant of the coefficients in Eqs. (2.27). In actual calculations the matrix of coefficients in Eqs. (2.27) is made to have a finite size by restricting m and n in these equations to run from -N to N. The value of N is increased until convergent results for the frequencies are obtained.

The results of the numerical calculations of the dispersion curves can be analyzed in terms of the flat-surface dispersion curves in both the extended- and reduced-zone schemes. In the extended-zone scheme of Fig. 5 the straight line $\omega = c_R k$ (shown with a solid and then a dotted segment) is the dispersion curve for a Rayleigh wave on a flat surface (c_R is the speed of such a wave), and the dashed lines are the lines $\omega = c_t|k+(2\pi/a)m|$, where either m = 0 (the transverse sound line) or m = ±1, ±2,... . Since any point (ω,k) in the region above the dashed lines, $\omega > c_t|k+(2\pi/a)m|$, will correspond to an imaginary $\alpha_t(k_m\omega)$, the displacement fields at such points will have radiative components. Thus, a Rayleigh wave initially on a flat surface with its (ω,k) on the dotted part of the dispersion curve in Fig. 5 will begin to radiate into the bulk at the moment the grating, however weak, is turned on. If a Rayleigh wave with (ω,k) on this radiative part of the dispersion curve is launched across the grating surface, it will decay with some characteristic lifetime or, equivalently, will acquire a finite mean free path. We will return to this point below in discussing the attenuation of Rayleigh waves on a grating. Gratings thus can act as transducers converting Rayleigh waves into bulk waves in a controlled manner. The Bloch-type surface waves that are true eigenmodes for the surface with a grating (i.e. possess an infinite lifetime) will thus be found only with (ω,k) beneath the dashed lines in Fig. 5. In other words, they originate out of the solid line part of the flat surface Rayleigh wave dispersion curve as the grating is turned on.

The flat surface dispersion curve with its solid and dotted line segments is folded back into the domain $-\pi/a < k < \pi/a$ (the first Brillouin zone for the grating) in the reduced zone scheme of Fig. 5. The nonradiative region is now beneath the single dashed line $\omega = c_t|k|$. At points like A, B, C,... on the flat surface dispersion curve of Fig. 5 we have two degenerate modes separated in

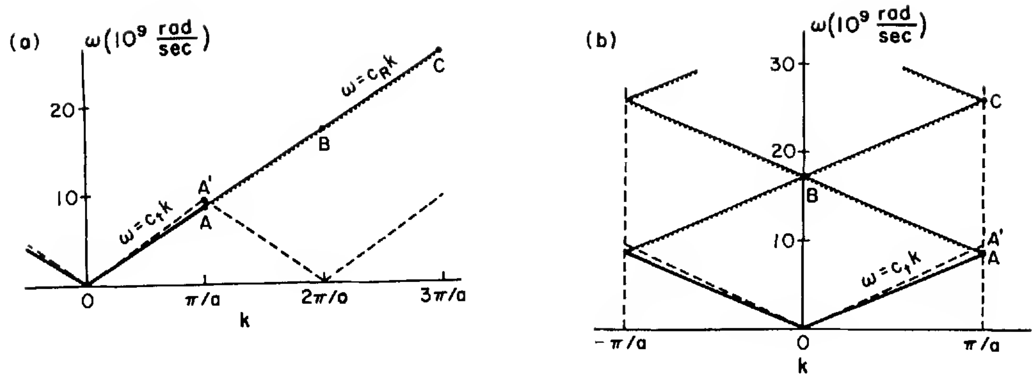

Fig. 5. The flat surface Rayleigh wave dispersion curve $\omega = c_R k$ in the nonradiative region (———) and in the radiative region (·····) defined by the boundary lines (- - - -) $\omega = c_t|k+(2\pi/a)m|$, where $m = 0, \pm 1, \pm 2, \ldots$, for a grating period of 10^{-6} m, and $c_\ell = 5 \times 10^3$ m/sec and $c_t = 3 \times 10^3$ m/sec. (a) the extended zone and (b) the reduced zone scheme.

wave vector by a multiple of $2\pi/a$, i.e. by a reciprocal lattice vector of the grating. If the Fourier coefficients of the grating profile function that correspond to these reciprocal lattice vectors are nonzero, then the degeneracy of the modes at the points A, B, C... will be lifted in the first order of perturbation theory in the surface profile function, and gaps will occur in the dispersion curves at these points in both the extended and reduced zone schemes.

From Eqs. (2.27) it is easy to show that this dispersion curve is an even function of k, and is periodic in k with period $2\pi/a$. Thus we confine our attention to the region $0 < k < \pi/a$, i.e. to half the one-dimensional first Brillouin zone defined by the periodicity of the grating.

The preceding qualitative results are what is observed in a typical dispersion curve, such as the one plotted in Fig. 6 for a sinusoidal surface profile function $\zeta(x_1) = \zeta_0 \cos 2\pi x_1/a$ with $\zeta_0/a = 0.3$. Values of N of about 10 were used in obtaining this result. In the long wavelength limit the dispersion curve osculates the dispersion curve for Rayleigh waves on a flat surface. With increasing k the curve bends away from the latter curve, into the nonradiative region. Both its group and phase velocity decrease

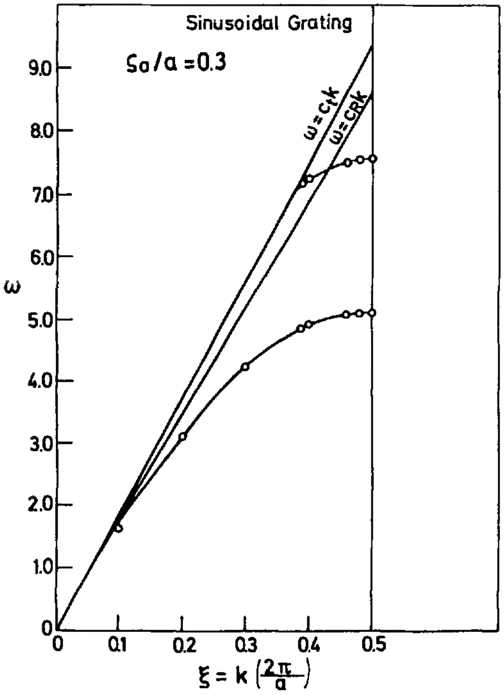

Fig. 6. Dispersion curve for Rayleigh waves propagating across a sinusoidal grating with corrugation strength $\zeta_0/a = 0.3$ on an isotropic elastic medium characterized by $c_\ell =$ 5×10^3 m/sec and $c_t = 3 \times 10^3$ m/sec.

below c_R. This is the phenomenon of wave slowing that occurs for Rayleigh waves on a grating. Wave slowing occurs because in contrast with the dispersion curve for a Rayleigh wave on a flat surface, which has a constant slope for all k, the dispersion curve for a Rayleigh wave on a grating is required to have zero slope at the Brillouin zone boundary $k = \pi/a$ due to its periodicity and continuity. This forces it to bend over into the nonradiative region of the (ω,k)- plane reducing its group velocity thereby. At the zone boundary a gap opens up in the dispersion curve, which defines a stop band for the propagation of Rayleigh waves on a grating. Knowledge of where this stop band occurs can be useful for the design of filters for Rayleigh waves. Finally, there is a high frequency branch to the dispersion curve above the gap, that terminates when it intersects the transverse sound line.

We now turn our attention to solutions of Eqs. (2.27) in the radiative region of the (ω,k)-plane, i.e. for (ω,k) above the transverse sound line $\omega = c_t k$, where $\alpha_t(k_n\omega)$ is imaginary, and for (ω,k) inside the gap in the Rayleigh wave dispersion curve at $k = \pi/a$ that is caused by the periodicity of the grating. In this region a Rayleigh wave can radiate energy into the bulk of the medium supporting it. By conservation of energy, the wave must be attenuated as it propagates across the grating. Consequently, if we assume that ω is real in these equations it is found that the corresponding wave number $k(\omega) = k_R(\omega) + ik_I(\omega)$ is complex, where $k_R(\omega)$ and $k_I(\omega)$ are real, positive functions of ω for a wave that travels in the $+x_1$-direction. The inverse attenuation length of the Rayleigh wave is then given by $\ell^{-1}(\omega) = 2k_I(\omega)$. In solving Eqs. (2.27) for ω real and k complex one has to be careful about the manner in which the branch cut defining the square root of $\alpha_{\ell,t}(k_n\omega)$ is chosen. The correct choice turns out to be along the positive imaginary axis, and one seeks solutions on the first sheet of the corresponding Riemann surface.* With this choice of branch cut we obtain a wave that radiates energy into the interior, is attenuated as it propagates along the surface, but in addition has an amplitude that grows exponentially with increasing distance into the medium. The latter feature of the resulting wave is an unavoidable consequence of the exponential growth in the amplitude of the Rayleigh wave on the surface of the medium as $x_1 \rightarrow -\infty$, due to the fact that $k_I(\omega) > 0$(13).

In Fig. 7 we show the experimental results of Rischbieter(14) for the attenuation of Rayleigh waves by symmetric sawtooth gratings ruled on an aluminum surface, together with the predictions of the first-order scattering theory of Sabine(15) (which follows the work of Brekovskikh(16)). In Fig. 8 we show the acoustical attenuation $(20 \log_e \lambda_s k_I)$ versus λ_s/a, where $\lambda_s/a = 2\pi c_t/\omega a$, for Rayleigh waves on symmetric sawtooth gratings with the same surface profile functions as in the experiments of Rischbieter. The latter results

---

* Equivalently, the branch cut can be chosen to coincide with the negative real axis, provided one then seeks solutions on the lower sheet of the corresponding Riemann surface.

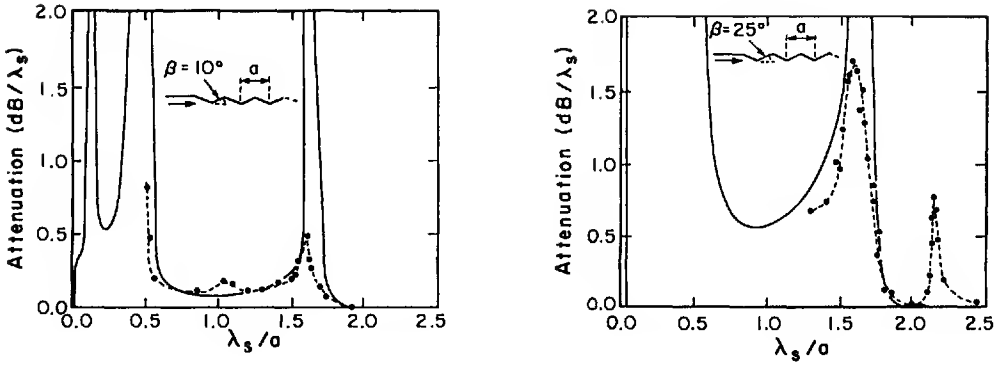

Fig. 7. Attenuation as a function of shear wavelength λ_s for Rayleigh waves on an Aℓ symmetric sawtooth grating, as measured by Rischbieter (-o-) and calculated by Sabine (———), for a Poisson ratio $\sigma = (1-2\lambda^2)/(2-2\lambda^2) = 0.33$, and (a) $\beta = 10^\circ$ and (b) $\beta = 25^\circ$ [Ref. 15].

were obtained by solving Eqs. (2.27) for $k_I(\omega)$ in the manner described above.(17) Comparisons of Figs. 7 and 8 show that the present theory gives the peak heights more accurately than the first order scattering theory, and finds all the experimental peaks, including (1) the sharp peaks at $\lambda_s/a = 2.15$, which correspond to solutions inside the first zone boundary gap, which are missed in any perturbative scattering theory; and (2) the higher frequency peaks, associated with the edges of the successively higher order gaps, also missed in previous theories.

2.2.2. Shear Horizontal Polarization

The displacement field of a surface acoustic wave propagating in the x_1-direction across the grating depicted in Fig. 4 has the form

$$\vec{u}(\vec{x};t) = (0,u_2(x_1x_3|\omega),0)\ \exp(-i\omega t) \tag{2.29}$$

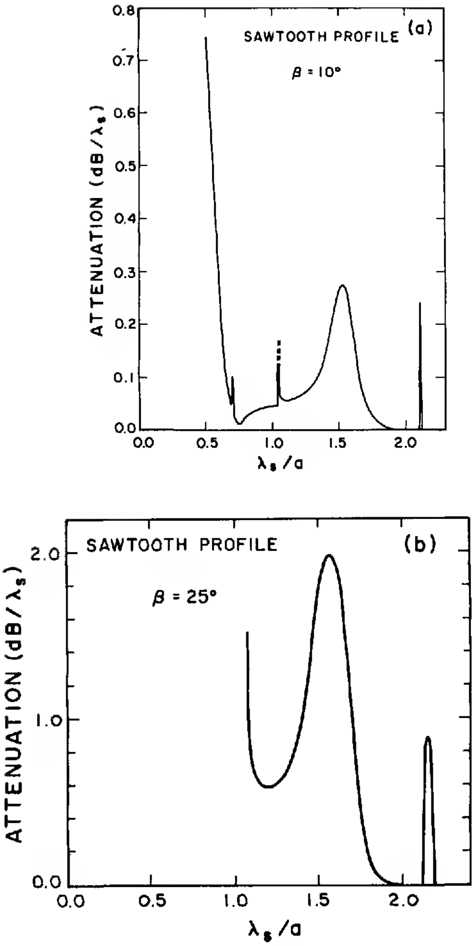

Fig. 8. Attenuation as a function of shear wavelength λ_s for Rayleigh waves on symmetric sawtooth gratings with (a) $\beta = 10^\circ$ and (b) $\beta = 25^\circ$, calculated for $c_t/c_\ell = 0.3$ [Ref. 17].

in the region $x_3 > \zeta(x_1)$. The time-independent equation of motion satisfied by $u_2(x_1 x_3|\omega)$ in this region is

$$-\omega^2 u_2 = c_t^2\left(\frac{\partial^2}{\partial x_1^2} + \frac{\partial^2}{\partial x_3^2}\right)u_2 \ . \tag{2.30}$$

The stress-free boundary condition at the surface $x_3 = \zeta(x_1)$ can be expressed in the form

$$\left(-\zeta'(x_1)\frac{\partial}{\partial x_1} + \frac{\partial}{\partial x_3}\right)u_2\Big|_{x_3=\zeta(x_1)} = 0. \tag{2.31}$$

In addition, we require that $u_2(x_1x_3|\omega)$ vanish as $x_3 \to \infty$.

The solution of Eq. (2.30) in the region $x_3 > \zeta(x_1)_{max}$ that satisfies the boundary condition at infinity can be written as the Fourier integral

$$u_2(x_1x_3|\omega) = \int\frac{dk}{2\pi}\, A(k\omega)e^{ikx_1-\alpha_t(k\omega)x_3}, \tag{2.32}$$

where $\alpha_t(k\omega)$ has been defined in Eq. (2.21).

We now invoke the Rayleigh hypothesis and substitute the expression (2.32) into the boundary condition (2.31). If we again use the representations (2.23)-(2.24), and equate to zero the k^{th} Fourier coefficient on the left hand side of the resulting equation, we obtain the following homogeneous integral equation for the Fourier coefficient $A(k\omega)$ of the displacement component $u_2(x_1x_3|\omega)$:

$$\int\frac{dq}{2\pi}\,\frac{I(\alpha_t(q\omega)\,|k-q)}{\alpha_t(q\omega)}\left(kq - \frac{\omega^2}{c_t^2}\, A(q\omega)\right) = 0. \tag{2.33}$$

Within the Rayleigh hypothesis this is the exact equation for $A(k\omega)$.

To apply this result to the case of a grating profile, we again assume that $\zeta(x_1)$ is a periodic function of x_1 with period a, and substitute the expansion (2.25) for $\alpha_t(k\omega)$ into Eq. (2.33) to obtain the following infinite set of homogeneous linear equations for the coefficients $\{A_n^{(t)}(k\omega)\}$:

$$\sum_{n=-\infty}^{\infty}\frac{I_{m-n}(\alpha_t(k_n\omega))}{\alpha_t(k_n\omega)}\left(k_mk_n - \frac{\omega^2}{c_t^2}\right)A_n^{(t)}(q\omega) = 0 \tag{2.34}$$

$$m = 0, +1, \pm 2, \pm 3, \ldots,$$

where $I_m(\alpha)$ has been defined in Eq. (2.28). The dispersion relation for shear horizontal surface acoustic waves on a grating is obtained by equating to zero the determinant of the coefficients in Eq. (2.34). Again, in practice the matrix of coefficients in Eq. (2.34) is made to have a finite size by restricting m and n to run from -N to N.

Dispersion curves for such waves are plotted in Fig. 9 for a sinusoidal grating defined by $\zeta(x_1) = \zeta_0\cos(2\pi x_1/a)$. Values of N of the order of 20 were used to obtain these results. For the same reasons that apply in the case of surface acoustic waves of sagittal polarization, we can restrict our attention to that portion of the dispersion curve corresponding to values of the wave vector k in the interval $0 < k < \pi/a$. We see that in the long wavelength limit these curves are tangent to the dispersion curve for bulk transverse waves with the same wave vector, $\omega = c_t k$, viz. the dispersion curve for surface skimming bulk transverse waves. (We have seen in Section 1 that surface acoustic waves of shear horizontal polarization cannot exist on a planar, stress-free surface of a semi-infinite isotropic elastic medium.) As the grating strength ζ_0/a increases, the dispersion curves bend away from the sound line at progressively lower frequencies, or smaller wave vectors, and display the phenomenon of wave slowing. For the values of ζ_0/a indicated in Fig. 9 there is only a single branch to the dispersion curve. Thus, the entire range of frequencies above the zone boundary frequency is a stop band for these waves.

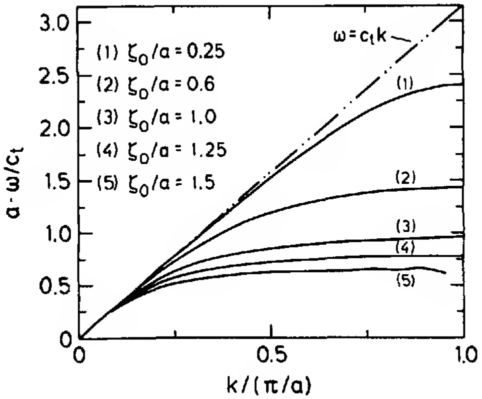

Fig. 9. Dispersion curves for shear horizontal surface acoustic waves propagating across a sinusoidal grating with a peirod of 500Å and $c_t = 3 \times 10^3$ m/sec, for several values of ζ_0/a.

We have here an example of surface roughness giving rise to surface acoustic waves that cannot exist in the absence of surface roughness.

These shear horizontal surface acoustic waves are weakly bound, however, at least in the limit of small k. A perturbation calculation starting from Eq. (2.34) shows that in this limit

$$\alpha_t(k\omega) = \pi(\zeta_0/a)^2(ka)^2k, \tag{2.35}$$

for a sinusoidal grating. Since the decay length of the wave into the elastic medium is $\alpha_t^{-1}(k\omega)$, we see that for $\zeta_0/a = 0.05$ and $ka = 0.1\pi$, the decay length is $(4 \times 10^5/\pi^4)\ a \sim 4000a$. Thus it penetrates far into the medium. As the wave vector increases, however, the wave becomes more tightly bound to the surface.

The determination of the attenuation of shear horizontal surface acoustic waves on a grating on the basis of Eq. (2.34) has not been carried out yet.

2.3. A Randomly Rough Surface

The results of the preceding subsection can also be used in the case that the surface defined by the equation $x_3 = \zeta(x_1)$ is randomly rough. We are therefore dealing with a random grating. In this case the surface profile function $\zeta(x_1)$ is not known in general, and we are forced to characterize it by certain statistical properties. Underlying this characterization is the assumption that there is not a single function $\zeta(x_1)$ but rather an ensemble of realizations of this function. Physical properties associated with a randomly rough surface are to be averaged over this ensemble, and it is assumed that this ensemble average does not differ significantly from the spatial average over a single realization of $\zeta(x_1)$.

We assume in this case that $\zeta(x_1)$ is a stationary stochastic process that is characterized by the properties

$$\langle\zeta(x_1)\rangle = 0 \tag{2.36}$$

$$\langle\zeta(x_1)\zeta(x_1')\rangle = \delta^2 W(|x_1-x_1'|). \tag{2.37}$$

In Eqs. (2.36)-(2.37) the angular brackets <...> denote an average over the ensemble of realizations of $\zeta(x_1)$. The quantity δ^2 appearing in Eq. (2.37) is the mean square departure of the surface from flatness,

$$\langle\zeta^2(x_1)\rangle = \delta^2. \tag{2.38}$$

We will also require the Fourier transform $\hat{\zeta}(Q)$ of $\zeta(x_1)$, which is defined by

$$\zeta(x_1) = \int \frac{dQ}{2\pi} \hat{\zeta}(Q)e^{iQx}. \tag{2.39}$$

With the aid of the Fourier inversion formula and Eqs. (2.36)-(2.37) it is readily established that $\hat{\zeta}(Q)$ possesses the following properties:

$$\langle\hat{\zeta}(Q)\rangle = 0 \tag{2.40}$$

$$\langle\hat{\zeta}(Q)\hat{\zeta}(Q')\rangle = 2\pi\delta(Q+Q')\delta^2 g(|Q|), \tag{2.41}$$

where

$$g(|Q| = \int dx_1\, e^{-iQx_1}\, W(|x_1|) \tag{2.42}$$

is called the surface structure factor.

The general results we obtain in this section will be given in terms of an arbitrary function $g(|Q|)$. However, in obtaining numerical results we will assume a Gaussian form for $W(|x_1|)$, viz.

$$W(|x_1|) = \exp(-x_1^2/a^2), \tag{2.43}$$

where the characteristic length a appearing in this expression is called the transverse correlation length. The form of $g(|Q|)$ that corresponds to the choice (2.43) is found from Eq. (2.42) to be

$$g(|Q|) = \pi^{1/2} a \exp(-a^2Q^2/4). \tag{2.44}$$

Finally, in obtaining the dispersion relation for surface acoustic waves on a random grating we will invoke the small roughness approximation, which is defined by the expansion

$$\begin{aligned} I(\alpha|Q) &= \int dx_1 e^{-iQx_1}[1-\alpha\zeta(x_1)+\ldots] \\ &= 2\pi\delta(Q)-\alpha\hat{\zeta}(Q)+\ldots \end{aligned} \tag{2.45}$$

Although it is possible to improve on this approximation, at the present time there appears to be little reason to do so.

We now consider the effects of random surface roughness on the dispersion curve of surface acoustic waves of sagittal and shear horizontal polarization in turn.

2.3.1. Sagittal Polarization

In the small roughness limit Eqs. (2.22) can be written in matrix form as

$$\sum_{\beta} M^{(o)}_{\alpha\beta}(k)A_{\beta}(k\omega) = \sum_{\beta} \int\frac{dq}{2\pi}\,\hat{\zeta}(k-q)M^{(1)}_{\alpha\beta}(k|q)A_{\beta}(q\omega), \qquad (2.46)$$

where the indices $\alpha,\beta,\ldots$ assume the values ℓ and t. The matrices $\overleftrightarrow{M}^{(o)}(k)$ and $\overleftrightarrow{M}(k|q)$ are given by

$$\overleftrightarrow{M}^{(o)}(k) = \begin{pmatrix} 2\alpha_{\ell}(k\omega) & \dfrac{k^2+\alpha_t^2(k\omega)}{\alpha_t(k\omega)} \\ \dfrac{k^2+\alpha_t^2(k\omega)}{k} & 2k \end{pmatrix} \qquad (2.47a)$$

$$\overleftrightarrow{M}^{(1)}(k|q) = \begin{pmatrix} \left[(k-q)\dfrac{\omega^2}{c_t^2} + 2k\alpha_{\ell}^2(q\omega)\right]\dfrac{1}{q} & 2kq-\dfrac{\omega^2}{c_t^2} \\ \left(2kq-\dfrac{\omega^2}{c_t^2}\right)\dfrac{\alpha_{\ell}(q\omega)}{q} & \dfrac{2kq^2-(k+q)\dfrac{\omega^2}{c_t^2}}{\alpha_t(q\omega)} \end{pmatrix}. \qquad (2.47b)$$

Equation (2.46) is a stochastic matrix integral equation because of the presence of the stochastic function $\zeta(x_1)$ in its kernel. The solutions $A_{\ell}(k\omega)$ and $A_t(k\omega)$ therefore are stochastic functions also. We will not seek the probability distribution functions of $A_{\ell,t}(k)$. Instead we will seek their first moments $\langle A_{\ell,t}(k)\rangle$, which describe the propagation of the mean wave across the random grating. This suffices for obtaining the dispersion relation of sagittally polarized surface acoustic waves across the random grating.

To extract the equation satisfied by $\langle A_{\alpha}(k\omega)\rangle$ from Eq. (2.46) we introduce the smoothing operator P that averages everything on which it acts over the ensemble of realizations of the surface profile function $\zeta(x_1)$: $Pf \equiv \langle f\rangle$. We also introduce the complementary operator $Q = 1-P$ that projects out the fluctuating part of everything on which it acts. We then apply these operators to both sides of Eq. (2.46) in turn:

$$\sum_{\beta} M^{(o)}_{\alpha\beta}(k)\,PA_{\beta}(k\omega) = \sum_{\beta}\int\frac{dq}{2\pi}\,P\hat{\zeta}(k-q)M^{(1)}_{\alpha\beta}(k|q)\,QA_{\beta}(q\omega) \tag{2.48a}$$

$$\sum_{\beta} M^{(o)}_{\alpha\beta}(k)\,QA_{\beta}(k\omega) = \sum_{\beta}\int\frac{dq}{2\pi}\,\hat{\zeta}(k-q)M^{(1)}_{\alpha\beta}(k|q)\,PA_{\beta}(q\omega). \tag{2.48b}$$

In writing these equations we have used the identity $A_{\beta}(q\omega) = PA_{\beta}(q\omega) + QA_{\beta}(q\omega)$ and the fact that $P\hat{\zeta}(k-q) = 0$. When we eliminate $QA_{\beta}(k\omega)$ from these equations we obtain the equation satisfied by $\langle A_{\alpha}(k\omega)\rangle$, viz.

$$\sum_{\beta} M^{(o)}_{\alpha\beta}(k)\langle A_{\beta}(k\omega)\rangle = \delta^2 \sum_{\beta\mu\nu}\int\frac{dq}{2\pi}\,\frac{g(|k-q|)}{D(q\omega)} \times$$

$$\times\, M^{(1)}_{\alpha\mu}(k|q)\,C_{\mu\nu}(q\omega)M^{(1)}_{\nu\beta}(q|k)\langle A_{\beta}(k\omega)\rangle \tag{2.49}$$

where we have used Eq. (2.41), and where

$$D(k\omega) = 4k^2\alpha_{\ell}(k\omega)\alpha_t(k\omega) - (k^2+\alpha_t^2(k\omega))^2, \tag{2.50}$$

while the matrix $\overleftrightarrow{C}(\vec{k}\omega) = D(k\omega)\overleftrightarrow{M}^{(o)-1}(k)$ is

$$\overleftrightarrow{C}(k\omega) = \begin{pmatrix} 2k^2\alpha_t(k\omega) & -k(k^2+\alpha_t^2(k\omega)) \\ -a_t(k\omega)(k^2+\alpha^2(k\omega)) & 2k\alpha_{\ell}(k\omega)\alpha_t(k\omega) \end{pmatrix}. \tag{2.51}$$

That Eq. (2.49) is an algebraic equation rather than an integral equation is due to the restoration of infinitesimal translational invariance by the averaging process.

The dispersion relation for sagittally polarized surface acoustic waves propagating across a random grating is obtained by equating to zero the determinant of the coefficients in Eq. (2.49). Correct to $O(\delta^2)$ this relation is$^{(18)}$

$$D(k\omega) = \delta^2\int\frac{dq}{2\pi}\,\frac{g(|k-q|)}{D(q\omega)}\sum_{\alpha\mu}\sum_{\beta\nu} C_{\alpha\mu}(k\omega)M^{(1)}_{\mu\beta}(k|q) \times$$

$$\times\, C_{\beta\nu}(q\omega)M^{(1)}_{\nu\alpha}(q|k). \tag{2.52}$$

The function $D(k\omega)$ vanishes when $\omega = c_R k$, where c_R, the speed of Rayleigh waves on a planar surface, is obtained from the smallest positive solution of Eq. (1.16). Thus, if we substitute

$$\omega = c_R k + c_R k \delta^2 \Delta(k) \tag{2.53}$$

into both sides of Eq. (2.52) and equate terms of $O(\delta^2)$ on both sides of the resulting equation, we find that

$$\Delta(k) = \frac{1}{\xi G(\xi,\lambda) k^4} \int \frac{dq}{2\pi}\, g(|k-q|) \times$$

$$\times \frac{\sum\limits_{\alpha\mu} \sum\limits_{\beta\nu} \left[C_{\alpha\mu}(k\omega) M^{(1)}_{\mu\beta}(k|q) C_{\beta\nu}(q\omega) M^{(1)}_{\nu\alpha}(q|k) \right]_{\omega = c_R k}}{D(q, c_R k)} \tag{2.54}$$

where

$$G(\xi,\lambda) = \frac{8\xi}{(2-\xi^2)^2} \left[\xi^4 - 2(3-2\lambda^2)\xi^2 + 6(1-\lambda^2) \right]. \tag{2.55}$$

The integral over q in Eq. (2.54) has to be evaluated numerically. It turns out to be complex,

$$\Delta(k) = \Delta_1(k) + i\Delta_2(k). \tag{2.56}$$

The imaginary part of $\Delta(k)$ arises from two sources. When $|q| < \omega/c_\ell$ both $\alpha_\ell(q\omega)$ and $\alpha_t(q\omega)$ are pure imaginary; when $\omega/c_\ell < |q| < \omega/c_t$ $\alpha_\ell(q\omega)$ is real while $\alpha_t(q\omega)$ is imaginary. The occurrence of imaginary $\alpha_{\ell,t}(q\omega)$ means that energy is being radiated into the interior of the solid from the surface due to the roughness-induced conversion of Rayleigh waves into bulk waves. By conservation of energy the Rayleigh wave is attenuated as it propagates along the random grating, and this is reflected in the presence of an imaginary part to its frequency that is proportional to $\Delta_2(k)$. For $|q| > \omega/c_t$ the function $D^{-1}(q, c_R k)$ has a simple pole at $|q| = k$, and circling this pole in a manner consistent with the analytic continuation of $\alpha_{\ell,t}(q\omega)$ defined by Eq. (2.21) yields a second contribution to the imaginary part of $\Delta_2(k)$. It is associated physically with the attenuation of the Rayleigh wave due to its roughness-induced scattering into other Rayleigh waves.

When the form for $(q|Q|)$ given by Eq. (2.44) is used, it is convenient to rewrite Eq. (2.53) in the form

$$\omega_S(k) = c_R k\left[1 + \frac{\delta^2}{a^2}\,\omega_1(x) - i\,\frac{\delta^2}{a^2}\,\omega_2(x)\right] \tag{2.57}$$

where $x = ka$ and

$$\omega_1(x) = a^2\Delta_1(k), \quad \omega_2(x) = -a^2\Delta_2(k). \tag{2.58}$$

The functions $\omega_1(x)$ and $\omega_2(x)$ are plotted in Figs. 10 and 11, respectively, for the particular choice $\lambda^2 = (1/3)$, for which $\xi = (2 - \frac{2}{3}\sqrt{3})^{1/2} = 0.9194$. In plotting $\omega_2(x)$ we have plotted both the

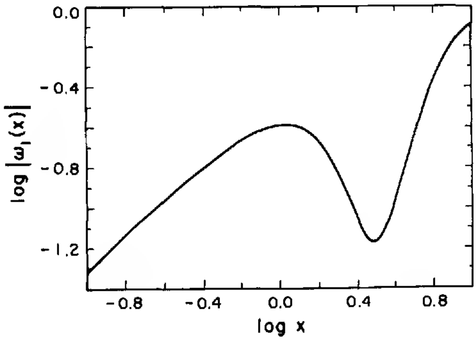

Fig. 10. The function $\omega_1(x)$ defined by Eqs. (2.47)-(2.58) of the text, for Rayleigh waves on a random grating, when $\lambda^2 = 1/3$.

contribution associated with the scattering of the Rayleigh wave into other Rayleigh waves, $\omega_2^{(s)}(x)$, (Fig. 11(b)), as well as the total function (Fig. 11(a)). It is clearly evident that the contribution $\omega_2^{(s)}(x)$ is dominated by the contribution associated with the scattering of the Rayleigh wave into bulk waves.

The function $\omega_1(x)$ is negative. This means that the Rayleigh wave on a random grating is slower than it is on a planar surface. The function $\omega_2(x)$ tends to zero (as x^3) when $x \to 0$ and also when $x \to \infty$, and has a maximum at an intermediate value of $x \approx 8$. This behavior is accounted for by the fact that as $x \to 0$ the wavelength of the Rayleigh wave is much larger than the transverse correlation length a and it therefore see a planar surface on which it is undamped. In the opposite limit of very short wavelengths the

Rayleigh wave rides adiabatically over what it sees as a locally flat surface and is again undamped.

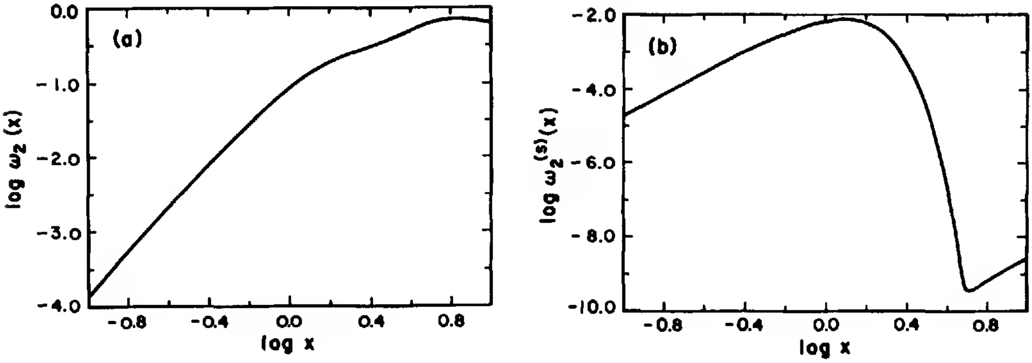

Fig. 11. (a) The function $\omega_2(x)$ defined by Eqs. (2.57)-(2.58) of the text for Rayleigh waves on a random grating, when $\lambda^2 = \frac{1}{3}$. (b) The contribution $\omega_2^{(s)}(x)$ to $\omega_2(x)$ that arises from the scattering of the Rayleigh wave into other Rayleigh waves.

The fact that $\omega_2(x)$ goes to zero as x^3 as $x \to 0$ means that the attenuation rate of a Rayleigh wave on a random grating, viz. $2\ c_R k\ (\delta^2/a^2)\omega_2(x)$ is proportional to $x^4 = (ka)^4 \propto \omega^4$ in this limit. The physical explanation for this dependence is that the frequency dependence of Rayleigh scattering in d dimensions is ω^{d+1}. The ridges and grooves responsible for the scattering of a Rayleigh wave in the present case are two-dimensional, since they are defined by the equation $x_3 = \zeta(x_1)$. Thus the Rayleigh scattering law in the present case gives us an ω^3 frequency dependence of the scattering rate in the low frequency, long wavelength limit. The remaining factor of ω arises because the penetration depth of the Rayleigh wave into the solid is of the order of its wavelength parallel to the surface(19) (see Section 1).

2.3.2. Shear Horizontal Polarization

The form Eq. (2.33) takes in the small roughness limit is

$$\alpha_t(k\omega)A(k\omega) = \int\frac{dq}{2\pi}\,\hat{\zeta}(k-q)\left(kq - \frac{\omega^2}{c_t^2}\right)A(q\omega) \quad . \tag{2.59}$$

When we apply the operators P and Q to both sides of this equation in turn and use the identity $A(q\omega) = PA(q\omega) + QA(q\omega)$, we obtain the pair of equations

$$\alpha_t(k\omega)PA(k\omega) = \int\frac{dq}{2\pi}\,P\hat{\zeta}(k-q)\left(kq - \frac{\omega^2}{c_t^2}\right)QA(q\omega) \tag{2.60a}$$

$$\alpha_t(k\omega)QA(k\omega) = \int\frac{dq}{2\pi}\,\hat{\zeta}(k-q)\left(kq - \frac{\omega^2}{c_t^2}\right)PA(q\omega) \quad . \tag{2.60b}$$

When we eliminate $QA(k\omega)$ from these equations we obtain the equation satisfied by $\langle A(k\omega)\rangle$:

$$\alpha_t(k\omega)\langle A(k\omega)\rangle = \delta^2\int\frac{dq}{2\pi}\,\frac{g(|k-q|)}{\alpha_t(q\omega)}\left(kq - \frac{\omega^2}{c_t^2}\right)^2\langle A(k\omega)\rangle. \tag{2.61}$$

The dispersion relation for shear horizontal surface acoustic waves on a random grating is therefore(20)

$$\alpha_t(k\omega) = \delta^2\int\frac{dq}{2\pi}\,\frac{g(|k-q|)}{\alpha_t(q\omega)}\left(kq - \frac{\omega^2}{c_t^2}\right)^2 \quad . \tag{2.62}$$

When $\delta = 0$ (a planar surface), this equation reduces to $\alpha_t(k\omega) = 0$. The solution of this equation, $\omega = c_t k$, is not the frequency of a surface acoustic wave, but instead is the frequency of a surface skimming bulk transverse acoustic wave. As we will now see, the effect of surface roughness on this wave will be to convert it into a surface acoustic wave.

The solution of Eq. (2.62) to lowest nonzero order in δ can be effected by setting

$$\frac{\omega^2}{c_t^2} = k^2 - \delta^4\Delta^2(k), \tag{2.63}$$

substituting this form of the dispersion relation into Eq. (2.62), and equating the coefficients of δ^2 on both sides of the resulting equation. The function $\Delta(k)$ obtained in this way has the form

$$\Delta(k) = \Delta_1(k) + i\Delta_2(k), \tag{2.64}$$

where

$$\Delta_1(k) = \int_{-\infty}^{-k} \frac{dq}{2\pi} \frac{g(|k-q|)}{(q^2-k^2)^{1/2}} (kq-k^2)^2 + \int_{k}^{\infty} \frac{dq}{2\pi} \frac{g(|k-q|)}{(q^2-k^2)^{1/2}} (kq-k^2)^2 \tag{2.65a}$$

$$\Delta_2(k) = \int_{-k}^{k} \frac{dq}{2\pi} \frac{g(|k-q|)}{(k^2-q^2)^{1/2}} (kq-k^2)^2 . \tag{2.65b}$$

The imaginary part of $\Delta(k)$ arises from the surface roughness induced conversion of the surface acoustic wave into bulk waves, which extracts energy from the surface wave and attenuates it as it propagates along the surface.

The integrals in Eq. (2.65) have to be evaluated numerically. When the form for $g(|Q|)$ given by Eq. (2.44) is used, the frequency of the shear horizontal surface acoustic wave obtained from Eqs. (2.63) and (2.64) can be expressed in the form

$$\omega_{SH}(k) = c_t k\left[1 + \frac{\delta^4}{a^4}\,\omega_1(x) - i\,\frac{\delta^4}{a^4}\,\omega_2(x)\right], \tag{2.66}$$

where $x = ka$ and

$$\omega_1(x) = -\frac{a^4}{2k^2}\left[\Delta_1^2(k) - \Delta_2^2(k)\right] \xrightarrow[x\to 0]{} -\frac{2}{\pi}\,x^2 + o(x^2) \tag{2.67a}$$

$$\omega_2(x) = \frac{a^4}{k^2}\,\Delta_1(k)\Delta_2(k) \xrightarrow[x\to 0]{} \frac{3}{2}\,x^4 + o(x^2) . \tag{2.67b}$$

The functions $\omega_1(x)$ and $\omega_2(x)$ are plotted in Fig. 12.

The shear horizontal surface acoustic wave obtained here displays the phenomenon of wave slowing ($\omega_1(x) < 0$) for small x, and indeed it is this wave slowing that binds it to the surface ($\mathrm{Re}\,\alpha_t(k\omega) > 0$). It follows that for larger values of $x (x \gtrsim 1)$, when $\omega_1(x)$ becomes positive, we no longer have a surface acoustic wave.

We also note that since in the absence of surface roughness a shear horizontal surface acoustic wave cannot exist, in the approximation maintained here the attenuation of the roughness-induced shear horizontal surface acoustic waves studied here is due entirely to

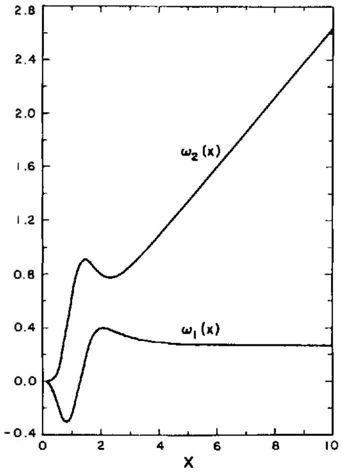

Fig. 12. The functions $\omega_1(x)$ and $\omega_2(x)$, defined by Eqs. (2.66)-(2.67) of the text, for shear horizontal surface acoustic waves on a random grating.

their scattering into bulk elastic waves. The $(ka)^5$ dependence of the attenuation rate $2c_t k(\delta^4/a^4)\omega_2(x)$ of these waves, in the long wavelength limit, can be understood as due to the ω^3 frequency dependence of Rayleigh scattering in the present case and to the fact that the penetration depth of this wave is proportional to the square of its wavelength parallel to the surface ($\alpha_t(k\omega)$ is proportional to k^2 in this case: see Eqs. (2.21), (2.66), and (2.67)).

The results obtained here provide one more example of how surface roughness can give rise to surface acoustic waves that have no counterparts in the case of a planar surface.

3. Effects of Nonstandard Boundary Conditions on Surface Acoustic Waves

As Velasco and Garcia-Moliner(21) have emphasized, the boundary conditions constitute the key features in any theory of surface waves. It is through them that one introduces in the analysis the physical consequences of specific surface effects, such as local changes of mass and stresses. In this way one goes beyond the simple case in which one matches a semi-infinite bulk medium to a semi-infinite vacuum. Up to this point our discussion of surface acoustic waves has been based on the assumption that the displacement field in the medium supporting the surface waves satisfies stress-free boundary conditions on the surface of that medium, irrespective of the shape of the surface. There are several situations, however, in which more general boundary conditions are appropriate. In this section we consider these situations, the corresponding boundary conditions, and the consequences of the latter for the surface acoustic waves on the surface bounding the media of interest.

3.1. Effects of an Adlayer on Surface Acoustic Waves

The study of elastic waves in layered media is of interest for seismology(22). In addition, a thin film deposited on a substrate can guide surface acoustic waves in the substrate(23-36). When the thickness of the film is very small the system of film plus substrate can serve as a model for a substrate with a small number of layers of foreign atoms adsorbed on it. In this limit it is convenient to simplify the study of surface or guided acoustic waves in such a structure by considering the vibrations of the substrate alone and requiring their displacement field to satisfy boundary conditions at its interface with the film that account for the presence of the film to first order in the latter's thickness.

Derivations of such boundary conditions were obtained by several authors in the late 1960's and 1970's.(21,26-29) More recently, Djafari-Rouhani *et al.*(30) and Dobrzynski and Djafari-Rouhani(31) have simplified the derivation of these boundary conditions, and have generalized the results of the earlier authors. In fact, the results obtained by Djafari-Rouhani *et al.*(30) and by Dobrzynski and Djafari-Rouhani(31) can themselves be simplified and generalized. In what follows we sketch out how this is done.

Consider the system that consists of an elastic medium (medium 1) characterized by a mass density $\rho^{(1)}$ and elastic moduli $C^{(1)}_{\alpha\beta\mu\nu}$ occupying the half-space $x_3 > 0$ and of a film (medium 2) characterized by a mass density $\rho^{(2)}(x_1)$ and elastic moduli $C^{(2)}_{\alpha\beta\mu\nu}(x_1)$ filling the region $-d < x_3 < 0$. (Fig. 13). The assumption that the material properties of the film depend on the coordinate x_1 allows the results to be obtained to be applied to surfaces on which steps, isolated strips, and parallel arrays of strips, for example, are present, as well as homogeneous films.

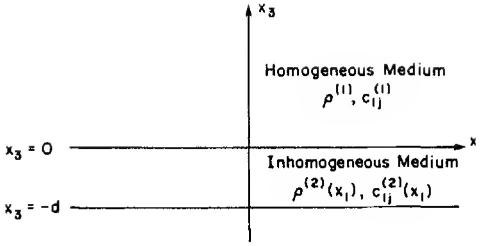

Fig. 13. An inhomogeneous layer of thickness d bonded to a semi-infinite, homogeneous substrate.

We assume that each of the media is a cubic medium with its cube axes parallel to the coordinate axes. We consider straight-crested waves propagating in the x_1-direction, so that the displacement field has the form

$$u_\alpha(x;t) = u_\alpha(x_1 x_3|\omega)\exp(-i\omega t) \quad \alpha = 1, 2, 3. \tag{3.1}$$

The equations satisfied by $u_\alpha(x_1 x_3|\omega)$ are

$$-\omega^2 \rho^{(1)} u_\alpha^{(1)} = \sum_{\beta\mu\nu} C_{\alpha\beta\mu\nu}^{(1)} \frac{\partial^2 u_\mu^{(1)}}{\partial x_\beta \partial x_\nu} \qquad x_3 > 0, \tag{3.2a}$$

and

$$-\rho^{(2)}(x_1)\omega^2 u_\alpha^{(2)} = \sum_{\beta\mu\nu} \frac{\partial}{\partial x_\beta} \left(C_{\alpha\beta\mu\nu}^{(2)}(x_1) \frac{\partial u_\mu^{(2)}}{\partial x_\nu}\right) \qquad -d < x_3 < 0. \tag{3.2b}$$

The boundary conditions satisfied by $u_\alpha^{(1,2)}(x_1 x_3|\omega)$ are

$$u_\alpha^{(1)}\Big|_{x_3=0} = u_\alpha^{(2)}\Big|_{x_3=0} \tag{3.3a}$$

$$\sum_{\mu\nu} C^{(1)}_{\alpha 3\mu\nu} \frac{\partial u_\mu^{(1)}}{\partial x_\nu}\Big|_{x_3=0} = \sum_{\mu\nu} C^{(2)}_{\alpha 3\mu\nu}(x_1) \frac{\partial u_\mu^{(2)}}{\partial x_\nu}\Big|_{x_3=0} \tag{3.3b}$$

$$\sum_{\mu\nu} C^{(2)}_{\alpha 3\mu\nu}(x_1) \frac{\partial u_\mu^{(2)}}{\partial x_\nu}\Big|_{x_3=-d} = 0. \tag{3.3c}$$

In addition, we require that $u_\alpha^{(1)}(x_1x_3|\omega) \to 0$ as $x_3 \to \infty$.

We begin by rewriting Eq. (3.3c) as

$$\sum_{\mu\nu} C^{(2)}_{\alpha 3\mu\nu}(x_1) \left[\frac{\partial u_\mu^{(2)}}{\partial x_\nu} - d\,\frac{\partial^2 u_\mu^{(2)}}{\partial x_\nu \partial x_3} + O(d^2)\right]_{x_3=0} = 0. \tag{3.4}$$

With the use of Eq. (3.3b) this equation becomes

$$\sum_{\mu\nu} C^{(1)}_{\alpha 3\mu\nu} \frac{\partial u_\mu^{(1)}}{\partial x_\nu}\Big|_{x_3=0} = d \sum_{\mu\nu} C^{(2)}_{\alpha 3\mu\nu}(x_1) \frac{\partial^2 u_\mu^{(2)}}{\partial x_\nu \partial x_3}\Big|_{x_3=0} + O(d^2). \tag{3.5}$$

Our task now is to eliminate $u_\mu^{(2)}$ from the right hand side of Eq. (3.5) in favor of $u_\mu^{(1)}$.

We rewrite the right hand side of Eq. (3.5) as

$$\text{RHS} = d \sum_{\mu\nu} \frac{\partial}{\partial x_3}\left(C^{(2)}_{\alpha 3\mu\nu}(x_1) \frac{\partial u_\mu^{(2)}}{\partial x_\nu}\right)\Big|_{x_3=0}. \tag{3.6}$$

Now, from Eqs. (3.1) and (3.2b) we find that

$$-\omega^2 \rho^{(2)}(x_1) u_\alpha^{(2)} = \sum_{\mu\nu} \frac{\partial}{\partial x_1}\left(C^{(2)}_{\alpha 1\mu\nu}(x_1) \frac{\partial u_\mu^{(2)}}{\partial x_\nu}\right) + $$

$$+ \sum_{\mu\nu} \frac{\partial}{\partial x_3}\left(C^{(2)}_{\alpha 3\mu\nu}(x_1) \frac{\partial u_\mu^{(2)}}{\partial x_\nu}\right) \qquad -d < x_3 < 0 . \tag{3.7}$$

Thus, Eq. (3.6) becomes

$$\text{RHS} = -d\left[\omega^2 \rho^{(2)}(x_1) u_\alpha^{(2)} + \sum_{\mu} \frac{\partial}{\partial x_1}\left(C^{(2)}_{\alpha 1\mu 1}(x_1) \frac{\partial u_\mu^{(2)}}{\partial x_1}\right) + \right.$$

$$\left. + \sum_{\mu} \frac{\partial}{\partial x_1}\left(C^{(2)}_{\alpha 1\mu 3}(x_1) \frac{\partial u_\mu^{(2)}}{\partial x_3}\right)\right]_{x_3=0} , \tag{3.8}$$

where we have used the fact that $u_\mu^{(2)}$ is a function of only x_1 and x_3. Now, since from Eq. (3.3a) u_α is continuous across the plane $x_3 = 0$, so are its tangential derivatives. Equation (3.8) can therefore be rewritten as

$$\mathrm{RHS} = -d\Big[\omega^2 \rho^{(2)}(x_1) u_\alpha^{(1)} + \sum_\mu \frac{\partial}{\partial x_1}\Big(C^{(2)}_{\alpha 1 \mu 1}(x_1)\frac{\partial u_\mu^{(1)}}{\partial x_1}\Big) + \sum_\mu \frac{\partial}{\partial x_1}\Big(C^{(2)}_{\alpha 1 \mu 3}(x_1)\frac{\partial u_\mu^{(2)}}{\partial x_3}\Big)\Big]_{x_3=0}. \tag{3.9}$$

To deal with the last term on the right hand side of this equation we turn to Eq. (3.3b), which we write as

$$\sum_{\mu\nu} C^{(1)}_{\alpha 3 \mu \nu}\frac{\partial u_\mu^{(1)}}{\partial x_\nu}\bigg|_{x_3=0} = \sum_\mu C^{(2)}_{\alpha 3 \mu 1}(x_1)\frac{\partial u_\mu^{(2)}}{\partial x_1}\bigg|_{x_3=0} + \sum_\mu \Gamma^{(2)}_{\alpha\mu}(x_1)\frac{\partial u_\mu^{(2)}}{\partial x_3}\bigg|_{x_3=0}, \tag{3.10}$$

where we have introduced the symmetric matrix $\Gamma^{(2)}_{\alpha\mu}(x_1) \equiv C^{(2)}_{\alpha 3 \mu 3}(x_1)$. For a cubic medium $\overleftrightarrow{\Gamma}^{(2)}(x_1)$ is a diagonal matrix,

$$\Gamma^{(2)}_{\alpha\mu}(x_1) = \delta_{\alpha\mu}\Gamma^{(2)}_\alpha(x_1), \tag{3.11a}$$

where

$$\Gamma^{(2)}_{11}(x_1) = \Gamma^{(2)}_{22}(x_1) = c^{(2)}_{44}(x_1);\ \Gamma^{(2)}_{33}(x_1) = c^{(2)}_{11}(x_1), \tag{3.11b}$$

in the Voigt notation. In view of Eq. (3.11a) we can rewrite Eq. (3.10) as

$$\frac{\partial u_\alpha^{(2)}}{\partial x_3}\bigg|_{x_3=0} = \frac{1}{\Gamma^{(2)}_\alpha(x_1)}\Big[\sum_{\mu\nu} C^{(1)}_{\alpha 3 \mu \nu}\frac{\partial u_\mu^{(1)}}{\partial x_\nu} - \sum_\mu C^{(2)}_{\alpha 3 \mu 1}(x_1)\frac{\partial u_\mu^{(1)}}{\partial x_1}\Big]_{x_3=0}, \tag{3.12}$$

where we have used the continuity of $\partial u_\alpha/\partial x_1$ across the plane $x_3 = 0$ in writing the second term on the right hand side of Eq. (3.12). It follows that

$$\sum_{\mu} C^{(2)}_{\alpha 1\mu 3}(x_1)\,\frac{\partial u^{(2)}_{\mu}}{\partial x_3}\Big|_{x_3=0}$$

$$= \sum_{\mu} \frac{C^{(2)}_{\alpha 1\mu 3}(x_1)}{\Gamma^{(2)}_{\mu}(x_1)}\Big[\sum_{\rho\sigma} C^{(1)}_{\mu 3\rho\sigma}\,\frac{\partial u^{(1)}_{\rho}}{\partial x_{\sigma}} - \sum_{\rho} C^{(2)}_{\mu 3\rho 1}(x_1)\,\frac{\partial u^{(1)}_{\rho}}{\partial x_1}\Big]_{x_3=0}. \qquad (3.13)$$

Equation (3.13) holds for all x_1. It is therefore the case that

$$\sum_{\mu} \frac{\partial}{\partial x_1}\Big(C^{(2)}_{\alpha 1\mu 3}(x_1)\,\frac{\partial u^{(2)}_{\mu}}{\partial x_3}\Big)\Big|_{x_3=0}$$

$$= \sum_{\mu} \frac{\partial}{\partial x_1}\Big(\frac{C^{(2)}_{\alpha 1\mu 3}(x_1)}{\Gamma^{(2)}_{\mu}(x_1)}\Big[\sum_{\rho\sigma} C^{(1)}_{\mu 3\rho\sigma}\,\frac{\partial u^{(1)}_{\rho}}{\partial x_{\sigma}} -$$

$$- \sum_{\rho} C^{(2)}_{\mu 3\rho 1}(x_1)\,\frac{\partial u^{(1)}_{\rho}}{\partial x_1}\Big]\Big)_{x_3=0}\ . \qquad (3.14)$$

When Eq. (3.14) is substituted into Eq. (3.9), the boundary conditions satisfied by $\vec{u}^{(1)}(x_1 x_3|\omega)$ become

$$\sum_{\mu\nu} C^{(1)}_{\alpha 3\mu\nu}\,\frac{\partial u^{(1)}_{\mu}}{\partial x_{\nu}}\Big|_{x_3=0} = -d\Big\{\omega^2\rho^{(2)}(x_1)u^{(1)}_{\alpha} +$$

$$+ \sum_{\mu} \frac{\partial}{\partial x_1}\Big[\Big(C^{(2)}_{\alpha 1\mu 1}(x_1) - \sum_{\rho} \frac{C^{(2)}_{\alpha 1\rho 3}(x_1)C^{(2)}_{\rho 3\mu 1}(x_1)}{\Gamma^{(2)}_{\rho}(x_1)}\Big)\,\frac{\partial u^{(1)}_{\mu}}{\partial x_1}\Big]\Big\}_{x_3=0} +$$

$$+ \sum_{\mu} \frac{\partial}{\partial x_1}\Big(\frac{C^{(2)}_{\alpha 1\mu 3}(x_1)}{\Gamma^{(2)}_{\mu}(x_1)}\sum_{\rho\sigma} C^{(1)}_{\mu 3\rho\sigma}\,\frac{\partial u^{(1)}_{\rho}}{\partial x_{\sigma}}\Big)\Big|_{x_3=0}\ . \qquad (3.15)$$

However, the last term on the right hand side of this equation is $O(d^2)$, in fact, because it contains the left hand side as a factor, and the latter is manifestly of $O(d)$. Thus we have finally for the boundary conditions satisfied by $\vec{u}^{(1)}(x_1 x_3|\omega)$ at the interface $x_3 = 0$

$$\sum_{\mu\nu} C^{(1)}_{\alpha 3\mu\nu}\,\frac{\partial u^{(1)}_{\mu}}{\partial x_{\nu}}\Big|_{x_3=0} = -d\Big\{\omega^2\rho^{(2)}(x_1)u^{(1)}_{\alpha} +$$

$$+ \sum_{\mu} \frac{\partial}{\partial x_1}\Big[\Big(C^{(2)}_{\alpha 1\mu 1}(x_1) - \sum_{\rho} \frac{C^{(2)}_{\alpha 1\rho 3}(x_1)C^{(2)}_{\rho 3\mu 1}(x_1)}{\Gamma^{(2)}_{\rho}(x_1)}\Big)\frac{\partial u^{(1)}_{\mu}}{\partial x_1}\Big\}_{x_3=0}\ . \qquad (3.16)$$

If we let α take the values 1, 2, 3 in turn, we obtain these conditions in explicit form:

$$c_{44}^{(1)}\left(\frac{\partial u_1^{(1)}}{\partial x_3} + \frac{\partial u_3^{(1)}}{\partial x_1}\right)_{x_3=0} = -d\{\omega^2\rho^{(2)}(x_1)u_1^{(1)} +$$

$$+ \frac{\partial}{\partial x_1}\left(\left[\frac{(c_{11}^{(2)}(x_1))^2-(c_{12}^{(2)}(x_1))^2}{c_{11}^{(2)}(x_1)}\right]\frac{\partial u_1^{(1)}}{\partial x_1}\right)\}_{x_3=0} \tag{3.17a}$$

$$c_{44}^{(1)}\left.\frac{\partial u_2^{(1)}}{\partial x_3}\right|_{x_3=0} = -d\{\omega^2\rho^{(2)}(x_1)u_2^{(1)} +$$

$$+ \frac{\partial}{\partial x_1}\left(c_{44}^{(2)}(x_1)\frac{\partial u_2^{(1)}}{\partial x_1}\right)\}_{x_3=0} \tag{3.17b}$$

$$\left(c_{12}^{(1)}\frac{\partial u_1^{(1)}}{\partial x_1} + c_{11}^{(1)}\frac{\partial u_3^{(1)}}{\partial x_3}\right)_{x_3=0} = -d\{\omega^2\rho^{(2)}(x_1)u_3^{(1)}\}_{x_3=0}. \tag{3.17c}$$

The approach outlined here can be extended to the case of a film depositied on a substrate of different symmetry and to propagation in an arbitrary direction on the surface.

3.1.1. Sagittal Polarization

To illustrate the uses of these boundary conditions let us consider first of all a Rayleigh wave on the surface of an isotropic medium covered by an isotropic, homogeneous adlayer $c_{12}^{(j)} = c_{11}^{(j)} - 2c_{44}^{(j)}$, $(j = 1, 2)$. The solutions of Eqs. (5.2a) in this case of sagittal polarization are

$$u_1(x_1x_3|\omega) = e^{ikx_1}[A_\ell e^{-\alpha_\ell x_3} + A_t e^{-\alpha_t x_3}], \tag{3.18a}$$

$$u_3(x_1x_3|\omega) = ie^{ikx_1}[\frac{\alpha_\ell}{k} A_\ell e^{-\alpha_\ell x_3} + \frac{k}{\alpha_t} A_t e^{-\alpha_t x_3}] \tag{3.18b}$$

where

$$\alpha_{\ell,t}(k\omega) = \left(k^2 - \frac{\omega^2}{c_{\ell,t}^2}\right)^{\frac{1}{2}} \qquad k^2 > \frac{\omega^2}{c_{\ell,t}^2}\ , \tag{3.19}$$

and we have defined

$$c_\ell^2 = \frac{c_{11}^{(1)}}{\rho^{(1)}}, \qquad c_t^2 = \frac{c_{44}^{(1)}}{\rho^{(1)}}\ . \tag{3.20}$$

When Eqs. (3.18) are substituted into Eqs. (3.17a) and (3.17c), we obtain the following pair of equations for the amplitudes $A_{\ell,t}$:

$$2\alpha_\ell A_\ell + \frac{k^2+\alpha_t^2}{\alpha_t} A_t = d\,\frac{\rho^{(2)}}{\rho c_t^2}\left[\omega^2 - \frac{4c_t'^2(c_\ell'^2-c_t'^2)k^2}{c_\ell'^2}\right](A_\ell+A_t) \tag{3.21a}$$

$$\frac{k^2+\alpha_t^2}{k} A_\ell + 2kA_t = d\,\frac{\rho^{(2)}}{\rho c_t^2}\,\omega^2\left[\frac{\alpha_\ell}{k} A_\ell + \frac{k}{\alpha_t} A_t\right]\ , \tag{3.21b}$$

where

$$c_\ell'^2 = \frac{c_{11}^{(2)}}{\rho^{(2)}}\ , \qquad c_t'^2 = \frac{c_{44}^{(2)}}{\rho^{(2)}}\ . \tag{3.22}$$

Equating to zero the determinant of the coefficients in Eqs. (3.21) yields the dispersion relation (to $O(kd)$)

$$D(k,\omega) = (kd)\,\frac{\rho^{(2)}\alpha_t\omega^2}{\rho c_t^2}\left[\frac{\omega^2}{kc_t^2}\left(1 + \frac{\alpha_\ell}{\alpha_t}\right) - \frac{4c_t'^2}{c_t^2}\,\frac{(c_\ell'^2-c_t'^2)k}{c_\ell'^2}\right] \tag{3.23}$$

where

$$D(k,\omega) = 4k^2\alpha_t\alpha_\ell - (k^2+\alpha_t^2)^2\ . \tag{3.24}$$

The solution of the equation $D(k,\omega)$ is $\omega = c_R k$, where c_R is the speed of Rayleigh waves on the stress-free surface of medium 1. It is obtained from the smallest root of the equation

$$\xi^6 - 8\xi^4 + 8(3-2\lambda^2)\xi^2 - 16(1-\lambda^2) = 0, \tag{3.25}$$

where we have put $\xi = c_R/c_t$, $\lambda = c_t/c_\ell$. The solution of Eq. (3.23) is

$$\omega_S(k) = c_R k\{1 - (kd)\frac{\xi}{G(\lambda,\xi)}\frac{\rho^{(2)}}{\rho}\beta_t \times$$

$$\times\ [\xi^2(1 + \frac{\beta_\ell}{\beta_t}) - 4\ (\frac{c_t'^2}{c_t})\ \frac{c_\ell'^2 - c_t'^2}{c_\ell'^2}] + O((kd)^2)\}, \tag{3.26}$$

where $\beta_{\ell,t} = [1-(c_R^2/c_{\ell,t}^2)]^{1/2}$ and

$$G(\lambda,\xi) = \frac{8\xi}{(2-\xi^2)^2}[\varepsilon^4 - 2(3-2\lambda^2)\varepsilon^2 + 6(1-\lambda^2)]. \tag{3.27}$$

Thus the correction to the frequency of a Rayleigh wave due to the presence of a thin overlayer of $O((kd)^2)$, and not of $O((kd)^3)$ as might have been expected.

3.1.2. Shear Horizontal Polarization

As a second example of the use of Eqs. (3.17), we apply them to obtain the dispersion curve of a wave of shear horizontal polarization propagating in the x_1-direction. The only nonzero component of the displacement field is $u_2(x_1x_3|\omega)$ which, from Eq. (3.2a), is found to be given by

$$u_2(x_1x_3|\omega) = e^{ikx_1}Ae^{-\alpha_t x_3}\ . \tag{3.28}$$

When this solution is substituted into Eq. (3.17b) the dispersion relation for this wave is obtained in the form

$$\alpha_t = d\frac{\rho^{(2)}}{\rho^{(1)}c_t^2}(\omega^2 - c_t'^2k^2) > 0. \tag{3.29}$$

The inequality here derives from the necessity of α_t being positive in order that Eq. (3.28) describe a surface wave. The solution of Eq. (3.29) is

$$\omega_{SH}(k) = c_t k[1 - \frac{1}{2}(kd)^2(\frac{\rho^{(2)}}{\rho^{(1)}})^2(1 - \frac{c_t'^2}{c_t^2})^2 + o((kd)^2)], \tag{3.30}$$

provided that $c_t'^2 < c_t^2$.

The result given by Eq. (3.30) coincides to the order in kd given with the frequency of the lowest branch (n=0) of the spectrum of Love waves in the structure considered (Fig. 14). This branch corresponds to a displacement field that has no nodes (as a function of x_3) within the film, i.e. it is the most smoothly varying branch within the film. Thus, the results obtained here, in addition to yielding surface wave frequencies that are exact only to the leading nonzero order in kd, are further limited to yielding the dispersion curve of only the mode that is the smoothest function of x_3 within the film. This is as it should be because the method used to derive Eqs. (3.17) implicitly assumes that the displacement field within the film is a slowly varying function of x_3.

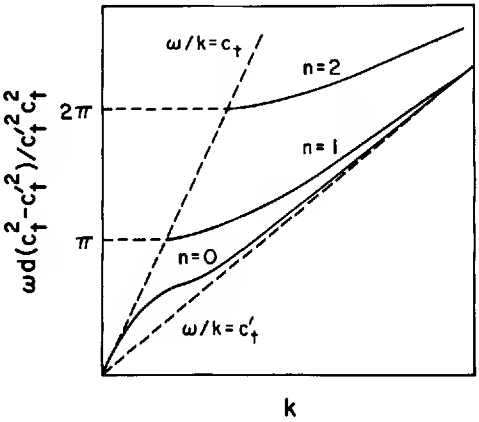

Fig. 14. The dispersion curves for the three lowest frequency Love waves associated with a layer of thickness d and material constants ρ', c_t' bonded to a semi-infinite substrate characterized by material constants ρ, c_t [Ref. 32].

The extension of the present analysis to the case of a piezoelectric film on either a piezoelectric or a nonpiezoelectric substrate would be useful, but has not been done yet.

3.2. Effects of Spatial Dispersion on Surface Acoustic Waves

The discreteness of a crystal structure has the consequence that the relation between stress and strain in it is nonlocal, i.e. the stress at any point in the medium is produced by the strains within a finite region of the medium surrounding that point. This nonlocal relation between stress and strain is often described by saying that the medium displays spatial dispersion. Spatial dispersion has interesting consequences for surface acoustic waves that we examine briefly here.

By passing to the long wave limit of the equations of motion of a simple cubic crystal with nearest and next nearest neighbor central and noncentral force interactions among atoms, the following continuum equations of motion are obtained, through fourth derivative terms$^{(6,8)}$:

$$\rho\ddot{u}_1 = [c_{11}\frac{\partial^2}{\partial x_1^2} + c_{44}\,(\frac{\partial^2}{\partial x_2^2} + \frac{\partial^2}{\partial x_3^2})]u_1 + (c_{12}+ c_{44})[\frac{\partial^2 u_3}{\partial x_1 \partial x_2} + \frac{\partial^2 u_3}{\partial x_1 \partial x_3}]+$$

$$+ a_o^2\{[\frac{1}{12}\,c_{11}\frac{\partial^4}{\partial x_1^4} + \frac{1}{12}\,c_{44}(\frac{\partial^4}{\partial x_2^4} + \frac{\partial^4}{\partial x_3^4}) + \frac{1}{2}\,c_{12}(\frac{\partial^4}{\partial x_1^2 \partial x_2^2} + \frac{\partial^4}{\partial x_1^2 \partial x_3^2})]u_1 +$$

$$+ \frac{1}{6}\,(c_{12}+ c_{44})[(\frac{\partial^4}{\partial x_1^3 \partial x_2} + \frac{\partial^4}{\partial x_1 \partial x_2^3})u_2 + (\frac{\partial^4}{\partial x_1^3 \partial x_3} + \frac{\partial^4}{\partial x_1 \partial x_3^3})u_3]\} \qquad (3.31a)$$

$$\rho\ddot{u}_2 = (c_{12}+ c_{44})\,\frac{\partial^2}{\partial x_2 \partial x_1}\,u_1 + [c_{11}\frac{\partial^2}{\partial x_2^2} + c_{44}\,(\frac{\partial^2}{\partial x_3^2} + \frac{\partial^2}{\partial x_1^2})]u_2 +$$

$$+ (c_{12}+ c_{44})\,\frac{\partial^2}{\partial x_2 \partial x_3}\,u_3 + a_o^2\,\{\frac{1}{6}\,(c_{12}+ c_{44})(\frac{\partial^4}{\partial x_2^3 \partial x_1} + \frac{\partial^4}{\partial x_2 \partial x_1^3})\,u_1 +$$

$$+ [\frac{1}{12}\,c_{11}\frac{\partial^4}{\partial x_2^4} + \frac{1}{12}\,c_{44}\,(\frac{\partial^4}{\partial x_3^4} + \frac{\partial^4}{\partial x_1^4}) + \frac{1}{2}\,c_{12}(\frac{\partial^4}{\partial x_2^2 \partial x_3^2} + \frac{\partial^4}{\partial x_2^2 \partial x_1^2})]u_2+$$

$$+ \frac{1}{6}\,(c_{12}+ c_{44})(\frac{\partial^4}{\partial x_2^3 \partial x_3} + \frac{\partial^4}{\partial x_2 \partial x_3^3})u_3\} \qquad (3.31b)$$

$$\rho\ddot{u}_3 = (c_{12}+ c_{44})[\frac{\partial^2 u_1}{\partial x_3 \partial x_1} + \frac{\partial^2 u_2}{\partial x_3 \partial x_2}]+[c_{11}\cdot\frac{\partial^2}{\partial x_3^2} + c_{44}(\frac{\partial^2}{\partial x_1^2} + \frac{\partial^2}{\partial x_2^2})]u_3+$$

$$+ a_o^2\{\frac{1}{6}\,(c_{12}+c_{44})[(\frac{\partial^4}{\partial x_3^3 \partial x_1} + \frac{\partial^4}{\partial x_3 \partial x_1^3})u_1 + (\frac{\partial^4}{\partial x_3^3 \partial x_2} + \frac{\partial^4}{\partial x_3 \partial x_2^3})u_2]+$$

$$+ [\frac{1}{12}\,c_{11}\frac{\partial^4}{\partial x_3^4} + \frac{1}{12}\,c_{44}(\frac{\partial^4}{\partial x_1^4} + \frac{\partial^4}{\partial x_2^4}) + \frac{1}{2}\,c_{12}(\frac{\partial^4}{\partial x_3^2 \partial x_1^2} + \frac{\partial^4}{\partial x_3^2 \partial x_2^2})]u_3\},$$

$$(3.31c)$$

where a_o is the lattice parameter. If the crystal is bounded by a stress-free (001) surface, the boundary conditions at the plane $x_3 = 0$ are found to be

$$c_{44}\left(\frac{\partial u_1}{\partial x_3} + \frac{\partial u_3}{\partial x_1}\right) - a_o \left\{\left[\frac{1}{2} c_{12} \frac{\partial^2}{\partial x_1^2} + \frac{1}{2} c_{44} \frac{\partial^2}{\partial x_3^2}\right]u_1 + \right.$$

$$\left. + \frac{1}{2} (c_{12} + c_{44}) \frac{\partial^2 u_3}{\partial x_1 \partial x_3}\right\} = 0 \qquad (3.32a)$$

$$c_{44}\left(\frac{\partial u_2}{\partial x_3} + \frac{\partial u_3}{\partial x_2}\right) - a_o \left\{\left[\frac{1}{2} c_{12} \frac{\partial^2}{\partial x_2^2} + \frac{1}{2} c_{44} \frac{\partial^2}{\partial x_3^2}\right]u_2 + \right.$$

$$\left. + \frac{1}{2} (c_{12} + c_{44}) \frac{\partial^2 u_3}{\partial x_2 \partial x_3}\right\} = 0 \qquad (3.32b)$$

$$c_{12} \left(\frac{\partial u_1}{\partial x_1} + \frac{\partial u_2}{\partial x_2}\right) + c_{11} \frac{\partial u_3}{\partial x_3} - a_o\left\{\frac{1}{2}(c_{12} + c_{44})\left(\frac{\partial^2 u_1}{\partial x_1 \partial x_3} + \frac{\partial^2 u_2}{\partial x_2 \partial x_3}\right) + \right.$$

$$\left. + \left[\frac{1}{2} c_{44}\left(\frac{\partial^2}{\partial x_1^2} + \frac{\partial^2}{\partial x_2^2}\right) + \frac{1}{2} c_{11} \frac{\partial^2}{\partial x_3^2}\right]u_3\right\} = 0. \qquad (3.32c)$$

Again, the leading nonzero terms in the lattice parameter have been kept.

In Eqs. (3.31) and (3.32) the terms containing the lattice parameter a_o are the terms describing the lowest order effects of spatial dispersion in the equations of motion and the boundary conditions, respectively.

We now apply Eqs. (3.31)-(3.32) to an investigation of surface acoustic waves of sagittal and shear horizontal polarization in turn.

3.2.1. Sagittal Polarization

In this subsection we consider a sagittally polarized surface acoustic wave propagating in the x_1-direction on the (001) surface of our crystal. This displacement field in this case can be written in the form

$$\vec{u}(\vec{x},t) = (\cos\theta f_1(x_3),\ 0,\ \sin\theta f_3(x_3)), \tag{3.33}$$

where $\theta \equiv kx_1 - \omega t$. When Eq. (3.33) is substituted into Eqs. (3.31) we obtain the following pair of equations for $f_{1,3}(x_3)$:

$$\begin{aligned}(c_{11}k^2 - \rho\omega^2)f_1 - c_{44}f_1'' - (c_{12}+c_{44})kf_3' \\ = a_o^2\{[\tfrac{1}{12}c_{11}k^4 - \tfrac{1}{2}c_{12}k^2\frac{d^2}{dx_3^2} + \tfrac{1}{12}c_{44}\frac{d^4}{dx_3^4}]f_1 + \\ + \tfrac{1}{6}(c_{12}+c_{44})(-k^3\frac{d}{dx_3} + k\frac{d^3}{dx_3^3})f_3\}\end{aligned} \tag{3.34a}$$

$$\begin{aligned}(c_{12}+c_{44})kf_1' + (c_{44}k^2 - \rho\omega^2)f_3 - c_{11}f_3'' \\ = a_o^2\{\tfrac{1}{6}(c_{12}+c_{44})(-k\frac{d^3}{dx_3^3} + k^3\frac{d}{dx_3})f_1 + \\ + [\tfrac{1}{12}c_{11}\frac{d^4}{dx_3^4} - \tfrac{1}{2}c_{12}k^2\frac{d^2}{dx_3^2} + \tfrac{1}{12}c_{44}k^4]f_3\}.\end{aligned} \tag{3.34b}$$

The boundary conditions at $x_3 = 0$ become

$$c_{44}(f_1' + kf_3) = a_o\{-\tfrac{1}{2}c_{12}k^2f_1 + \tfrac{1}{2}c_{44}f_1'' + \tfrac{1}{2}(c_{12}+c_{44})kf_3'\} \tag{3.35a}$$

$$-c_{12}kf_1 + c_{11}f_3' = a_o\{-\tfrac{1}{2}(c_{12}+c_{44})kf_1' - \tfrac{1}{2}c_{44}k^2f_3 + \tfrac{1}{2}c_{11}f_3''\}. \tag{3.35b}$$

In Eqs. (3.34) and (3.35) primes denote differentiation with respect to x_3.

In what follows we will assume the isotropy condition $c_{12} = c_{11} - 2c_{44}$ in order to simplify the analysis.

If we make the Ansatz

$$f_1(x_3) = Ae^{-\alpha x_3},\quad f_3(x_3) = Be^{-\alpha x_3}, \tag{3.36}$$

the equation for the amplitudes A and B takes the form

$$\begin{pmatrix} c_{11}\,k^2 - \rho\omega^2 - c_{44}\alpha^2 + 0(a_o^2) & (c_{11}-c_{44})k\alpha + 0(a_o^2) \\ -(c_{11}-c_{44})k\alpha + 0(a_o^2) & c_{44}k^2-\rho\omega^2-c_{11}\alpha^2 + 0(a_o^2) \end{pmatrix} \begin{pmatrix} A \\ B \end{pmatrix} = 0 \tag{3.37}$$

The solvability condition for this system can be written as

$$(\alpha^2 - \alpha_\ell^2(k\omega))(\alpha^2 - \alpha_t^2(k\omega)) = 0(a_o^2) \tag{3.38}$$

where

$$\alpha_{\ell,t}^2(k\omega) = k^2 - \frac{\omega^2}{c_{\ell,t}^2}, \tag{3.39}$$

with $c_\ell^2 = c_{11}/\rho$, $c_t^2 = c_{44}/\rho$. Thus, if we write

$$\omega = \omega_o + a_o\omega_1 + 0(a_o^2) \tag{3.40a}$$

$$\alpha = \alpha_o + a_o\alpha_1 + 0(a_o^2), \tag{3.40b}$$

then to this order in a_o the two solutions of Eq. (3.38) are

$$\alpha = \alpha_\ell(k\omega) = \alpha_{o\ell} - a_o\frac{\omega_o\omega_1}{c_\ell^2\alpha_{o\ell}} + 0(a_o^2) \tag{3.41a}$$

and

$$\alpha = \alpha_t(k\omega) = \alpha_{ot} - a_o\frac{\omega_o\omega_1}{c_\ell^2\alpha_{ot}} + 0(a_o^2). \tag{3.41b}$$

The solution of Eqs. (3.34) is therefore

$$f_1(x_3) = A_\ell e^{-\alpha_\ell x_3} + A_t e^{-\alpha_t x_3} \tag{3.42}$$

$$f_3(x_3) = -\frac{\alpha_\ell}{k}A_\ell e^{-\alpha_\ell x_3} - \frac{k}{\alpha_t}A_t e^{-\alpha_t x_3}. \tag{3.43}$$

Substitution of these solutions into Eqs. (3.35) yields the equation

$$\begin{pmatrix} 2\alpha_\ell & \frac{\alpha_t^2+k^2}{\alpha_t} \\ \frac{\alpha_t^2+k^2}{k} & 2k \end{pmatrix}\begin{pmatrix} A_\ell \\ A_t \end{pmatrix} + \frac{1}{2}a_o\begin{pmatrix} (\alpha_t^2+k^2) & (\alpha_t^2+k^2) \\ -\frac{\omega^2}{c_t^2}\frac{\alpha_\ell}{k} & -\frac{\omega^2}{c_t^2}\frac{k}{\alpha_t} \end{pmatrix}\begin{pmatrix} A_\ell \\ A_t \end{pmatrix} = 0. \tag{3.44}$$

Since the second term on the left hand side of this equation is explicitly proportional to a_o, we can replace ω and $\alpha_{\ell,t}$ in it by ω_o and $\alpha_{o\ell,t}$, respectively. However, terms of $O(a_o^o)$ and of $O(a_o)$ from Eqs. (3.41a)-(3.41b) must be retained in the first matrix on the left hand side. The solvability condition for the resulting equation then yields the dispersion relation for Rayleigh waves to lowest order in the lattice parameter as

$$\omega(k) = c_R|k|\left[1 - \frac{1}{8}(2-\xi^2)^2 \frac{(2-\xi^2)(1-\xi^2)^{1/2} - \xi^2(1-\lambda^2\xi^2)^{1/2}}{4(1-\lambda^2)-4(3-2\lambda^2)\xi^2+6\xi^4-\xi^6} a_o|k| + \right.$$
$$\left. + O((a_o k)^2)\right]. \qquad (3.45)$$

In writing this equation we have denoted by c_R the speed of Rayleigh waves in the absence of spatial dispersion, and have used the notation $\xi = c_R/c_t$, $\lambda = c_t/c_\ell$. $c_R(\lambda)$ is obtained from these definitions in terms of the smallest root of the Rayleigh equation, Eq. (1.16).

We see from Eq. (3.45) that in the presence of spatial dispersion Rayleigh waves are dispersive. This is due to the presence of a characteristic length in the problem, viz. the lattice parameter a_o.

A similar result has been obtained on the basis of a slightly different crystal model by Djafari-Rouhani et al.(30) and by Dobrzynski and Djafari-Rouhani(31).

3.2.2. Shear Horizontal Polarization

The effect of spatial dispersion in the case of sagittal polarization discussed in the preceding subsection is to render dispersive a surface acoustic wave that exists even in the absence of spatial dispersion. A more dramatic consequence of spatial dispersion is that it can give rise to a surface acoustic wave of shear horizontal polarization that, as we have seen earlier, cannot exist in the absence of spatial dispersion. To see this, we assume a displacement field of the form

$$\vec{u}(\vec{x},t) = (A,-A,0)\exp\left[\frac{ik}{\sqrt{2}}(x_1+x_2)-\alpha x_3-i\omega t\right], \qquad (3.46)$$

that describes a shear horizontal surface acoustic wave propagating in the [110] direction on the (001) surface of our crystal. When we substitute Eq. (3.46) into Eqs. (3.31) we obtain a single independent equation, viz.

$$\omega^2 = \frac{1}{\rho}\left[\frac{1}{2}(c_{11} - c_{12})\, k^2 - c_{44}\alpha^2\right] -$$

$$- \frac{a_o^2}{\rho}\left[\frac{1}{48}\,(c_{11} + 2c_{12} - 3c_{44})k^4 - \frac{1}{4}\, c_{12}k^2\alpha^2 + \frac{1}{12}\, c_{44}\, \alpha^4\right]. \qquad (3.47)$$

Then if we expand ω^2 and α^2 in powers of a_o according to

$$\omega^2 = \omega_o^2 + a_o\omega_1^2 + a_o^2\omega_2^2 + \ldots \qquad (3.48a)$$

$$\alpha^2 = \alpha_o^2 + a_o\alpha_1^2 + a_o^2\alpha_2^2 + \ldots \qquad (3.48b)$$

we obtain the set of equations

$$\omega_o^2 = \frac{c_{11}-c_{12}}{2\rho}\, k^2 - \frac{c_{44}}{\rho}\, \alpha_o^2 \qquad (3.49a)$$

$$\omega_1^2 = - \frac{c_{44}}{\rho}\, \alpha_1^2 \qquad (3.49b)$$

$$\omega_2^2 = - \frac{c_{44}}{\rho}\, \alpha_2^2 - \frac{1}{\rho}\left[\frac{1}{48}\,(c_{11}+2c_{12} - 3c_{44})k^4 - \frac{1}{4}\, c_{12}k^2\alpha_o^2 + \frac{1}{12}\, c_{44}\alpha_o^4\right]. \qquad (3.50)$$

From the boundary conditions (3.32) we also obtain a single equation, which can be written as

$$\alpha^2 = a_o^2\left[\frac{1}{4}\,\frac{c_{12}}{c_{44}}\, k^2 - \frac{1}{2}\, \alpha^2\right]^2 . \qquad (3.51)$$

By equating terms of the same order in a_o on both sides of this equation we obtain the set of equations

$$\alpha_o^2 = 0 \qquad (3.52a)$$

$$\alpha_1^2 = 0 \qquad (3.52b)$$

$$\alpha_2^2 = \left(\frac{1}{4}\,\frac{c_{12}}{c_{44}}\, k^2 - \frac{1}{2}\, \alpha_o^2\right)^2 \qquad (3.52c)$$

From Eqs. (3.49), (3.52) and (3.48) we obtain

$$\omega^2(k) = \frac{c_{11}-c_{12}}{2\rho}\, k^2 - \frac{a_o^2}{48\rho}\,(c_{11}+2c_{12} - 3c_{44})k^4 - \frac{a_o^2}{16\rho}\,\frac{c_{12}^2}{c_{44}}\, k^4 + O(k^6)$$

(3.53a)

$$\alpha^2(k) = \frac{a_o^2}{16}\frac{c_{12}^2}{c_{44}^2}k^4 + 0(k^6). \tag{3.53b}$$

We can simplify Eq. (3.53a) if we note that by setting $\alpha = 0$ in Eqs. (3.46) and (3.47) we obtain the square of the frequency of the bulk transverse acoustic wave propagating in the [110] direction (in the presence of spatial dispersion):

$$\omega_{110}^2(k) = \frac{(c_{11} - c_{12})}{2\rho}k^2 - \frac{a_o^2}{48\rho}(c_{11} + 2c_{12} - 3c_{44})k^4 + 0(k^6). \tag{3.54}$$

Thus we have that

$$\omega^2(k) = \omega_{110}^2(k) - \frac{a_o^2}{16\rho}\frac{c_{12}^2}{c_{44}}k^4 + 0(k^6). \tag{3.55}$$

The fact that $\omega^2(k) < \omega_{110}^2(k)$, and hence lies outside the band of frequencies allowed the normal modes of the bulk crystal, is the reason for the localization of this mode to the crystal surface. Because $\alpha(k) = (a_o/4)(c_{12}/c_{44})k^2$, rather than being of $0(k)$ as in the case of Rayleigh waves, this mode penetrates more deeply into the crystal than does a Rayleigh wave.

Future work on the effects of spatial dispersion on surface acoustic waves will undoubtedly employ phenomenological equations of motion and boundary conditions that are not based on specific crystal models. Some steps in this direction have been taken recently(33). Nevertheless, theories based on such models can provide very useful insights into the form such phenomenological theories must take.

4. Nonlinear Surface Acoustic Waves

All elastic media are nonlinear to a greater of lesser extent. The consequences of this nonlinearity for surface acoustic waves are several. It can give rise to such effects as second and third harmonic generation of surface acoustic waves(34,35), or the nonlinear mixing of two or more surface acoustic waves to produce a new surface acoustic wave.(36) In contrast with these consequences of elastic nonlinearity in which changes in the frequency or frequencies of the participating surface acoustic waves occur, there are other consequences that occur at constant frequency. For example, nonlinear surface acoustic waves can exist that propagate along the surface without change of form.(37-42) In this section we consider such nonlinear surface waves and a consequence of their existence that has been little discussed in the literature up to the present time.

We have pointed out in Section 1 that the displacement field of a Rayleigh surface acoustic wave is essentially nonzero only at distances into the medium supporting it that are smaller than its wavelength parallel to the surface. The energy in such a surface acoustic wave is similarly localized in the vicinity of the surface. The elastic energy density of the Rayleigh wave in this region is therefore much higher than that of the bulk elastic waves, particularly in the case of high-frequency Rayleigh waves, and the effects of the nonlinearity of the medium on the propagation of these waves are correspondingly enhanced. We have also seen in the preceding section that the discreteness of the structure of a real crystal, or the presence of an adlayer of a different material, can make Rayleigh waves dispersive. It is well known that a balance between the spreading tendency of dispersion and the contracting tendency of nonlinearity in the propagation of a wave through a nonlinear dispersive medium can result in the formation of a stable solitary wave, that travels through the medium without change of form and have some localized form. Consequently, one may expect that under suitable conditions a surface acoustic solitary wave (or surface acoustic soliton*) can exist.

Surface acoustic solitons based on Rayleigh waves have been studied in a series of papers by Sakuma and coworkers(43-46). Similarly, surface acoustic solitons based on Love waves have been studied by Bataille and Lund(47). There are, however, some unsatisfactory features to both of these sets of studies. In each case, the dispersion of the linear surface acoustic wave is introduced into the problem in a somewhat ad hoc fashion and, in the case of Refs 43-44, incorrectly in view of the results of Sections 3.1.1 and 3.2.1. In the case of sagittal polarization Sakuma and Kawanami(43) begin with a Hamiltonian for a semi-infinite elastic medium written ins second quantized form in terms of creation and annihilation operators for Rayleigh waves. The equations of motion of these operators are rewritten in a coherent state representation, and a nonlinear wave equation for the normal component of the (classical) elastic displacement field at the surface of the medium is extracted from them. Finally, the reductive perturbation method of Taniuti and Yajima(48) is used to obtain a nonlinear Schrodinger equation from this nonlinear wave equation. The nonlinear Schrodinger equation has well-known soliton solutions.(49) This approach to obtaining surface acoustic solitons seems unnecessarily complicated for a classical nonlinear system.

---

* Strictly speaking, a soliton is a solitary wave that has the property that when it collides with another solitary wave each passes through the other without change of form and only a small change in the phase of each. However, since the term "surface acoustic soliton" has entered the literature, and since it is less clumsy than the term "surface acoustic solitary wave," we will use the former here.

In this section we obtain surface acoustic solitons in a system supporting Love waves by an approach that requires obtaining first the dispersion relation for the nonlinear surface acoustic waves supported by that system, and that appears to be free of the kinds of objections that can be raised against the work cited above.

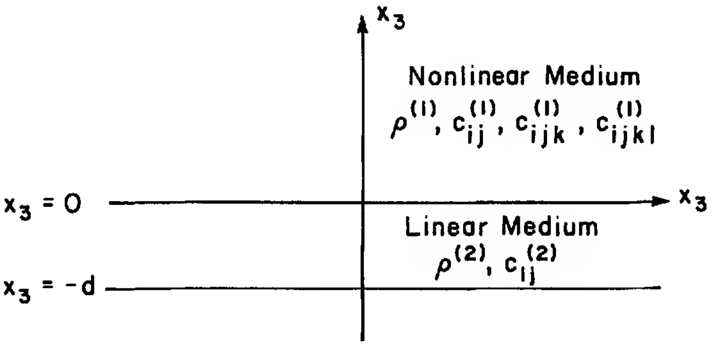
x_3
Nonlinear Medium
$\rho^{(1)}, c_{ij}^{(1)}, c_{ijk}^{(1)}, c_{ijkl}^{(1)}$
$x_3 = 0$
x_3
Linear Medium
$\rho^{(2)}, c_{ij}^{(2)}$
$x_3 = -d$

Fig. 15. A layer of thickness d of a linear cubic elastic medium bonded to a semi-infinite, nonlinear cubic elastic medium.

The system we consider is depicted in Fig. 15. It consists of a semi-infinite cubic elastic medium, characterized by a mass density $\rho^{(1)}$ and linear and nonlinear elastic moduli $c_{ij}^{(1)}$, $c_{ijk}^{(1)}$, $c_{ijk\ell}^{(1)}\ldots$, in the contracted, Voigt notation, that occupies the region $x_3 > 0$, to which is bonded a thin plate of cubic symmetry, characterized by a mass density $\rho^{(2)}$ and linear elastic moduli $c_{ij}^{(2)}$, that fills the region $-d < x_3 < 0$. It will be assumed that the cube axes coincide with the coordinate axes. Thus we assume that only the substrate is a nonlinear elastic medium. In this system we seek straight-crested, shear horizontal acoustic waves that propagate in the x_1-direction and are localized to the interface $x_3 = 0$. The form of the displacement field we study is therefore

$$\vec{u}(\vec{x};t) = (0,\ u_2(x_1x_3;t),0). \tag{4.1}$$

The choice of system and form of the displacement field was prompted by the following considerations. The fact that there is only a single nonzero component of the displacement field means that there is only a single nonlinear partial differential equation that has to be solved and only a single boundary condition that has to be satisfied, in contrast with the two coupled nonlinear partial differential equations and two boundary conditions that are encountered in the case of sagittal polarization (see below). The analysis is simplified somewhat as a result. In addition, for the orientation of the medium with respect to the coordinate axes assumed here, the lowest order nonlinear terms in the elements of the stress tensor of the nonlinear medium are of third order in the displacement component $u_2(x_1x_3;t)$, i.e. of the form $(\partial u_2/\partial x_3)(\partial u_2/\partial x_1)^2$, rather than of second order, i.e. of the form $(\partial u_2/\partial x_3)(\partial u_2/\partial x_1)$, as in the case of sagittal polarization. As a result, the lowest order nonlinear terms in the equation of motion of the nonlinear medium are also of third order in $u_2(x_1x_3;t)$, i.e. of the form $(\partial^2u_2/\partial x_1^2) \times (\partial u_2/\partial x_1)^2$, rather than of second order, i.e. of the form $(\partial^2u_2/\partial x_1^2)(\partial u_2/\partial x_1)$, as in the case of sagittal polarization. This circumstance considerably simplifies the derivation of the nonlinear dispersion relation for the shear horizontal waves we are studying. Finally, the thin overlayer occupying the region $-d < x_3 < 0$ has been introduced in order to give rise to surface acoustic waves in the linear theory, viz. the Love waves, that are absent in the absence of the overlayer and that are dispersive. In this way the dispersion is introduced into the linear dispersion relation in a physical, and controllable, way rather than being introduced in an *ad hoc* fashion.

It may be thought, however, that the introduction of the overlayer in fact complicates the problem of obtaining the nonlinear dispersion relation for the nonlinear shear horizontal waves we seek, by giving rise to boundary conditions at the interface $x_3 = 0$ as well as at the surface $x_3 = -d$. This, however, is not the case due to the way in which we treat the overlayer in the present work. The approach used here consists of replacing the overlayer by a modified boundary condition on the displacement field in the substrate at the plane $x_3 = 0$. This boundary condition is exact to first order in the thickness d of the overlayer. Thus, we have to solve the nonlinear equation of motion in the substrate alone, and we use the solution in a single boundary condition, which is the only way in which the properties of the substrate now enter the problem. As we have seen in Section 3.1.2, the overlayer is sufficient to introduce dispersion into the frequency of the linear surface wave supported by the structure depicted in Fig. 15 . It also has the effect of giving rise to only the lowest frequency Love wave in this structure, rather than to the infinite number that can exist when the finite thickness of the overlayer is taken into account.

A repetition of the analysis presented in Section 3.1 yields for the modified boundary condition at the plane $x_3 = 0$

$$T^{(1)}_{23}\Big|_{x_3=0} = d\left[\rho^{(2)} \frac{\partial^2 u_2^{(1)}}{\partial t^2} - c^{(2)}_{44} \frac{\partial^2 u_2^{(1)}}{\partial x_1^2}\right]_{x_3=0} , \tag{4.2}$$

where the left hand side is the stress in the nonlinear medium ($x_3 > 0$) at the plane $x_3 = 0$. We turn now to obtaining the solution of the nonlinear equation of motion of the substrate and from it the stress that enters the left hand side of Eq. (4.2). The satisfaction of the latter equation yields the nonlinear dispersion relation sought.

4.1. The Nonlinear Dispersion Relation

In Lagrangian coordinates$^{(50)}$ the Lagrangian (or Piola-Kirchhoff) stress tensor of an arbitrary nonlinear elastic medium can be written in the form$^{(51)}$

$$\begin{aligned} T_{\alpha\beta} = \sum_{\mu\nu} C_{\alpha\beta\mu\nu} \frac{\partial u_\mu}{\partial x_\nu} + \sum_{\mu\nu\rho\sigma} C^{(s)}_{\alpha\beta\mu\nu\rho\sigma} \frac{\partial u_\mu}{\partial x_\nu} \frac{\partial u_\rho}{\partial x_\sigma} + \\ + \sum_{\mu\nu\rho\sigma\kappa\lambda} C^{(s)}_{\alpha\beta\mu\nu\rho\sigma\kappa\lambda} \frac{\partial u_\mu}{\partial x_\nu} \frac{\partial u_\rho}{\partial x_\sigma} \frac{\partial u_\kappa}{\partial x_\lambda} + \cdots \end{aligned} \tag{4.3}$$

through the first two nonlinear contributions, where

$$C^{(s)}_{\alpha\beta\mu\nu\rho\sigma} = \frac{1}{2} C_{\alpha\beta\mu\nu\rho\sigma} + \frac{1}{2} C_{\alpha\beta\sigma\nu}\delta_{\mu\rho} + C_{\sigma\beta\mu\nu}\delta_{\alpha\rho} \tag{4.4a}$$

$$C^{(s)}_{\alpha\beta\mu\nu\rho\sigma\kappa\lambda} = \frac{1}{6} C_{\alpha\beta\mu\nu\rho\sigma\kappa\lambda} + \frac{1}{2} C_{\alpha\beta\mu\nu\lambda\sigma}\, \delta_{\rho\kappa} + \frac{1}{2} C_{\lambda\beta\mu\nu\rho\sigma} \delta_{\alpha\kappa} + \frac{1}{2} C_{\sigma\beta\lambda\nu} \delta_{\alpha\rho} \delta_{\mu\kappa}, \tag{4.4b}$$

and $C_{\alpha\beta\mu\nu\rho\sigma}$ and $C_{\alpha\beta\mu\nu\rho\sigma\kappa\lambda}$ are elements of the third and fourth order elastic modulus tensors, respectively. The equations of motion of the medium, to the same order in the nonlinearity, are given by$^{(52)}$

$$\begin{aligned}\rho_o \frac{\partial^2 u_\alpha}{\partial t^2} &= \sum_\beta \frac{\partial T_{\alpha\beta}}{\partial x_\beta} \\ &= \sum_{\beta\mu\nu} C_{\alpha\beta\mu\nu} \frac{\partial^2 u_\mu}{\partial x_\beta \partial x_\nu} + \sum_{\beta\mu\nu\rho\sigma} C^{(f)}_{\alpha\beta\mu\nu\rho\sigma} \frac{\partial^2 u_\mu}{\partial x_\beta \partial x_\nu} \frac{\partial u_\rho}{\partial x_\sigma} + \\ &\quad + \sum_{\beta\mu\nu\rho\sigma\kappa\lambda} C^{(f)}_{\alpha\beta\mu\nu\rho\sigma\kappa\lambda} \frac{\partial^2 u_\mu}{\partial x_\beta \partial x_\nu} \frac{\partial u_\rho}{\partial x_\sigma} \frac{\partial u_\kappa}{\partial x_\lambda} + \dots \end{aligned} \tag{4.5}$$

where ρ_o is the mass density of the undeformed medium, and

$$C^{(f)}_{\alpha\beta\mu\nu\rho\sigma} = C_{\alpha\beta\mu\nu\rho\sigma} + C_{\alpha\beta\sigma\nu} \delta_{\rho\mu} + C_{\sigma\beta\mu\nu} \delta_{\alpha\rho} + C_{\nu\beta\rho\sigma} \delta_{\alpha\mu} \tag{4.6a}$$

$$\begin{aligned} C^{(f)}_{\alpha\beta\mu\nu\rho\sigma\kappa\lambda} &= \frac{1}{2} C_{\alpha\beta\mu\nu\rho\sigma\kappa\lambda} + C_{\alpha\lambda\mu\nu\rho\sigma} \delta_{\beta\kappa} + C_{\alpha\beta\lambda\nu\rho\sigma} \delta_{\mu\kappa} + \\ &\quad + \frac{1}{2} C_{\alpha\beta\mu\nu\lambda\sigma} \delta_{\rho\kappa} + \frac{1}{2} C_{\alpha\nu\rho\sigma\kappa\lambda} \delta_{\beta\mu} + \\ &\quad + C_{\alpha\sigma\lambda\nu} \delta_{\beta\rho} \delta_{\mu\kappa} + \frac{1}{2} C_{\alpha\nu\lambda\sigma} \delta_{\beta\mu} \delta_{\rho\kappa} \; . \end{aligned} \tag{4.6b}$$

In the particular case considered in this section the equation of motion (4.5)-(4.6) simplifies to

$$\begin{aligned} \frac{1}{c_t^2} \frac{\partial^2 u}{\partial t^2} &= \frac{\partial^2 u}{\partial x_1^2} + \frac{\partial^2 u}{\partial x_3^2} + \left[\alpha\left(\frac{\partial u}{\partial x_1}\right)^2 + \beta\left(\frac{\partial u}{\partial x_3}\right)^2\right] \frac{\partial^2 u}{\partial x_1^2} + \\ &\quad + 4\beta \frac{\partial^2 u}{\partial x_1 \partial x_3} \frac{\partial u}{\partial x_1} \frac{\partial u}{\partial x_3} + \left[\beta\left(\frac{\partial u}{\partial x_1}\right)^2 + \alpha\left(\frac{\partial u}{\partial x_3}\right)^2\right] \frac{\partial^2 u}{\partial x_3^2} , \end{aligned} \tag{4.7}$$

where $c_t^2 = c^{(1)}_{44}/\rho^{(1)}_o$, and

$$\alpha = \frac{1}{c^{(1)}_{44}} \left(\frac{1}{2} c^{(1)}_{4444} + 3c^{(1)}_{344} + \frac{3}{2} c^{(1)}_{11}\right) \tag{4.8a}$$

$$\beta = \frac{1}{c_{44}^{(1)}} \left(\frac{1}{2} c_{4466}^{(1)} + c_{144}^{(1)} + 2c_{456}^{(1)} + c_{44}^{(1)} + \frac{1}{2} c_{12}^{(1)}\right) \tag{4.8b}$$

To simplify the notation, in writing Eq. (4.7) we have replaced $u_2^{(1)}(x_1x_3;t)$ by $u(x_1x_3;t)$. The boundary condition (4.1) becomes

$$c_{44}^{(1)}\left[1 + \beta\left(\frac{\partial u}{\partial x_1}\right)^2 + \frac{1}{3}\,\alpha\left(\frac{\partial u}{\partial x_3}\right)^2\right]\frac{\partial u}{\partial x_3}\bigg|_{x_3=0}$$

$$= d\left[\rho^{(2)}\,\frac{\partial^2 u}{\partial t^2} - c_{44}^{(2)}\,\frac{\partial^2 u}{\partial x_1^2}\right]_{x_3=0} . \tag{4.9}$$

We seek a solution of Eq. (4.7) in the form of a wave that propagates in the x_1-direction without changing its form, viz.

$$u(x_1x_3;t) = v(\theta;x_3), \tag{4.10}$$

where $\theta = kx_1-\omega t$. The equation satisfied by $v(\theta;x_3)$ is

$$-\left(k^2 - \frac{\omega^2}{c_t^2}\right)\frac{\partial^2 v}{\partial \theta^2} - \frac{\partial^2 v}{\partial x_3^2} = \alpha k^4\left(\frac{\partial v}{\partial \theta}\right)^2\frac{\partial^2 v}{\partial \theta^2} +$$

$$+ \beta k^2\left[\left(\frac{\partial v}{\partial x_3}\right)^2\frac{\partial^2 v}{\partial \theta^2} + 4\,\frac{\partial v}{\partial \theta}\,\frac{\partial v}{\partial x_3}\,\frac{\partial^2 v}{\partial \theta \partial x_3} + \left(\frac{\partial v}{\partial \theta}\right)^2\frac{\partial^2 v}{\partial x_3^2}\right] + \alpha\left(\frac{\partial v}{\partial x_3}\right)^2\frac{\partial^2 v}{\partial x_3^2} . \tag{4.11}$$

To solve this equation we set

$$v(\theta;x_3) = \varepsilon v_1(\theta;x_3) + \varepsilon^3 v_3(\theta;x_3) + \ldots \tag{4.12}$$

and

$$\omega^2 = \omega_o^2 + \varepsilon^2\omega_2^2 + \ldots, \tag{4.13}$$

where ε is an ordering parameter that can be set equal to unity at the end of the calculation. When we substitute Eqs. (4.12)-(4.13) into Eq. (4.11) and equate terms of the same order in ε on both sides of the equation, we obtain the following set of equations:

$$-\gamma_o^2\,\frac{\partial^2 v_1}{\partial \theta^2} - \frac{\partial^2 v_1}{\partial x_3^2} = 0 \tag{4.14a}$$

$$-\gamma_o^2 \frac{\partial^2 v_3}{\partial \theta^2} - \frac{\partial^2 v_3}{\partial x_3^2} = -\frac{\omega_2^2}{c_t^2}\frac{\partial^2 v_1}{\partial \theta^2} + \alpha k^4 \left(\frac{\partial v_1}{\partial \theta}\right)^2 \frac{\partial^2 v_1}{\partial \theta^2} +$$

$$+ \beta k^2 \left[\left(\frac{\partial v_1}{\partial x_3}\right)^2 \frac{\partial^2 v_1}{\partial \theta^2} + 4 \frac{\partial v_1}{\partial \theta}\frac{\partial v_1}{\partial x_3}\frac{\partial^2 v_1}{\partial \theta \partial x_3} + \right.$$

$$\left. + \left(\frac{\partial v_1}{\partial \theta}\right)^2 \frac{\partial^2 v_1}{\partial x_3^2}\right] + \alpha \left(\frac{\partial v_1}{\partial x_3}\right)^2 \frac{\partial^2 v_1}{\partial x_3^2} \qquad (4.14b)$$

. . . .

where

$$\gamma_o^2 = k^2 - \frac{\omega_o^2}{c_t^2} . \qquad (4.15)$$

The solution of Eq. (4.14a) that vanishes as $x_3 \to \infty$ can be written as

$$v_1(\theta;x_3) = a \cos\theta \, e^{-\gamma_o x_3} , \qquad (4.16)$$

where a is a constant amplitude, provided that $k^2 > (\omega_o^2/c_t^2)$. Equation (4.14b) thus takes the form

$$-\gamma_o^2(k\omega)\frac{\partial^2 v_3}{\partial \theta^2} - \frac{\partial^2 v_3}{\partial x_3^2} = \cos\theta \left[a \frac{\omega_2^2}{c_t^2} e^{-\gamma_o x_3} + \right.$$

$$\left. + a^3\left(-\tfrac{1}{4}\alpha k^4 + \tfrac{1}{2}\beta k^2 \gamma_o^2 + \tfrac{3}{4}\alpha \gamma_o^4\right) e^{-3\gamma_o x_3} \right] +$$

$$+ \cos 3\theta \, a^3\left(\tfrac{1}{4}\alpha k^4 - \tfrac{3}{2}\beta k^2 \gamma_o^2 + \tfrac{1}{4}\alpha \gamma_o^4\right) e^{-3\gamma_o x_3} . \qquad (4.17)$$

If we assume a solution of this equation of the form

$$v_3(\theta;x_3) = \cos\theta A(x_3) + \cos 3\theta B(x_3) , \qquad (4.18)$$

The equations satisfied by $A(x_3)$ and $B(x_3)$ are

$$\frac{d^2 A}{dx_3^2} - \gamma_o^2 A = -a \frac{\omega_2^2}{c_t^2} e^{-\gamma_o x_3} + a^3\left(\tfrac{1}{4}\alpha k^4 - \tfrac{1}{2}\beta k^2 \gamma_o^2 - \tfrac{3}{4}\alpha \gamma_o^4\right) e^{-3\gamma_o x_3} \qquad (4.19a)$$

$$\frac{d^2 B}{dx_3^2} - 9\gamma_o^2 B = -a^3\left(\tfrac{1}{4}\alpha k^4 - \tfrac{3}{2}\beta k^2 \gamma_o^2 + \tfrac{1}{4}\alpha \gamma_o^4\right) e^{-3\gamma_o x_3} \qquad (4.19b)$$

whose solutions that vanish as $x_3 \to \infty$ are

$$A(x_3) = \frac{a}{2\gamma_o}\frac{\omega_2^2}{c_t^2} x_3 e^{-\gamma_o x_3} + \frac{a^3}{8\gamma_o^2}\left(\tfrac{1}{4}\alpha k^4 - \tfrac{1}{2}\beta k^2 \gamma_o^2 - \tfrac{3}{4}\alpha \gamma_o^4\right) e^{-3\gamma_o x_3} \qquad (4.20a)$$

$$B(x_3) = C\, e^{-3\gamma_o x_3} + \frac{a^3}{6\gamma_o}\left(\frac{1}{4}\,\alpha k^4 - \frac{3}{2}\,\beta k^2\gamma_o^2 - \frac{1}{4}\,\alpha\gamma_o^4\right)x_3\, e^{-3\gamma_o x_3}. \tag{4.20b}$$

In writing the solution of Eq. (4.19b) we have added in a solution of the corresponding homogeneous equation with a coefficient C. It should be noted that the presence of secular terms in the solutions given by Eqs. (4.20) does not violate the boundary condition at infinity.(53)

The boundary condition satisfied by $v(\theta;x_3)$ is obtained from Eq. (4.9) as

$$c_{44}^{(1)}\left[1 + \beta k^2\left(\frac{\partial v}{\partial\theta}\right)^2 + \frac{1}{3}\,\alpha\left(\frac{\partial v}{\partial x_3}\right)^2\right]\frac{\partial v}{\partial x_3}\bigg|_{x_3=0}$$

$$= d\left[\rho^{(2)}\omega^2 - c_{44}^{(2)}k^2\right]\frac{\partial^2 v}{\partial\theta^2}\bigg|_{x_3=0} \quad . \tag{4.21}$$

When the expansions (4.12)-(4.13) are substituted into this equation, and terms of the same order in ε on both sides of the resulting equation are equated, we obtain the following system of equations at $x_3 = 0$:

$$c_{44}^{(1)}\frac{\partial v_1}{\partial x_3} - d\left[\rho^{(2)}\omega_o^2 - c_{44}^{(2)}k^2\right]\frac{\partial^2 v_1}{\partial\theta^2} = 0 \tag{4.22a}$$

$$c_{44}^{(1)}\frac{\partial v_3}{\partial x_3} - d\left[\rho^{(2)}\omega_o^2 - c_{44}^{(2)}k^2\right]\frac{\partial^2 v_3}{\partial\theta^2}$$

$$= - c_{44}^{(1)}\left[\beta k^2\left(\frac{\partial v_1}{\partial\theta}\right)^2 + \frac{1}{3}\,\alpha\left(\frac{\partial v_1}{\partial x_3}\right)^2\right]\frac{\partial v_1}{\partial x_3} + d\rho^{(2)}\omega_2^2\,\frac{\partial^2 v_1}{\partial\theta^2} \quad . \tag{4.22b}$$

. . . .

The substitution of Eq. (4.16) into Eq. (4.22a) yields the value of $\omega_o^2(k)$, viz.

$$\omega_o^2(k) = c_t^2 k^2\left[1 - \left(\frac{\rho^{(2)}}{\rho^{(1)}} - \frac{c_{44}^{(2)}}{c_{44}^{(1)}}\right)^2 (kd)^2\right] \tag{4.23}$$

to lowest nonzero order in d, provided that $(\rho^{(2)}/\rho^{(1)}) > (c_{44}^{(2)}/c_{44}^{(1)})$. Equation (4.23) is just the dispersion curve for the lowest frequency Love wave, obtained in Section 3.1.2, as it must be. The substitution of $v_3(\theta;x_3)$, as given by Eqs. (4.18) and (4.20) into

Eq. (4.22b) yields both the coefficient C and $\omega_2^2(k)$:

$$C = -\frac{a^3}{144\gamma_o^2}\alpha(k^4-\gamma_o^4) \tag{4.24}$$

$$\omega_2^2(k) = c_t^2 \frac{a^2}{8\left(1 - 2\frac{\rho^{(2)}}{\rho^{(1)}}\gamma_o\right)}(\alpha k^4 + 2\beta k^2\gamma_o^2 + \alpha\gamma_o^4). \tag{4.25}$$

If we note from Eqs. (4.15) and (4.23) that

$$\gamma_o = d\left(\frac{\rho^{(2)}}{\rho^{(1)}} - \frac{c_{44}^{(2)}}{c_{44}^{(1)}}\right)k^2 + 0(d^3), \tag{4.26}$$

and work only to the lowest order in d, we obtain for the nonlinear dispersion curve

$$\omega(k) = c_t k\{1 - \frac{1}{2}[(\frac{\rho^{(2)}}{\rho^{(1)}} - \frac{c_{44}^{(2)}}{c_{44}^{(1)}})^2 - \frac{\alpha}{8}(\frac{a}{d})^2 \cdot (kd)^2\}, \tag{4.27}$$

while the corresponding displacement field is given by

$$v(\theta;x_3) = a\cos\theta e^{-\gamma_o x_3} + a^3\frac{ak^4}{16\gamma_o^2}\left(\gamma_o x_3 e^{-\gamma_o x_3} + \frac{1}{2}e^{-3\gamma_o x_3}\right)\cos\theta -$$

$$- a^3\frac{ak^4}{144\gamma_o^2}\left(1 - \frac{1}{6}\gamma_o x_3\right)e^{-3\gamma_o x_3}\cos 3\theta. \tag{4.28}$$

We see from Eq. (4.27) that if the phase velocity of this nonlinear wave is to be slower that c_t, for the wave to be localized to the surface, we must have

$$\left(\frac{a}{d}\right) < \left(\frac{8}{\alpha}\right)^{1/2}\left(\frac{\rho^{(2)}}{\rho^{(1)}} - \frac{c_{44}^{(2)}}{c_{44}^{(1)}}\right), \tag{4.29}$$

an inequality that is easily satisfied, since the right hand side is typically of order unity.

We now turn to the application of Eq. (4.27) to the determination of surface acoustic solitons.

4.2. Surface Acoustic Solitons

It is not expected that the kind of nonlinear surface acoustic wave studied in the preceding subsection exhausts the surface waves possible on the surface of a nonlinear elastic medium. In particular, for reasons described in the introduction to this section, it is of considerable interest to look for surface acoustic solitons. These are pulse envelope waves that have the nature of solitary waves propagating along the surface of a nonlinear elastic medium. In this subsection we apply the results of the preceding subsection to an examination of the question of whether such excitations can exist in the structure depicted in Fig. 15.

Let $a(x,t)$ be the (real) amplitude of a component of the elastic displacement field at the surface of a nonlinear elastic medium in contact with vacuum. (A precise definition of a will be given below.) The fact that we have assumed that $a(x,t)$ dependes only on the coordinate x ($\equiv x_1$) in the direction of propagation of the wave on the surface and is independent of the transverse coordinate z ($\equiv x_3$) normal to the surface means that the transverse variation of the elastic displacement field enters the final pulse evolution equation to be obtained here (Eq. (4.43) below) through the nonlinear surface wave dispersion relation. This is an adiabatic assumption in which at any point (x,t) the transverse variation of the elastic displacement field is given by the nonlinear CW surface acoustic wave solution. This means, physically, that as the wave propagates along the surface the system adjusts to the self-consistent nonlinear field distribution at a rate faster than the time scale over which the wave changes.(54) Any wave propagating along the surface can be expressed in terms of a complex amplitude $a(x,t)\exp i\theta(x,t)$, where $\theta(x,t)$ is a generalized phase factor. In a simple CW case $\theta(x,t)$ is $kx - \omega t$, so that the derivatives of θ with respect to x and t are just the wave number $k = \theta_x$ and frequency $\omega = -\theta_t$, where the subscripts denote partial derivatives. In this case k and ω are constants. In the more general nonlinear case considered here they are functions of both x and t.

The equations determining $a(x,t)$ are(55-57):

the energy equation

$$\frac{\partial a^2}{\partial t} + \frac{\partial}{\partial x}\left(\frac{\partial \omega}{\partial k}\, a^2\right) = 0; \tag{4.30}$$

the dispersion relation

$$\omega(k,a) = \omega_0(k) - \frac{1}{2}\,\frac{\partial^2 \omega_0(k)}{\partial k^2}\,\frac{a_{xx}}{a} + \omega_2(k)a^2; \tag{4.31}$$

the consistency equation

$$k_t + \omega_x = 0. \tag{4.32}$$

We note that in the absence of the second term on the right hand side of Eq. (4.31) the dispersion relation given by the latter has the form of the nonlinear dispersion curve to $O(a^2)$ obtained in the CW case in the preceding subsection. The term $-\frac{1}{2}(\partial^2\omega_o(k)/\partial k^2)(a_{xx}/a)$ has been shown by Yuen and Lake$^{(56)}$ to be present when the wave amplitude a is a slowly varying function of x and t.

We now introduce the phase function $\theta(x,t)$ and require that

$$\theta_t = -\omega, \qquad \theta_x = k, \tag{4.33}$$

so that Eq. (4.32) is automatically satisfied. We next set

$$\omega = \omega_o + \overline{\omega}, \qquad k = k_o + \overline{k}, \tag{4.34}$$

where ω_o and k_o are constants. It follows that

$$\theta = \theta_o + \overline{\theta} \tag{4.35}$$

where

$$\theta_o = k_o x - \omega_o t \tag{4.36}$$

and

$$\overline{\theta}_t = -\overline{\omega}, \qquad \overline{\theta}_x = \overline{k}. \tag{4.37}$$

If we expand the dispersion relation (4.31) about $k = k_o$, using the second of Eqs. (4.34),

$$\omega(k_o + \overline{k}, a) = \omega_o(k_o) + \overline{k}\left(\frac{\partial\omega_o}{\partial k}\right)_o + \frac{1}{2}\overline{k}^2\left(\frac{\partial^2\omega_o}{\partial k^2}\right)_o - $$

$$-\frac{1}{2}\left(\frac{\partial^2\omega_o}{\partial k^2}\right)\frac{a_{xx}}{a} + \omega_2(k_o)a^2, \tag{4.38}$$

where the subscript o means that the derivative is evaluated at $k = k_o$, and use the first of each of Eqs. (4.34) and (4.37), and the second of Eqs. (4.37) we find that

$$\overline{\theta}_t = -\left(\frac{\partial\omega_o}{\partial k}\right)_o \overline{\theta}_x - \frac{1}{2}\left(\frac{\partial^2\omega_o}{\partial k^2}\right)\left(\overline{\theta}_x^2 - \frac{a_{xx}}{a}\right) - \omega_2(k_o)a^2. \tag{4.39}$$

From Eqs. (4.30) and (4.38) we obtain the result that

$$a_t = -\left(\frac{\partial\omega_o}{\partial k}\right)_o a_x - \frac{1}{2}\left(\frac{\partial^2\omega_o}{\partial k^2}\right)(\overline{\theta}_{xx}a + 2\overline{\theta}_x a_x), \tag{4.40}$$

where we have used the result that

$$\frac{\partial^2\omega}{\partial x\partial k} = \overline{\theta}_{xx}\left(\frac{\partial^2\omega_o}{\partial k^2}\right)_o \tag{4.41}$$

which follows from Eqs. (4.38) and the second of Eqs. (4.37).

We can combine Eqs. (4.39) and (4.40) into a single equation if we introduce the complex amplitude A(x,t) by

$$A(x,t) = a(x,t)\ \exp i\overline{\theta}(x,t). \tag{4.42}$$

By the use of Eqs. (4.39) and (4.40) it is easy to show that A(x,t) satisfies the nonlinear Schrodinger equation

$$i\left(A_t + \left(\frac{\partial\omega_o}{\partial k}\right)_o A_x\right) + \frac{1}{2}\left(\frac{\partial^2\omega_o}{\partial k^2}\right)_o A_{xx} - \omega_2(k_o)\,|A|^2\,A = 0. \tag{4.43}$$

The condition that Eq. (4.43) have stable soliton solutions is that $(\partial^2\omega_o/\partial k^2)_o\ \omega_2(k_o) < 0.$(58) A solution of this equation is

$$A(x,t) = \left(-\frac{(\partial^2\omega_o/\partial k^2)_o}{\omega_2(k_o)}\right)^{1/2} \frac{e^{i\delta t}}{|v_g\Delta|}\ \mathrm{sech}\left(\frac{t-(x/v_g)}{\Delta}\right) \tag{4.44}$$

where

$$\delta = \frac{(\partial^2\omega_o/\partial k^2)_o}{2v_g^2\Delta^2}, \qquad v_g = \left(\frac{\partial\omega_o}{\partial k}\right)_o, \tag{4.45}$$

and Δ is the half-width of the pulse represented by Eq. (4.44).

The nonlinear dispersion relation obtained in the preceding subsection (Eq. (4.27)) yields the following results for the functions $\omega_o(k)$ and $\omega_2(k)$ appearing in Eq. (4.31):

$$\omega_o(k) = c_t k\left[1 - \frac{1}{2}\left(\frac{\rho^{(2)}}{\rho^{(1)}} - \frac{c_{44}^{(2)}}{c_{44}^{(1)}}\right)^2 (kd)^2 {}_\approx \tag{4.46a}$$

$$\omega_2(k) = c_t k^3\,\frac{\alpha}{16}, \tag{4.46b}$$

from which it follows that

$$v_g = c_t[1 - \frac{3}{2} (\frac{\rho^{(2)}}{\rho^{(1)}} - \frac{c_{44}^{(2)}}{c_{44}^{(1)}})^2 (kd)^2 \approx \qquad (4.47a)$$

$$(\frac{\partial^2 \omega_o}{\partial k^2})_o = -3c_t(\frac{\rho^{(2)}}{\rho^{(1)}} - \frac{c_{44}^{(2)}}{c_{44}^{(1)}})^2 \ kd^2 < 0. \qquad (4.47b)$$

Thus, if we identify $a(x,t)$ with the amplitude of the displacement field of the nonlinear shear horizontal surface acoustic wave at the surface $x_3 = 0$, whose CW value was denoted by a in the preceding subsection, we see that a stable surface acoustic soliton is possible in the system considered in this section if $\alpha > 0$.

There are questions about such solitons that remain to be answered. For example, how can they be excited and detected? What is the evolution distance for these pulses, that is, what is the distance a pulse of arbitrary form established at $t = 0$ travels before it evolves into the form given by Eq. (4.44)? It is hoped that these and other questions concerning surface acoustic solitons will be raised and answered in future work on these excitations.

Acknowledgements

I am grateful to Patriciann Ryann for preparing Figs. 1 and 3; to Xuemei Huang for Figs. 10-12; and to Dr. W. Zierau for Fig. 9. I am also grateful to the Graduate Council of the University of California, Irvine, for travel funds that made my participation in this School possible. This work was supported in part by NSF Grant No. DMR85-17634.

References

1. Lord Rayleigh, Proc. Lond. Math. Soc. 17, 4 (1885).
2. See, for example, W. Prager, Introduction to Mechanics of Continuua (Ginn and Co., Boston, 1961), p. 91.
3. See, for example, L. D. Landau and E. M. Lifshitz, Theory of Elasticity (Pergamon Press, New York, 1970), p. 102.
4. I. A. Viktorov, Akust. Zhur. 25, 1 (1979) [Soviet Physics - Acoustics 25, 1 (1979).]
5. A. A. Maradudin, in Modern Problems of Surface Physics, ed. I. J. Lalov (Bulgarian Academy of Sciences, Sofia, 1981), p. 11.
6. A. A. Maradudin, in Nonequilibrium Phonon Dynamics, ed. W. Bron (Plenum, New York, 1985), p. 395.
7. A. A. Maradudin, in Surface Waves in Plasmas and Solids, ed. S. Vukovic (World Scientific, Singapore, 1986), p. 220.

8. A. A. Maradudin, in Proceedings of the International Symposium on Surface Waves in Solids and Layered Structures, Novosibirsk, July 1-4, 1986 (to appear).

9. See, for example, A. A. Maradudin and W. M. Visscher, Z. Phys. B60, 215 (1985).

10. P. Ryan and A. A. Maradudin (unpublished work).

11. Lord Rayleigh, Philos. Mag. 14, 70 (1907); Theory of Sound, vol. II, 2nd Ed. (Dover, New York, 1945), p. 89.

12. N. E. Glass, R. Loudon, and A. A. Maradudin, Phys. Rev. B24, 6843 (1981).

13. K. A. Ingebrigtsen and A. Tonning, Phys. Rev. 184, 942 (1968).

14. F. Rischbieter, Acustica 16, 75 (1965).

15. P. V. H. Sabine, Electron. Lett. 6, 149 (1970).

16. L. M. Brekhovskikh, Akust. Zhur. 5, 288 (1959) [Soviet-Physics-Acoustics 5, 288 (1960)].

17. N. E. Glass and A. A. Maradudin, J. Appl. Phys. 54, 796 (1983).

18. Xuemei Huang and A. A. Maradudin (unpublished work).

19. A. A. Maradudin and D. L. Mills, Ann. Phys. (New York) 100, 262 (1976).

20. A. A. Bulgakov and S. I. Khankina, Solid State Commun. 44, 55 (1982).

21. V. R. Velasco and F. Garcia-Moliner, Physica Scripta 20, 111 (1979).

22. W. M. Ewing, W. S. Jardetsky, and F. Press, Elastic Waves in Layered Media (McGraw-Hill, New York, 1957).

23. A. E. H. Love, Some Problems of Geodynamics (Cambridge Univ. Press, London, 1911).

24. R. Stoneley, Proc. Roy. Soc. (London) A106, 416 (1924).

25. K. Sezawa, Bull. Earthquake Res. Inst. 3, 1 (1927).

26. H. F. Tiersten, J. Appl. Phys. 40, 770 (1969).

27. I. Murdoch, J. Mech. Phys. Solids 24, 237 (1976).

28. G. W. Farnell, in Acoustic Surface Waves, ed. A. A. Oliner (Springer-Verlag, New York, 1978), p. 13.

29. S. V. Bogdanov, M. D. Levin, and I. B. Yakovkin, Akust. Zhur. 15, 12 (1969) [Soviet Physics-Acoustics 15, 10 (1969)].

30. B. Djafari-Rouhani, L. Dobrzynski, V. R. Velasco, and F. Garcia-Moliner, Surf. Sci. 110, 129 (1981).

31. L. Dobrzynski and B. Djafari-Rouhani, in Vibrations at Surfaces, eds. R. Dandano, J. M. Gilles, and A. A. Lucas (Plenum, New York, 1982), p. 1.

32. B. A. Auld, Acoustic Fields and Waves in Solids, vol. II (John Wiley and Sons, New York, 1973), p. 101.

33. V. V. Krylov, Kristallografiya 27, 791 (1982) [Soviet Physics - Crystallography 27, 475 (1982)].
34. R. Normandin, M. Fukui, and G. I. Stegeman, J. Appl. Phys. 50, 81 (1979).
35. R. Normandin, M. Fukui, and G. I. Stegeman, J. Appl. Phys. 50, 1131 (1979).
36. See, for example, P. J. Vella, T. C. Padmore, G. I. Stegeman, and V.M. Ristic, J. Appl. Phys. 45, 1993 (1974).
37. N. Kalyanasundaram, Int. J. Engng. Sci. 19, 279 (1981).
38. N. Kalyanasundaram, Int. J. Engng. Sci. 19, 287 (1981).
39. N. Kalyanasundaram, J. Acoust. Soc. Am. 72, 1518 (1982).
40. D. F. Parker and F. M. Talbot, in Nonlinear Deformation Waves, eds. U. Nigul and J. Engelbrecht (Springer-Verlag, New York, 1983), p. 397.
41. D. F. Parker, Physica 16D, 385 (1985).
42. D. F. Parker and F. M. Talbot, J. Elasticity 15, 389 (1985).
43. T. Sakuma and Y. Kawanami, Phys. Rev. B29, 869 (1984).
44. T. Sakuma and Y. Kawanami, Phys. Rev. B29, 880 (1984).
45. T. Sakuma and T. Miyazaki, Phys. Rev. B33, 1036 (1986).
46. T. Sakuma and O. Saito, Phys. Rev. B35, 1294 (1987).
47. K. Bataille and F. Lund, Physica 6D, 95 (1982).
48. T. Taniuti and N. Yajima, J. Math. Phys. 14, 1389 (1973).
49. See, for example, R. K. Dodd, J. C. Eilbeck, J. D. Gibbon, and H. C. Morris, Solitons and Nonlinear Wave Equations (Academic Press, New York 1982), Chap. 8.
50. See, for example, D. R. Bland, Nonlinear Dynamic Elasticity (Blaisdell, Waltham, MA, 1969), p. 2ff.
51. Ref. 50, Eq. (1.30) and the expansion of the internal energy in terms of the Lagrangian finite strain parameters given, e.g. by K. Brugger, Phys. Rev. 133, A1611 (1964).
52. Ref. 50, Eq. (1.16).
53. Some authors, however, object to the presence of such terms. See, for example, R. W. Lardner, J. Appl. Phys. 55, 3251 (1984).
54. A. D. Boardman, G. S. Cooper, A. A. Maradudin, T. P. Shen, Phys. Rev. B34, 8273 (1986).
55. G. B. Witham, Linear and Nonlinear Waves (John Wiley and Sons, New York, 1974), p. 363.
56. H. C. Yuen and B. M. Lake, Phys. Fluids 18, 956 (1975).
57. V. I. Karpman and E. M. Krushkal', Zh. Eksp. i. Teor. Fiz. 55, 530 (1968) [Soviet Physics - JETP 28, 277 (1969)].
58. Ref. 49, p. 504ff.

Acoustic phonons in infinite and semi-infinite superlattices

B. Djafari Rouhani
Université de Haute Alsace, 4 rue des Frères Lumière 68093 MULHOUSE Cédex, France.

1. Introduction

A great deal of work have been devoted during the last decades to the study of wave propagation in layered media [1]. There is a renewal of interest in this domain due to fabrication of artificial crystals made of alternating layers of two (or more) different materials, and the measurements of phonons in these periodically modulated structures. Due to the larger periodicity of the superlattice in the direction perpendicular to the layers, there are many phonon branches in the folded Brillouin zone ; these branches are separated by gaps where localized modes associated to defects, and in particular to the surface of a semi-infinite superlattice, may exist. In this paper, we present a review of the theoretical calculations on the bulk and surface phonons in superlattices, using either an elastic continuum approach or some particular atomic models ; we will mainly limit our discussion to the phonons belonging to the acoustic domains of the constituent crystals.

Let us mention that the experimental demonstration of acoustic zone folding was first given [2] by using superconducting tunnel junctions as sources and detectors of quasi-monochromatic phonons and probing the selective transmission of high frequency phonons by a GaAs-GaAlAs superlattice. The frequencies of the few first folded acoustic modes were then obtained by Raman spectroscopy in different type of superlattices [3-9] ; the dispersion curves of these phonon branches were also probed [10,5] and even umklapp processes were observed in long period superlattices [11]. These experiments (which have been discussed within an elastic continuum approach) are only dealing with phonons propagating along the axis of the superlattice. On the other hand, concerning the surface phonons, Brillouin scattering has been used as a tool to investigate Rayleigh waves localized at the surface of metallic [12,13] or semiconductor [4] superlattices.

2. Elastic continuum approach

2.1. Bulk acoustic waves

Each constituent of the superlattice is characterized by its elastic constants $C_{\alpha\beta\mu\nu}$ and mass density ρ. This continuum description can only be applied if the thicknesses of the films ($d_1 = 2h_1$ and $d_2 = 2h_2$) as well as the acoustic wavelengths are large compared to the interatomic distances. The equations of motion of the elasticity theory can then be written

$$\rho(x_3)\,\frac{\partial^2 u_\alpha(\vec{x},t)}{\partial t^2} = \sum_\beta \frac{\partial}{\partial x_\beta}\left[\sum_{\mu\nu} C_{\alpha\beta\mu\nu}(x_3)\,\frac{\partial u_\mu(\vec{x},t)}{\partial x_\nu}\right] \quad (\alpha = 1,2,3) \qquad (1)$$

where x_3 is along the axis of the superlattice and ρ and $C_{\alpha\beta\mu\nu}$ are periodic functions of x_3. To obtain the dispersion relations of the bulk (and also of the surface) acoustic waves in the superlattice one can use a transfer matrix method |14,17| ; first the solution to the displacement field can be obtained in each film from eq. (1) ; for example in the first type of film belonging to the nth cell of the superlattice

$$u_i^{(n)}(\vec{x},t) = \sum_{j=1}^{3}\left[A_{ij}^{(n)}\exp(\alpha_j x_3^{(n)}) + B_{ij}^{(n)}\exp(-\alpha_j x_3^{(n)})\right] e^{i(\vec{k}_{/\!/}\cdot\vec{x}-\omega t)} \qquad (2)$$

where ω is the frequency and $\vec{k}_{/\!/}$ the wavevector parallel to the interfaces. The reduced coordinate $x_3^{(n)} = x_3 - (n-1)D$ (where $D = d_1 + d_2$ is the period of the superlattice) is introduced for convenience and ranges from $-h$ to $+h$. The parameters α_j are the solutions of a secular determinant of rank 3 while the coefficients $A_{ij}^{(n)}$ (or $B_{ij}^{(n)}$) are the eigenvectors of the corresponding matrix. There are consequently six unknown multiplicative constants, let us say $A_{1j}^{(n)}$ and $B_{1j}^{(n)}$ ($j = 1,2,3$) which have to be determined by using the boundary conditions on the displacements and on the stresses at the different interfaces. By writing these six coefficients as a column vector $|\psi_n>$, the boundary conditions easily give

$$|\psi_{n+1}> = \overleftrightarrow{T}\,|\psi_n> \qquad (3)$$

where $\overleftrightarrow{T}$ is a 6x6 transfer matrix. For an infinite superlattice, the application of the Bloch theorem in the x_3 direction, with a wave vector k_3, gives the eigenvalues as solutions of the determinantal equation

$$\det(\overleftrightarrow{T} - e^{ik_3D}\,\overleftrightarrow{I}) = 0 \qquad (4)$$

where $\overleftrightarrow{I}$ is a 6x6 unit matrix. For given ω and $\vec{k}_{/\!/}$, this equation gives six roots for k_3 associated two by two, corresponding to propagation in positive or negative x_3-direction ; in a bulk band these solutions are real while in a gap they have an imaginary part.

A simplification arises in the above general theory in some particular cases, for example when the films in the superlattice are isotropic |14,16|, or |17| when they are (0001) oriented hexagonal slabs, or still if they are (001) oriented cubic slabs with $\vec{k}_{/\!/}$ along [100] or [110] ... In these cases the shear horizontal modes decouple from those polarized in the sagittal plane ; then the $\overleftrightarrow{T}$ matrix becomes a juxtaposition of a 2x2 and a 4x4 matrix. Moreover, we showed that the eigenvalue problem for this last matrix can be solved analytically by introducing the matrix $\overleftrightarrow{M} = \frac{1}{2}(\overleftrightarrow{T}+\overleftrightarrow{T}^{-1})$ when the displacements (eq. (2)) are expressed in terms of $\cosh(\alpha_j x_3^{(n)})$ and $\sinh(\alpha_j x_3^{(n)})$ rather than in terms of exponentials ; indeed, the matrix $\overleftrightarrow{M}$ can be block

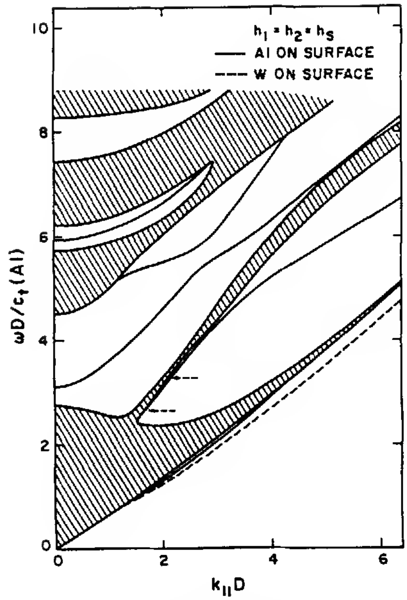

Fig. 1. Bulk bands and surface wave dispersion for an Al-W superlattice. The shaded areas are the bulk bands. The surface modes are presented either for an Al layer (solid line) or a W layer (dashed line) at the surfaces. $c_t(Al)$ is the transverse velocity of sound in Al. After ref. |15|.

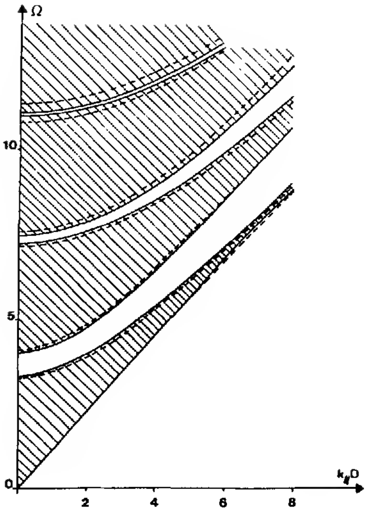

Fig. 2. Comparison of the elastic waves band structure in a two-component (A_1A_2) and in a four-component ($A_1A_3A_2A_3$) superlattice, where A_3 is a mixture of A_1 and A_2 due to the interdiffusion of the films ; $\Omega = \omega D/c_t$ is a reduced frequency. The shaded areas (limited by the full lines) are the bulk bands of the four-component superlattice ; the dashed lines give the band limits of the two component superlattice. After ref. |18|.

diagonalized into two 2x2 submatrices.

As a matter of example the dispersion relation of the transverse waves in the case of hexagonal slabs mentioned above becomes |17|

$$\cos k_3 D = \cosh(\alpha_1 d_1)\cosh(\alpha_2 d_2) + F \sinh(\alpha_1 d_1)\sinh(\alpha_2 d_2) \qquad (5)$$

$$\text{with } F = \frac{1}{2}\left(\frac{C_{44}^{(1)}\alpha_1}{C_{44}^{(2)}\alpha_2} + \frac{C_{44}^{(2)}\alpha_2}{C_{44}^{(1)}\alpha_1}\right) \; ; \; \alpha_i^{\,2} = \frac{C_{11}^{(i)}-C_{12}^{(i)}}{2C_{44}^{(i)}} k_{/\!/}^2 - \frac{\rho_i\omega^2}{C_{44}^{(i)}} \; (i = 1,2) \qquad (6)$$

For cubic slabs, this same relation holds when $\vec{k}_{/\!/}$ is along [110] while $\frac{C_{11}-C_{12}}{2}$ has to be changed to C_{44} when $\vec{k}_{/\!/}$ is parallel to [100]. The dispersion relation of the sagittal waves is more complicated when $k_{/\!/} \neq 0$; however at $k_{/\!/} = 0$ the sagittal modes decouple into longitudinal and shear horizontal modes and one obtains dispersion relations similar to (5). An illustration of the sagittal bulk bands is given in figure 1 (shaded area) for an Al-W superlattice |16|. This band structure is not only dependent on the parameters of the constituents but also on the relative thickness of the two media. Concerning the example displayed in fig. 1, let us also point out that at an interface between two semi-infinite Al and W crystals there is a Stoneley (interface) wave, with an eigenfunction localized near the interface and decaying exponentially on both side into the interior of the crystals. In the superlattice this gives rise, in the limit of thick layers, to bulk bands at the frequency of the Stoneley mode ; indeed for $k_{/\!/}D \gg 1$ the velocities of the first bulk bands approach the velocity of the Stoneley wave (at about 2800 m/s).

A generalization of the above calculations to a superlattice composed of N different layers (instead of two) is possible ; in particular an analytic dispersion relation was derived in the case of shear horizontal waves |17,18|. Figure 2 gives |18| a comparison of the corresponding bulk bands in a two-component (A_1A_2) superlattice and in a four-component ($A_1A_3A_2A_3$) superlattice, where A_3 is a mixture of A_1 and A_2 due to the diffusion near the interfaces of one film into another.

2.2. Surface acoustic waves

The surface acoustic waves in a superlattice have been investigated by assuming the surface to be either parallel |14-17,19| or perpendicular to the laminations |20|. In the first case, one can use the transfer matrix method |14-17| to search for surface modes, which have their frequencies inside the gaps separating the bulk bands. Such a mode has to be sought in the form of a linear combination of three out of the six solutions of eq. (4), i.e. those corresponding to the attenuation of the wave far from the surface.

$$u_i^{(n)}(\vec{x},t) = \sum_{\mu=1}^{3} R_\mu \sum_{j=1}^{3} [A_{ij}^{(n)(\mu)}\exp(\alpha_j x_3^{(n)}) + B_{ij}^{(n)(\mu)}\exp(-\alpha_j x_3^{(n)})]\, e^{i(\vec{k}_{/\!/}.\vec{x}-\omega t)} \qquad (7)$$

R_μ ($\mu = 1,2,3$) are arbitrary coefficients introduced to make a linear combination of the three possible solutions. The surface mode solution must also fulfill the vanishing of the stresses at the free surface of the superlattice. This leads to three linear homogeneous equations in the coefficients R_μ, whose determinant has the frequencies of the surface modes as its roots. In fig. 1 we have presented the dispersion curves of the surface modes (polarized in the sagittal plane) either for an Al layer or a W layer at the surface of the superlattice. The thickness of the surface layer is assumed to be the same as that of the corresponding films in the bulk. However the existence and frequencies of the surface waves are very dependent on this thickness which may be varied experimentally |14-17|.

The Rayleigh waves on a superlattice have also been investigated in a geometry in which the surface is perpendicular to the alternating layers |20|. A new method has been developped which consists of first Fourier analyzing the equations of motion (1) in the direction x_3 perpendicular to the layers so as to include automatically the boundary conditions at the different interfaces. For each value of the wave vector k perpendicular to the layers, this gives an infinite set of wave vectors parallel to the layers (i.e. perpendicular to the surface). Then a surface wave is constructed

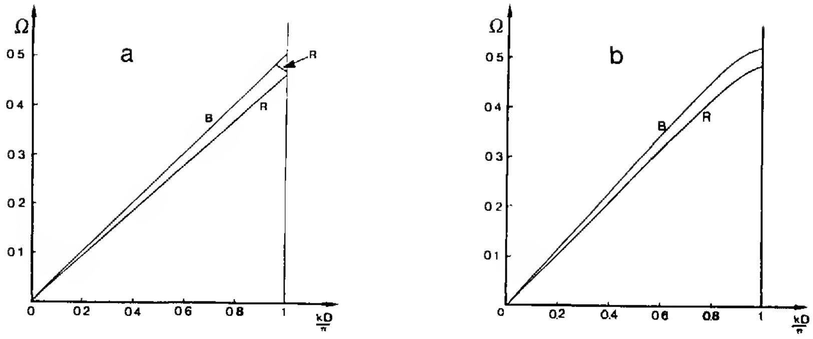

Fig. 3. Dispersion of the bottom of the bulk bands (B) and of the Rayleigh waves (R) in the reduced Brillouin zone associated with the superlattice. The two media in the superlattice differ only by their mass density, with (a) $\frac{\rho'}{\rho} = 0.95$ and (b) $\rho'/\rho = 0.5$, $\Omega = \omega D/2\pi c_t$ is a reduced frequency, where c_t is the transverse speed of sound in the first medium. After ref. |20|.

from a superposition of these solutions. The frequencies of the surface Rayleigh wave are obtained by using the Fourier-analysed conditions of vanishing stresses at the free surface. Numerical calculations are performed by limiting the number of Fourier components taken into account. For two relatively similar layers in the superlattice, there are two different Rayleigh branches near the Brillouin zone boundary which result from the folding of the dispersion curve for a Rayleigh wave on a homogeneous medium (fig. 3a). The higher branch can disappear when the two layers differ significantly in their elastic properties (fig. 3b). The magnitude of the gap between the two Rayleigh branches may also be varied by changing the relative thickness of the two layers.

2.3. Piezoelectric superlattices

The transfer matrix method has been applied to the study of shear horizontal waves in infinite and semi-infinite superlattices, composed of two piezoelectric media of hexagonal symmetry |21|. There is a new possibility afforded by these systems due to the coupling between the acoustic waves and the electric field. Let us mention that the homogeneous piezoelectric materials have already found many practical applications and also they exhibit surface waves (the Bleustein Gulyaev wave (BGW)) which have no analogue in purely elastic media. Figure 4 gives an illustration of the shear horizontal bulk bands (shaded area) and surface modes in a CdS-ZnO superlattice. The effect of the piezoelectric coupling is to rise the frequencies by a few per cent compared to those in the purely elastic system. An other effect of this coupling is the existence of BGW ; the behaviour of the surface modes below the bottom of the bulk bands is then qualitatively different in the two, piezo and non-piezoelectric, cases. Besides the surface waves are sensitive to the nature of the film at the surface, its thickness,

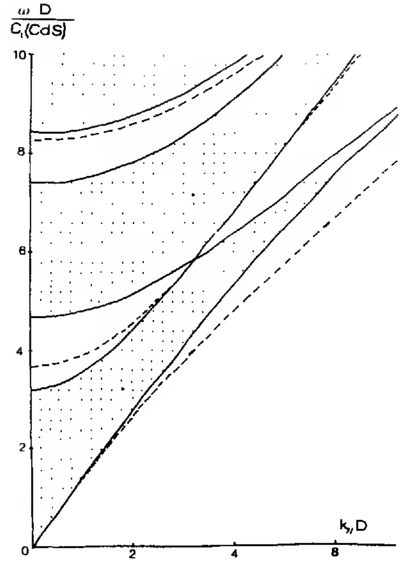

Fig. 4. Same as in fig. 1 for a piezoelectric CdS-ZnO superlattice. The dashed curves represent the surface modes when a non-metallized CdS film is at the surface. For a metallized surface, the results are slightly different. When a ZnO film is at the surface (metallized or non-metallized) there is only one surface wave very near to the bottom of the bulk bands over a small range of $k_{/\!/}D$. After ref. |21|.

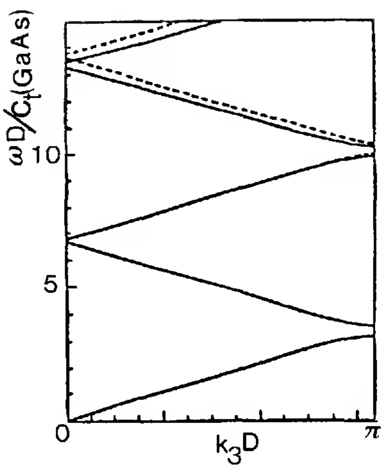

Fig. 5. Illustration of the first acoustic phonon branches in a GaAs-AlAs superlattice, for propagation perpendicular to the layers, using the continuum model (----) or a linear chain model with five monolayers in each film (____). After ref. |14|.

and also to the electrical boundary conditions at the surface (metallized or non-metallized surface).

2.4. Effective medium approximation

In the long wavelength regime, i.e. when the acoustic or optic wavelengths become large compared to the period D, the superlattice behaves like an effective homogeneous medium in which the waves are dispersionless. This medium is characterized by elastic, dielectric, photoelastic ... constants which can be expressed as functions of the parameters of the constituents in the superlattice. Besides the earlier work of Rytov |22| assuming the layers in the superlattice to be isotropic, the effective elastic constants have been recently calculated for layers of cubic |23,24|, hexagonal |24| or orthorhombic |25| symmetries, and finally given formally for any symmetry of the layers |26|. This formal theory has been generalized to piezoelectric superlattices |21| in which the effective elastic, dielectric and piezoelectric constants are coupled together (neglecting piezoelectricity, one finds independently the elastic and dielectric constants). The result can be expressed as

$$\overleftrightarrow{C}^{e} = \langle \overleftrightarrow{C}\,\overleftrightarrow{P}^{-1} \rangle (\langle \overleftrightarrow{P}^{-1} \rangle)^{-1} \tag{8}$$

where

$$\overleftrightarrow{C} = \begin{pmatrix} C_{11} & C_{12} & C_{13} & C_{14} & C_{15} & C_{16} & -e_{11} & -e_{21} & -e_{31} \\ C_{12} & C_{22} & C_{23} & C_{24} & C_{25} & C_{26} & -e_{12} & -e_{22} & -e_{32} \\ C_{13} & C_{23} & C_{33} & C_{34} & C_{35} & C_{36} & -e_{13} & -e_{23} & -e_{33} \\ C_{14} & C_{24} & C_{34} & C_{44} & C_{45} & C_{46} & -e_{14} & -e_{24} & -e_{34} \\ C_{15} & C_{25} & C_{35} & C_{45} & C_{55} & C_{56} & -e_{15} & -e_{25} & -e_{35} \\ C_{16} & C_{26} & C_{36} & C_{46} & C_{56} & C_{66} & -e_{16} & -e_{26} & -e_{36} \\ e_{11} & e_{12} & e_{13} & e_{14} & e_{15} & e_{16} & \varepsilon_{11} & \varepsilon_{12} & \varepsilon_{13} \\ e_{21} & e_{22} & e_{23} & e_{24} & e_{25} & e_{26} & \varepsilon_{12} & \varepsilon_{22} & \varepsilon_{23} \\ e_{31} & e_{32} & e_{33} & e_{34} & e_{35} & e_{36} & \varepsilon_{13} & \varepsilon_{23} & \varepsilon_{33} \end{pmatrix} \tag{9}$$

$$\overleftrightarrow{P} = \begin{pmatrix} 1 & 0 & 0 & 0 & 0 & 0 & 0 & 0 & 0 \\ 0 & 1 & 0 & 0 & 0 & 0 & 0 & 0 & 0 \\ C_{13} & C_{23} & C_{33} & C_{34} & C_{35} & C_{36} & -e_{13} & -e_{23} & -e_{33} \\ C_{14} & C_{24} & C_{34} & C_{44} & C_{45} & C_{46} & -e_{14} & -e_{24} & -e_{25} \\ C_{15} & C_{25} & C_{35} & C_{45} & C_{55} & C_{56} & -e_{14} & -e_{25} & -e_{35} \\ 0 & 0 & 0 & 0 & 0 & 1 & 0 & 0 & 0 \\ 0 & 0 & 0 & 0 & 0 & 0 & 1 & 0 & 0 \\ 0 & 0 & 0 & 0 & 0 & 0 & 0 & 1 & 0 \\ e_{31} & e_{32} & e_{33} & e_{34} & e_{35} & e_{36} & \varepsilon_{13} & \varepsilon_{23} & \varepsilon_{33} \end{pmatrix} \tag{10}$$

and the symbol < > means average over the constituents of the superlattice, each film having a weight proportional to its thickness.

It is interesting to note that the effective constants are involved into expressions which are averages of the corresponding expressions in the two constituents.

A similar conclusion holds for the effective photoelastic constants |27| which play a major role in the scattering of light by long wavelength phonons.

3. Atomic models

It is necessary to go beyond the elastic continuum model in several respects, for example if the layers in the superlattice are only a few monolayers thick, or in order to describe the high frequency phonons (in particular optical phonons), or still, to obtain the dispersion curves in the whole two dimensional Brillouin zone parallel to the layers.

To deal only with phonons propagating along the axis of the superlattice the simplest approach is to use a linear chain model ; then the general equation of motion for an atom ℓ may be written as

$$M_\ell \ddot{u}_\ell = \gamma(\ell,\ell+1)(u_{\ell+1}-u_\ell) + \gamma(\ell-1,\ell)(u_{\ell-1}-u_\ell) \tag{11}$$

where only interactions between nearest neighbors are taken into account and the force constants γ are relative either to the bulk of each material or to the interfaces. Different linear chain models have already been set up |5,14,28-31| and several numerical or analytical results obtained. In figure 5, the few first folded acoustic branches calculated in the continuum model (dashed line) are compared to those obtained by using a linear chain model (full line) in which the films contain respectively five monolayers of GaAs and AlAs. One can notice that some deviations appear between the two results for higher phonon branches. However the linear chain models have often been used in connection with optical phonons in semiconductor superlattices, especially in GaAs-AlAs superlattices where several experimental data are available. Also a linear chain calculation |31| showed the existence of interface phonons (see § 2.1. above) in a GaSb-InAs superlattice, with a crucial dependence of the results on the nature of the interfaces (In-Sb or Ga-As).

Using a Green's function technique, the qualitative behaviour of phonons in a three dimensional, infinite or semi-infinite, superlattice was studied |32| within a Montroll-Potts model of monoatomic cubic crystals. An example of the bulk bands and surface modes, as functions of $\vec{k}_{//}$, is given in figure 6. Let us point out that at each value of $\vec{k}_{//}$ some of the bulk bands are relatively wide while others are very narrow ; this means that as functions of k_3 (wave vector along the superlattice axis) the bands may show some dispersion or be very flat. These behaviours can be explained in the following way ; for a given $\vec{k}_{//}$, the frequency range of a bulk band may fall into the spectral domains of both (resp. only one) constituents in the superlattice and consequently the eigenfunctions of the corresponding phonons are extended (resp. localized) over both (resp. only one) type of films. On the other hand, the surface modes may exist everywhere in the Brillouin zone, and are dependent on the nature of the film at the surface and on the number of atomic layers it contains.

The quantitative calculations of phonons propagating along the axis ($\vec{k}_{//} = 0$) of a GaAs-AlAs superlattice have been treated in two papers, using either a bond charge model |33| or a rigid ion model |34|. Some differences exist between the results of the two calculations which however give qualitative conclusions similar to those of linear chain models. Finally a recent calculation |34|

Fig. 6. Band structure of a superlattice, with two atomic planes in each film $(L_1=L_2=2)$. The two crystals have the same atomic masses $(M_1 = M_2)$ and different force constants $(\gamma_1 = 2\gamma_2$ or $\gamma_2 = 2\gamma_1)$; at the interfaces $\gamma = (\gamma_1+\gamma_2)/2$. The film labeled as 1 is at the surface. The shaded areas represent the bulk bands (four of each value of $\vec{k}_{/\!/}$). Surface modes are present (absent) for a surface layer containing two (one) atomic planes. The N_1, N'_1, N''_1 modes (____) refer to $\gamma_1 = 2\gamma_2$, the N_2, N'_2, N''_2 modes (----) to $\gamma_1 = \gamma_2/2$.

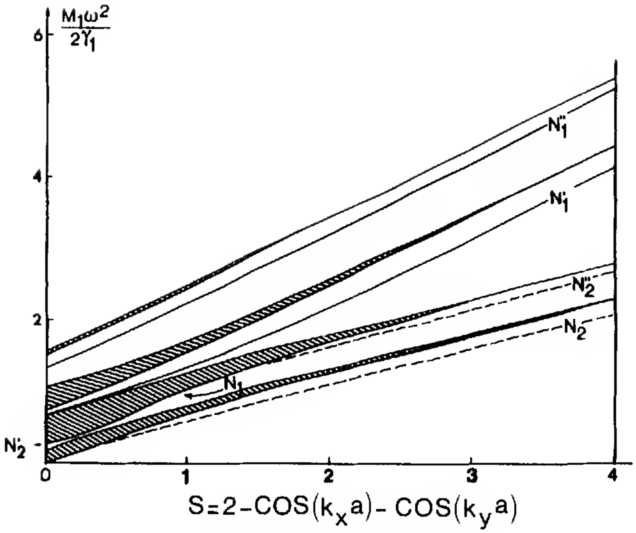

was also dealing with phonons in a GaAs-Ga_xAl_{1-x}As superlattice where one of the compound is a ternary disordered alloy ; in this paper, the recursion method was used to obtain the densities of phonon states near the wave vector $\vec{k} = 0$.

4. Conclusion

By studying the acoustic phonons of a superlattice within both continuum and discrete models, we have shown that the eigenfunctions may be extended over both type of slabs, localized in only one type of slab, or localized around the interfaces. The overall bulk band structure is dependent on the elastic parameters of the superlattice and the relative thickness of the two layers. In a semi-infinite superlattice, surface modes may exist inside the gaps, depending on the composition of the surface layer, its thickness and possibly on specific surface boundary conditions. These general physical conclusions still hold for optical phonons in superlattices, and in particular the ideas of extended, confined |36,37|, or interface |38,39,31| phonons have been more extensively discussed in connection with optical modes.

We are certainly going to know more extensive quantitative calculations of phonons in superlattices, including the effects of different types of disorder, the analyses of intensities and lineshapes in Raman scattering or other experiments. These and other vibrational properties may be handled through the knowledge of the Green's function |15,32,40| which can be calculated for instance by using the recent interface response theory |41|.

Acknowledgments.- The author would like to thank Drs. L. Dobrzynski and J. Sapriel for a critical reading of the manuscript .

References

1. W.M. Ewing, W.S. Jardetzky and F. Press, Elastic waves in layered media (Mc Graw Hill, New York, 1957) ; L.M. Brekhovskikh, Waves in layered media (Academic, New York, 1960).
2. V. Narayanamurti, H.L. Stormer, M.A. Chin, A.C. Gossard and W. Wiegmann, Phys. Rev. Lett. 43, 2012 (1979).
3. C. Colvard, R. Merlin, M.V. Klein and A.C. Gossard, Phys. Rev. Lett. 45, 298 (1980) ; J. Phys. (Paris) C6, 631 (1981).
4. J. Sapriel, J.C. Michel, J.C. Toledano, R. Vacher, J. Kervarec and A. Regreny, Phys. Rev. B28, 2007 (1983).
5. C. Colvard, T.A. Gant, M.V. Klein, R. Merlin, R. Fisher, H. Morkoc and A.C. Gossard, Phys. Rev. B31, 2080 (1985).
6. B. Jusserand, F. Alexandre, J. Dubard and D. Paquet, Phys. Rev. B33, 28 (1986).
7. J. Sapriel, J. Chavignon, F. Alexandre and R. Azoulay, Phys. Rev. B34, 7118 (1986
8. P. Santos, M. Hundhausen and L. Ley, Phys. Rev. B33, 1516 (1986).
9. H. Brugger, G. Abstreiter, H. Jorke, H.J. Herzog and E. Kasper, Phys. Rev. B33, 5928 (1986).
10. B. Jusserand, D. Paquet, A. Regreny and J. Kervarec, Solid State Commun. 48, 499 (1983).
11. M.W.C. Dharma-Wardana, D.J. Lockwood, J.M. Baribean and D.C. Houghton, Phys. Rev. B34, 3034 (1986).
12. A. Kueny, M. Grimsditch, K. Miyano, I. Banerjee, C.M. Falco and I.K. Schuller, Phys. Rev. Lett. 48, 166 (1982).
13. R. Darmer, R.P. Huebener, C.S.L. Chun, M. Grimsditch and I.K. Schuller, Phys. Rev. B33, 3696 (1986).
14. J. Sapriel, B. Djafari Rouhani and L. Dobrzynski, Surf. Sci. 126, 197 (1983).
15. R.E. Camley, B. Djafari Rouhani, L. Dobrzynski and A.A. Maradudin, Phys. Rev. B27, 7318 (1983).
16. B. Djafari Rouhani, L. Dobrzynski, O. Hardouin Duparc, R.E. Camley and A.A. Maradudin, Phys. Rev. B28, 1711 (1983) ; J. Phys. (Paris), C5, 151 (1984).
17. A. Nougaoui and B. Djafari Rouhani, Surface Science (1987), to be published.
18. B. Djafari Rouhani and L. Dobrzynski, Solid State Communications (1987), to be published.
19. B.A. Auld, G.S. Beaupre and G. Herrmann, Elec. Lett. 13, 525 (1977) ; B.A. Auld in Moderns problems in elastic wave propagation, ed. J. Miklowitz and Jan D. Achenbach (John Wiley and Sons, Inc., New York, 1978), p. 459.
20. B. Djafari Rouhani, A.A. Maradudin and R.F. Wallis, Phys. Rev. B29, 6454 (1984).
21. A. Nougaoui and B. Djafari Rouhani, Surf. Science (1987), to be published.
22. S. Rytov, Akust Zh. 2, 71 (1956) |Sov. Phys. Acoust. 2, 68 (1956)|.
23. F. Nizzoli in Proceedings of the International Conference on the Physics of Semiconductors, San Francisco (1984).
24. B. Djafari Rouhani, J. Sapriel, L. Dobrzynski and A. Nougaoui. Proceedings of the Second International Conference on Phonon Physics, Budapest (World Scientific, 1985) p. 555.
25. M. Grimsditch, Phys. Rev. B31, 6818 (1985).
26. M. Grimsditch and F. Nizzoli, Phys. Rev. B33, 5891 (1986).
27. B. Djafari Rouhani and J. Sapriel, Phys. Rev. B34, 7114 (1986).

28. A.S. Barker Jr., J.L. Merz and A.C. Gossard, Phya. Rev. B17, 3181 (1978).

29. B. Djafari Rouhani, J. Sapriel and F. Bonouvrier, Superlattices and Microstructures, 1, 29 (1985).

30. S.R.P. Smith. Proceedinga of the Second International Conference on Phonon Physics, Budapest (World Scientific, 1985) p. 531.

31. A. Fasolino, E. Molinari and J.C. Maan, Phys. Rev. B33, 8889 (1986).

32. B. Djafari Rouhani, L. Dobrzynski and O. Hardouin Duparc, J. Elect. Spectr. and Related Phenomena 30, 119 (1983).
L. Dobrzynski, B. Djafari Rouhani and O. Hardouin Duparc, Phya. Rev. B29, 3138 (1986).

33. Sung-Kit Yip and Yia-Chung Chang, Phys. Rev. B30, 7037 (1984).

34. G. Kanellis, Phya. Rev. B35, 746 (1987).

35. A. Kobayashi and A. Roy, Phys. Rev. B35, 2237 (1987).

36. B. Juaaerand, D.Paquet and A. Regreny, Phys. Rev. B30, 6245 (1984).

37. A.K. Sood, J. Menendez, M. Cardona and K. Ploog, Phys. Rev. Lett. 54, 2111 (1985).

38. A.K. Sood, J. Menendez, M. Cardona and K. Ploog, Phys. Rev. Lett. 54, 2115 (1985).

39. P. Lambin, J.P. Vigneron, A.A. Lucaa, P.A. Thiry, M. Liehr, J.J. Pireaux and R. Caudano, Phys. Rev. Lett. 56, 1842 (1986).

40. M. Babiker, D.R. Tilley, E.L. Albuquerque and C.E.T. Gonçalvea da Silva, J. Phya. C18, 1269 (1985).

41. L. Dobrzynaki, Surface Science 175, 1 (1986) ; Surface Science Reporta 6, 119 (1986).

PHONONS IN SUPERLATTICES

John M. Worlock
Bell Communications Research, Inc.
Red Bank, NJ, 07701-7020, USA

Superlattices are artificially and periodically layered materials, with periodicities chosen and controlled by their makers. Together with their cousins, the heterojunctions and the quantum wells, they have shown great promise for new electronic and optoelectronic phenomena. Superlattices are routinely grown by various epitaxial techniques, from crystalline semiconductor materials and metals, and even occasionally as amorphous (sic) superlattices. Intercalation of graphite is another technique for the generation of superlattices, and there are also a few analogous structures which are found ready-made in nature. Periods of grown superlattices range from a few atomic layers upward, and probably the most precise control is obtained using molecular beam epitaxy. While it is possible and very useful to grow and study superlattices of materials not well matched in lattice constant, the best developed materials are lattice-matched, and of these the most widely studied is the combination GaAs - $Al_xGa_{1-x}As$.

Semiconductor superlattices were conceived in 1969 by Leo Esaki and Raphael Tsu[1], but a few years of gestation passed before they began to be taken seriously. Phonons in these new structures have caught the interest of investigators almost from their earliest beginnings, and both acoustic and optical modes have now been widely studied by Raman spectroscopy. These studies have been used to develop the ideas of zone-folding and mode confinement, but have contributed as well to the characterization of the quality of the interfaces between layers.

Two recent reviews are available, and so much of the material covered in the lectures can be found there. They are: "Phonons in Semiconductor Superlattices," by M. V. Klein[2], and "Phonons in Superlattices," by J. M. Worlock[3]. In addition, I can recommend B. Jusserand's lecture notes on "Confined and Propagative Vibrations in Superlattices," from the Winter School in March 1985, at Les Houches, France[4]. Both Klein and Jusserand are leaders in the exploration and the exposition of the subject. Two recent international conferences have had symposia on superlattice phonons, and their proceedings are most useful[3,5]. Finally, C. Colvard, M. V. Klein, and coworkers have provided an excellent and readable account of the development of the field and their contributions to it as of late 1984[6].

Generally, superlattices are one-dimensional in the sense that the superperiod has a unique axis, which is the axis of growth. This fact, coupled with the fact that the momentum transfer in the normal Raman experiment is along that axis, has enabled us to understand many properties of superlattice phonons using one-dimensional, linear chain, models. A further very useful simplification is the assumption of nearest-neighbor interactions: the mathematics for the dispersion curves becomes identical to that of the Kronig-Penney model for electronic dispersion in a one-dimensional lattice. Knowledge of the dispersion of the constituents of the superlattice allows the easy calculation of the superlattice modes.

So let us begin with a quick review of the Kronig-Penney model. In Figure 1 we show a one-dimensional

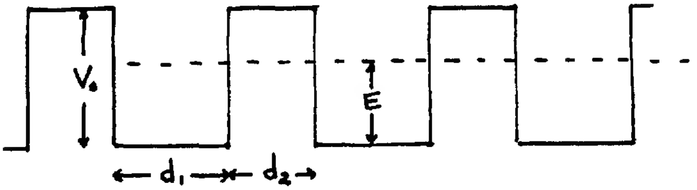

Figure 1. Periodic potential for Kronig-Penney particle model.

periodic potential, with abrupt edges, and period $d = d_1 + d_2$. We are interested in calculating the dispersion relation q(E), giving the dependence of wave vector q on the energy E, for a particle of mass m moving in that potential. We have learned to construct wave functions by joining known solutions in the different sections: in section 1, as shown in Figure 2, the particle's energy is such that its wave vector k_1 is real, while in section 2, because we have chosen $E < V_0$, the wave vector κ_2 is imaginary. In other words, in section 1 the wave function is sinusoidal, while in section 2 it is exponential or hyperbolically-sinusoidal. In joining the pieces of wave function together, we must follow some simple boundary conditions, which guarantee continuity of the wave function and its first derivative.

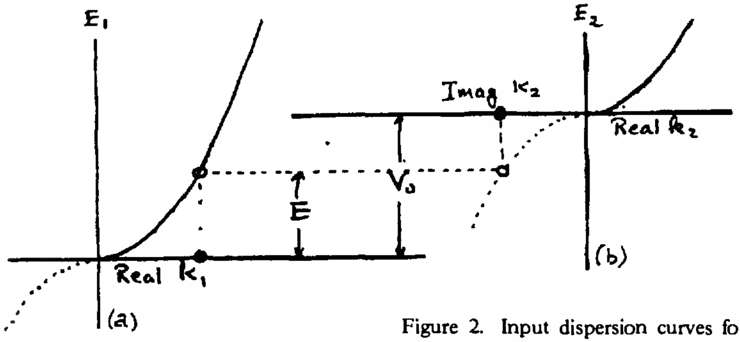

Figure 2. Input dispersion curves for a particle in the Kronig-Penney model. (a) is for section 1, while (b) is for section 2, offset in energy by V_0. At the energy E depicted, the wave vector is real in section 1, imaginary in section 2.

The required dispersion relation is then given by:

$$\cos(qd) = \cos(k_1d_1)\cosh(\kappa_2d_2) + 1/2[\kappa_2/k_1 - k_1/\kappa_2]\sin(k_1d_1)\sinh(\kappa_2d_2).$$

In this relation, the energy, E, is contained implicitly in k_1 and κ_2 through the dispersion relations shown pictorially in Figure 2. For those values of E for which $|\cos(qd)| < 1$, two real values of q emerge as solutions, within the range $|qd| < \pi$, representing two counterpropagating sinusoidal waves.

Figure 3 is a sketch of a dispersion curve which represents such solutions. For values of E for which $|\cos(qd)| > 1$, q must be complex, indicating that there are no propagating solutions. The gaps in the energy spectrum depend on all the input parameters: m, V_0, d_1, and d_2. For very strong barriers, i.e. large values of κ_2 and d_2, the energy bands in Fig.3 will be quite flat, corresponding to particles strongly confined between barriers.

Now we are going to do the same exercise for *phonons* in a one-dimensional superlattice. We construct a superlattice from segments of diatomic chains, as shown in Figure 4. The dispersion curves for LO and LA phonons in each segment are also shown in this figure. They are quite familiar, except that we must also use the portions of the curve which have imaginary and complex wave vectors, just as we did above for the particle which must tunnel between wells. The superlattice will be found to have modes at frequencies which are normally not found in one or the other of its constituents. In these, the phonon has to "tunnel" through the barriers to connect segments where it can propagate freely.

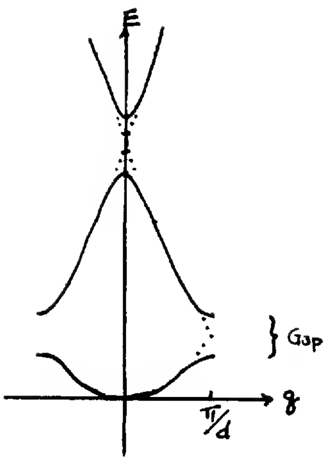

Figure 3. Resulting dispersion curve for a particle in the Kronig-Penney model. The periodic potential has allowed us to shrink our span of view to the range $|q| < \pi/d$, and has opened gaps in the energy spectrum at $q = 0$ and π/d.

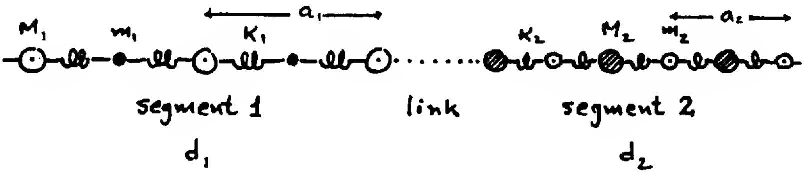

Figure 4. Model for constructing linear chain superlattice. Each of the two segments is diatomic, and has dispersion curves as shown, depending on masses and spring constants. The frequency is real so the wave vectors must be complex in the frequency "gaps."

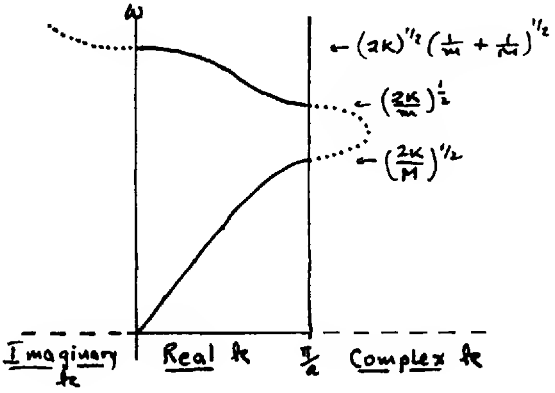

Assuming an elastic link between neighboring segments, the boundary conditions analogous to those for the particle's wave function can be stated, in terms of continuity of displacement and force. Now the superlattice phonon dispersion curve can be found:

$$\cos(qd) = \cos(k_1 d_1)\cos(k_2 d_2) + [*\#*!]\sin(k_1 d_1)\sin(k_2 d_2).$$

The form of this equation is identical to that found above, except that the term in the brackets, [*#*!], is somewhat more disagreeable, owing to the extra complication of the diatomic lattices. In this case, two separate amplitudes, whose complex ratio is frequency dependent, must be kept in mind, and in the equations. The serious student is urged to study carefully the explication of this subject by Colvard, et al.[6]

Figure 5 shows how the dispersion curve for the superlattice is related to those of its constituents. It is taken from Colvard, et al,[6] and is meant to represent the longitudinal modes of a GaAs-AlAs superlattice with d_1(GaAs) = 5a and d_2(AlAs) = 4a, where GaAs and AlAs share the lattice parameter a. The dashed lines are AlAs modes and the full lines those of GaAs.

The first thing to notice is that the Brillouin Zone for the superlattice is 9 times smaller than that of the constituents, for propagation along the growth axis. The most immediate and general consequence of a superlattice structure is Brillouin *zone-folding,* quite independent of models or computational techniques. A superperiod leads immediately to a reduced Brillouin zone. In principle there is then a multiplicity of zone-center modes, giving rise to new Raman-active modes among both acoustic and optical branches. While their existence is model-independent, their explication is not, and their observation and behavior depend on the real physical properties of the constituents, their interfaces, and their interaction, just as the gaps in electronic spectra as in Figure 3 depend on the real physical parameters.

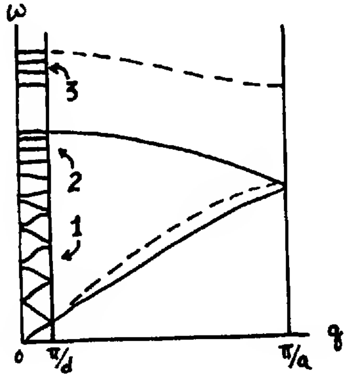

Figure 5. Dispersion relation for superlattice phonons, within the reduced zone $|q| < \pi/d$, showing both zone-folding of acoustic phonons (1) and confinement of optical phonons (2) and (3). Constructed to resemble a GaAs-AlAs superlattice by Colvard, et al[6].

Most of these phenomena were predicted by Rytov[7], who considered vibrations in layered elastic continuous media. In the long wavelength, low frequency limit, the ugly bracket above becomes simple:

$[*\#*!] = -(1 + r^2)/2r$, where $r = \rho_2 v_2/\rho_1 v_1$, with ρ being density and v velocity.

The zone-folded longitudinal acoustic modes (arrow 1 in Figure 5) are now well studied by Raman spectroscopy and well understood in semiconductor superlattices with sharp interfaces, and are being used to study the quality of as-grown interfaces, as well as the interdiffusion of constituents upon annealing. Gaps in the frequency spectra are expected at zone-edge and zone-center and have been observed in Raman spectroscopy.

In one of the earliest experiments on acoustic superlattice phonons, Narayanamurti, et al[8], used a superconducting junction phonon spectrometer to show gaps in the spectrum of propagating, ballistic phonons in a GaAs-AlGaAs superlattice. This technique has lain dormant, but has recently been revived and improved by the addition of time-resolved phonon imaging by Hurley, Tamura, Wolfe, and Morkoc.[9] They were able to observe the phonon stop-bands for high frequency LA and TA phonons which were brought on by the zone-edge and zone-center gaps, and in addition found a new intrazone stop-band due to off-axis coupling between LA and TA modes.

Longitudinal optical modes are also rather well studied. Here, the basic phenomenon, in addition to zone-folding, is *confinement*, strongly analogous to the electronic confinement mentioned above. Arrows 2 and 3 in Figure 5 are pointing to confined optical modes: at 2, the frequencies are those of GaAs, so GaAs is the confining well and AlAs is the barrier; while at 3, the opposite is the case. At arrow 3 are depicted four confined optical modes: they can be indexed by the number of half-waves of optical phonon which fit into the segment of AlAs. The flatness of their dispersion curves expresses the weak coupling between AlAs segments: these are frequencies at which the GaAs wave vector is imaginary and very large, and so there is little or no "tunneling" through the GaAs segments. Confined optical modes of many orders have been observed,[10] and their frequencies compared with the simple models, leaving some small but worrisome discrepancies. The models calculate the mode wavelengths within the layers, taking account of finite tunneling, and try to relate the observed frequencies to the bulk mode frequencies at that wavelength, using known dispersion curves. It is not yet known whether the discrepancies are in the models or in the bulk dispersion curves, which are not generally well determined. The most striking defect of the models is their failure to allow for any long-range, or even moderate-range, interactions: the frequency spectrum is assumed to be a local property of a chain segment. Long-range interactions provide, I believe, one of the most important unsolved theoretical problems in understanding superlattice phonons. For propagation obliquely or perpendicular to the axis, in superlattices made of polar semiconductors, there is as yet no adequate description of the optical modes. Some attempts will be described later.

One of the most notable recent contributions to the study of axial or one dimensional phonons in superlattices is the work of Merlin, et al[11], on quasi-periodic structures. Inspired by much recent work on icosahedral quasi-periodic "crystals," they set out to study epitaxially grown structures with a quasi-periodicity in the growth direction. Their recipe was the Fibonacci sequence: layer n is identical to the sum of layers n-2 and n-1... Such structures they called Fibonacci superlattices, and they are interesting because although they have no periodicity, they do have well defined Fourier transforms, with delta-function "Bragg peaks." Thus, though there is no Brillouin zone, there should be a well defined structure to their Raman spectra, analogous to the well defined X-ray diffraction patterns that they possess.

A Fibonacci superlattice, because of its quasi-periodicity, has no reciprocal lattice, but a multitude of quasi-reciprocal-lattice points, given by the expression:

$$q = q_{n,m} = 2\pi(m + n\tau)/(d_2 + \tau d_1),$$

where d_1 and d_2 are the thicknesses of the first two layers in the sequence, τ is the golden mean, $\tau = (1 + \sqrt{5})/2$, and m and n are Fibonacci numbers. This implies that acoustic modes with such wave vectors should be zone-folded back to the center of the Brillouin Zone, and might thereupon become Raman active. They might also, in analogy with the folded-zone acoustic modes in periodic superlattices, have gaps in their spectra.

Both phenomena appear to have been observed. Merlin, et al, studying Raman spectra of a GaAs - AlAs Fibonacci superlattice, found a continuum response in the acoustic frequency range attributable to defect-activated scattering, but with gaps in the spectra which they were able to index with the expected "strong" quasi-reciprocal-lattice points found to be those with neighboring Fibonacci numbers and having the form :

$$q = 2\pi/(d_2 + \tau d_1)\tau^p.$$

More recently Dharma-wardana, et al,[12] have observed peaks in Raman spectra of Fibonacci superlattices of Si - Ge_xSi_{1-x}, which were similarly identifiable as the new pairs of Raman peaks brought near zone center by the "strong" quasi-zone-folding. There seems to be genteel agreement that both results are reasonable, given the differences in the structures and the experiments.

I have constructed Figure 6, to represent the quasi-zone-folding found in Fibonacci superlattices. Since reciprocal space is dense with "Bragg peaks," it is reasonable to choose a few which are suspected of being "strong." Following Dharma-wardana, et al, I have chosen to portray those with p = 0, ± 1. The circles and crosses then represent their observed frequencies. Merlin, et al, can then be supposed to have observed the partial gaps in the acoustic continuum.

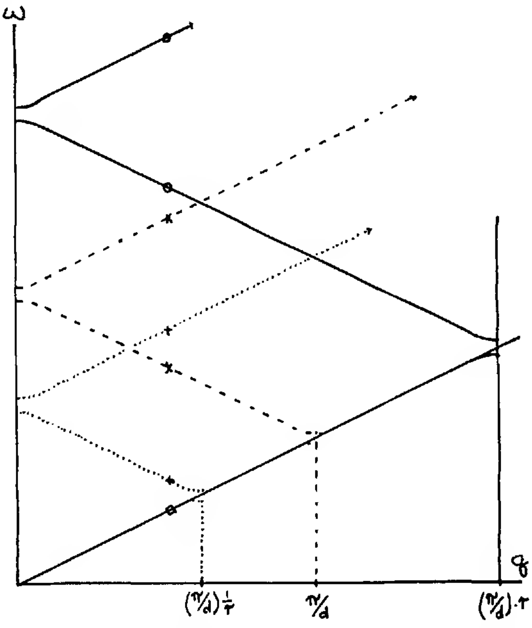

Figure 6. Schematic folding of the Brillouin Zone for the axial LA phonon in a Fibonacci superlattice. Three foldings are shown, corresponding to quasi-reciprocal-lattice points (qrl points) $q = 2\pi/d)(1/\tau)$ - dotted line; $q = 2\pi/d$ - dashed line; and $q = (2\pi/d)(\tau)$ - full line. The corresponding pairs of Raman lines are shown as vertical crosses, diagonal crosses, and circles, and the Brillouin scattered line is marked with the open box. Note that each branch folds only once, suggesting that the harmonics of the qrl points are not themselves qrl points. The gaps in the frequency spectrum shown are probably realistic, i.e. non-zero, but perhaps there should also be gaps where the branches cross each other. Who knows?

There has been some work on periodic superlattices with more than two layers per period, and these are sometimes referred to as *polytypes.*[13] They seem to me to be curiosities showing no essentially new phenomena not seen in the bi-layer superlattices, except perhaps that a thin layer connecting two dissimilar thick layers can be made as a model of controlled interface properties.

Once we depart from the simple, one-dimensional world, with propagation along the axis, the phonons of superlattices look much more complicated. I know of no lattice-dynamical calculation which even attempts to comprehend oblique propagation, starting with an atomic-level model.

Several experiments, however, suggest that it is possible to observe non-axial phonons by Raman scattering. Zucker, et al,[14] in a unique experiment measuring light scattered perpendicular to the superlattice axis, were able to observe confined optical modes with finite in-plane wave vector. Because of the confinement, the modes observed occurred with reversed polarization selection rules: the mode with polarization along the propagation direction had a TO frequency, while the mode polarized along the axis was LO in character. S. A. Lyon and I have sought to reinterpret these results in a slightly different way.[15] We suppose that the modes observed may not be confined, but may have a large apparent axial wave vector because of the resonant, and confined, excitation. If this is the case, then when the layers between excitation regions are alloy, this technique affords a novel way to probe the vibrations of alloys, by exciting optical modes at the surfaces of the alloy layers.

The other class of observations that is interpreted in terms of non-axial modes involves *interface phonons.* Since their initial invocation by Sood, et al,[16], they have been noticed in several different systems, though their appearance is somewhat mysterious. An interface mode is expected at the interface between two dissimilar dielectrics, as for example the surface mode found at the interface between a vacuum and a polar crystal. Such modes propagate along the interface, with exponential spatial dependence perpendicular to the interface, and with frequency intermediate between LO and TO. In a superlattice of many interfaces there are many interface modes which interact to provide a continuum of possibilities, with wave vector both axial and in-plane.

Pokatilov and Beril[17] have worked out dispersion expressions for these interface modes in superlattices. By now it will surprise no one to learn that the dispersion is given in implicit form by:

$$\cos(k_z d) = \cosh(k_x d_1)\cosh(k_x d_2) + [(\eta^2 + 1)/2\eta]\sinh(k_x d_1)\sinh(k_x d_2),$$

where η is the ratio of the frequency-dependent dielectric functions, k_z and k_x are axial and in-plane propagation vectors, d_1 and d_1 are the layer thicknesses, and d is the superlattice period.

The mystery associated with observation of interface modes arises because they have been observed in axial back-scattering experiments, in which there is little or no in-plane momentum transfer, so one has to posit a defect mechanism in order to generate theoretical interface modes with the observed frequencies.[18] Perhaps the interfaces, themselves, possess enough roughness to account for the observation of interface modes, but eventually one would like some correlation between the intensity of the interface-mode scattering and some other physical property.

Other continuum theories of superlattice phonons have been suggested, notably that of Merlin, et al,[19] who model the superlattice as a strongly uniaxial dielectric, with dielectric functions depending on those of the constituents. The zeroes and poles give the LO and TO frequencies, in the long wavelength limit.

The real problem, of course, is to take account, in the same theory, of both the atomic nature of the superlattice with details of the short-range interactions, and the long-range, Coulomb interactions, especially for polar semiconductors.

Phonons propagating obliquely and in-plane in semiconductor heterostructures and superlattices, while not yet well understood, are among the most important from the point of view of their practical consequence. They are the ones, of course that interact with carriers, providing thermalization and momentum relaxation. This makes them interesting not only to the academic physicist but also important to the applied physicist wishing to understand modern electronic devices.

ACKNOWLEDGMENTS

I wish to thank Prof. T. Paszkiewicz and the other organizers of the 23rd Winter School of Theoretical Physics at Karpacz for their generosity and hospitality; I am grateful to the students at both the Winter School and the Karpacz Kindergarten for their enthusiasm; I acknowledge many enlightening conversations with R. E. Nahory, M. V. Klein, and S. A. Lyon; and I thank L. Farrow, A. H. MadDonald, D. Hurley, J. P. Wolfe, and their coworkers for giving me access to their work prior to its publication.

REFERENCES

1. L. Esaki and R. Tsu, IBM Journ. Res. Develop. 14, 61 (1970).
2. M. V. Klein, IEEE J. Quantum Electron. QE-22, 1760 (1986).
3. J. M. Worlock, in Proceedings of the Second International Conference on Phonon Physics, Budapest, 1985, edited by J. Kollár, N. Kroó, N. Menyhárd, and T. Siklós, World Scientific Publishing Co, (Singapore) 1985.
4. B. Jusserand, in Lecture Notes for Winter School at Les Houches, France, "Superreseau et Heterojunctions de Semiconducteurs," Springer-Verlag, 1985.
5. Proceedings of the Tenth International Conference on Raman Spectroscopy, Eugene, OR, 1986, edited by W. L. Peticolas and B. Hudson, University of Oregon Printing Department, (Eugene, OR) 1986.
6. C. Colvard, T. A. Gant, M. V. Klein, R. Merlin, R. Fischer, H. Morkoc, and A. C. Gossard, Phys. Rev. B31, 2080 (1985).
7. S. M. Rytov, Akust. Zh. 2, 71 (1956) [Soviet Physics-Acoustics 2, 67 (1956)].
8. V. Narayanamurti, H. L. Stormer, M. A. Chin, A. C. Gossard, and W. Wiegmann, Phys. Rev. Letters 43, 2012 (1979).
9. D. C. Hurley, S. Tamura, J. P. Wolfe, and H. Morkoc, private communication.

10. See, for example, A. K. Sood, J. Menendez, M. Cardona, and K. Ploog, Phys. Rev. Letters 54, 2111 (1985).

11. R. Merlin, K. Bajema, R. Clarke, F.-Y. Juang, and P. K. Bhattacharya, Phys. Rev. Lett. 55, 1769 (1985).

12. M. W. C. Dharma-wardana, A. H. MacDonald, D. J. Lockwood, J. -M. Baribeau, and D. C. Houghton, Phys. Rev. Letters 58, 1761 (1987).

13. M. Nakayama, K. Kubota, S. Chika, H. Kato, and N. Sano, Solid State Commun. 58, 475 (1986).

14. J. Zucker, A. Pinczuk, D. S. Chemla, A. C. Gossard, and W. Wiegmann, Phys. Rev. Letters 53, 1280 (1984).

15. S. A. Lyon and J. M. Worlock, to be published.

16. A. K. Sood, J. Menendez, M. Cardona, and K. Ploog, Phys. Rev. Letters 54, 2115 (1985).

17. E. P. Pokatilov and S. I. Beril, phys. stat. solidi (b)110, K75 (1982) and (b)118, 567 (1983). Similarly, superlattice plasmons were explored by R. E. Camley and D. L. Mills, Phys. Rev. B29, 1695 (1984).

18. G. P. Schwartz, G. J. Gualtieri, W. A. Sunder, and L. A. Farrow, Phys. Rev. B, to be published.

19. R. Merlin, C. Colvard, M. V. Klein, H. Morkoc, A. Y. Cho, and A. C. Gossard, Appl Phys. Letters 36, 43 (1980).

NONERGODIC BEHAVIOUR AND PHONON LOCALIZATION AT STRUCTURAL PHASE TRANSITIONS

N.M. Plakida
Joint Institute for Nuclear Research, Dubna, USSR

A dynamical ergodic-nonergodic phase transition as a result of the localization of order-parameter fluctuations (soft phonons freezing) at structural phase transitions is discussed. Connection between the nonergodic behaviour and appearance of precursor clusters and central peak phenomena is considered.

1. INTRODUCTION

Recent experimental and theoretical investigations/1,2/ have shown that under certain conditions a crossover from a displacive (soft mode behaviour) to an order-disorder regime takes place near structural phase transitions (SPT). This results in a two-time scale behaviour with a slow relaxation of the Ising-type (central peak phenomena) and a frozen soft mode. As the renormalization group calculations show/3,4/, there exists some temperature $T_g > T_o (T_c$ - is the phase transition temperature) where this crossover occurs. $T_g - T_c$ becomes the larger the lower the lattice dimensionality and the shorter the range of forces.

As a reason for such a peculiar critical behaviour the existence of precursor clusters is now generally accepted. A direct proof of this picture is possible now only for low demensional system that allow analytical solutions. As was shown in/5/ the critical behaviour of the one-dimensional system is determined by the dynamics of virtual domain walls whose diffusion results in a central peak in the scattering function. A qualitative change occurs also in the behaviour of the soft phonon mode/6/.

However, at present there is no unique answer to the question whether there exist stable formations of the type of clusters of short-range order in the real three-dimensional space. For this reason it is rather difficult to interpret the experimental data many of which point to the existence of clusters in the real systems/2/. Therefore, it would be very desirable to establish a general criterion for the appearance of clusters of short-range order which show the Ising-like behaviour.

For this purpose let us consider the nonergodicity of a local atomic displacement above T_c as a characteristic feature of the Ising-like behaviour of the system. For nonergodic systems the usual thermodynamical averaging and the time averaging lead to different results. In particular, as has been shown by Kubo[7], the isothermal thermodynamical susceptibility χ^T_{AB} is not equal to the isolated one χ^K_{AB}, and a general equation holds:

$$\beta L_{AB} = \chi^T_{AB} - \chi^K_{AB} = \lim_{t\to\infty} \beta \langle \Delta A(t) \Delta B\rangle \neq 0, \qquad (1)$$

where $\Delta A = A - \langle A\rangle$, $\langle\ldots\rangle$ is the thermodynamical average, $\chi^T_{AB} = \partial\langle A\rangle/\partial h_B$, (h_B is the field conjugated to the thermodynamical variable $\langle B\rangle$), $\chi^K_{AB} = -\langle\langle A|B\rangle\rangle_{\omega=0}$, $\langle\langle A|B\rangle\rangle$ is the commutator Green function (see e.g.[8]). According to Suzuki[9] integrals of motion cause nonvanishing long-time correlations that bring about the difference between the isothermal and isolated susceptibilities:

$$L_{AB} = \sum_{\nu} \langle \Delta A K_\nu\rangle \left(\langle K_\nu^2\rangle\right)^{-1} \langle K_\nu \Delta B\rangle \geqslant 0 \qquad (2)$$

where K_ν compose an orthogonal set of integrals of motion, i.e. $[K_\nu, H] = 0$ and $\langle K_\nu K_\mu\rangle = \delta_{\mu,\nu}\langle K_\nu^2\rangle$. Therefore, the condition (1), $L_{AB} \neq 0$ as was proposed in[10], can be considered as a criterion for the appearance of nonergodic Ising-like behaviour of the system. As has been pointed out by Schreiber[11], the criterion (1) can be considered also as a criterion of localization since it is indeed connected with the existence of local integrals of motion in eq.(2).

The proposed criterion for the appearance of clusters of short-range order in a certain sense is a generalization of the idea by Feder[12] who has proved that above T_c order-parameter clusters yield difference between the isothermal and adiabatic susceptibility. The origin of the nonergodicity in this case can be thought of as due to a local spontaneous symmetry breaking inside the clusters. The only difference with the nonergodicity in a low symmetry phase where the order parameter is a nonergodic quantity[13] is that the clusters have finite sizes and lifetimes (for discussions see[1]).

A microscopic self-consistent theory for a dynamical ergodic-nonergodic phase transition has first been developed by Götze[14] and applied recently for discussions of localization in a number of models (see[15]).

In the present lecture the nonergodic behaviour is discussed in two models of structural phase transition: scalar lattice φ^4 model [9,16] and the transversal Ising model[17].

2. CALCULATION OF LOCALIZATION CONSTANT

We consider a model of coupled anharmonic oscillators usually used to study structural phase transitions both of the displacive and order-disorder types (see[1]):

$$H = \sum_{\ell} \left(\frac{1}{2}\Pi_\ell^2 - \frac{1}{2} A Q_\ell^2 + \frac{1}{4} B Q_\ell^4 \right) + \frac{1}{4} \sum_{\ell\kappa} C_{\ell\kappa} \left(Q_\ell - Q_\kappa \right)^2 \tag{3}$$

where Π_ℓ and Q_ℓ are canonically conjugated local normal momenta and coordinates. The single-site potential in (3) describes an anharmonic oscillator with the negative harmonic force constant $- A < 0$ and the quartic anharmonic interaction of strength B . The harmonic force constant $C_{\ell\kappa}$ couple these oscillators on a d-dimensional lattice, $\ell = 1, \dots, N$.

To study relaxation processes in the model we introduce the isothermal relaxation function[18]

$$\phi_{\ell\kappa}(t) \equiv \left(u_\ell(t) | u_\kappa \right) = \int_0^\beta d\tau \langle u_\ell(t - i\tau)\, u_\kappa \rangle \tag{4}$$

where $\langle \dots \rangle$ defines the thermodynamical average, $u_\ell(t) = Q_\ell(t) - \langle Q_\ell \rangle$ is the time-dependent displacement operator. The initial value of (4) determines the static isothermal susceptibility: $\phi_{\ell\kappa}(t=0) = \chi^T_{\ell\kappa}$. If the displacements $u_\ell(t)$ do not behave ergodically, their correlation function does not decay in the limit $t \to \infty$. The corresponding localization (or nonergodicity) constant (1) can be determined in the following way:

$$\begin{aligned} L_{\ell\kappa} &= \lim_{\varepsilon \to 0} \varepsilon \int_0^\infty dt\, e^{-\varepsilon t} \langle u_\ell(t)\, u_\kappa \rangle = \\ &= \frac{1}{\beta} \left(\chi^T_{\ell\kappa} - \chi^K_{\ell\kappa} \right) = \lim_{z \to i0^+} z\, \phi_{\ell\kappa}(z) \end{aligned} \tag{5}$$

where $\phi_{\ell\kappa}(z) \equiv ((u_\ell | u_\kappa))_z = -i \int_0^\infty dt\, e^{izt}\, \phi_{\ell\kappa}(t)$ is the Laplace transformation of (4).

By applying the projection-operator technique/18/ that is equivalent to the continued fraction expansion of Mori, one obtains for the relaxation function in the q -representation:

$$\Phi_q(z) = \sum_l \Phi_{kl}(z)\, e^{i\vec{q}\vec{l}} = \chi_q^T \frac{1}{z - \dfrac{1/\chi_q^T}{z - M_q(z)}} \tag{6}$$

The relaxation kernel $M_q(z)$, or the self-energy operator, is given by the irreducible part of the second order (see/18/) and in the mode coupling approximation (cf./15/) can be written as:

$$M_{lk}(z) = B^2 ((u_l^3 / u_k^3))_z^{(2)} \approx -i B^2 \int_0^\infty dt\, e^{izt} \int_0^\beta d\tau \langle u_l(t-i\tau)\, u_k\rangle^3 \tag{7}$$

where the correlation function is given by:

$$\langle u_l(t)\, u_k\rangle = -\frac{1}{\pi}\int_{-\infty}^{\infty} d\omega\, e^{-i\omega t} \frac{\omega}{1-e^{-\beta\omega}}\, \mathrm{Im}\, \Phi_{lk}(\omega+i\epsilon)\ . \tag{8}$$

In this approximation the corrections of vertices are neglected which we believe to be unimportant at least outside the critial region, since the bare anharmonic interaction in the model (3) is a nonsingular function.

The static limit for the relaxation function (6) yields the nonergodicity constant (5) in the form

$$\beta L_q = \lim_{z\to i0} [z\,\Phi_q(z)] = \chi_q^T - \left(1/\chi_q^T + S_q\right)^{-1} \tag{9}$$

where $S_q = \lim_{z\to i0} z\, M_q(z)$.

The singular part of (7) is defined by the nonergodic contribution (5) of the correlation function (8) and after integration the q -representation of eq.(7) can be written as

$$M_q(z) = \frac{1}{z}\, 6\beta B^2 \frac{1}{N^2} \sum_{q_1 q_2} L_{\vec{q}_1} L_{\vec{q}_2} L_{\vec{q}_1+\vec{q}_2-\vec{q}} + M_q^{reg}(z) \tag{10}$$

where $M_q^{reg}(z)$ is the regular part of the relaxation kernel: $\lim_{z\to i0} z\, M_q^{reg}(z) \to 0$. Now, assuming that the static isothermal susceptibility is known, one obtains a closed set of equations (9),(10) for the nonergodicity constant L_q .

3. NONERGODIC PHASE TRANSITION

Let us first discuss qualitatively the self-consistent equation (9) for the nonergodicity constant L_q . If we assume the system (3) to undergo a SPT of the ferrodistortive type at some temperature T_c, then its susceptibility at $\tau = T/T_c - 1 \to 0$ can be written in the form:

$$\chi_q^T = \left(a|\tau|^\gamma + C_0 - C_q \right)^{-1} \tag{11}$$

where $C_q = \sum_\ell C_{K\ell} \exp(i\vec{q}\vec{\ell})$, $C_0 = C_{q=0}$.

For further discussions the self-consistent eq.(9) can be written in a more convenient form (cf./15/):

$$\frac{\beta L_q / \chi_q^T}{1 - \beta L_q / \chi_q^T} = \chi_q^T S_q \approx \chi_q^T 6\beta B^2 \frac{1}{N^2} \sum_{q_1 q_2} L_{\vec{q}_1} L_{\vec{q}_2} L_{\vec{q}_1 + \vec{q}_2 - \vec{q}} \tag{12}$$

Since $L_q \geqslant 0$ solutions of eq.(12) can be obtained only in the interval: $0 \leqslant \beta L_q/\chi_q^T \leqslant 1$. A simple graphical analysis of eq.(12)shows that there is always a trivial solution $L_q = 0$; but for a sufficiently high susceptibility χ_q^T and coupling constant B a pair of nonzero solutions, $L_q^{(1)} \leqslant L_q^{(2)}$ is also possible. Particularly, for $q = 0$ and $\tau \to 0$ the susceptibility (11) on the right-hand side of eq.(12) becomes divergent that brings about the solution $\beta L_q/\chi_q^T \to 1$ on the left-hand side of eq.(12). For $\beta L_q \approx \chi_q^T$ one can prove that $S_q \sim \ln|\tau|$ which even enhances this divergences as $\tau \to 0$.

Therefore, in the vicinity of T_c($\tau \to 0$) the long-wave-length fluctuations in the system undergoing a SPT should be described as nonergodic (Ising-like) ones, $\chi_q^T \approx \beta L_q$, with the Kubo susceptibility being finite, $\chi_q^K = [1/\chi_q^T + S_q]^{-1} \ll \chi_q^T$. For a sufficiently small susceptibility χ_q^T, e.g. far from the phase transition temperature T_c, there is only the trivial solution $L_q = 0$ of eq.(12) and the Kubo susceptibility is equal to the isothermal one: $\chi_q^K = \chi_q^T$.

This simple analysis of eq.(12) clearly shows that the model (3) should exhibit a dynamical phase transition from an ergodic ($L_q = 0$) to a nonergodic ($L_q \neq 0$) state at some temperature T_g with a nonzero solution in the temperature range $T_c \leqslant T \leqslant T_g$. As in the liquid-glass transition with nonlinear coupling/15/ the nonzero solutions $L_q^{(1)} \leqslant L_q^{(2)}$ appear discontinuously at $T = T_g$: $L_q^{(1)}(T_g) = L_q^{(2)}(T_g)$ where only a large solution $L_q^{(2)}$ is stable.

The numerical investigation of eq.(9) was performed in a single-site approximation for the relaxation kernel (7): $M_{\ell K}(z) \approx \delta_{\ell K} M(z)$. This results in the $\vec{q}$-independent S_q : $S = 6\beta B^2 L^3$, where the single-site nonergodic constant $L = L_{KK}$ was calculated self-consistently from eq.(9): $L = 1/N \sum_q L_q$. For integration over $\vec{q}$ in this equation the static susceptibility (11) with a=A, γ =1 and anisotropic spectrum of order parameter fluctuations $C_0 - C_q = C_0(\varkappa^2 K_\perp^2 + K_z^2)$ were used (here $K_\perp = q_\perp / q_0$ and $K_z = q_z / q_0$ are the dimensionless wave vectors, z -axis is directed along the displacements u_l and $\varkappa$ is the anisotropy constant).

The results of numerical solution for $l(\tau) = L(\tau)/(A/B)$ are shown in Figs. 1,2 for some parameters $f_0 = C_0/A$ and $\varkappa$.

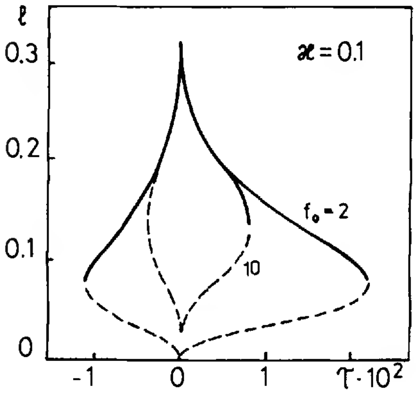

Fig.I.

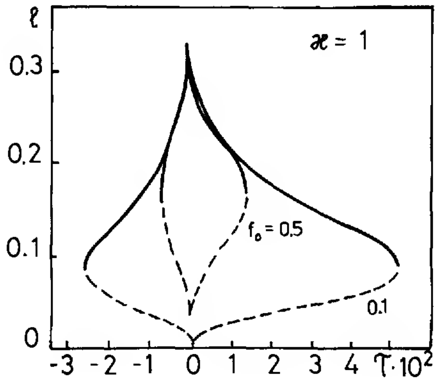

Fig. 2.

At $\tau = \tau_g(f_0, \varkappa)$ the nonergodic solutions $l_1 = l_2 = l_g$ appear discontinuously and for $\tau < \tau_g$ we have $l_1 < l_g < l_2$. The lesser solution l_1 (broken curve) is dynamically unstable/15/ and only l_2 (full curve) has the physical meaning. The nonzero solutions exist only for certain values of f_0 : $f_0 < f_g$ where the value of f_g increases with the anisotropy $\varkappa$: e.g. $f_g \approx 0.85$ for $\varkappa = 1$ and $f_g = 20$ for $\varkappa = 0.1$ (for details see/10/).

The influence of defects on the phase transition to a nonergodic state in the model (3) was investigated in/16/ by introducing the random parameters A_l , B_l : $A_l = A_D \lessgtr 0$, $B_l = B_D > 0$ at defect sites l and $A_l = A > 0$, $B_l = B > 0$ otherwise. The presence of defects considerable increases τ_g (and, correspondingly, f_g) whereas the maximum value of $l = l(\tau = 0)$ depends only slightly on the defect concentration. The transition to the nonergodic state becomes also "more continuous": $l_g \to 0$ with increasing the defect concentration (for details see/16/).

The comparison of our results with computer simulations and

and with experimental results (see/1,2/) suggests that the nonergodic behaviour of the model is connected with the apearance of precursor order clusters as discussed in the introduction. The size of these clusters is given by the spatial dependence of the nonergodicity constant. By the Fourier transformation of (9) one obtains with $S_q \approx S = 6\beta B^2 L^3$ and $\varkappa = 1$

$$L_{\ell K} = L(R) \sim \frac{1}{R}\left\{\exp(-R/\xi_0) - \exp(-R/\xi_1)\right\}, \quad R = q_0 |\vec{l} - \vec{K}| \qquad (13)$$

where $\xi_0 = f_0/\tau$, $\xi_1 = f_0/(\tau + \Delta)$, $\Delta = S/A$.

In this way the appearance of the localization constant (5) yields a quantitative criterion of the corssover from the soft mode dynamics to the Ising-like behaviour. For $f_0 > f_g$ there is only a pure displacive regime (if one neglects $L_{q=0}(\tau = 0) \neq 0$) but for $f_0 < f_g$ the localization constant $L_{KK} = (1/N)\sum_q L_q$ appears discontinuously at some temperature T_g which also determines the temperature of the crossover from the displacive to order-disorder (Ising-like) behaviour.

The nonergodic behaviour and the existence of precusor clusters naturally explains the observed narrow central peak in neutron scattering experiments: $S_{cp}(q,\omega) = (T/T_1)\,\mathrm{Im}\,\phi_q^{cp}(\omega + i\varepsilon) = L_q\,\delta(\omega)$, where L_q is given by eq.(9). The elastic central peak of the present theory idealizes the real situation. Physically, this central peak corresponds to the Ising-like behaviour of the φ^4-model in the critical region as it has been detected by the static renormalization group technique/3,4/. In order to get the critical dynamics for an Ising-system, additional relaxational mechanisms have to be included (cf. the Glauber-model).

In conclusion we briefly discuss some results of the investigation/17/ of the transversal Ising-model that is an extreme limit(for $f_0 = C_0/A \ll 1$) of the model (3). The two parameters of the model: the tunnelling frequency Ω and the effective coupling constant $J_{\ell K} = 4C_{\ell K}\cdot(A/B)$, define the dynamical ergodic-nonergodic phase transition. By applying the method of calculation described in Sec.2 for the relaxation functions $\phi_{\ell K}^{\alpha\beta}(t) = (S_\ell^\alpha(t)|S_K^\beta)$ and the nonergodic constants $L_{\ell K}^{\alpha\beta}$ for the pseudo-spin operators $S_\ell^\alpha(t)$, $\alpha = x, y, z$ the following results were obtained.

For a sufficiently small transversal field ($\Omega < \Omega_c^0 \approx 0.05\,J_0$) the system behaves nonergodically at any temperature in paraphase:

both L_{kk}^{zz} and L_{kk}^{xx} are nonzero for $T_c \leqslant T < \infty$ (T_c is the temperature of phase transition to the ordered state with $\langle S_\ell^z \rangle \neq 0$). For $\Omega > \Omega_c^0$ a nonergodic behaviour is possible only for $T_c \leqslant T \leqslant T_g$, where $T_g \to T_c$ for $\Omega \to \Omega_c$ (Ω_c is an upper critical value: $T_c = 0$ for $\Omega > \Omega_c \approx 0.5 J_0$). The latter nonergodic behaviour seems to be due to the appearance of short-range-order clusters in the vicinity of phase transition as in the case of φ^4-model described above.

The last remark is that the nonergodic behaviour discussed in this lecture has much in common with the nonergodic dynamics in glasses and spin glasses (see e.g., /15,18/).

Acknowledgement

The author is indebted to Professor W.Götze for many valuable discussions.

REFERENCES

1. A.D.Bruce, R.A.Cowley. Structural Phase Transitions. Taylor and Francis, London, 1981.
2. K.A.Müller. In: Statics and Dynamics of Nonlinear Systems. Springer, Berlin, 1983, p. 68.
3. P.D.Beale, S.Sarker, J.A.Krumhansl. Phys.Rev. B24, 266 (1981).
4. G.A.Barker (Jr), A.R.Bishop. J.Phys. A15, L201 (1982).
5. J.A.Krumhansl, J.R.Schrieffer. Phys.Rev. B11, 3535 (1975).
6. V.L.Aksenov, A.Yu.Didyk. Phys.Lett., A105, 368 (1984).
7. R.Kubo. J.Phys.Soc.Japan, 12, 570 (1957).
8. D.N.Zubarev. Nonequilibrium Statistical Thermodynamics, Plenum, New York, 1974, § 16.
9. M.Suzuki. Physica 51, 277 (1971).
10. V.L.Aksenov, M.Bobet, N.M.Plakida, J.Schreiber. J.Phys. C, 1987.
11. J.Schreiber. In: Proc. of Int.Seminar on Localization, Johnsbach, Teubner-Texte, Leipzig, 1983, p. 138;
    In: Proc. 5th Int.Seminar on Magnetism, Wissenschaftliche Zeitschrift der HfV, Dresden, 1984, p. 31.
12. J.Feder. Solid St.Comm. 9, 2021 (1971).
13. H.Thomas. In: Anharmonic Lattices, Structural Transitions and Melting. Noordhoff, Leiden, 1974, p. 231.
14. W.Götze. Solid St. Comm. 27, 1393 (1978); J.Phys. C12, 1279 (1979).

15. W.Götze. Zeit.Phys. B56, 139 (1984); In: Lectures delivered at Nato Advanced Study Institute on Amorphous and Liquid Materials (Italy, 1985). (Ed. M.Nijhoff) Dordrecht, 1986.
16. V.L.Aksenov, M.Bobet, N.M.Plakida, J.Schreiber. JINR, P17-86-299, Dubna, 1986.
17. V.L.Aksenov, M.Bobet, N.M.Plakida. Ferroelectrics, 1986.
18. S.L.Ginzburg. JETP 90 , 754 (1986).

SPECTRUM OF LOCAL FREQUENCIES FOR ORDERLESS SOLIDS

A. Czachor

Institute of Physics
Polish Academy of Sciences
02-668 Warsaw, Poland

Spectrum of local frequencies (Einstein frequencies) $E(\omega)$ is perhaps the best and the most direct measure of disorder ever invented: it is a distribution of a finite width, whereas for a crystal it consists of one or a few peaks of the δ- function type. This fact has been generally disregarded so far.

For monoatomic systems it has been shown that the spectrum of the normal mode frequencies $g(\omega)$ can be derived from $E(\omega)$. On taking the first order Raman spectrum for amorphous silicon as approximate representation of $g(\omega)$, the local frequency spectrum $E(\omega)$ has been found, for the first time. Neutron inelastic scattering also can be used to determine $E(\omega)$ for monoatomic systems. For multiatomic orderless solids these experiments lead to the function - $\mathrm{Im}\langle L(\omega + i\varepsilon)\rangle$, where $\langle L\rangle$ is the average locator Green's function for such system.

1. Definition of the local (Einstein) frequency

As a thought experiment let us freeze all atoms of a solid at their equilibrium positions, and then disturb one of them slightly. It begins to oscillate about its equilibrium position $\vec{R}$. We have the following equation of motion for its displacement $\vec{u}_{\vec{R}}$

$$M_{\vec R}\,\ddot{\vec u}_{\vec R} = -\overleftrightarrow{\Psi}_{\vec R}\,\vec u_{\vec R} \tag{1}$$

where $M_{\vec R}$ is the mass of the atom and $\overleftrightarrow{\Psi}_{\vec R}$ is the so called self-force matrix, characterizing the restoring force at $\vec R$. Such an equation describes oscillatory motion with the frequencies $\omega_{\vec R\nu}$ such that

$$\omega^2_{\vec R\nu} = \Psi_{\vec R\nu}/M_{\vec R}\ , \quad \nu = 1, 2, 3, \tag{2}$$

where the numbers $\Psi_{\vec R\nu}$ are the eigenvalues of the (symmetric and real) matrix $\overleftrightarrow{\Psi}_{\vec R}$. We shall call them the local frequencies or Einstein frequencies.

For many decades physicists have studied mainly crystals, where atoms have just one, or a few types of neighborhood, and one or a few local frequencies. For example, for a monoatomic crystal of a regular structure $M_{\vec{R}} = M$, $\overleftrightarrow{\Psi}_{\vec{R}} = \overleftrightarrow{1}\Psi$ and we have just one Einstein frequency $\omega_E = (\Psi/M)^{1/2}$, e.g. for Al $\omega_E = 3.83_{10}13$ rad/s. Figures for other crystals are to be found in Leibfried's papers [1]. This quantity, ω_E, has so far been of little interest as a characteristic of crystal dynamics, except perhaps for the Mossbauer effect. True, for monoatomic crystals of regular structure it is known to be related to the spectrum of the normal-mode frequencies $g(\omega)$ [2]

$$\omega_E^2 = \int g(\omega)\, \omega^2\, d\omega \equiv \langle \omega^2 \rangle_{BZ} \;.$$

Still, being such an average, ω_E carries little information about crystal dynamics, as compared with the abundance of information displayed in the available phonon spectra for crystals.

2. Spectrum of local frequencies

Contrary to crystals, in orderless (disordered) solids the neighborhoods of atoms are in general different. This results in different self-force matrices $\overleftrightarrow{\Psi}_{\vec{R}}$. Besides, we may have different atomic masses $M_{\vec{R}}$. It follows, there are many different local frequencies, their total number being the number of degrees of freedom for the system, 3N. We can introduce the spectrum of these frequencies, $E(\omega)$, such that $\int E(\omega)\, d\omega = 1$ and $3N\, E(\omega)\, d\omega$ is the number of local frequencies in the range $d\omega$. We expect that the local frequency spectrum for, e.g., an orderless Al, should compare with that for the crystal Al in the way shown schematically in Fig.1.

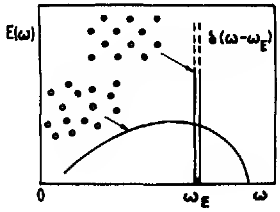

Fig.1.
Local frequency spectrum for a monoatomic crystal and for a corresponding orderless solid, schematically.

This picture shows that such a spectrum, by its very nature, should be a perfect notion to express a fundamental distinction between crystals and orderless solids - it is the difference between the δ-function (or a few of them) and a broad quasi-continuous distribution. The $E(\omega)$ provides us with statistical information on the fields of force the atoms move in. In the theory of solids we have no other physical characteristic, which would be more sensitive to the distinction between order and disorder than $E(\omega)$; perhaps only the distributions of the atomic-level stresses have a similar merit [3,4]. Therefore, this spectrum deserves attention and one should look for methods allowing one to establish it for orderless systems.

It is clear that one can determine $E(\omega)$ numerically, for finite harmonic systems, as a side product within the molecular dynamics scheme. So far, however, the importance of this spectrum has been generally disregarded and little attention has been paid to collect such data. The only such spectrum known to me is the one computed by von Heimendahl [5], Fig.2, for the $Mg_{70}Zn_{30}$ cluster of 800 atoms interacting with pair potentials derived from first principles.

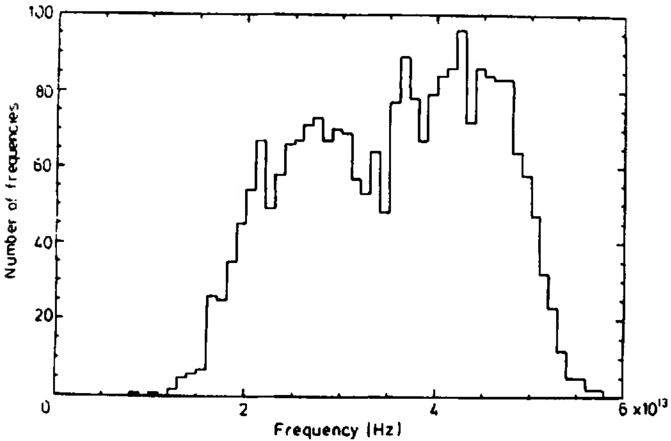

Fig.2
Local frequency spectrum computed for the $Mg_{70}Zn_{30}$ cluster of 800 atoms [5] .

It has been shown merely in order to demonstrate that the relaxation procedure used in this work does not lead to unphysical "extreme" atomic configurations at the cluster surface.

In this lecture, apart from emphasizing the importance of $E(\omega)$, we shall show that one can determine it experimentally, using neutron inelastic scattering (NIS), at least for monoatomic systems with short-range interactions between atoms. Besides, we derive an approximate relation between the normal-mode frequency spectrum $g(\omega)$ and the local frequency spectrum $E(\omega)$. This gives the possibility of determining $E(\omega)$ from optical spectra.

3. Scattering of neutrons and light in orderless solids

In order to show that $E(\omega)$ is a physical observable, we have to present the theory of inelastic scattering of neutrons and light by orderless systems [6,7] . We shall concentrate our attention on monoatomic systems with configurational disorder and interatomic coupling disorder.

For monoatomic systems the frequency spectrum of normal modes, $g(\omega)$, can be expressed exactly, and the neutron inelastic scattering (NIS), the first-order Raman (FOR), and the infrared absorption (IRA) spectra can be expressed approximately in terms of the Fourier transform of the displacement-displacement Green's function (GF)

$$\langle \overleftrightarrow{G}_{\vec q}(\omega)\rangle = \int dt\, e^{i\omega t}\, N^{-1}\sum_{\vec R \vec R'} \overleftrightarrow{G}_{\vec R\vec R'}(t)\, \exp[i\vec q\cdot(\vec R-\vec R')] \tag{3}$$

where

$$\overleftrightarrow{G}_{\vec R\vec R'}(t-t') = \langle\langle \vec u_{\vec R}(t), \vec u_{\vec R'}(t')\rangle\rangle \tag{4}$$

where $\vec u_{\vec R}(t)$ is the displacement at time t of an atom from its average position $\vec R$. For example, the (squared) frequency spectrum is $(\lambda \sim \omega^2)$

$$G(\lambda) \sim \sum \mathrm{Im}\,\mathrm{Tr}\,\langle \overleftrightarrow{G}_{\vec{Q}}(\omega+i\varepsilon)\rangle \tag{5}$$

i.e. the frequency spectrum is $g(\omega) = 2\,\omega\, G(\lambda)$, whereas the NIS cross section has roughly the form

$$\frac{d^2\sigma^{NIS}}{d\Omega\, d\omega} \sim n(\omega)\vec{Q}\vec{Q}\left(-\mathrm{Im}\langle \overleftrightarrow{G}_{\vec{Q}}(\omega+i\varepsilon)\rangle\right) \tag{6}$$

where $\hbar\vec{Q}$ and $\hbar\omega$ are momentum and energy transfers in the scattering, respectively, and $n(\omega)$ is the Bose-Einstein factor. Similar expressions appear in the FOR and IRA cases. Poles of the function $\langle \overleftrightarrow{G}_{\vec{q}}(\omega)\rangle$ in the ω-Q plane represent dispersion relations for the plane-wave excitations of the system.

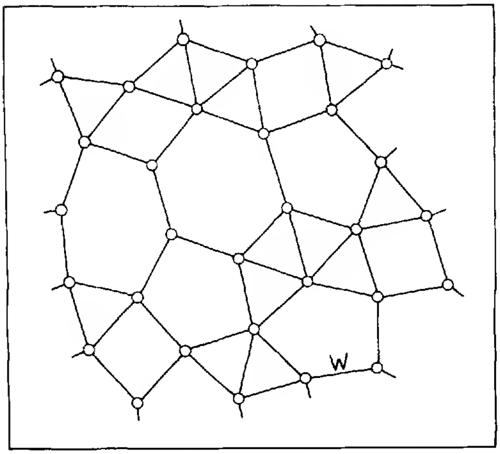

Fig.3.
Example of a monoatomic orderless structure with the n.n. distance W fixed.

The GF (4) obeys the following equation of motion

$$\omega^2 M_{\vec R}\,\overleftrightarrow{G}_{\vec R\vec R'} - \sum_{\vec R''}\overleftrightarrow{\Phi}_{\vec R\vec R''}\,\overleftrightarrow{G}_{\vec R''\vec R'} = \overleftrightarrow{1}\,\delta_{\vec R\vec R'} \tag{7}$$

where $\overleftrightarrow{\Phi}_{\vec R\vec R'}$ is the force constant matrix between atoms at $\vec R$ and $\vec R'$. As an auxiliary notion, useful for future perturbation treatment of this problem, we introduce the locator GF

$$\overleftrightarrow{L}_{\vec R\vec R'}(\omega) = \left(\omega^2 M_{\vec R}\overleftrightarrow{1} - \overleftrightarrow{\Psi}_{\vec R}\right)^{-1}\delta_{\vec R\vec R'} \equiv \overleftrightarrow{L}_{\vec R}\,\delta_{\vec R\vec R'} \tag{8}$$

where the self-force matrix $\overleftrightarrow{\Psi}_{\vec R}$ obeys the relation following from the translational invariance of the adiabatic potential of the system as a whole

$$\overleftrightarrow{\Psi}_{\vec R} = -\sum_{\vec R'}\overleftrightarrow{\Phi}_{\vec R\vec R'}\,. \tag{9}$$

Essential information on the local dynamics is stored in the locator - its poles occur at the (squared) local frequencies $\omega^2_{\vec R\nu}$. Using it, we arrive at the Dyson equation

$$\overleftrightarrow{G}_{\vec R\vec R'} = \overleftrightarrow{L}_{\vec R}\,\delta_{\vec R\vec R'} + \sum_{\vec R''}\overleftrightarrow{L}_{\vec R}\,\overleftrightarrow{C}_{\vec R\vec R''}\,\overleftrightarrow{G}_{\vec R''\vec R'} \tag{10}$$

where $\overleftrightarrow{C}_{\vec R\vec R'}$ is a perturbation matrix, $\overleftrightarrow{C}_{\vec R\vec R'} = (1-\delta_{\vec R\vec R'})\,\overleftrightarrow{\Phi}_{\vec R\vec R'}$. On multiplying (10) by $\exp\left[i\vec{Q}\cdot(\vec R-\vec R')\right]$ and summing over $\vec R$ and $\vec R'$ we obtain the equation for the GF we need:

$$\langle \overleftrightarrow{G}_{\vec q}\rangle = \langle \overleftrightarrow{L}\rangle + \langle (\overleftrightarrow{L}\,\overleftrightarrow{C}\,\overleftrightarrow{G})_{\vec q}\rangle \tag{11}$$

where

$$\langle (\overleftrightarrow{L}\,\overleftrightarrow{C}\,\overleftrightarrow{G})_{\vec{q}}\rangle = N^{-1}\sum_{\vec{R}\vec{R}'\vec{R}''} \overleftrightarrow{L}_{\vec{R}}\,\overleftrightarrow{C}_{\vec{R}\vec{R}''}\,\overleftrightarrow{G}_{\vec{R}''\vec{R}'}\, e^{i\vec{q}\cdot(\vec{R}-\vec{R}')} \tag{12}$$

To solve it, we apply an approximation of the mean-field type, the average local-information transfer approximation (ALITA) [6], $\langle LCG\rangle = \langle LC\rangle\langle G\rangle$. We arrive immediately at the GF

$$\langle \overleftrightarrow{G}_{\vec{q}}(\omega)\rangle = \left[\omega^2 \langle \overleftrightarrow{L}\rangle^{-1}\langle M\overleftrightarrow{L}\rangle - \langle \overleftrightarrow{L}\rangle^{-1}\langle(\overleftrightarrow{L}\,\overleftrightarrow{\Phi})_{\vec{q}}\rangle\right]^{-1} \tag{13}$$

where

$$\langle M\overleftrightarrow{L}\rangle = N^{-1}\sum_{\vec{R}} M_R\,\overleftrightarrow{L}_{\vec{R}}\,, \tag{14}$$

$$\langle (L\,\Phi)_{\vec{q}}\rangle = N^{-1}\sum_{\vec{R}\vec{R}'} \overleftrightarrow{L}_{\vec{R}}\,\overleftrightarrow{\Phi}_{\vec{R}\vec{R}'}\,\exp\left[i\vec{q}\cdot(\vec{R}-\vec{R}')\right]. \tag{15}$$

These averages can be calculated for some systems of physical interest. Here we assume central coupling between nearest neighbors (n.n.) at the fixed distance W, see Fig.3.

$$\overleftrightarrow{\Phi}_{\vec{R}\vec{R}'} = \overleftrightarrow{\Phi}_{\vec{R},\vec{W}_{\vec{R}}} = \begin{cases} -l\,\hat{W}\hat{W} & \text{for } |\vec{W}_{\vec{R}}| = W, \\ 0 & \text{otherwise}, \end{cases} \tag{16}$$

where $\vec{W}_{\vec{R}}$ is the distance vector between the atom at $\vec{R}$ and one of its nearest neighbors, $\hat{W}_{\vec{R}} = \vec{W}_{\vec{R}} / W$. If, in addition, we take all self-force matrices scalar and identical, $\overleftrightarrow{\Psi}_{\vec{R}} = \overleftrightarrow{1}\Psi$, $\Psi = n\,l$, where n is the n.n. number (fixed), then for a monoatomic system we have purely configuration disorder, characterized by the following dispersion curves

$$\begin{aligned} \omega_L^2 &= \frac{2nl}{M}\,h_2(p)\,, \\ \omega_T^2 &= \frac{nl}{M}\left(h_0(p) - h_2(p)\right), \end{aligned} \tag{17}$$

where we have introduced the useful dimensionless variable p=QW and

$$\begin{aligned} h_0(p) &= \frac{1}{2}\left[1 - \frac{\sin p}{p}\right], \\ h_2(p) &= \frac{1}{6}\left[1 + 6\,\frac{\sin p - p\cos p}{p^3} - 3\,\frac{\sin p}{p}\right]. \end{aligned} \tag{18}$$

Isotropy and macroscopic size of the system considered were essential for the derivations.

These curves are displayed in Fig. 4. At large p both curves oscillate about average local frequency. In particular the T-curve is almost flat there. This results in a strong concentration of mode vibrations about this frequency, i.e. in a peak in the frequency spectrum $g(\omega)$. It should be stressed once more that no coupling disorder is involved in the result (17), but only the configurational disorder.

4. Coupling disorder

Isotropy results in the following form of the GF(3) for a monoatomic solid.

$$\left\langle \overleftrightarrow{G}_{\vec{Q}}(\omega) \right\rangle = \frac{\hat{Q}\hat{Q}}{M\omega^2 - \phi^L_Q(\omega)} + \frac{\overleftrightarrow{1} - \hat{Q}\hat{Q}}{M\omega^2 - \phi^T_Q(\omega)} \equiv \hat{Q}\hat{Q}\Gamma^L_Q + (\overleftrightarrow{1} - \hat{Q}\hat{Q})\Gamma^T_Q \,, \tag{19}$$

where $\hat{Q} = \vec{Q}/Q$. With the central coupling between nearest neighbors (16) we find in the case of the coupling disorder, [7]

$$\begin{aligned} \phi^L_Q(\omega) &= 2\,A(\omega)\,h_2(p) \,, \\ \phi^T_Q(\omega) &= A(\omega)\left[h_0(p) - h_2(p)\right] \,, \end{aligned} \tag{20}$$

where $A(\omega)$ is an effective n.n. coupling constant, given by

$$A(\omega) = 3\left(M\omega^2 - 1/\langle L \rangle\right) \tag{21}$$

As $A(\omega)$ depends, through $\langle L \rangle$, only on the self-force matrices $\overleftrightarrow{\Psi}_{\vec{R}}$, we can say that within this model the problem of force disorder reduces to the problem of the self-force disorder.

Now the only thing to do is to calculate the average locator $\langle L \rangle$. Let the eigenvalues of the matrices $\overleftrightarrow{\Psi}_{\vec{R}}$ be $\Psi_{\vec{R}\nu}$, $\nu = 1,2,3$. We assume the distribution of all eigenvalues to be extended and continuous in a certain range about an average value Ψ_0 ; we shall call it the distribution of self-forces, equivalently we may speak of the distribution of (squared) local frequencies (2). Using these notions we can introduce the dimensionless locator $\Lambda(\lambda)$

$$\begin{aligned} \langle L(\omega + i\varepsilon) \rangle &= \frac{1}{3N} \sum_{\vec{R},\nu} \frac{1}{M(\omega + i\varepsilon)^2 - \Psi_{\vec{R}\nu}} = \\ &= \frac{1}{\Psi_0}\left[\mathcal{P}\int_0^\infty \frac{\rho(\lambda')}{\lambda - \lambda'}\,d\lambda' - i\,\mathrm{sgn}(\varepsilon\omega)\,\pi\,\rho(\lambda)\right] \equiv \frac{1}{\Psi_0}\left[\Lambda_1(\lambda) - i\,\Lambda_2(\lambda)\right] \end{aligned} \tag{22}$$

where $\lambda = (\omega/\omega_0)^2$, $\omega_0^2 = \Psi_0/M$ and $\rho(\lambda)$ is the distribution of the eignevalues in the units ω_0^2, i.e. the distribution of (squared) local frequencies. It is related to the spectrum of local frequencies by the obvious formula

$$E(\omega) = 2\,\omega\,\rho\left(\frac{\omega^2}{\omega_0^2}\right). \tag{23}$$

Now we insert (22) into (19) and obtain the following formula for Im $\Gamma_q(\omega+i\varepsilon)$ in the band of coupling disorder, $\varrho(\lambda) \neq 0$

$$-\mathrm{Im}\,\Gamma_q^{L,T}(\omega+i\varepsilon) = \frac{f_p^{L,T}(f_p^{L,T}+1)}{\Psi_0\,\lambda}\;\frac{\pi\lambda\varrho(\lambda)}{\left[f_p^{L,T}+\lambda\Lambda_1(\lambda)\right]^2+\left[\pi\lambda\varrho(\lambda)\right]^2} \qquad (24)$$

where

$$f_p^L = \frac{6\,h_2(p)}{1-6\,h_2(p)}\,, \qquad f_p^T = \frac{3(h_0(p)-h_2(p))}{1-3(h_0(p)-h_2(p))}\,. \qquad (25)$$

For a frequency outside the range of the band of disorder, $\varrho(\lambda) = 0$, we can take the limit $\pi\lambda\varrho(\lambda) \to 0$ in (24) to arrive at

$$-\mathrm{Im}\,\Gamma_q^{L,T}(\omega+i\varepsilon) = \frac{f_p^{L,T}(f_p^{L,T}+1)}{\Psi_0\,\lambda}\,\pi\,\delta\!\left(f_p^{L,T}+\lambda\Lambda_1(\lambda)\right) \qquad (26)$$

Having these, we can calculate the NIS profiles (6), see Fig.4, and the frequency spectrum (5) . It follows that $\varrho(\lambda)$ is a primary dynamical characteristic for monoatomic orderless system.

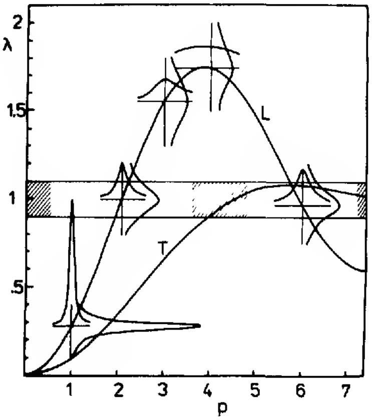

Fig.4
Dispersion curves for the n.n. central-coupling model of solid with purely configurational disorder and the broadening of the NIS profiles for the Lorentzian spectrum of self-forces $\varrho(\lambda)$, characterized by the width parameter a = 0.1 .

5. Determination of E(ω) by neutron scattering

According to (19) it is the function Γ_q^L , which appears in the NIS cross section (6) . By definition, the function $f_p^L \to \infty$ whenever $6h_2(p) \to 1$, i.e. when the dispersion curve ω_L approaches the average local frequency. We find immediately, that in such cases, in the band of disorder [7]

$$-\mathrm{Im}\,\Gamma_q^L(\omega+i\varepsilon) \sim \varrho(\lambda) \tag{27}$$

i.e. the NIS cross section is, by (19) and (6), proportional to $\omega\, n(\omega)E(\omega)$.

Therefore, the local frequency spectrum $E(\omega)$ can be in principle determined by neutron inelastic scattering.

The above condition for f_p^L is certainly fulfilled when $p \sim Q \rightarrow \infty$, which is a limit too extreme. But the L-dispersion curve (17a) in Fig.4 oscillates about the level $\lambda = 1$ and the first crossover occurs at $p = QW \simeq 2$, the second at $p \simeq 6$, etc. It follows that one can determine the form of $E(\omega)$ with the Q-constant scan at, e.g, the neutron momentum transfer $Q \simeq 2/W$,. It should be stressed that for multiatomic systems such a procedure leads to the function $-\mathrm{Im}\,\langle L(\omega + i\varepsilon)$, which is somewhat different. One can distinguish the corresponding curves among the calculated dynamical structure factors, reported by several authors [4,5], about the above special value of Q.

6. Derivation of g(ω) from E(ω)

We can now use the derived GF (19, 24) in the formula (5) to calculate the spectrum of the normal-mode frequencies $g(\omega) = 2\omega\, G(\lambda)$. Interestingly, we find that $G(\lambda) \sim \varrho(\lambda)\; I(\lambda)$, where $I(\lambda)$ is smooth, i.e. possible sharp features in $\varrho(\lambda)$ can show up in $G(\lambda)$.

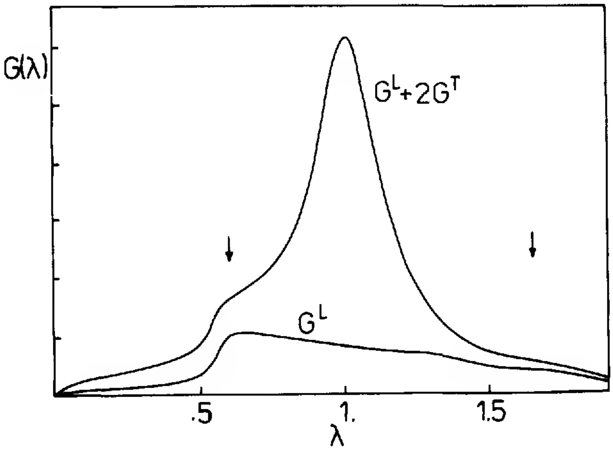

Fig.5
Spectrum of (squared) frequencies of the normal modes for the orderless system characterized by the Fig.4.
The $G^L(\lambda)$ curve is the contribution due to the L dispersion curve.

To make the $\vec{Q}$ - integration in (5) convergent, one has to multiply the integrand by a cut off function F(Q), decreasing fast for $Q \to \infty$. Using the analogy with crystals, where we may consider such a function to be F = 1 for $\vec{Q} \in BZ$, zero otherwise, we have chosen [7]

$$F(Q) = \exp\left[-(p/p_0)^2\right] \quad , \quad p = Q\,W, \tag{28}$$

with $p_0 = 2\times6^{1/3}\times\pi^{1/6}$. For mathematical convenience we have taken the Lorentzian distribution of self-forces

$$\rho(\lambda, a, b) = \frac{1}{\pi}\,\frac{a}{a^2 + (\lambda - b)^2} \tag{29}$$

with the width parameter a = 0.1 and b = 1. To calculate $\Lambda_1(\lambda)$ we have extended the lower limit of integration in (22) to $-\infty$; this matters little if the distribution is narrow enough.

The corresponding NIS profiles (27) are shown in Fig. 4. They contribute independently to the partial, L and T, spectra of squared frequencies, $G(\lambda) = G^L(\lambda) + 2G^T(\lambda)$, as shown in Fig.5. Besides the long expected peak near the average local (squared) frequency, $\lambda = 1$, there appears also the L-bump at $\lambda = 0.6$, due to the first minimum in the L-dispersion curve in Fig.4.

7. Derivation of E(ω) from optical spectra

We have shown that the following approximate relation holds between the frequency spectrum of monoatomic system, g(ω), and the first-order Raman and the infrared absorption spectra [6] .

$$g(\omega) \sim \gamma^{FOR}(\omega) + \alpha\,\gamma^{IRA}(\omega), \tag{30}$$

where α is expected to be small or zero.

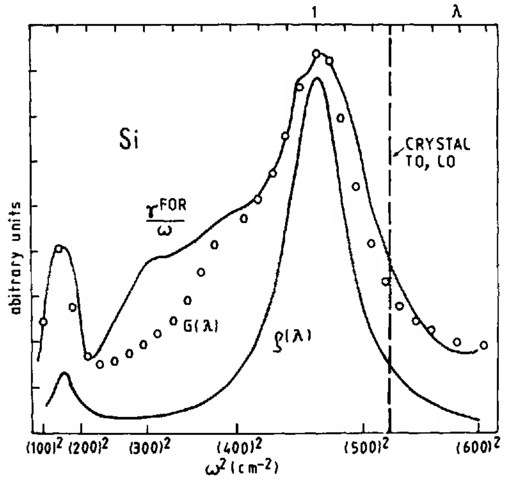

Fig.6
The two-Lorentzian spectrum of self-forces $\rho(\lambda)$ for amorphous Si, as obtained by fitting the derived from it spectrum of normal mode frequencies $G(\lambda)$, open circles, to the corresponding experimental spectrum, derived from the Raman spectrum [8] .

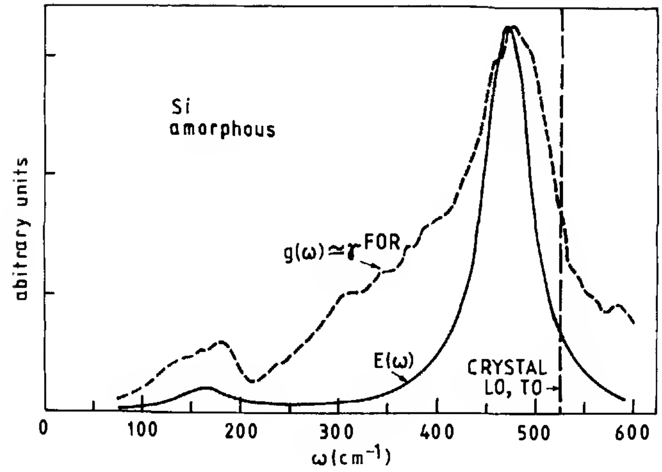

Fig.7.
Spectrum of local frequencies $E(\omega)$ for amorphous Si derived from the function $\varrho(\lambda)$ shown in Fig.6, and the first - order Raman spectrum [8], assumed here to be a fair representation of $g(\omega)$.

Having such experimental $g(\omega)$ we may try to invert the above procedure and to derive the spectrum of local frequencies $E(\omega)$ from the optical spectra. So far, only preliminary results for amorphous Ge and Si have been obtained. The Raman spectrum [8] has been taken as the representation of $g(\omega)$. $\varrho(\lambda)$ has been assumed to consist of two Lorentzians (29), $C_1 + C_2 = 1$

$$\varrho(\lambda) = c_1\, \varrho(\lambda, a_1, \lambda_1) + c_2\, \varrho(\lambda, a_2, \lambda_2)\,, \qquad (31)$$

so the calculation was aimed at fitting the calculated $G(\lambda)$ to the one following from the experimental spectrum, by varying the parameters in (31). By a trial and error method we have arrived at the following numbers for Si: $\lambda_1 = 1.$ $\lambda_2 = 0.115$, $a_1 = 0.12$, $a_2 = 0.05$, $c_1 = 0.94$, corresponding to the curve given by open circles in Fig. 6 ; very close numbers appear for Ge. With just two Lorentzians and the dispersion curves corresponding to the above described n.n. central--force model no essentially better fit can be achieved, it seems. A more satisfactory iterative procedure for deriving $\varrho(\lambda)$ straightforwardly from $g(\omega)$ is expected to be available soon.

There are two peaks in the derived spectrum $E(\omega)$ for Si, Fig.7, and Ge. The big one is obviously due to atoms vibrating much the same way as in crystals, probably with 4 nearest neighbors forming somewhat deformed tetrahedra. The small one correspond to the eigenvalues of the $\Psi_{\vec{R}}$ matrices, which are ~ 10 times smaller than the typical ones. It seems they may be due to atoms coupled to 3 nearest neighbors, the central atom being almost in plane with them; the restoring forme for vibrations perpendicular to the plane can then be small.

To conclude, we have shown that the spectrum $E(\omega)$, or $\varrho(\lambda)$, is a well-conceived primary characteristic. Several observables depend on its form. It can be determined experimentally for monoatomic orderless solids. It has been approximately established for amorphous Si and Ge.

Acknowledgment

Author is grateful to Professor J. Worlock for his helpful remarks on the manuscript.

References

1. G. Leibfried and W. Ludwig, Solid State Physics 12, 275 (1961)
2. A. Czachor, Atomic Vibrations in Solids, Polish Scientific Publishers, Warsaw, 1982 (in Polish).
3. T. Egami, K. Maeda and V. Vitek, Philos. Mag. A41, 883 (1980)
4. J. Hafner, Phys. Rev. B27, 678 (1983)
5. L. von Heimendahl, J. Phys. F:Metal Physics 9, 161 (1979)
6. A. Czachor, Phys. Rev. B32, 5628 (1985), Acta Physica Polonica A69, 281 (1986)
7. A. Czachor, Phys. Rev. B 34, 4521 (1986)
8. R. Alben, D. Weaire, J. Smith and M.H. Brodsky, Phys.Rev. B11, 2271 (1975).

INTERACTION OF PHONONS AND POINT DEFECTS AND ITS INFLUENCE ON DEFECT MOBILITY

H.R. Schober
Institut für Festkörperforschung der Kernforschungsanlage Jülich
D-5170 Jülich, Federal Republic of Germany

The theory of lattice dynamics of crystals with point defects in its modern form originates in the work of Lifshits 1943 [1]. Since then the theory has been worked out in great detail and numerous review articles of earlier work were published, e.g. [2-5]. In the present contribution the theory can only be outlined and illustrated by a few recent results. On the material side we restrict ourselves to metallic and similar systems and do not touch upon the interesting effects of long range interactions of charged defects. Point defects are in this context those defects which do not destroy the topology of the host lattice and where the ideal host lattice can be used as a convenient reference system, i.e. vacancies, substitutional and interstitial atoms and finite clusters. After a short introductory section on the defect statics and elastic properties we give an outline of Green's function techniques to calculate the dynamics of the defect itself and of the crystal as a whole. These effects will be illustrated by results from neutron and Raman scattering experiments. In the final sections lattice dynamics will be applied to calculate classical migration activation energies, defect tunneling rates and quantum diffusion.

1. DEFECT STRUCTURE AND ELASTIC CONSTANTS

Before calculating the dynamics it is in general necessary to calculate the structure of the defect crystal. This is usually done by computer simulation techniques. General properties on the other hand are more conveniently discussed in the framework of Green's function techniques where an ideal harmonic crystal is taken as the reference system. The total potential energy of the crystal with the defect at its origin is expanded as

$$E = U_0(\{\mathbf{r}\}) + \frac{1}{2}\sum_{\mathbf{mn}} s_\alpha^{\mathbf{m}} \Phi_{\alpha\beta}^{\mathbf{mn}} s_\beta^{\mathbf{n}} + V^{anh}(\{\mathbf{R}\}) + \sum_{\mathbf{m}} V^d(\mathbf{R}^{\mathbf{m}}) \tag{1.1}$$

where $\mathbf{R}^{\mathbf{m}} = \mathbf{r}^{\mathbf{m}} + \mathrm{s}^{\mathbf{m}}$ is the lattice vector of atom $\mathbf{m}$ displaced by the static displacement $\mathrm{s}^{\mathbf{m}}$ from its ideal lattice position $\mathbf{r}^{\mathbf{m}}$. $U_0(\{\mathbf{r}\})$ is the ground state potential energy of the ideal crystal and Φ the coupling constant matrix. V^{anh} stands for the anharmonic part of the host-host interaction. Finally V^d is the defect host potential in the case of interstitial defects or the difference to the ideal host potential for substitutional defects and vacancies. For the sake of simplicity possible internal degrees of freedom, explicit volume dependencies and quantum effects have been omitted. The lattice equilibrium condition at T=0 is obtained by differentiation with respect to the atomic positions

$$-\frac{\partial}{\partial R^{\mathbf{m}}_{\alpha}} V^{d}(\mathbf{R}^{\mathbf{m}}) - \frac{\partial}{\partial R^{\mathbf{m}}_{\alpha}} V^{anh}(\mathbf{R}^{\mathbf{m}}) \equiv K^{\mathbf{m}}_{\alpha} = \sum_{\mathbf{n}\beta} \Phi^{\mathbf{mn}}_{\alpha\beta} s^{\mathbf{n}}_{\beta} \tag{1.2}$$

K^m_α is a generalized Kanzaki force, which is defined as that force which causes in the ideal harmonic crystal the same displacements as does the real force in the real crystal. Eq. (1.2) can be solved by the Green's function, $\mathring{G}^{\mathbf{mn}}_{\alpha\beta}$, of the ideal lattice [6,7]

$$s^{\mathbf{m}}_{\alpha} = \sum_{\mathbf{n}\beta} \mathring{G}^{\mathbf{mn}}_{\alpha\beta} K^{\mathbf{n}}_{\beta} \tag{1.3}$$

For large distances from the defect the lattice Green's function converges towards its continuum counterpart $\mathring{G}_{\alpha\beta}(\mathbf{R})$ which is a function of the elastic constants. For a description of the long range displacement field the force pattern may be expanded into multipoles. The zero moment (the sum over all Kanzaki forces) vanishes due to translational invariance and the first moment, the dipole contribution, is the leading term

$$s_{\alpha}(\mathbf{R}^{\mathbf{m}}) \simeq \textstyle\sum_{\mathbf{n}\beta} \mathring{G}_{\alpha\beta}(\mathbf{r}^{\mathbf{m}} - \mathbf{r}^{\mathbf{n}}) K^{\mathbf{n}}_{\beta} \simeq \displaystyle\sum_{\beta\gamma} \frac{\partial}{\partial r^{\mathbf{m}}_{\gamma}} \mathring{G}_{\alpha\beta}(\mathbf{r}^{\mathbf{m}}) P_{\alpha\gamma} \tag{1.4}$$

with the (force) dipole tensor

$$P_{\alpha\beta} = \sum_{\mathbf{n}} r^{\mathbf{n}}_{\beta} K^{\mathbf{n}}_{\alpha} \tag{1.5}$$

The symmetry of $P_{\alpha\beta}$ is determined by the point symmetry of the defect. Since the Green's function falls off as $1/R$ the displacements decay slowly as $1/R^2$. They are in general anisotropic due to the anisotropy of the host lattice, through $\mathring{G}_{\alpha\beta}(\mathbf{r})$ and additionally for many types ofinterstitial and off-centre substitutional atoms due to the anisotropy of P. In the latter case difference of the longrange displacement fields of differently oriented defects will also be $\propto 1/R^2$. The Kanzaki forces are localized at the defect, their range given by the defect force and the lattice anharmonicity. The latter is important for "large" defects such as self interstitial atoms [7]. So far we have tacitly assumed an infinite crystal. In a finite crystal there is an additional lattice expansion, ΔV^{im}, by the so called image forces, i.e. due to the missing restoring forces at the surface. Independent of the crystalline shape the defect relaxation volume is given by [8]

$$\Delta V = \sum_{\alpha} P_{\alpha\alpha}/(3\kappa) = \Delta V^{\infty} + \Delta V^{im} \tag{1.6}$$

with κ the bulk modulus and ΔV^{∞} the defect relaxation volume in an infinite crystal. The various relaxation volumes are related by the Eshelby factor γ ($\Delta V^{\infty} = \gamma \Delta V$) which is e.g. for Cu $\gamma = 0.69$. The (diaelastic) change of the elastic constants, ΔC, due to a random distribution of noninteracting defects is obtained from the energy change under an applied external strain ϵ. Inserting (1.4) into (1.1) and expanding in ϵ we obtain

$$V_c \Delta C_{\alpha\beta\gamma\delta} = -c \frac{\partial P_{\alpha\beta}}{\partial \epsilon_{\gamma\delta}} - c \Delta V^{im} \kappa \frac{\partial C_{\alpha\beta\gamma\delta}}{\partial p} \tag{1.7}$$

with V_c the cell volume, c the defect concentration and p pressure. Here the first term represents the defects polarizability and the second one the contribution of the image volume expansion. Especially interstitial defects are often highly polarizable under strain causing values of $\Delta C/C \sim -100c$ [3]. This is caused by resonant defect vibrations, see next section.

In analogy with electrostatics there can be in addition to this diaelastic polarizability also a paraelastic one due to the reorientation of anisotropic defects in a external strain field [9].

$$V_c \Delta C^{para}_{\alpha\beta\gamma\delta} = -\frac{c}{kT} \{ \langle P_{\alpha\beta} P_{\gamma\delta} \rangle - \langle P_{\alpha\beta} \rangle \langle P_{\gamma\delta} \rangle \} \tag{1.8}$$

where $\langle\rangle$ indicates averaging over initially equivalent orientations. This effect is, contrary to the diaelastic one, strongly temperature dependent. It can only be observed when the defect can reorientate either by thermally activated hopping or by tunneling. The resulting temperature and frequency dependance is utilized in ultrasonic attenuation experiments.

2. SINGLE DEFECT DYNAMICS

In the harmonic theory of defect vibrations one studies the vibrations of the crystal atoms around their equilibrium positions given by (1.2). A second order expansion of the potential energy with respect to the dynamic displacements $\mathbf{u}$ from their static equilibrium positions $\mathbf{R} = \mathbf{r} + \mathrm{s}$ gives for substitutional defects the equation of motion:

$$(\mathbf{M} + \Delta\mathbf{M})\ddot{\mathbf{u}} + (\mathbf{\Phi} + \Delta\mathbf{\Phi})\mathbf{u} = \mathbf{f}. \tag{2.1}$$

Here and in the following indices have been dropped and matrix notation is adopted with $\mathbf{M} = m^{\mathbf{m}}\delta_{\mathbf{mn}}\delta_{\alpha\beta}$ the mass matrix of the ideal host crystal, $\Delta\mathbf{M}$ the matrix of mass changes, $\mathbf{\Phi}$ the force constant matrix of the ideal crystal and $\Delta\mathbf{\Phi}$ the matrix of force constant changes. $\Delta\mathbf{\Phi}$ contains not only the direct couplings due to the defect but also contributions from the anharmonic host potential V^{anh}. After Fourier transformation with respect to time (2.1) can be written as

$$(\mathbf{L} + \Delta\mathbf{L})\mathbf{u} = \mathbf{f} \tag{2.2}$$

where the ideal host lattice terms have been combined to $\mathbf{L} = -\mathbf{M}\omega^2 + \mathbf{\Phi}$ and the perturbation terms to $\Delta\mathbf{L} = -\Delta\mathbf{M}\omega^2 + \Delta\mathbf{\Phi}$. (2.1) can formally be solved by a Green's function

$$\mathbf{G} = (\mathbf{L} + \Delta\mathbf{L})^{-1}. \tag{2.3}$$

Experimentally observable quantities can be conveniently expressed by this Green's function. E.g. the local frequency spectrum $z_\alpha^{\mathbf{m}}$ of atom $\mathbf{m}$ for vibrations in direction α is given by:

$$z_\alpha^{\mathbf{m}} = \frac{2\omega m^{\mathbf{m}}}{\pi} Im G_{\alpha\alpha}^{\mathbf{mm}}(\omega) \tag{2.3}$$

the imaginary part being defined by setting $\omega \rightarrow \omega + i\eta$.

Various ways to calculate $\mathbf{G}$ are currently in use:

i) The most simple one is to do a straightforward diagonalization of (2.3) for a finite crystallite. On modern computers this can be done for several hundred atoms in a couple of minutes. The resultant frequencies and eigenvectors will be accurate for localized and short wavelength vibrations. Long wavelength accustic vibrations can be estimated from their static limit, i.e. from the elastic constants.

ii) In recent years the recursion techniques, proposed by Haydock et al. [10] for tight binding electronic calculations, is used frequently for lattice dynamical calculations of point defects and disordered systems. This method is based on the fact that it is possible to construct for a quadratic Hamiltonian a set of basis states $|n\rangle$ which are coupled by a three point symmetric recursion relation

$$(\mathbf{L} + \Delta\mathbf{L})|n\rangle = a_n|n\rangle + b_{n+1}|n+1\rangle + b_n|n-1\rangle \tag{2.5}$$

The a_n and b_n are determined by orthogonality and normalization. In this basis $(\mathbf{L}+\Delta\mathbf{L})$ is tridiagonal and the inversion (2.3) can be done by an infinite continued fraction to obtain the Green's function element corresponding to $|0\rangle$

$$G_{|0\rangle} = \cfrac{1}{a_0 - \cfrac{b_1}{a_1 - \cfrac{b_2}{a_2 - \cfrac{b_3}{\cdots}}}} \tag{2.6}$$

Dependent on the size of the problem the continued fraction is terminated at a given level by some appropriate closure procedure. This causes the discrete spectrum of a finite fraction to be replaced by a smooth continuous one. Usually ten to twenty levels are sufficient for convergence comparable to experimental resolution [11]. Different elements of $\mathbf{G}$ are calculated by chosing different states $|0\rangle$, e.g. the x-displacement of atom 0.

iii) Eq. (2.3) can be expanded in terms of locators where the locator is the one particle Green's function in the Einstein approximation for this particle [12].

iv) An exact solution of (2.3) for the single defect case can be given by T-matrix techniques where $\mathbf{G}$ is expressed by the ideal host lattice Green's function $\mathring{\mathbf{G}}$ and the perturbation $\Delta\mathbf{L}$. Whereas for the previously discussed methods the splitting int $\mathbf{L}$ and $\Delta\mathbf{L}$ was more ore less formal in T-matrix theory care has to be taken when interstitial or complex substitutional defects introduce additional degrees of freedom not present in the host lattice. Let us first discuss the case of a simple substitutional defect without that added difficulty and later on ammend the results for the more complicated case. We introduce the ideal host Green's function

$$\mathring{\mathbf{G}}(\omega) = \mathbf{L}(\omega)^{-1} \tag{2.7}$$

which can be readily calculated by Fourier transformation to q-space and integration over the Brillouin zone, see e.g. [13]. From (2.3) follows

$$\mathbf{G} = \mathring{\mathbf{G}} - \mathring{\mathbf{G}}\,\Delta\mathbf{L}\,\mathbf{G} = \mathring{\mathbf{G}} - \mathring{\mathbf{G}}\,\mathbf{t}\,\mathring{\mathbf{G}} \tag{2.8}$$

with the single defect T-matrix

$$\mathbf{t} = \Delta\mathbf{L}(1 + \mathring{\mathbf{G}}\,\Delta\mathbf{L})^{-1} = \Delta\mathbf{L} - \Delta\mathbf{L}\,\mathring{\mathbf{G}}(1 + \Delta\mathbf{L}\,\mathring{\mathbf{G}})^{-1}\mathring{\mathbf{G}}. \tag{2.9}$$

The matrix $\mathbf{t}$ has the same dimension as the defect matrix $\Delta\mathbf{L}$ whence (2.9) can be fairly easily evaluated for "small" defects whereas for "large" defects mostly approximate methods are preferred. The point symmetry of the defect subspace can be utilized to speed up the inversion in (2.9) and to gain extra insight into the physics behind $\mathbf{G}$.

Complex and interstitial defects can be dealt with by a projection technique [14]. The degrees of freedom involved in the problem are divided into those present in the host crystal and the additional ones introduced by the defect. Such a split-up is not unique. A complex substitutional defect e.g. can be described by its centre of mass (host degree of freedom) plus its internal motion or alternativly as a host vacancy plus a complex interstitial with all its degrees of freedom. We can now write $\mathbf{G}$ and $\mathbf{L} + \Delta\mathbf{L}$ as hyper-matrices in the space of host (H) and added (A) degrees of freedom:

$$\begin{pmatrix} \Delta\mathbf{L}_{AA} & \Delta\mathbf{L}_{AH} \\ \Delta\mathbf{L}_{HA} & \mathbf{L}_{HH} + \Delta\mathbf{L}_{HH} \end{pmatrix} \begin{pmatrix} \mathbf{G}_{AA} & \mathbf{G}_{AH} \\ \mathbf{G}_{HA} & \mathbf{G}_{HH} \end{pmatrix} = \begin{pmatrix} \mathbf{1} & \mathbf{0} \\ \mathbf{0} & \mathbf{1} \end{pmatrix} \tag{2.10}$$

We obtain three linear equations for the Green's function. By elimination we get

$$[(\mathbf{L}_{HH} + \Delta\mathbf{L}_{HH} - \Delta\mathbf{L}_{HA}(\Delta\mathbf{L}_{AA})^{-1}\Delta\mathbf{L}_{AH}]\mathbf{G}_{HH} = [\mathbf{L}_{HH} + \Delta\mathbf{L}^{eff}_{HH}]\mathbf{G}_{HH} = \mathbf{1}. \tag{2.11}$$

The additional degrees of freedom lead to an effective, frequency dependent coupling change to be used in the T-matrix equation (2.9). A similar expression is gained for $\mathbf{G}_{AA}$ where the effective coupling will contain terms containing the host lattice Green's function which in turn causes the sharp frequency levels of the additional degrees of freedom to be broadened into a continuous spectrum.

From (2.9) one sees that large effects have to be expected if $Det|\mathbf{1} + \Delta\mathbf{L}\ \hat{\mathbf{G}}| \simeq 0$. The determinand can only vanish exactly if the real and imaginary part vanish simultaneously. The imaginary part stems from the imaginary part of the host's Green's function $\hat{\mathbf{G}}$ and vanishes therefore for all frequencies outside the bands of ideal lattice frequencies. For those frequencies where also the real part vanishes (2.8) δ-shaped contributions to the spectrum result. These vibrational modes are spatially localized and whence called localized modes. For Bravais lattices such modes are to be expected for defects with either small mass (e.g. H in metals) or very strong couplings (e.g. intramolecular vibrations of substitutional molecules). If the real part of the determinant vanishes while the imaginary part is small one has a resonant mode. Such a mode is not as strongly localized around the defect and its frequency is broadened with the width given by the imaginary part. Since $Im\hat{\mathbf{G}}(\omega) \sim \omega$ for small ω such resonant vibrations occur at low frequencies and therefore for either heavy (e.g. Ag in Al) or weakly coupled defects. In fig. 1 typical local vibrational spectra for a neighbour to a vacancy and of a self-interstitial atom in Cu are shown. As to be expected the spectrum shows in the vacancy case a general softening due to the missing couplings but neither resonant nor localized modes. By contrast the spectrum of the self-interstitial atom is made up mainly from such modes.

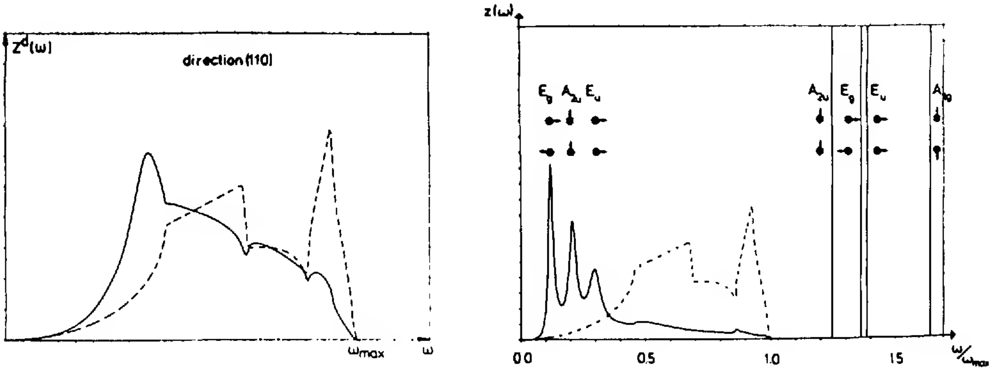

Fig. 1 Local frequency spectrum of a nearest neighbour atom to a vacancy for vibrations in (110)-direction (left) and of a self interstitial atom (right) in fcc Cu. Broken line ideal host spectrum. [3].

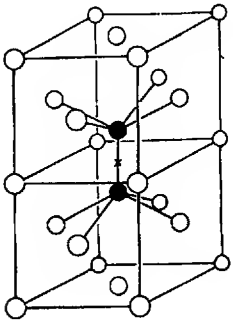

Fig. 2 Schematic view of the self-interstitial, (100)-dumbbell, configuration in Cu. The configuration can also be seen as an octahedral interstitial which has been displaced in (001)-direction (100-off-centre interstitial configuration). There are six equivalent such positions for each octahedral site in an fcc lattice.

Fig. 2 shows the configuration of the self-interstitial. For our purposes it can be envisaged as a substitutional Cu_2 molecule where the two atoms are strongly coupled causing a localized bond stretching vibration (A_{1g}). At the same time the restoring forces against libration (E_g) or translation (A_{2u}) of the molecule as a whole are weak causing resonant vibrations. This example shows the importance of the tensor character of the coupling. The simultaneous occurance of localized and resonant modes is typical for "large" defects which compress the lattice locally and thus cause a tendency to instability in some directions. The defect configuration can even become instable and is then often split into configurations of lower symmetry. The configuration of fig.2 is actually a result of such an instability in the octahedral configuration which would have higher symmetry. In cases where the local vibrational spectrum of the defect has only little contribution from the eigenfrequencies of the ideal lattice the Green's function of the defect, $\mathbf{G}^{dd}$, can to a good approximation be described by the resonant and localized modes alone:

$$\mathbf{G}^{dd} = \sum_{\sigma} \frac{|\sigma\rangle\langle\sigma|}{m^{\sigma}\omega_{\sigma}^{2} - m^{\sigma}\omega^{2} - im^{\sigma}\gamma^{\sigma}(\omega)\omega} \tag{2.12}$$

where $|\sigma\rangle$ represents the eigenvector of the mode σ in the defect subspace, ω_{σ} and γ^{σ} are the mode frequency and damping and m^{σ} its effective mass. The latter is a measure of the participation of the other atoms in the vibration, i.e. of the localization of the mode. For localized modes one has $\gamma^{\sigma} = 0$ and $m^{\sigma} \simeq m^{d}$. For resonant modes of interstitial atoms the effective mass is $m^{\sigma} = m^{d} + x\, m^{h}$ with x typically varying between 1 and 5 and m^{h} the host atom mass. The mean square thermal displacements of the defect can be calculated from the local spectrum and whence from the Greens function:

$$\begin{aligned} \langle (u_{\alpha}^{d})^{2} \rangle &= \int_{0}^{\infty} d\omega (\hbar/2m^{d}\omega) \coth(\hbar\omega/2kT) z_{\alpha}^{d}(\omega) \\ &\simeq kT G_{\alpha\alpha}^{dd}(\omega = 0) \;\; \text{for} \;\; kT \geq \hbar\omega_{resonance}. \end{aligned} \tag{2.13}$$

For not too low temperatures the mean square thermal displacement is given by the $\langle\omega^{-2}\rangle$ moment of the spectrum and therefore, is determined mainly by the resonant vibrations. Localized vibrations play only a minor role in classical motion.. The mean square velocity on the other hand would be given mainly by the localized modes. From (2.13) one sees that interstitials will have in general, due to their resonance modes, strongly enhanced Debye-Waller factors.

Defect vibrations are often used to identify defect structure. Such an investigation was carried out to identify the configurations of Ag_2 in noble gas matrices [15]. There exist one, two or three distinct such configurations for matrices of Ar, Kr and Xe respectively. These could be identified by a comparison of experiment with the results of structure calculations followed by a calculation of the Ag_2 vibrations. Fig. 3 shows the spectra seen by resonance Raman scattering on Ag_2 trapped in Kr.

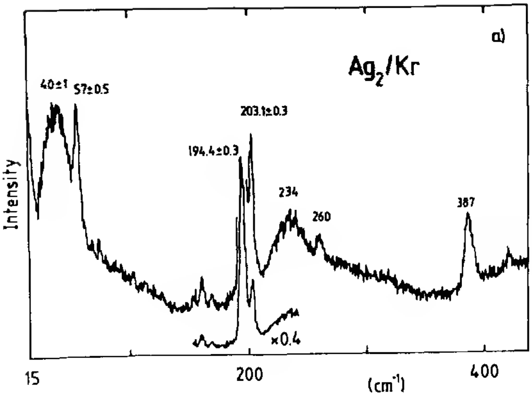

Fig. 3 Resonance Raman spectrum of Ag_2 in Kr, demonstrating the simultaneous occupation of two trapping sites and the correlation of modes [15]. The internal Ag_2 bond-stretching modes are at 194 and 203 cm^{-1},respectively. The species with the 203 cm^{-1} mode also has a broad in-band contribution at 40 cm^{-1} and a combination band at 234 cm^{-1}. The other configuration has a localized mode at 57 cm^{-1} with a combination band at 260 cm^{-1}.

3. FINITE DEFECT CONCENTRATION

So far we have discussed the dynamics of isolated defects . When the concentration of defects increases the dynamics of the defects will be modified and, in addition, their effects on host lattice properties will become noticeable. An example of the former is the evolution of the optic phonon bands in metal hydrides from the localized modes of the isolated H-impurity. The latter is exemplified in the change of the elastic constants discussed earlier. Both these types of effect can be described by average Green's functions as long as defect-defect correlations can be neglected. We consider a concentration of defects sufficiently small so that overlap effects are negligible. The total perturbation $\Delta\mathbf{L}$ can then be split into the contributions of the single defects

$$\Delta\mathbf{L}(\omega) = \sum_i \Delta\mathbf{L}^i(\omega). \tag{3.1}$$

The Green's function can again be calculated exactly in terms of a T-matrix (2.8). This formal solution is however not very useful. Macroscopic properties such phonon dispersion curves will not depend on the exact positions of all defects but only on their configurational or volume averages. We are therefore interested in an average Green's function, $\langle\mathbf{G}\rangle$, which from (2.8) is determined by an average T-matrix

$$\langle\mathbf{G}(\omega)\rangle = \mathring{\mathbf{G}} - \mathring{\mathbf{G}}\langle\mathbf{T}\rangle\mathring{\mathbf{G}}. \tag{3.2}$$

Due to the averaging $\langle\mathbf{G}\rangle$ is translationally invariant and can be conveniently epressed in terms of a self energy matrix $\mathbf{\Sigma}$:

$$\langle\mathbf{G}(\omega)\rangle = (\mathbf{L}(\omega) + \mathbf{\Sigma}(\omega))^{-1} \tag{3.3}$$

with

$$\mathbf{\Sigma}(\omega) = \langle\mathbf{T}(\omega)\rangle(\mathbf{1} - \mathring{\mathbf{G}}(\omega)\langle\mathbf{T}(\omega)\rangle)^{-1} \tag{3.4}$$

To lowest order in the concentration the self energy is given by the configurational average of the single defect T-matrices, $\mathbf{t}^{(i)}$

$$\boldsymbol{\Sigma}(\omega) \simeq c \sum_i \mathbf{t}^{(i)} = N_d \langle \mathbf{t} \rangle \tag{3.5}$$

In general the configuration average will include averaging over equivalent defect orientations. $\langle \mathbf{G} \rangle$ can now be expanded in plane waves. For the main crystallographic directions where the polarization vectors are determined by symmetry alone

$$\langle \mathbf{G} \rangle = \frac{1}{N_0} \sum_{\mathbf{k},j} \frac{|\mathbf{k},j\rangle\langle\mathbf{k},j|}{m\omega_0^2(\mathbf{k},j) - m\omega^2 + ct(\mathbf{k},j,\omega)}. \tag{3.6}$$

We expect especially large effects when $t(\mathbf{k},j,\omega)$ has contributions from resonant modes. Wether a particular resonance couples to a particular phonon is determined by symmetry. For very low concentrations (3.6) will still have well defined phonon solutions whereas for higher concentrations a description in terms of hybridized phonon and resonance states is more adequate, fig. 4. Both kinds of behaviour have been observed in experiment [3].

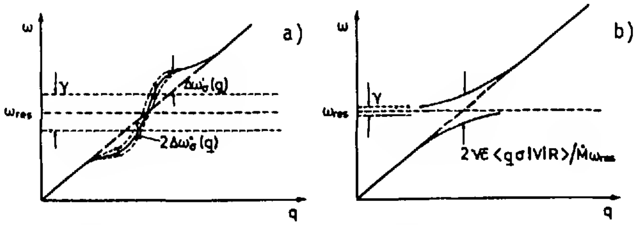

Fig. 4 Effects of resonance vibrations on the phonon dispersion curves.

a) mere distortion of the phonon line being shifted by $\Delta\omega_\sigma'$ and broadened by $\Delta\omega_\sigma''$ (valid if $2\Delta\omega_\sigma'' << \gamma$).

b) hybridization of the ideal phonon line with the resonance mode resulting in a split of the dispersion curves (valid if $2\Delta\omega_\sigma'' >> \gamma$).

To see the influence of defects on long wavelength phonons one expands $|\mathbf{k},j\rangle$ for small k. One sees easily that only resonance modes with even symmetry couple to long wavelength phonons to order k^2 whereas "uneven" resonances couple only to order k^4. These latter ones will therefore not contribute to the change of elastic constants, sect. 1.

Whereas phonon dispersion curves are generally easy to measure since all atoms of the crystal contribute to their intensity the shifts induced by the defects are small $\sim c$. Since the defect lattice lacks translational invariance $Im\langle\mathbf{G}\rangle$, which is essentially measured in neutron scattering experiments, will have additional contributions with intensity $\sim c$ in the whole Brillouin zone. The distribution of this "diffuse" intensity is determined by the structure factors of the vibrational modes. For different resonant modes these vary as functions of $\mathbf{k}$ and ω, see fig. 5, which

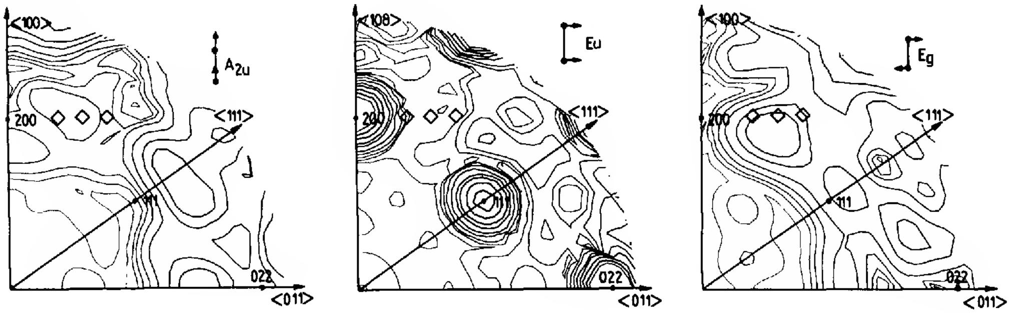

Fig. 5 Plot of the structure factors of resonant modes of the self interstitial atom, fig. 2. The plots are only valid off the phonon lines.

can be utilized to identify individual defect vibrations [15]. At higher concentrations additional information about defect ordering could thus be gained. Such measurements have been done for H in Nb [17].

The "single T-matrix approximation" (STA), (3.5), is only valid in the low concentration limit. It also does not give a finite width to the spectrum of localized vibrations as has to be expected from disorder. For diagonal (pure isotope) disorder one can improve the STA by an "average T-matrix" approximation (ATA) which uses an average lattice as reference system, and further by the self consistent "coherent potential approximation" (CPA) [18]. With off-diagonal (force constant) disorder these approximations are due to the translational condition only possible with restrictions on the force constants, e.g. $\Phi^{(AB)} = \frac{1}{2}(\Phi^{(AA)} + \Phi^{(BB)})$. This difficulty could be avoided by switching to an augmented space [19] which has, however, only been utilized for model systems. For realistic systems an alternative is to create configurations by Monte Carlo methods, let them relax to equilibrium and finally evaluate the dynamics by recursion procedures [11].

Finally it should be pointed out that often not the displacement- displacement Green's function itself but some weighted average is measured in experiment. E.g. in neutron scattering experiments the Green's function is weighted by the scattering length. These weight factors do not influence the shape of the phonon line but the diffuse intensities and have then to be included in the averaging procedure [3].

1. CLASSICAL DIFFUSION

The diffusion constant in classical defect diffusion processes is often found to be given by an Arrhenius law with an only weakly temperature dependent prefactor times Boltzmann factor

$$D = D_0 \exp(-E_a/kT) \tag{4.1}$$

The microscopic picture is that of an atom (interstitial or a neighbour atom to a vacancy) hopping over a potential barrier formed by the other atoms. The classical activation energy, E_a, is the minimal energy needed for that process. It corresponds to the energy necessary to move the atom adiabatically to the saddle point seperating its initial and final equilibrium configurations. E_a is, therefore, the difference of the potential energies with the hopping particle in the saddle point and equilibrium configurations, respectively, and the rest of the lattice fully relaxed. There is a large number of approximate formulae relating E_a to other lattice quantities. Employing a Debye model Flynn [20] gave a formula for E_a in terms of the elastic constants and a single parameter depending on geometry. The local Green's function of the defect allows one to relate E_a to lattice dynamics going beyond the elastic limit. One can thus check models qualitatively for consistency by relating their predictions to measured quantities. The energy needed to displace an atom, d, from its equilibrium site with the other atoms relaxing adiabatically is given by

$$E(\mathbf{s}^d) = (1/2)\mathbf{s}^d[\mathbf{G}^{dd}(\omega=0)]^{-1}\mathbf{s}^d \tag{4.2}$$

Assuming a smooth, *sin*-like, shape of the potential surface along the "reaction" coordinate to the saddle point (4.2) can be extrapolated to give

$$E_a \simeq (2/\pi^2)\mathbf{d}[\bar{\mathbf{G}}^{dd}(\omega=0)]^{-1}\mathbf{d} \tag{4.3}$$

where $\mathbf{d}$ is the distance vector to the saddle point and $\bar{\mathbf{G}} = (1/2)(\mathbf{G}_{equilibrium} - \mathbf{G}_{saddle})$. Tests of this relation with computer models gave an error of $< 1\%$. Taking the experimental values of the activation energies for vacancy diffusion in fcc and bcc metals one finds that $\bar{\mathbf{G}}$ is about 1.8 its ideal lattice counterpart. For bcc metals one has to take into account that the saddle point is split and $|\mathbf{d}|$ thus reduced. We have seen that the defect Green's function for interstitial atoms is often determined by low lying resonance vibrations. In such a case (4.3) reduces to a sum over these resonances

$$E_a \simeq 2/\pi^2 \sum_r m^r \omega_r^2 d_r^2 \tag{4.4}$$

where d_r is the projection of $\mathbf{d}$ onto the eigenvector of the resonance mode with effective mass m^r and frequency ω_r. (4.4) establishes the observed correlation between the occurance of low lying resonance modes and low activation energies.

5. TUNNELING AND QUANTUM DIFFUSION

At very low temperatures one expects tunneling to contribute to particle motion. The magnitude of the tunnel splitting, ΔE_T, for a particle in a onedimensional double well potential is determined essentially by an exponential factor $\exp(-gm\omega d^2/\hbar)$ where g is a geometrical factor of order unity, m the mass, $\frac{1}{2}\hbar\omega$ the ground state energy and $2d$ the well separation. From (5.1) it is evident that tunneling will be important for particles of either low mass (e.g. H or μ) or moving in a soft potential with small d. Tunneling of an atom in a crystal cannot be described by a simple onedimensional double well potential. The atom experiences the potentials exerted by its neighbours which in turn move in the potential of their neighbours and so on. The potential in which the atom tunnels thus becomes N-dimensional ($N \to \infty$). In tunneling between the two minima the atom carries its displacement cloud with it - it is "dressed".

For heavy interstitial atoms with pronounced resonant vibrations it has been shown that similar to the classical activation energy also the tunnel splitting energy can be approximated by these resonances [21]:

$$\Delta E_T \sim \exp[-g \sum_r m^r \omega_r d_r^2/\hbar] \tag{5.1}$$

From the dependence on the effective resonance mass m^r one sees that the dependence on the interstitial mass and whence the isotope effect is much reduced. Such a close connection between the occurance of resonance vibrations and tunneling has also been observed in glasses [22].

For very light interstitials in a heavy matrix the tunnel splitting energy is made up from two parts: a term giving the tunnelsplitting, J, in some average fixed potential which shows the full isotope effect of the tunneling particle and a term describing the dressing by the lattice, $\exp(-S)$.

$$\Delta E_T = J \exp(-S) \tag{5.2}$$

Eqs. (5.1) and (5.2) describe "coherent" tunneling at $T = 0$, i.e. the tunneling particle can be envisaged to move periodically between the two wells. With increasing temperature ΔE_T is replaced by a thermal average, $\Delta E_T(T) = \langle \Delta E_T \rangle_T$ since there will be also tunneling between states with excited phonons. This temperature dependency is rather weak for low temperatures. Eventually the coherent tunneling breaks down and "incoherent" processes become dominant, i.e. transitions between states with different phonon occupation numbers. In metals there are in addition to these phononic processes at low temperatures also electronic dressing effects and these actually determine the temperature dependences at very low temperatures, see below.

In the following we will study the "incoherent" tunneling which is the elementary step in quantum diffusion (phonon assisted tunneling). As a model system we have chosen H and D in Nb at low concentration which have been studied extensively both theoretically and experimentally, see e.g. the recent review by Fukai and Sugimoto [23]. H occupies tetrahedral sites in the Nb lattice, fig.6. Its dynamics is characterized by localized vibrations at 27 and 43 THz [24]. These account for $\simeq$ 99% of the local spectral intensity. Additionally it has strongly enhanced in-band-modes which determine the temperature dependence of the mean square thermal amplitude (2.13) at intermediate temperatures [25]. At low temperatures a tunnel splitting of $E_T \simeq 0.2meV$ has been observed for H trapped at O-impurities in Nb [26]. This value is thought to be fairly representative also for the pure H-Nb-system since the localized H-vibrations change only marginally upon trapping of the H at the O-impurity [27]. At higher temperatures, in the pure H-Nb-system, two distinct diffusion regimes are observed. In both regimes diffusion follows an Arrhenius law with activation energies of $68meV$ $(T < 250K)$ and $108meV$ $(T > 250K)$ [28], respectively.

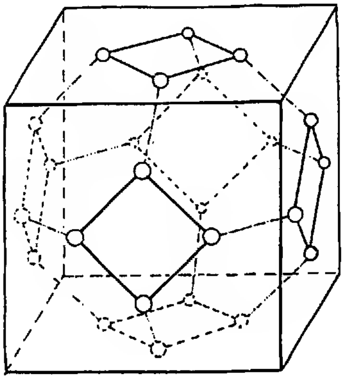

Fig. 6 Tetrahedral sites in the bcc lattice. There are four sites surrounding an octahedral site on each side of the bcc cube. The symmetry of the tetrahedral sites is D_{2d}. The H will therefore have two localized vibrations, the higher frequency one being degenerate.

The standard approach in the calculation of absolute diffusion rates is that of Flynn and Stoneham [29]. It involves several distinct ideas. The first is that of "sensibly localized" states between which transitions occur. The second, related idea, is that of self trapping: the interstitial causes a distortion of the host lattice which in turn immobilizes the interstitial. The transition probability is then found by the usual "golden rule expression"

$$W^{if} = \langle\langle w^{if} \rangle\rangle_m \tag{5.3}$$

$$w^{if} = (2\pi/\hbar)|\langle \Psi_i(m)|H - E_{im}|\Psi_f(n)\rangle|^2 \delta(E_{im} - E_{fn}) \tag{5.4}$$

where Ψ_i and Ψ_f are the initial and final state many body wavefunctions, m and n denote the respective excitational states, $\langle\langle \; \rangle\rangle_m$ denotes thermal averaging over the initial states m and summation over the final states n and finally $E_{im} = \langle \Psi_i(m) H \Psi_i(m) \rangle$. To be able to evaluate (5.3) a number of approximations are made. The hydrogen atom is assumed to follow the lattice vibrations adiabatically and the lattice phonons themselves are coupled linearly to the hydrogen. The matrix element in (5.3) is thus split into a "naked" tunneling element, J, of the hydrogen atom in the potential built by the host atoms and a dressing lattice-overlap term, σ, accounting for the change of the displacement field. To simplify the evaluation even further the dependence of the naked H-tunneling element on the state of the host lattice is neglected (Condon approximation) and one finally arives at a simple expression

$$W^{if} = (2\pi/\hbar)|J|^2|\sigma^{if}|^2. \tag{5.5}$$

Neglecting the deformation of the phonon spectrum by the H (5.5) can be evaluated using the ideal phonon states as basis

$$|\sigma^{if}|^2 = (\hbar/2\pi) \int_{-\infty}^{+\infty} du \exp[-\sum_{\mathbf{q}} S_{\mathbf{q}}(2n_{\mathbf{q}} + 1)] \times [\exp(-\sum_{\mathbf{q}} \frac{\cos \omega_{\mathbf{q}} u}{\sin \hbar\omega_{\mathbf{q}}/2kT}) - 1] \tag{5.6}$$

with $n_{\mathbf{q}}$ the phonon occupation number and the "Huang-Rhys factors"

$$S_{\mathbf{q}} = (1/2)|s_{\mathbf{q}}^{+} - s_{\mathbf{q}}^{-}|^2 m\omega_{\mathbf{q}}/\hbar \tag{5.7}$$

which describe the coupling of the displacement change to the phonon field, $s_{\mathbf{q}}^{+}$ and $s_{\mathbf{q}}^{-}$ being the displacement components of the host atoms with the H-atom at $+\mathbf{d}$ and $-\mathbf{d}$, respectively. For small $\mathbf{q}$ one has $S_{\mathbf{q}} \sim q$ or q^{-1} for isotropic defects or anisotropic defects which change their orientation in the tunneling process, respectively (1.4). In evaluating (5.5) one has to omit the diagonal transitions $\{m_i\} = \{n_i\}$. This leads to the -1 on the rhs. of (5.6). Diagonal transitions correspond to coherent tunneling without phonon creation or absorption. Their inclusion would cause a divergence due to their weak coupling to the long wavelength phonons, given by $S_{\mathbf{q}}$ combined with a vanishing density of states, $Z(\omega) \sim \omega^2$. A golden rule formula cannot describe coherent processes adequately. (5.6) yields in the isotropic case a T^7 law at low temperatures and an Arrhenius behaviour at high temperatures

$$W^{if} = (\pi/4\hbar^2 E_c kT)^{1/2}|J|^2 \exp(-E_c/kT) \tag{5.8}$$

The activation energy, E_c, in (5.8) is the so called coincidence energy, i.e. the minimal energy necessary to deform the lattice such that the initial and final configurations - of H plus lattice - are equivalent. This coincidence energy is different from the "classical" activation energy which is the energy needed to transpose the H atom quasistatically from its initial to its final position. It has been shown by Kondo [30] that in the low temperature limit the nonadiabacity of the interstitial-electron interaction becomes decisive. The resulting low temperature behaviour of the hopping rate shows a minimum at low temperatures, for details we have to refer to the original literature. For calculations at low temperatures where the linear coupling approximation, with the coupling to the electrons added, describes the temperature behaviour adequately, Feynman path integral methods have been found to be an ideal method, see eg. [31,32] . We will not discuss these methods here but concentrate on phononic effects in (5.4), thus keeping within the adiabatic (Born-Oppenheimer) approximation as regards the electrons. The electronic effects would be superimposed on our results.

There are numerous extensions to the simple linear coupling model, mainly aimed at improving upon the concept of a constant J. Even keeping the strict splitting into a hydrogen and a lattice wavefunction J will be temperature dependent due to the larger tunneling probability between excited states. Still within the adiabatic approximation but improving on the Condon approximation is the occurence probability approach [33,34] where one evaluates J for all coincidence configurations and averages with respect to lattice energy and excitation of the localized H-vibrations. These approximations explain the observed H-diffusion at least qualitatively.

Whereas the approximations discussed so far relied on a weak hydrogen-phonon interaction we want to drop this restriction which is inconsistent with the occurence of resonant vibrations and comparatively large self-trapping energies. To accomodate the resonant vibrations, which are tantamount to a strong hydrogen-phonon coupling, we treat the hydrogen and lattice degrees of freedom simultaneously, starting from (5.3) and (5.4) but avoiding the adiabatic and Condon approximations. The evaluation of the rates (5.4) is outlined in [21] it can be broken down into the following stages: i) choice of interaction model, ii) calculation of structures, energies and eigenmodes, iii) evaluation of the tunnel splitting and of the transition probabilities w^{if} and the total rate W^{if}. For the interaction we used the model by Sugimoto and Fukai [35] where the H-Nb interaction is via a truncated double exponential potential and the Nb-Nb interaction is via Born-von Karman parameters .

In agreement with experiment the stable configuration of the hydrogen interstitial is tetrahedral. We find for H a self-trapping energy of $E_{ST} = 470meV$ where $300meV$ is potential energy and the change of the zero point vibrations contributes $170meV$. The minimal coincidence configuration energy is $E_c = 41meV$ ($31meV$ potential energy and $10meV$ zero point motion) and the classical saddle point energy is $E_a = 61meV$ (potential energy only). As eigenstates in the initial and final configurations we take as a first approximation the harmonic ones obtained by diagonalizing the dynamic matrix for clusters of 6 to 21 atoms. Using these eigenmodes and a correction term for the rest of the lattice [21] we find at $T = 0K$ a tunnel splitting of $\Delta E_T = 0.01meV$ smaller than the value of $0.2meV$ observed for H trapped in Nb-O. This underestimate may be due to a slightly different geometry for Nb-O-H as compared to Nb-H. We have assumed that the tunneling occurs only between a pair of adjacent sites. In general there is an additional geometric factor. Our value will be an underestimate due to the too small overlap of the harmonic wavefunctions. Assuming a sinusoidal potential shape one gains a correction factor of 1.3. If we write ΔE_T as in (5.2) as $\Delta E_T = J\exp(-S)$ we find changing the isotopic masses a dressing factor of 0.15 in accordance with the usual estimates. The total tunnel splitting is, however, larger by a factor 5 as compared to a seperate calculation of the two terms. This indicates a rearrangement of the contributions of the localized modes, included in J, and of the band modes, determining S. The temperature dependence of (5.2) as gained by thermal averaging over the occupation numbers with $m_i = n_i$, is totally different from the one expected in the weak coupling model.

The total transition rate sums over all possible initial and final mode occupancies with energy conservation as the only restriction. With increasing temperature the number of terms diverges rapidly. In order to evaluate (5.4) we, therefore, divide the modes into strongly and weakly coupling ones. The latter ones we treat by the usual small polaron formalism whereas we sum over the strongly coupled ones explicitely. Eq. (5.4) is transformed into

$$w^{if} = 2\pi/\hbar|\langle\Psi_i(m)|H - 1/2(E_{im} + E_{fn})|\Psi_f(n)\rangle|^2 G(E_{im} - E_{fn}) \qquad (5.9)$$

Here the δ-function is replaced by a shape function which consists of two distinct factors. One comes from the line broadening, i.e. it accounts for the broadening of the sharp modes of the atomic cluster by the embedding lattice. We take a form

$$G_v(\omega) = (1/\sqrt{\pi})W_v \exp[-(\omega - \Omega)^2 W_v^2] \tag{5.10}$$

where $W_v = \sum_\sigma w^\sigma(m_\sigma + n_\sigma)$ is the total width and $\hbar\Omega = \sum_\sigma \hbar\omega^\sigma(m_\sigma - n_\sigma)$ is the difference in vibrational energy between the initial and final states. As widths, w^σ, of the individual modes σ we took $0THz$ and $0.5THz$ for the localized and band modes, respectively. The second factor in the shape function stems from the change in mean displacement of the weakly coupled modes outside of the cluster as the hydrogen atom jumps. It corresponds to the dressing terms in (5.5). Its magnitude is, however, strongly reduced since we have included the bulk of the dressing explicitely in (5.9). To simplify the evaluation we take the high temperature limit of this term

$$G_R(\omega) = (16\pi E_R kT)^{-1/2} \exp[-(\hbar\omega + 4E_R)^2/16E_R kT] \tag{5.11}$$

where we estimate from the overlap at $T = 0K$ that $E_R = 6meV$.

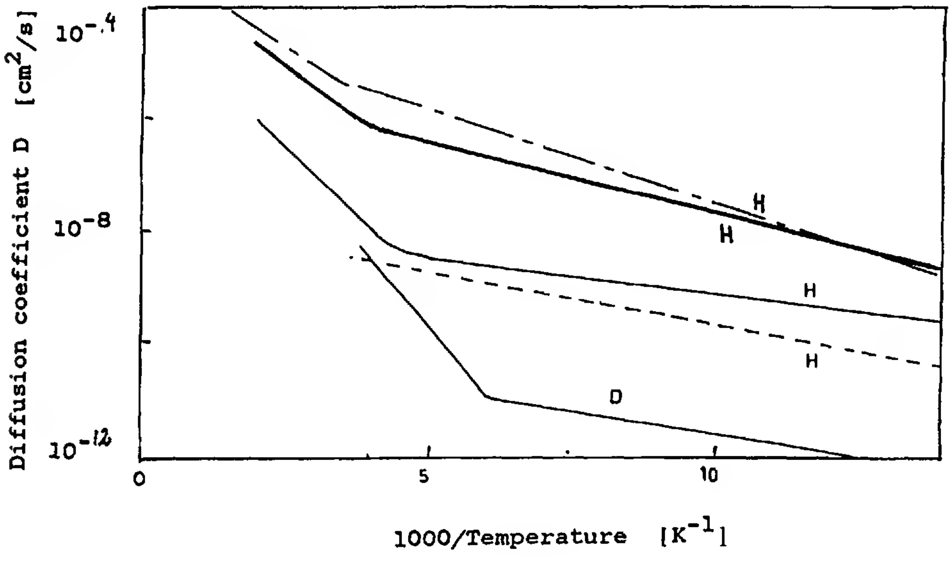

Fig. 7 Diffusion constants of H and D in Nb.—— - ——experimental value [28], — — — according to (5.8), ——— full calculation harmonic wavefunctions, ▬▬▬ full calculation with anharmonic wavefunctions.

Fig. 7 shows our results for the diffusion coefficients of H and D together with the values for H derived from (5.7) and experiment. From $T \simeq 10K$ upwards we find an Arrhenius behaviour with a sudden change in activation energy at $T \simeq 250K$. This kink can be understood from the partial rates, w^{if}. At low temperatures transitions are only possible without exciting the localized vibrations of the H. At higher temperatures scattering from the band states into the localized states becomes allowed, $m_{loc} = 0 \rightarrow n_{loc} = 1$. These transitions with an excited localized state have much larger tunneling elements and whence become dominating.

The model so far is able to describe the general behaviour. To get a better quantitative agreement we have to improve on the wavefunctions. For this we studied the anharmonic expansion parameters of the potential energy and added a first order correction to the harmonic wavefunctions. Two types of anharmonic terms were found to be important:
i) Fourth order terms in the localized H-vibrations $(\phi^{(4)}u_{loc}^4)$. Including these terms leads to an increased tunneling rate at $T = 0$ and a slight increase in the high temperature activation energy. These effects can be estimated from low dimensional models including only the localized modes.
ii)third order couplings between localized and band modes $(\phi^{(3)}u_{band}u_{loc}^2)$. These terms are important for the low temperature behaviour. They account for the reduction of the localized frequencies when the surrounding lattice is appropriately deformed.
Including these anharmonic contributions we get also quantitatively good agreement with the experimental values, fig.7, and we conclude that we have demonstrated that a lattice dynamical model of quantum diffusion is applicable. The advantage of such a model is the possibility to study in detail the influence of the single processes contributing to diffusion. The importance of anharmonic effects will probably be reduced for heavier interstitials where one does not have the interplay between localized and resonance modes.

1. I. M. Lifshitz, J.Phys.Ussr. **7**, 215 and 249, (1943).
2. A. A. Maradudin, E. W. Montroll, G. H. Weiss and I. P. Ipatova, *Theory of Lattice Dynamics in the Harmonic Approximation*, Solid State Physics, Suppl. 3, 2nd ed., (Academic Press, New York 1971).
3. P. H. Dederichs and R. Zeller in *Point Defects in Metals II*, Springer Tracts in Modern Physics 87, (Springer Verlag, Berlin 1980).
4. R. F. Wood, in *Methods in Computational Physics 15*, p.119, (Academic Press, New York 1976).
5. R. M. Nicklow, in *Treatise in Material Science and Technology*, p.191 , (Academic Press, New York 1979).
6. V. K. Tewary, Adv.Phys. **22**, 758, (1973).
7. H. R. Schober and K. W. Ingle, J.Phys.F **10**, 575, (1980).
8. G. Leibfried and N. Breuer, *Point Defects in Metals I*, Springer Tracts in Modern Physics

81, (Springer Verlag, Berlin 1978).

9. K.-H. Robrock, Report JÜL 1077-FF, (1974).
10. R. Haydock, V. Heine and M. J. Kelly, J.Phys.C **5**, 2845, (1972).
11. G. Punz and J. Hafner, Z.Phys.B **61**, 231, (1985).
12. A. Czachor, Phys.Rev.B **21**, 4458, (1980) and this volume.
13. H. R. Schober, M. Mostoller and P. H. Dederichs, Phys.Stat.Sol. (b)n **64**, 173, (1974).
14. J. A. Krumhansl and J. A. D. Mathews, Phys.Rev. **166**, 856, (1968).
15. P. S. Bechthold, U. Kettler, H. R. Schober and W. Krasser, Z.Phys.D **3**, 263, (1986).
16. R. Urban, P. Ehrhart, W. Schilling, H. R. Schober and H. Lauter in *Vacancies and Interstitials in Metals and Alloys 1986*, Materials Science Forum in print.
17. S. M. Shapiro, D. Richter, Y. Noda and H. Birnbaum, Phys.Rev.B **23**, 1594,(1981).
18. R. J. Elliot, J. A. Krumhansl and P. L. Leath, Rev.Mod. Phys. **46**, 465 (1974).
19. H. W. Diehl and P. L. Leath, Phys.Rev.B **19**, 587 and 596, (1979); H. W. Diehl, P. L. Leath and T. Kaplan, Phys.Rev.B **19**, 5044, (1979).
20. C. P. Flynn, Phys.Rev. **171**, 682, (1968).
21. H. R. Schober and A. M. Stoneham, Phys.Rev.B **26**' 1819, (1982).
22. U. Buchenau, M. Prager, N. Nücker, A. J. Dianoux, N. Ahmad and W. A. Phillips, Phys.Rev.B **34**, 5665, (1986).
23. Y. Fukai and H. Sugimoto, Adv.Phys. **34**, 263, (1985).
24. T. Springer in *Hydrogen in Metals*, Basic Properties in Applied Physics **28** (G. Alefeld and J. Völkl eds.), (Springer, Berlin 1978).
25. V. Lottner, H. R. Schober and W. J. Fitzgerald, Phys.Rev.Lett. **17**, 1162, (1979).
26. H. Wipf, A. Magerl, S. M. Shapiro, S. K. Satija and S. K. Thomlinson, Phys.Rev.Lett. **46**, 947, (1981); H. Wipf and K. Neumaier, Phys.Rev.Lett. **52**, 1308, (1984).
27. A. Magerl, J. J. Rush, J. M. Rowe, D. Richter and H. Wipf, Phys.Rev.B **27**, 927, (1983).
28. Zh Qi, J. Völkl, R. Lässer and H. Wenzl, J.Phys.F **13**, 2053, (1983).
29. C. P. Flynn and A. M. Stoneham, Phys.Rev.B **1**, 3966, (1970).
30. J. Kondo, Physica **125B**, 279, (1984); Hyperfine Interactions **31**, 117, (1986).
31. H. Grabert, U. Weiss and H.R. Schober, Hyperfine interactions **31**, 147 (1986).
32. P. Hedegard, Phys.Rev.B **35**, 533 (1987).
33. D. Emin, M. I. Baskes and W. D. Wilson, Phys.Rev.Lett. **42**, (1979).
34. H. Teichler and A. Klamt, Phys.Lett. **108A**, 63, (1985).
35. H. Sugimoto and Y. Fukai, Phys.Rev.B **22**, 670, (1980).

EQUIVALENCE OF EULERIAN AND LAGRANGIAN PHONONS: SOUND PRESSURE AND TWO-FLUID EQUATIONS

A. Thellung
Institut für Theoretische Physik der Universität
Zürich, Schönberggasse 9, 8001 Zürich, Switzerland

Abstract: In correspondence to the two different descriptions of hydrodynamic motion by Euler and by Lagrange, there are two natural ways of defining phonons and the corresponding classical sound waves. Eulerian phonons turn out to have a momentum $\hbar \underline{k}$ ($\underline{k}$ = wave vector), whereas Lagrangian phonons carry no momentum. This might suggest that the two definitions lead to different physical effects. That this is not the case is shown in detailed discussions of two examples: the sound pressure and the derivation of two-fluid equations.

1. INTRODUCTION

Fluid motion can be described in terms of Eulerian (local) or Lagrangian (material) coordinates [1]. Due to the nonlinear terms in the equations of motion of an ideal fluid, an initially purely sinusoidal sound wave will change its shape in the course of time, but with suitable boundary conditions its momentum is a constant of the motion. It vanishes for a purely sinusoidal sound wave in Lagrangian coordinates and is different from zero for a purely sinusoidal sound wave in Eulerian coordinates.

At any instant of time the irrotational motion of an ideal fluid can be Fourier decomposed into sinusoidal sound waves (with slowly varying amplitudes as a consequence of the nonlinearities), whose momenta vanish in one case and are different from zero in the other case. In either case any amount of momentum can be obtained from the mode with wave number $\underline{k} = 0$, i.e. from a uniform translational motion.

The quantized theory leads to similar results: A Lagrangian phonon has no momentum, an Eulerian phonon of wave vector $\underline{k}$ carries a momentum $\hbar \underline{k}$.

This might make one believe that the two formulations of hydrodynamics would lead to different physical results. An example is the sound pressure when it is calculated along the same lines as the light pressure in electrodynamics, which can be found by determining the momentum of an incoming light wave transferred to an absorbing or reflecting screen. Another example is the microscopic derivation of the two-fluid equations for liquid He II (see e.g. [2]-[5]) for which it looks essential that an elementary excitation - like a phonon - of wave vector $\underline{k}$ carries a momentum $\hbar \underline{k}$. This point of view is put forward e.g. in [6].

On the other hand, physically observable effects cannot depend on the choice of the variables - Lagrangian or Eulerian - which are both legitimate and give complete descriptions of hydrodynamic motion. Indeed, a careful analysis shows that for well-defined physical situations both descriptions lead to the same result. In this paper we are going to demonstrate this in full detail for the sound pressure. As to the derivation of the two-fluid equations, the equivalence of the two formulations has been shown earlier [7],[8]. We repeat here the essential facts.

In Section 2, the differences between Euler's and Lagrange's formulations of hydrodynamics are laid out, and classical sound waves in the two cases are compared. In Section 3 we remind the reader of the calculation of the light pressure in electrodynamics. The calculation of the sound pressure is more delicate because of the non-linearities and because what might be called "lateral boundary conditions" play a rôle (compare [9]). We derive a general formula which is then applied to various physical situations. In Section 4 quantization is carried out in Euler's and Lagrange's formalisms, giving the two kinds of phonons. Finally, in Section 5, we sketch the differences in the derivation of the two-fluid equations and show that they do not affect the final result. It is important to remark that the two-fluid equations themselves are always written in local coordinates, referring to the laboratory frame of reference, whether their derivation is based on Eulerian or Lagrangian phonons; otherwise the two cases cannot be easily compared.

2. CLASSICAL SOUND WAVES IN EULERIAN AND LAGRANGIAN COORDINATES

A Lagrangian coordinate $\underline{a}$ - also called material coordinate - labels a given element of fluid (independent of its present position); it equals e.g. its equilibrium position when the fluid is at rest. An Eulerian coordinate $\underline{x}$ - also called local coordinate - characterizes a given point in space (independent of which element of fluid passes through that point). The connection between $\underline{x}$ and $\underline{a}$ is made by saying that $\underline{x}$ is the position at time t of the element of fluid whose equilibrium position is $\underline{a}$. Therefore the relation between $\underline{x}$ and $\underline{a}$ is

$$\underline{x} = \underline{a} + \underline{\xi}(\underline{a},t) \ , \tag{2.1}$$

where $\underline{\xi}(\underline{a},t)$ is the displacement vector at time t of the element of fluid labeled by $\underline{a}$. In Euler's formulation of hydrodynamics, $\underline{x}$ and t are taken as the independent variables; in Lagrange's formulation, the independent variables are $\underline{a}$ and t .

By means of (2.1) any function φ of $\underline{x}$, t can be expressed as a function φ^* of $\underline{a}$, t and vice versa,

$$\varphi(\underline{x}(\underline{a},t),t) =: \varphi^*(\underline{a},t) \ . \tag{2.2}$$

The vector field

$$\frac{\partial}{\partial t}\,\underline{x}(\underline{a},t) = \frac{\partial}{\partial t}\,\underline{\xi}(\underline{a},t) = \underline{v} \tag{2.3}$$

as a function of $\underline{a}$, t is the velocity of the element of fluid labeled by $\underline{a}$; expressed as a function of $\underline{x}$, t it is ths hydrodynamic velocity at point $\underline{x}$.

Now we look at longitudinal sound waves in the two formulations of the hydrodynamics of a nonviscous fluid [1]. We assume periodic boundary conditions in order to allow for travelling waves. For small amplitudes one can taks the linearized version of the squations of motion, and a possible solution in Lagrangian coordinates is

$$\underline{\xi} = \underline{A}\,\sin(\underline{k}\underline{a} - \omega_{\underline{k}}t + \alpha) \ . \tag{2.4}$$

Such a purely sinusoidal wave will of course not persist for all times because of the nonlinear terms in the equations of motion, but we can assume it as an exact initial state of the liquid at a certain moment, and for a little while it will remain a good approximation, if ths amplitude $\underline{A}$ is small. Obviously the momentum of such a wave is zero,

$$\int d^3a\,\varrho_0\,\dot{\underline{\xi}} = 0 \ , \tag{2.5}$$

and will stay so since it is a constant of the motion. ($\varrho_0 d^3a$ is the mass contained in the element of volume d^3a; ϱ_0 = const for a homogensous fluid).

For later comparison with purely sinusoidal waves in Eulerian coordinates, we express the velocity field due to (2.4) in Eulerian coordinates. Using (2.1), we have

$$\begin{aligned} \underline{v}_L &= \dot{\underline{\xi}} = -\,\underline{A}\omega_{\underline{k}}\cos(\underline{k}\underline{a} - \omega_{\underline{k}}t + \alpha) \\ &= -\,\underline{A}\omega_{\underline{k}}\cos(\underline{k}\underline{x} - \underline{k}\,\underline{\xi} - \omega_{\underline{k}}t + \alpha) \ . \end{aligned} \tag{2.6}$$

Substitution of (2.4) and expansion in powers of the (small) amplitude $\underline{A}$ yields

$$\underline{v}_L = -\underline{A}\omega_{\underline{k}} \cos(\underline{k}\underline{x} - \omega_{\underline{k}} t + \alpha) - \underline{A}\omega_{\underline{k}}(\underline{k}\underline{A}) \sin^2(\underline{k}\underline{x} - \omega_{\underline{k}} t + \alpha) + O(A^3) , \qquad (2.7)$$

which is not purely sinusoidal in $\underline{x}$. The (Eulerian) density

$$\rho(\underline{x},t) = \rho_0 + \rho'(\underline{x},t) \qquad (2.8)$$

is calculated by observing that

$$\rho\, d^3x = \rho_0 d^3a . \qquad (2.9)$$

In Euler's formulation, ρ_0 plays the role of the average or equilibrium density, and we have

$$\int d^3x\, \rho'(\underline{x},t) = 0 . \qquad (2.10)$$

Equation (2.9) shows that ρ/ρ_0 is given by the Jacobian of the transformation (2.1), (2.4), which yields, calculated to first order in $\underline{A}$,

$$\rho = \rho_0 - \rho_0(\underline{A}\underline{k}) \cos(\underline{k}\underline{x} - \omega_{\underline{k}} t + \alpha) + O(A^2) . \qquad (2.11)$$

The momentum of the sound wave (2.4) must of course also vanish when it is calculated in Eulerian coordinates. In fact, it is easily checked, at least to second order in $\underline{A}$, that the spatial average (average over $\underline{x}$, denoted by a bar) of the momentum density $\rho\underline{v}$, calculated from (2.11) and (2.7) vanishes,

$$\overline{(\rho\underline{v})}_L = 0 . \qquad (2.12)$$

Later, we shall need the spatial average of the velocity (average again over $\underline{x}$) . From (2.7) it is seen to be

$$\overline{\underline{v}}_L = - \tfrac{1}{2} \underline{A}\omega_k(\underline{k}\underline{A}) \qquad (2.13)$$

to second order in $\underline{A}$, which is different from zero for a longitudinal wave.

Next we look at a purely sinusoidal wave in Eulerian coordinates,

$$\underline{v}_E = - \underline{B}\omega_{\underline{k}} \cos(\underline{k}\underline{x} - \omega_{\underline{k}} t + \alpha) . \qquad (2.14)$$

It is a solution of the linearized Eulerian equations of motion. Due to the nonlinear terms in the fundamental equations, it will not persist for all times, but again we can take it as an exact state of the liquid at a given moment, and for a little while it will remain a good approximation if $\underline{B}$ is small. The corresponding density can be calculated from the equation of continuity.

$$\frac{\partial}{\partial t}\rho(\underline{x},t) = - \mathrm{div}_{\underline{x}}(\rho\underline{v}_E) . \qquad (2.15)$$

Calculating ρ' [Eq.(2.8)] to first order in $\underline{B}$, we obtain the result (2.11) with $\underline{A}$ replaced by $\underline{B}$. The spatial average of the momentum density is now

$$\overline{(\rho\underline{v})_E} = \tfrac{1}{2}\rho_0(\underline{B}\underline{k})\underline{B}\omega_{\underline{k}} \tag{2.16}$$

to second order in $\underline{B}$. On the other hand, the average velocity vanishes,

$$\overline{\underline{v}}_E = 0 . \tag{2.17}$$

Now consider the general irrotational motion of a liquid. Still assuming periodic boundary conditions, we can decompose $\underline{v}$ and ρ into spatial Fourier series at any instant of time. That means the motion can be considered as a superposition of sinusoidal longitudinal sound waves (with slowly time-varying amplitudes) plus a uniform translational motion, corresponding to the mode $\underline{k} = 0$. No transverse modes will occur if the motion is irrotational.

If we do the Fourier decomposition in Lagrangian coordinates, the velocity field will be a sum of terms of the type (2.6) and (2.7), plus a uniform translational velocity $\underline{U}_L$, and the density deviation $\rho' = \rho - \rho_0$ will be a sum of terms corresponding to (2.11). Forming spatial averages as before (averages over $\underline{x}$), the cross terms due to different $\underline{k}$'s cancel, and taking into account (2.10), we get to second order in the Fourier amplitudes $\underline{A}_{\underline{k}}$ the following generalizations of (2.12) and (2.13):

$$\overline{(\rho\underline{v})_L} = \rho_0\underline{U}_L \tag{2.18}$$

$$\overline{\underline{v}}_L = \underline{U}_L - \sum_{\underline{k}} \tfrac{1}{2}\underline{A}_{\underline{k}}\omega_{\underline{k}}(\underline{k}\underline{A}_{\underline{k}}) . \tag{2.19}$$

Thus, the Lagrangian sound modes (with $\underline{k} \neq 0$) do not contribute to the momentum of the liquid, but they contribute to the average velocity.

If we Fourier decompose the motion in Eulerian coordinates, we obtain the generalizations of (2.16) and (2.17), i.e.,

$$\overline{(\rho\underline{v})_E} = \rho_0\underline{U}_E + \sum_{\underline{k}} \tfrac{1}{2}\rho_0\underline{B}_{\underline{k}}\omega_{\underline{k}}(\underline{k}\underline{B}_{\underline{k}}) , \tag{2.20}$$

$$\overline{\underline{v}}_E = \underline{U}_E . \tag{2.21}$$

Thus, the Eulerian sound modes (with $\underline{k} \neq 0$) give a contribution to the momentum of the liquid, but not to the average velocity.

3. LIGHT PRESSURE AND SOUND PRESSURE

3.1. LIGHT PRESSURE

There are two ways of calculating the pressure exerted by an electromagnetic wave on an absorbing or reflecting screen. One can either integrate the force densities on the charges and currents in the screen or use the law of conservation of momentum. The second method is much simpler and will be illustrated by the following examples.

Consider a plane electromagnetic wave incident normally on a perfectly absorbing flat screen. In a plane travelling wave the magnitudes of the electric field $\underline{E}$ and of the magnetic field $\underline{B}$ are equal, and the energy density,

$$u = \frac{1}{8\pi}\left(\underline{E}^2 + \underline{B}^2\right) , \tag{3.1}$$

and the momentum density,

$$\underline{g} = \frac{1}{4\pi c}\left[\underline{E}, \underline{B}\right] , \tag{3.2}$$

are related by

$$\underline{g} = \frac{u}{c}\,\underline{n} . \tag{3.3}$$

($\underline{n}$ is a unit vector in the direction of propagation, c is the speed of light.) If A is the area of the screen, then in time dt electromagnetic radiation within a volume $Ac\,dt$ is absorbed and its momentum of magnitude $|\underline{g}|\,Ac\,dt = u\,A\,dt$ is transferred to the screen. According to Newton's law it equals dt times the force acting on the screen, which can be written $dt\,pA$, where p is the pressure. This shows that $p = u$. The light pressure is the time average of p,

$$\bar{p} = \bar{u} . \tag{3.4}$$

(Throughout this section we designate by a bar the time average.)

If, instead of absorption, one has perfect reflection the momentum of the incident wave is reversed, twice as much momentum is transferred to the screen, and the light pressure is

$$\bar{p} = 2\,\bar{u}^{in} . \tag{3.5}$$

Here $\bar{u}^{in}$ is the energy density of the incident wave. It equals the energy density $\bar{u}^{r}$ of the reflected wave. Therefore (3.4) is still valid if $\bar{u}$ means the total energy density, $\bar{u}^{in} + \bar{u}^{r}$.

For perfect reflection and incidence at an angle ϑ one finds

$$\bar{p} = 2\,\bar{u}^{in}\cos^2\vartheta . \tag{3.6}$$

(Only the normal component of $\underline{g}$, $|\underline{g}| \cos \vartheta$, is reversed, and only a light beam of cross section $A \cos \vartheta$ hits the screen.)

For an isotropic distribution of plane waves one has to average $\cos^2 \vartheta$ over all directions. This leads to the formula, valid in particular for black body radiation,

$$\bar{p} = \frac{1}{3} \bar{u} \, , \tag{3.7}$$

where $\bar{u}$ again is the total energy density.

All these results can of course also be derived from the concept of photons with energy $\varepsilon = \hbar\omega$ and momentum $\underline{p} = \hbar \underline{k} = \frac{\varepsilon}{c} \underline{n}$.

In view of the above derivation of the light pressure one would expect that in hydrodynamics, too, it is the momentum of a wave that determines the pressure on an absorbing or reflecting surface and that therefore Eulerian and Lagrangian sound waves lead to different results. We are now going to show that in hydrodynamics the problem is more subtle and that Eulerian and Lagrangian sound waves give the same result.

3.2 SOUND PRESSURE

Let us consider a plane longitudinal sound wave propagating in the x-direction and incident normally on a flat wall W (Fig. 1) located at

$$x = a + \xi(a,t) \, . \tag{3.8}$$

x coincides with the Eulerian coordinate of an element of fluid right

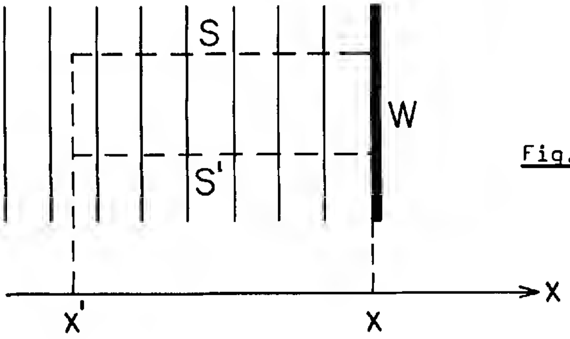

Fig. 1

at the wall, whose Lagrangian coordinate a gives its equilibrium position and that of the wall. Special cases are (i) the fixed rigid wall, $\xi \equiv 0$, $x \equiv a$, giving rise to complete reflection, or

(ii) ξ corresponding exactly to the motion an element of fluid would carry out in the absence of the wall (this is equivalent to complete absorption). The pressure on W is $p(x,t) = p^*(a,t)$.

Now we write down the momentum balance for the fluid in a cylinder of unit area of cross section, with axis in the x-direction, between the wall W and an arbitrary plane $x' =$ const. (Fig.1):

$$\frac{d}{dt}\int_{x'}^{a+\xi(a,t)} dx\, \varrho v_x = p(x',t) - p^*(a,t) + \varrho v_x^2(x',t) , \qquad (3.9)$$

where the last term represents the flux of momentum across the surface at x' . Let us assume a stationary (periodic in time) situation. If we take the time average of (3.9) the left hand side vanishes, and we have

$$\overline{p^*}(a) = \bar{p}(x') + \overline{\varrho v_x^2}\,(x') . \qquad (3.10)$$

This shows that the quantity determining the pressure is not the momentum, but the flux of momentum. x' is arbitrary and we can take a spatial average over x' , which we shall indicate by a second bar. $\overline{p^*}(a)$ not being affected by this average, we obtain

$$\overline{p^*}(a) = \overline{\overline{p}} + \overline{\overline{\varrho v_x^2}} . \qquad (3.11)$$

If the sound wave is propagating in an arbitrary direction with respect to the wall the result (3.11) is still valid because the contributions from the lateral surfaces S, S' (Fig. 1) cancel on the average.

This shows that quite generally the (time average of the) pressure on a wall equals the space-time average in the sound field of the pressure plus twice the kinetic energy of the motion perpendicular to the wall. In an actual physical situation it is a well-defined quantity that cannot depend on the mathematical description (Lagrangian or Eulerian) of the fluid motion. Different formulae for the sound pressure occurring in the literature stem from the fact that the value of $\overline{\overline{p}}$ depends on what one might call "lateral boundary conditions". This has been pointed out in an elucidating paper by Richter [9]. We are giving a somewhat generalized version of his arguments.

Suppose that in a liquid between a sound transmitter T and a (reflecting or absorbing or partly reflecting) wall W a stationary (periodic) sound field has been established as shown in Fig. 2. For sufficiently small wave length the sound field practically fills only the region between T and W . In particular at the backside of W the liquid is at rest and we have the normal static pressure p_0 and

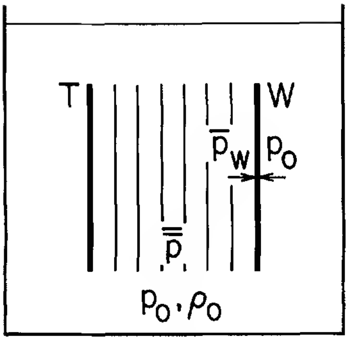

Fig. 2: Sound field in open connection with liquid at rest.

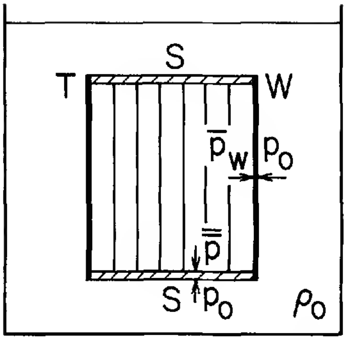

Fig. 3: Sound field confined by lateral walls S .

the equilibrium density ρ_0 . If one has doubts about the sound field remaining confined to the region between T and W one can imagine that side walls S have been put in (Fig.3).

Evidently, the sound pressure on the wall W is the time average of the difference between the pressures p_w and p_0 to the left and right of the wall. Using formula (3.11) for $\overline{p^*(a)} \equiv \overline{p}_w$ we have

$$\overline{p}_w - p_0 = \overline{\overline{p}} - p_0 + \overline{\overline{\rho v_x^2}} \; . \tag{3.12}$$

Fig. 2 shows that

$$\overline{\overline{p}} = p_0 \; ; \tag{3.13}$$

otherwise a flow of liquid would take place through the region separating the sound field from the liquid at rest. In Fig. 3 we assume the lateral walls S to be mobile; then in a stationary situation they have taken such positions that $\overline{\overline{p}} = p_0$. Thus in either case the sound pressure is

$$\overline{p}_w - p_0 = \overline{\overline{\rho v_x^2}} \; . \tag{3.14}$$

In general the space-time average of the density ρ in the sound field will differ from ρ_0 . To see this we use the (adiabatic) equation of state giving the pressure as a function of ρ . We write it as a Taylor series in powers of $\rho - \rho_0$,

$$p = f(\rho) = p_0 + f_0'(\rho - \rho_0) + \tfrac{1}{2} f_0''(\rho - \rho_0)^2 + \dots \tag{3.15}$$

From (3.13) it follows that

$$\overline{\overline{\rho}} - \rho_0 = -\frac{1}{f_0'}\left[\tfrac{1}{2} f_0'' \; \overline{\overline{(\rho - \rho_0)^2}} + \frac{1}{3!} f_0''' \; \overline{\overline{(\rho - \rho_0)^3}} + ..\right]. \tag{3.16}$$

Depending on the sign of f''_o (f'_o is always positive) liquid will flow into or out of the region between T and W (Fig. 2) while the sound field is being set up. In the case of Fig. 3 the lateral walls S will shift to appropriate positions.

On the other hand, if the lateral walls S (Fig. 3) are kept fixed while the sound field is set up one has

$$\overline{\overline{\rho}} = \rho_o \, . \tag{3.17}$$

In that case

$$\overline{\overline{p}} - p_o = \tfrac{1}{2} f''_o \; \overline{\overline{(\rho - \rho_o)^2}} + \dots \tag{3.18}$$

and the sound pressure (3.12) becomes

$$\overline{p_w} - p_o = \overline{\overline{\rho v_x^2}} + \tfrac{1}{2} f''_o \; \overline{\overline{(\rho - \rho_o)^2}} + \frac{1}{3!} f'''_o \; \overline{\overline{(\rho - \rho_o)^3}} + \dots \tag{3.19}$$

In the rest of this section we specialize our results to the case of small sound amplitudes and take only terms up to second order in $\rho - \rho_o$ and $\underline{v}$. We introduce the density of the potential energy

$$E_p = -\rho \int_{1/\rho_o}^{1/\rho} (p - p_o) \, d \left(\frac{1}{\rho}\right) , \tag{3.20}$$

which, calculated to second order by means of (3.15), is

$$E_p = \frac{1}{2\rho_o} f'_o \; (\rho - \rho_o)^2 \, . \tag{3.21}$$

Furthermore, since in the sound fields discussed here $v_x = v$ is the full velocity of the liquid, the expression ρv_x^2 in our equations equals twice the kinetic energy density, which to second order is

$$E_k = \tfrac{1}{2} \rho_o \, v^2 \, . \tag{3.22}$$

In this approximation (3.14) gives

$$\overline{p_w} - p_o = 2 \, \overline{\overline{E_k}} \, , \tag{3.23}$$

(3.16) yields

$$\overline{\overline{\rho}} - \rho_o = -2 \, \frac{\gamma}{f'_o} \overline{\overline{E_p}} \tag{3.24}$$

with

$$\gamma = \frac{f''_o \, \rho_o}{2 \, f'_o} \, , \tag{3.25}$$

and finally (3.19) takes the form

$$\overline{p_w} - p_o = 2 \, \overline{\overline{E_k}} + 2 \, \gamma \, \overline{\overline{E_p}} \, . \tag{3.26}$$

Since we want to calculate $\overline{p_w} - p_o$ and $\overline{\overline{\rho}} - \rho_o$ only to second order in the amplitudes it suffices to calculate the right hand sides of eqs.

(3.23), (3.24) and (3.26) by substituting in E_k and E_p the first order values of $\underline{v}$ and $\rho - \rho_o$, i.e. the solutions of the linearized equations of motion. These are the same in Euler's and Lagrange's formalism !

In this approximation

$$\overline{\overline{E}}_k = \overline{\overline{E}}_p = \tfrac{1}{2}\,\overline{\overline{E}} \tag{3.27}$$

holds, where E is the total energy density. Using this, we arrive at the final result for the sound pressure (3.23),

$$\overline{p_w} - p_o = \overline{\overline{E}}\ , \tag{3.28}$$

valid for a sound field in open connection with liquid at rest (Fig.2) or with mobile lateral walls (Fig. 3). In the case of fixed lateral walls (3.26) can be written

$$\overline{p_w} - p_o = (1 + \gamma)\ \overline{\overline{E}}\ . \tag{3.29}$$

The second order formulae (3.28), (3.29) have been derived by Richter [9] by integrating Euler's equation of an ideal fluid under the assumption that everywhere - also in the intermediate region between the sound field and the liquid at rest (Fig. 2) - the motion is vortex-free.

4. QUANTIZED SOUND WAVES

4.1. EULERIAN PHONONS

Quantization of the irrotational motion of a nonviscous fluid was carried through in Eulerian coordinates [10]. We summarize the main aspects of the theory.

Consider a fluid in a cube of volume V with periodic boundary conditions. The equations of motion can be brought into a canonical form with Hamiltonian

$$\mathcal{H}_E = \int_V d^3x\ (\tfrac{1}{2}\,\underline{v}\,\rho\,\underline{v} + E_p(\rho))\ , \tag{4.1}$$

where the velocity $\underline{v}$ is written in the form

$$\underline{v} = \underline{U}_E - \underline{\nabla}\,\varphi \tag{4.2}$$

($\underline{U}_E$ = uniform translational velocity, φ = velocity potential) and the potential energy $E_p(\rho)$ is defined by (3.20) with p a given function of ρ. φ and ρ are canonically conjugate fields. The canonical field equations,

$$\dot{\varphi} = \frac{\delta\mathcal{H}}{\delta\rho}\ , \qquad \dot{\rho} = -\frac{\delta\mathcal{H}}{\delta\varphi}\ , \tag{4.3}$$

give the Bernoulli equation and the equation of continuity. We take $\mathcal{H}_E$ exact in $\underline{u}_E$ but only up to second order in φ and $\rho - \rho_0$ (harmonic approximation). The higher order terms are treated as a perturbation. This yields (compare (3.21) with $f'_0 = c^2_0$, where c_0 is the speed of sound at density ρ_0)

$$\mathcal{H}_E = \int_V d^3x \left\{ \tfrac{1}{2} \rho_0 \underline{u}_E^2 - \underline{u}_E \cdot \tfrac{1}{2} (\rho \underline{\nabla} \varphi + \underline{\nabla} \varphi \rho) + \tfrac{1}{2} \rho_0 (\underline{\nabla} \varphi)^2 + \frac{c^2_0}{2\rho_0} (\rho - \rho_0)^2 + \dots \right\} . \tag{4.4}$$

The total momentum is given by

$$\underline{\mathcal{P}}_E = \int_V d^3x \, \tfrac{1}{2} \left\{ \rho (\underline{u}_E - \underline{\nabla} \varphi) + (\underline{u}_E - \underline{\nabla} \varphi) \rho \right\} . \tag{4.5}$$

In the quantized version the field commutators are

$$[\rho(\underline{x}), \varphi(\underline{x}')] = \frac{\hbar}{i} \delta(\underline{x} - \underline{x}') , \tag{4.6}$$

the other commutators vanishing. The quadratic Hamiltonian (4.4) can be diagonalized by standard methods [7], [10] (Fourier transformation of φ and ρ), yielding

$$\mathcal{H}_E = \tfrac{1}{2} \rho_0 V \underline{u}_E^2 + \underline{u}_E \sum_{\underline{k}} \hbar \underline{k} n_{\underline{k}} + \sum_{\underline{k}} \varepsilon_{\underline{k}} n_{\underline{k}} , \tag{4.7}$$

where $n_{\underline{k}}$ can take the values 0,1,2,... and is the number of phonons of wave vector $\underline{k}$ and

$$\varepsilon_{\underline{k}} = \hbar \omega_{\underline{k}} = \hbar c_0 k \tag{4.8}$$

their energies. The zero point energy has been omitted in (4.7). The momentum (4.5) takes the form

$$\underline{\mathcal{P}}_E = \rho_0 V \underline{u}_E + \sum_{\underline{k}} \hbar \underline{k} n_{\underline{k}} , \tag{4.9}$$

and the spatially averaged velocity, which will be called $\underline{u}_s$ from now on, is seen from (4.2) to be

$$\underline{u}_{sE} = \underline{u}_E . \tag{4.10}$$

For later purposes we replace $\underline{u}_E$ by $\underline{u}_{sE}$ in (4.7) and obtain

$$\mathcal{H}_E = \tfrac{1}{2} \rho_0 V \underline{u}^2_{sE} + \sum_{\underline{k}} n_{\underline{k}} (\varepsilon_{\underline{k}} + \hbar \underline{k} \, \underline{u}_{sE}) . \tag{4.11}$$

The terms of third and higher order (anharmonic terms) in the Hamiltonian (4.1) are treated by perturbation theory. They lead (i) to a modification of the phonon energy spectrum (4.8) (dispersion) and (ii) to transitions between different phonon states (scattering, annihilation, and creation of phonons).

The expressions for the momentum (4.9) and for the average velocity (4.10) are exact; they are not affected by the anharmonic terms in the Hamiltonian. Equations (4.9) and (4.10) mean that Eulerian phonons give a contribution ($\hbar \underline{k}$ per phonon) to the momentum, but no contribution to the average velocity. Equations (4.9) and (4.10) are the quantum analogs of the classical results (2.20) and (2.21).

4.2 LAGRANGIAN PHONONS

We do now the same thing in Lagrangian coordinates. The velocity field can be written as $\underline{U}_L - \underline{\nabla}_{\underline{a}} \phi$.

First we assume $\underline{U}_L = 0$. In their linearized forms, the equations of motion as well as the continuity equation are the same in the Euler and Lagrange formalisms. Therefore the harmonic part of the Hamiltonian is the same as in (4.4) with $\underline{x}$ replaced by $\underline{a}$, and we have

$$\mathcal{H}_L^o = \int_V d^3a \left\{ \tfrac{1}{2} \rho_o (\underline{\nabla}_{\underline{a}} \phi)^2 + \frac{c_o^2}{2\rho_o} (\rho - \rho_o)^2 + \dots \right\}, \tag{4.12}$$

ϕ and ρ being canonically conjugate. The anharmonic terms in the Hamiltonian will of course look different in the Lagrange and Euler descriptions. The total momentum is

$$\underline{\mathcal{P}}_L^o = - \int_V d^3a \, \rho_o \, \underline{\nabla}_{\underline{a}} \phi = 0 \tag{4.13}$$

for periodic boundary conditions, and the spatially averaged velocity (spatial average again in Eulerian coordinates $\underline{x}$) is

$$\underline{u}_{sL}^o = - \frac{1}{V} \int_V d^3x \, \underline{\nabla}_{\underline{a}} \phi = - \frac{1}{V} \int_V d^3a \left\{ \frac{\rho_o}{\rho} , \underline{\nabla}_{\underline{a}} \phi \right\}$$

$$= - \frac{1}{V} \int_V d^3a \left\{ \left(1 - \frac{\rho - \rho_o}{\rho_o}\right), \underline{\nabla}_{\underline{a}} \phi \right\} + \dots , \tag{4.14}$$

where higher-order powers in $(\rho - \rho_o)/\rho_o$ have been neglected. $\{a,b\} := \frac{1}{2}(ab+ba)$ is the symmetrized product, introduced in order to obtain self-adjoint operators. The commutation relations are

$$[\rho(\underline{a}), \phi(\underline{a}')] = \frac{\hbar}{i} \, \delta(\underline{a} - \underline{a}') \; . \tag{4.15}$$

The quadratic Hamiltonian (4.12) can be diagonalized as before (Fourier transformation of ϕ and ρ this time in Lagrangian variables), yielding

$$\mathcal{H}_L^o = \sum_{\underline{k}} \varepsilon_{\underline{k}} \, n_{\underline{k}} \tag{4.16}$$

apart from the zero point energy. Here $n_{\underline{k}}$ is the number of Lagrangian phonons of wave number $\underline{k}$, their energies $\varepsilon_{\underline{k}}$ being again given by (4.8). The average velocity (4.14) takes the value

$$\underline{u}^{0}_{sL} = -\frac{1}{\rho_0 V}\sum_{\underline{k}} \hbar\underline{k}\, n_{\underline{k}} + \dots \tag{4.17}$$

Now a translational motion at uniform velocity $\underline{U}_L$ is superimposed. Each atom that before had a velocity $\underline{v}$ now has a velocity $\underline{v} + \underline{U}_L$. From (4.13) and (4.17) the momentum and the average velocity now become

$$\underline{\mathcal{P}}_L = \rho_0 V \underline{U}_L \,, \tag{4.18}$$

$$\underline{u}_{sL} = \underline{U}_L - \frac{1}{\rho_0 V}\sum_{\underline{k}} \hbar\underline{k} n_{\underline{k}} + \dots \,, \tag{4.19}$$

which can be treated as a c-number in this approximation, and the energy is

$$\mathcal{H}_L = \mathcal{H}^{0}_{L} + \underline{U}_L \underline{\mathcal{P}}^{0}_{L} + \tfrac{1}{2}\rho_0 V \underline{U}^2_L = \mathcal{H}^{0}_{L} + \tfrac{1}{2}\rho_0 V \underline{U}^2_L \,,$$

since $\underline{\mathcal{P}}^{0}_{L} = 0$, or

$$\mathcal{H}_L = \sum_{\underline{k}} \varepsilon_{\underline{k}} n_{\underline{k}} + \tfrac{1}{2}\rho_0 V \underline{U}^2_L \,. \tag{4.20}$$

Equations (4.18)and (4.19)show that Lagrangian phonons have zero momentum, but give a contribution $(-(1/\rho_0 V)\hbar\underline{k}$ per phonon) to the average velocity. These results are the quantum analogs of the classical equations (2.18) and (2.19).

5. TWO-FLUID EQUATIONS

We consider liquid He II at temperatures below 0.6°K, where the thermal excitations consist entirely of phonons. Since their wavelength is considerably larger than the interatomic distance they can be obtained in a good approximation from a continuum theory, and our results of Section 4 can be applied.

We start with some kinematic considerations. If the background medium carrying a phonon is at rest, isotropic conditions prevail and the energy $\varepsilon_{\underline{k}}$ depends only on the magnitude k of the vector $\underline{k}$ (compare (4.8)). If, however, the background is moving with a velocity $\underline{u}_s$ with respect to the laboratory frame of reference, the wave vector $\underline{k}$ (whose magnitude is 2π divided by the wavelength and whose direction is perpendicular to the wave fronts) stays the same,

$$\underline{k}' = \underline{k} \,, \tag{5.1}$$

whereas the energy of the phonon in the laboratory frame will be

$$\varepsilon'_{\underline{k}} = \varepsilon_{\underline{k}} + \hbar\, \underline{k}\, \underline{u}_s \,. \tag{5.2}$$

This is just the formula for the Doppler shift,

$$\omega'_{\underline{k}} = \omega_{\underline{k}} + \underline{k}\, \underline{u}_s \,, \tag{5.3}$$

multiplied by $\hbar$, and is independent of whether a momentum is associated with a phonon or not.

The crucial point now is that $\underline{u}_s$, the velocity of the background, in (5.2) and (5.3) is not only due to a uniform translational motion of the background medium, but there may be additional contributions from all the small ripples of the other phonons present, leading to average velocities (average in the laboratory frame, i.e. in local coordinates) as we have calculated them in Sections 2 and 4. Therefore $\underline{u}_s$ in (5.2) and (5.3) has to be identified with (4.10) for Eulerian or with (4.19) for Lagrangian phonons, the $n'_{\underline{k}}$ s being the occupation numbers of the other phonons.

Since the total energy, $E' = \sum_{\underline{k}} n_{\underline{k}}(\varepsilon_{\underline{k}} + \hbar\underline{k}\underline{u}_s)$, and the sum of the wave vectors, $\underline{K} = \sum_{\underline{k}} n_{\underline{k}}\underline{k}$, are conserved in collisions between phonons in a liquid, the general canonical distribution is

$$\rho = Ce^{-(E' - \underline{u}_n \cdot \hbar \underline{K})/k_B T} \,,$$

where $\underline{u}_n$ is an arbitrary vector. By the general methods of statistical mechanics, one concludes that in thermodynamic equilibrium the mean phonon number is given by

$$\langle n_{\underline{k}} \rangle = [e^{(\varepsilon_{\underline{k}} + \underline{u}_s \cdot \hbar \underline{k} - \underline{u}_n \cdot \hbar \underline{k})/k_B T} - 1]^{-1} \,. \tag{5.4}$$

The physical meaning of $\underline{u}_n$ is that of the drift velocity of the phonon gas. The mean wave vector density of the phonons in thermal equilibrium is

$$\frac{1}{V} \sum_{\underline{k}} \underline{k} \langle n_{\underline{k}} \rangle = \frac{1}{(2\pi)^3} \int d^3k\, \underline{k}\, \langle n_{\underline{k}} \rangle =: \frac{1}{\hbar} \rho_n (\underline{u}_n - \underline{u}_s) \,. \tag{5.5}$$

The last equation defines ρ_n, the so-called density of the normal component in the two-fluid model.

In order to deal with transport phenomena the phonons are to be taken as wave packets with a distribution function $f(\underline{x},\underline{k},t)$ obeying the Boltzmann equation [4],[5],

$$\frac{\partial f}{\partial t} + \frac{\partial f}{\partial \underline{x}} \dot{\underline{x}} + \frac{\partial f}{\partial \underline{k}} \dot{\underline{k}} = \left(\frac{\partial f}{\partial t}\right)_{\text{coll}} \,, \tag{5.6}$$

where (compare (5.3))

$$\dot{\underline{x}} = \frac{\partial \omega'_{\underline{k}}}{\partial \underline{k}} = \frac{\partial \omega_{\underline{k}}}{\partial \underline{k}} + \underline{u}_s \tag{5.7}$$

is the group velocity at which the wave packet travels in the laboratory frame, and $\dot{\underline{k}}$ can be found on purely kinematic grounds by using the geometric meaning of the wave vector (without any reference to $\hbar\underline{k}$ being a momentum), yielding [3],[7]

$$\dot{\underline{k}} = - \frac{\partial \omega_{\underline{k}}}{\partial \rho} \underline{\nabla} \rho - \underline{\nabla} (\underline{u}_s \cdot \underline{k}) . \tag{5.8}$$

Expression (5.4), divided by the volume, may still be a good approximation for $f(\underline{x},\underline{k},t)$ if $\underline{u}_s$, $\underline{u}_n$, T (and also ρ_0) are functions of $\underline{x}$ and t , corresponding to local thermal equilibrium.

The two-fluid equations are just the balance equations (always written in local coordinates) for the following conserved quantities:

(i) energy of the phonons,
(ii) wave vector of the phonons,
(iii) momentum of the liquid as a whole,
(iv) mass.

In order to obtain the balance equations for (i) and (ii), one multiplies the Boltzmann equation (5.6) by the collisional invariants $\varepsilon'_{\underline{k}}$ and $\underline{k}$, respectively, and integrates over $\underline{k}$ [4],[5]. The right hand sides vanish. No difference arises between Eulerian and Lagrangian phonons, and the resulting two-fluid equations are the same. If irreversible effects and nonlinear terms in the velocities are neglected they read [4]

$$\frac{\partial S}{\partial t} = - \operatorname{div}(S\, \underline{u}_n) \tag{5.9}$$

and

$$\frac{\partial\, \rho_n(\underline{u}_n - \underline{u}_s)}{\partial t} = - S\, \underline{\nabla}\, T , \tag{5.10}$$

where S is the entropy density. These results can also be obtained without reference to the Boltzmann equation [3],[7].

In order to deal with (iii) the expression for the momentum density of the whole liquid (phonons + background medium) is needed. In the presence of Eulerian phonons it is according to (4.9) and (5.5) (assuming local equilibrium)

$$\rho_0\, \underline{u}_E + \rho_n\, (\underline{u}_n - \underline{u}_s) .$$

Since $\underline{u}_E = \underline{u}_s$ by (4.10), the momentum density is

$$\rho_0\, \underline{u}_s + \rho_n (\underline{u}_n - \underline{u}_s) = \rho_n\, \underline{u}_n + \rho_s\, \underline{u}_s , \tag{5.11}$$

where the usual definition $\rho_s := \rho_o - \rho_n$ of the so-called density of the superfluid component has been employed.

In the presence of Lagrangian phonons the momentum density of the whole liquid is, according to (4.18), $\rho_o \underline{u}_L$. However, by using (4.19) and (5.5), we obtain

$$\rho_o \underline{u}_L = \rho_o \underline{u}_s + \rho_n (\underline{u}_n - \underline{u}_s) = \rho_n \underline{u}_n + \rho_s \underline{u}_s ,$$

i.e. again expression (5.11). So in both cases one obtains the momentum balance equation [5]

$$\frac{\partial}{\partial t} (\rho_n \underline{u}_n + \rho_s \underline{u}_s) + \underline{\mathrm{Div}}\, \Pi = 0 , \tag{5.12}$$

where Π is the momentum flux tensor. If irreversible effects are neglected (5.12) reduces to [3],[4]

$$\frac{\partial}{\partial t} (\rho_n \underline{u}_n + \rho_s \underline{u}_s) + \underline{\nabla}\, p = 0 \tag{5.13}$$

with p being the pressure.

Finally, we have to consider the conservation of mass (iv). It is described by the equation of continuity

$$\frac{\partial \rho_o}{\partial t} = -\mathrm{div}\ \underline{j} , \tag{5.14}$$

where $\underline{j}$ is the mass current density. Thus one has to find $\underline{j}$ in the two cases. However, for a system of massive particles, mess current density and momentum density are the same thing. Therefore, $\underline{j}$ is given by Eq.(5.11) in both cases, and (5.14) can be written in the form

$$\frac{\partial \rho_o}{\partial t} = -\mathrm{div}(\rho_n \underline{u}_n + \rho_s \underline{u}_s) . \tag{5.15}$$

We can conclude that the whole set of two-fluid equations is identical for Eulerian and Lagrangian phonons. For the reversible equations (5.9), (5.10), (5.13) and (5.15) this has already been shown in [7] and [8] .

ACKNOWLEDGMENTS

The author would like to thank D. Loss, H. Schoeller and J. Vigfusson for e helpful discussion.

REFERENCES

1. H. Lamb, "Hydrodynamics", Cambridge Univ. Press, London/New York, 1957
2. L.D. Landau, J.Phys. USSR 5, 71 (1941)
3. R. Kronig, Physica 19, 535 (1953)
4. J. de Boer, "Liquid Helium", ed. G. Careri, Academic Press, New York, 1963, p.1
5. I.M. Khalatnikov, "Introduction to the Theory of Superfluidity", Benjamin, New York, 1965
6. J. Wilks, "The Properties of Liquid and Solid Helium", Oxford Univ.Press (Clarendon), London, 1967
7. A. Thellung, Annals of Physics 127, 289 (1980)
8. A. Thellung, "Phonon Scattering in Condensed Matter", ed. H.J. Maris, Plenum Press, New York, 1980, p. 125
9. G. Richter, Z.Phys. 115, 97 (1940)
10. R. Kronig and A. Thellung, Physica 18, 749 (1952)

SQUEEZED STATES OF LIGHT AND SOUND

Iwo Bialynicki-Birula
Institute for Theoretical Physics, Polish Academy of Sciences
Lotnikow 32/46, 02-668 Warsaw, Poland

I. INTRODUCTION

The description of light and sound in quantum theory is very similar. Both these phenomena may be viewed as resulting from the motions and transmutations of the corresponding quanta: photons and phonons. Alternatively, both can be described in terms of coupled harmonic oscillators. After the decomposition into the normal modes, these oscillators become decoupled. In the language of the normal modes the description of photons, phonons and also other elementary excitations is mathematically identical as long as we can neglect the interaction of these excitations leading to their transmutations via various nonlinear processes. The big physical difference, of course, is that for the photons in the vacuum, the nonlinear effects (due to the phenomena of the vacuum polarization) are negligible even for the highest available beam intensities whereas for the phonons their free propagation (ballistic phonons) is achieved only under exceptional conditions (low temperatures, perfect crystals etc.). In these lectures I shall only deal with the description in the harmonic approximation, when the harmonic oscillator serves as a universal model of every (bosonic) elementary excitation. Using this very model, I would like to discuss the squeezed states of the quantized harmonic oscillator, which have recently come into prominence in quantum optics. In view of the universality of the harmonic oscillator model, the squeezed states of the phonons and other "-ons" are easily envisaged.

The general definition of a squeezed state of a harmonic oscillator or of a harmonic mode of any vibrating system is based on the values of the dispersions of the two canonically conjugate variables: x and p for the harmonic oscillator or their counterparts for the harmonic modes. If either of these values is lower than the ground state value (or the vacuum value), we call the state for which it happens: the squeezed state. The name squeezed state can be understood with the help of the distribution function representing the state in question in the phase space.

I shall discuss it later in terms of the Wigner distribution function. The definition of the squeezed state given above is very broad. Almost in any family of quantum states that is characterized by a set of parameters we will find some squeezed states for certain values of these parameters. For example, Wodkiewicz, Knight, Buckle, and Barnett (1987) found squeezed states among the states that are formed by superposing several photon number states. I will go in a different direction and look at squeezed states as natural generalizations of the coherent states. This will lead us to the states described by Gaussian wave functions. Ordinary coherent states belong, clearly, to this category but they do not exhaust all such states.

II. GAUSSONS OF THE HARMONIC OSCILLATOR

The states described by Gaussian wave functions are exceptional in several ways. They saturate the Heisenberg uncertainty relations and the entropic uncertainty relations (Bialynicki-Birula and Mycielski 1975). They are the only states for which the Wigner distribution function is positive everywhere (Hudson 1974), i.e. they are as classical as possible. This last property makes them also very useful for the discussion of the classical limit of the quantum theory (Bialynicki-Birula 1971, Hepp 1974).

What makes the Gaussian states a natural generalization of the coherent states is the mechanism of their formation. The coherent states are produced by applying an external, time-dependent force to the oscillator in its ground state or the field in its vacuum state. The states of the harmonic oscillator described by Gaussian wave functions, on the other hand, are produced when the frequency of the applied harmonic force is time dependent. The transition from the regime producing the coherent states to the regime producing the Gaussian states of the oscillator corresponds, therefore, to the transition from ordinary resonance to parametric resonance. When we pass from the quantum mechanical oscillator to the oscillator-like harmonic modes of a quantum field - electromagnetic or acoustic - the quantum states of the field corresponding to the states of the oscillator described by the Gaussian wave functions give us an interesting class of squeezed states with unique mathematical and physical properties. They certainly deserve the name of ideal squeezed states, but some authors just restrict the name squeezed states to these exceptional states. In my lecture, I shall also discuss only the Gaussian states. I will call these states Gaussons of the electromagnetic field, partly to avoid the term Gaussian which is used in optics in a different context (Gaussian beams) and partly for historical reasons, because that was the name we introduced for the Gaussian solutions of the Schrodinger equation with the logarithmic nonlinearity (Bialynicki-Birula and Mycielski 1976).

Gaussons of the electromagnetic field were more and more frequently discussed in the literature over last twenty years in the simplest context of one or two relevant modes of the radiation. For a detailed analysis of the mathematical properties of one and two mode squeezed states I refer the reader to a paper by Schumaker (1986), whereas the applications to optics are discussed in a review paper by Yamamoto and Haus (1986).

In my lecture I would restrict myself to a general discussion of generic squeezed states (Gaussons) first for multidimensional harmonic oscillators and then briefly for the full electromagnetic field. I shall follow here to some extent my earlier contribution on that subject (Bialynicki-Birula 1986).

Already in the very early days of quantum mechanics it was found (Kennard 1927) that oscillating Gaussian wave packets become exact solutions of the Schrödinger equation when the real and the imaginary parts of the quadratic form in the exponent are given a proper time dependence. Kennard's solution was the first example of a squeezed state. I will generalize here this result to the n-dimensional harmonic oscillator, where some new phenomena will appear.

Let us consider the Schrödinger equation for such an oscillator

$$i\partial_t\psi(\vec{r},t) = \tfrac{1}{2}(-\Delta + \vec{r}\cdot\Omega^2\cdot\vec{r})\ \psi(\vec{r},t), \tag{1}$$

where Δ is the n-dimensional Laplacian and the n x n frequency matrix Ω is positive but otherwise quite arbitrary; it may even be time dependent. The most general Gaussian wave function can be described in terms of a complex symmetric matrix and a complex vector. From the normalizability of this wave function it follows that the real part of this matrix is positive definite. After some simple rearrangements, this wave function can be written in the form

$$\psi(\vec{r}) = N\ \exp[-\tfrac{1}{2}(\vec{r} - \vec{\xi})\cdot(A + iB)\cdot(\vec{r} - \vec{\xi}) + i\vec{\pi}\cdot\vec{r}], \tag{2}$$

where the two symmetric matrices A and B and the two vectors $\vec{\xi}$ and $\vec{\pi}$ are all real. The new parameters $\vec{\xi}$ and $\vec{\pi}$ have now a simple physical interpretation of the mean position and the mean momentum vectors, respectively. This is seen, for example, from the form of the Wigner function corresponding to the wave function (2),

$$W(\vec{r},\vec{p}) = \pi^{-2}\exp[-(\vec{r} - \vec{\xi})\,(A + BA^{-1}B)\,(\vec{r} - \vec{\xi})$$

$$-(\vec{p} - \vec{\pi})\cdot A^{-1}\cdot(\vec{p} - \vec{\pi}) - 2(\vec{r} - \vec{\xi})\cdot BA^{-1}\cdot(\vec{p} - \vec{\pi})]. \tag{3}$$

This distribution in the phase space is, in general, not only shifted and squeezed as compared to its form corresponding to the ground state, but also rotated with respect to the r and p axes.

All the properties of state described by the Gaussian wave function can be expressed in terms of its parameters. For the average values of some of the important physical variables we obtain

$$\langle\vec{p}^{\,2}\rangle = \vec{\pi}^{2} + \tfrac{1}{2}\mathrm{Tr}(A + BA^{-1}B), \tag{4a}$$

$$\langle\vec{r}\cdot\Omega^{2}\cdot\vec{r}\rangle = \vec{\xi}\cdot\Omega^{2}\cdot\vec{\xi} + \tfrac{1}{2}\mathrm{Tr}(\Omega A^{-1}\Omega), \tag{4b}$$

$$\langle r_i p_k - r_k p_i\rangle = \xi_i \pi_k - \xi_k \pi_i + \tfrac{1}{2}[B, A^{-1}]_{ik}. \tag{4c}$$

In all the quadratic variables, in addition to the classical part built from the average positions and momenta, we also have quantum correction built from the matrices A and B.

The time evolution of the wave function can also be expressed as a set of equations for its parameters

$$\dot{\vec{\xi}} = \vec{\pi}, \qquad \dot{\vec{\pi}} = -\Omega^{2}\cdot\vec{\xi}, \tag{5a}$$

$$\dot{A} = AB + BA, \qquad \dot{B} = B^{2} - A^{2} + \Omega^{2}. \tag{5b}$$

These equations are equivalent to the original Schrodinger equation for the wave functions of the Gaussian form. The solutions of these equations describe the Gaussons: oscillating and moving around, but non-spreading Gaussian wave functions. The equations of motion for the center of mass variables $\vec{\xi}$ and $\vec{\pi}$ are completely decoupled from the equations for the matrices A and B describing the internal degrees of freedom.

It may be interesting to observe that not only the equations for the center of mass motion can be viewed as canonical equations of a Hamiltonian system – a well known fact from classical mechanics – but that the same is true for the equations describing the internal motion. This is achieved by choosing the average quantum energy of the system as the Hamiltonian of the system,

$$H = \langle E \rangle = \tfrac{1}{2}(\vec{\pi}^2 + \vec{\xi}\cdot\Omega^2\cdot\vec{\xi}) + \tfrac{1}{4}\mathrm{Tr}(A + BA^{-1}B + \Omega A^{-1}\Omega), \qquad (6)$$

and by identifying the independent elements of the symmetric matrices A^{-1} and B as canonical coordinates and momenta, respectively.

The general solution of the equations of motion for the center of mass variables are well known from classical mechanics. In the simplest case, when the frequency matrix Ω is time independent, the general solution of the set of two coupled nonlinear equations for the matrices A and B can also be written in a closed form. To this end I shall rewrite the equations of motion in terms of the original complex matrix $K = A + iB$,

$$\dot{K} = -iK^2 + i\Omega^2, \qquad (7)$$

This equation can be linearized by the following Ansatz

$$K(t) = \Omega D^{-1}(t)N(t), \qquad (8)$$

where N and D are two complex matrices satisfying the equations

$$\dot{N} = iD\Omega, \qquad \dot{D} = iN\Omega. \qquad (9)$$

From the general solution of these linear equations we can immediately construct the general solution of the equation for K,

$$K(t) = (\cos\Omega t + iK_0\Omega^{-1}\sin\Omega t)^{-1}(K_0\cos\Omega t + i\Omega\sin\Omega t), \qquad (10)$$

where K_0 is the initial condition.

In one dimension this is just the solution obtained by Kennard, but in more dimensions, if only the matrices A and B do not commute, their time dependence may be quite intricate. This means that the shape of the Gausson will be changing in time in a complicated manner as its center follows a trajectory of a classical harmonic oscillator. All this "breathing and tumbling" of the Gausson may be viewed as a generalization of simple squeezing for a single mode of radiation i.e. for a one dimensional oscillator.

There is only one static solution of the evolution equation for K, namely $K = \Omega$. Ordinary coherent states are obtained when this solution is combined with any choice of the center of mass variables: the components of the complex vector $\vec{\xi} + i\vec{\pi}$ are to be identified with the eigenvalues of the annihilation operators in the standard definition of the coherent states. As seen from the formulas (3b-3d), all the quadratic physical variables for the coherent state have their average values given by the corresponding classical expressions (up to additive constants). This ceases to be true for general Gausson states for which the fluctuations in the r and p variables are time dependent and not just equal to their ground state or the vacuum values.

The production of general Gausson states from the initial ground state requires a time dependent parametric coupling or, in other words, a time dependent frequency. A time dependent external force will only produce ordinary coherent states of the harmonic oscillator.

III. GAUSSONS OF THE ELECTROMAGNETIC AND THE ACOUSTIC FIELD

All that I said about the Gaussons of the harmonic oscillator in n dimensions applies without modifications to the Gausson states of various bosonic excitations treated in the harmonic approximation. The quantum theory of such excitations is in its mathematical form equivalent to the quantum mechanics of the harmonic oscillator. We usually write down the Hamiltonian as a sum of the contributions representing different normal modes of the system,

$$H = \tfrac{1}{2}\sum(P_\alpha^2 + Q_\alpha^2). \tag{11}$$

In order to make the correspondence with the previous analysis as close as possible I shall use the wave functions in the Schrodinger representation instead of a more commonly used Fock representation (photon or phonon number states) to describe the states of the system. In the Fock representation the connection with the Gaussian wave packets is not transparent and some nice features, in my opinion, are not clearly seen. In the Schrodinger representation the quantum state of the system is described by a wave function depending on all the coordinate-like variables Q_α. Should I have named these coordinates r_i, this theory would be indistinguishable from the theory of the harmonic oscillator in quantum mechanics. I will keep this notational distinction, however, to remind us of a different physical content in the two cases.

The general description of the Gaussons of the electromagnetic field has been given in my previous publication (Bialynicki-Birula 1986) and their production by space- and time-dependent material coefficients is discussed elsewhere (Bialynicka-Birula and Bialynicki-Birula 1987). Here I shall restrict myself to the simplest case when the matrices A and B are present and owing to their noncommutativity we may encounter some new and interesting phenomena. I will consider a two-mode state of either the photon or the phonon field with the two modes having the same wave vector and differing only in their polarization. Such states can be studied with the use of only two terms in the Hamiltonian (10) representing the energy of the two relevant modes; the system is effectively a two-dimensional harmonic oscillator. The general Gausson state of such a system is characterized by the two amplitudes constructed from the average values of the position and momentum variables - the same as for coherent states - and by two two-dimensional real matrices A and B. They are equal to the real and the imaginary part of the complex matrix K obtained by specializing the general solution (9) to the present situation (K is now a 2 x 2 matrix and ω is the wave frequency),

$$K(t) = (\cos\omega t + iK_0\omega^{-1}\sin\omega t)^{-1}(K_0\cos\omega t + i\omega\sin\omega t), \qquad (12)$$

This solution describes a squeezed state whose squeezings in the direction of each polarization oscillate with the frequency of the wave. One special case is particularly interesting since it describes a pure rotation of the ellipse representing the squeezed state in the plane perpendicular to the wave vector. Such a solution has the form

$$K = \omega + \kappa\sigma e^{-2i\omega t}, \qquad \kappa < \omega, \qquad (13)$$

where σ is the following linear combination of the Pauli matrices

$$\sigma = \sigma_3 + i\sigma_1, \qquad \sigma^2 = 0. \qquad (14)$$

When this form of the matrix K is combined with the circularly polarized wave describing the average field (the center of mass motion in the language of the harmonic oscillator), we obtain a state which will have an exceptional property: in the frame of reference co-rotating with the average field it will be permanently squeezed in one direction. For example, we can produce in this manner a wave whose electric field will have at all times a smaller spread than in the vacuum. In order to see this I write down below the probability density for the wave function (2) of the two-dimensional oscillator in which the matrix K is of the form (12) and the average trajectory describes a rotating motion

$$\rho(x,y,t) = \exp[-(\omega + \kappa)(x\cos\omega t + y\sin\omega t - a)^2$$
$$-(\omega - \kappa)(y\cos\omega t - x\sin\omega t)^2], \qquad a = |\vec{\xi}| . \qquad (15)$$

When expressed in terms of the rotating variables x(t) and y(t), the probability density becomes

$$\rho(x(t),y(t)) = \exp[-(\omega + \kappa)(x(t) - a)^2 - (\omega - \kappa)y^2(t)]. \qquad (16)$$

Using the methods developed in a related context (Bialynicki-Birula and Mycielski 1979), one can prove that the solutions (13) are the only ones which represent a Gausson that is undergoing a steady rigid rotation. Thus, we can permanently reduce the spread in one of the quadrature components, but at most by a factor of $\sqrt{2}$, regardless of the value a of the amplitude of the average oscillations. For the circularly polarized electromagnetic waves we can achieve in this way a permanent reduction below the vacuum value of the quantum fluctuations, say, of the electric field. For the acoustic waves the circular polarization is not usually considered, but for uniaxial crystals it should in principle be possible. The permanently squeezed state with lower than the ground state value of the quantum fluctuations of the displacement can in that manner be constructed.

I have shown in this lecture that there is an advantage in using the coordinate representation of the wave function in the description of the squeezed states. The squeezed states of photons, phonons and othere harmonic excitations can be related to Gaussian wave functions of the harmonic oscillator in one or more dimensions. This simple mode of description of the squeezed states does not by itself solve any important physical problems concerning the production and the applications of these states, but helps to understand the basic physical principles involved.

References

Bialynicki-Birula, I., 1986, in Coherence, cooperation and fluctuations, edited by F.Haake, L.M.Narducci and D.Walls (Cambridge University Press, Cambridge 1986), all occurences of the imaginary unit i in this paper should be replaced by -i.

Bialynicka-Birula, Z., and I.Bialynicki-Birula, 1987, JOSA B(to appear).

Bialynicki-Birula, I., and J.Mycielski, 1975, Comm.Math.Phys.44,129.

Bialynicki-Birula, I., and J.Mycielski, 1976, Ann.Phys.100,62.

Bialynicki-Birula, I., and J.Mycielski, 1979, Physica Scripta 20,539.

Hepp, K., 1974, Comm.Math.Phys.35,265.

Hudson, R.L., 1974, Rep.Math.Phys.6,249.

Kennard, E.H., 1927, Z.Phys.44,326.

Schumaker, B.L., 1986, Physics Reports 135,317.

Wodkiewicz, K.,P.L.Knight, S.J.Buckle and S.M.Barnett, 1987, Phys.Rev.A.

Yamamoto, Y., and H.A.Haus, 1986, Rev.Mod.Phys.58,1001.

ULTRASHORT TRANSIENT DYNAMICS OF PHONONS AND ELECTRONS IN SEMICONDUCTORS

W.E. Bron
Department of Physics
University of California, Irvine
Irvine, CA 92717, USA

I. Introduction

The field of phonon and electron dynamics in solids, and in semiconductors in particular, has rapidly expanded in recent years. Progress has been spurred through the advent of pulsed laser light with time duration from microseconds all the way to the femtosecond (10^{-15}s) regime. These ultrashort duration laser pulses have been used to generate nonequilibrum primary excitations of the electronic and vibrational states of the solid, and, moreover, to study, directly in time domain, the decay of the primary excitations into secondary excitations and eventually the return of the solid to thermal equilibrium.

This field of research is barely one decade old but has already blossomed into a literature much too extensive to be covered in detail here. I have chosen instead to cover the subject in terms of a series of illustrative examples.

2. Theoretical Background

2.1 Phonons

It is important from the start to be aware of the natural timescale associated with phonon dynamics; namely, the "lifetime" over which the excitations exist. It is now known that the lifetime of optical phonons in a simple solid is of the order of picoseconds, whereas those of acoustic phonons varies strongly with phonon frequency (ν) and phonon branch. Typically, the lifetimes (τ) of 1 THz longitudinal acoustic (LA) phonons is of the order of microseconds and varies with the inverse fifth power of the frequency [1], such that $\tau(\nu) \sim 10^{54}\ \nu^{-5}$. On the other hand, in the absence of any impurity scattering it has been postulated that some transverse acoustic (TA) phonons in the dispersive regime may have lifetimes of the order of seconds [2].

The above noted "lifetimes" arise primarily from anharmonic processes involving three-phonon interactions provided that the phonon energy $\hbar\omega << k_BT_A$ (k_B is the Boltzmann constant, and T_A is the ambient temperature and $\hbar$ refers to h-bar.

The rate, Γ, at which a given nonequilibrium phonon (with wavevector a and energy ω_q) decays into secondary excitations is governed by the strength of the three particle interaction; namely,

$$\Gamma(q,\omega_q) = 2\pi \sum_{q'q''} \frac{|V_{qq'q''}|^2}{\omega_q\omega_{q'}\omega_{q''}} \delta(\omega_q-\omega_{q'}-\omega_{q''})\{1+n_T(\omega_{q'})+n_T(\omega_{q''})\} . \quad (1)$$

In Eq. (1) $\omega_q,\omega_{q'},\omega_{q''}$, refer to energies of, and q,q',q'' refer to the wavevectors of, the three phonons involved, $V_{qq'q''}$ is the appropriate matrix element for the third order anharmonic process, and at thermal equilibrium $n_T(\omega_{q'}) = (\exp(\hbar\omega_{q'}/k_BT)-1)^{-1}$.

Several attempts [2-6] have been made to reduce Eq. (1) to analytical expressions which can be compared to experimental results. It will be of interest for later discussions to note some of the simplest of these analytical expressions. A case in point is a phonon of given frequency ω and belonging to the longitudinal acoustic, LA, dispersion branch decaying into two phonons of lower frequency, one belonging to the LA, and the other to the transverse acoustic branch, TA. For this case an analytic expression has been formulated by Orbach and Vredevoe [2] from a perturbative treatment of the anharmonic lattice. In this formulation the anharmonic interaction is described in terms of linear combinations of second- and higher-order elastic constants, C_i, and in terms of the density of states available to the decay phonons which is taken to be that of an isotropic dispersionless Debye solid. It is found that

$$\tau^{-1}(\omega) = \frac{\hbar[(C_1+C_2 + \frac{3}{2}(C_2+C_5)]^2}{16\pi\rho^3 v_\ell^6 v_t^3}(1-\beta^2)(\beta^2-\beta+\tfrac{3}{8})\omega^5 . \quad (2)$$

In equation (2), T_A is assumed to be 0^oK, ρ is the mass density of the crystal in which the phonons propagate, v_ℓ and v_t are, respectively, the propagation velocity of phonons belonging to the LA and TA branches, and $\beta = v_t/v_\ell$. It is important to note at this point that the

LA phonon lifetime varies with frèquency as ω^{-5}, i.e., high-frequency LA phonons are predicted to decay much more rapidly than low-frequency phonons. The frequency dependence indicated in equation (2) has recently been partially verified by Baumgartner et al. [2] for CaF_2 for phonons with $\nu < 3.5$ THz.

A related expression has been formulated by Klemens [6] for the spontaneous decay of a LA phonon into two TA phonons. In this case it is found, again for $T_A \approx 0$, that

$$\tau^{-1}(\omega) = \frac{3\pi}{4\sqrt{2}} \gamma^2 \omega \left(\frac{\hbar\omega}{Mv_\ell^2}\right) \left(\frac{\omega}{\omega_o}\right)^3 \beta \tag{3}$$

in which M is the atomic mass, and γ is the Grueneisen constant.

The above expressions describe the decay of nonequilibrium LA phonons in an ambient environment in which the temperature $T_A \approx 0$ K. In an experimental technique, to be described later, it is possible to lift this constraint on T_A which can then take on any value. Moreover, in this case it is the spontaneous decay of optical phonons into pairs of lower energy acoustic phonons which is probed. An approximate analytic expression for the decay time of optical phonons in a crystal held at any temperature has been obtained by Klemens [5], and is

$$\tau^{-1} = \omega_o \frac{J}{24\pi} \gamma^2 \frac{\hbar\omega_o}{Mv_o^2} \frac{a^3\omega_o^3}{v_g^3} \tag{4}$$
$$\times \left[(n_0+1)(n'n'')-n_o(n'+1)(n''+1)\right]$$

in which the subscript o stands for the optical phonon which decays into two acoustic phonons denoted by superscript prime and double prime, v_g is the group velocity of the acoustic phonons, a^3 is the volume per atom, the n is the phonon occupation number, and J is a number between 1 and 6. One word of caution. Expression (4) was derived for a monoatomic lattice, such as crystalline silicon. The expression cannot be expected to be directly applicable for diatomic lattices as, for example, GaAs, etc.

Phonons also scatter elastically from crystal imperfections such as isotopic and foreign-ion impurities. Theoretical expressions for the scattering rates at point imperfections are in general quite complicated. A qualitative insight into the scattering probability can, however, be gained through the assumption that the scattering is of Rayleigh type [4], that the crystal is an isotropic dispersionless Debye solid, and that the disturbance is limited to the local change in mass, ΔM. Under these assumptions the elastic scattering rate, τ^{*-1}, becomes

$$\tau^{*-1} = (N/\eta)(\Delta M/M)^2 \omega^4 (4\pi v^3)^{-1} \tag{5}$$

in which N is the defect concentration, η is the number of atoms per unit volume, and v is the average group velocity of the acoustic phonons, Note should be taken that high-frequency phonons are predicted to be also elastically scattered more strongly than low-frequency phonons.

It is worth noting further that, according to equation (5), elastic impurity scattering of acoustic phonons can be approximated by $\tau^* \approx A^* \omega^{-4}$, whereas equations (2) and (3) predict that spontaneous anharmonic scattering of LA phonons can be approximated by $\tau \approx A\omega^{-5}$. Average values of A*, obtainable from the literature for crystals containing ≈ 100 ppm imperfections, are of the order of 10^{39} s^{-3}. As has already been noted above, A is found in insulators to be typically of the order of 10^{-54} s^{-4}. On the assumption that the phonon propagation velocity is approximately constant and equal to 5×10^3 ms^{-1}, one concludes that the mean free path against impurity and anharmonic scattering is much less than the dimensions of typically sized samples only if the phonon frequency $\nu > 1$ THz.

Optical phonon lifetimes against anharmonic decay typically lie in the picosecond regime, and thereby dominate the observable transport properties of these phonons.

B.2 Electronic Carriers

The primary electronic excitation to be considered here is that produced in a semiconductor by photoexcitation of an electron from the valence band to the conduction band as is illustrated by the dark vertical arrow in Fig. 1. A "hole" is simultaneously produced in the valence band. This nonequilibrium excitation then decays into secondary excitation, and eventually returns to the ground state through electron-hole recombination.

A number of sign-posts exist in our knowledge of these dynamics. For example, it has been known for some time that highly excited free

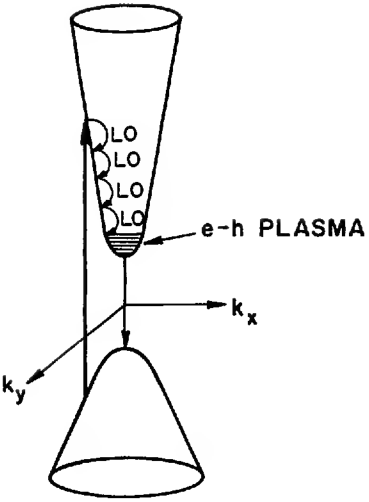

Figure 1. Excitation and decay processes for a hypothetical semiconductor with a simple band structure.

carriers, i.e., electron-hole pairs, in polar semiconductors decay into lower energy states via the emission of low wavevector, longitudinal optical (LO) phonons primarily through the so-called "Frohlich Interaction" [7]. The decay proceeds through a cascade of carrier-phonon interactions eventually producing an electron-hole plasma (gas or liquid) at some minimum of the conduction band [8], followed by electron-hole recombination. Figure 1 is an illustration of the excitation and decay in a hypothetical direct gap semiconductor with simple parabolic bands.

There are a number of auxiliary features to note in connection with the dynamics of the decay process. For typical polar semiconductors the electron effective mass is approximately $m^* \approx 0.25\ m_e$ [9]. This means that the curvature of a simple parabolic conduction band is such that the LO phonon which can interact with an electron in the cascade must possess a wave vector, $\vec{q}$, of the order of $10^5\ \mathrm{cm}^{-1}$ and that this value needs to change as the cascade proceeds. This conclusion holds true for electrons with energies of up to 20 LO phonon energies above the band minimum. As will be discussed later, measurements of the decay by time resolved, incoherent Raman scattering, or by multiple-wave mixing experiments, such as the CARS method, all need to be performed in the backward scattering geometry if phonons with such relatively high wavevectors are to be detected. The effects of more complicated band structures has also been considered [6].

It has also been predicted [7] that the average time interval between successive steps in the cascade is of the order of 100 to 200 femtoseconds which is shorter than the carrier-carrier scattering time

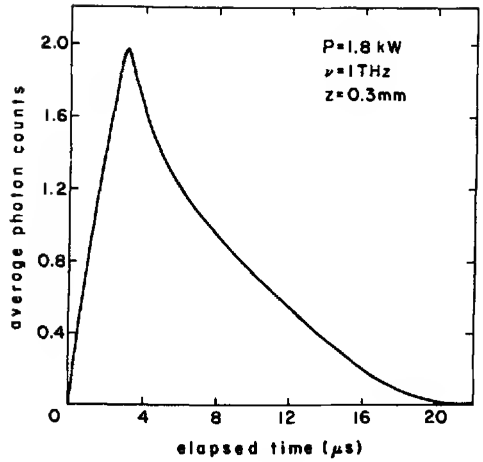

Figure 2. Vibronic sideband intensity as a function of elapsed time, t.

in semiconductors with carrier concentrations of less than 10^{17} cm^{-3} [7].

The interaction of phonons with the electron-hole plasma, on the other hand, is not well understood. It has been found [10] experimentally in GaP that the LO phonon frequency increases as the plasma concentration exceeds about 0.5 x 10^{18} cm^{-3}, but that little effect is observed below that concentration and that, curiously, no change in the phonon lifetime is observed up to concentrations of about 5 x 10^{18} cm^{-3}. The observed frequency shifts have been attributed to coupled plasmon-phonon modes.

We have already noted that in polar semiconductors, such as GaP, that the LO phonons themselves decay into acoustic phonons in times of

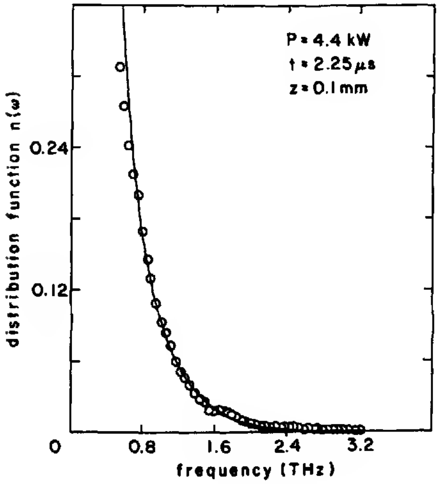

Figure 3. The variation of the observed phonon distribution, n(ω,R,T), with phonon frequency. Circles are data points. The solid line is a best fit Planck distribution to the data.

the order of picosecond and that the dominant decay mechanism, at least at low temperatures, are three-phonon anharmonic processes. Finally, a recent investigation [11] on systems which contain an electron-hole plasma with concentration less than 0.5 x 10^{-18} cm^{-3}, indicates an additional effect is present, namely, that the strength of nonlinear phonon generation, such as coherent Raman excitation (CRE), is effected by the presence of the plasma.

It should already be apparent to the reader that the dynamics of electrons and phonons in these materials exhibits many interesting and multifaceted properties.

3. Experimental Results and Discussion

3.1 Acoustic Phonon Transient Dynamics

A general review of the experimental methods to be illustrated here may be found in reference [12] and [13].

Research in the field of transient phonon dynamics arises from the early experiments on nonequilibrium phonon transport by the heat pulse method. This important step was taken by von Gutfeld and Nethercot [14]. The heat pulse technique differs from thermal conductivity measurements in that a nonequilibrium short-duration pulse of phonons is transported across the solid rather than a steady-state thermalized phonon distribution. The technique's primary advantage is that the "time of flight" for phonons to traverse a solid sample can be directly measured and which, since the length of a given sample is constant, translates into a measurement of the effective phonon group velocity, v_g. Moreover, since v_g is normally different from longitudinally and transversely polarized phonons, the technique permits a separation of the phonon distribution into polarization (dispersion) branches.

The "heat pulse" technique has a number of drawbacks. First, the method does not resolve the spectral content of the heat pulse; in fact, the very words "heat pulse" involves an assumption that the phonons in the pulse possess a Planck frequency distribution even though the pulse itself is not in thermal equilibrium with the host crystal. Moreover, the technique possesses no spatial resolution since the heater film and phonon detector are fixed to opposing faces of the sample.

These constraints were removed by the introduction of the vibronic sideband phonon spectroscopy (VSPS) [15]. The basis for the technique

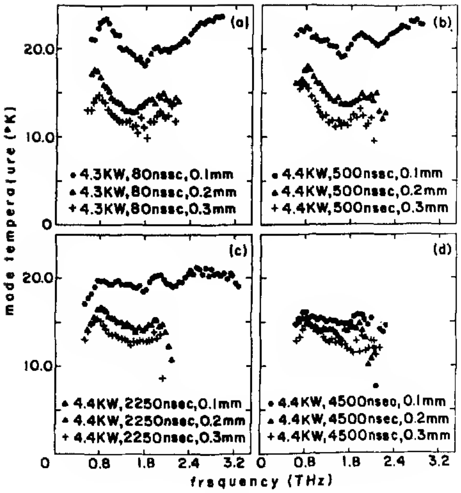

Figure 4. Variation of the mode temperature as a function of phonon frequency, detector displacement, z, and elapsed time, t. The inserts contain the values of P, t, and z. Note that the elapsed time increases in the series 4a to 4d.

has been reviewed elsewhere [12] and will not be discussed further here. Let it suffice to point out that this technique permits resolution of the spectral, spatial and temporal distribution of the heat pulse in any nonequilibrium phonon distribution. The technique which uses optical sources as phonon generators and/or detectors has been applied to a number of problems [13]. I will here illustrate the application of VSPS to the case of phonon dynamics in dispersive media, specifically, to the case of quasidiffusion.

The term "quasidiffusive" phonon dynamics was coined by Kasakovtsev and Levinson [16-18] to describe a new transport mode which nonequilibrium phonons undergo in a dispersive medium in the presence of anharmonic phonon-phonon interactions. The special requirement of "quasidiffusive" vs. "quasiballistic" transport is that in the former the rate of elastic scattering τ^{*-1} is faster than that for anharmonic scattering τ^{-1} and vice versa.

Unfortunately, space does not permit a discussion of our first experiment on "quasidiffusion" [19] in which monochromatic phonons were injected into a sample of sapphire containing V^{4+} ions which acts as phonon scattering sites.

We turn, instead, to quasidiffusive transport of a broadband phonon distribution [20]. In fact, we return to the case, discussed earlier, of phonons generated by the "heat pulse" method and propagating in a sample of $SrF_2:Eu^{2+}$. Moreover, we again apply the vibronic sideband spectrometer to obtain a more quantitative evaluation of the phonon transport than was available to Bron and Grill [15].

Before proceeding we briefly review the characteristics of quasidiffusive transport extracted from the experiment using monochromatic phonons. Among these characteristics are: (1) as a result of the strong elastic scattering, the high frequency component of the phonon distribution undergoes random deflections and, accordingly, propagates diffusively, hence (ii) the high frequency component propagates only slowly away from the phonon source, and (iii) since anharmonic processes are present, the spectral composition of the phonon distribution changes with time, and consequently since Γ^* is a strong function of ν, the effective diffusion rate changes with time and displacement from the phonon source.

The experimental arrangement employed is similar to the one used by Grill and Bron [15]. Major refinements were achieved, however, in the signal to noise recovery. This procedure (see equation (2) of reference [15]) makes it possible to report the absolute (rather than relative) values of the phonon distribution function $n(\omega,R,t)$, for phonons of a given frequency ω, at various positions R relative to z=0 and at any time t after t=0. Alternatively, we may transform to the "mode temperature" $T(\omega,R,t)$ since

$$T(\omega,R,t) \equiv \frac{\hbar\omega}{k_B} [\ln(n(\omega,R,t)^{-1} + 1)]^{-1} \quad . \tag{6}$$

As in the previous work, the actual signal recovered is the vibronic sideband intensity when the broadband phonon distribution is present less that when only ambient phonons are present. Thus to within linear effects, only the signal due to the nonequilibrium phonon distribution is observed here.

Figure 2 is an example of the observed vibronic sideband signal intensity plotted as a function of the elapsed time after the heater pulse has been injected at t=0, z=0. This "time of flight" spectrum was measured for ν = 1 THz, at a detector column located at z=0.3 mm, after a voltage pulse of 40 ns duration, such that a peak power, P, of 1.8 KW, was passed through the heater film. The lack of sharp structure plus the broad temporal distribution of this signal is usually assigned to "diffusive" phonon propagation brought on by elastic scattering at lattice imperfections. We now show, however, that other experimental evidence requires that anharmonic scattering processes are also present. Figure 3 is an example of the observed phonon distribution function, $n(\omega,R,t)$, here presented as a function of ν, as observed immediately behind the heater after 80 ns have elapsed after a 4.3 KW (40 ns duration) pulse was passed through the heater film. The solid line is a best fit to a Planck distribution (T=22.2 K). Note $n(\omega)$ for small phonon frequencies reaches values greater than

0.3. Also note that the overall agreement with a black body distribution is good, but that definite deviations from that distribution exist. These deviations can be more readily observed in figure 4 which is a plot of $T(\omega,R,t)$ as a function of ν for $t=80$ ns and various values of z. In this representation a true Planck distribution would be a straight horizontal line.

Deviations from the Planck distribution are easily recognized, particularly when $z=0.1$ mm. These deviations are always observed under our experimental conditions and are fully repeatable in every detail. After increasing periods of time (figures 4a to 4d) the deviations are seen to disappear. Another observation is that at any fixed time, for $z < 0.01$ the low frequency component of the distribution tends to be at a slightly higher mode temperature than the high frequency component. Moreover, the high frequency component is almost at a constant mode temperature; i.e., phonons of $\nu > 1.6$ THz tend to form a local quasiequilibrium among themselves. Finally, at early times the highest mode temperatures occur near $z = 0$, but as time progresses this difference disappears such that at $t = 4.5$ μs a more complete spatial quasiequilibrium is forming albeit at a mode temperature of nearly 3 times the ambient temperature of 5 K. A true thermal equilibrium at the ambient temperature of 5 K is reached at a much slower rate and is completed only in times of the order of milliseconds [21]. This result reflects the slow heat conduction from the sample to the cold finger to which it is attached. It is for this and other reasons that the heater pulse repetition rate is kept to less than 50 Hz.

To summarize the observed experimental features of the transport of the broadband phonon distribution we note; (i) the "time of flight" spectrum follows that usually assigned to purely diffusive phonon transport, (ii) at the time of injection immediately behind the injection surface, the phonon distribution is almost a black body source but with marked deviations, (iii) the deviations from the Planck distribution disappear as the elapsed time after injection increases, (iv) in the interior of the sample and for $t \lesssim 2.25$ μs the mode temperature of the low frequency component of the phonon distribution is slightly higher than the high frequency component, with the latter component tending to form a local quasiequilibrium, and (v) as time progresses a more complete spatial quasiequilibrium begins to form.

In order to make headway in interpreting these experimental results it is necessary to return to a discussion of the underlining theoretical formalism. It has already been pointed out that the theory of transport of nonequilibrium phonons in dispersive media under the presence of anharmonic processes has been discussed by Kazakovtsev and Levinson [16-18] and by Schaich [22], [23].

The basic starting point in the theoretical formulations is the diffusion equation modified by anharmonic collision terms. At low ambient- and mode-temperatures such that $\hbar\omega < kT$, we expect three-phonon interaction processes to dominate the anharmonic interactions. Hence, for this regime, an expression for quasidiffusive phonon transport is

$$\begin{aligned} \frac{\partial n(\omega,z,t)}{\partial t} - D(\omega)\,\frac{\partial^2 n}{\partial z^2} = &-\frac{1}{2}\int \partial\omega'\rho' \int \partial\omega''\rho'' A(\omega;\omega',\omega'') \\ &\times \delta(\hbar\omega - \hbar\omega' - \hbar\omega'')\,[n(1+n')(1+n'') \\ &- (1+n)n'n''] - \int d\omega'\rho' \int d\omega'\rho'' A(\omega';\omega',\omega) \\ &\times \delta(\hbar\omega'' - \hbar\omega' - \hbar\omega)\,[nn'(1+n'') \\ &- (1+n)(1+n')n''] \quad . \end{aligned} \tag{7}$$

In expression (7), the coefficients A describe the strengths of the three-phonon creation and annihilation processes. Recombination processes involving n', n" may not be neglected as is clear from the high values of n indicated in figure 3 for low frequency phonons.

Two attempts have been made to solve equation (7) in analytical form. The first by Levinson [24] considers an instantaneous temperature increment located somewhere inside an infinite medium. The second approach by Wilson and Schaich [23], which is closer to our experimental conditions, considers an arbitrary time-dependent temperature perturbation at the boundary of a semi-infinite medium. However, in order to obtain an analytical solution in either approach, it is necessary to further restrict the temperature increment of the source to a small fraction of the ambient temperature. This restriction is not obeyed in the present experiment since it is clear from the results displayed in figure 4, that the mode temperature excursion is of the order of 20 K compared to an ambient temperature of about 5 K.

A similar, albeit numerical, approach to the solution of equation (7) has been taken by Schaich [22]. Here the integral equation (7) is supplanted by a series of equations which describe the response of a small set of Einstein modes, $\ell = 0,1,2,3,4$, with frequencies $\nu_\ell = 2^\ell \nu_0$

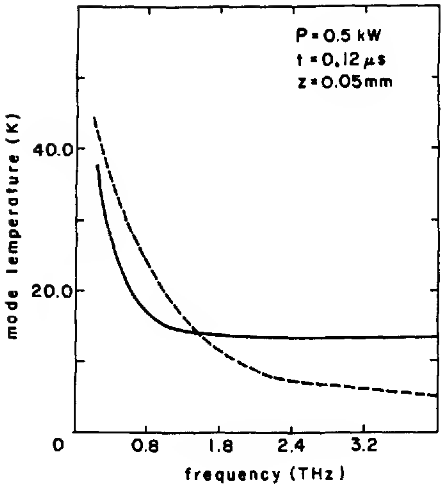

Figure 5. Comparison between the theoretically predicted mode temperature as a function of phonon frequency with only elastic scattering (dashed line) and with quasidiffusive transport (solid line).

with $\nu_0 = 1/4$ THz. These modes are weighted by a factor ρ_ℓ which is a measure of the integrated number of states for the complete set of lattice modes assuming that $\rho(\nu) \propto \nu^2$ hence $\rho_\ell \propto \nu_\ell{}^3$. A further restriction to processes such that $\nu_\ell \rightleftarrows 2\nu_{\ell-1}$, leads to

$$\frac{\partial n_\ell}{\partial t} + D_\ell \frac{\partial^2 n_\ell}{\partial x^2} = - R_\ell^-[n_\ell(1+n_{\ell-1})^2 - (1+n_\ell)n_{\ell-1}^2] \quad (8)$$

$$+ bR_\ell^+[n_{\ell+1}(1+n_\ell)^2 - (1+n_{\ell+1})n_\ell^2] \quad .$$

where R^+ and R^- are now the relevant rate constants. The factor b=16 ensures that anharmonic scattering conserves total energy. A numerical solution of expression [8], with boundary conditions which reflect our experiment, has been shown by Schaich to predict a temporal variation of the heater film which is similar to that previously observed experimentally [21]. A number of other properties of the transport which are predicted in this way are discussed by Schaich. Those which bear most directly on the results of the present experiment are (i) components of the phonon distribution, which can interact anharmonically with each other during the experimental time span, reach a common mode temperature, (ii) only the lowest frequency component of the phonon distribution (which elastically scatters the least) can penetrate rapidly into the sample, but since low frequency phonons interact anharmonically only infrequently during the time span of the experiment their mode temperatures remain high compared to that of the quasiequilibrium, (iii) the high frequency component, because of strong elastic scattering, penetrates into the sample rather slowly at a rate determined by the diffusion constant, D_ℓ, of essentially the

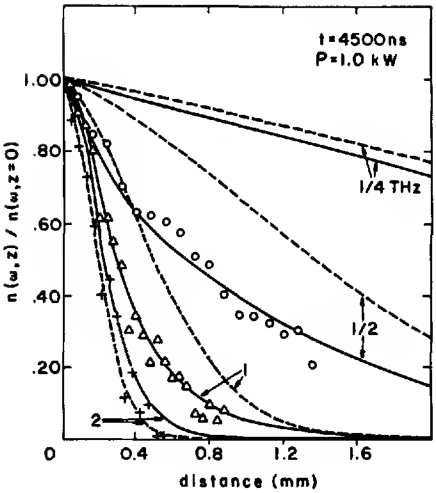

Figure 6. Normalized distribution function as a function of the detector displacement distance, z, and phonon frequency ν = 1/4, 1/2, 1, and 2 THz. The symbols represent experimental data, the dashed lines are theoretically predicted values for elastic scattering only. The solid lines are theoretically predicted values for quasidiffusive transport.

lowest frequency component of the quasiequilibrium. The existence of (i) and (ii) is illustrated in figure 5 which displays the predicted mode temperature as a function of phonon frequency as calculated at z = 0.5 mm, t = 0.12 μs after a pulse of 0.5 KW has passed through the heater film. In the absence of anharmonic processes (dashed line) no quasiequilibrium forms (for all t and z) whereas in the presence of anharmonic processes (solid line) a quasiequilibrium forms among phonons with ν > 1 THz. In contrast, the low frequency component remains "hot" and does not form a quasiequilibrium. This situation corresponds qualitatively to the experimental results indicated in figures 4a and 4b for z > 0.2 mm.

A further comparison between data and the predicted properties (i) to (iii) above is illustrated in figure 6. The symbols represent the observed values of the normalized phonon distribution function $n^o = n(\omega,z,t=4.5\ \mu s)/n(\omega,z=0,t=4.5\ \mu s)$ as a function of z for ν = 1/2, 1 and 2 THz with P = 1 KW. For comparison, figure 6 contains the theoretically predicted values obtained via equation (8) for quasi-diffusive transport (solid lines) and those obtained for transport under elastic scattering only (dashed lines).

The agreement, illustrated by figure 6, between experiment and theory when both elastic and anharmonic processes are taken into account, and the lack of agreement when anharmonic processes are neglected, together with the qualitative agreement between the observed and predicted properties of the transport, yield strong evidence that the quasidiffusive process is present in the transport of the broadband phonon distribution reported here.

Since even most "pure" crystals contain elastic scattering centers in the form of isotopic impurities we suspect that some level of quasidiffusion occurs in most systems. If this is the case, then much of the earlier work on "heat-pulse" propagation may need to be reexamined. A case in point is our earlier work [15, 21] on the $SrF_2:Eu^{2+}$ system. Here we were led by the observed temporal evolution of the high-frequency component of a heat pulse distribution to conclude that the lifetimes of high-frequency acoustic phonons are anomalously long [25]. However, it is now clear that the temporal evolution of the high-frequency phonon component does not reflect pure anharmonic decay, but rather the rate at which energy is extracted from the quasiequilibrium. The extraction is controlled by the low frequency phonon component, which alone can readily leave the area adjacent to the phonon source. However, since the density of states of these phonons is low, the amount of energy they can carry away is small, and hence the apparent slow decay of the high-frequency component.

3.2 Optical Phonon Transient Dynamics

The standard technique to determine the "lifetime" of optical phonons is to determine the spectral width of the incoherent Raman scattering cross section. Since spectral width and temporal duration are related by a Fourier transformation, information on the temporal duration of the optical phonon excitation can, in principle, be obtained in this way. More recently it has become apparent that we may circumvent the transformation by simply making measurements of the optical phonon dynamics directly in the time domain. Since, however, optical phonon "lifetimes" are of the order of picoseconds, experimental techniques capable of resolution within that very short temporal domain have had to be developed. Modern synchronously pumped mode-locked dye laser systems have proven to be the answer. (For a general review of the subject, see, for example, Demdroter [26]).

I shall again illustrate the results obtainable in terms of a small number of examples. Since phonon energies correspond to the far infrared (FIR) region of the electromagnetic spectrum, it would be necessary to construct a picosecond source in this spectral range. Unfortunately, to date no such source has been demonstrated. On the other hand, many pico- and even femto-second lasers with energies in the visible spectrum have been demonstrated. It is, therefore, possible to use nonlinear difference mixing of two visible laser frequencies to form a FIR excitation source of phonons providing the phonons involved are Raman active [26]. The apparatus involves dual synchronously pumped dye lasers which produce synchronized trains of pulses with picosecond (and subpicosecond) duration at two different wavelengths. We have used such laser systems to generate near-zone-center coherent optical phonons in GaP and ZnSe through coherent Raman excitation (CRE), and to study the subsequent dynamics of the coherent longitudinal optical (LO) phonon state, plus the response of the electronic system to nonlinear excitation. These investigations were carried out directly in the time domain through time resolved coherent anti-Stokes Raman scattering (TRCARS) [27-30]. Only the results on GaP will be discussed here.

Coherent Raman excitation (CRE) and coherent anti-Stokes Raman scattering (CARS) are particular forms of nonlinear mixing of laser fields [26]. Two electromagnetic fields $\vec{E}_\ell$ and $\vec{E}_s$, with photon energies $\hbar\omega_\ell$ and $\hbar\omega_s$ and wavevectors $\vec{k}_\ell$, $\vec{k}_s$, can in general give rise to a series of nonlinear interactions in a solid. One interaction leads to a virtual excitation of the electronic system at a frequency $\omega_\ell-\omega_s$. Of particular interest here is the case in which $\omega_\ell-\omega_s$ corresponds to a Raman active vibrational excitation. In the resultant CRE, the energy $\hbar(\omega_\ell-\omega_s)$ and wavevector $\vec{q}=\vec{k}_\ell-\vec{k}_s$ of the active mode are in the ideal case exactly specified, and the phase space available to the excited vibrations is severely limited. In this sense it differs markedly from stimulated and spontaneous Raman scattering for which the available phase space is much larger. Thus, the occupation probabilities of the components of the coherent state produced through CRE may be very high as compared to those of incoherent Raman excitation. Generation of intense coherent oscillations by CRE was first described for molecular systems by Garmire, et al. [31]. Large amplitude coherent excitation of lattice vibrations was soon thereafter described by Giordmaine and Kaiser [32].

The coherent excitation may be probed by a third laser field, $\vec{E}_p$, whose energy $\hbar\omega_p$ is taken for convenience to be $\hbar\omega_\ell$. The nonlinear interaction of this field, with the coherent lattice vibrations results in yet another nonlinear polarization [33] which drives an electromagnetic field with energy $\hbar\omega_c=\hbar(2\omega_\ell-\omega_s)$. It is further required through wavevector conservation (the phase-matching condition) that $\vec{k}_c=\vec{k}_p+\vec{k}_\ell-\vec{k}_s$, where $\vec{k}_p$ and $\vec{k}_c$ are the wavevectors associated with the probe pulse and the anti-Stokes pulse, respectively. The probe technique clearly involves coherent anti-Stokes Raman scattering, giving rise to the CARS designation for the entire nonlinear process.

The coherent phonon state mentioned above is defined by a superposition of states of different occupation probabilities, but whose component states have, at least initially, a fixed relative phase relationship among each other. The resultant excitation of the solid resembles most closely a classical harmonic oscillator [34].

We first concentrate here on the coherent LO phonon state. A discussion of TO phonons appears elsehwere [35]. We describe the coherent LO phonon state in terms of the following classical equation of motion for the coherent amplitude <Q>:

$$\mu\ (\ddot{Q}^{+} + \Gamma\ \dot{Q}^{+} + \omega^{2}{}_{LO}Q^{+}) = \hat{q}\cdot[\bar{R}\ \vec{E}_{\ell}^{+}\vec{E}_{s}^{-} - \frac{4\pi e^{*}}{\varepsilon_{\infty}}\ \vec{P}_{NL}^{+}] \quad . \tag{9}$$

In Eq. (9), μ is the reduced lattice mass, Γ a phenomenological damping rate, ω_{LO} the LO phonon frequency, $\hat{q}$ the unit polarization vector of LO phonon, ε_{∞} the high frequency dielectric constant, $\bar{R}$ the appropriate Raman tensor, e* the effective lattice charge, $\vec{P}_{NL}$ the nonlinear polarization due to the interaction of the two electromagnetic fields and the superscript "+" refers to the Fourier component $\exp[i(\vec{k}\cdot\vec{r}-\omega t)]$ and "-" refers to its complex conjugate. Equation (9) implies that the amplitude <Q> of the coherent state is driven by a force involving a Raman interaction and by a force associated with the longitudinal component of a nonlinear polarization which acts as a depolarization field. If only the lowest order of P_{NL} (i.e. of second order in the fields) is considered, the driving force, F{j}, in Eq. (9) is reduced to

$$F\{j\} = R_{A}\{j\}\ E_{\ell}^{+}E_{s}^{-}\ , \tag{10}$$

where $R_{A}\{j\} = (\bar{R}_{A}\cdot\hat{q})\hat{\ell}\hat{s}$ and $\bar{R}_{A} = \bar{R} - \frac{4\pi e^{*}}{\varepsilon_{\infty}}\ \bar{\chi}^{(2)}$. Here, {j} is an index for the geometrical configuration of the polariztion of the two ℓ- and s-laser beams with respect to the crystal axes, $\bar{\chi}^{(2)}$ the second order nonlinear susceptibility tensor, and $\hat{\ell}$ and $\hat{s}$ are the unit polarization vectors of the fields E_{ℓ}, E_{s}.

The experimentally observable parameter in the CARS experiment is the intensity of the TRCARS signal at the energy $\hbar\omega_{c}=\hbar(2\omega_{\ell}-\omega_{s})$. This intensity is proportional to the absolute square of the nonliner polarization induced in the vibrational and electronic systems due to the three laser fields $\vec{E}_{\ell}$, $\vec{E}_{s}$ and $\vec{E}_{p}$. Thus an expression for this quantity can be written as [29],

$$I_{c}(\Delta t) = AS \int_{-\infty}^{\infty} dt\ |\vec{E}_{p}^{+}(t+\Delta t)\times[N(\bar{R}_{A}\cdot\hat{q})Q^{+}(t)+\bar{\chi}_{eff}^{(3)}\vec{E}_{\ell}^{+}(t)\vec{E}_{s}^{-}(t)]|^{2}\quad , \tag{11}$$

where

$$A=2\pi\omega_c^2 L^2/c\epsilon_c,\quad S=\sin^2(\Delta\vec{k}\cdot\vec{L}/2)/(\Delta\vec{k}\cdot\vec{L}/2)^2 \text{ and } \vec{\Delta}=\vec{k}_c-(\vec{k}_\ell+\vec{k}_p-\vec{k}_s) \quad .$$

In Eq. (11), the factor S goes to unity as the phase mismatch $\Delta\vec{k}$ goes to zero, L is the length of the spatial overlap within the sample of all three laser fields, c is the speed of light, ϵ_c the dielectric constant of the medium at ω_c, Δt is the temporal difference between the probe pulse and that of $\vec{E}_\ell$ and $\vec{E}_s$ (which are set as close as possible to the exact time overlap $\delta t=0$), N is the number of primitive cells per unit volume, $\bar{\chi}_{eff}^{(e)}$ is the effective third-order nonlinear electronic susceptibility.

It is clear from Eq. (11) that there are two contributions to $I_c(\Delta t)$, i.e., one due to the response of the lattice and one to the response of the electronic system and that the relative contributions of the phonon part to the electronic part depend on the geometrical configuration {j} of the polarization direction of the three laser beams and that of an analyser (placed in the CARS field) with respect to the crystal axes. The explicit expressions for the response of the vibrational and electronic systems, for the seven possible configurations for the present case, can be found in reference [30]. The parameter $\chi^{(3)}$ may be complex, and the lattice term is purely imaginary at resonance, i.e., at $\omega_{LO}=\omega_\ell-\omega_s$. Thus, interference between these contributions are expected.

The components of the coherent phonon state described above are expected to dephase relative to each other after the excitation fields $\vec{E}_\ell$ and $\vec{E}_s$ cease. In general, phonon dephasing in solids results from scattering at boundaries, lattice imperfections, carriers, or through population decay brought about by anharmonic interactions. Near-zone-center LO phonons possess, however, nearly zero group velocities so that their generation in the bulk of the solid (as is done here) eliminates boundary scattering as an active dephasing mode. Impurity scattering may also be neglected in high quality crystals. We demonstrate below that the experimental results support this supposition. Carrier scattering may also be neglected for observations in excess of a few picoseconds after carrier generation. This conclusion stems from the recently obtained knowledge [36], [37] that hot carriers decay in this time scale to an electron-hole plasma at a conduction band minimum. As already discussed above, the LO phonon off which the electron-hole plasma can scatter (and conserve energy and crystal momentum) must possess a wavevector of the order of 10^5 cm^{-1}, which is two orders of magnitude greater than the wavevector of the LO phonons under investigation here. Thus, contrary to the assumptions we made in Ref. [28], we now assume that, under our experimental conditions, only anharmonic phonon decay can be expected to contribute to the dephasing time.

It has been generally accepted that the phonon dephasing time, $T_2/2$, obtained from TRCARS measurements, is related to the spectral linewidth $\delta\nu$(in cm^{-1}) of the incoherent spontaneous Raman scattering cross-section. The relation is $T_2/2=(2\pi\delta\nu)^{-1}$ provided that the Raman scattering lineshape is homogeneously broadened [38], i.e., it possesses a Lorentzian profile. Moreover, if the lineshape is Lorentzian one would predict that in the temporal domain the amplitude of the coherent phonon state decays exponentially. Thus, one would predict that the phonon contribution of $I_c(\Delta t)$ (which is proportional to $<Q>^2$) decays as $\exp(-2t/T_2)$.

The experimental apparatus has been discussed in reference [35]. Samples of GaP of dimension a few millimeters on each edge were held over a range of temperatures from 5-300K to within an accuracy of about ±0.5K. The GaP sample contains about 4×10^{16} cm^{-3} isoelectronic nitrogen impurities. Standard measurements were also performed on the linewidth of the incoherent spontaneous Raman scattering intensity. For this purpose the cw Argon ion laser line at 514 nm and backward scattering geometries are used. In the TRCARS measurements, a part of the ℓ-laser beam was split off to produce a probe pulse train whose total optical path length to the crystal could be varied through an optical delay such that its arrival at the sample preceded or lagged behind the arrival time of pulses from the ℓ- and s-lasers.

Figure 7 illustrates typical normalized TRCARS intensities as a function of the time delay Δt between the two pump beams (E_ℓ, E_s) relative to the probe beam (E_p) for the case of GaP held at 4.2K and 300K, and with $\omega_\ell-\omega_s=\omega_{LO}$ so that the coherent LO phonon state is excited. The two components of $I_c(\Delta t)$ are clearly visible. The first component near $\Delta t=0$, which can be independently observed when $\omega_\ell\omega_s\neq\omega_{LO}$, is a slightly asymmetric "bell-shaped" curve displayed as the dash-dotted curve in Fig. 10. This component of $I_c(\Delta t)$ is attributed to the nonlinear, electronic response of the crystal, $I_c^e(\Delta t)$. The remaining part of $I_c(\Delta t)$ decreases exponentially with delay time for $\Delta t>>o$ and can be observed to do so over several orders of magnitude. Thus for these experimental conditions the time interval over which the coherent phonon state is observed to decay is long compared to the time interval over which the purely electronic signal

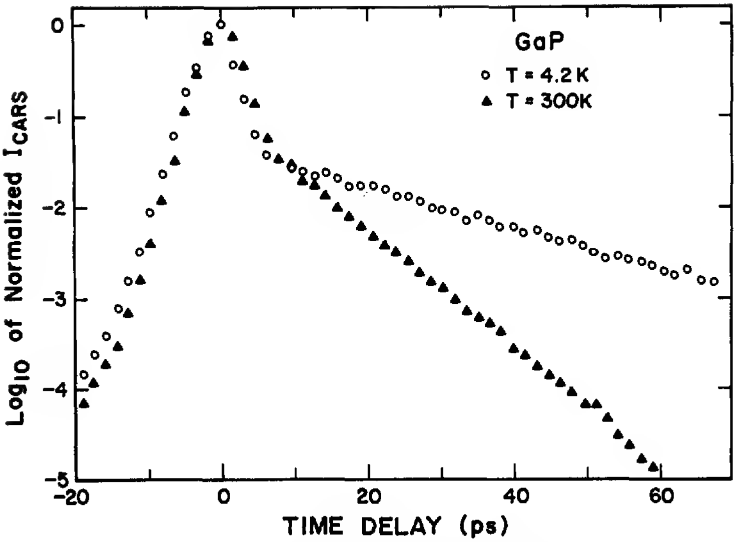

Figure 7. Temporal evolution of the CARS intensity at the LO phonon resonance of GaP for sample temperatures of 4.2 and 300 K.

is observed. The slope of the "phonon" part of $I_c(\Delta t)$ is then equal to the dephasing time $T_2/2$. The experimental results on the temperature dependences of $T_2/2$ for coherent LO phonon dephasing in GaP are indicated as solid circles in Fig. 9.

Similar measurements for the dephasing time of coherent TO phonons were also attempted by setting $\omega_\ell-\omega_s=\omega_{TO}$. For all temperatures in both GaP and ZnSe we find only the "bell shaped" electronic response. We conclude that the dephasing time for coherent TO phonons is less than the lower limit of our temporal resolution (1-2 ps), i.e., it corresponds to a steeper (negative) slope than that of the positive Δt component of the purely electronic response and is, therefore, hidden.

The temperature dependence of $T_2/2$ has also been determined through linewidth measurements of the spontaneous Raman scattering intensity. The results are displayed in Fig. 9 as crosses for LO phonons and as solid triangles for TO phonones in GaP. For completeness we also include similar data for a different crystal of GaP as reported by Bairamov, et al. [39], [40].

Note should be taken of the following additional results depicted in Fig. 9. Namely, (i) the temperature dependence of TO phonon dephasing is less than that of LO dephasing, (ii) the results of the linewidth studies agree among the two experimental groups, and (iii) agreement also exists between the results obtained from the linewidth and from the temporal measurements. It should be further noted that

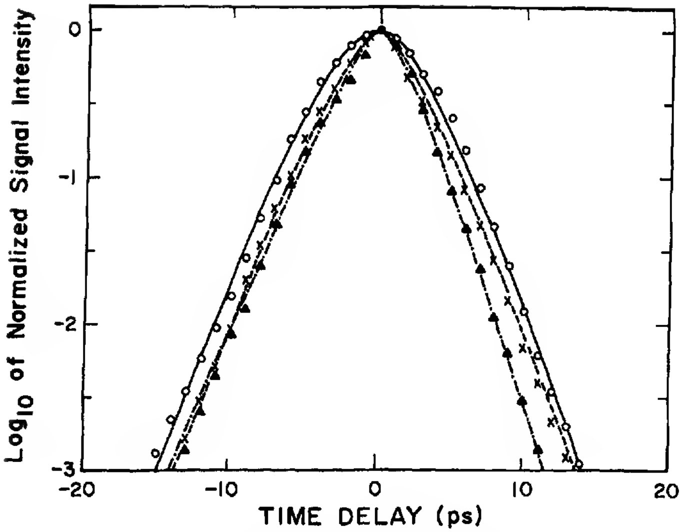

Figure 8. Temporal evolution of the intensity of the autocorrelation signal (dashed line); of the cross-correlation signal (solid line); and the three-wave mixing signal (dotted line).

the temporal measurements show quite clearly that the coherent LO phonon state is not destroyed as a result of the dephasing process, rather $<Q>^2$ presists through many orders of $I_c(\Delta t)$ and simply decreases its magnitude exponentially.

The dephasing time $T_2/2$ may include contributions from all dephasing phenomena such as elastic scattering from free electronic carriers and from phonon-phonon scattering.

Whatever the effect of elastic impurity scattering is on the dephasing rate, to a good approximation, we can assume it to be temperature independent in comparison to that of anharmonic phonon-phonon scattering, since the former is proportional $n_T(\omega_{LO})$ [41] as compared to the latter which is proportional to $2n_T(\omega_{LA})$ (see Eq. 1).

In the low temperature regime, for which $\hbar\omega >> k_BT$, three phonon interactions should dominate [42] anharmonic interactions. Of the possible interactions only LO phonon decay into acoustic phonons (and their recombination) needs to be considered. Combination of a longitudinal optical phonon at the zone center with an acoustic phonon cannot occur since this would produce a phonon with $\omega > \omega_{LO}(q=0)$ which cannot exist in GaP. Moreover, the phonon dispersion relations of GaP, [43] plus energy and crystal momentum conservation, rule out all interactions except

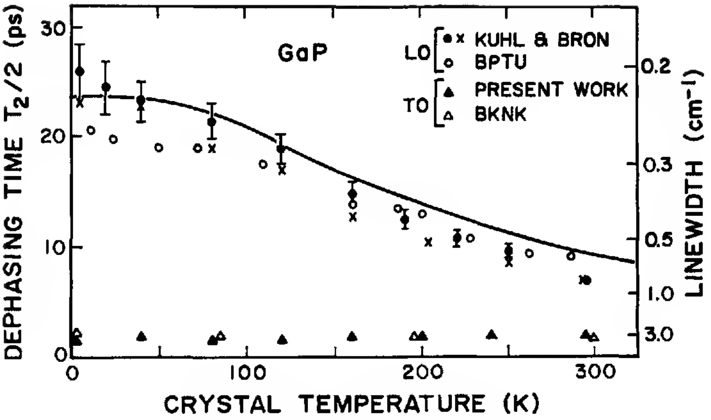

Figure 9. Temperature dependence of $T_2/2$ and of the Raman bandwidth of LO and TO phonons in GaP. The solid circles and crosses refer to data taken from different sources.

$$LO(\omega_{LO},0) \longleftrightarrow LA(\omega_{LO}/2,\vec{q}\,') + LA(\omega_{LO}/2,-\vec{q}\,')$$

Here, $\vec{q}\,'$ is the wavevector of the LA phonon at half the LO phonon energy. We shall refer to this interaction as the "Klemens' channel" [5].

If only the Klemens channel is considered the expression, Eq. (4), for the population decay time (τ) can be further simplified to

$$\tau(T) = \frac{1}{\Gamma} = \frac{\tau_o}{1+2n_T(\omega_{LO}/2)} , \qquad (12)$$

where τ_o is the population decay time at zero temperature. Hence, the general dephasing time becomes

$$\frac{2}{T_2} = \frac{1}{T_{im}} + \frac{1+2n_T(\omega_{LO}/2)}{\tau_o} , \qquad (13)$$

where T_{im} is dephasing time due to elastic scattering from imperfections.

The solid curve given in Fig. 9 indicates the temperature variation of the dephasing time for GaP as obtained from Eq. (13) with the best fit values for $T_{im} = \infty$ and for $\tau_o = 24.6$ ps. Thus impurity scattering does not play an important role even in the presence of nitrogen impurities of the order of $10^{16}/cm^3$ in our crystal of gaP.

The experimental observation of a more rapid decay with increasing temperature than that predicted by Klemens implies that higher order phonon-phonon interactions are beginning to play a role. Since it is impossible at this time to enumerate all the possible decay channels and the corresponding strengths accurately due to insufficient knowledge of the anharmonic potential [44], [45], a complete analysis of the dephasing time including its absolute value cannot yet be done.

Particular note should be taken that a comparison of the dephasing time obtained from the Raman linewidth measurements to that from the CARS measurements, indicates that the two different methods yield identical results within experimental error. This observation has been foreshadowed by previously derived theoretical expressions for $T_2/2$ for each case which are also found to be identical in every way [41]. These predictions assume, as is the case here, that the acoustic phonons produced in the decay of the LO phonons do not appreciably increase $n(\omega_{LA})$ beyond its value at thermal equilibrium $n_T(\omega_{LA})$. It remains to be seen what happens when $n(\omega_{LA}) >> n_T(\omega_{LA})$ for which phonon breakdown [46] and phonon renormalization [47] effects have been predicted to be of importance.

3.3 Electron-Phonon Dynamics

In this final section, I want to briefly introduce experimentation which has recently been conducted on the interaction of (mostly) optical phonons with electronic carriers. I had already mentioned in the introduction that strong electron-phonon interaction in polar semicondcutors can only occur for optical phonons with wavevectors $> 10^5$ cm^{-1}.

The first experiment along these lines which I wish to cite was performed in GaAs by von Der Linde, et al. [36] who used time-resolved Raman scattering to study the dynamics of nonequilibrium incoherent optical phonons and their interaction with photoexcited hot electrons and holes.

In the experiment photoexcited electron-hole pairs (e-h pairs) were generated with light from pulses from dye-lasers with autocorrelation duration of 2.5 ps. The electron-hole pair excess energy was 17 times the LO-phonon energy of 36.5 meV. Subsequent dynamics of the e-h pairs and of the LO phonons produced by the pair cascade, as illustrated in Fig. 1, was monitored by a probe pulse (of the same laser frequency) which preceded or followed in time the pump pulse. The Raman (backward) scattering off the LO phonon distribution as measured by time delayed probe pulse is accordingly a function of the temporal evolution of the LO phonons (with $\vec{q} > 10^5$ cm^{-1}).

The experiment was repeated by Kash, et al. [37] through incoherent Raman scattering measurements in the spectral domain, but carried out

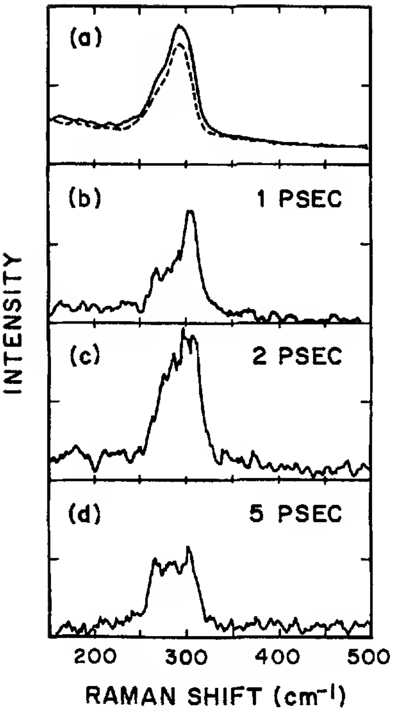

Figure 10. Time resolved anti-Stokes Raman difference signal for Δt = 1, 2 and 5 ps.

with a probe pulse after various delays relative to the pump pulse. In this experiment the laser pulse duration was only 0.6 ps (600 fs). The pump and probe pulses were polarized perpendicularly to each other as was the LO phonon Raman (backward) scattering excited by the pump and the probe pulses. However, the pump pulse was observed to also produce a spectrally broad but unpolarized emission band. This emission, plus the signal from stray laser light and detector dark current, were compensated for by taking difference measurements between spectra taken with the probe delay time, Δt, fixed at various values less than obtained when Δt << 0 ps.

The results are illustrated in Fig. 10 which shows the intensity of the anti-Stokes Raman signal as a function of Raman shift for various values of Δt for a molecular-beam epitaxially grown GaAs sample held at room temperature. In Fig. 10a the solid line is observed for Δt = 1 ps, whereas the dashed line is observed for Δt = -20 ps. Similar differences for Δt = 1, 2 and 5 ps as indicated in Fig. 10b,c,d. It is found that the total cascade consists of 12 cascade steps each of approximately 165 fs long; in very good agreement with predictions [7]. The phonon decay time near 80K was found to be 7.5 ps, in good agreement with the earlier results of von der Linde, et al. [36].

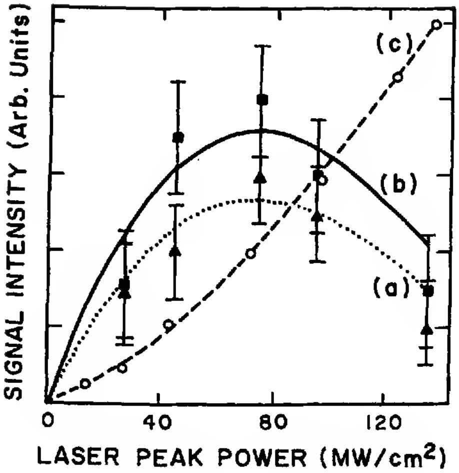

Figure 11. Anti-Stokes vibronic intensity as a function of the s-laser peak power for (a) the LO peak, and (b) the LA peak frequency. (The data marked c is not discussed in this paper.) Symbols are experimental points, solid and dotted lines are theoretical fits to the data. The peak power of the ℓ-laser is fixed at 135 MW/cm^3.

The observed decay time, τ, is related to the fundamental phonon lifetime only in a remote way. As should be apparent from Fig. 1, the e-h pair decay produces an ensemble of optical phonons with a spread of $\vec{q}$. The decay of such an ensemble may well differ from the decay of a well-defined coherent phonon state as recently reported by Kuhl and Bron [13,28].

3.4 Effects of Electron-Hole Plasma

We now turn our attention to the interaction of phonons with an electron-hole plasma, i.e., to the situation which prevails once the "hot" electrons have decayed to some minimum of the conduction band. The lifetime of e-h pairs against recombination varies from many nanoseconds to microseconds, thus the dynamics of the interaction should easily be observable with modern picosecond laser spectroscopy.

We have reported above detailed CARS measurements of the dephasing time of coherent optical phonons in GaP containing very low carrier concentrations. The observed phonon dephasing time is attributable solely to anharmonic phonon-phonon interactions. The interaction, at least in GaP, results only in the creation of longitudinal acoustic (LA) phonons of half the energy of the LO phonons. These experiments have been repeated with the addition of an electron-hole plasma produced by absorption of additional laser light in a manner similar to that illustrated in Fig. 1. Since the effective wavevector of the LO phonon produced by our CARS technique is $\lesssim 3 \times 10^3$ cm^{-1}, and since the temporal resolution of the CARS measurements were limited to $\lesssim$ 1.3 ps, no observation could be made on the interaction during the free carrier cascade. Similarly, since the concentration of the e-h plasma produced by the cascade was less than ~ 10^{17} cm^{-3}, no shift in the LO phonon frequency or change in dephasing time could be expected. None was in fact observed. However, we were surprised to find that a strong (approximately 10-20%) decrease was observed in the magnitude of the CARS signal associated with the coherent phonon state. Although the plasma does not in this limit form a coupled state with the phonons, the results imply that it does apparently interfere with the production of the coherent phonons.

The last mentioned phenomenon has been recently investigated in more detail by Rhee and Bron [28]. In this experiment coherent phonon generation proceeds through nonlinear interaction in GaP of pulse trains emitted from two dye lasers driven simultaneously by 5 ns duration pulses from a N_2-laser. One dye laser is operated at a frequency ω_ℓ = 18,275 cm^{-1}, which together with another laser at ω_s = 18,322 cm^{-1}, makes up the difference frequency $\omega_{LO} = \omega_\ell - \omega_s$ = 403 cm^{-1} required to excite coherent LO phonons. The maximum energy per laser pulse is ~ 60 μJ resulting in an initial LO phonon concentration $n_{LO} \approx 5 \times 10^{16}$ cm^{-3}, located within the overlap volume of the two laser beams.

The laser operating at ω_ℓ also serves to excite the luminescence from the bound exciton in GaP (zero phonon line at 18,688 cm^{-1}) with which the vibronic sidebands are associated. In figure 11 we present the observed dependence of the anti-Stokes vibronic sideband intensity, as measured at the LO and the LA peak frequencies, as a function of the power in the s-laser when the power of the ℓ-laser is fixed at 135 MW/cm^2.

It can be shown [35] that the intensity of the anti-Stokes vibronic sideband should be proportional to the product of the power of the two lasers (ℓ and s lasers) which drive the coherent phonon generation. The results shown in Fig. 11 obviously disagree with this prediction. The origin of the discrepancy arises from the presence of competing forces within the driving force, F_{LO}, through which the coherent LO phonons are generated. The pertinent expression for the driving force is

$$F_{LO} \propto \left[R + \frac{8\pi e^* \, |\chi^{(2)}|}{\varepsilon_\infty} \{1 - \frac{24\pi \, \chi^{(3)}}{0.017} (|\vec{E}_\ell|^2 + |\vec{E}_s|^2)\}\right] E_\ell E_s, \qquad (14)$$

where we have made the simplification $\chi^{(3)} = \chi^{(3)}_{1111} = \chi^{(3)}_{1122} = \chi^{(3)}_{1221}$ for the elements of the third order nonlinear electronic susceptibility, $(c/\omega)^2[(2\vec{k}_\ell - \vec{k}_s)^2 - \varepsilon(\omega)] \approx -0.017$ with $\vec{k}_i$ being the corresponding wavevector of the laser light, $\varepsilon(\omega)$ is the dielectric constant at the frequency ω, c is the speed of light, and R is the effective Raman tensor element, $\chi^{(2)}$ and E_ℓ and E_s are the field intensities of the ℓ- and s-lasers. In the event of high enough values of the laser power it becomes possible for the higher order terms to lead to a net decrease in F_{LO}, which in turn results in a decrease in the production of coherent LO phonons, and hence to a decrease in the anti-Stokes intensity.

The most significant contribution comes from $\chi^{(3)}$ which contains the response of bound electrons, $\chi_b^{(3)}$, and that from the carriers in the plasma $\chi_f^{(3)}$. The major contribution comes from terms in $\chi_f^{(3)}$, i.e.,

$$\chi_f^{(3)} \propto N^*(\sigma_\ell |E_\ell|^2 + \sigma_s |E_s|^2), \tag{15}$$

in which N* is the concentration of bound excitons which is itself proportional to the laser power, and σ_ℓ and σ_s are, respectively, the cross section for the excitation of a bound exciton to form a carrier through a further absorption of ℓ- or s-laser light. Thus, the nonlinearity in the last term of Eq. 14 (produced by the nonlinearity as expressed in Eq. 15) can account for the observed variation in the anti-Stokes sideband intensity, as is shown by the calculated dependence on the s-laser power indicated by the solid and dotted lines of Fig. 13.

Thus, although the effect of an electron-hole plasma on phonon lifetimes and frequency can be observed only at high plasma densities, the interference of lower density plasma with the formation of optical phonons can be readily observed and explained.

4. Conclusions

I have reviewed a small number of experiments in order to illustrate recent progress in the field of transient dynamics of phonons and electrons in semiconductors.

The field has in the past few years experienced a rebirth spurred on by ever more sophisticated experimental techniques which have made it possible to delve deeper into the complex interactions which control nonequilibrium dynamics in real systems. In this lecture I have used as examples the interplay of impurity based scattering and anharmonic interactions to demonstrate quasidiffusive transport dynamics. I have also emphasized phonon dephasing effects and the interaction of electrons and optical phonons and the "screening" of coherent phonon excitations by an electron-hole plasma. The depth of the knowledge so gained cannot be obtained by the more traditional experimental methods of electron and phonon transport.

I trust that I have demonstrated both the vitality and the complexity of this field of research.

I wish to make a final point. The material which I presented involves some experimental results which have outpaced their theoretical basis, not in the sense that a theoretical basis does not exist, but rather that its application to the experimental situation is either too cumbersome to carry out or some components of the analysis, such as crystal potential or electronic polarizabilities, are not sufficiently known. Thus, I further trust that this lecture will stimulate new attacks on the theoretical basis of transient dynamics.

Acknowlegements

I would like to acknowledge the contributions of the many collaborators in the research program which I have described. I would like to specifically acknowledge the work of J. Kuhl, B. K. Rhee, and T. Wilson. The work presented here has been carried out in part through the support of ARO Contracts DAAG 29-83-K-0091, DAAL03-86-K-0142 and NSF DMR 8603888.

V. References

1. P. Baumgartner, M. Englehardt and K. F. Renk, Phys. Rev. Lett. 47, 1403 (1981).
2. R. Orbach and L. A. Vredevoe, Physics 1, (1964).
3. P. C. Kwok and P. B. Miller, Phys. Rev. 146, 592 (1966).
4. P. G. Klemens, "Solid State Physics," Vol. 1, ed. F. Seitz and D. Turnbull (Academic Press: NY) 1958.
5. P. G. Klemens, Phys. Rev. 148, 845 (1966).
6. P. G. Klemens, J. Appl. Phys. 38, 4573 (1967).
7. E. M. Conwell and M. D. Vassel, IEEE Trans. Electron Devices 13, 22 (1966).
8. C. L. Collins and P. Y. Yu, Phys. Rev. B30, 4501 (1984).
9. E. M. Conwell, "High Field Transport in Semiconductors" (Springer: Berlin, Heidelberg, NY) 1967.
10. J. E. Kardontchick and E. Cohen, Phys. Rev. Lett. 42, 669 (1979).
11. B. K. Rhee and W. E. Bron, Phys. Rev. B34, 7107 (1986).
12. W. E. Bron, Rep. Prog. Phys. 43, 301 (1980).
13. W. E. Bron, in "Nonequilibrium Phonon Dynamics," ed. W. E. Bron (Plenum: NY) 1985.
14. R. G. von Gutfeld and A. H. Nethercot, Phys. Rev. Lett. 12, 641

(1964).
15. W. E. Bron and W. Grill, Phys. Rev. B16, 5303 and 5315 (1977).
16. D. V. Kazakovtzev and Y. B. Levinson, JETP Lett. 27, 181 (1978).
17. __________, Phys. Status Solidi (b) 96, 117 (1979).
18. __________, J. Low Temperature Physics 45, 49 (1981).
19. W. E. Bron, Y. B. Levinson and J. M. O'Connor, Phys. Rev. Lett. 49, 209 (1982).
20. T. E. Wilson, F. M. Lurie and W. E. Bron, Phys. Rev. B30, 6103 (1984).
21. W. E. Bron, J. C. Patel and W. C. Schaich, Phys. Rev. B20, 5394 (1979).
22. W. C. Schaich, Sol. State Comm. 49, 55 (1984).
23. T. E. Wilson and W. C. Schaich, Sol. State Comm. 50, 3 (1984).
24. Y. B. Levinson, Sov. Phys. JETP 52, 70 (1980).
25. W. E. Bron, Phys. Rev. B21, 2627 (1980).
26. W. Demdroter, "Laser Spectroscopy" (Springer: Berlin, Heidelberg and New York) 1981.
27. J. Kuhl and D. von der Linde, "Picosecond Phenomena III," ed. K. B. Eisenthal, R. M. Hockstrasser, W. Kaiser and A. Lauberau (Springer: Berlin, Heidelberg and New York) 1982, pp. 201-4.
28. J. Kuhl and W. E. Bron, Solid State Commun. 49, 935 (1984), Physica 117B/118B, 532 (1983).
29. B. K. Rhee, W. E. Bron and J. Kuhl, Phys. Rev. B30, 7358 (1984).
30. B. K. Rhee and W. E. Bron, Phys. Rev. B34, 7107 (1986).
31. E. Garmire, F. Panderese and C. H. Townes, Phys. Rev. Lett. 11, 160 (1963).
32. T. A. Giordmaine and W. Kaiser, Phys. Rev. 144, 676 (1966).
33. M. D. Levenson and N. Bloembergen, Phys. Rev. B10, 4447 (1974).
34. See e.g., L. L. Schiff, "Quantum Mechanics," 3rd edition (McGraw-Hill: NY) 1970, pp. 408.
35. W. E. Bron, J. Kuhl and B. K. Rhee, Phys. Rev. B34, 6961 (1986).
36. D. von der Linde, J. Kuhl and H. Klingenberg, Phys. Rev. Lett. 44, 1505 (1980).
37. J. A. Kash, J. C. Tsang and J. M. Hvam, Phys. Rev. Lett. 54, 2151 (1985).
38. See e.g., A. Lauberau and W. Kaiser, Rev. Mod. Phys. 50, 607 (1978).
39. B. Kh. Bairamov, D. A. Parshin, V. V. Toporov and Sh. B. Ubaidullav, Sov. Tech. Phys. Lett. 5, 466 (1979).
40. B. Kh. Bairamov, Yu. E. Kitaev, V. K. Negoduiko and Z. M. Kashkhozhev, Sov. Phys. Sol. State 16, 1323 (1975).
41. P. Carruthers and K. S. Dy, Phys. Rev. 147, 214 (1966), A. A. Maradudin and A. E. Fein, Phys. Rev. 128, 2589 (1962).
42. R. Orbach and L. A. Vredevoe, Physics 1, 91 (1964).
43. H. Bilz and W. Kress, "Phonon Dispersion Relations in Insulators" (Springer: Berlin) 1979.
44. A. S. Pine and P. E. Tannenwald, Phys. Rev. 178, 1424 (1968).
45. T. R. Hart, R. L. Aggraval and B. Lax, Phys. Rev. 81, 638 (1970).
46. R. Orbach, IEEE Transactions on Sonics and Ultrasonics, SU-14, 140 (1967).
47. S. A. Bulgadaev and I. B. Levinson, Zh. Eksp. Teor. Phys. 67, 2341 (1974), Sov. Phys. JETP 40, 1161 (1974).

CROSSING EFFECTS IN PHONON SCATTERING

L.J. Challis
Department of Physics, University of Nottingham, Nottingham, NG7 2RD, England.

1. Introduction

Phonons have been used very effectively by many groups for the spectroscopic study of impurities and defects in solids [1]. The impurity can give rise to resonant scattering through transitions between its electronic states and the resonant frequency and scattering strength provide information about the eigenvalues and eigenstates of the system. In general, the resonant scattering from a phonon beam or current will occur at more than one frequency either because an impurity has more than one transition within the spectral range of the beam or because more than one type of impurity is present. If all these frequencies are well separated, the scattering from the beam is merely the sum of the scattering due to each process, but if this is not the case, various forms of "interference" can occur which are called crossing effects. This lecture is intended to provide a qualitative introduction to these effects and is illustrated by our own data. A more complete discussion giving proper acknowledgement to other work in the field can be found elsewhere [2].

2. Frequency Crossing

If a heat current passes through a pure crystal, the phonon spectrum of the current has the form shown in fig 1(a). The phonon mean free path equals the diameter of the crystal and is independent of frequency. If the crystal contains magnetic ions producing resonant scattering at a frequency $\nu_1 = g\beta B/h$, the spectrum has the form shown in fig 1(b). A "hole" appears at a frequency ν_1 which can be moved by changing the field.

Suppose now there is also a second type of ion present which gives rise to resonant scattering at a frequency ν_2 which is independent of magnetic field. The spectrum now contains two holes (fig 1(c)) which can be made to coincide by adjusting the field until $\nu_1 = \nu_2$. This is called a frequency crossing and it gives rise to a minimum in the thermal resistance, W, and so in the temperature gradient along the

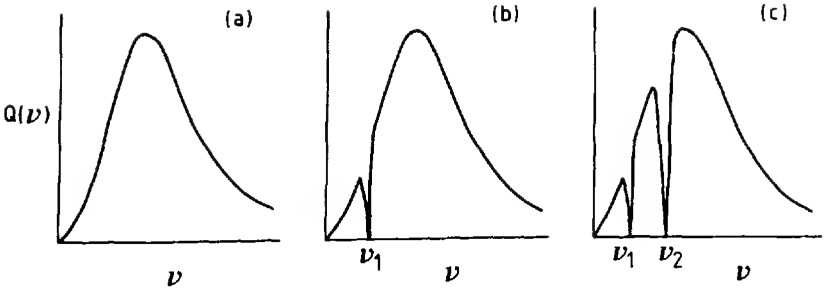

Fig 1 : The spectral distribution of a heat current (a) a pure crystal, (b) a crystal containing magnetic ions resonant at ν_1 (c) with ions resonant at ν_1 and ν_2.

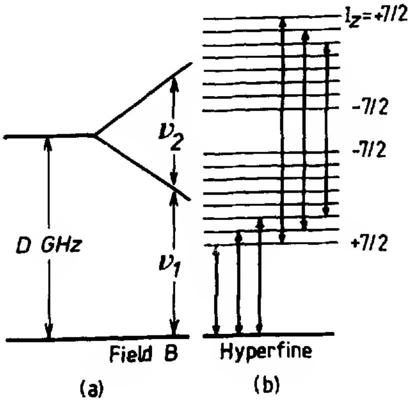

Fig 2 : Energy level diagram for V^{3+} in Al_2O_3 (a) splitting due to a field B||c (b) hyperfine splittings (not to scale); also shown are the phonon transitions allowed by the selection rule $\Delta I_z = 0$. [3].

crystal because the effect of the two holes on the total heat current is less when they are merged than when they act independently.

We illustrate this by looking at a frequency crossing signal caused by V^{3+} ions in Al_2O_3. Their energy levels for fields parallel to the c-axis are shown in fig 2(a). If hyperfine splitting is neglected, we can see that a frequency crossing occurs when $\nu_1 = \nu_2$ ($D - g\beta B = 2g\beta B$) and the resulting signal is shown in fig 3 [3]. The structure arises because the levels are actually split by hyperfine interaction as shown in fig 2(b). The hyperfine splitting constant $A_H \sim 10^{-3} D$ (D = 249GHz) and as a result the "holes" at ν_1 and ν_2 are each split into 8. Since $\Delta I_z = 0$ for phonon scattering, the 8, $\Delta M = 1$ holes are split by A_H

while the $\Delta M = 2$ holes are split by $2A_H$; this is shown schematically in fig 4. [4]. Structure in frequency crossing signals can conveniently be enhanced by differentiation and fig 5 shows the differential of the signal in fig 3 obtained by modulating the magnetic field using two small superconducting coils on either side of the sample [5].

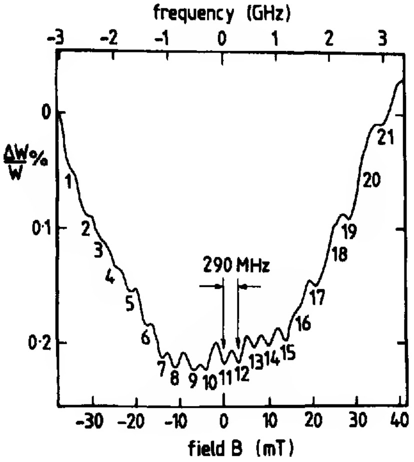

Fig 3 : Frequency crossing signal due to 70ppm of V^{3+} in Al_2O_3. The structure is due to hyperfine interaction. [3].

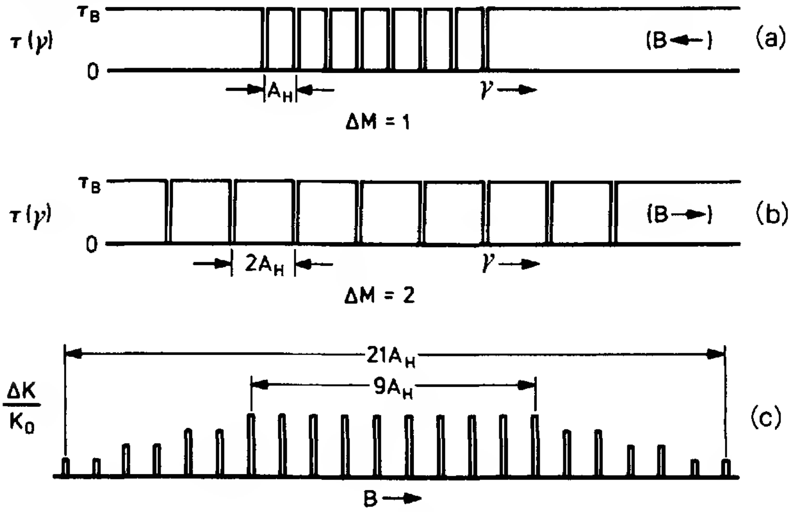

Fig 4 : The hyperfine structure of frequency crossing signals from V^{3+} in Al_2O_3 using a "rectangular hole" model. (a) and (b) show the holes in $\tau(\nu)$ (the relaxation time) caused by the $\Delta M=1$ and 2 transitions respectively and (c) shows the 22 lines of the crossing. The different sizes are caused by differences in the number of overlapping holes. [4] and the maxima in ΔK correspond to minima in ΔW.

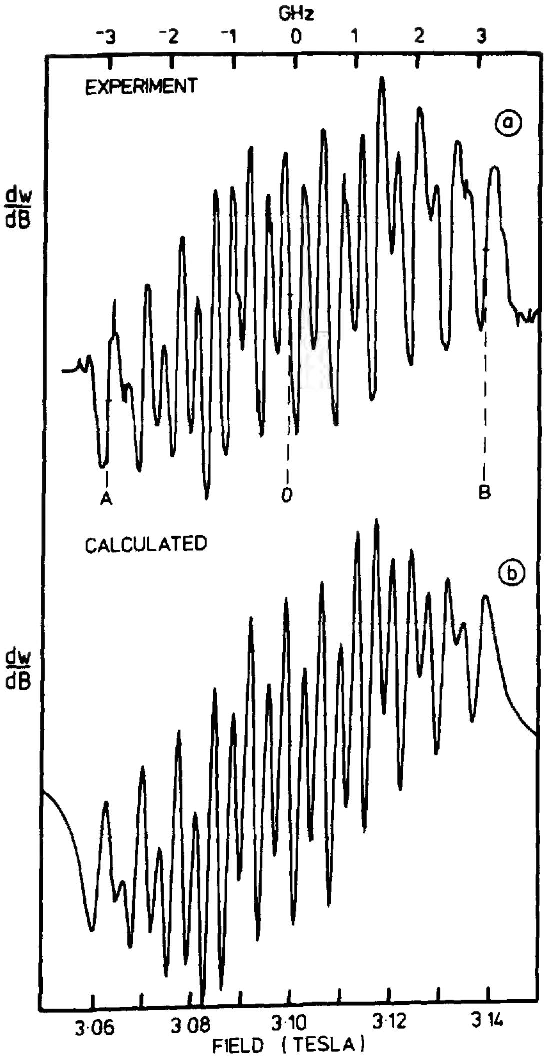

Fig 5 : (a) The differential of the frequency crossing signal in fig 3 obtained by field modulation (b) computed curve. [5].

These experiments show that frequency crossing can be quite a high resolution technique. Its sensitivity is demonstrated by experiments on V^{3+}/V^{3+} pairs in Al_2O_3. If the concentration of V^{3+} is c, then that of a particular pair is c^2 if the ions are randomly distributed. The energy levels are easily calculated if we assume isotropic exchange coupling $J\underline{S}_1 . \underline{S}_2$ and the lower levels of the pair are shown in fig 6. The resulting transition frequencies are shown in fig 7 for J=8.7 GHz [6]. The most noticeable feature is the septet of frequency crossings

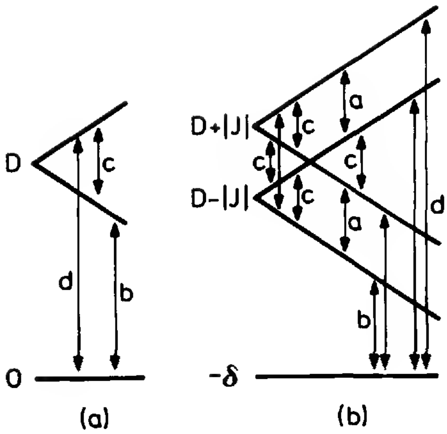

Fig 6 : The lower energy levels of V^{3+} in Al_2O_3 (a) ions and (b) exchange coupled pairs. [6].

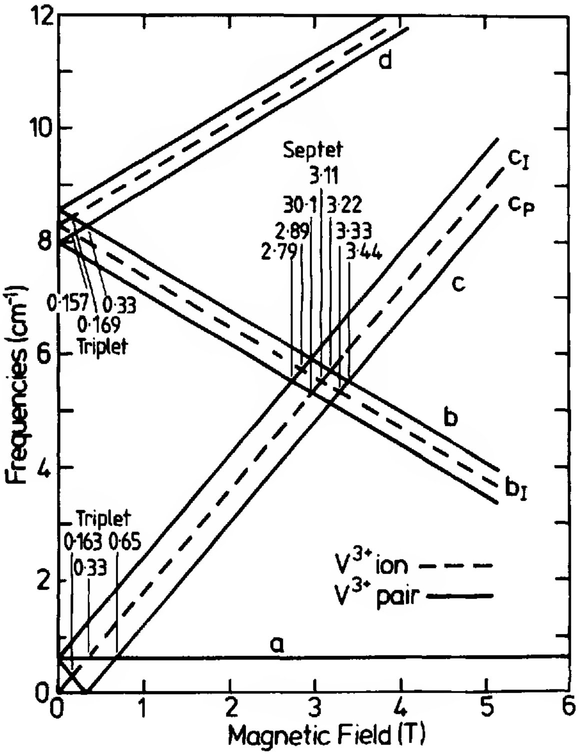

Fig 7 : The transition frequencies of V^{3+} ions and V^{3+}/V^{3+} pairs for B||C and J=8.7 GHz. Note particularly the septet of equally spaced lines at 3.1T. [6].

centered on the single ion crossing. A doped crystal will contain a whole set of pairs each with a different value of J corresponding to various possible Al-Al neighbours in the lattice. So the pair spectrum is quite complicated. Fig 8 shows the thermal magnetoresistance of an Al_2O_3 sample containing 1170ppm of V^{3+} [6]. The septet around 3.1T is very apparent and from the splitting we deduce a value of J=8.7 GHz. Further work showed that the spectrum was dominated by crossings from 4 pair systems (J=9.0 ±1.5, 44 ±1.5, 37 ±1.5 and 50 ±1.2 GHz) [7] and could be rather well explained using an isotropic interaction. As the concentration is decreased, the pair lines (concentration $\propto c^2$) fall more rapidly in size than the single ion line as expected, (fig 9), and at 70ppm where $c^2 \sim 5\times10^{-3}$ppm, it was necessary to use signal averaging to see the pair line shown. V^{3+} is fairly weakly coupled to the lattice and pairs of more strongly coupled ions should be readily seen at this concentration if they are not inhomogeneously broadened by random strain.

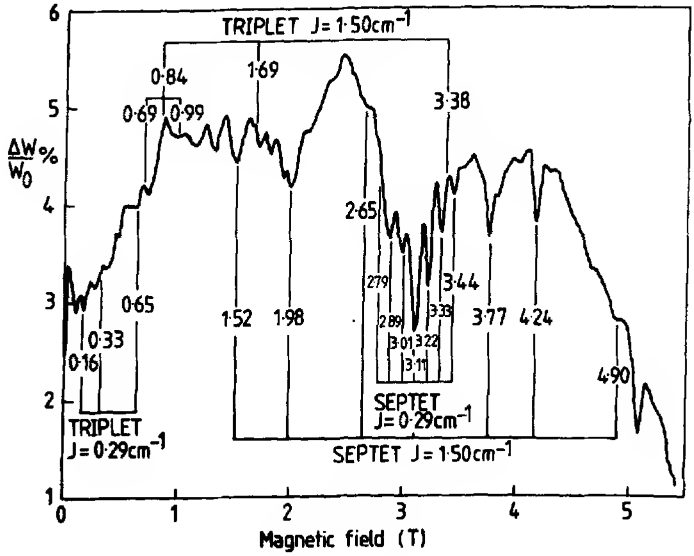

Fig 8 : The frequency crossing pair spectrum in Al_2O_3 containing 1170 ppm V^{3+} showing assignments for two pairs (J=0.29 cm^{-1} = 8.7GHz and J=1.5cm^{-1} = 45GHz). [6].

Further information can be obtained by investigating the angular dependence of the signals. Fig 10 shows values of the crossing fields for Fe^{2+} in Al_2O_3 which were used to obtain the first accurate value of the ground state splitting [8] and the solid line shows that the angular dependence was in agreement with previous values of g for this

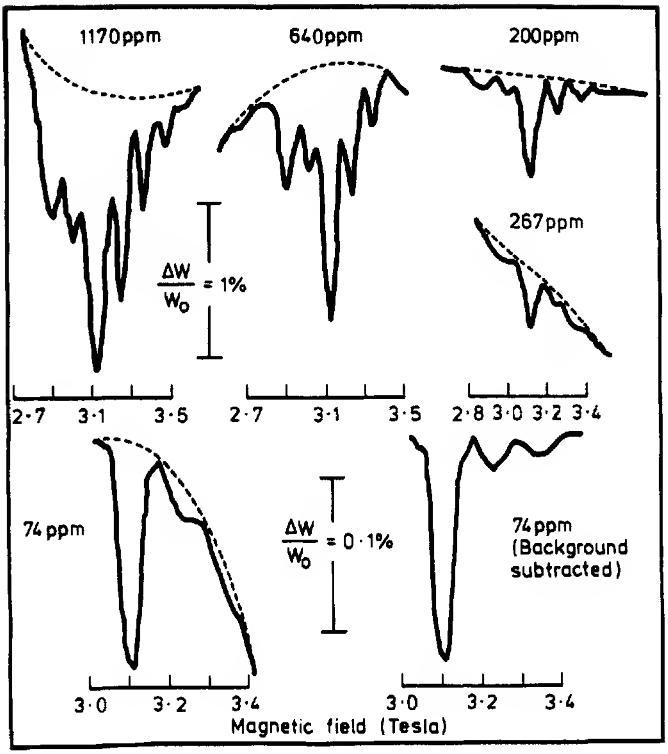

Fig 9 : The septet of crossing signals due to V^{3+} pairs in Al_2O_3 for different V^{3+} concentrations. [6].

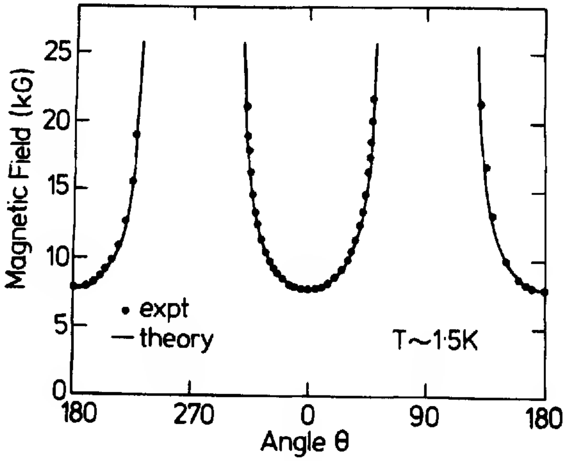

Fig 10 : The angular dependence of a frequency crossing signal for Fe^{2+} in Al_2O_3 compared with calculation (solid line). [8]. (The energy levels are shown in fig 13).

system. Not all the signals observed in Al_2O_3 samples are well understood however, and fig 11 includes crossings from a number of unidentified centres, some of which may be strongly coupled defects rather than impurities. [9].

Frequency crossing can also be used to investigate inelastic

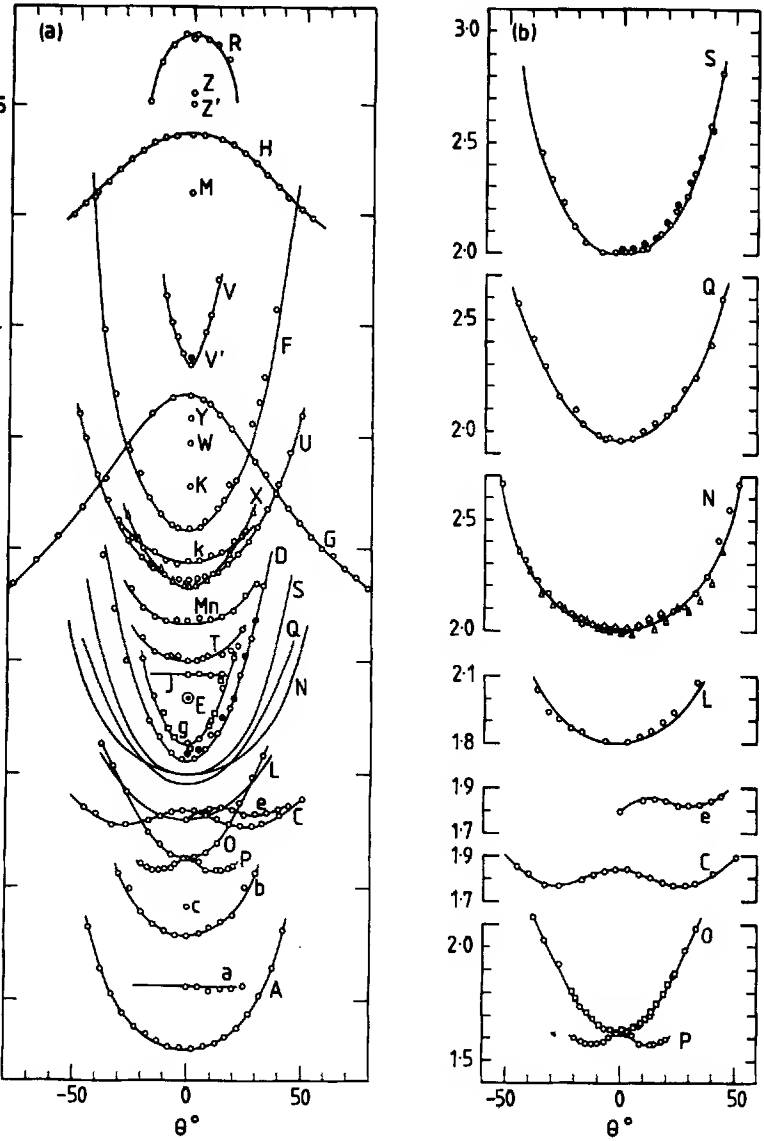

Fig 11 : (a) Examples of the angular dependence of crossing signals seen in Al_2O_3. (b) some of the same signals shown on an expanded scale [9].

scattering. We have seen that when a heat current passes along a doped crystal, holes are burned at the resonant frequencies ν_i of the dopant ions. If now the current leaves the doped part of the crystal and enters an undoped region (or a differently doped region) the spectrum of the phonon current will gradually change towards the new equilibrium form. This means in particular that the holes at ν_i will decay to zero or in practice to a smaller size set by the trace impurity level. The distance over which this change take place is determined by the mean free path for inelastic phonon scattering. It can be measured by using a probe ion in the second half of the crystal. The size of the decaying hole due to ions in the first half is measured by crossing it with the hole of constant size due to ions in the second. An example is shown in fig 12. The solid circles show the size of the signal as a function of the distance from the interface between the two halves of the crystal. The open circles show the limiting value set by traces of the first dopant present in the second half. This was measured by injecting heat into the second half only. [10].

3. Level Crossing and Anticrossing

Undoubtedly the most interesting crossing effects occur when two levels either cross or anticross (repel). Anticrossing requires that there should be an off-diagonal matrix element between the states so that crossings may turn into anticrossings if the magnetic field is moved away from a symmetry axis. Fig 13 shows this effect for Fe^{2+} in Al_2O_3 and fig 14 shows the signal that results. [8]. Phonon scattering is occurring between the two anticrossing levels and a third level, and the mixing of states gives rise to the beautiful Lorentzian maximum in the thermal resistance seen in the plot at $\vartheta=2°$. At this angle the minimum separation of the two states is larger than the combined width of the two holes but this is no longer the case at $\vartheta=0°$. So now the two holes partially overlap and a small frequency crossing signal can be seen rather like a volcanic crater on top of the anticrossing maximum! Level crossing effects have still to be seen. These are genuine interference effects arising from the coherent excitation of two states by a single phonon (or photon) when they are separated by less than their natural widths. The process is analogous to a two slit experiment and as in that case, interference does not cause a change in the total scattering (or transmission) but does change its angular distribution. Level crossing was seen in light scattering by Hanle as long ago as 1924 and more recently has been used very effectively for high resolution spectroscopy. However, it has still to be

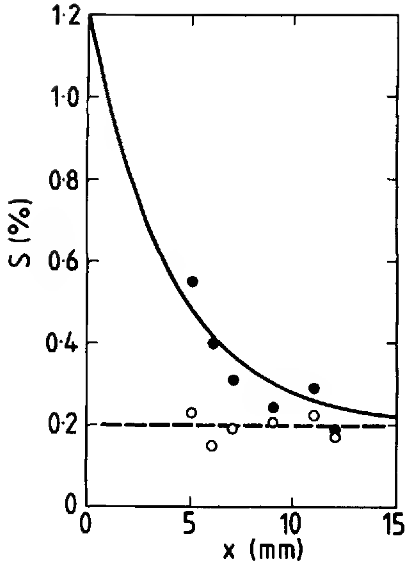

Fig 12 : The solid circles show the decrease in size of a frequency crossing as a function of distance from an interface. The open circles show the limiting value obtained by injecting heat into the second half of the sample. [10].

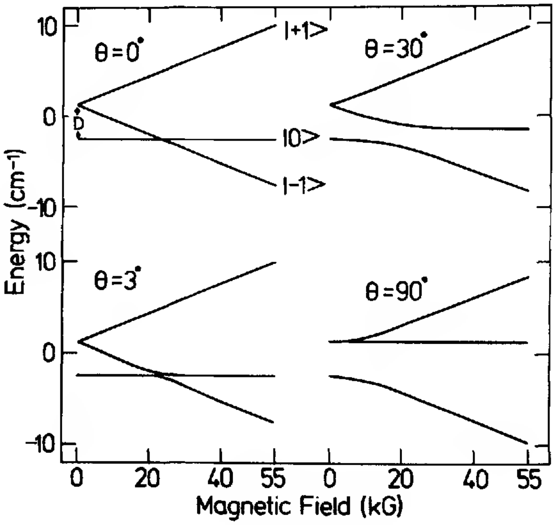

Fig 13 : The energy levels of the ground state triplet of Fe^{2+} in Al_2O_3 for various angles ϑ of field relative to the c-axis. The two lower levels anticross as ϑ increases from 0°. [8].

seen in phonon scattering. It will be a difficult experiment but a possible technique is suggested in Fig. 15. A heat pulse is fired at magnetic ions restricted to a small region of the crystal as shown. (It should be possible to do this by using a pencil of γ-rays to convert ions in a weakly coupled valence state into "active" ions).

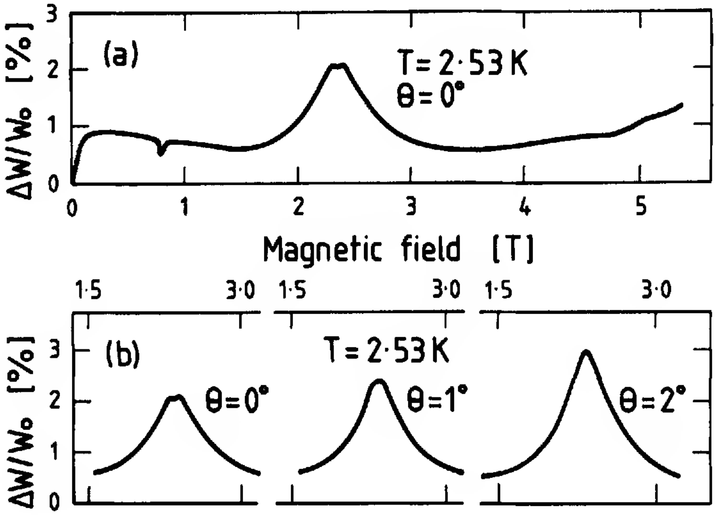

Fig 14 : The magnetothermal resistivity of Fe^{2+} in Al_2O_3 showing (a) the anticrossing at 2.4 T for ϑ= 0°. (The minimum at 0.8T is a frequency crossing signal whose angular dependence is shown in fig 10) (b) the angular dependence of the anticrossing signal showing the development of the frequency crossing minimum at the peak ϑ—>0. [8].

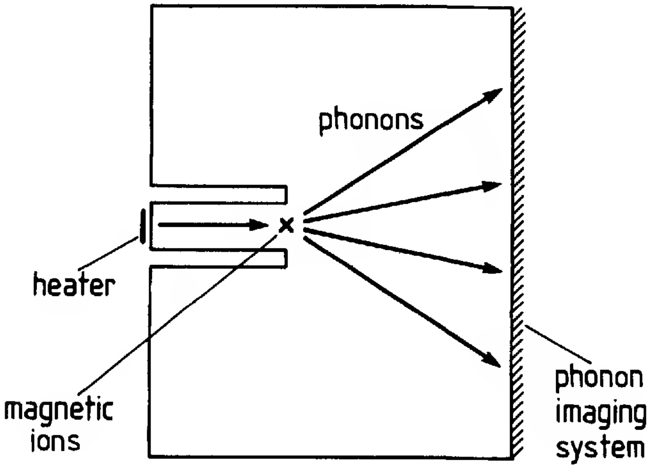

Fig 15 : Proposed arrangement for observing level crossing signals.

Phonon imaging could then be used to study the change in the angular distribution of the scattered phonons when a magnetic field takes the system through the level crossing.

4. CONCLUSION

Frequency crossing effects in phonon scattering can be used to provide spectroscopic information on ions or defects and to study inelastic scattering at surfaces. Particularly interesting effects occur when levels cross or anticross.

5. ACKNOWLEDGEMENTS

I am very grateful to all my collaborators in this work and to the Science and Engineering Research Council for their support.

6. REFERENCES

[1]. L.J. Challis and A.M. de Goër : Phonon Spectroscopy of Jahn-Teller ions, in "The Dynamical Jahn-Teller Effect in Localised Systems", Modern Problems in Condensed Matter Sciences, Vol. 7, eds. Yu. E. Perlin and M.Wagner (North-Holland, Amsterdam) p533, 1984.

[2]. L.J. Challis : Crossing Effects in Phonon Scattering, in "Nonequilibrium Phonons in Nonmetallic Crystals", Modern Problems in Condensed Matter Sciences, Vol. 16, eds W.Eisenmenger and A.A. Kaplyanskii (North-Holland, Amsterdam) p145, 1986.

[3]. A.P. Heraud, A.A. Ghazi and L.J. Challis 1982, unpublished ; see ref [2].

[4]. L.J. Challis and D.L. Williams : J.Phys. C 11, 3787, 1978.

[5]. M.N. Wybourne, L.J. Challis and A.A. Ghazi : J.Phys. C 13, 6495, 1980.

[6]. L.J. Challis, A.A. Ghazi, D.J. Jefferies, D.L. Williams and M.N. Wybourne : Phys.Rev.Letts 40, 519, 1978.

[7]. A.P. Heraud, L.J. Challis and A.A. Ghazi in Proc. 2nd Int. Conf. on Phonon Physics, Budapest, 1985 eds J. Kollar, N. Kroo, N. Menyhard and T. Silkos (World Scientific, Singapore) p723, 1985.

[8]. B.R. Anderson and L.J. Challis : J.Phys. C6, L226, 1973.

[9]. A.A. Ghazi and L.J. Challis : J.Phys.C18, 6719, 1985.

[10]. L.J. Challis, S.V.J. Kenmuir, A.P. Heraud and P.A. Russell, Proc 5th Int. Conf. on Phonon Scattering in Condensed Matter, Urbana, Illinois 1986, eds A.C. Anderson and J.P. Wolfe (Springer, Berlin) p180, 1986, and S.V.J. Kenmuir, L.J. Challis, A.P. Heraud and P.A. Russell, J. Phys. C20, 1987 in the press.

THEORY OF FORMATION, DYNAMICS AND EXPLOSION OF A PHONON HOT SPOT

D.V.Kazakovtsev* and Y.B.Levinson**

*Institute of Solid State Physics, USSR Academy of Sciences;
**Institute of Problems of Microelectronics Technology and Superpure Materials, USSR Academy of Sciences;
142432, Chernogolovka, Moscow region, USSR

1. Introduction.

This lecture presents some theoretical models of high energy phonon propagation at low, say, helium bath temperatures in semiconductor or dielectric pure crystals. Phonon relaxation in these crystals is determined by two scattering mechanisms: impurity or isotope scattering, and anharmonic phonon-phonon interactions.

For a long time heat pulse experiments dealt with "weak" excitation, i.e., the frequencies of generated nonequilibrium phonons were the same as those of thermal bath phonons, $\omega \sim \omega_{T_B}$, and the energy density of nonequilibrium phonons, $\mathcal{E}$, was small, compared to the bath energy density, $\mathcal{E}_{T_B}$. The experiments [1-3] on electron-hole drop propagation in crystals due to phonon wind and [4] were likely to be among the first ones with "strong" excitation of phonon system, i.e., with $\omega \gg \omega_{T_B}$ and $\mathcal{E} \gg \mathcal{E}_{T_B}$. A most pronounced feature of these experiments was formation of some highly excited region near the irradiated surface of the crystal, called "hot spot" by Hensel and Dynes [1]. At the same time the rest of the crystal seemed to remain almost at the bath temperature.

Speaking of a hot spot one usually has in mind some nonequilibrium temperature T of excited region of the crystal, with $T > T_B$. This temperature, however, can be established only as a result of phonon-phonon collisions. The process of temperature T formation needs some time τ_T, that is the scale time of the anharmonic processes at $\omega = \omega_T$. During this time the phonons with ω_T propagate in a diffusive or ballistic manner, and are displaced for the distance ℓ_T in space. That is, only in the case, when the size of heated region L satisfies the condition

$$L \gg \ell_T \qquad (1)$$

the nonequilibrium temperature is a well defined quantity. We shall use the term "hot spot" only for such situation. As we shall see below, this is not always the case at liquid helium temperatures. Thus, one of the questions we are going to analyse is that of temperature existence in the excited region, i.e., hot spot existence, and its possible destruction due to temperature space gradients, violating the condition (1).

But space inhomogeneity is not the only reason for temperature not to be a well-defined notion. One can generate phonons with $\omega \gg \omega_{T_B}$, as in the case of optical excitation, when predominantly phonons with $\omega \sim \omega_{\mathfrak{D}}$, the Debye frequency, are produced via thermalization of hot electrons exited high into the band. Then even for a spatially homogeneous source at least the initial phonon distribution can drastically differ from a Planckian one with any possible temperature T. We are going to follow this distribution time evolution to see when and how it changes into a Planckian one, if at all. This question acquires new aspects in a spatially inhomogeneous case.

2. Phonon source.

We shall deal, as we have already mentioned, with nonequilibrium phonons generated by light excited electron system of the crystal, as, e.g., in experiments [2,3,5]. The interband light produces hot electrons high in the band in a thin $\sim$1-10μm layer near the surface of the crystal. In the process of cooling these electrons emit optical or intervalley phonons and diffuse for a distance of the order of 1μm. Due to the Klemens (sometimes it is called Orbach) mechanism optical phonons decay very fast into $\omega^* \sim \omega_{\mathfrak{D}}/2$ acoustic ones. So, a layer of thickness $d \sim 1-10\mu m$ serves as a source of high energy acoustic phonons. Strictly speaking, this source power depends on the distance z from the surface, and has no abrupt edge at z=d. But for our purpose we can use a model of phonon source, producing phonons uniformly in a surface layer $0 < z < d$ of the crystal. The lateral dimensions of the source are those of light focusing, usually its area A is $(30\mu m)^2$-$(1mm)^2$. As for the time duration θ, its lower limit is the sum of the thermalization time of hot carriers and the lifetime of optical phonons, that is, $\sim$10-50ps, and the upper limit, determined by the light pulse duration, can be $\sim$100ns or even more. The typical energy imparted per pulse is $E \lesssim 10\mu J$.

The acoustic phonons ω^* of the source can propagate in the crystal, this propagation being governed mainly by two scattering mechanisms, mentioned above. Now we put aside all the fast processes, resulting in ω^* phonon emission, and focus ourselves on proceeding evolution of the acoustic phonon frequency and space distribution. We consider this evolution in a semiinfinite crystal, filling the halfspace $z > 0$.

3. Acoustic phonon scattering mechanisms.

In order to understand, what mode of acoustic phonon propagation is realized in the crystal, we have to estimate the phonon relaxation times due to the two above-mentioned scattering mechanisms. For the first one, the elastic phonon scattering leading to momentum relaxation only, it is $\tau'(\omega)$. In the case of pure crystals it is determined by isotope scattering, $\tau'(\omega)$ follows the well-known Rayleigh law, written conveniently in the form

$$1/\tau'(\omega) = \eta\omega_{\mathcal{D}}(\omega/\omega_{\mathcal{D}})^4 \tag{2}$$

The values of numerical parameter η vary from $4.2\cdot10^{-4}$ for SrF_2 to $27\cdot10^{-4}$ for Ge, those for Si, GaAs and CaF_2 lie inside this range, according to [6,7]. This gives for $\tau'(\omega^*) \sim 0.1-0.8$ ns.

The second scattering mechanism we take into account is that of three-phonon anharmonic processes, i.e., the splitting of a phonon into two ones, the total energy and momentum being conserved, and the inverse process of two phonon coalescence into one, obeing the same conservation laws. For instance, splitting can be schematically depicted as

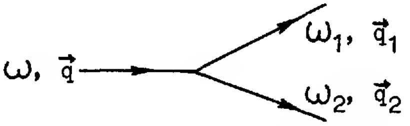

$$\omega = \omega_1 + \omega_2$$
$$\vec{q} = \vec{q}_1 + \vec{q}_2$$

For the Debye model spectrum the corresponding relaxation time can be presented in the form

$$1/\tau(\omega) = \gamma\omega_{\mathcal{D}}(\omega/\omega_{\mathcal{D}})^5 \tag{3}$$

The relevant values of numerical parameter γ are of the same order of magnitude for all the above-mentioned crystals and lie in the range $3.6\cdot10^{-5}$ (Ge) - $7.1\cdot10^{-5}$ (CaF_2), according to [6,8].

The relative importance of splitting and coalescence depends on phonon occupation numbers in the frequency domain, where the main part of the whole energy is contained. If these are $n \ll 1$, then splitting, proportional to n dominates over coalescence proportional to n^2, the whole distribution being shifted to lower frequencies. This regime was analysed in [9]. If it is accompanied by phonon cloud spreading in space, it is called quasidiffusion. When the dominant phonon occupation numbers are $n \sim 1$, then splitting and coalescence are equally important, and they compensate one another. This means now $\tau_T \equiv \tau(\omega_T)$ is the time characteristic not of decays only, but of coalescence of thermal phonons, too. On the other hand, such compensation of splitting and coalescence is a typical feature of local equilibrium, i.e., a local temperature existence. One can see it from somewhat different viewpoint. The phonons of a Planck distribution with temperature T have typical energy $\hbar\omega_T = \alpha T$, where $\alpha = 2.82$ if we identify ω_T with the maximum of spectral energy density. Then we obtain directly from the Planck formula $n_T \equiv n(\omega_T) \sim 1$. So the condition $n \sim 1$ for dominant phonon frequencies means, on the one hand, a local temperature formation, and on the other hand - the end of quasidiffusion or any other regime with dominant phonon frequency decrease.

4. Hot spot formation.

Using (2) and (3) with η and γ from Section 3, we obtain that $\tau'(\omega^*) \ll \tau(\omega^*)$ or at least $\tau'(\omega^*) < \tau(\omega^*)$. With ω decreasing the inequality becomes more and more strict, because $\tau(\omega)$ grows faster then $\tau'(\omega)$ while ω decreases. This means elastic phonon scattering dominates for initial acoustic phonons ω^*, and all the more does for phonons with lower frequencies. So all of them propagate in a diffusive manner with frequency-dependent diffusion coefficient $\mathcal{D}(\omega) = s^2\tau'(\omega)/3$. As phonons with frequency ω have a finite lifetime $\tau(\omega)$ due to anharmonic processes, their diffusion length by this time is $\ell(\omega) = [\mathcal{D}(\omega)\tau(\omega)]^{1/2} = \sqrt{s^2\tau(\omega)\tau'(\omega)/3}$. For ω^* phonons in the crystals considered it gives $\ell(\omega^*) \sim 3\text{-}7\,\mu\text{m}$. As it is approximately the same, as the source layer depth, we can say, that the initial acoustic phonons do not leave the source layer during their lifetime.

Let the light pulse be very short, so that after the fast relaxation processes described in Section 2 all the imparted energy P per surface unit of the crystal is contained in ω^* phonons. It means their number per 1 cm^3 of the excited layer is $P/d\hbar\omega^*$. To find $n(\omega^*)$, we divide this number by the phase volume occupied by phonons, $b\rho(\omega^*)\omega^*$. Such an expression comes from the energy density of phonons with $n \sim 1$, average frequency ω and distributed over frequency interval $\Delta\omega\sim\omega$:

$$\varepsilon(\omega) = b\hbar\omega\rho(\omega)\omega, \quad b = \pi^4/15\alpha^4 = 0.10 , \tag{4}$$

where $\rho(\omega)$ is the state density, and the numerical factor b is chosen the expression (4) to give for $\omega=\omega_T\ll\omega_{\mathfrak{D}}$ the energy density of the three-mode Planck distribution for the Debye linear spectrum. So we obtain $n(\omega^*)\sim P/\ d\hbar\omega^* b\rho(\omega^*)\omega^* = P/d\varepsilon(\omega^*)$. Taking $d = 5\mu m$ we obtain, e.g., for Ge at a very high pump level $P= 200\ \mu J/mm^2$ occupation numbers $n(\omega^*)\sim 0.1$. Nevertheless, at the lowest pump level, $P= 2\cdot 10^{-4}\mu J/mm^2$ we still have $n(\omega^*)\sim 10^{-7}$, while at $T_B=4.2K$ the equilibrium values are $n_{T_B}(\omega^*)\sim 10^{-21}\ll n(\omega^*)$. It means, that in a wide range of energies imparted the excitation is strong in the sence determined in Introduction, and at the same time the initial occupation numbers of phonons are $n(\omega^*)\ll 1$, and these initial phonons propagate in a quasidiffusive manner, if at all. Because the excitation is strong we can neglect the bath phonons n_{T_B} and assume initial bath temperature $T_B= 0$, considering the nonequilibrium phonon evolution itself. The situation is essentially the same for all crystals mentioned in Section 3.

In the process of quasidiffusion phonon frequency distribution shifts to lower frequencies, so the phase space, occupied by phonons, diminishes, and their occupation numbers increase. At the same time phonon cloud can spread in real space, this resulting in decrease of phonon occupation numbers. A simple pattern of phonon generations [9] goes as follows. Initial phonons ω^* split into approximately half frequency $\omega^*/2$, these again split into $\omega^*/4$, and so on. Every generation spreads in space over additional $\ell(\omega)$ length. As $\ell(\omega)\propto\omega^{-9/2}$, the total spreading is always determined by that of the last generation involved. So a generation with frequency ω occupies a layer of $\ell(\omega)$ thickness.

It is natural to determine a boundary frequency ω_d such that $\ell(\omega_d) = d$. As phonon generations with $\omega>>\omega_d$ can spread only over a distance $\ell(\omega)\ll d$, they occupy just the initially excited layer of thickness d. Those with $\omega\ll\omega_d$ easily escape from this layer and occupy the depth $\ell(\omega)\gg d$. Until $(\omega)\ll A^{1/2}$ the phonon propagation is one-dimensional, going only in z direction. While the distribution dominant frequency is $\omega\gg\omega_d$, we can neglect the spatial propagation and write

$$n(\omega) = P\ /\ d\varepsilon(\omega). \tag{5}$$

If the energy P satisfies the oondition

$$P > P_o \ , \quad P_o = d\mathcal{E}(\omega_d), \tag{6}$$

then before the decreasing phonon frequency reaches the boundary "escape frequency" ω_d, occupation numbers reach unity. The regime with dominant splitting terminates, and a nonequilibrium temperature T of the hot spot is established. It can be obtained from

$$P = d\mathcal{E}(\omega_{\bar{T}}). \tag{7}$$

The time needed for this process can be obtained from the analysis similar to that of phonon spreading in space. The time for ω generation to dominate is $\tau(\omega^*) + \tau(\omega^*/2) + \dots + \tau(2\omega) \sim \tau(2\omega)$ is also determined by the last term of the sum. This gives for the frequency ω_t dominant at the t time moment

$$\tau(\omega_t) = t, \quad \omega_t \propto t^{-1/5} \tag{8}$$

So the temperature T needs the time $\tau(\omega_{\bar{T}})$ to be established, and if (6) is valid, this happens before phonon distribution reaches ω_d, i.e., before phonons begin to escape from the initial excited layer d at the time

$$\theta_o = \tau(\omega_d). \tag{9}$$

Using (8), (9), and P_o definition from (6), one can rewrite (5) in the form

$$n(t) \sim (P/P_o)(t/\theta_o)^{4/5}, \tag{10}$$

directly demonstrating the occupation number increase with time before these numbers reach unity at time $\tau(\omega_{\bar{T}})$. Introducing T_d by the condition $T_d = \hbar\omega_d$, we can obtain from (7) the temperature of the hot spot formation

$$\bar{T} = T_d(P/P_o)^{1/4}. \tag{11}$$

If, on the contrary to (6), $P < P_o$, then even at the time $t = \theta_o$ the inequality $n \ll 1$ holds, splitting goes on, now accompanied by phonon spreading in space. This is quasidiffusion, analysed in [9], and here

$$n(\omega) = P/\ell(\omega)\mathcal{E}(\omega) = (P/P_o)(\theta_o/t)^{1/10}. \tag{12}$$

We see that now the occupation numbers decrease with time t, and as at $t = \theta_o$ they were $n(\omega_d) \ll 1$, they will never reach unity, while quasidiffusion goes on, and no phonon temperature in the excited region can be established.

Analysing in a similar way different possible cases of the pulse duration θ and the total energy input P per 1 cm^2 of the crystal surface, one can obtain instead of (10) and (12) two more time dependences for phonon occupation numbers. The results of such analysis are concisely presented in θ, P plane, see Fig.1. The equations of the boundaries between the different regions of this plane are

$$\begin{array}{ll} 1/2 & P/P_o = 1 \\ 2/3 & P/P_o = (\theta/\theta_o)^{-4/5} \\ 3/4 & P/P_o = \theta/\theta_o \\ 4/1 & P/P_o = (\theta/\theta_o)^{1/10} \end{array} \tag{13}$$

According to [10], P_o equals 45 μJ/mm^2 for Ge, and respectively 77 and 130 μJ/mm^2 for GaAs and Si. The θ_o values for these crystals are correspondingly 31, 12 and 10 ns.

In the hatched region 1 (weak pumping, arbitrary pulse length) a hot spot does not form. The above analysed case $P<P_o$ with the expression(12) for $n(\omega)$ falls into this domain of θ, P plane. In the region 2 (intermediate values of P, brief pumping) $n(\omega)$ reach unity, and a temperature is formed after the end of pumping but before the phonons have escaped from layer d. Here the occupation numbers are (10), and the temperature established at the end of the regime with dominant splitting is (11). Regions 3 and 4 have been analysed elsewhere [10]. In region 3 (high pump, intermediate pulse duration) the temperature

$$T = T_d(W/W_o)^{1/9}, \tag{14}$$

with $W = P/\theta$, $W_o = P_o/\theta_o$ is established in layer d for the time

$$\bar{t} = \theta_o(W/W_o)^{-5/9} \tag{15}$$

before the end of the pump

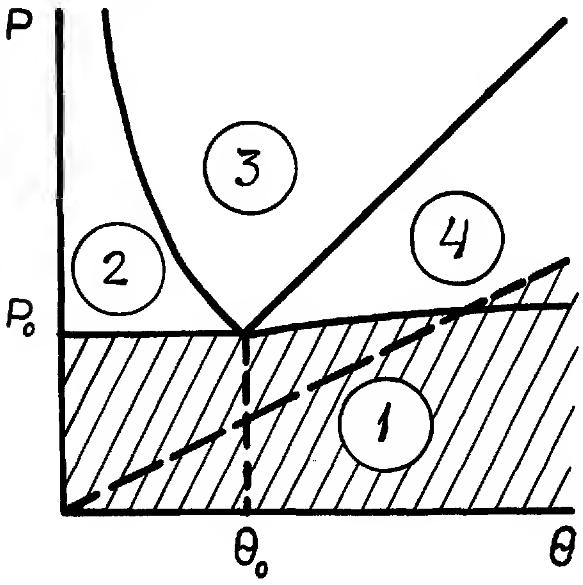

Fig. 1. Conditions for the formation of a hot spot. Heavy solid lines are boundaries (13) between different regime domains. One of the dashed ones is the plane geometry limit $P/P_o = (d/A^{1/2})(\theta/\theta_o)$.

pulse and before a significant part of energy have left layer d. In region 4 (intermediate values of P, prolonged pumping) the temperature is formed in the layer of thickness $\bar{z} = d(W/W_o)^{-1} \gg d$ before the end of the pumping.

When $\ell(\omega)$ becomes larger than lateral dimensions of light focusing $A^{1/2}$, the above considered plane geometry regime changes into 3-dimensional spherical one. Now the space volume of the phonon cloud grows as $\ell^3(\omega)$. That's why even if the heating pulse is on, $n(\omega)$ decreases in time as $t^{-9/10}$, and even as $t^{-19/10}$ after the end of the pulse [10]. As in 3-dimensional case n can only decrease with time, no hot spot with a local temperature can form itself in this regime.

5. Nonlocal heat transfer (NLHT).

Up to now we dealt with quasidiffusion which could under certain conditions result in a hot spot formation. Now we assume it is formed, and so there is some nonequilibrium temperature in the excited part of the crystal, $T(z,t)$, or, more generally, $T(\vec{r},t)$. Let the dominant mechanisms of phonon scattering be those described in Section 3. As we saw there, in the case of temperature existence the phonon coalescence processes are of the same magnitude as decays, τ_T being the characteristic for all anharmonic prooesses with dominant, i.e., now thermal phonons.

Following Levinson [11], one can show that in the case of dominant Rayleigh scattering the heat transfer is nonlocal. Some experimental hints for such regime can be found in this volume in the lecture by W.E.Bron. These are relatively high occupation numbers of low energy phonons in the bulk of the crystal with respect to those corresponding to the high energy phonon temperature. Here we give an idea of nonlocal heat transfer, because under conditions considered the evolution of the hot spot, once it has been formed, goes in this regime.

It must be mentioned that the problem itself is a classical one, being mentioned by Peierls in 1929 [12]. It arises from the following mathematical fact. If one writes energy balance equation in the form

$$\frac{\partial \varepsilon}{\partial t} + \operatorname{div} \vec{W} = 0, \qquad (16)$$

with

$$\varepsilon(T) = \int_0^\infty d\omega \rho(\omega) \omega n_T(\omega) = \frac{\pi^2}{15} \rho(\omega_T) T^2 \propto T^4,$$

and then tries to obtain energy flux $\vec{W}$ in a straight manner

$$\vec{W} = \nabla T \int_0^\infty d\omega \rho(\omega)\omega \mathcal{D}(\omega) \left[\partial n_T(\omega)/\partial T\right], \qquad (17)$$

the integral appears to diverge at the lower limit. It means, on the one hand, that although almost all phonon energy is contained in the spectral region of $\omega \sim \omega_T$, the energy flux is transfered not by these thermal phonons, but by subthermal phonons with $\omega \ll \omega_T$ due to their relatively large diffusion coefficient. On the other hand, it means that real phonon distribution at $\omega \ll \omega_T$ is not a Planckian one.

In [11] Levinson has stated and solved the problem of calculating the real phonon distribution at $\omega \ll \omega_T$ using the following phonon propagation equation

$$\left[\partial/\partial t - \mathcal{D}(\omega)\nabla^2 + 1/\hat{\tau}(T,\omega)\right] n(\omega, \vec{r}, t) = w(T). \qquad (18)$$

Assuming phonons with $\omega \gtrsim \omega_T$ have a temperature distribution we can obtain for subthermal ones equation (18) with

$$w(T) = 1/\tau(\omega_T) \propto T^5,$$

$$\hat{\tau}(T,\omega) = \tau(\omega_T)(T/\omega) \gg \tau(\omega_T).$$

The terms $w(T)$ and $n(\omega,\vec{r},t)/\hat{\tau}(T,\omega)$ in (18) result from subthermal phonon scattering by thermal phonon bath, that is

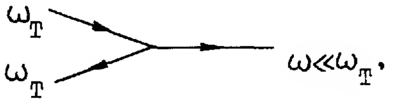

and vice versa.

Now if (18) is solved, and $n(\omega,\vec{r},t)$ thus obtained for $\omega \ll \omega_T$ are substituted into the energy balance equation (16), where instead of (17) the energy flux is

$$\vec{W} = \int_0^\infty d\omega \rho(\omega)\omega \left[-\mathcal{D}(\omega)\nabla n(\omega, \vec{r}, t)\right. ,$$

the NLHT equation for temperature can be obtained and solved. The process appears to be quasistationary, i.e., the flux $\vec{W}$ is established rapidly in comparison with the overall process duration, so one can neglect the term $\partial/\partial t$ in (18), as we do below.

6. Hot spot dynamics and explosion.

Here we will use the NLHT equations to follow the hot spot temporal evolution, first in the one-dimensional case, when the depth of the spot L is small as compared to its lateral dimension $A^{1/2}$. Then, following Esipov&Levinson [13], we find a self-similar solution describing the hot spot one-dimensional expansion in z coordinate. It is a solution of the equation (18) without $\partial/\partial t$ in the right hand. One can present it in the form

$$n(\omega, z, t) = (t')^{-\lambda} g(\zeta, \eta),$$
$$T(z, t) = T^{+}(t')^{-\mu} f(\zeta), \qquad (19)$$

with dimensionless self-similar cordinates

$$\eta = \omega'(t')^{\alpha}, \qquad \zeta = z'(t')^{-\beta},$$
$$\omega' = \hbar\omega/T^{+}, \qquad z' = z/\ell(\omega_{T+}), \qquad t' = t/\tau(\omega_{T+}).$$

Here T^{+} is a characteristic temperature depending on the total hot spot energy. It has a physical sence of the lowest possible temperature for the notion of temperature in the hot spot to be well defined. Equations for unknown functions $g(\zeta, \eta)$ and $f(\zeta)$, not given here (see [10]), contain no physical parameters. So the relevant values of ζ, η, and f,g are of the order of unity. Then the front of the hot spot moves according to

$$L \sim \ell_{T+}(t/\tau(\omega_{T+}))^{\beta}, \qquad (20)$$

and its typical temperature changes as

$$T \sim T^{+}(t/\tau(\omega_{T+}))^{-\mu}. \qquad (21)$$

The state of the hot spot can be represented by an image point in T,L plane, see Fig.2 with a numerical example. Corresponding to (20) and (21), this point moves along the curve

$$L/\ell_{T+} = (T/T^{+})^{-\beta/\mu}. \qquad (22)$$

From the energy conservation law one can obtain two sets of parameters $\alpha, \beta, \lambda, \mu$. The first one corresponds to constant heating of the crystal surface by light of power W per 1 cm^2. This is W-trajectory

$$\alpha = 2/7, \quad \beta = 3/7, \quad \lambda = -3/7, \quad \mu = -1/7. \qquad (23)$$

After light excitation terminates, the hot spot moves along another, so called P-trajectory with

$$\alpha = 4/21, \quad \beta = 20/21, \quad \lambda = 1/21, \quad \mu = 5/21. \qquad (24)$$

Sooner or later the hot spot thickness L exceeds the lateral dimensions $A^{1/2}$ of light focusing. Then the propagation geometry changes into spherical symmetry 3-dimensional case. This alter, of course, the set of parameters; now for P-trajectory

$$\alpha = 4, \quad \beta = -20, \quad \lambda = -19, \quad \mu = -15,$$

and solution (19) becomes physically meaningless, for it corresponds to a time decrease of the hot spot radius with increase of temperature. So (19) must be changed by replacing t' by $(t_o - t)/\tau_{T+}$, where t_o is a time parameter of the order of time the plane geometry propagation regime needs to change into spherical one. It means that $L(t_o) = A^{1/2}$, and t_o can be found as a function of A and the total energy input E. Now instead of (20) and (21) we have for the hot spot radius

$$r \sim \ell_{T+} \left((t_o - t)/\tau_{T+}\right)^{-20} , \qquad (25)$$

and for typical temperature

$$T \sim T^{+} \left((t_o - t)/\tau_{T+}\right)^{15} . \qquad (26)$$

Solution (25)-(26) shows explosive behaviour at finite time $t = t_o$. It means that at $t \rightarrow t_o$ the hot spot in a spherical regime of expansion is abruptly destructed. In Section 4 we saw the hot spot cannot form itself in a 3-dimensional case. Now we see that even if it has been formed before, in a 3-dimensional case it destructs rapidly. These two facts seems to be in agreement one with another.

7. Numerical example.

Consider the formation and dynamics of a hot spot in Ge pumped with the light pulse of energy $E = 1\,\mu J$, duration $\theta = 75$ ns, focused in the area $A = (0.1\,mm)^2$. These values approximately correspond to those from experiment [5]. The depth of ω^* phonon source, described in Section 2, is $d = 5\,\mu m$. Since $P = 150\,\mu J/mm^2$ and $W = 2\ kW/mm^2$, the pulse with such parameters falls into region 3 in Fig. 1. Then, according to (14) and (15), the hot spot with initial temperature $T_o = 62$ K is formed in the layer d at $t = 25$ ns. So the point $T=T_o$, $L = d$ is a starting one for the trajectory of image point, representing the hot spot evolution in T, L plane (see Fig.2). After being created, the hot spot moves without considerable expansion along $L = d$ trajectory, with T(t) given by the condition $d\mathcal{E}_T/dt = W/d$. At $t_1 = 46$ ns with $T_1 = 73$ K the energy flux from the layer d becomes of the order of W, the spot moves to W-trajectory (22) with the set of parameters (23) and follows it until the pumping pulse ends at $t_2 = \theta = 75$ ns with corresponding depth $L_2 = 14\,\mu m$ and $T_2 = 103$ K, according to (20) and (21). At point 2 the spot changes W-trajectory for the P-one, (22) with parameters (24) and follows this one up to $t_3 = 1.4\,\mu s$ with $T_3 = 38$ K. Here its depth

L = L_3 attains its lateral size $A^{1/2}$, the expansion becomes 3-dimensional, and the spot moves along P-trajectory (25-26), reaches by the time $\sim t_3$ point 4, where it is destroyed at $T_4 = T^+ = 28$ K and radius $r_4 \sim \ell_{T^+} = 140\,\mu$m.

One should not take too literally the obtained values characterizing different points of the hot spot trajectory. First, all the equations used here are estimates with numerical factors of the order of unity remaining unknown. Next point is that simplified power laws (2-4) are valid at $\omega \sim \omega_{\mathfrak{D}}$ only as order of magnitude estimates. Finally, scattering mechanisms other than isotope scattering may become of importance, as is really the case in Ge at $T \gtrsim 70$ K.

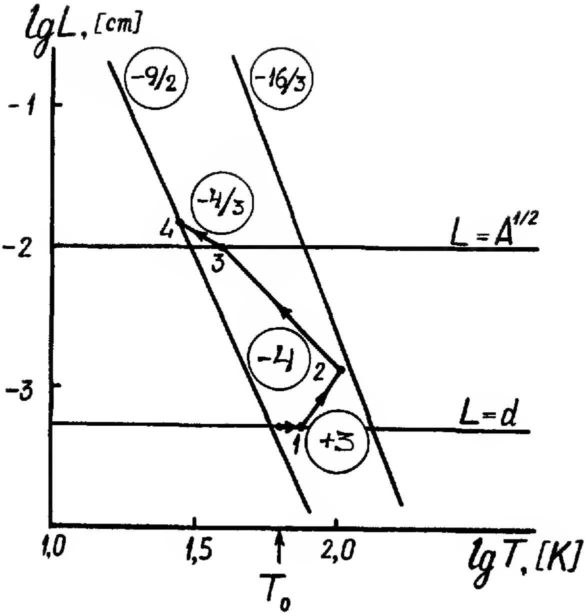

Fig. 2. Dynamics of a hot spot in Ge. The temperature does not exist to the left of the line $L = \ell_T$ with slope -9/2. The line with slope -16/3 restricts the right part of the plane with more complicated NLHT regime [14]. The lines with slopes +3, -4, and -4/3 are trajectories (23), (24) and (25-26), respectively.

References.

1. J.C.Hensel and R.C.Dynes, Phys.Rev.Lett. 39, 969 (1977).
2. N.V.Zamkovets, N.N.Sybeldin, V.B.Stopachinsky, and V.A.Tsvetkov, Zh.Eksp.Teor.Fiz. 74, 1147 (1978).
3. V.S.Bagaev, G.Bel'skaya-Levandovskaya, M.M.Bonch-Osmolovskii, T.I.Galkina, S.Yu.Levandovskii, G.N.Mikhaĭlova, A.G.Poyarkov, and G.Young, Zh.Eksp.Teor.Fiz. 77, 2117 (1979)[Sov.Phys. JETP 50, 1013 (1979)].

4. V.L.Broude et al , Zh.Eksp.Teor.Fiz. 74, 314 (1978)[Sov.Phys. JETP 47, 161 (1978)].
5. M.Greenstein, M.A.Tamor, and J.P.Wolfe, Phys.Rev. B26, 5604 (1982).
6. D.V.Kazakovtsev and Y.B.Levinson, Phys.Stat.Solidi (b), 136, 425 (1986).
7. S.Tamura, Phys.Rev. B30, 849 (1984).
8. S.Tamura, Phys.Rev. B31, 2574 (1985).
9. D.V.Kazakovtsev and Y.B.Levinson, Pis'ma Zh.Eksp.Teor.Fiz. 27, 194 (1978)[Sov.Phys. JETP Letters 27, 181 (1978)]; Phys. Stat. Solidi (b), 96, 117 (1979).
10. D.V.Kazakovtsev and Y.B.Levinson, Zh.Eksp.Teor.Fiz. 88, 2228 (1985)[Sov.Phys. JETP 61, 1318 (1985)].
11. Y.B.Levinson, Zh.Eksp.Teor.Fiz. 79, 1394 (1980)[Sov.Phys. JETP 52, 704 (1980)].
12. R.Peierls, Ann.Phys. (Germany) 3, 1055 (1929).
13. S.E.Esipov and Y.B.Levinson, Pis'ma Zh.Eksp.Teor.Fiz. 34 , 218 (1981)[Sov.Phys. JETP Letters 34, 210 (1981)].
14. N.M.Guseĭnov and Y.B.Levinson, Zh.Eksp.Teor.Fiz. 82, 1936 (1982)[Sov.Phys. JETP 55, 1114 (1982)].

SUPERCONDUCTING TUNNEL JUNCTIONS, VERY HIGH FREQUENCY PHONONS, AND THE KAPITZA RESISTANCE

H. Kinder
Fakultät für Physik
Technische Universität München
D-8046 Garching

Introduction

Spectroscopy of solids is usually done by sending a beam of particles, e.g. photons, neutrons, or electrons, into the sample and analyzing the scattered particles for energy and momentum. Similar experiments can also be made with phonons in the sample itself, because they propagate ballisticly at low temperatures.

Several techniques for the generation and detection of phonons are available. Ultrasound with frequencies up to ≈30 GHz can be generated and detected by the piezoelectric effect. Higher frequencies are most simply obtained by pulse heating of a metal film evaporated onto the sample surface. The heat pulses propagate with sound velocity across the sample and are detected by a superconducting bolometer at the far crystal surface. While their power and frequency can be quite high, the heat pulses have a broad thermal distributon. Spectroscopy with narrow band tunable phonons is achieved with superconducting tunnel junctions.[1] Among other existing techniques for monochromatic phonons,[2] superconducting junctions have proven to be extremely versatile, and they have been applied to a great number of different problems.[3]

There are two different ways to generate monochromatic tunable phonons by superconducting tunnel junctions, namely the "bremsstrahlung" and the "Josephson" technique. The latter is experimentally more difficult, but allows for extremely high frequency resolution. Both techniques will be presented, together with some selected applications in Part I of this lecture. As a major application then, I shall concentrate in Part II on surface scattering of phonons which is related to the Kapitza resistance, i.e. the heat transport through surfaces into liquid helium.

Part I. Monochromatic Phonons

Generation of Phonon Bremsstrahlung

A superconducting junction is fabricated by evaporating a metal film, say Sn, oxidizing, and depositing a second metal film on top. At low temperature, the I-V-characteristic develops a sharp gap, see Fig. 1.

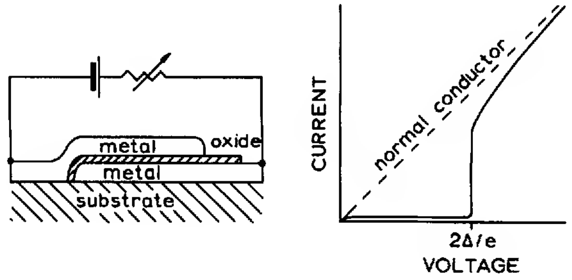

Fig. 1. Superconducting tunnel junction and I-V-Characteristic.

At voltages below $2\Delta/e$, almost no current can flow, because most of the electrons are in the Cooper pair condensate. Only if the battery supplies the minimum energy 2Δ required to "break" pairs, single electrons can tunnel while their partners are left behind. This leads to the steep current rise.

At voltages above 2Δ, the electrons attain additional kinetic energy, eV-2Δ, which is randomly distributed among both partners so that a continuous distribution of electrons (quasiparticles) is excited in both films. These fast quasiparticles slow down, i.e. relax, by phonon emission ("bremsstrahlung") to the gap edge.

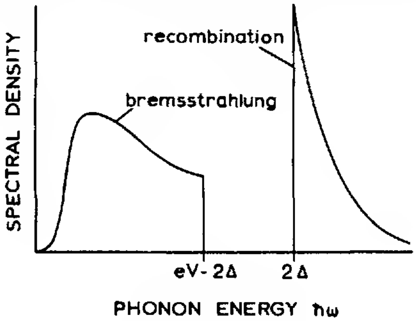

Fig. 2. Phonon spectrum (schematic) emitted by the junction.

The resulting spectrum (Fig. 2) has a sharp upper edge at the maximum kinetic energy, eV-2Δ. Also shown in Fig. 2 is the spectrum due to the eventual recombination of the quasiparticles, into the pair condensate.[4]

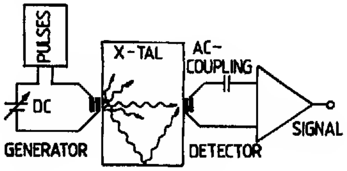

Fig. 3. Circuit diagram of the modulation technique.

Because the "bremsstrahlung" edge is tunable, a modulation technique can be used to isolate a narrow band of quasi monochromatic phonons. Fig. 3 shows the circuit diagram. The generator junction has a dc bias V to determine the position of the edge which is then modulated by small superposed pulses, δV. Thus, the junction emits a dc shower of phonons whose spectrum is given by V, and small superposed phonon pulses whose spectrum is the difference between those for V and for V+δV. This differential spectrum is hatched in Fig. 4. It has a tunable monochromatic part due to the bremsstrahlung edge and a fixed background of recombination phonons whose number is modulated by δI.

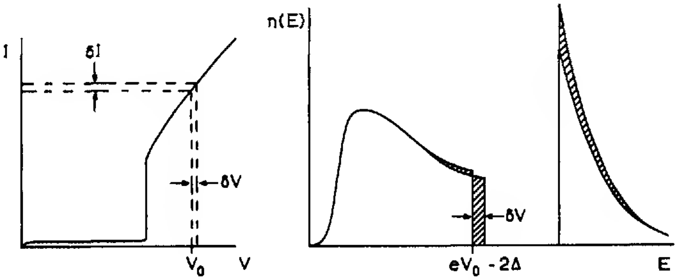

Fig. 4. The modulated spectrum is quasi monochromatic and tunable.

The phonons propagate ballisticly to the far crystal face where they are detected by a second tunnel junction (see below). Then, the pulse and dc signals are simply separated by ac coupling (Fig. 3). A typical pulse signal is shown in Fig 5. Longitudinal (L) and transverse (T) phonon pulses are easily distinguished by their times of flight.

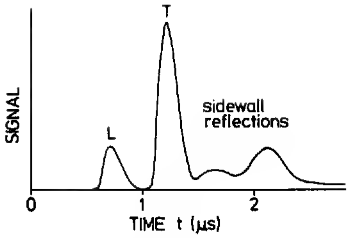

Fig. 5. Phonon pulse pattern reveals polarizations and transits.

The frequency resolution corresponds to the sharpness of the energy gap of the superconductors used, typically 1 to 5 %. The frequency range is limited by reabsorption of phonons at energies above 2Δ. This limit is 300 GHz for Sn and 870 GHz for PbBi. Only in Al, the reabsorption is weak enough so that frequencies as high as 2.8 THz have been observed.[5] A lower frequency limit is imposed by the detector, if a tunnel junction is used.

Tunnel junction detector

If a junction is biased to voltages below 2Δ, no quasiparticles will be excited from the pair condensate, but existing quasiparticles can tunnel with no energy threshold. So, the current is a measure of quasiparticle density in the junction. Incident phonons with energy $\hbar\omega > 2\Delta_D$ are absorbed by pair breaking and so increase the quasiparticle density. This leads to an enhancement of the current or, for finite load resistor, to a decrease in voltage, as indicated in Fig 6.[4]

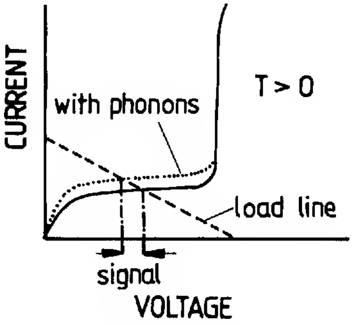

Fig. 6. The junction at small bias voltage as a phonon detector.

The sensitivity of junctions is roughly 10 times higher than that of bolometers. Since phonons with $\hbar\omega \lesssim 2\Delta_D$ are not absorbed at sufficiently low temperature, the junction detector (with both gaps equal) has a threshold of $2\Delta_D$. Therefore, a superconductor with small gap (Al) is most oftenly used. The frequency range for spectroscopy then extends from $2\Delta_D$ to $2\Delta_G$, i.e. from the detector to the generator gap.

Spectroscopy of impurities

Only a few applications will be presented in this lecture. A more elaborate version is given in Ref. 2. The very first application was the study of V^{3+} ions in Al_2O_3 (sapphire).[1] The two electrons of V^{3+} form an $S = 1$ state with quenched orbital momentum. This state is split by spin-orbit coupling into a lower singlet and an upper Kramers doublet, ≃1 meV apart. The doublet has a small hyperfine splitting which is presently neglected. Phonons can couple to the system via the Van Vleck mechanism and cause transitions, if their energy is at resonance. Thus, ballistic phonons travelling from the generator to the detector junction will be resonantly scattered. The resulting absorption lines for various phonon directions and polarizations are shown in Fig. 7.

The step at 150 GHz demonstrates the frequency threshold, $2\Delta_D/h$, of the detector junction. Below this frequency, only recombination phonons with the fixed frequency $2\Delta_G/h$ are detected. By extrapolation, this background can be subtracted everywhere.

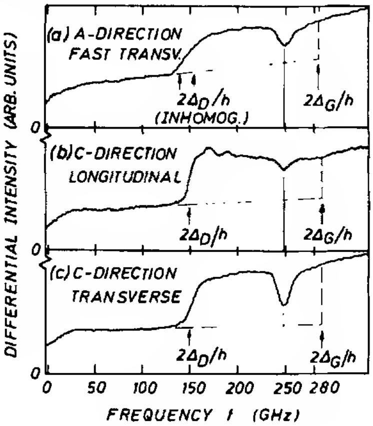

Fig. 7. Resonance scattering at 248 Ghz by V^{3+} ions in sapphire

A second example is OH$^-$ in NaCl. The OH$^-$dipole has 6 equivalent orientations along the cubic axes, and the potential barrier for reorientation is small. Tunneling between the 6 directions then leads to new, delocalized eigenstates whose energy levels are shown in the inset of Fig. 8 for cubic symmetry, and for tetragonal distortion by uniaxial stress.

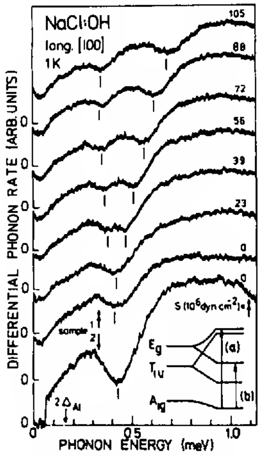

Fig. 8. Spectroscopy of OH$^-$ in NaCl with uniaxial stress.

The result of phonon spectroscopy is shown in Fig. 8.[6] Although the concentration of OH$^-$ was less than 0.1 ppm, a strong line is seen due to the allowed A_{1g}–E_g transition which splits into two by uniaxial stress.

Many more impurities in a variety of crystals have been studied by this technique. Here I mention only one further system, boron acceptors in silicon, because it is used as a phonon spectrometer.

Spectrometer for phonons

Boron in silicon is a shallow acceptor. At low temperatures the hole forms a hydrogen like bound state at the B^- ion. The hole can be light or heavy, and have spin up or down, so that its ground state is fourfold degenerate in cubic symmetry. By uniaxial stress, the quartet splits into two Kramers doublets. This tunable two-level system can be used as a phonon spectrometer.[7]

Consider any phonon source emitting an unknown spectrum into the Si crystal containing $5 \cdot 10^{13}$ cm^{-3} boron. At zero stress, the bound hole states are degenerate, the phonons are not scattered, and can reach the detector where they produce a 100% signal. At a finite stress, the splitting is finite, too, and the phonons with corresponding frequency are partially blocked. The signal is thus reduced by an amount which depends on the contribution of these phonons to the total spectrum. The difference from 100 %, as a function of the stress splitting, is thus a replica of the unknown phonon spectrum. There were many applications of this spectrometer yet, but here I present only the most spectacular one, to Josephson junctions.

Josephson phonons

So far, we have discussed only tunneling of single electrons. Josephson has shown that pairs can tunnel with a comparable probability. These effects are usually suppressed by a magnetic field of $\simeq 2$ mT. In weaker magnetic fields, 0.1 to 0.5 mT, the junction exhibits the ac Josephson effect at finite voltage, i.e. electromagnetic waves with frequency $f = 2\,eV/h$ are generated inside the junction. Only a minute fraction (10^{-4}) of the electromagnetic power is radiated into free space. All the rest is dissipated. The resulting phonons were investigated with the Si:B spectrometer. Fig. 9 shows the results.[8]

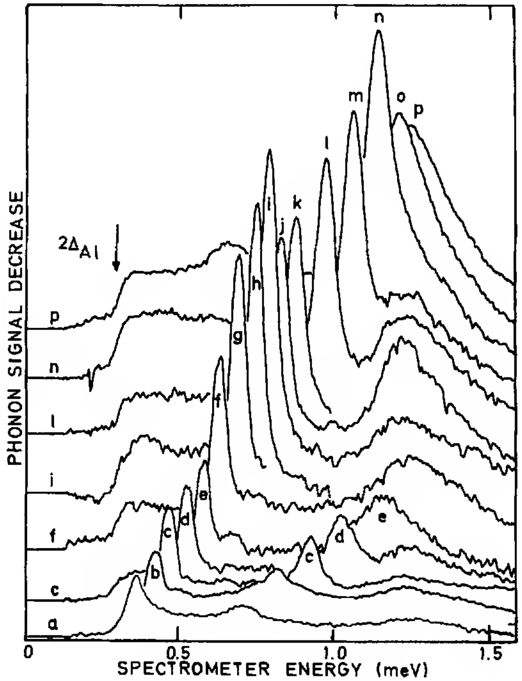

Fig. 9: Phonon spectra emitted by a Josephson junction at various bias voltages.

The salient feature is a peak in each trace, whose position coincides exactly with the Josephson frequency. This corresponds to a 1:1 conversion of the photons into phonons. The mechanism is dielectric loss in the glassy oxide of the junction, which is equivalent to disorder induced infrared activity.

The Josephson frequency can easiliy be tuned by the magnitude of the weak magnetic field. Since the frequency is controlled by the voltage, a stable voltage leads to a very high frequency resolution. This was experimentally tested by investigating V^{3+} in Al_2O_3 once again. While the "bremsstrahlung" technique could only resolve a single line, the Josephson technique now allows to observe the hyperfine splitting, see Fig. 10.[9] The frequency resolution is $\Delta f/f = 2\cdot 10^{-4}$ in this experiment, two orders of magnitude better than with "bremsstrahlung" phonons.

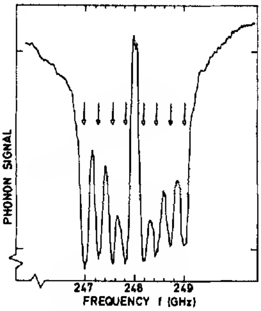

Fig. 10. Hyperfine spectrum of V^{3+} in Al_2O_3, resolved by Josephson phonons

Part II. Surface Scattering and Kapitza Resistance

So far, all experiments described were done in the bulk of solids. But phonons are also well suited for the study of surfaces. This was found in the course of experiments on the Kapitza resistance. The Kapitza resistance is a thermal boundary resistance between liquid helium and solids. Its magnitude depends on the mechanism of heat transfer across the interface. If this mechanism were an acoustic transmission of phonons,[10] the Kapitza resistance would be rather high, and cooling would be difficult at helium temperatures. Fortunately, the conduction is two orders of magnitude better in practice. But the actual mechanism was not understood for decades, and is still under debate.

Phonon pulse experiments

To our present knowledge of the mechanism, phonon pulse experiments have largely contributed. A typical experiment is shown in Fig. 11.[11]

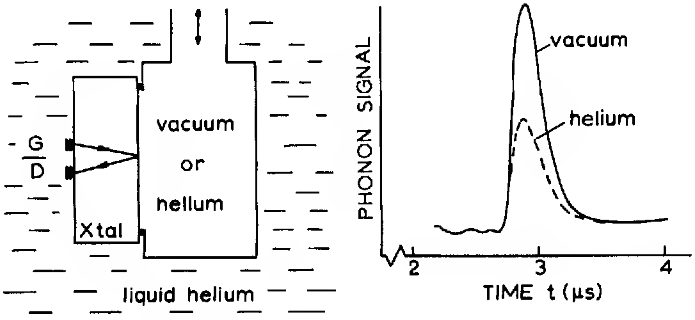

Fig. 11. Typical pulse experiment for Kapitza measurement.

In this experiment, the reflected phonon pulses are recorded for vacuum in the chamber on the back side of the crystal, and then with helium. On a typical surface which was held in air and "cleaned" with organic solvents before mounting, the signal is 50 % less with helium. In contrast, the coefficient for acoustic transmission would be 0.5 %. This is in accordance with the high thermal Kapitza conductance.

Such experiments [12] have shown that transverse phonons are transmitted even more than longitudinal ones and that helium films of 3 monolayers already permit the full transmission, and no further change of the signal is observed with bulk liquid, with helium under pressure, or even with solid helium. Saturation of the Kapitza transmission was observed at high phonon intensities.[13] And experiments on transmission of phonon pulses have revealed that the angular distribution in the helium obeys a cosθ law.[12]

Phonon scattering at clean surfaces

Many of these features suggested that surface impurities are involved in the mechanism. Therefore we have made pulse experiments with clean surfaces. Fig. 12 shows the results for a surface prepared in situ by cleaving at low temperatures, as indicated in the inset.[14] Before cleaving, only the pulse in vacuum is shown in the figure, but the helium effect was also typically 50 % on these surfaces. After cleaving, the crystal is shorter, and so is the time of flight. The helium effect on this fresh surface has vanished for the first (transverse) pulse and is very small for the second (oblique) one. Later results on NaF were even better.[15] In some instances, however, the cleaving was less successful, with a surface full of little steps and flaws. The resulting phonon pulses for such a surface are shown in Fig. 13.[14]

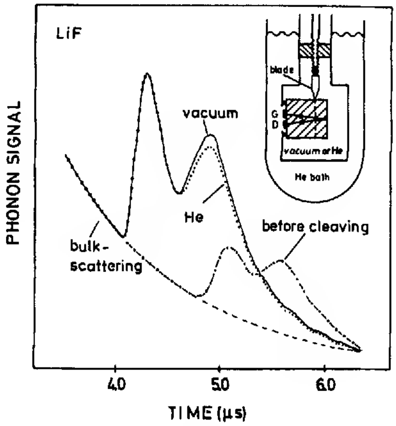

Fig. 12. Helium effect on freshly cleaved LiF surface

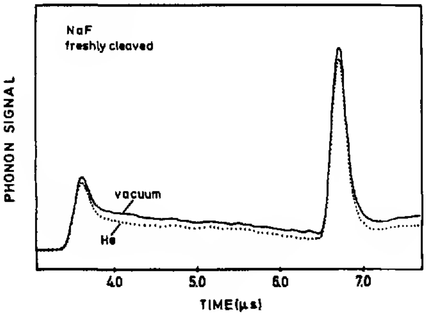

Fig. 13. Cleaved NaF. Diffusive surface scattering is mostly affected by helium.

The pulses are due to spectularly reflected longitudinal and transverse phonons who travel on the shortest path, while the long tails correspond to diffusely scattered phonons which have longer paths. Clearly, these are mostly affected by the helium. Similar phenomena were also observed on polished sapphire surfaces.[16].

As a new technique for cleaning Si crystals at low temperatures, we have used laser annealing.[17] Now, the vacuum chamber has an optical window, and the surface is melted for 20 ns in a layer of 100 nm by a focused ruby laser pulse while the crystal face with the junctions is in liquid helium. A scanning technique is used to clean a large surface area. The results are shown in Fig. 14.

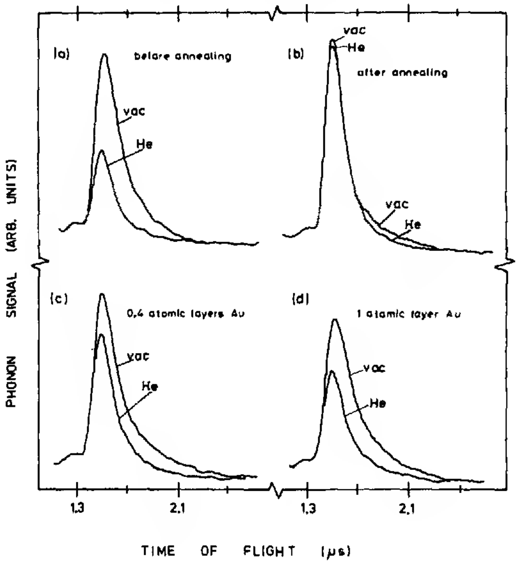

Fig. 14. Effect of laser annealing and Au deposition on a Si surface.

Before annealing (a), the helium effect is typical. After annealing (b), the result is similar as in the case of cleaving.

Clean surfaces with adsorbates

We were able to "comtaminate" the clean surface of Fig. 14 by evaporating a few gold atoms with the help of the same laser. The effect of 0.4 atomic layers (c) and of 1 atomic layer (d) is shown. Clearly, there is again a large helium effect due to these few atoms.

Gold on Si may form special surface states. A more general contamination on all surfaces is a water film. Therefore, we have next constructed a small effusion cell which allows the evaporation of H_2O molecules at controlled rates onto the cleaned Si surface.[18] Very similar results were obtained, see Fig. 15.

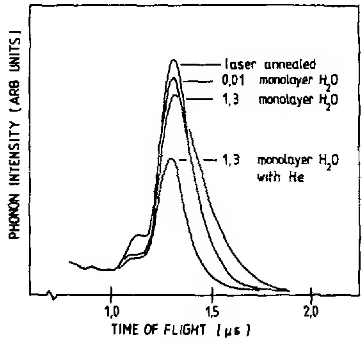

Fig. 15. Effect of H_2O molecules on the annealed surface without He and with He.

For a very small amount of water on the surface, the pulses already change from specular to somewhat diffuse (longer tails), without any helium on the surface. This shows that the impurities alone scatter the phonons, and no peculiar states of the helium near the interface need to be assumed.[19] We have also observed absorption lines at coverages of ≃1 monolayer.[18] This demonstrates that surface spectroscopy with phonons is now possible. No other surface spectroscopy extends down to the meV region, so that more new phenomena are hoped to be found.

Theory

The effect of surface impurities on phonon scattering and Kapitza resistance can be quite simply understood without any specific assumptions on their microscopic nature.

In the bulk of solids, the average effect of defects with random positions is characterized by a complex elastic constant, if they couple via deformation potential to the strain field of the phonons.[20] On the other hand, mass defects which couple to the acceleration field, are characterized by a complex mass density. Either the elastic or the inertial loss leads to damped plane waves. The energy thus derived from a wave emerges as a random field of scattered waves (reemitted phonons). In the same way, we now treat the surface impurities as a thin layer of lossy material which can have a complex elastic constant or, alternatively, a complex density. If the layer is assumed to be homogenous throughout, this is a problem of classical acoustics which can be solved exactly for anisotropic solids, for all angles of incidence, and for arbitrary attenuation strength.[21] As a result, the absorption coefficients of any incident phonons, from the solid or from the helium, are obtained.

For the numerical results presented here, the solid was taken to be Si with the surface normal in [111]-direction. The absorbing layer had the same elastic constants and density, but one of them with a loss angle of 45^0. The frequency was f = 200 GHz, while the layer thickness, a, was varied. But the results actually depend only on the product f*a, as long as the loss angle is constant. In Fig. 16, the energy flux absorption coefficients for longitudinal (L), fast transverse (FT), and slow transverse (ST) phonons incident from the solid are plotted for a layer with a = 0.7 nm as a function of $s_{||} = q_{||}/\omega$, the parallel component of the slowness. The latter is a measure of the angle of incidence. Elastic loss was assumed in this case.

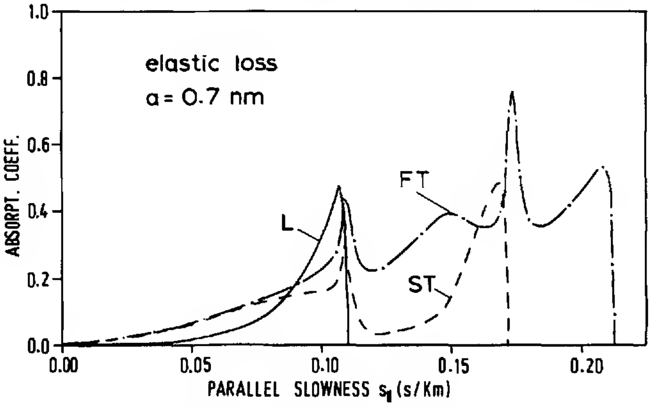

Fig. 16. Absorption coefficient of a thin lossy surface layer

Obviously, the absorption coefficients can be quite high, ≃50 %. For comparison, the transmission coefficient into helium is ≃0.6 % for longitudinal waves, and even smaller for the (oblique) transverse waves. For $s_{||} = 0$, i.e. perpendicular incidence, the absorption vanishes for all polarizations. This is because a perpendicularly incident wave has the same phase everywhere on the surface so that the layer is not strained parallel to the surface and no losses arise. For oblique incidence, the phase does vary along the layer, and so the absorption coefficient increases with increasing angle, or $s_{\parallel}$. There are also some interesting peaks at larger angles due to the impedance of the silicon surface.

While in Fig. 16 the thickness was much smaller than the wavelengths involved, a layer of 1.7 nm shows effects of finite thickness already, see Fig. 17. Even at normal incidence, there is now a substantial absorption because of the finite normal strain components below the free surface. The effect is stronger for transverse waves because of their shorter wave lengths.

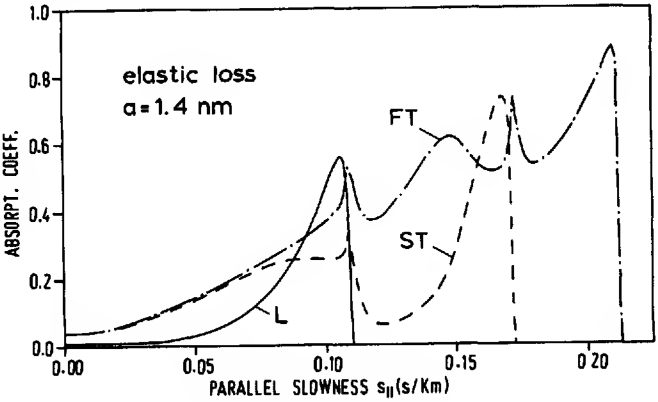

Fig. 17. Absorption of thicker layer is finite for $s_{\parallel} = 0$.

Since the effects discussed so far are specific to elastic loss, i.e. to complex elastic constants, it is interesting to consider now inertial loss, i.e. complex mass density, for comparison. Fig. 18 shows the corresponding results for the layer with a = 0.7 nm (cf. Fig. 16). As expected, the absorption does not much depend on the angle at all, because the acceleration field of the wave is always finite at the free surface. This behavior allows to test experimentally whether the impurities couple by deformation potential, or as "mass-spring-systems".

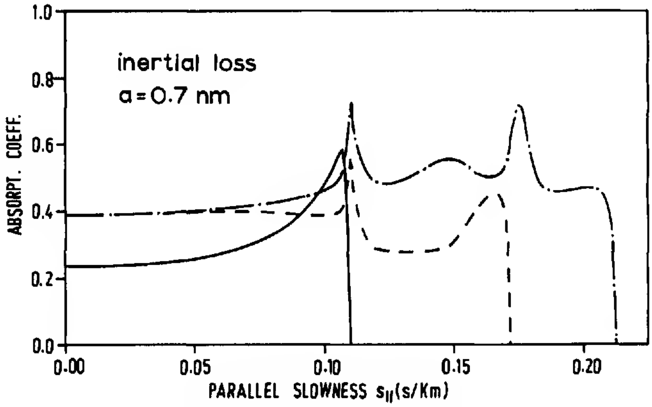

Fig. 18. Mass-spring-systems have distinctly different angular distribution

One simple experimental test of the variation of the absorption coefficient near to the normal direction (cf. Figs. 16-18) with frequency and/or surface condition was already made.[22] The results were in qualitative agreement with Figs. 16 and 17, while Fig. 18 was clearly excluded. This means that the impurities are no resonance modes, but rather localized states with deformation potential coupling ("two level systems"). Further experiments are planned to measure the full angular distribution of phonons transmitted into the solid.

Phonons incident from the helium side are also absorbed by the layer. For the thickness of 0.7 nm, the energy flux absorption coefficient is plotted in Fig. 19. It is rather weak, $\simeq 10^{-3}$, because the surface impedance is large. The peaks indicate a softening of the impedance, e.g. by Rayleigh waves. But all important is the fact that the absorption remains finite for all angles of incidence, i.e. for evanescent waves with $s_{\parallel}$ much larger than the "critical cone" set by the slowness of the solid at $s_{\parallel} \simeq 0.2$ s/km.

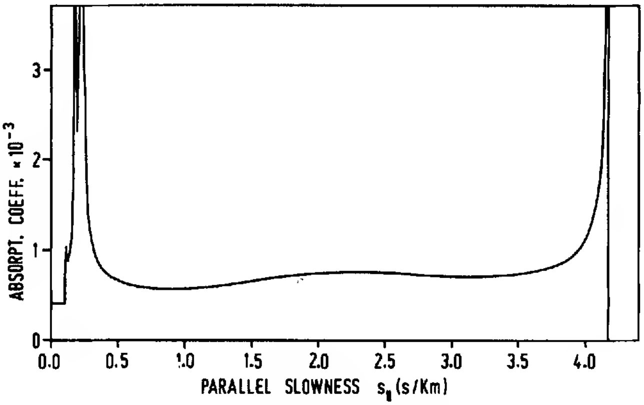

Fig. 19. Absorption of phonons incident from liquid helium.

The fact that the layer absorbs phonons from both, the helium and the solid opens up the new mechanism for Kapitza conduction. In the thermal equilibrium situation, there is detailed balance between absorption and emission of phonons from each side and for any given wave vector and polarization. Thus, the emission distribution of the layer is immediately known from the absorption coefficients. For a temperature difference, the Kapitza conductance is found by summing over the absorbed and emitted distributions on either side of the layer. It turns out that the small absorption coefficients for the helium side do not cause a bottleneck, because they are compensated by the large phase space, i.e. the large $\vec{s}_{\parallel}$-area on that side. For this reason, the large absorption coefficients of the solid side give rise to an equally large Kapitza conductance, about 50 times larger that of acoustic transmission, indeed.

This phenomenological model can in fact explain most of the existing experiments. The transmission has the correct magnitude and tends to be larger for transverse waves. The material properties of the helium (^{3}He, ^{4}He, solid He, films) do not enter as long as there is no bottleneck on the helium side. Diffuse reflection of phonons is understood as absorption and emission: with the surface in vacuum, the reemission is entirely forced back into the solid where it shows up as diffuse reflection. With helium in contrast, most of the energy is emitted out, i.e. effectively Kapitza-transmitted. The magnitude of the loss angle can be justified if the surface imperfections are assumed to form a distribution of two-level-systems[23] similar to those found in glasses, and these do couple to phonons by deformation potential indeed.[20] Yet, a microscopic picture is still lacking. Probably there will be as many microscopic mechanisms as there are defects at surfaces, and the problem of Kapitza resistance will eventually merge into general surface physics.

References

1. H. Kinder, Phys. Rev. Lett. 28, 1564 (1972).
2. For a recent review, see H. Kinder in: Nonequilibrium Phonon Dynamics, ed. by W.E. Bron, (Plenum 1985), p. 129.
3. see, e.g. Phonon Scattering in Condensed Matter V, ed. by A.C. Anderson and J. P. Wolfe (Springer 1986)
4. W. Eisenmenger and A.H.Dayem, Phys. Rev. Lett. 18, 125 (1967).
5. K. Laßmann and P. Burger in: Phonon Scattering in Condensed Matter V, ed. by A.C. Anderson and J. P. Wolfe (Springer 1986), p. 116.
6. R. Windheim and H. Kinder, Phys. Lett. 51A, 475 (1975).
7. P. Berberich and H. Kinder, J. Physique C6-42, 374 (1981); P. Berberich and M.Schwarte, Z. Phys. B 64, 1 (1986).
8. P. Berberich, R. Buemann, and H. Kinder, Phys. Rev. Lett. 49, 1500 (1982).
9. A. Schick, P. Berberich, and H. Kinder in: Phonon Scattering in Condensed Matter, ed. by W. Eisenmenger, K. Lassmann, and S. Döttinger (Springer 1984), p. 40.
10 I. M. Khalatnikov, Zh. Eksp. Teor. Fiz. 22, 687 (1952).
11. J. Weber, W. Dietsche, and H. Kinder, Phys. Lett. 64A, 202 (1977).
12. For a review, see A.F.G. Wyatt in: Nonequilibrium Superconductivity, Phonons, and Kapitza Boundaries, ed. by K.E. Gray (Plenum 1981), p. 31.
13. H. Schubert, P. Leiderer, and H. Kinder, Phys. Rev. B 26, 2317 (1982).
14. J. Weber, W. Sandmann, W.Dietsche, and H. Kinder, Phys. Rev. Lett. 40, 1469 (1978).
15. H. Kinder, J. Weber, and W. Dietsche in: Phonon Scattering in Condensed Matter, ed. by H.J. Maris (Plenum 1980), p. 173.
16. P. Taborek and D. Goodstein, J. Phys C 12, 4737 (1979)
17. H.C. Basso, W. Dietsche, and H. Kinder in: LT 17 (Contributed Papers), ed. by U. Eckern, A. Schmid, W. Weber, and H. Wühl (North Holland 1984), p. 465.
18. L. Köster, S. Wurdack, W. Dietsche, and H. Kinder in: Phonon Scattering in Condensed Matter V, ed. by A.C. Anderson and J. P. Wolfe (Springer 1986), p. 171.
19. T. Nakayama, Phys. Rev. B 32, 777 (1985).
20. J. Jäckle, L. Piche, W. Arnold, and S. Hunklinger, J. Noncryst. Sol. 20, 365 (1976).
21. H. Kinder and K. Weiss in: Phonon Scattering in Condensed Matter V, ed. by A.C. Anderson and J. P. Wolfe (Springer 1986), p. 218, and to be publ.
22. H. Kinder, A. De Ninno, D. Goodstein, G. Paterno', and F. Scaramuzzi, Phys. Rev. Lett. 55, 2441 (1985).
23. H. Kinder, Physica 107B, 549 (1981).

PHONON FOCUSSING IN CRYSTALS

K.S.Viswanathan
(Department of Physics, University of Kerala,
Kariavattom, Trivandrum 695 581, INDIA).

1. THE HEAT PULSE EXPERIMENTS

The heat pulse experiments carried out by various workers [1,5] during the last two decades demonstrated that phonons show a tendency to propagate ballistically rather than diffusively at very low temperatures. In these experiments, a thin metallic film is coated on one surface of a crystal and phonons are generated by passing a short electrical or laser pulse over the film. The phonons arriving at the opposite face of the crystal are detected by a fast superconducting bolometer. Pulses of the phonons of different polarizations arrive at the detector at different times and can be studied independently.

Taylor, Maris and Elbaum [2] studied the characteristics of phonon propagation at very low temperatures in the range $2^{\circ}K \leq T \leq 3.6$. They produced pulses of phonons by passing a short duration pulse (10^{-7}sec) of current through a resistive film evaporated on a selected area of the crystal. The phonon pulses travelled through the crystal ballistically and arrived at the face opposite to the source. The arriving phonons were detected by measuring the change in the electrical resistance of a superconducting film kept near its transition temperature. This temperature can be varied through the use of a magnetic field. These authors observed that pulses due to transverse and longitudinal phonons arrived at different times in view of the difference in their velocities.

Northrop and Wolfe [4,5] devised a novel technique of phonon imaging to study the focussing of phonons. They produced the heat pulse by a pulsed laser beam and the heat pulse was accurately scanned in two dimensions across the surface of the crystal. The method produced a two dimensional map of phonon intensities emanating from a point source in the crystal and gave a precise map of the phonon flux singularities. A typical two dimensional map of the phonon intensities is given in Fig. 1. Bright regions are points of high phonon flux arriving at (100) face of the Germanium crystal. Here the phonon source is at the centre of this pattern in the opposite face.

2. ANISOTROPY OF ELASTIC WAVE PROPAGATION

The phenomenon of ballistic propagation of phonons in crystals at very low temperatures can best be understood if we remember that elastic wave propagation in a crystal is highly anisotropic [6,7]. The dispersion equation for elastic wave propagation has been known for over a century. It is sufficient to recall that three types of elastic waves propagate in any direction inside a crystal, which we call the quasilongitudinal L, the fast shear (FT) and slow shear (ST) modes. An important consequence of the elastic anisotropy of crystals is that the group velocity is not collinear with the wave vector except along a few symmetry directions. The group velocity and wave velocity vectors are related by means of the relation [6]

$$\vec{v}.\vec{n} = s \qquad (1)$$

This group velocity vector is alternatively called the ray vector and signifies the direction of transport of elastic energy in the medium. The angle between the group and wave velocity vectors though normally small, can assume very high values.

The elastic waves inside a crystal are not strictly longitudinal or transverse, except in a few directions depending on the symmetry of the crystal. Pure modes [8] occur along directions related to the symmetry axes and symmetry planes or along certain non-symmetry directions determined by the elastic constants of the crystal. Generally waves propagating along three-fold, four fold or six-fold axes are pure, and besides there exists one pure shear mode normal to a plane of symmetry.

The anisotropy of elastic wave propagation in crystals can be best understood by studying either the sections or a three dimensional computer graphics of the inverse velocity surface [7,9]. This is defined as the locus of all radius vectors given by $\vec{r} = \vec{n}|\vec{v}$, where $\vec{n}$ is a unit vector in the direction of wave propagation and v is the velocity of propagation in that direction. Corresponding to the three different modes of propagation, the inverse velocity surface exhibits three sheets. Another surface known as the energy surface or group velocity surface represents the envelope of all points reached by the energy flux of a disturbance starting at the origin after unit time. The radius vector from the source to any point on this surface represents the distance travelled by the energy in unit time in that direction or the group velocity of the waves. By the method of phonon imaging, Northrop and Wolfe [45] have plotted a three dimensional representation of the energy surface. Their experiments show that the energy surface exhibits ramps and ridges. A typical view of the energy surface given by them is reproduced in Fig. 2.

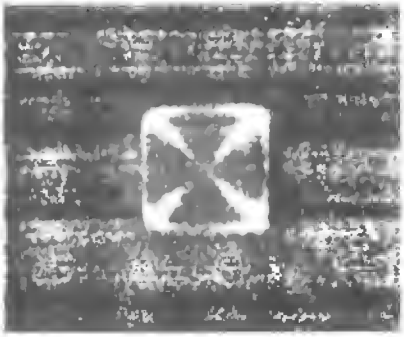

Fig. 1.
Ballistic phonon image for Germanium (after Northrop and Wolfe)

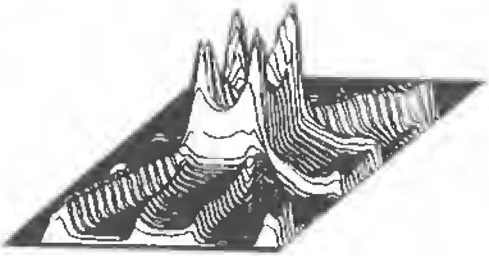

Fig.2
Three dimensional representation of the ramp and ridge structures exhibited by the energy surface (After Northrop and Wolfe).

3. CUSPIDAL EDGES FOR ENERGY SURFACES

Sections of the energy surface for the slow shear mode for cubic crystals by a principal plane invariably exhibits cusps along one of the symmetry axes. Since the group velocity is not a single valued but a many valued function of the wave vector, there could exist several wave vectors corresponding to a single group velocity vector. In figure 3 we reproduce some typical sections [9] of the inverse velocity as well as the energy surface by the principal (001) plane for Lithium. The cuspidal edges are present for the two quasi shear modes only; the quasi longitudinal wave sheet does not exhibit a cusp. In Fig.4 we give a three dimensional view of the inverse velocity surface for the slow transverse mode for He^3, which is a quantum crystal. The cusps arise from the convoluted form of the quasishear inverse velocity surface in the vicinity of the cubic axes of the

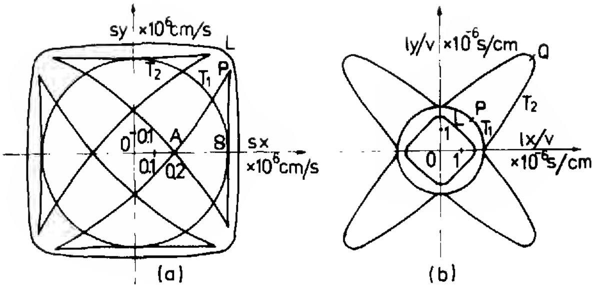

(a)

(b)

Fig.3
Section of (a) the ray velocity surface and (b) the inverse velocity surface for Lithium by the (0 0 1) plane.

crystal. The semi angle, width and other parameters related to a cusp have been calculated and tabulated for over sixty crystals by Jacob Philip and Viswanathan [9]. For sections by the principal plane for a cubic crystal, the existence of a cusp along the cubic axes or face diagonal direction depends on the anisotropy factor $A = \frac{2C_{44}}{(C_{11}-C_{12})}$. If A > 1, a cusp occurs along the cubic axes; otherwise it occurs along the face diagonal.

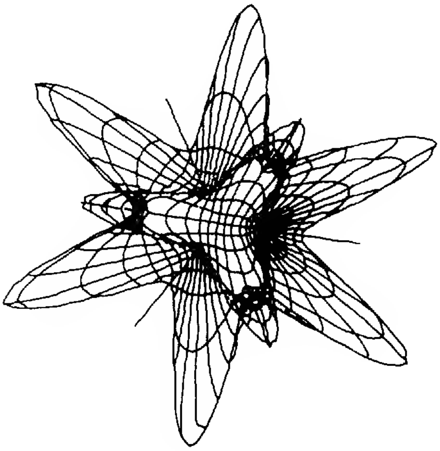

Fig.4
Three dimensional view of the inverse velocity surface for the ST mode for solid Helium 3 viewed about the (1 1 1) direction (After Narasimha Iyer)

The elastic wave surfaces are interesting for the A-15 compounds which undergo a phase transition [10] at low temperatures above the superconducting critical temperatures. These substances are noted generally for their high superconducting critical temperatures and other anomalous properties. For all these crystals $C_{11} \rightarrow C_{12}$ near this critical temperature so that the pure shear mode propagating along the (110) direction with (1 $\bar{1}$ 0) polarization becomes soft. In Fig.5, we have reproduced the sections by the (1 0 0) plane for V_3Si, which is one of the A-15 compounds.

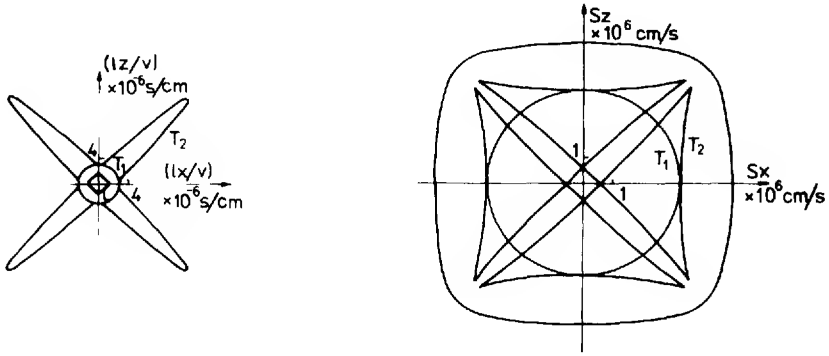

Fig.5(a)
Inverse velocity surface of V_3Si at 4.2°K in the (0 0 1) plane (b) Ray velocity surface of V_3Si at 4.2° K in the (0 0 1) plane.

The presence of cuspidal edges give rise to a large phonon amplification factor. Mc Curdy [11] has found that the amount of enhancement is related to the width of the cusp - the narrower the cusp, the higher the phonon intensity.

4. THE PHONON MAGNIFICATION FACTOR

We have mentioned earlier the results of the heat pulse experiments which demonstrated that at low temperatures, phonons propagate ballistically rather than diffusively. Even though the hot region in the experiments was generated as an incoherent source of phonons with isotropic angular distribution of wave vectors, the group velocity vectors emerged with high anisotropy. Phonons are focussed in certain directions, and some regions in the crystal are bereft of phonons at all.

The ballistic propagation of phonons at temperatures below the superconducting critical temperature for metals can be understood if we remember that at these low temperatures thermal transport is carried by phonons only as there are negligible normal state electrons to carry heat. By choosing a pure specimen free from defects, impurity scattering can also be reduced to the minimum. The mean freepath will then be limited by the linear dimensions of the sample and phonons, will propagate ballistically.

Maris et al [2,3,12] pointed out that a phonon magnification factor A can be defined by taking the ratio of the solid angles in the wave vector space to the solid angle in the group velocity space [10]

$$\frac{1}{A} = \frac{d\Omega_s}{d\Omega_q} = \frac{\sin\theta_s d\theta_s\, d\phi_s}{\sin\theta\, d\theta\, d\phi}\ , \qquad (2)$$

where (θ_s, ϕ_s) denote the polar angles of the group velocity vector.

Phonon magnification factor PMF is proportional to the phonon energy flux. Phonon energy emanating from a heated point source in the crystal is concentrated along directions for which A is large. The phonon magnification factor was computed for a large number of crystals by Mc Curdy [11] and others [2] by evaluating the above ratio numerically. Maris et al [2] calculated the directions of the group velocity vector associated with a large number of wave vectors, which were taken in intervals of 1.25° for θ and ϕ. The number of group velocity vectors for each of the three modes lying within a solid angle was enumerated and from this, the PMF was determined as the ratio of the phonon intensity to the intensity expected in an isotropic solid.

If the dispersion relation for elastic wave propagation is written in the form [8]

$$\Omega\,(k_x,\ k_y,\ k_z,\ \omega) = 0 \qquad (3)$$

an expression for the group velocity of the waves is given by

$$\vec{S} = -\operatorname{grad}_k \Omega / \partial\Omega/\partial\omega\ . \qquad (4)$$

From this the components of the group velocity vector can be written and one finds that the polar angles (θ_s, ϕ_s) signifying the direction of propagation of the group velocity are given by the equations

$$\tan\theta_s = \frac{(S_x^2 + S_y^2)^{1/2}}{S_z} = \frac{(D_x^2 + D_y^2)^{1/2}}{D_z} \qquad (5)$$

and

$$\tan\phi_s = \frac{S_y}{S_x} = \frac{D_y}{D_x}\ . \qquad (6)$$

The expressions for D_x, D_y, D_z are [13]

$$
\begin{aligned}
{}_x = {} & 2A_0 \operatorname{Sin}^3 \theta \cos^2 \theta \sin^2 \phi \cos \phi \\
& + B\,(2 \sin^5 \theta \sin^4 \phi \cos \phi + 4 \sin^5 \theta \cos^3 \phi \\
& \quad \sin^2 \phi + 2 \sin \theta \cos^4 \theta \cos \phi + 4 \cos^2 \theta \sin^3 \theta \cos^3 \phi) \\
& - 2(\rho v^2)\,[C(\sin^3 \theta \cos \phi \sin^2 \phi + \sin \theta \cos^2 \theta \cos \phi) + 2D \sin^3 \theta \cos^3 \phi] \\
& + 2E(\rho v^2)^2 \sin \theta \cos \phi + 6F \sin^5 \theta \cos^5 \phi
\end{aligned}
\qquad (7)
$$

$$
\begin{aligned}
D_y = {} & 2A_o \sin^3 \theta \cos^2 \theta \sin \phi \cos^2 \phi \\
& + 2B(\sin \theta \cos^4 \theta \sin \phi + 2 \sin^3 \theta \cos^2 \theta \sin^3 \phi \\
& + \sin^5 \theta \sin \phi \cos^4 \phi + 2 \sin^5 \theta \sin^3 \phi \cos^2 \phi) \\
& - 2(\rho v^2)\,[C(\sin \theta \cos^2 \theta \sin \phi + \sin^3 \theta \sin \phi \cos^2 \phi) \\
& \qquad + 2D \sin^3 \theta \sin^3 \phi] \\
& + 2E(\rho v^2)^2 \sin \theta \sin \phi + 6F \sin^5 \theta \sin^5 \phi
\end{aligned}
\qquad (8)
$$

and

$$
\begin{aligned}
D_z = {} & 2A_o \sin^4 \theta \cos \theta \sin^2 \phi \cos^2 \phi \\
& + 2B(\sin^4 \theta \cos \theta \cos^4 \phi + 2 \sin^2 \theta \cos^3 \theta \cos^2 \phi \\
& + \sin^4 \theta \cos \theta \sin^4 \phi + 2 \sin^2 \theta \cos^3 \theta \sin^4 \phi) \\
& - 2(\rho v^2)\,[C(\cos \theta \sin^2 \theta \cos^2 \phi + \cos \theta \sin^2 \theta \sin^2 \phi) \\
& + 2D \cos^3 \theta] + 2E(\rho v^2)^2 \cos \theta + 6F \cos^5 \theta
\end{aligned}
\qquad (9)
$$

where

$$
\begin{aligned}
A_o &= C_{11}^3 + 2C_{12}^3 + 4C_{44}^3 + 6C_{12}\,C_{44}^2 \\
&\qquad + 6C_{12}^2\,C_{44} - 3\,C_{11}C_{12}^2 \; - 6C_{11}C_{12}C_{44} \\
B &= (C^2_{11}C_{44} + C_{11}C_{44}^2 - C_{12}^2\,C_{44} - 2C_{12}C_{44}^2) \\
C &= (C_{11}^2 - C_{12}^2 + 2C_{44}^2 + 2\,C_{11}\,C_{44} - 2C_{12}\,C_{44}) \\
D &= C_{44}(2C_{11} + C_{44}), \quad E = (C_{11} + 2C_{44}) \\
F &= C_{11}\,C_{44}^2
\end{aligned}
\qquad (10)
$$

From these expressions it follows that θ_s and ϕ_s are functions of the polar angles (θ, ϕ) of the wave vector. It was pointed out by the present author and Jacob Philip [13] that the ratio $\dfrac{d\theta_s \; d\phi_s}{d\theta \;\; d\phi}$ is none other than the Jacobian of the transformation

$\frac{\partial(\theta_s,\phi_s)}{\partial(\theta,\phi)}$ between the variables (θ_s, ϕ_s) and (θ, ϕ)

$$\text{Now } J = \frac{d\theta_s \, d\phi_s}{d\theta \, d\phi} = \frac{\partial\theta_s}{\partial\theta}\frac{\partial\phi_s}{\partial\phi} - \frac{\partial\theta_s}{\partial\phi}\frac{\partial\phi_s}{\partial\theta} . \qquad (11)$$

To evaluate the Jacobian, it is necessary to obtain the four partial derivatives $\frac{\partial\theta_s}{\partial\theta}$, $\frac{\partial\theta_s}{\partial\phi}$, $\frac{\partial\phi_s}{\partial\theta}$ and $\frac{\partial\phi_s}{\partial\phi}$, and these can be obtained by direct partial differentiation of (5) and (6) with respect to θ and ϕ. Thus the PMF can be evaluated analytically and is given by

$$\frac{1}{A} = J \frac{\sin\theta_s}{\sin\theta} . \qquad (12)$$

A programme can be written to evaluate the Jacobian J, and even with the aid of a small computer, the magnification $A(\theta,\phi)$ can be evaluated for different directions for any crystal. A geometrical interpretation of the [14] Jacobian J is that $J = K k^2 \cos\sigma$, where K is the Gaussian curvature of the slowness surface and σ is the angle between the wave and group velocity vectors. The Jacobian is dimensionless and is inversely proportional to the PMF. Regions of small curvature in the inverse surface correspond to directions having high values for the PMF.

Numerical calculations show that the phonon magnification can be as very high for certain directions in crystals. The magnification has been found to be high for symmetry directions, though it is not restricted to them; large values have been noticed for other nonsymmetry directions too. To compare the calculated values with the experimental results, it may be often convenient to study $A(\theta_s,\phi_s)$ rather than $A(\theta,\phi)$. This could be achieved by sorting the computer output for $A(\theta,\phi)$ in ascending values for the parameters θ_s and ϕ_s.

Computer calculations indicate that the PMF can assume very high values normally for the slow shear mode. Though the PMF does not assume high values for the longitudinal mode generally, an exception is the case of Xenon [17] for which A= 139903 for propagation along the direction $\theta_s = 81.89^\circ$ and $\theta_s = 136.41^\circ$. High values of the PMF are related to the shape of the energy surface or the curvature of the slowness surface. The curvature tends to be very small along directions showing large values for the PMF. For propagation along the principal planes, the group velocity vector also lies in the same plane and one can study the variation of the PMF either with respect to ϕ or ϕ_s in these planes. In Fig.7, we give the variation of A with ϕ_s for the (0 0 1) plane for the FTA mode in diamond. As can be seen from the figure, the PMF shows maximum values along the directions $\theta_s = 0$ or $\pi/2$. Similarly in Fig. 8, we plot the relation between A and ϕ_s in the (0 0 1) plane for the slow shear mode for Nb_3Sn at 40^{o}K.

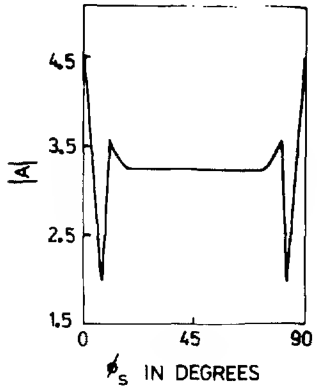

Fig. 6
Relation between A and ϕ_s in the (001) plane for the FTA mode in diamond.

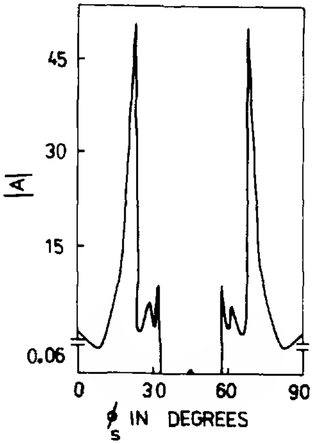

Fig. 7
Relation between A and ϕ_s in the (001) plane for the STA mode for Nb_3Sn at 40K.

Secondly the distribution of the polar variables of the group velocity vector (θ_s ϕ_s) may be densely populated around certain directions. This feature can be brought out best by plotting the distribution of the angles θ_s and ϕ_s in the polar Schmidt net with pole at ($\pi/2$, $\pi/2$) meant for studying the distribution of directions on a unit sphere. In Fig. 8, we show the polar Schmidt net for the STA mode for diamond. The figure shows that the density of group velocity vectors is not uniform in space, being high along the diagonal directions and edges of the square, and it is low elsewhere. However the intensity of the focussing is high along the (0 0 1) or equivalent directions. The figure also exhibits the cubic symmetry of the density of the phonons. In Fig. 9 we show the polar Schmidt net for the FTA mode for Nb_3Sn at 40^{o}K before the phase transition. This figure shows islands that are empty of phonons. The defocussing is in fact as much important as the focussing phenomenon itself.

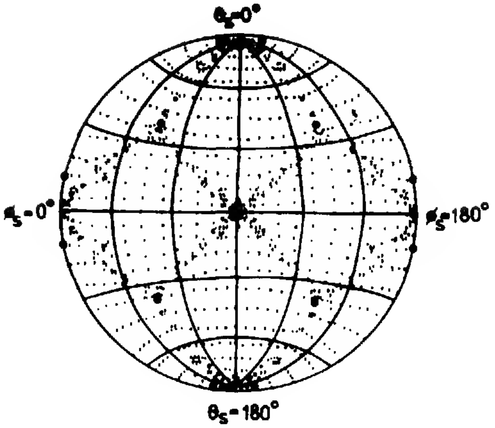

Fig. 8
Polar Schmidtnet with Pole at (π/2, π/2) for the STA phonons in diamond.

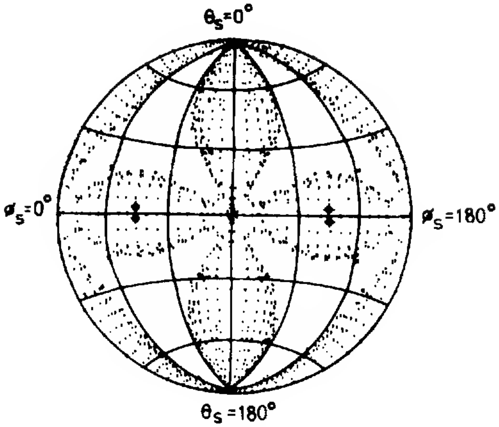

Fig. 9
Polar Schmidtnet with pole at (π/2, π/2) for the FTA phonons in nontransforming Nb Sn_3 at 40K

5. PHONON WIND INTERACTION WITH ELECTRONHOLE DROPLETS.

Non equilibrium phonons which are produced in the phonon focussing experiments have been used to propel electron-hole droplets, that are formed at low temperatures in semiconductors. In analogy with the solar wind in space physics, this flux of phonons is called the phonon wind. Experiments on the phonon wind have helped to understand several phenomena such as the absorption of non equilibrium phonons by the e-h liquid in the metal, the characteristics of phonon focussing and the scattering of phonons. Hensel et al [16] studied the motion of electron-hole droplets using phonons generated through the heat pulse technique. If F is the force on a droplet due to the phonon wind and τ_p is the scattering time, which is of the order of 10^{-9} sec, the velocity of the droplet is given by

$$V_d = (F\tau_p/M) \qquad (13)$$

where M is the inertial effective mass of the droplet. The force exerted on the electron-hole drop by the phonon results when the drop absorbs a phonon of momentum $\vec{q}$ and gets scattered across the Fermi surface. The force has been found to be a maximum when $\vec{q}$ is oriented along the major axis of the Fermi surface. Hensel showed that LA phonons were attenuated by 35% by the droplets whereas the

TA phonons were not absorbed at all. They obtained a value of the drift velocity V_d of the droplet as

$$V_d = 1.0 \times 10^5 \text{ cm/sec} \qquad (14\text{ a})$$

which is to be compared with the velocity V_L of the longitudinal phonons along the face diagonal,

$$V_L = 5.62 \times 10^5 \text{ cm/sec.} \qquad (14\text{ b})$$

Modern developments in electronics and measuring instruments, cryogenics, lasers and computers have all contributed much to the progress in the physics of phonons and especially on nonequilibrium phenomena. On the applied side, there are rays of hopes for success in the invention of phonon spectrometers or phonon masers. Far from being a century old or closed subject, the physics of phonons has retained its vitality, and promises still new developments, discoveries or inventions.

REFERENCES

(1)	R.J. VonGutfeld and A.H. Nethercot	Phys. Rev. Lett. 12, 641 (1964)
(2)	B. Taylor, H.J. Maris C. Elbaum	Phys. Rev. Lett. 23, 416 (1969)
(3)	B. Taylor, H.J. Maris and C. Elbaum	Phys. Rev. B3 1462 (1971)
(4)	Northrop, G.A. and Wolfe, J.P.	Phys. Rev. Lett. 43, 1424 (1979)
(5)	Northrop, G.A. and Wolfe, J.P.	Phys. Rev. B 22, 6196 (1980)
(6)	F.I. Federov	Theory of Elastic Waves in Crystals (Plenum, New York 1968)
(7)	M.J.P. Musgrave	Crystal Acoustics (Holden-Day, San Francisco 1970)
(8)	Auld, B.A.	Acoustic Fields and Waves in Solids (New York: Wiley Interscience)
(9)	Philip J and Viswanathan, K.S.	Pramana 8, 348 (1977)
(10)	Testardi, L.R.	Physical Acoustics - Principles and Methods (eds) W.P. Mason and R.N. Thurston (New York: Academic Press) Vol. X 1973.
(11)	A.K. McCurdy	Phys. Rev. 69, 466 (1974)

(12) Maris, H.J. J. Acoust. Soc. Am. 50,

(13) Philip J and Viswanathan, K.S. Pramana 24, 875 (1985)

(14) Lax M and Narayanamurti, V. Phys. Rev. B 22, 4876 (1980)

(15) Pushpahasan, A and Viswanathan, K.S. Pramana 24, 875 (1985)

(16) Hensel, J.C. and Dynes, R.C. Phys. Rev. Lett. 43, 1033 (1979)

(17) Narasimha Iyer, V and Viswanathan, K.S. J. Phys. C (under publication)

PHONON SCATTERING AT PLANE INTERFACES AND SURFACES

O. Weis
Abteilung Festkörperphysik
Universität Ulm
D-7900 Ulm
Federal Republic of Germany

Abstract

Phonon pulses propagate with group velocity. Therefore, the concept of group velocity is discussed in the range of continuum acoustics and in the general frame of lattice dynamics, too. The rather complicated problem of phonon reflection and refraction at a plane boundary is presented with the help of frequency surfaces in $\vec{q}$-space. This treatment emphasizes the underlying geometrical properties and gives an understanding of the excited wavemodes. The explicit determination of the phonon-scattering probabilities requires extensive numerical computation.

Content

1. Introduction
2. Mechanical Poynting vector and group velocity
3. Coherent and incoherent phonon radiators
4. Phonon scattering at plane interfaces and surfaces within continuum acoustics
5. Phonon scattering at plane interfaces and surfaces within lattice dynamics.

1. Introduction

Phonons are quanta of mechanical vibrations. In the special case of plane mechanical waves, they are characterized by the wave vector $\vec{q}$ and by the polarization index σ. Standard treatments can be found in references [1-5]. The dependence of phonon frequency $\omega_\sigma(\vec{q})$ on wave vector $\vec{q}$ or the same dependence on phonon energy, respectively,

$$\varepsilon_\sigma(\vec{q}) = \hbar\cdot\omega_\sigma(\vec{q}) \tag{1.1}$$

is called dispersion relation. For high symmetry directions, this relation has been measured by means of inelastic neutron scattering for the most important crystals during the last thirty years. As an example, Fig. 1 and Fig. 2 show the lowest polarization branches of quartz (α-SiO_2), sapphire (Al_2O_3) and diamond together with all six existing branches of silicon, germanium and gallium arsenide in directions of highest symmetry.

Plane lattice waves are Bloch waves and have therefore all properties which can be derived for Bloch waves. In particular, the phase velocity $\vec{c}_\sigma(\vec{k})$ of a Bloch wave $|\vec{k},\sigma>$ is given by

$$\vec{c}_\sigma(\vec{k}) = e_n\cdot\varepsilon_\sigma(\vec{k})/\hbar k \quad \text{with} \quad \vec{e}_n \equiv \vec{k}/k \quad \text{and} \quad k = |\vec{k}| \ , \tag{1.2a}$$

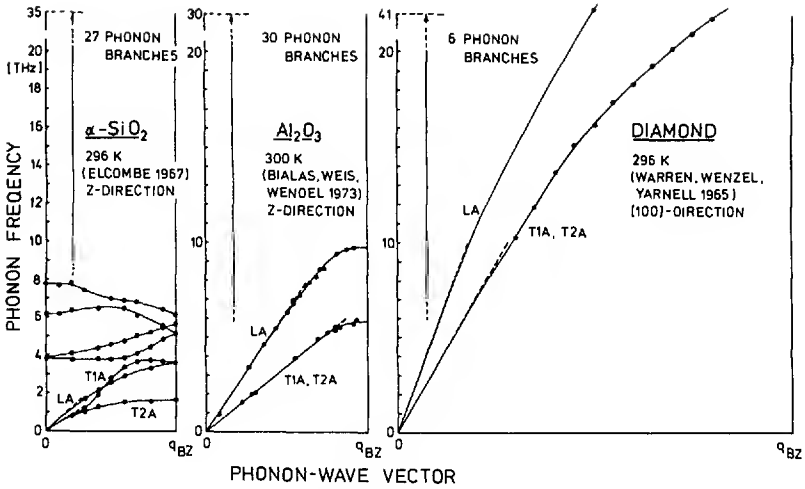

Fig. 1. Phonon dispersion in technical important insulators measured by inelastic neutron scattering

where $\vec{e}_n$ denotes the wave normal. On the other hand, the group velocity $\vec{v}_\sigma(\vec{k})$ of a wave packet ('lokalized' particle) is determined by the gradient at the energy surface in $\vec{k}$-space:

$$\vec{w}_\sigma(\vec{k}) = \frac{1}{\hbar}\cdot\nabla_{\vec{k}}\varepsilon_\sigma(\vec{k}) \; . \tag{1.3a}$$

Replacing $\vec{k}$ by $\vec{q}$ and using (1.1) we get for phonons the phase velocity

$$\vec{c}_\sigma(\vec{q}) = \vec{e}_n\cdot\varepsilon_\sigma(\vec{q})/\hbar q = \vec{e}_n\cdot\omega_\sigma(\vec{q})/q \quad \text{with} \quad \vec{e}_n \equiv \vec{q}/q \; , \quad q = |\vec{q}| \tag{1.2b}$$

and the group velocity

$$\vec{w}_\sigma(\vec{q}) = \frac{1}{\hbar}\cdot\vec{\nabla}_{\vec{q}}\varepsilon_\sigma(\vec{q}) = \vec{\nabla}_{\vec{q}}\omega_\sigma(\vec{q}) . \tag{1.3b}$$

According to (1.3a) the phase velocity can be taken directly from dispersion plots like those of Fig. 1 and Fig. 2 by determining the slope of the straight line between origo and point $\omega_\sigma(\vec{q})$. In the three acoustic branches LA, T1A and T2A, at sufficient low frequencies, this slope and hence the phase velocity are independent on frequency. This 'dispersionless' region is well described by continuum acoustics which uses only the measured elastic constants instead of fitted atomic force constants as is done in lattice dynamics.

The frequency range in which continuum acoustics is applicable is quite different for the crystals considered in Fig. 1. Dispersion starts in a remarkable extent in quartz already below 1 THz (= 10^{12} Hz) whereas for diamond continuum acoustics may be valid up to 10 THz. In any case, the frequency range of continuum acoustics measured in frequency decades is far larger than the actual region for lattice dynamics. This is an important point:

- As a consequence of Bose-Einstein-distribution function, low-frequency phonons are

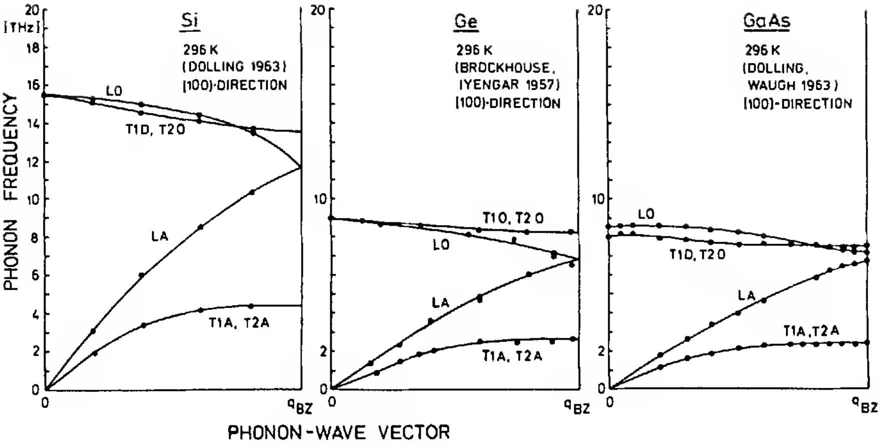

Fig. 2. Phonon dispersion in some semiconductors measured by inelastic neutron scattering. For better comparison, the units are the same as in the diagrams of Fig. 1

more excited in thermal equilibrium than high-frequency phonons. Therefore, interactions with thermal phonons, as appear for example in transport phenomena like thermal and electrical conductivity, are mainly governed by acoustic phonons which are usually described by simplified isotropic models of continuum acoustics.

- In the past, almost all phonon-pulse experiments have been performed with phonon frequencies in the range of continuum acoustics and need therefore no interpretation by lattice dynamics.
- The progress in experimental methods [6] make it now indispensable to study also phonon propagation in the typical lattice-dynamics region.

The principle arrangements of phonon-pulse experiments is sketched in Fig. 3. Such experiments are performed either in a transmission or in a reflection configuration. They demand a transmission material allowing a macroscopic free path for the phonon beam. Therefore, strong interactions with electrons, thermal phonons and static defects must be avoided carefully. Usually, only insulating monocrystals of high quality are used. The measured thermal conductivity is a good guide for choosing suitable crystals with large free phonon path.

If metal films are used as phonon generators (for instance: thermal phonon radiators, superconducting tunneling junctions) or are used as phonon detectors (superconducting bolometers and tunneling junctions), we have inevitable interfaces between two

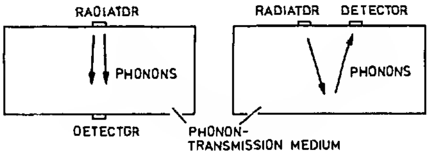

Fig. 3. Principal arrangement of radiator and detector in phonon-pulse experiments

dissimilar media which must be crossed by the detected phonons. Moreover, in the reflection experiments the scattering occurs also at the free crystal surface.
It is the main purpose of my contribution to discuss what we know theoretically about the scattering of phonons at such interfaces and surfaces. This is done first within continuum acoustics [7] and thereafter from the standpoint of lattice dynamics. Of course, we have to make some restrictions for handling this rather complex problem:

- Description is done within linear theory
- Phonon damping is neglected
- Interfaces and surfaces are assumed to be plane at an atomic scale. In the case of continuum acoustics this means an abrupt change in the elastic constants and mass densities. In the lattice dynamical treatment we assume a slab containing some atomic layers with properties different from the bulk, but showing lateral periodicity with a two-dimensional supercell commensurable with the unit cells of the bulk.

The last item is the most important one, since it is hardly be fulfilled in experimental work at present. Commercial carfully lapped and polished crystals show in general a damage layer which may extent to depth of some micrometer. Fig. 4 gives an impression of such a damage layer in a polished Cu crystal. Analogous damage layers can be found in hard crystals like quartz and sapphire. The atoms near the surface are in amorphous state or form microscopic crystallites. This part is called Beilby layer [9]. The adjacent region contains a lot of crystal defects produced by the mechanical treatment like sawing, grinding, lapping and polishing. The damage layer can be removed only by special methods. Etching is sometimes applicable, but often roughens the surface. Silicon crystals in air are covered by an oxid layer. In addition, the evaporated metal films, serving as phonon generator or detector, are at present polycrystalline and have to be replaced by heteroepitaxially grown monocrystals in order to get clear unequivocal conditions for experimental phonon scattering at such interfaces.

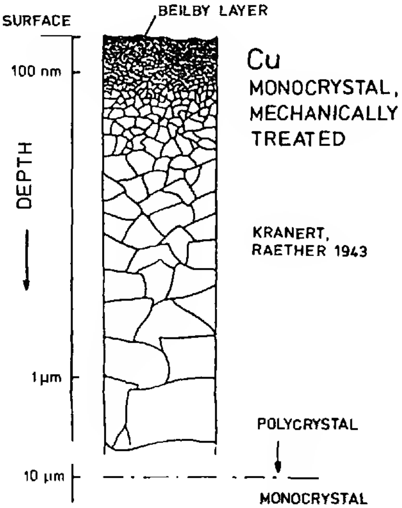

Fig. 4. Damage layer in a mechanically treated Cu crystal according to Kranert and Raether [8]

2. Mechanical Poynting vector and group velocity

The instantaneous local energy-current density in an arbitrary electromagnetic field is given by the Poynting vector

$$\vec{S}(\vec{r},t) = \vec{E}(\vec{r},t) \times \vec{H}(\vec{r},t) \tag{2.1}$$

which depends only on the electric field $\vec{E}$ and on the magnetic field $\vec{H}$.

There exists also an expression for the mechanical Poynting vector within continuum acoustics

$$\vec{S}(\vec{r},t) = - \vec{\vec{\sigma}}(\vec{r},t)\cdot\vec{v}(\vec{r},t), \tag{2.2}$$

where $\vec{\vec{\sigma}}$ denotes the stress tensor and $\vec{v}$ the particle velocity,
In a discrete mechanical system like a Born-von Kârmân lattice, the mechanical energy-current density can only be given as an average over a unit cell. This may be the smallest unit cell, the elementary cell, or a larger conventional unit cell in a periodic lattice. But also nonperiodic atomic arrangements have to be taken into account. In a recent paper [10] it could be shown that in the special case of a harmonic system, the unit-cell averaged Poynting vector can be written

$$\vec{S}(\mathbf{n},t) = \sum_{\mathbf{n}'} \frac{\vec{R}_{\mathbf{n}}-\vec{R}_{\mathbf{n}'}}{4\cdot V_d} \sum_{\nu,\nu'} \left(\dot{\vec{u}}\binom{\mathbf{n}}{\nu}\cdot\vec{\vec{\phi}}\binom{\mathbf{n}\mathbf{n}'}{\nu\nu'}+\dot{\vec{u}}\binom{\mathbf{n}'}{\nu'}\cdot\vec{\vec{\phi}}\binom{\mathbf{n}'\mathbf{n}}{\nu'\nu}\right)\cdot\left(\vec{u}\binom{\mathbf{n}}{\nu}-\vec{u}\binom{\mathbf{n}'}{\nu'}\right) . \tag{2.3}$$

V_d denotes in this expression the volume of the unit cells and $\mathbf{n} \equiv (n_1,n_2,n_3)$ identifies the unit cell $\mathbf{n}$ which has the position vector

$$\vec{R}_{\mathbf{n}} = n_1\cdot\vec{a}_1 + n_2\cdot\vec{a}_2 + n_3\cdot\vec{a}_3 \qquad \text{with vector basis} \quad \{\vec{a}_i\}. \tag{2.4}$$

The atoms in each unit cell are identified by the index ν. The general force-constant tensor $\vec{\vec{\phi}}\binom{\mathbf{n}\mathbf{n}'}{\nu\nu'}$ needs not to be symmetric nor is the translation invariance required for deriving (2.3). The atomic displacement $\vec{u}$ is taken from the equilibrium position which does not appear explicitely in (2.3).
In the special case of a Bravais-type lattice, we have $\nu = \nu' = 1$ and the force-constant tensor $\vec{\vec{\phi}}(\mathbf{n},\mathbf{n}')$ becomes symmetric:

$$\vec{S}(\mathbf{n},t) = \sum_{\mathbf{n}'} \frac{\vec{R}_{\mathbf{n}}-\vec{R}_{\mathbf{n}'}}{4\cdot V_d}\cdot\left(\dot{\vec{u}}(\mathbf{n}) + \dot{\vec{u}}(\mathbf{n}')\right)\cdot\vec{\vec{\phi}}(\mathbf{n},\mathbf{n}')\cdot\left(\vec{u}(\mathbf{n})-\vec{u}(\mathbf{n}')\right) . \tag{2.5}$$

The energy velocity $\vec{w}(\vec{r},t)$ can be introduced by defining

$$\text{Poynting vector} \equiv \text{energy density} \cdot \text{energy velocity}. \tag{2.6}$$

It is wellknown that expression (2.6) yields in the electromagnetic case as well as in continuum acoustics for plane waves in the time average

$$\overline{\vec{S}(\vec{r},t)}^{\,t}_{\text{plane wave}} = \text{energy density} \cdot \text{group velocity}, \tag{2.7}$$

i.e. the group velocity is identical with the energy velocity for plane waves. This can also be shown for plane lattice waves [10] starting from expression (2.3).
In continuum acoustics a plane wave $|\vec{q},\sigma>$ is described by the displacement field

$$\vec{s}_{\vec{q}\sigma}(\vec{r},t) = \vec{e}_\sigma\cdot\hat{s}_{\vec{q}\sigma}\cdot e^{-i\cdot\vec{q}\cdot\vec{r}}\cdot e^{i\cdot\omega\cdot t} + \text{c.c.} , \tag{2.8}$$

where $\hat{s}_{\vec{q}\sigma}$ is the complex amplitude and $\vec{e}_\sigma$ the polarization vector. If the wave normal

$\vec{e}_n = \vec{q}/q$ is prescribed, the possible polarizations $\{\vec{e}_\sigma\}$ follow from the eigenvalue equation

$$\{\vec{q}\cdot{}^{4}\vec{c}\cdot\vec{q} - \rho\cdot\omega^2\}\vec{e}_\sigma = 0 \ , \tag{2.9}$$

where ${}^{4}\vec{c}$ means the tensor of elastic constants and ρ the mass density. Dividing (2.9) by $\vec{q}^{\,2} = \omega^2/c_\sigma^2(\vec{e}_n)$ we get the equivalent eigenvalue equation

$$\{\vec{e}_n\cdot{}^{4}\vec{c}\cdot\vec{e}_n - \rho\cdot c_\sigma^2(\vec{e}_n)\}\vec{e}_\sigma = 0 \tag{2.10}$$

which gives the three phase velocities $\vec{c}_\sigma(\vec{e}_n)$, σ = L,T1 and T2, as eigenvalues. The three polarizations $\{\vec{e}_\sigma\}$ are eigenvectors and therefore orthogonal in $\vec{r}$-space to each other. Now, these results allow us to construct the frequency surfaces in $\vec{q}$-space, since the radius vector to this surface is given by

$$\vec{q} = \vec{e}_n\cdot\omega/c_\sigma(\vec{e}_n) \qquad \text{(corresponding to 1.2b)} \ . \tag{2.11}$$

From (2.11) follows that all frequency surfaces or energy surfaces of a given polarization are similar within continuum acoustics and blow up in size proportional to frequency. As an example, Fig. 5 illustrates these surfaces in normalized form for quartz [11]. According to (1.3b) the gradient at these surfaces represents the group velocity. It is obvious, that in general the direction of the group velocity deviates from the direction of the phase velocity $\vec{c}_\sigma(\vec{e}_n)$ which is always parallel to $\vec{q}$.

An analytic expression for the group velocity can be derived either from equation (2.7) combined with (2.8) or from equation (1.3b) combined with (2.9). In both cases, one obtaines

$$\vec{w}_\sigma(\vec{e}_n) = \vec{e}_\sigma\cdot{}^{4}\vec{c}:\vec{e}_\sigma\vec{e}_n/\rho\cdot c_\sigma(\vec{e}_n) \ . \tag{2.12}$$

Taking $\vec{w}_\sigma(\vec{e}_n)$ as a radius vector, one obtains the group-velocity surfaces [11]. Fig. 6 shows these surfaces for quartz. They are also called 'wave surfaces' since a delta pulse excitation at the origin gives rise to wave fronts in $\vec{r}$-space having the same shape.

In the case of lattice dynamics the particle displacement in a plane wave is given for an arbitrary atom $\binom{\mathbf{n}}{\nu}$ by

$$\vec{u}_{\vec{q}\sigma}\binom{\mathbf{n}}{\nu} = \sqrt{\frac{M}{N}}\cdot\hat{U}_{\vec{q}\sigma}\cdot\frac{\vec{d}_{\vec{q}\sigma}(\nu)}{\sqrt{M_\nu}}\cdot e^{i\cdot\vec{q}\cdot\vec{R}_{\mathbf{n}}}\cdot e^{-i\cdot\omega_{\vec{q}\sigma}\cdot t} + \text{c.c.} \ , \tag{2.13}$$

where $M \equiv \sqrt[s]{M_1\cdot M_2\cdot\ \cdot M_s}$ and s is the number of atoms per elementary cell. N is the number of elementary cells in the volume chosen for cyclic boundary conditions. The set of s polarization vectors $\{\vec{d}_{\vec{q}\sigma}(\nu)\}$ for each solution σ represents an eigenvector of the eigenvalue equations

$$\sum_{\boldsymbol{\ell},\nu'} \frac{\vec{\vec{\phi}}\binom{\mathbf{0}\ \boldsymbol{\ell}}{\nu\ \nu'}}{\sqrt{M_\nu\cdot M_{\nu'}}}\cdot\vec{d}_{\vec{q}\sigma}(\nu')\cdot e^{i\cdot\vec{q}\cdot\vec{R}_{\boldsymbol{\ell}}} - \omega_{\vec{q}\sigma}^2\cdot\vec{d}_{\vec{q}\sigma}(\nu) = 0, \quad \nu = 1,2,\ldots s \tag{2.14}$$

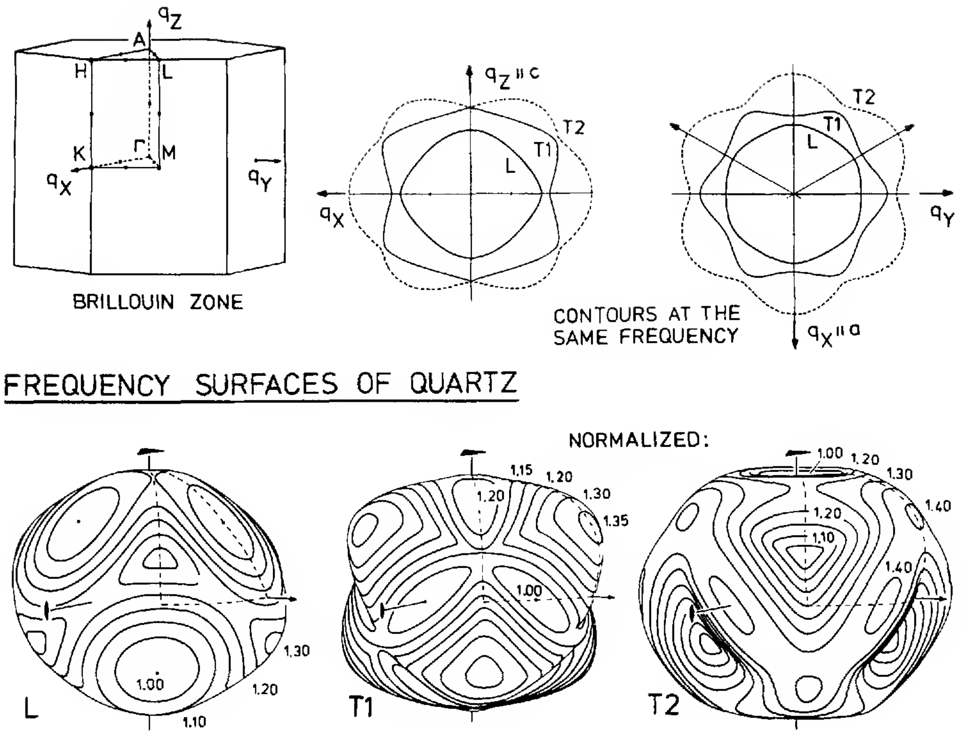

Fig. 5. Frequency surfaces of quartz for long-wavelength acoustic phonons within the validity of continuum acoustics. The frequency surfaces are always single-valued surfaces. The T1- and T2-surfaces have contacts at points of degeneracy which define the acoustic axes. The shortest radius vector is taken to be 1.00 in the normalized surfaces.

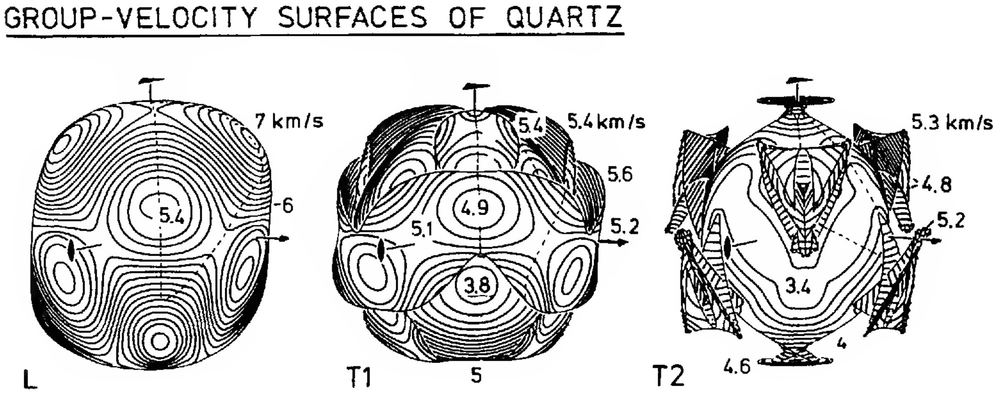

Fig. 6. Group-velocity surfaces of quartz for long-wavelength acoustic phonons within the validity of continuum acoustics. Both surfaces of the transverse phonons are many-valued surfaces.

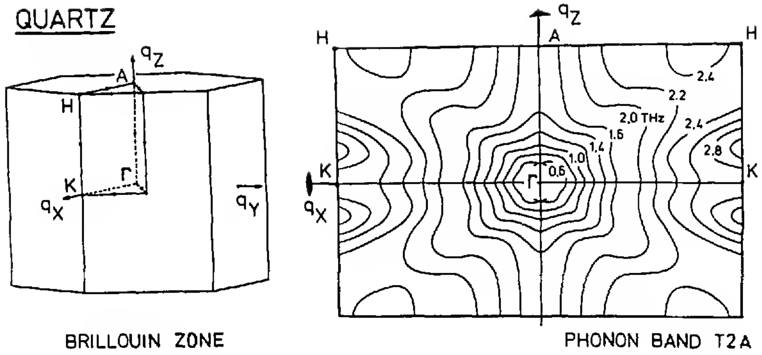

Fig. 7. Contours of phonon-frequency surfaces in the XZ-cross section through the Brillouin zone of the T2A-polarization band of quartz (after [12])

Since these are 3s scalar homogeneous equations, the secular equation of (2.14) gives rise to 3s eigenvalues $\{\omega_{\vec{q}\sigma}\}$ for each $\vec{q}$ vector.

Calculating these frequencies for all $\vec{q}$-vectors within the Brillouin zone, i.e. for the fundamental $\vec{q}$-range of Bloch waves, we are able to represent this dispersion relation by frequency surfaces. In order to avoid ambiguities, each polarization band σ is represented in a seperate Brillouin zone. This procedure requires the knowledge of all force-constant tensors appearing in (2.14). On the other hand, one can determine the whole frequency surfaces or parts of them by inelastic neutron scattering. Due to the tremendous work involved, only a few investigations of this kind have been done in the past. Fig. 7 shows one measured cut through the frequency surfaces of the T2A-phonon band in quartz [12]. The low-frequency surfaces around the Γ point are similar to each other and are identical in shape with the cuts gained by the continuum model in Fig. 5.

The group velocity $\vec{w}_{\vec{q}\sigma}$ for a plane wave $|\vec{q},\sigma\rangle$ may be pictured again by the gradients at the corresponding $\vec{q}$-point at the frequency surface. An analytic expression can also be derived [10] for the group velocity of a general plane lattice wave by combining (2.14), (1.3b) and the orthonormalization of the polarization vectors

$$\sum_{\nu=1}^{s} \vec{d}^{*}_{\vec{q}\sigma}(\nu)\cdot \vec{d}_{\vec{q}\sigma'}(\nu) = \delta_{\sigma\sigma'} \quad . \tag{2.15}$$

One obtains the general expression

$$\vec{w}_{\vec{q}\sigma} = \frac{1}{2\cdot\omega_{\vec{q}\sigma}} \cdot \sum_{\ell} i\cdot\vec{R}_{\ell}\cdot e^{i\cdot\vec{q}\cdot\vec{R}_{\ell}} \cdot \sum_{\nu,\nu'} \frac{\vec{d}^{*}_{\vec{q}\sigma}(\nu)\cdot\vec{\phi}\binom{0\ell}{\nu\nu'}\cdot\vec{d}_{\vec{q}\sigma}(\nu')}{\sqrt{M_{\nu}\cdot M_{\nu'}}} \tag{2.16}$$

which reduces in the case of a Bravais-type lattice ($\nu = \nu' = 1$, $M_{\nu} = M_{\nu'} \equiv M$) to

$$\vec{w}_{\vec{q}\sigma} = \frac{1}{2\cdot M\cdot\omega_{\vec{q}\sigma}} \cdot \sum_{\ell} i\cdot\vec{R}_{\ell}\cdot e^{i\cdot\vec{q}\cdot\vec{R}_{\ell}}\cdot\{\vec{e}_{\vec{q}\sigma}\cdot\vec{\Phi}(0\,\ell)\cdot\vec{e}_{\vec{q}\sigma}\}\ , \tag{2.17}$$

where we have replaced $\vec{d}_{\vec{q}\sigma}(1)$ by the unit vector $\vec{e}_{\vec{q}\sigma}$.

Conclusion: From the considerations of this section we conclude that not only wave packets but also the energy density of plane mechanical waves $|\vec{q},\sigma\rangle$ travel with group velocity. This implies that phonons in the plane wave state also propagate with group velocity. Phase velocity and group velocity can be taken from geometric properties of the frequency surfaces but analytic expressions are also available.

3. Coherent and incoherent phonon radiators

The difference between (spatial) coherent and incoherent phonon radiation from a generator can be explained best with the help of Fig. 8. If the transmission medium is an isotropic solid like quartz glass, we have pure longitudinal and pure transverse plane waves, the group velocity of which is always parallel to the wave normal or wave vector, respectively. We consider first a coherent phonon radiator, i.e. a sound radiator (for instance an electromechanical transducer) which is characterized by a well-defined phase relationship between the field quantities at all elements of the radiator area. This coherent phonon radiator emits a pulse, for example, of 50 ns duration. For convenience, we take an excitation with equal phase over the radiator area, and the diameter of the radiating area is assumed to be very large in

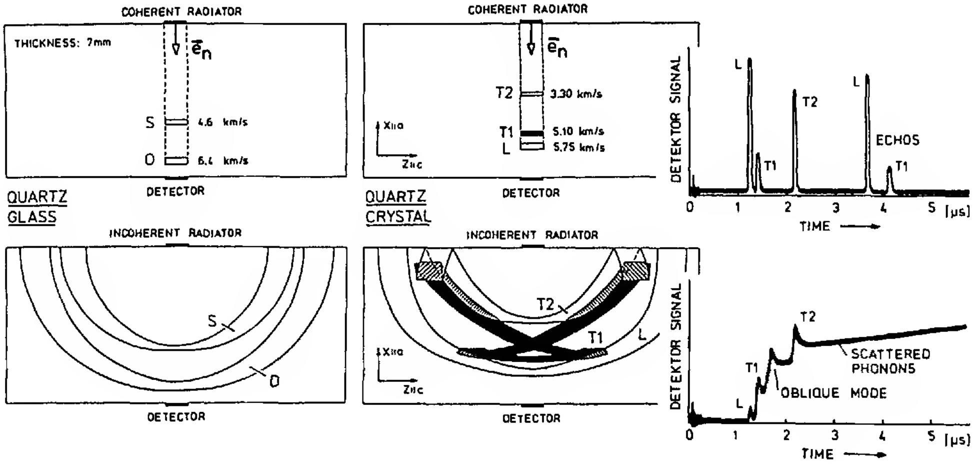

Fig. 8. Momentary phonon positions 1 μs after phonon-pulse emission (pulse duration is 50 ns) from coherent and from incoherent phonon radiators. The phonon propagation in an isotropic solid (quartz glass) is compared with the propagation in an anisotropic solid (quartz crystal, X-cut). The time dependent detector signals are given for the last case.

comparison to the sound wavelengthes. Therefore, the emitted phonon pulses are highly collimated and fall with their whole power onto the detector - as long as no scattering events occur during transmission.

On the contrary, the power is spread over the whole halfspace by using a totally incoherent phonon radiator, i.e. a radiator where no phase relation exists between emitting elements of the radiator area. This is analogous to photon emission from a flash lamp (incoherent photon radiator) and to photon emission from a pulsed laser (coherent photon radiator).

This simplicity in propagation is lost in crystals due to the anisotropy which gives rise to the deviation between group and phase velocity. Only along pure mode axes like the twofold X-axis in quartz (Fig. 8) the group velocity and the phase velocity coincides and all three possible phonon pulses meet the phonon detector after each other. Using a general crystal cut, the coherent radiator sets only the wave normal $\vec{e}_n$ normal to the radiator area and gives of course the frequency or frequency spectrum of excitation. The propagation directions of the collimated beams are then in general oblique and fixed by the group velocities associated with $\vec{e}_n$, the polarizations σ and frequencies ω. In general, if a detector is brought into the appropriate position for the detection of one phonon pulse, the other phonon pulses will be missed.

An incoherent phonon radiator in contact with an X-cut quartz (Fig. 8) gives, a certain time interval after phonon-pulse emission, a superposition of all wavefronts of each independently emitting element of the radiator area. On the other hand, we know the shapes of each wavefront since they are proportional to the group-velocity surfaces of Fig. 6. In our case, we have to take the XZ-cut for constructing the region in which phonons can be found. These regions and also the detector signals given in Fig. 8 show that in addition to the three pulses, arriving at the same time as the coherent pulses, there exists a forth pulse ('oblique mode') in X-direction which is associated with $\vec{q}$-vectors not parallel to the twofold axis (see Fig. 9). Actually, we have prescribed the radiator/detector direction or group-velocity direction $\vec{e}_{\vec{w}}$, respectively, by the experiment and have to look for the whole set $\{|\vec{q}_\nu,\sigma>\}$ of wave vectors which contribute in $\vec{e}_w$-direction for each polarization σ. This inverse problem is rather cumbersome, since, at present, no analytic method is known for determining this set. But this set can of course be calculated by a computer. Using a sufficient large memory, the

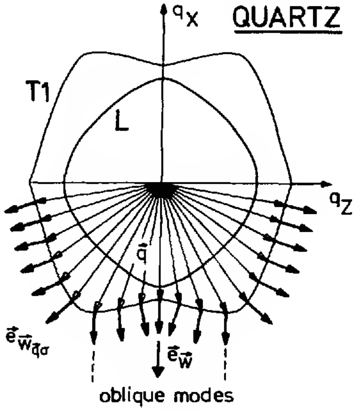

Fig. 9. Direction of group velocities for phonon states $|\vec{q},T1>$ in the q_Xq_Z-plane of quartz (compare with the corresponding cut in Fig. 5). This plane is a mirror plane for phonons and hence all group velocities lie in this plane

group velocities are evaluated for a fine net of discrete $\vec{q}$-vectors in advance. Comparing these group-velocity directions with $\vec{e}_{\vec{w}}$, one gets some solid angles in $\vec{q}$-space where the wanted $\vec{q}$-vectors may exist. By a systematic reduction of these solid angles in a sequence of intervals, the whole set can be determined.

All the $\vec{q}$-vectors contributing to group velocities in a prescribed direction $\vec{e}_{\vec{w}}$ can be visualized in a qualitative way by shining from the observer in $-\vec{e}_{\vec{w}}$-direction a parallel light beam onto a specularly reflecting model of a frequency surface (like those of Fig. 5) and observing the spots at the frequency surface which reflect back to the observer. By turning around the model, all $\vec{e}_{\vec{w}}$-directions can be investigated after each other.

Now, we proceed to the difficult question: how are the emitted phonons distributed over the regions marked in Fig. 8? Since all these phonons have crossed the interface between radiator (1) and crystal (0), we first ask for the chance for phonons in (1) to cross the interface. The following discussion is done with the help of Fig. 10. For this discussion, we assume in the radiator material a certain $\vec{q}$-space phonon distribution $f_\sigma(\omega)$ which depends only on frequency. Therefore, all $\vec{q}$-states between the frequency surfaces ω_σ and $\omega_\sigma + d\omega$ are occupied with the same probability. From these phonons, only those will meet ballistically the interface radiator/substrate which have a group velocity pointing towards that interface. Phonons which have crossed the interface can only be found in $\vec{q}$-states having a group velocity pointing away from the interface. Hence, we have a $\vec{q}$-space source distribution in the substrate near the interface consisting of totally unoccupied and somehow occupied states. Knowing this source distribution, one can calculate the momentary phonon distribution in the crystal at each time after emission and also the most interesting time-dependent irradiation of the detector area [13]. Experiments [14,15] are in excellent accordance with these calculations.

The simple but fundamental case of an incoherent point source located in the substrate and having an isotropic source distributions, was investigated in great detail [11]. The calculated phonon-intensity characteristics for quartz are shown

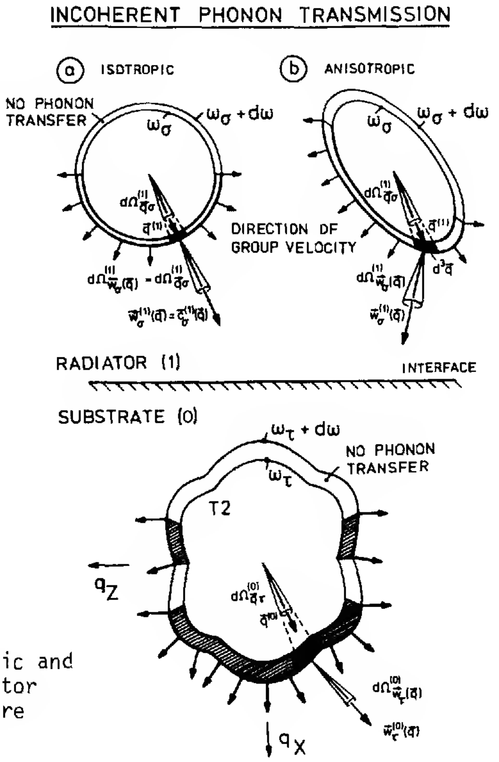
INCOHERENT PHONON TRANSMISSION
ⓐ ISOTROPIC
ⓑ ANISOTROPIC
NO PHONON TRANSFER
ω_σ
$\omega_\sigma + d\omega$
$d\Omega^{(1)}_{\vec{q}\sigma}$
$\vec{q}^{(1)}$
DIRECTION OF GROUP VELOCITY
$d\Omega^{(1)}_{\vec{w}_\sigma}(\vec{q}) \cdot d\Omega^{(1)}_{\vec{q}\sigma}$
$\vec{w}^{(1)}_\sigma(\vec{q}) = \vec{\xi}^{(1)}_\sigma(\vec{q})$
$d^3\vec{q}$
$d\Omega^{(1)}_{\vec{w}_\sigma}(\vec{q})$
$\vec{w}^{(1)}_\sigma(\vec{q})$
RADIATOR (1)
INTERFACE
SUBSTRATE (0)
$\omega_\tau + d\omega$
ω_τ
NO PHONON TRANSFER
T2
q_Z
$d\Omega^{(0)}_{\vec{q}\tau}$
$\vec{q}^{(0)}$
$d\Omega^{(0)}_{\vec{w}_\tau}(\vec{q})$
$\vec{w}^{(0)}_\tau(\vec{q})$
q_X

Fig. 10. Phonon emission from a) an isotropic and b) an anisotropic incoherent radiator into an X-cut quartz substrate where only the T2-phonons are shown with their frequency surfaces

in Fig. 11. These rather anisotropic radiation characteristics were verified experimentally [16]. Such an angular dependent enhancement of intensity is called 'phonon focusing' and was first explained by Taylor et al. [17]. The physical ground is the change of curvature of the frequency surfaces with direction: for example, the frequency surfacesT2 of quartz in Fig. 10 show parts which are nearly flat and hence give rise to a phonon enhancement in the corresponding group-velocity direction whereas other very convex regions give rise to a strong reduction of phonon flow in comparison to the flow in an isotropic solid with its constant curvature. Since phonon focusing is associated with the propagation of incoherent phonons in the bulk of the crystal but not directly with the phonon transfer across an interface, we will not discuss further this very interesting phenomenon. A recent review article on phonon focusing was written by Maris [18].

We return to the interface problem of Fig. 10 and ask for a quantitative description of the $\vec{q}$-space source distribution in the crystal near the interface. This problem can be solved [19,7], if the two materials and their relative orientation are known as well as the phonon distribution in the radiator. Furthermore, one needs an expression for the phonon-transfer probabilities $t_{\sigma\tau}^{(10)}(\vec{q}^{(1)})$ for incident phonons $|\vec{q}^{(1)},\sigma>$ in medium (1) into phonons of polarization τ in medium (0). The remaining sections of this paper are devoted to this phonon scattering problem. The phonon-transitions probabilities must be calculated for each incident phonon and thereafter all transmitted phonons can be superposed to give the $\vec{q}$-space distribution looked for. This procedure has been done for various material combinations [19] using continuum acoustics. Fig. 12 shows the result for X-cut quartz excited by an isotropic constantan radiator. The direction dependent $\vec{q}$-space phonon number is given in a normalized form,

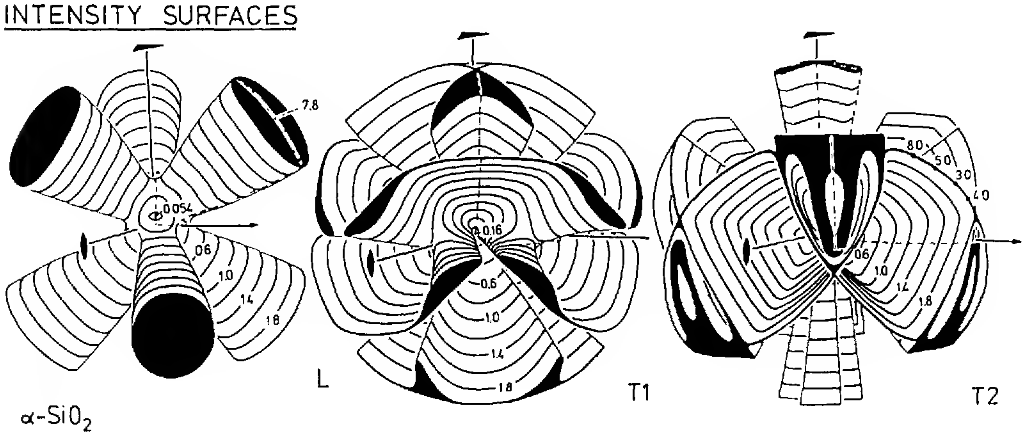

Fig. 11. Intensity surfaces for an incoherent point source with isotropic $\vec{q}$-space source distribution in quartz within the validity of continuum acoustics. The intensities (= power per solid angle) are normalized to an isotropic $\vec{r}$-space emitter of the same power (according to [11]). The intensity peaks are cut away for clarity.

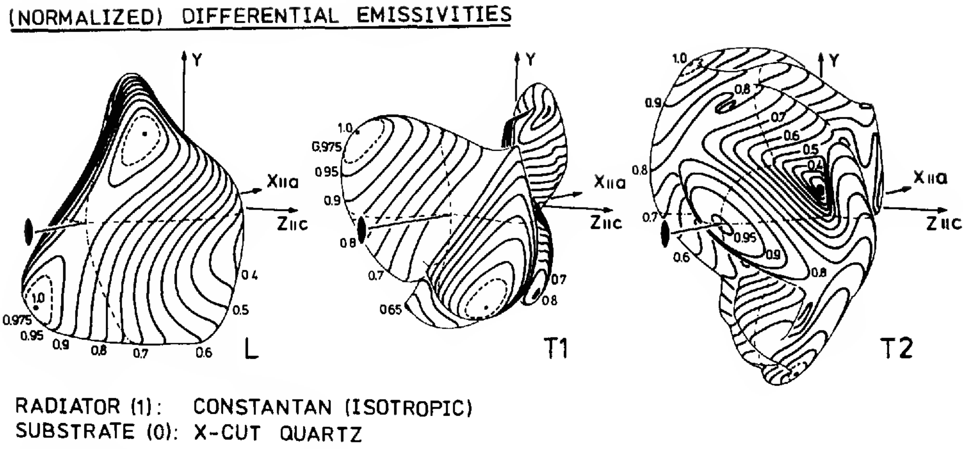

Fig. 12. Calculated differential emissivities in X-cut quartz excited by a constantan radiator (according to [19]). These directional characteristics have a radius vector proportional to the number of phonons in $\vec{q}$-space between two frequency surfaces ω_σ and $\omega_\sigma + d\omega$.

where 1.0 represents the highest value for each polarization. The deviation from an isotropic source distribution or from the cosine law of a Lambert radiator is evident.

4. Phonon scattering at plane interfaces and surfaces within continuum acoustics

We start the discussion of phonon scattering at plane interfaces by considering the reflection, refraction and mode conversion of a plane incident sound wave falling from medium (1) onto the interface [7]. The ratio of the Poynting-vector component normal to the interface of a generated wavemode τ to the same component of the incident wave σ is called

power-reflection coefficient $$r^{(11)}_{\sigma\tau} \equiv \vec{e}_\perp \cdot \overline{\vec{S}^{(1)}_\tau(\vec{r},t)}^{\,t} / (-\vec{e}_\perp \cdot \overline{\vec{S}^{(1)}_\sigma(\vec{r},t)}^{\,t}) \tag{4.1a}$$

or

power-transmission coefficient $$t^{(10)}_{\sigma\tau} \equiv -\vec{e}_\perp \cdot \overline{\vec{S}^{(0)}_\tau(\vec{r},t)}^{\,t} / (-\vec{e}_\perp \cdot \overline{\vec{S}^{(1)}_\sigma(\vec{r},t)}^{\,t}) \;, \tag{4.2a}$$

where $\vec{e}_\perp$ denotes the unit vector perpendicular to the interface pointing into medium (1).

According to conservation of energy, we expect the relation

$$\sum_\tau r^{(11)}_{\sigma\tau} + \sum_\tau t^{(10)}_{\sigma\tau} = 1 \;. \tag{4.3}$$

Since these plane sound waves consist of phonons of the same frequency ω and since phonons do not split up at the interface, we have to interpret (4.1) and (4.2) as

$$\text{phonon-reflection probability} \qquad r_{\sigma\tau}^{(11)} \equiv t_{\sigma\tau}^{(11)} \quad \text{and} \tag{4.1b}$$

$$\text{phonon-transmission probability} \qquad t_{\sigma\tau}^{(10)} \quad , \tag{4.2b}$$

where conversion in polarization of phonons is included. This treatment of phonon scattering at interfaces within continuum acoustics is called 'acoustic mismatch model'. It was first used by Khalatnikov [20] for calculating phonon transfer from an isotropic solid to superfluid helium and vice versa. Little [21] treated the phonon transfer across an interface between two isotropic solids and Weis [22] extended to phonon scattering at anisotropic/anisotropic interfaces.

In order to determine the phonon-transfer probabilities from (4.1) and (4.2) we use for the incident plane wave the displacement field (2.8) but add the superscript (1) to denote the medium. The wave vector can be split in a component parallel and perpendicular to the interface

$$\vec{q}_{\sigma}^{(1)} = \vec{q}_{\parallel} + q_{\sigma\perp}^{(1)} \cdot \vec{e}_{\perp} \; , \qquad\qquad \vec{q}_{\parallel} = q_{\parallel} \cdot \vec{e}_{\parallel} \; ,$$

where $\vec{e}_{\parallel}$ is the unit vector of the 'trace' which is common to the plane of incidence and to the interface. The (real) displacement field of the incident wave is therefore

$$\vec{s}_{\sigma}^{(1)}(\vec{r},t) = \vec{e}_{\sigma}^{(1)} \cdot \hat{s}_{\sigma}^{(1)} \cdot e^{i(-\vec{q}_{\parallel}\cdot\vec{r} + \omega\cdot t)} \cdot e^{-i\cdot q_{\sigma\perp}\cdot r_{\perp}} + \text{c.c.} \tag{4.4}$$

with $r_{\perp} \equiv \vec{r}_{\perp}\cdot\vec{e}$. The associated stress field

$$\overset{\rightrightarrows}{\sigma} = {}^{4}\vec{c} : \overset{\rightrightarrows}{\varepsilon} = {}^{4}\vec{c} : \left[(\partial s_i/\partial x_K + \partial s_K/\partial x_i)/2\right] \tag{4.5}$$

reads by introducing (4.2)

$$\overset{\rightrightarrows}{\sigma}_{\sigma}^{(1)}(\vec{r},t) = -i\cdot {}^{4}\vec{c}^{(1)} : \vec{q}_{\sigma}^{(1)} \vec{e}_{\sigma}^{(1)} \cdot \hat{s}_{\sigma}^{(1)} \cdot e^{i\cdot(-\vec{q}_{\parallel}\cdot\vec{r} + \omega\cdot t)} \cdot e^{-i\cdot q_{\sigma\perp}\cdot r_{\perp}} + \text{c.c.} \quad . \tag{4.6}$$

This incident wave causes a field at the plane boundary ($r_{\perp} = 0$) which can be taken from (4.4) and (4.6) by setting $r_{\perp} = 0$. The remaining twodimensional trace field is time- and space-dependent and is the cause for all excited wavemodes which must have therefore the same trace field. Hence, the displacement and stress field of the excited wavemodes of polarization τ in medium (K) = (0) or (1) can be written

$$\vec{s}_{\tau}^{(K)}(\vec{r},t) = \vec{e}_{\tau}^{(K)} \cdot \hat{s}_{\tau}^{(K)} \cdot e^{i\cdot(\vec{q}_{\parallel}\cdot\vec{r} + \omega\cdot t)} \cdot e^{-i\cdot q_{\tau\perp}^{(K)}\cdot r_{\perp}} + \text{c.c.} \; , \tag{4.7}$$

$$\overset{\rightrightarrows}{\sigma}_{\tau}^{(K)}(\vec{r},t) = -i\cdot {}^{4}\vec{c}^{(K)} : \vec{q}_{\tau}^{(K)} \vec{e}_{\tau}^{(K)} \cdot \hat{s}_{\tau}^{(K)} \cdot e^{i\cdot(\vec{q}_{\parallel}\cdot\vec{r} + \omega\cdot t)} \cdot e^{-i\cdot q_{\tau\perp}^{(K)} r_{\perp}} + \text{c.c.} \quad . \tag{4.8}$$

where the polarization vector may be complex in order to allow elliptic polarization

$$\vec{e}_{\tau}^{\,(K)} \equiv \vec{e}_{\tau}^{\,\prime(K)} + i\cdot\vec{e}_{\tau}^{\,\prime\prime(K)} \quad . \tag{4.9}$$

Inserting (4.7) in the wave equation of continuum acoustics yields the homogeneous vector equation

$$\{(\vec{q}_{\parallel} + q_{\tau\perp}^{(K)}\cdot\vec{e}_{\perp})\cdot{}^{4}\vec{c}^{\,(K)}\cdot(\vec{q}_{\parallel} + q_{\tau\perp}^{(K)}\cdot\vec{e}_{\perp}) - \omega^{2}\cdot\rho^{(K)}\cdot\overset{\rightrightarrows}{e}\}\cdot(\vec{e}_{\tau}^{\,\prime(K)} + i\cdot\vec{e}_{\tau}^{\,\prime\prime(K)}) = 0 \tag{4.10}$$

or after division by ω^2

$$\{(g\cdot\vec{e}_{\parallel} + h_{\tau}^{(K)}\cdot\vec{e}_{\perp})\cdot{}^{4}\vec{c}^{\,(K)}\cdot(g\cdot\vec{e}_{\parallel} + h_{\tau}^{(K)}\cdot\vec{e}_{\perp}) - \rho^{(K)}\cdot\overset{\rightrightarrows}{e}\}\cdot(\vec{e}_{\tau}^{\,\prime(K)} + i\cdot\vec{e}_{\tau}^{\,\prime\prime(K)}) = 0, \tag{4.11}$$

where

$$g \equiv q_{\parallel}/\omega = 1/c \ , \qquad h_{\tau}^{(K)} \equiv q_{\tau\perp}^{(K)}/\omega \tag{4.12}$$

and c denotes the 'trace velocity'.

Nontrivial solution of (4.11) exist only if the coefficient determinant is zero which leads to a secular equation of sixth degrees in $h_{\tau}^{(K)}$ with real coefficients. Therefore, the six roots $\tau = 1,2,..,6$ may be real or may appear as conjugate complex pairs. According to (4.12) and (4.7) we get a plane wave for a real $h_{\tau}^{(K)}$ and exponentially decaying or rising fields for a complex root. But only three of these six solutions can be excited in each halfspace by the incident wave since the excited waves must have a group velocity pointing away from the interface and the excited exponential waves must decay, i.e. represent nearfields. The excited plane waves can easily be visualized in $\vec{q}$-space using a cut parallel to the plane of incidence. Examples are given for the reflected waves in an isotropic medium in Fig. 13 and for an anisotropic medium in Fig. 14. The phonon scattering at a crystal/crystal inter-

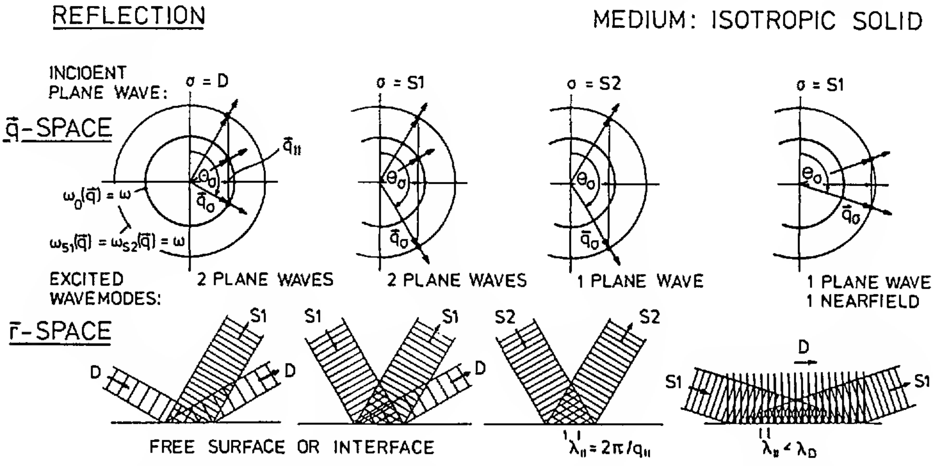

Fig. 13. Geometric illustration of generated wavemodes due to plane wave excitation of a plane boundary in an isotropic solid.

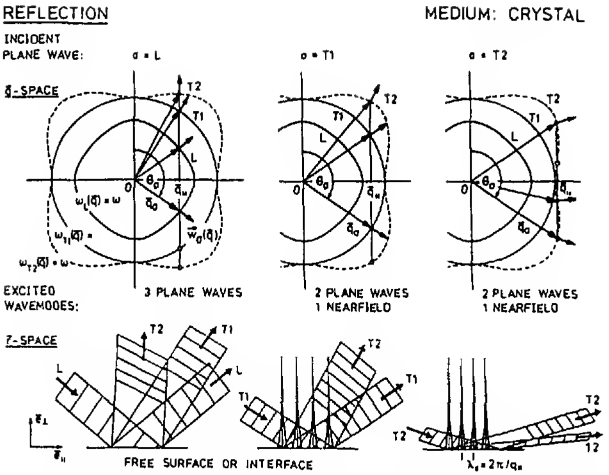

Fig. 14. Geometric illustration of generated wavemodes due to plane wave excitation of a plane boundary in an anisotropic solid. A mirror plane is chosen as plane of incidence which implies that all group velocities lie in the plane of incidence. The three incident waves differ only in polarization, whereas frequency and wavenormal are unchanged.

face is outlined in Fig. 15. The incident plane wave with wave vector $\vec{q}_\sigma$ produces at the plane boundary a trace field governed by the wave vector $\vec{q}_{\parallel}$ which is common to all excited waves. This property allows to deduce geometrically all possible generated plane waves by considering in $\vec{q}$-space the cut between the plane of incidence and all frequency surfaces having the same frequency as the incident wave. We take from these cuts the angle of reflection $\Theta_\tau^{(1)}$ of an excited plane wave of polarization τ in (1) as well as the angle of transmission $\Theta_\tau^{(0)}$ of an excited plane wave of polarization τ in (0). They are connected with $q_{\parallel}$ or q_σ and Θ_σ of the incident wave, respectively, by

$$q_{\parallel} = q_\sigma\cdot\sin\Theta_\sigma = q_\tau^{(1)}\cdot\sin\Theta_\tau^{(1)} = q_\tau^{(0)}\cdot\sin\Theta_\tau^{(0)} . \tag{4.13}$$

which is Snell's law for anisotropic media, if we divide by ω:

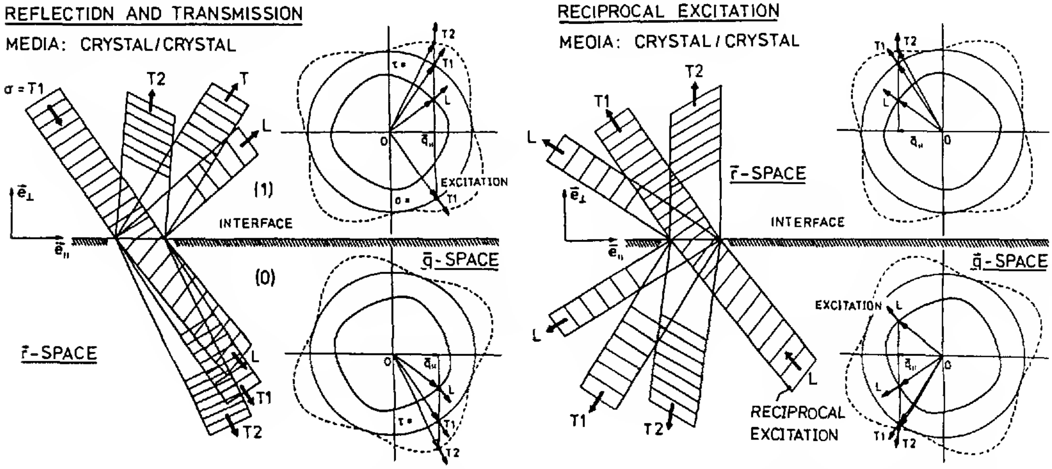

Fig. 15. Geometric illustration of generated wavemodes due to plane wave excitation of an interface between two anisotropic solids. In order to make the diagrams as simple as possible, we use a plane interface between identical, but rotated crystals ('grain boundary') and choose in addition a mirror plane as plane of incidence

$$1/c = \sin\Theta_\sigma / c_\sigma(\vec{e}_{n\sigma}^{\,(1)}) = \sin\Theta_\tau^{(1)} / c_\tau(\vec{e}_{n\tau}^{\,(1)}) = \sin\Theta_\tau^{(0)} / c_\tau(\vec{e}_{n\tau}^{\,(0)}) \; . \tag{4.14}$$

If $q_\parallel$ is too large to allow an excitation of a plane longitudinal wave, a corresponding exponential nearfield occurs as solution (see Fig. 13 and Fig. 14). Rising further the magnitude of $q_\parallel$, the emission of plane T1-waves stops and again a corresponding nearfield occurs. It is interesting to note that under certain circumstances (see Fig. 14) this second nearfield can be replaced by a second plane T2-wave.

The group-velocity directions are indicated in the $\vec{q}$-space cuts by short arrows normal to the frequency surfaces for each plane wave involved in the scattering problem. These directions occur in $\vec{r}$-space as propagation direction of sound beams, whereas each wave-front pattern is perpendicular to the $\vec{q}$-vector.

The wave amplitudes and hence the transition probabilities of the scattered phonons cannot be taken from these pure geometrical considerations. They must be calculated by fulfilling the boundary conditions of continuum acoustics which demand continuity of the displacement-vector field and of the stress-vector field across the interface $r_\perp = 0$. According to (4.4) and (4.7) we get for the displacement field

$$\vec{e}_\sigma^{\,(1)} \cdot \hat{s}_\sigma^{(1)} + \sum_{\tau=1}^{3} \vec{e}_\tau^{\,(1)} \cdot \hat{s}_\tau^{(1)} = \sum_{\tau=1}^{3} \vec{e}_\tau^{\,(0)} \cdot \hat{s}_\tau^{(0)} \tag{4.15}$$

and for the stress-vector field $\vec{\vec{\sigma}} \cdot \vec{e}_\perp$ according to (4.6) and (4.8)

$$\vec{e}_\perp \cdot {}^4\vec{c}^{\,(1)} : \vec{q}_\sigma^{\,(1)} \vec{e}_\sigma^{\,(1)} \cdot \hat{s}_\sigma^{(1)} + \sum_{\tau=1}^{3} \vec{e}_\perp \cdot {}^4\vec{c}^{\,(1)} : \vec{q}_\tau^{\,(1)} \vec{e}_\tau^{\,(1)} \cdot \hat{s}_\tau^{(1)} = \sum_{\tau=1}^{3} \vec{e}_\perp \cdot {}^4\vec{c}^{\,(0)} : \vec{q}_\tau^{\,(0)} \vec{e}_\tau^{\,(0)} \cdot \hat{s}_\tau^{(0)} \, . \tag{4.16}$$

These six scalar equations (4.15) and (4.16) represent an inhomogeneous system of equations from which the six unknown amplitudes $\{\hat{s}_\tau^{(\;)}\}$ can be computed numerically. Using these amplitudes, one gets from (4.1) and (4.2) the desired phonon transition probabilities.

Furthermore, there exist general relations which can be proofed analytically [7]:

- the phonon-transfer probabilities vanish, if τ represents a nearfield
- the sum over all transition probabilities is equal one as was expressed in (4.3)
- the following theorem of reciprocity holds (K,L = 0 or 1)

$$t_{\tau\sigma}^{(KL)}(-\vec{e}_{n\tau}^{\,(K)}) = t_{\sigma\tau}^{(LK)}(\vec{e}_{n\sigma}^{\,(L)}) \; , \tag{4.16}$$

expressing the fact, that we have the same phonon-transition probability for the direct transition and for the reversed transition where generator and detector are interchanged as well as polarizations. This is illustrated in Fig. 15 for the transition probabilities $t_{LT1}^{(01)}(-\vec{e}_{nL}^{\,(0)}) = t_{T1L}^{(10)}(\vec{e}_{nT1}^{\,(1)})$.

Of course, interfaces between simpler materials like isotropic solids, fluids and the reflection at a free surface are special cases and included in the above treatment. Medium (1) is vacuum for a free surface, i.e. the right side of (4.16) is zero and (4.15) is not needed since there is no restriction to the surface displacement.

There remains only to solve the following three scalar equations where we have dropped the superfluent superscript (1)

$$\vec{e}_{\perp}\cdot {}^{4}\vec{c}:\vec{q}_{\sigma}\vec{e}_{\sigma}\cdot\hat{s}_{\sigma} + \sum_{\tau=1}^{3} \vec{e}_{\perp}\cdot {}^{4}\vec{c}:\vec{q}_{\tau}\vec{e}_{\tau}\cdot\hat{s}_{\tau} = 0. \tag{4.17}$$

5. Phonon scattering at plane interfaces and surfaces within lattice dynamics

Going over to plane lattice waves, we have to remember that a crystal with s atoms per elementary cell possesses 3s phonon bands which can be represented by frequency surfaces in 3s Brillouin zones. As an example, Fig. 16 shows a $\vec{q}$-space cut through the six bands of a crystal with s=2 atoms per elementary cell. Only the contours of the frequency surfaces $\omega_{\sigma}(\vec{q}) = \omega$ are drawn. The frequency ω of the incident plane lattice wave of polarization σ = T1A is chosen high enough in order to allow in the given phonon-band structure a generation of acoustic waves as well as optical lattice waves. As in continuum acoustics, the trace field of the incident wave is the source field for all excited wavemodes which are all characterized by the transverse wave vector $q_{\parallel}$. Again, the whole set of outgoing plane lattice waves can be determined by pure geometric construction in $\vec{q}$-space. We find two emerging LA-waves, one T1A- and two T2O-waves. In the excited LA-wave, the wave vector $\vec{q}$ comes out to be nearly antiparallel to the group velocity.

The question, how many wavemodes can be excited by an incident plane lattice wave, was answered by Feuchtwang [23], who investigated in two important papers the reconstruction of the surface layer of a semi-infinite crystal and the reflection of an

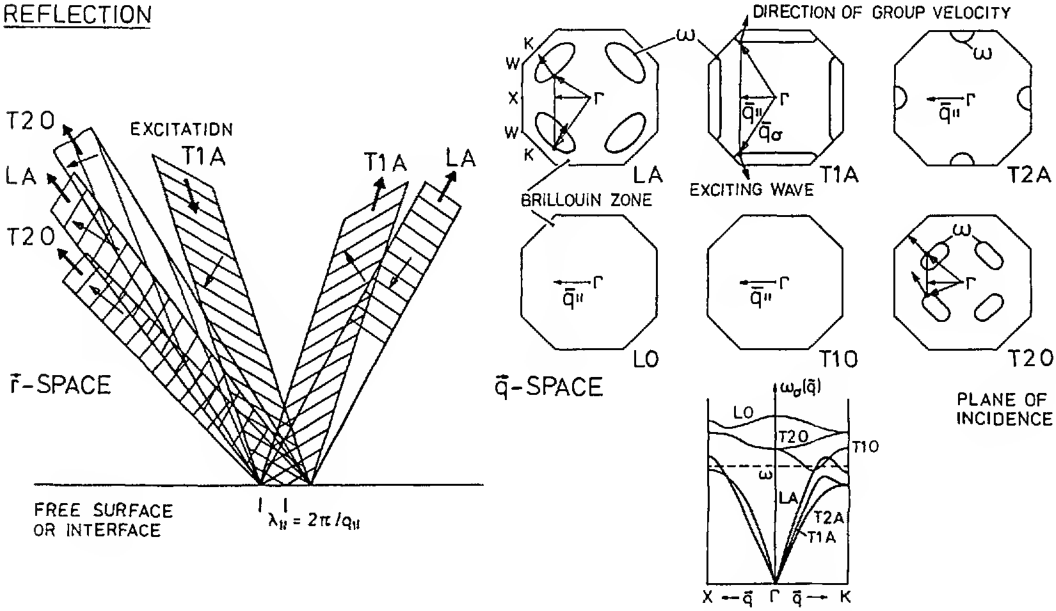

Fig. 16. Geometric illustration of generated wavemodes due to plane wave excitation of a plane boundary in lattice dynamics

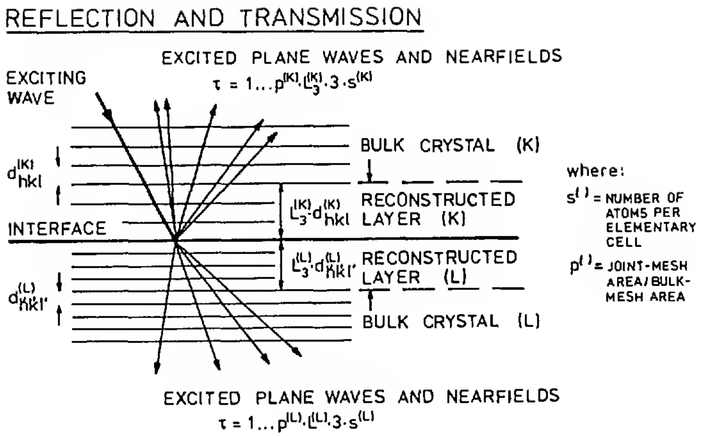
REFLECTION AND TRANSMISSION
EXCITED PLANE WAVES AND NEARFIELDS
$\tau = 1 \ldots p^{(K)} \cdot L_3^{(K)} \cdot 3 \cdot s^{(K)}$
EXCITING WAVE
$d_{hkl}^{(K)}$
BULK CRYSTAL (K)
$L_3^{(K)} \cdot d_{hkl}^{(K)}$
RECONSTRUCTED LAYER (K)
INTERFACE
$L_3^{(L)} \cdot d_{h'k'l'}^{(L)}$
RECONSTRUCTED LAYER (L)
$d_{h'k'l'}^{(L)}$
BULK CRYSTAL (L)
EXCITED PLANE WAVES AND NEARFIELDS
$\tau = 1 \ldots p^{(L)} \cdot L_3^{(L)} \cdot 3 \cdot s^{(L)}$
where:
$s^{(\,)}$ = NUMBER OF ATOMS PER ELEMENTARY CELL
$p^{(\,)}$ = JOINT-MESH AREA/BULK-MESH AREA

Fig. 17. Excited wavemodes at a reconstructed interface within the Born-Kārmān model

incident plane lattice wave at such a free surface. With the help of Fig. 17 we extend his discussion immediately to the phonon transitions at a plane interface between two semi-infinite crystals. In any case, the interface is parallel to a lattice plane (hkl) in the upper crystal (K) and also parallel to a lattice plane (h'k'l') in the lower crystal (L). If these lattice planes are important planes, Miller's indices will be small integers. The associated basis vectors $\vec{a}_1^{(\,)}$, $\vec{a}_2^{(\,)}$ and $\vec{a}_3^{(\,)}$ of the elementary cell of the bulk are chosen in the following manner: $\vec{a}_1^{(\,)}$ and $\vec{a}_2^{(\,)}$ are always parallel to the interface whereas $\vec{a}_3^{(\,)}$ points away from the interface and has a component in normal direction being just the distance d_{hkl} and $d_{h'k'l'}$ between the lattice planes parallel to the interface.

We assume a common twodimensional periodicity parallel to the interface, characterized by the two basis vectors

$$\vec{a}_1 \equiv N_1^{(K)} \cdot \vec{a}_1^{(K)} = N_1^{(L)} \cdot \vec{a}_1^{(L)}, \qquad \vec{a}_2 \equiv N_2^{(K)} \cdot \vec{a}_2^{(K)} = N_2^{(L)} \cdot \vec{a}_2^{(L)}, \tag{5.1}$$

where the $N_1^{(\,)}$, $N_2^{(\,)}$ should be small integers. Hence, the joint-mesh area $\vec{a}_1 \times \vec{a}_2$ of both lattices contains $p^{(\,)} = N_1^{(\,)} \cdot N_2^{(\,)}$ bulk-mesh areas $\vec{a}_1^{(\,)} \times \vec{a}_2^{(\,)}$ and the new unit cells contain $p^{(\,)} \cdot s^{(\,)}$ atoms.

If we assume force constants with an interaction ranging in $\vec{a}_3^{(\,)}$-direction over $L_3^{(\,)}$ elementary cells, the reconstructed layer can be taken to have the same thickness. In this case, one can deduce from the investigations of Feuchtwang that just

$$p^{(\,)} \cdot L_3^{(\,)} \cdot 3 \cdot s^{(\,)} \quad \text{wavemodes} \tag{5.2}$$

are connected with a trace field of a given $\vec{q}_{\parallel}$. Of course, most of these wavemodes are nearfields and only a few represent outgoing plane lattice waves. In continuum acoustics we found three excited wavemodes in each halfspace. This number ist only achieved in lattice dynamics for perfect lattice match ($p^{(\,)} = 1$), next-neighbour interaction ($L_3^{(\,)} = 1$) and a Bravais-type structure ($s^{(\,)} = 1$).

QUASI-PARTICLE INTERACTION AND ANOMALIES IN THE EXCITATION SPECTRA OF METALS

H. Eschrig *)
Zentralinstitut fuer Festkoerperphysik und Werkstoffforschung der AdW der DDR, DDR-8027 Dresden, GDR

M. I. Kaganov *)
Institute of Physical Problems, Academy of Sciences of USSR, Moscow

The low-energy excitation spectrum of a paramagnetic metal in the absence of an external magnetic field consists of phonons filling the whole quasi-momentum space and of electrons in a thin layer around the Fermi surface. The interaction of these quasi-particles results in a renormalization of the energies and in a finite lifetime. The renormalization contains a variety of anomalies - divergencies of the spectra or its derivatives, the group velocities - in which the local geometry of the Fermi surface manifests. The divergencies are cut off due to various damping processes, it is however to be expected that peaks remain some of which being experimentally detected. The phenomena discussed are general, i.e. to be expected present in any metal. The given treatment continues the semi-phenomenological theory of metals developed by I. M. Lifshits and his school.

1. Quasi-particles

The excitation spectrum of condensed matter is usually described as a quasi-particle spectrum (though such a picture is not universal). Quasi-particles are quasi-stationary excitations: if the system at time t=0 was excited from the quantum state $|\Psi\rangle$ into the state $\hat{\Phi}^{+}(0)|\Psi\rangle$, then, at t>0, it may be found in the same propagated state $\hat{\Phi}^{+}(t)|\Psi\rangle$ with a quantum mechanical probability

---

*) Essential parts of this paper were prepared during a stay of both authors at the International Laboratory of High Magnetic Fields and Low Temperatures, Wroclaw, in 1986.

$$w_\alpha(t) = |\langle\Psi|\hat{\Phi}_\alpha(t) \quad \hat{\Phi}^+_\alpha(0)|\Psi\rangle|^2 , \qquad t>0 . \tag{1.1a}$$

The propagation of "hole type excitations" from t<0 to t=0 is likewise described by

$$w_\alpha(t) = |\langle\Psi|\hat{\Phi}^+_\alpha(0) \quad \hat{\Phi}_\alpha(t)|\Psi\rangle|^2 , \qquad t<0 . \tag{1.1b}$$

Both types are combined into

$$w_\alpha(t) = |G_\alpha(t)|^2 ,$$

$$G_\alpha(t) = -i\langle\Psi|T\hat{\Phi}_\alpha(t)\hat{\Phi}^+_\alpha(0)|\Psi\rangle , \tag{1.2}$$

where T is Dyson's (Wick's) time ordering operator for bosons (fermions). A quasi-particle with energy ξ_α and lifetime τ_α was created if the Green function $G_\alpha(t)$ contains a term

$$G_\alpha(t) = \mp i Z_\alpha \, e^{i\xi_\alpha t/\hbar} \, e^{-|t|/\tau_\alpha} + \ldots \equiv \mp i Z_\alpha \, e^{\pm i(\varepsilon_\alpha-\mu)t/\hbar} + \ldots , \tag{1.3}$$

where ε_α is the complex quasi-particle energy, and

$$\xi_\alpha = \pm(\mathrm{Re}\,\varepsilon_\alpha - \mu) \quad \text{for} \quad \begin{matrix}\text{particles}\\ \text{holes}\end{matrix} , \tag{1.4}$$

$$\tau_\alpha = -\frac{\hbar}{\mathrm{Im}\,\varepsilon_\alpha}\,\mathrm{sign}(\mathrm{Re}\,\varepsilon_\alpha - \mu) . \tag{1.5}$$

The Fourier transform of the Green function then contains a term

$$G_\alpha(\omega) = \frac{\hbar}{\omega - \varepsilon_\alpha + \mu} + \ldots , \tag{1.6}$$

and the equation

$$G^{-1}_\alpha(\varepsilon_\alpha - \mu) = 0 \tag{1.7}$$

determines the complex quasi-particle energy.

Once the various types of quasi-particles and their gross characteristics are known one tries to find a model Hamiltonian

$$\hat{H} = \sum_\alpha (\varepsilon^{(0)}_\alpha - \mu)\hat{a}^+_\alpha \hat{a}_\alpha + \hat{H}_{int} = \hat{H}_0 + \hat{H}_{int} \tag{1.8}$$

which is capable of reproducing that quasi-particle spectrum within the frame of perturbation theory (see [1] for details):

$$\hat{G}^{(0)}(\omega) = \hbar(\omega - \hat{H}_0)^{-1} , \qquad (1.9)$$

$$\hat{G}^{(0)}(\omega)^{-1} - \hat{G}(\omega)^{-1} \equiv \hat{\Sigma}(\omega)/\hbar , \qquad (1.10)$$

$$\hat{G}(\omega) = \hat{G}^{(0)}(\omega) + \hat{G}^{(0)}(\omega) \frac{\hat{\Sigma}}{\hbar} \hat{G}^{(0)}(\omega) + \dots , \qquad (1.11)$$

$$G_\alpha(\omega) \quad \frac{\hbar}{\omega - \varepsilon_\alpha^{(0)} - \mu - \Sigma_{\alpha\alpha}(\omega)} , \qquad \varepsilon_\alpha = \varepsilon_\alpha^{(0)} + \Sigma_{\alpha\alpha}(\varepsilon_\alpha) . \qquad (1.12)$$

The connection between $\hat{\Sigma}$ and $\hat{H}_{int}$ depends on the form of the coupling terms contained in $\hat{H}_{int}$ (see below). It is important to note that the diagonalization of the Hamiltonian (1.8) makes little physical sense in any *realistic* model: it would yield the highly complicated stationary quantum states instead of the quasi-particles [2]. Hence the term H_{int} unavoidably appears in any realistic model Hamiltonian (it is especially necessary in order to have kinetics).

2. The excitation spectrum of a metal

The basic characteristics of a metal are the number of conduction electrons n and the number of ions n_i per volume, connected by the valency Z of the metal according to $n = Zn_i$. If the electrons are assumed free, then from n we get the Fermi momentum p_F, the Fermi energy ε_F, and the Fermi velocity v_F:

$$\begin{aligned} p_F &= (3\pi^2 n)^{1/3}\hbar = (3\pi^2 Z)^{1/3}\hbar/a , \\ \varepsilon_F &= p_F^2/2m , \quad v_F = p_F/m , \end{aligned} \qquad (2.1)$$

where $a^3 = 1/n_i$, and m is the free electron mass.

The ionic excitations are the phonons, in the simplest model propagating with the sound velocity $s = \omega/k$ (ω – frequency, k – wave number) and having three independent polarizations for each wave vector k. The number of modes must equal the number of degrees of freedom of the ions leading to the maximum wave number $k_m = (6\pi^2)^{1/3}/a$ corresponding to the Debye frequency ω_D or to the Debye temperature

$$\Theta = \hbar\omega_D = (6\pi^2)^{1/3}\hbar s/a . \qquad (2.2)$$

The metallic bond which keeps the ions near their equilibrium positions is mainly the result of a competition between Coulomb energy and kinetic energy of the electrons, so that $M\omega_D^2 a^2/2 \sim \varepsilon_F \sim e^2/a$, where M is the ion mass. From this estimate together with (2.1-2) we have immediately

$$\frac{s}{v_F} \sim \left(\frac{m}{M}\right)^{1/2} \ll 1\ , \qquad \frac{\Theta}{\varepsilon_F} \sim \left(\frac{m}{M}\right)^{1/2} \ll 1. \tag{2.3}$$

These estimates remain valid also in more realistic models and play a fundamental role in any theory of the metallic state, especially they allow for the application of perturbation theory to the adiabatic approximation [3]. The simple excitation spectrum (2.1-2) is shown in fig. 1a).

In a real metal the excitation spectrum is qualitatively different (fig. 1b). The phonon branches are curved and additional optical branches eventually appear. Depending on the direction of p, in the same crystal several values p_F or no p_F may appear due to the high anisotropy of the bandstructure even in monovalent metals. Besides the electrons and phonons there are of course other quasi-particles. The plasmons have comparatively high energies h_{pl} $_F$. If a magnetic field is applied then the electron motion changes qualitatively resuling in a discrete level quantization in two dimensions and allowing for the propagation of undamped modified photons which are called helicons, dopplerons, and so on, with energies Θ [4-6]. If the metal has a spin structure, magnons appear with characteristic energies $\lesssim\Theta_C$ (Curie temperature for ferromagnets) or $\lesssim\Theta_N$ (Neel temperature for antiferromagnets). Usually $\Theta_C, \Theta_N \ll \varepsilon_F$.

In the rest of this paper we are concerned with low energy excitations $\varepsilon \lesssim \Theta$ of non-magnetic metals in the absence of external fields. Then we are left with electrons and phonons having a spectrum of fig. 1b) and being described by a model Hamiltonian

$$\hat{H} = \sum_{\alpha p} \xi_\alpha(p)\ \hat{a}^+_{\alpha p}\hat{a}_{\alpha p} + \sum_{\nu k} \hbar\omega_\nu(k)\ \hat{b}^+_{\nu k}\hat{b}_{\nu k} + \hat{H}_{int}\ , \tag{2.4}$$

where $\hat{a}^+_{\alpha p}$, $\hat{a}_{\alpha p}$ create and annihilate electrons or holes in states $|\alpha p\rangle$ with spin index included in α, and $\hat{b}^+_{\nu k}$, $\hat{b}_{\nu k}$ create and annihilate phonons in states $|\nu k\rangle$. The changes of the spectra due to the transition into the superconducting state are small on the energy scale of fig. 1 and are unimportant for our considerations.

If the electron subsystem of the metal is perturbed out of equilibrium, then, after damping out the electric field accompanying the

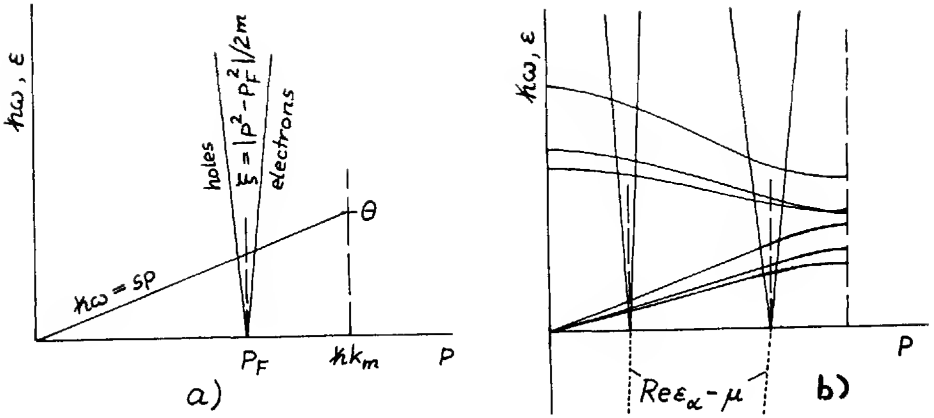

Fig. 1. The low-energy excitation spectrum of a metal; a) the simplest model, b) realistic case.

relaxation process, each k-component of the electron distribution function $f_k(p,t)$ vibrates with the frequency $\omega = k\cdot v(p)$ [7]. The degeneracy of the electron liquid singles out v_F of all velocities resulting in "quasi-waves" with

$$\omega = k\cdot v_F\ ,\qquad v_F = v(p_F)\ , \tag{2.5}$$

p_F being on the ordinary Fermi surface for a small perturbation. We shall come back to this later.

3. Interaction, renormalization, and anomalies

The interaction term $\hat H_{int}$ of (2.4) contains the Fermi liquid interaction $\hat H_{e-e}$ of the electrons and holes, the phonon-phonon interaction $\hat H_{ph-ph}$ due to the anharmonic ion-ion forces, and the electron-phonon interaction $\hat H_{e-ph}$:

$$\hat H_{e-e} = \sum_{1234} \Psi_{1,2;3,4}\,\hat a_1^+\hat a_2^+\hat a_3\hat a_4 + \dots\ , \tag{3.1}$$

$$\hat H_{ph-ph} = \sum_{123} \Phi_{1;2,3}\,\hat b_1^+\hat b_2\hat b_3 + h.c. + \dots\ , \tag{3.2}$$

$$\hat H_{e-ph} = \sum_{123} \Lambda^{I}_{1,2,3}\,\hat a_1^+\hat a_2\hat b_3 + \sum_{123} \Lambda^{II}_{1,2,3}\,\hat a_1^+\hat a_2\hat b_3^+ + \dots\ , \tag{3.3}$$

The summations run over all branches of the spectra and over all quasi-momenta (first Brillouin zone), the conservation law of quasi-momenta

$$p_1 = p_2 + p_3 + \hbar G \ , \ \dots \ , \qquad p_i = \hbar k_i \tag{3.4}$$

being contained in the interaction matrix elements $\mathfrak{A}\dots$, $\Phi\dots$, $\Lambda\dots$.

From the estimates of the previous section we have

$$v_F \sim \frac{\hbar}{a\,m} \ , \qquad s \sim \frac{\hbar}{a\sqrt{mM}} \ , \qquad \omega_D \sim s/a \ , \qquad a \sim \frac{\hbar^2}{e^2 m} \ , \tag{3.5}$$

which relations may be combined to

$$v_F \sim \frac{c}{\alpha} \ , \qquad s \sim \frac{c}{\alpha}\sqrt{\frac{m}{M}} \ , \qquad \Theta \sim \frac{mc^2}{\alpha^2}\sqrt{\frac{m}{M}}$$
$$\alpha = \frac{\hbar c}{e^2} \approx 137 \ , \qquad p_F \sim \frac{mc}{\alpha} \ . \tag{3.6}$$

Noticing for the operator of the atomic displacement

$$\hat{U}_i \sim \left(\frac{1}{M_i N}\,\frac{\hbar}{\omega_\nu(k)}\right)^{1/2} \frac{1}{2}\,(\hat{b}^+_{\nu k} + \hat{b}_{\nu k}) \ ,$$

where N is the number of unit cells (and therefore also the number of different quasi-momenta to be summed up), one may obtain [8]

$$\Phi\dots \sim \Theta\sqrt{\frac{\Theta}{Ms^2}} \ , \qquad \Lambda\dots \sim \sqrt{\Theta\epsilon_F} \ . \tag{3.7}$$

In addition to (3.7), the matrix elements depend on the quasi-momenta which dependence may essentially reduce them in the long-wavelength limit (e.g. $\Lambda\dots \sim ak$ [9], § 79).

While Φ contains the small parameter $(\Theta/Ms^2)^{1/2} \sim (\Theta/\varepsilon_F)^{1/2} \sim$ $\sim (m/M)^{1/4} \ll 1$, (3.1) and (3.3) do not contain formally a small parameter justifying a perturbation treatment. In practice, however, apart from the exceptions discussed below these interactions effectively also prove to be small due to the large mass difference between electrons and ions. Thereby either T/ε_F (T – temperature) or ξ/ε_F appears as the small parameter, that is, essential is the degeneracy of the metal electron gas because of which the number of excited electrons and holes is always small thus keeping down the interaction energy.

The theoretical idealization of an infinite defectfree monocrystalline metal at T = 0 allows for the study of the intrinsic damping mechanisms limiting the quasi-particle lifetimes $\tau_\alpha(p)$ due to their mutual interaction. Comparison to the lifetime due to defect scattering makes the quantitative definition of a "defectfree crystal" possible. Besides, the assumption that T = 0 appears natural in a study of properties of a single quasi-particle.

According to the philosophy sketched in section 1. $\xi_\alpha(p)$ and $\omega_\nu(k)$ of (2.4) are not the quasi-particle energies seen in experiment. The interaction contained in $\hat{H}_{int}$ leads to a renormalization $\delta\xi_\alpha$ and $\delta\omega_\nu$ of these energies and to a finite lifetime (imaginary part of $\delta\xi_\alpha$ and $\delta\omega_\nu$). Before discussing the effects of interaction, some remarks are necessary regarding the Hamiltonian (2.4). We remind you that $\xi_\alpha(p)$ is usually obtained by completely neglecting the ionic motion (bandstructure calculation). As a result it is a (manyvalued) analytic function of p on any analytic curve through the quasi-momentum space [10]. $\xi_\alpha(p)$ must therefore be renormalized with the full electron-phonon Hamiltonian (3.3) including the adiabatic (deformation potential) as well as nonadiabatic terms. Contrary, the phonon frequencies $\omega_\nu(k)$ are calculated including already all virtual adiabatic (without retartion) electron-phonon processes. Therefore, $\omega_\nu(k)$ is to be renormalized only with the non-adiabatic part of (3.3) removing mainly the infinite group velocities appearing (because retartion is neglected) on some places in the adiabatic spectra (see section 5). The lifetimes of both electrons and phonons on the other hand may in lowest order be calculated with the full Hamiltonian (3.3) because the adiabatic interaction results in a real effective ion-ion potential and has no lifetime effect. It may seem to be inconsistent to construct the Hamiltonian (2.4) in such a manner, but if one wants to use perturbation theory one is forced to do so because the adiabatic renormalization of the phonons is very strong, e.g. shifting the longitudinal acoustic branch at k = 0 from the ionic plasma frequency to zero [11]. Forgetting about this special character of (2.4) one may end up with completely wrong conclusions (see [11,12] for a comprehensive discussion).

Using the correction terms to the imaginary parts of $\varepsilon_\alpha(p)$ and $\omega_\nu(k)$ and obtaining from them the anomalies in the real parts of the dispersion relations with the help of generalized Kramers-Kronig relations we by-pass the problems discussed above. For a qualitative discussion, furthermore, the lowest perturbation order is sufficient. Thus we have with the same abbreviations as in (3.1-3)

$$\operatorname{Im}\,\delta\varepsilon_1 = -\pi\sum_{23} |M^3_{1,2}|^2 \,(1-n_2)\,\Delta_{1,-2,-3}\ ,$$

$$\operatorname{Im}\,\delta\omega_1 = -\frac{\pi}{\hbar}\sum_{23} |M^1_{2,3}|^2 \,(n_2-n_3)\,\Delta_{1,2,-3}\ , \tag{3.8}$$

$$\Delta_{1,2,3} \equiv (2\pi\hbar)^3\,\delta(p_1+p_2+p_3+\hbar G)\,\delta(\varepsilon_1+\varepsilon_2+\varepsilon_3)\ ,$$

where G must be chosen such that the quasi-momenta p_i are in the first Brillouin zone, and $\sum_1 \equiv \sum_{\alpha_1}\int d^3p_1/(2\pi\hbar)^3$. (The subscript -2, e.g., means $(-p_2, -\varepsilon_2)$.) The structure of M is

$$M^3_{1,2} = \sqrt{2}\,\Lambda^3_{1,2}\,|p_1 - p_2|/(\varrho\hbar\omega_3)^{1/2}\ , \tag{3.9}$$

where ϱ is the mass density of the metal, and $\Lambda^3_{1,2}$ goes over into the deformation potential as 2→1 and therefore is of the order of ε_F [13,14]. n_i is the Fermi step function, its appearence in (3.8) is connected with the use of ε instead of ξ which is convenient for geometrical interpretations.

The electron-electron and phonon-phonon interactions (3.1-2) of course also contribute to Im ε_1 and Im ω_1, however, we will not further consider them. In fact, for $|\varepsilon_1 - \varepsilon_F| < ms^2$ the electron-electron interaction dominates leading to a quadratic increase of Im ε_1 [13,14]:

$$\operatorname{Im}\,\varepsilon_1 \sim \varepsilon_F\left(\frac{\varepsilon_1-\varepsilon_F}{\varepsilon_F}\right)^2\ . \tag{3.10}$$

4. Anomalies in the electron-hole spectrum

The influence of electron-phonon interaction on the electron-hole spectrum was first investigated by Migdal [14] in the simple model of fig. 1a). In [13] the case of a general dispersion law is treated.

Besides the technical aspects discussed in the last section the physical consequence of renormalization due to interaction is a fine structure in the spectra well localized in momentum space at places determined by the Fermi surface. This allows to express the renormalization of Re ε as a Fermi surface integral [14] (cf. (3.8))

$$\operatorname{Re}\,\delta\varepsilon_1 = \sum_{\nu}\oint\frac{dS}{\bar{v}(\bar{p}^{E}_{F})}\,|M^{\nu}_{1,F}|^2\,\ln\left|\frac{\varepsilon_1-\varepsilon_F-\hbar\omega_\nu(p_1-p_F)}{\varepsilon_1-\varepsilon_F+\hbar\omega_\nu(p_1-p_F)}\right| \tag{4.1}$$

where the integral is over all sheets of the Fermi surface. From this we have

$$\mathrm{Re}\,\delta\varepsilon \sim \begin{cases} \varepsilon - \varepsilon_F & \\ (\varepsilon - \varepsilon_F)^{-1} & \end{cases} \quad \text{for } |\varepsilon - \varepsilon_F| \begin{matrix} \ll \\ \gg \end{matrix} \hbar\omega_D \,. \tag{4.2}$$

As was to be expected, renormalization takes essentially place in an interval $\Delta p \sim \hbar\omega_D/v_F \sim \sqrt{m/M}\,\hbar/a \sim ms$ where the relative change of the electron velocity is large (compared to $\sqrt{m/M}$). As was shown in [13] and will be discussed in the following, the transition from one dependence in (4.2) to the other goes necessarily through an anomaly if not through several ones.

Comming back to (3.8) we see that the δ-functions in combination with the factor $(1 - n_2)$ limit the p_2-integration to the parts of the surfaces

$$\varepsilon_{\alpha_1}(p_1) = \varepsilon_{\alpha_2}(p_2) + \hbar\omega_\nu(p_1 - p_2) \tag{4.3}$$

outside of the Fermi surface (i.e. in the electron region of ε_2). The surface (4.3) is near to the isoelectronic surface

$$\varepsilon_{\alpha_1}(p_1) = \varepsilon_{\alpha_2}(p_2) \;, \tag{4.4}$$

and if an acoustic branch ω_ν is considered it touches the latter in the point p_1 (fig. 2). It is easily seen that (3.8) leads in this case to the generalization of Migdal's result

$$\mathrm{Im}\;\delta\varepsilon_1 \approx \lambda(p_F)\;|\varepsilon_1 - \varepsilon_F|^3 \;, \qquad |\varepsilon_1 - \varepsilon_F| \ll \hbar\omega_D \;. \tag{4.5}$$

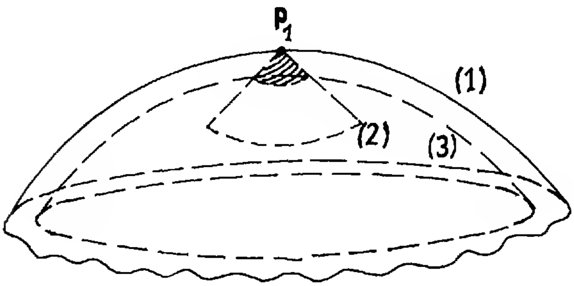

Fig. 2. Integration domain in (3.8) according to (4.3) for $|\varepsilon_2 - \varepsilon_1| \to 0$ (dashed surface). (1) – surface (4.4), (2) – surface (4.3), (3) – Fermi surface.

If, however, the Fermi surface contains a conical point p_F^c in which the Fermi velocity vanishes, then (4.5) is no longer valid. It may be seen that there is a small region around p_F^c where no damping due to electron-phonon interaction takes place. The reason for this "switching off" the damping is that an electron whose velocity is smaller than the sound velocity may not emit or absorb a phonon.

For $|\varepsilon_1 - \varepsilon_F| \gg \hbar\omega_D$ the surface (4.3) lies completely outside of the Fermi surface, and $\mathrm{Im}\,\delta\varepsilon_1$ saturates. Again the transition from the cubic law to saturation goes necessarily through anomalies. An unavoidable anomaly appears at $p = p_c$ when one surface (4.3) leaves the Fermi surface completely (fig. 3). The excitation spectra of electrons and phonons determine the locus of all points p_c around all sheets of the Fermi surface, a distance of about ms away from the latter. Near p_c, for $\varepsilon \lesssim \varepsilon_c \equiv \varepsilon_\alpha(p_c)$, the intersection line of the surface (4.3) with the Fermi surface is an ellipse, and the singular part (S) of $\mathrm{Im}\,\varepsilon$ may be calculated [13] to give

$$S\ \mathrm{Im}\,\delta\varepsilon = \begin{cases} \dfrac{\pi |M_c|^2}{v_c}\, m_c^*\, (\varepsilon_c - \varepsilon) & \qquad\qquad < \\ & \text{for} \qquad\quad {}_c \\ 0 & \qquad\qquad > \end{cases} \tag{4.6}$$

with $m_c^* \sim (mM)^{1/2}$ as a mass parameter. Physically the anomaly (4.6) is caused by dying out (or setting in) of a certain scattering process due to the Pauli principle.

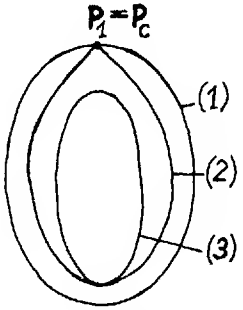

Fig. 3. The same surfaces as in fig. 2 for $p_1 = p_c$.

For each optical branch of the phonon spectrum at least two anomalies of the type (4.6) appear – when the surface (4.3) enters the fermi surface and when it leaves it. If the Fermi surface has humps or dips additional anomalies may appear. The same holds if the phonon spectrum contains several local maxima (or minima). Among them especially interesting are those corresponding to topological changes of the intersection line between the surface (4.3) and the Fermi surface. According to [13] an singular part at the corresponding point p_c'

$$S\ \mathrm{Im}\,\delta\varepsilon = K_c'\,\Delta \ln \frac{\varepsilon_F}{|\Delta|}\,, \qquad \Delta \equiv \varepsilon - \varepsilon_\alpha(p_c') \tag{4.8}$$

is obtained where the prefactor K_c' again contains a mass parameter.

As was already mentioned the anomalies of the real and imaginary parts of the dispersion relations are connected via generalized

Kramers-Kronig relations, especially:

Im	step of derivative	$\Delta \ln(\varepsilon_F/\lvert\Delta\rvert)$
Re	$\Delta \ln(\varepsilon_F/\lvert\Delta\rvert)$	step of derivative

In connection with this we see from (4.8) that the electron-hole spectrum Re unavoidably seems to contain anomalies of the type $\Delta \ln|\Delta|$ formally corresponding to an infinite group velocity $v = \partial\varepsilon/\partial p$ at p_c (even in cubic alkaline metals with a spherical Fermi surface there are saddlepoints in the phonon spectrum.) In the present case this is not connected with neglecting retartion effects but simply indicates the usual breakdown of perturbation theory at points where the perturbed quantity behaves non-analytically. As a rule, the setting in of the anomal dependence is, however, correctly described. In the present situation the reason for the infinity is that in the zero order (p) damping is neclected. Having this in mind we see from (4.5) that the logarithm is to be cut at $\ln(\varepsilon_F/\Theta) \sim \ln(M/m)$.

5. Anomalies in the phonon spectrum

Whereas the phonons may excite electrons only in a thin layer of thickness ms around the Fermi surface, the electrons interact with all phonons. Pecularities because of interaction may therefore appear at the most various places in quasi-momentum space [15].

In order not unnecessarily to sophisticate the analysis (see [16]) we simplify (3.8) taking into account the smallness of the phonon energies compared to ε_F:

$$\mathrm{Im}\ \delta\omega_\nu(\mathbf{q}) = \pi\omega_\nu(q)\sum_{\alpha\beta}^{--}\int d^3p\,|M^{\nu q}_{\alpha p,\beta p+q}|^2\,\delta(\varepsilon_\alpha(p)-\varepsilon_F)\,\delta(\varepsilon_\beta(p+\mathbf{q})-\varepsilon_F)\ , \tag{5.1}$$

where $q = \hbar k$ (in (3.8) we put $(n_2 - n_3) \approx \hbar\omega_1\delta(\varepsilon_2 - \varepsilon_F)$). As long as the Fermi surface and its copy shifted by $-q$ intersect ($q < 2p_F$ in the case of a Fermi sphere) the integral in (5.1) is non-zero, and as is well known [17,18],

$$\frac{\mathrm{Im}\ \delta\omega}{\omega} \sim \frac{s}{v_F} \sim \left(\frac{m}{M}\right)^{1/2} . \tag{5.2}$$

When two pieces of the Fermi surface leave each other (in dependence of q, in the case of a sphere this happens at $q_c = 2k_F$) the integral value of (5.1) behaves non-analytically resulting in the real part of the spectrum in a singularity of the type $\Delta \ln|\Delta|$, where Δ is the distance of q from the critical value q_c measured in the direction perpendicular to the Fermi surfaces ($\Delta = q - 2p_F$ in the spherical case – the Migdal-Kohn anomaly [14,19]). Depending on the dimensionality [20] or the local geometry [21] of the Fermi surface even stronger anomalies are possible. Physically these anomalies may be interpreted as a resonance interaction of the phonons with the accompanying screening cloud the Friedel oscillations in the assymptotics os which have just the wave-vector $q_c/\hbar$.

Of course, the phonon velocity again is not infinite: the finite electron lifetime leads to the cut-off of $\ln(\hbar/a|\Delta|)$ at $\ln(M/m)$ as long as q_c is large so that electrons with energies $\sim\hbar\omega_D$ above the Fermi level are involved (see (3.8)).

Again, if the Fermi surface has humps or dips or is open – more precisely if it has lines of parabolic points (where the gaussian curvature is zero) – additional anomalies appear at $q = q_c'$ where the intersection line of the Fermi surface with its shifted copy makes a topological change (Taylor anomalies [22]). Contrary to the previous case, where the Fermi surface normal and that of the shifted copy are generally antiparallel in the touching point, now they are parallel (if the Fermi surface consists of several sheets, the normals may be parallel also in the first case). A more distinguishing property of the Taylor anomalies is that their locus necessarily extents to $q_c' = 0$ with definite directions $e_c = q_c'/q_c'$ (fig. 4), whereas the Migdal-Kohn

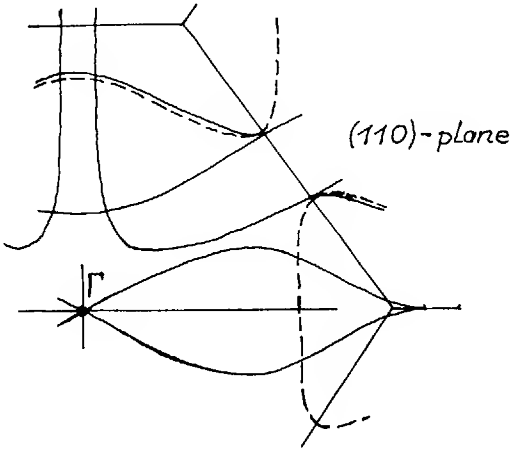

Fig. 4. The Fermi surface of Cu (broken line) and the loci of phonon anomalies in the (110)-plane.

anomalies may approach $q_c \approx 0$ only by chance. The locus and character of the Taylor anomalies was investigated in [15]. For $q \to 0$ see [24,25]. As an example, in fig. 4 a (110)-cut of the Fermi surface of copper together with the loci of anomalies is shown. Experimentally the Taylor anomaly was found for the first time in [23].

6. Quasi-waves in metals

An incident electromagnetic wave excites in a metal electromagnetic vibrations dying off in a skin depth. In the collisionless limit (no defects) the metal can be treated as an electron plasma the dielectric function of which is in the classical approximation ($\hbar\omega \ll \varepsilon_F$, $T = 0$) expressed by a Fermi surface integral:

$$\varepsilon_{ik}(\omega,k) = \delta_{ik} + \frac{4\pi e^2}{\omega}\langle v_i \; R \; v_k\rangle \,, \tag{6.1}$$

$$R = \frac{1}{i(kv - \omega) + 0} \,, \qquad \langle \ldots \rangle = \frac{2}{(2\pi\hbar)^3} \oint \frac{dS_F}{v(p_F)} \ldots \,.$$

As was already discussed, in a metal there are no low-frequency free plasma vibrations, so that the dispersion equation

$$D(\omega,k) = \boldsymbol{\varepsilon}(\omega,k) \; E(\omega,k) = 0 \tag{6.2}$$

obtained from (6.1) has only complex solutions. As is well known, the asymptotics of the electric field in the depth of the metal is not always determined by the nodes of $\boldsymbol{\varepsilon}$. If $\boldsymbol{\varepsilon}(\omega,k)$ has a singularity at $k_z = k_z^c$ (as a function of k_z for $k_x = k_y = \mathrm{Im}\,\omega = 0$, the z-axis pointing normal into the depth of the metal, and normal incidence of the electromagnetic wave is assumed), then the asymptotic field is [26,25]

$$E \sim e^{-i(\omega t - k_z^c z)} \, (k_z^c z)^{-\alpha} \,, \tag{6.3}$$

where α is determined by the character of the singularity.

From (6.1) we see that singularities of $\boldsymbol{\varepsilon}(\omega,k_z)$ are produced by multiple nodes in the denominator of R, i.e.

$$k_z^c = \frac{\omega}{(\mathbf{e}\mathbf{v}_F)_{\mathrm{extr.}}} \,, \qquad \mathbf{e}\mathbf{v}_F > 0 \,, \qquad \mathbf{e} = \mathbf{e}_z \,, \tag{6.4}$$

where the extremum is taken on the Fermi surface. In the case of a spherical Fermi surface there is only one $k_z^c = \omega/v_F$. A more complicated Fermi surface may give rise to several values. If $\mathbf{e} = \mathbf{e}_c$ has a critical direction where the curve $ev_F = 0$ on the Fermi surface makes a topological change, then $(e_c v_F)_{extr.} = 0$. As shown in [16], in this case quantum corrections must be considered. (See also [27].)

References:

[1] L. D. Landau, E. M. Lifshits, and L. P. Pitaevskii, "Statistical Physics" (part II), Pergamon Press, London, 1980.
[2] M. I. Kaganov and H. Eschrig, Usp. fiz. nauk, to be published.
[3] M. Born and Kun Huang, "Dynamical Theory of Crystal Lattices", Clarendon Press, Oxford, 1954.
[4] E. A. Kaner and V. G. Skobov, Usp. fiz. nauk 89, 367 (1966).
[5] V. Ya. Demikhovskii and A. P. Protanganov, Usp. fiz. nauk 118, 101 (1976).
[6] P. M. Platzman and P. A. Wolff, "Waves and Interactions in Solid State Plasmas", Academic Press, New York, 1973.
[7] L. D. Landau, Zh. exp.teor. fiz. 16, 574 (1946).
[8] V. L. Gurevich, "Kinetika fononikh sistem", Moscow, Nauka, 1980, chap. 1, §6.
[9] E. M. Lifshits and L. P. Pitaevskii, "Physical Kinetics", Pergamon Press, London, 1981.
[10] H. Eschrig in: P Ziesche (ed.), Proc. 4th Symp. Electronic Structure, TU Dresden, p.17, 1974.
[11] E. G. Brovman and Yu. M. Kagan in: G. K. Horton and A. A. Maradudin (ed.), "Dynamical Properties of Solids", vol. 1, p. 191, North-Holland, Amsterdam, 1974.
[12] E. G. Maksimov, Zh. exp. teor. fiz. 69, 2236 (1975).
[13] M. I. Kaganov and Y. Yu. Lisovskaya, Zh. exp. teor. fiz. 80, 2445 (1981).
[14] A. B. Migdal, Zh. exp. teor. fiz. 34, 1438 (1958).
[15] M. I. Kaganov, A. G. Plyavenek, and M. Hietschold, Zh. exp. teor. fiz. 82, 2030 (1982).
[16] M. I. Kaganov and A. G. Plyavenek, Zh. exp. teor. fiz. 88, 249 (1985).
[17] A. B. Pippard, Phil. Mag. 2, 1147 (1957).
[18] A. I. Akhieser, M. I. Kaganov, and G. Ya. Lyubarskii, Zh. exp. teor. fiz. 32, 837 (1957).
[19] W. Kohn, Phys. Rev. Letters 3, 393 (1959).
[20] A. M. Afanas'ev and Yu. M. Kagan, Zh. exp. teor. fiz. 43, 1456 (1962).
[21] M. I. Kaganov and A. I. Semenenko, Zh. exp. teor. fiz. 50, 630 (1966).
[22] P. L. Taylor, Phys.Rev. 131, 1995 (1963).
[23] L. Weiss and H. Eschrig, phys. stat. sol. (b) 114, 419 (1982); L. Weiss, H. Eschrig, and M. I. Kaganov in: P. Ziesche (ed.), Proc. 13th Symp. Electronic Structure, TU Dresden, p. 103, 1983.
[24] G. T. Afanesyan, M. I. Kaganov, and T. Yu. Lisovskaya, Pisma Zh. exp. teor. fiz. 25, 381 (1977); Zh. exp. teor. fiz. 75, 1786 (1978).
[25] M. I. Kaganov, V. M. Kontorovich, T. Yu. Lisovskaya, and N. A. Stepanova, Zh. exp. teor. fiz. 85, 1675 (1983).
[26] G. E. H. Reuter and E. H. Sondheimer, Proc. Roy. Soc. 195A, 336 (1948); G. I. Ivanovskii and M. I. Kaganov, Zh. exp. teor. fiz. 83, 2320 (1982); V. G. Peshanskii, V. S. Lekhtsier, and A. Tada, Fiz. met. met. 56, 855 (1983).
[27] M. I. Kaganov and A. G. Plyavenek, Pisma Zh. exp. teor. fiz. 38, 94 (1983).

ACOUSTIC PHONON INTERACTION WITH A TWO-DIMENSIONAL ELECTRON GAS (2DEG)

L. J. Challis, G. A. Toombs and F. W. Sheard
Department of Physics, University of Nottingham, Nottingham,
NG7 2RD, U.K.

1. Introduction and Electron Transport

Interaction between a 2DEG and acoustic phonons can be studied in a variety of ways. The simplest, in principle, is to measure the electron mobility, μ, in a temperature region where it is strongly affected by collisions with acoustic phonons. It is not easy in practice however to separate the acoustic phonon scattering from other processes and also, at the high temperatures at which phonon scattering is strong, the system is beginning to lose its 2D character [1]. A better technique is to heat the 2DEG at low temperatures by passing a current through it; it then loses its energy predominantly by acoustic phonon emission ($kT_e \ll \hbar\omega_{LO}$). The electron temperature T_e can be determined, for example, from the amplitude of the Shubnikov-de Haas oscillations in the magnetoresistance (with the complication though that T_e will vary with B) or from the far infra-red spectrum into which a small fraction of the energy loss occurs and the loss rate into the phonons is given by $P = AN_s e\mu E_{sd}^2$ where A is the area of the 2DEG, N_s its carrier density per unit area, e the electronic charge and E_{sd} the applied electric field [2]. An example is shown in figure 1. The electron-phonon interaction can also be studied through the phonon-drag term of the thermoelectric power. In the presence of a temperature gradient there is a net flow of phonons and so of phonon momentum in the direction of $\underline{\nabla}T$. Part of this is continually being transferred to the electrons producing a current which is eventually opposed by an electric field. The result is the phonon drag thermopower, S_{ph}, which is expected to vary as T^3. The measured thermopower also includes a diffusion term $S_d \alpha T$ due to the electrons themselves, but in bulk semiconductors at low temperatures, the total heat flow and momentum flow is very largely due to phonons and it is not surprising therefore that the phonon drag term dominates in the thermopower. It is becoming clear that this is also the case in a 2DEG coupled to a 3D phonon system as might be expected and that the

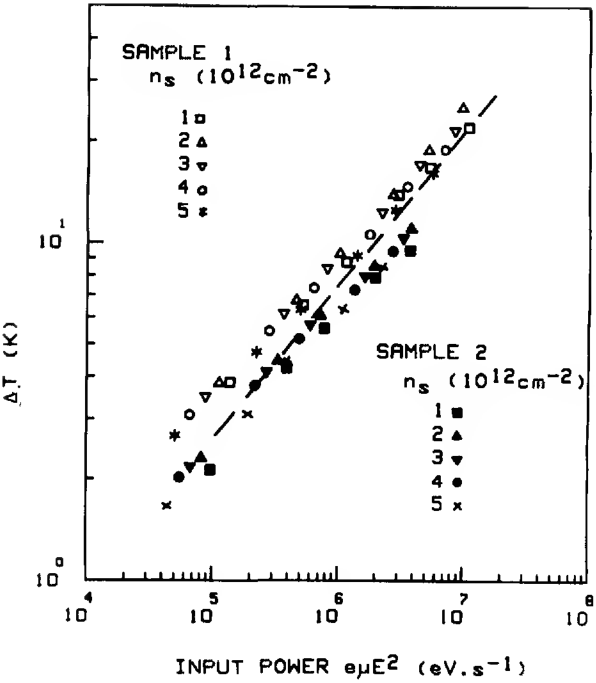

Fig 1 : The acoustic phonon emission per electron (this is assumed = total power loss $e\mu E^2_{sd}$) as a function of $\Delta T=T_e-T$ for 2DEGs in Si MOSFETS; Höpfel et al [2]. The dashed line shows $P\alpha(\Delta T)^2$.

measurements could therefore provide useful information on the electron-phonon interaction. The first experiments demonstrating the predominance of phonon drag were by Zavaritsky et al [3] and these were followed by a number of experiments e.g. Nicholas et al [4], Fletcher et al [5] and Gallagher et al [6]; Nicholas [7], who was unaware of Zavaritsky's work, independently stressed the importance of phonon drag. The samples include Ge bicrystals, Si MOSFETS, and GaAs/AlGaAs heterostructures. Recent theoretical treatment of phonon drag on a 2DEG by Cantrell and Butcher [8] seems in good agreement with the experiments of Fletcher et al on GaAs/AlGaAs. The treatment has been modified to apply to Si by Gallagher et al and comparison with their experimental results is shown in Fig 2.

Extension of this work to magnetic fields is of particular interest and a number of experiments have already been made (e.g. Fletcher et al [5]).

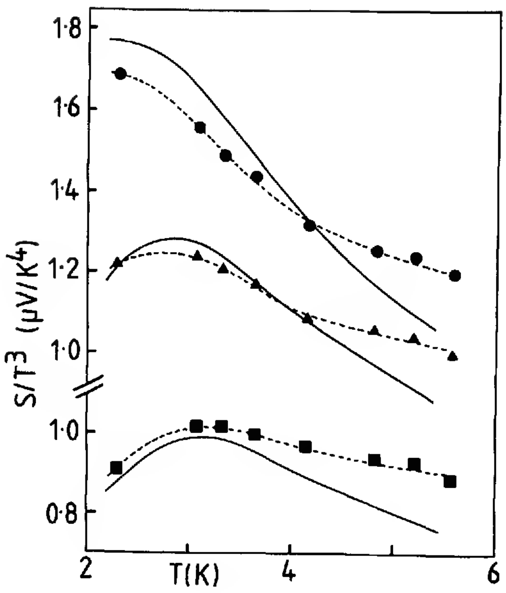

Fig 2: The reduced thermopower S/T^3 as a function of temperature for a Si MOSFET: N_s=9.8x10^{11} cm^{-2} (■) , 7.8x10^{11} cm^{-2} (▲) and 6.1x10^{11} cm^{-2} (●). The dashed lines are drawn through the experimental points and the solid lines show calculated values (Gallagher et al [6]).

All of these techniques give very useful but averaged information about the total rate of energy or momentum transfer between the electron system and all the phonon modes $\underline{q}_s$ (s is the polarization index). To obtain more detailed information on the electron-phonon interaction we need to look directly at the phonons emitted from a hot 2DEG or absorbed by a cold 2DEG. We need to know for example how the power emitted into a small solid angle, $P(\omega,s,\vartheta,\phi)d\Omega d\omega$ at a frequency ω and polarization s, varies with the angle ϑ that $\underline{q}$ makes with the normal to the plane of the 2DEG and with the angle ϕ that $q\sin\vartheta$ makes with a symmetry axis in the plane. We should also expect that P will depend, weakly, on the direction of the drift velocity of the electrons because of phonon drag and, strongly, on magnetic fields applied perpendicular to the plane because of quantization effects. Complementary studies to these investigations of emission can be made by looking at the phonon absorption by a cold 2DEG of bulk or surface acoustic phonons, again as a function of ω,s,ϑ and ϕ. These lectures are concerned largely with these phonon techniques and we start by considering emission.

2. Phonon Emission

2.1 $B = 0$

As an example, we discuss the phonon emission from a 2DEG in the (001) plane of a Si MOSFET. This discussion follows closely that given recently by Toombs et al [9]; see also Rothenfusser et al [10]. In bulk Si, the 6 degenerate minima in the conduction band lie along the <100> directions. The energy surfaces are ellipsoids with that along [001] described by

$$E = \hbar^2[(k_x^2+k_y^2)/2m^*_t + k_z^2/2m^*_l]$$

The effect of the surface potential V(z) is to replace the z-component of the energy for this valley $\hbar^2 k_z^2/2m^*_l$, by discrete eigenvalues whose energies $\propto - m^*_l$. The result is that the energies of the 2 valleys along the z-axis ($m^*=m_l=0.916m_o$) are lower in energy relative to the other 4 ($m^*=m^*_t=0.190m_o$). The ground state energies are therefore

$$E=E_o + \frac{\hbar^2}{2m^*_t}(k_x^2 + k_y^2)$$

with a valley degeneracy factor $g_v=2$ and a spin degeneracy factor $g_s=2$.

The energies are affected by strain and, as would be expected, the energy shifts within these ellipsoidal valleys depend on the direction of the strain relative to their axes: z in the present case. So we can write

$$V_{ep}(\underline{r}) = a\left(\frac{\partial u_x}{\partial x} + \frac{\partial u_y}{\partial y}\right) + b\left(\frac{\partial u_z}{\partial z}\right) \qquad \text{or, more conveniently,}$$

$$V_{ep}(\underline{r}) = \Xi_d \underline{\nabla}\cdot\underline{u} + \Xi_u \frac{\partial u_z}{\partial z}$$

where typical values are $\Xi_u=9.0$eV and $\Xi_d = -6.0$eV. Phonons provide an oscillating strain arising from a displacement $\underline{u}(\underline{r})$ whose instantaneous value is given by

$$\underline{u}(\underline{r}) = \left(\frac{\hbar}{2\rho V\omega_{q,s}}\right)^{\frac{1}{2}} \left(a_{q,s} e^{i\underline{q}\cdot\underline{r}} + a^{+}_{q,s} e^{-i\underline{q}\cdot\underline{r}}\right) \underline{\varepsilon}_{q,s}$$

where a_q, a^{+}_q are annihilation and creation operators, $\underline{\varepsilon}_{q,s}$ is the polarization vector and ρ and V, the density and volume of the Si respectively. (This expression for $\underline{u}(\underline{r})$, in which the phonon modes are those for bulk Si, assumes that the 2DEG is imbedded in a large volume V and neglects the fact that it is rather near to the interface between the Si and the SiO_2 layer. Calculations suggest that this should be a reasonable approximation [11]).

So the Hamiltonian for phonon emission is

$$V_{ep}(\underline{r}) = -i\left(\frac{\hbar}{2\rho V\omega_{q,s}}\right)^{\frac{1}{2}} \Xi_u \left(q_z \varepsilon_{q,s,z} - D\underline{q}\cdot\underline{\varepsilon}_{q,s}\right) a^{+}_{q,s} e^{-i\underline{q}\cdot\underline{r}}$$

where $D = -\Xi_d/\Xi_u$. For an isotropic (Debye) model, we can choose, without loss of generality, the 2TA modes for each $\underline{q}$ to be polarized within and perpendicular to the plane of incidence for which the z-component of $\underline{\varepsilon}$, $\varepsilon_{q,s,z} = \sin\vartheta$ and 0 respectively. So if we write

$$\chi_s^{\frac{1}{2}}(\vartheta) = (q_z \varepsilon_{qs,z} - D\underline{q}\cdot\underline{\varepsilon}_{q,s})/q$$

then $\chi_s^{\frac{1}{2}}(\vartheta) = \cos^2\vartheta - D$ LA modes

$= \sin\vartheta\cos\vartheta$ TA modes (in plane)

$= 0$ TA modes (out of plane)

and $V_{ep} = -i\left(\frac{\hbar\omega_{q,s}}{2\rho V v_s}\right)^{\frac{1}{2}} \Xi_u \chi_s^{\frac{1}{2}}(\vartheta) a^{+}_{q,s} e^{-i\underline{q}\cdot\underline{r}}$

where v_s = sound velocity of mode s.

This perturbation induces transitions between electronic states $\underline{k}$, $\underline{k}'$ with the emission of a phonon so that there is a continuous energy transfer from a hot electron gas into phonon modes $\underline{q}$ at a rate

$$P = g_s g_v \sum_{\underline{k},\underline{k}'} \hbar\omega_{\underline{q},s} f_{\underline{k}} (1 - f_{\underline{k}'})(n_{\underline{q},s} + 1) W_{\underline{k}}^{\underline{k}',\underline{q},s}$$

where $W_{\underline{k}}^{\underline{k}',\underline{q},s} = \frac{2\pi}{\hbar} \left|M_{\underline{k}}^{\underline{k}',\underline{q},s}\right|^2 \delta(E_{\underline{k}} - E_{\underline{k}'} - \hbar\omega_{\underline{q},s})$; $M_{\underline{k}}^{\underline{k}',\underline{q},s} = \langle\underline{k}'|V_{ep}|\underline{k}\rangle$,

and $f_{\underline{k}}$ and $n_{\underline{q},s}$ are the usual Fermi-Dirac and Bose-Einstein functions. Energy is also transferred in the reverse direction but we can neglect this if $T_e \gg T$, the lattice temperature. The expression for P assumes that the electrons are in equilibrium as a a result of electron-electron scattering. To evaluate it we suppose free-electron behaviour in the plane so that the eigenfunctions can be written

$$\psi(\underline{r}) = (L_x L_y)^{-\frac{1}{2}} \exp(ik_x x)\exp(ik_y y)\psi_o(z)$$

where, for the bound state wavefunction, we take

$$\psi_o(z) = (2a^3)^{-\frac{1}{2}} z \exp(-z/2a) \text{ with } a \sim 1\text{nm. [1]}$$

The matrix elements are the products of 3 integrals. Those over x and y give $\delta_{\underline{k},\underline{k}' + \underline{q}_{\parallel}}$ corresponding to conservation of wave-vector in the plane of the 2DEG while that over z gives

$$F(q_z) = \int_0^{\infty} \psi_o^2(z) e^{-iq_z z} dz = 1/(1-iq_z a)^3 \text{ so that } |F(q_z)|^2 = (1+q_z^2 a^2)^{-3}$$

showing that there is an effective limit to the magnitude of the wave-vector q_z that can be emitted. The fact, expressed by $F(q_z)$, that q_z does not have to be zero is a consequence of the Uncertainty Principle resulting from the localization of the electron in a distance $\Delta z \sim a$.

The next task is to sum the emission into mode $\underline{q}_s$ from all the initial k- states that are allowed by energy and wave-vector conservation. For $kT \ll \hbar\omega_q$ and a 2DEG of area A

$$P \simeq 2g_v \frac{\pi\hbar\omega^2}{\rho V v_s} \Xi_u^2 \chi_s(\vartheta) |F(q\cos\vartheta)|^2 \frac{A}{4\pi^2} \int f_k(1-f_{k'})\delta_{\underline{k},\underline{k}'+\underline{q}_{\parallel}} \delta(E_k - E_{k'} - \hbar\omega_q) d^2\underline{k}$$

$\delta_{\underline{k},\underline{k}'+\underline{q}_{\parallel}}$ requires $k'^2 = k^2 + q_{\parallel}^2 - 2kq_{\parallel}\cos\phi$, where ϕ is the angle between k and $q_{\parallel}$. We write $y = E - E' - \hbar\omega_q = \frac{\hbar^2}{2m^*}(k^2 - k'^2 - \frac{2m^*}{\hbar^2}\hbar\omega)$ and

$k_o = q_{\parallel}/2 + m^* v_s/\hbar\sin\vartheta$ and substituting for k' obtain

$y = \frac{\hbar^2 q_{\parallel}}{m^*}(k\cos\phi - k_o)$, so $y = 0$ requires $k\cos\phi_o = k_o$ and hence

$k_o \lesssim k_F$ or $q_{\parallel} \lesssim 2k_F - 2m^* v_s/\hbar\sin\vartheta$ which requires $q_{\parallel} \lesssim 2k_F$ except at the smallest angles. We next transform

$$dy = -\frac{\hbar^2 q_{\parallel}}{m^*}\sin\phi \, k d\phi \quad \text{and} \quad d^2\underline{k} = k d\phi dk = \frac{-m^*}{\hbar^2 q_{\parallel}} \frac{dkdy}{\sin\phi}$$

So the integral becomes $\frac{-2m^*}{\hbar^2 q\sin\vartheta}\int f_k(1-f_{k'})dk\int\frac{\delta(y)dy}{\sin\phi}$

$$= \frac{-2m^*}{\hbar^2 q\sin\vartheta}\int_{k_o}^{\infty}\frac{f_k(1-f_{k'})kdk}{(k^2-k_o^2)^{\frac{1}{2}}}$$

(the factor of 2 before the integral counts the two values of ϕ_o satisfying $y=0$ and we are assuming that it is a reasonable approximation that the second integral $\simeq(\sin\phi_o)^{-1}$ throughout the range).

So finally we can write down the power emitted per unit area of the 2DEG into phonons of polarization s in a range of frequencies $d\omega$ in a small solid angle $d\Omega$ at an angle ϑ from the normal to the 2DEG when $T_e >> T$, $Pd\Omega d\omega$ where

$$P = \frac{m^* g_v \Xi_u^2 \chi_s(\vartheta)\,|F(q\cos\vartheta)|^2\omega^3}{8\pi^4\rho\hbar v_s^3\sin\vartheta}\int_{k_o}^{\infty}\frac{f_k(1-f_{k'})kdk}{(k^2-k_o^2)^{\frac{1}{2}}}$$

The integral can be evaluated numerically and fig 3 shows the total energy emitted as a function of ϑ for TA modes (after Toombs et al [9]), showing that it is fairly strongly peaked in the forward direction ($\vartheta \sim 0$). The angular distribution measured would also be quite strongly modified by phonon focussing due to the elastic anisotropy of Si. This can be allowed for by including a function $F(\vartheta,\phi)$ so that the measured distribution is the product $P(\vartheta)F(\vartheta,\phi)$. However in these lectures we do not consider $F(\vartheta,\phi)$ further and concentrate on the emission function $P(\vartheta)$ although we note that $F(\vartheta,\phi)$ has a strong peak centred at $\vartheta=0$. Evidently $P(\vartheta)$ must drop to zero at $\vartheta=0$ since the necessary perturbation in the plane disappears when $q_{\parallel}=0$. For LA modes it also vanishes at $\vartheta=36°$ ($\cos^2\vartheta=D$). The frequency spectrum also depends on ϑ and s (ν(cut - off) $\sim k_F V_s/\pi\sin\vartheta - m^* V_s^2/\pi\hbar\sin^2\vartheta$) increasing in high frequencies as ϑ falls. The temperature dependence of the total power is also of interest. At 'low'-electron temperatures, and for all but the smallest angles, the cut-off occurs at much higher frequencies than can be emitted thermally ($\sim 4kT_e/\hbar$) and the emission is determined mainly by the

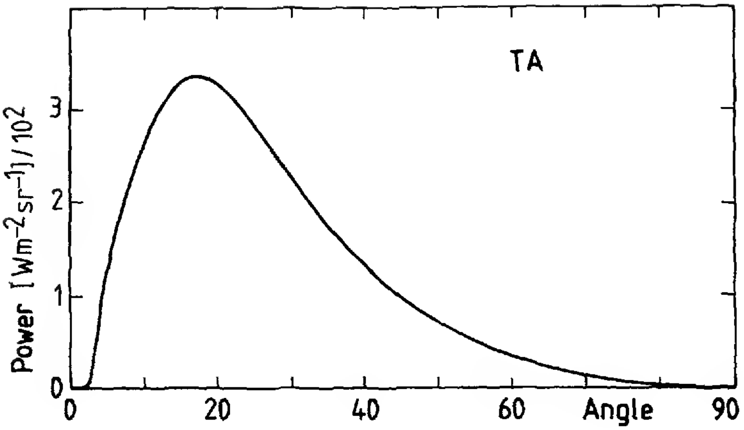

Fig 3 : The angular dependence of the phonon emission per unit solid angle from a hot 2DEG in Si for B=0 (Toombs et al [9]). (No allowance has been made for phonon focussing). The parameters assumed are $N_s=5\times10^{11}cm^{-2}$ (E_F=3.0 meV) and T_e= 15K(kT_e=1.3 meV).

phonon distribution function. So P α T_e^5 (or $T_e^5-T^5$ if T cannot be neglected) as can be seen from the ω³dω dependence of the prefactor and the integral which αω in this limit. This is a good approximation to the total power dependence when the fraction emitted at small angles can be neglected which is the usual situation. At 'high' electron temperatures however, the cut-off will have a dominant effect and PαT_e. Experimental conditions lie between these two limits so that a wide range of temperature dependences seem possible; we note that the F(qcosϑ) cut-off can also play a role.

This calculation by Toombs et al was largely made for comparison with the B≠ 0 case discussed later and looks to be essentially the same as Rothenfusser et al, although this latter paper does not give a final expression for P. There have also been several other calculations of P(T) for a hot 2DEG in zero field (although P(ϑ) does not appear to have been written out explicitly before) with an interesting variation of temperature dependences! Our low temperature dependence seems consistent with Shinba et al [12] and with Payne et al [12] who follow Shinba et al, but note that the emission must be multiplied by ql, when ql<l as in their experiments, giving PαT_e^6. But weaker dependence have been derived and we are presently comparing these calculations in detail.

One aspect that we have not yet discussed is the role of electron screening. Rothenfusser et al allow for it by reducing the deformation potentials by a dielectric constant $\varepsilon(q_{\parallel},\omega)$ taken from the dynamic Linhard theory for a 2D system (see ref [1]). So their phonon emission is less than ours by $\varepsilon^2(q_{\parallel},\omega)$ and since $q_{\parallel}$ (phonons)$\lesssim q_s$, the screening wave-vector ($q_s \sim 1.2\text{x}10^7 \text{cm}^{-1}$ in the long wavelength, low temperature limit which equals that of TA phonons at 1100 GHz) this would affect the magnitude and the angular and frequency distributions. However it is not clear to us at present that this is an appropriate procedure because of the differences between a deformation potential, that is a potential distribution arising from a strain, and a potential distribution resulting from an external electric field (we also note that the screening is reduced by scattering) and for the moment we have neglected screening in these calculations.

Experimental evidence showing the striking differences in the phonon emission from a 2DEG in a Si MOSFET from that from a 3DEG has recently been obtained by Rothenfusser et al [10], by Dietsche [13] and by Kent et al [14]. The arrangement used by Rothenfusser et al is shown in fig 4(a). 100ns pulses were applied across a 1mm^2 2DEG through capacitively connected source and drain contacts. The power dissipated in the 2DEG ($R \sim 1\text{k}\Omega$) was typically 1mW/mm^2 and the resulting phonon pulses were detected by Al or Pb superconducting tunnel junctions on the opposite face at various angles, ϑ, to the normal. The samples were thicker than the usual wafers (3mm rather than 0.5mm) to spread out the time of flight spectrum. Phonons travel ballistically in Si for $\nu \lesssim 800$ GHz (the limit is set by isotope scattering) and this feature plus the lower detection limit set by the energy gap of the junctions means that the Al junctions detect ballistic phonons from 100-800 GHz while the Pb junctions detect those between 650 and 800 GHz. Examples of their results for TA phonons detected using Pb junctions are shown in fig 5 for three different angles ϑ to the normal. The data were taken using a fixed E_{sd} and show the effect of increasing the carrier density N_s.

Before discussing these data we first consider what would be expected at constant power with a narrow band detector at ν_o. Theoretically there should be a rather sharp peak in the emitted intensity just before the cut off at $q \simeq 2k_F/\sin\vartheta$ so that since $k_F=(\pi N_s)^{\frac{1}{2}}$ the detected signal should have a maximum at $N_s = \pi(\nu_o \sin\vartheta / v_s)^2 = 4.9\text{x}10^{12} \sin^2\vartheta \text{ cm}^{-2}$ for $\nu_o = 725$ GHz. (v_s for TA modes $= 5.8\text{x}10^3 \text{ms}^{-1}$). The experimental

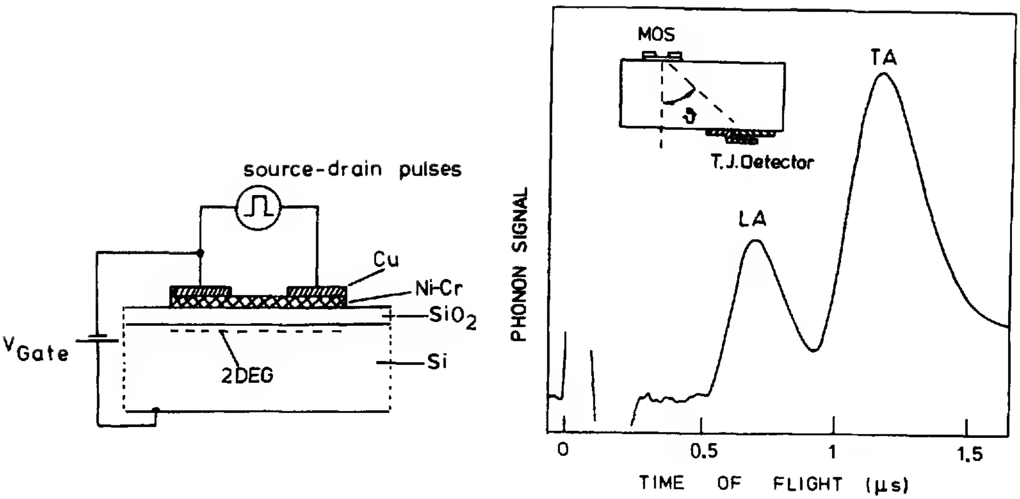

(a)

(b)

Fig 4(a) : The experimental arrangement used by Rothenfusser et al [10]). The 2DEG forms just below the Si-SiO$_2$ interface when a voltage is applied to the Ni-Cr gate. (b): The phonon signal detected by the tunnel junction as a function of time of flight. The insert shows the geometry of the emitter and detector [10];

situation was inevitably slightly more complicated than this. In particular, since E_{sd} was constant, the total power ($AN_s e\mu E_{sd}^2$) increased as N_s was increased. The calculated signals are shown by the broken curves in fig 5. (The absolute values are scaled). The peaks are shifted to somewhat higher values of N_s than those given by the simplified expressions but the angular dependence remains. The agreement with the position of the first peak found experimentally is striking and clear evidence of the 2D features of the emission. Some features have still to be explained however, in particular the peak at $N_s=5\times10^{12}cm^{-2}$ detectable at $\vartheta = 39°$ and very marked at 23°. The authors also detected phonon drag effects in the emission: the signals depended on the direction of E_{sd} and so the electron drift velocity.

The angular dependence was also investigated by this group using an extended superconducting tunnel junction covering an area of 6x4mm² on the opposite face of the Si substrate [13]. The sensitivity of the

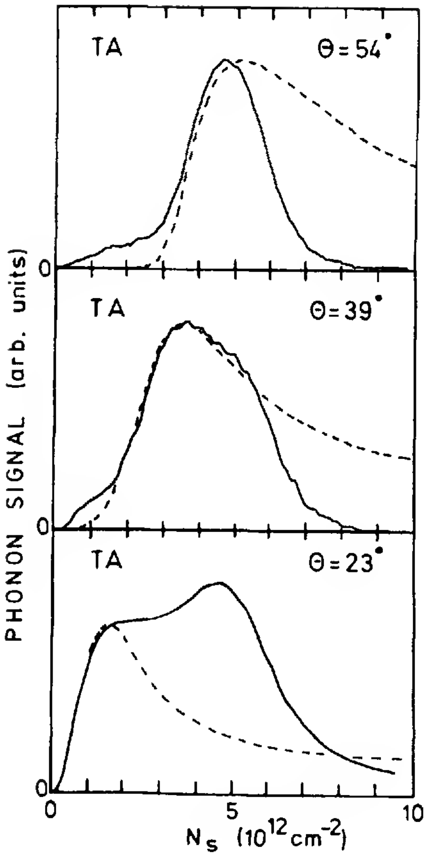

Fig 5: Phonon emission from a hot 2DEG in the frequency range 650-800GHz at 3 different angles ϑ from the normal to the 2DEG (solid lines). The source-drain voltage was held constant while N_s was changed. The broken lines show theoretical results [10].

detector can be increased by illumination,and by raster scanning a laser beam across the junction, a 'phonograph' was obtained of the phonon emission (TA). The most noteworthy feature was a strong peak in the forward direction ($\vartheta \sim 0^\circ$) which, as they note, is partly at least due to focussing. (This is perhaps the reason why they do not see the 'hole' at $\vartheta=0$ predicted by the theory).

Some zero field measurements of phonon emission from a 2DEG in a Si MOSFET have also been reported recently by Kent et al [13]. These form part of a study of emission in magnetic fields up to 7T and use CdS bolometers which are relatively field insensitive (unlike of course superconducting tunnel junctions) and have a broad band response. Kent et al also found that the phonon emission was strongly peaked in the forward direction and that the intensity fell sufficiently sharply with angle that it could not be detected at $\vartheta > 40°$. This is in contrast with the findings of Rothenfusser et al, who as we have seen, were able to detect these weaker signals at larger angles. This is probably because of the greater sensitivity of tunnel junctions compared with bolometers although there may also be modest differences in the focussing function $F(\vartheta,\phi)$ since the values of ϕ were different in the two experiments. We note too an interesting difference in the variation of P with N_s, for E_{SD} constant, measured with broad band detectors at 54° [13] and spanning 0-34° [14]. If indeed most of the emission falls within a solid angle $\vartheta < 34°$, then the signal seen at the small angle detector should be proportional to the total emission $P = N_s e \mu E_{SD}^2$ i.e. $P \propto N_s$ and this was indeed observed by Kent et al [14]. However at $\vartheta = 54°$ we are in the tail of the angular distribution. So the detected signal depends on the shape of $P(\vartheta,\phi)$ which in turn depends on k_F, i.e. N_s. So in this case, $P \not\propto N_s$ but will be a more complicated function as observed by Rothenfusser et al [13].

The first experiments on phonon emission by a 2DEG were in fact not in a Si MOSFET but in a GaAs/AlGaAs heterostructure (Chin et al [15]). Phonons emitted at $\vartheta \sim 10°$ to the normal to the 2DEG were detected by an Al superconducting bolometer on the opposite face of the 0.5mm substrate. They found that for low powers, $\lesssim 2\mathrm{mW/mm^2}$ when $T_e \lesssim 40K$, the detected signal was very largely due to TA phonons which would have been emitted by piezoelectric coupling (TA phonon emission via deformation potential coupling is not possible in GaAs because of the parabolic energy bands). The results are shown in fig 6. At higher powers when $T_e > 40K$, an increasing proportion of the signal arrived appreciably later than the TA phonons as a broad slow pulse (SP). This was attributed to the increasing importance of LO phonon emission as T_e increases ($\hbar\omega_{LO}/k \sim 400K$). The LO phonons are known to decay rapidly into high energy TA phonons at the zone boundary but these travel slowly since the dispersion curve is flat and they are unable to decay easily into faster moving phonons because of difficulties in satisfying the selection rules for energy and momentum conservation. Qualitatively similar effects were observed by Chin et al [16] in the phonon emission from a 2D hole gas. They also showed that in GaAs, the holes are substantially more strongly coupled to the phonons than are the electrons.

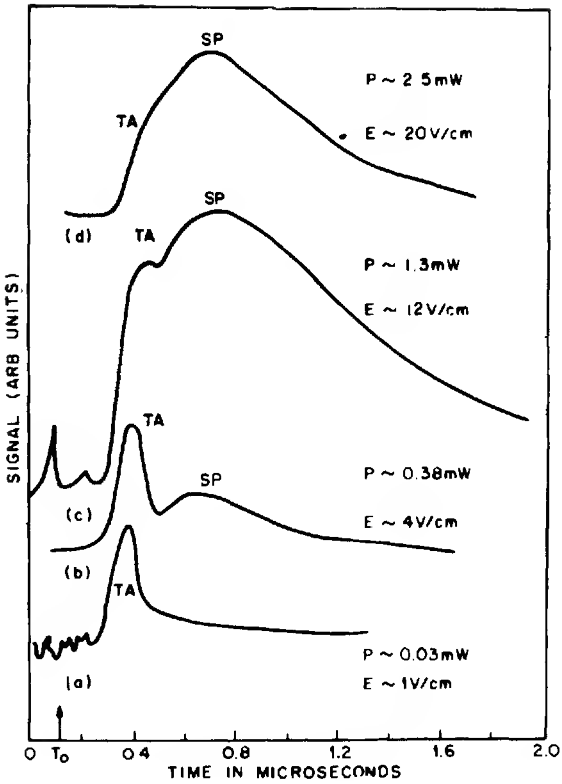

Fig 6 : Phonon emission from a 2DEG in a GaAs/AlGaAs heterojunction (∿30ns pulses) for a range of source-drain fields E_{sd}. The detected signal is shown as a function of the time of flight [15].

2.1 B ≠ 0

We next discuss the interesting changes in the phonon emission anticipated as a result of magnetic field quantization. The most striking is that the emission now takes place at the cyclotron frequency and its harmonics. Cyclotron phonon emission by a 3DEG and its possible use as a tunable phonon source has been discussed by Slater and Tremblay [9] and the considerable advantages of a 2DEG for this were pointed out by Challis & Rampton [9] and independently by Slater [9]. Calculations of the emission spectrum have recently been made by Toombs et al [9] and we follow their discussion.

In a magnetic field B along the z-axis represented by the vector potential A=(0, Bx, 0), - the assymetric Landau gauge - the electron eigenstates and eigenvalues may be written

$$\psi_{n,k_y}(x,y,z) = u_n(x-X_{k_y})L_y^{-\frac{1}{2}}\exp(ik_y y)\psi_0(z); \qquad E_n = (n+\tfrac{1}{2})\hbar\omega_c$$

where n=0,1,2,.... labels the Landau levels and $u_n(x)$ is the nth eigenstate of a simple harmonic oscillator whose frequency is $\omega_c = eB/m^*$. (We have not included spin splitting in E_n. This does not change the frequency spectrum of the phonon emission since the electron-phonon interaction cannot change the spin but it will make a small difference to the intensities because of its effect on the thermal populations). The eigenfunction is centred at $X_{k_y} = -l_B^2 k_y$ where $l_B = (\hbar/eB)^{\frac{1}{2}}$ is the magnetic length which provides the scale of the S.H.O. wavefunctions. Since $-L_x/2 < x < L_x/2$ and k_y is restricted to values $m(2\pi/L_y)$ with m=0,1,2,..., each Landau level contains $g_s g_v L_x L_y/2\pi l_B^2$ states.

The calculation of the phonon emission can be carried out as in zero field. The matrix element integrals over y and z are unaffected by the field but the x-integral becomes

$$\int_{-L_x/2}^{+L_x/2} u_{n'}(x-X_{k_y'})\,e^{-iq_x x}\,u_n(x-X_{k_y})\,dx$$

Since S.H.O. states are localized, the limits can be extended to $\pm\infty$, and, by moving the origin to the orbit centre X_{k_y} and noting that

$X_{k_y'} - X_{k_y} = l_B^2(k_y - k_y') = l_B^2 q_y$, the integral can be written

$e^{-iq_x X_{k_y'}}\, I_{n'n}(q_x,q_y)$ where

$$I_{n'n}(q_x,q_y) = \int_{-\infty}^{-\infty} u_{n'}(x)\,e^{-iq_x x}\,u_n(x+l_B^2 q_y)\,dx$$

The integral may be evaluated using the generating function for the Hermite polynomials [17] and we obtain the result for the power per unit area PdΩ emitted into modes $\omega_{\underline{q},s} = (n-n')\omega_c$ in a small solid angle dΩ at angle ϑ to the normal. (Note that this expression is for all frequencies while that given earlier for zero field was for a frequency range $d\omega$):

$$P = \frac{m^* g_v \Xi_u^2 \chi_s(\vartheta) \left|F(q\cos\vartheta)\right|^2 \omega^4 \omega_c}{8\pi^3 \rho \hbar v_s^5} \left|I_{n',n}(q_x,q_y)\right|^2 f_n(1-f_{n'})$$

and $$\left|I_{n',n}(q_x,q_y)\right|^2 = \left(\frac{n'!}{n!}\right)\left(\frac{\xi^2}{2}\right)^{n-n'} e^{-\xi^2/2}\left[\sum_{r=0}^{n'} \frac{(-\xi^2/2)^r}{r!} \frac{n!}{(n'-r)!(n-n'+r)!}\right]^2$$

and $\xi = q l_B \sin\vartheta$

Examples of the angular dependence of the emission from a (100) 2DEG in a Si MOSFET given by this expression are given by Toombs et al and reproduced in fig 7 and 8 for B=5T and 0.5T respectively for $N_s = 5\times10^{11}\,\mathrm{cm}^{-2}$ (E_F= 3.0meV), and T_e=15K(kT_e=1.3meV).

As in zero field, the intensity falls to zero at ϑ =0 and $\cos^2\vartheta = D$ (LA phonons) and indeed the angular dependences at B=0 and 0.5T are very similar apart from the structure (the peak values differ by ~ 30% partly due to computing procedures; this is being checked).At the higher values of field the angular dependence is dominated by the overlap integral which has a maximum near $\sin\vartheta \sim \sqrt{2}(n-n')^{\frac{1}{2}}/ql_B$. This angle can be quite small for high magnetic fields and for example $\vartheta \sim$ 13° and 9° for LA and TA modes respectively for the conditions for figure 7. The fall off in intensity with angle can again be linked to the Uncertainty Principle. The electrons are now localised in the x-direction with $\Delta x \sim l_B \sim (\hbar/eB)^{\frac{1}{2}}$ so that $q\sin\vartheta < (eB/\hbar)^{\frac{1}{2}}$. Since $q \propto B$, $(\sin\vartheta)_{max} \cong B^{-\frac{1}{2}}$ so that the energy is pushed closer to the normal as B increases. We note that this calculation does not include any screening effects which are even more complicated in these non-zero fields.

Experiments to examine these effects in detail are underway in Nottingham and preliminary work appeared broadly consistent with quantised emission (Kent et al [14]). These first experiments were carried out on a Si MOSFET 2DEG of rather modest mobility (~1500cm²$V^{-1}s^{-1}$) so substantial Landau level broadening would be present at lower fields : $\omega_c\tau = \mu B$ = 1 at B~6T. Phonon emission following a current pulse through the 2DEG was investigated using a bolometer centred at ϑ ~17°. At constant power, no change was observed in the detected signal for B<5T, but it started to fall at

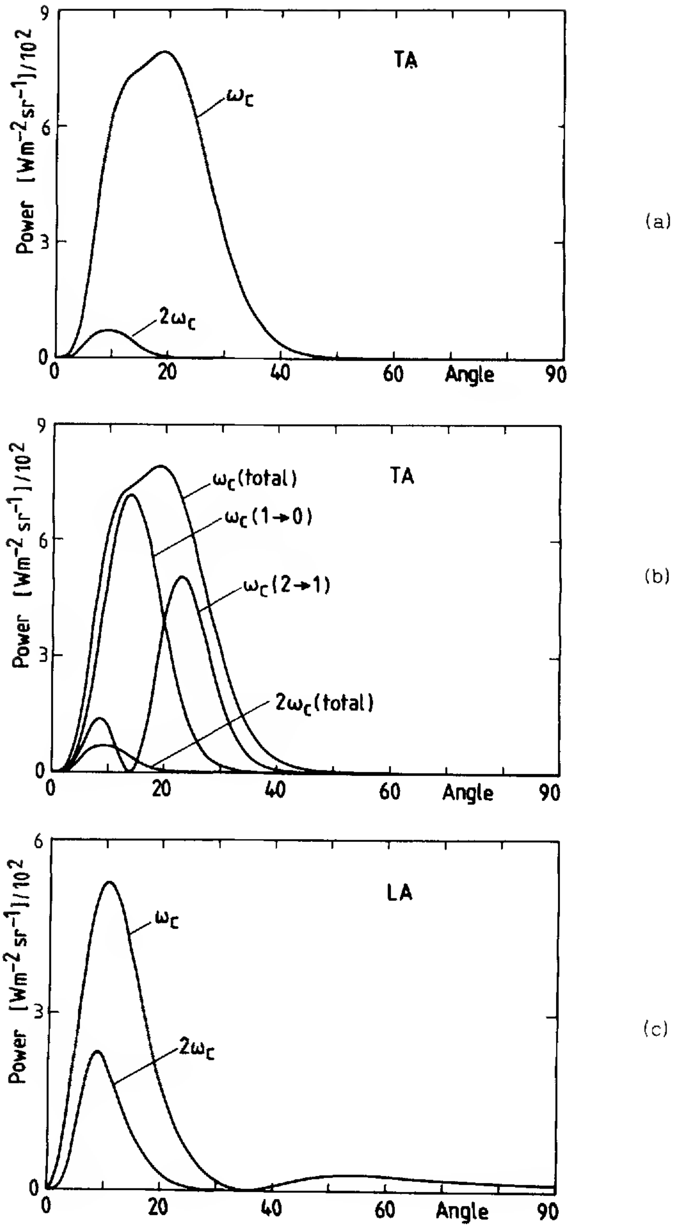

Fig 7: Angular dependence of phonon emission at 5T: ν_c = 740GHz, ($\hbar\omega_c$=3.0meV), $q_c l_B$(TA) = 9.2, $q_c l_B$(LA)=6.1. (a): The total TA emission at ω_c and $2\omega_c$. Note the absence of emission at ϑ=0° and the fall in P(ϑ) when $q_c \sin\vartheta > l_B^{-1}$. (b): This shows the separate contributions to the TA emission at ω_c from 1—>0 and 2—>1 inter-Landau level transitions. These give rise to the structure in the total emission at ω_c. Note the 2 peaks in the 2—>1 transition caused by the structure in the $u_2(x)$ S.H.O. function. (c): The total

LA emission at ω_c and $2\omega_c$. The fall in $P(\vartheta)$ is weaker than for TA modes ($q_c l_B(LA)<q_c l_B(TA)$) but note that $P(\vartheta)=0$ when $\cos^2\vartheta=D$. The structure due to the separate transitions is not apparent in this case.

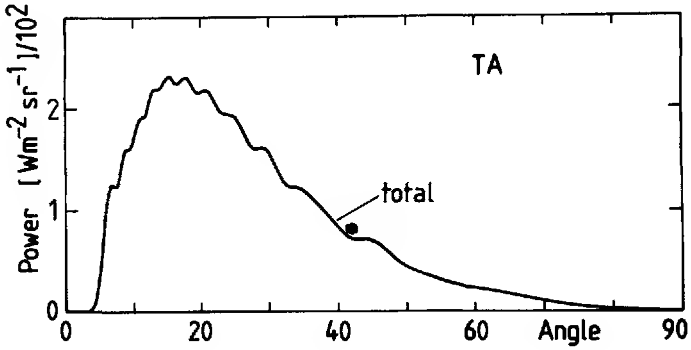

Fig 8: Angular dependence of the total TA phonon emission at 0.5T. $\nu_c=74$ GHz ($\hbar\omega_c$ = 0.3meV). The emission is strongest for transitions $(n-n')\omega_c \sim kT_e/\hbar$ as in the zero field case. The large number of harmonics and transitions involved results in the structure in $P(\vartheta)$.

higher fields where $\nu_c>700$GHz. This is consistent with the cyclotron peak in the emission moving to frequencies where it is strongly scattering by isotopes.

3. Phonon Absorption

Phonon absorption can take place by a similar process to emission and a theoretical analysis for absorption in zero field is given by Hensel et al [18]. (The analysis is presently being extended in Nottingham to magnetic fields when, in the absence of level broadening, the absorption is restricted to inter-Landau level transitions i.e. to $\omega=(n-n')\omega_c$)). The treatment is similar to that given above and for T_e=0K, the absorption from a beam of phonons with wave-vector q is given in the notation of these lectures, by

$$\frac{\Delta I}{I} = \frac{m^* g_v \Xi_u^2 \chi_s(\vartheta)\,|F(q\cos\vartheta)|^2 A(q_{\parallel})}{\pi\rho\hbar^2 v_s^2 \cos\vartheta\sin\vartheta}$$

$A(q_{\parallel})$ and so ΔI are zero for $q_{\parallel}>2k_F+2m^*v_s/\hbar\sin\vartheta$, and $A(q_{\parallel}) = \beta_-(q_{\parallel})$, $2k_F-2m^*v_s/\hbar\sin\vartheta<q_{\parallel}<2k_F+2m^*v_s/\hbar\sin\vartheta$

and $A(q_{\parallel}) = \beta_-(q_{\parallel})-\beta_+(q_{\parallel})$, $q_{\parallel}<2k_F-2m^*v_s/\hbar\sin\vartheta$

where $\beta_\pm(q_{\parallel}) = \left|k_F^2-\left(q_{\parallel}/2\pm\frac{m^*v_s}{\hbar\sin\vartheta}\right]^2\right)^{\frac{1}{2}}$

So at low $q_{\parallel}$ (and $m^*v_s/\hbar\sin\vartheta$) we can expand the brackets in $\beta_\pm(q_{\parallel})$ and find $\Delta I \propto q_{\parallel}$. This steepens sharply as $q_{\parallel}$ approaches $2k_F - 2m^*v_s/\hbar\sin\vartheta$ and then falls to zero for a further increase in $q_{\parallel}$ of $4m^*/v_s\hbar\sin\vartheta$. This is shown in figure 9. The angular dependence of ΔI depends on the magnitude of q and we note that $\Delta I \rightarrow 0$ as $\vartheta \rightarrow 0$ as expected.

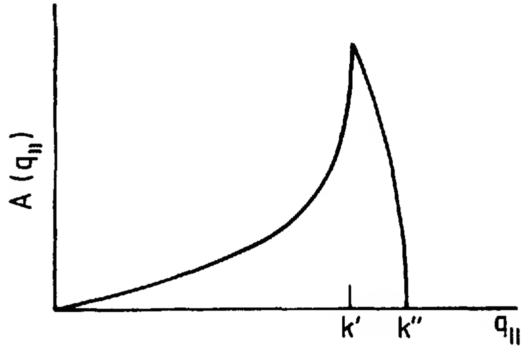

Fig 9: $A(q_{\parallel})$, from Hensel et al [18]. (In their notation $G(q_{\parallel}) = (2m^*/{}^2\hbar^2)(A(q_{\parallel}))$; $k'=2k_F-2m^*v_s/\hbar\sin\vartheta$; $k''=2k_F+2m^*v_s/\hbar\sin\vartheta$.

Hensel et al carried out the first experimental measurements of phonon absorption and these were also the first experiments in which the phonon interaction with a 2DEG was measured directly. The arrangement is shown in fig 10.

90ns heat pulses were generated by shining a laser pulse onto a constantan film and were detected by a superconducting Al bolometer after reflection from the $Si-SiO_2$ interface of a Si MOSFET. The phonons pass twice through the 2DEG at an angle $\vartheta=55°$ to the normal and its effect on the detected signal could clearly be seen by modulating the carrier density between 0 and some value N_s. The

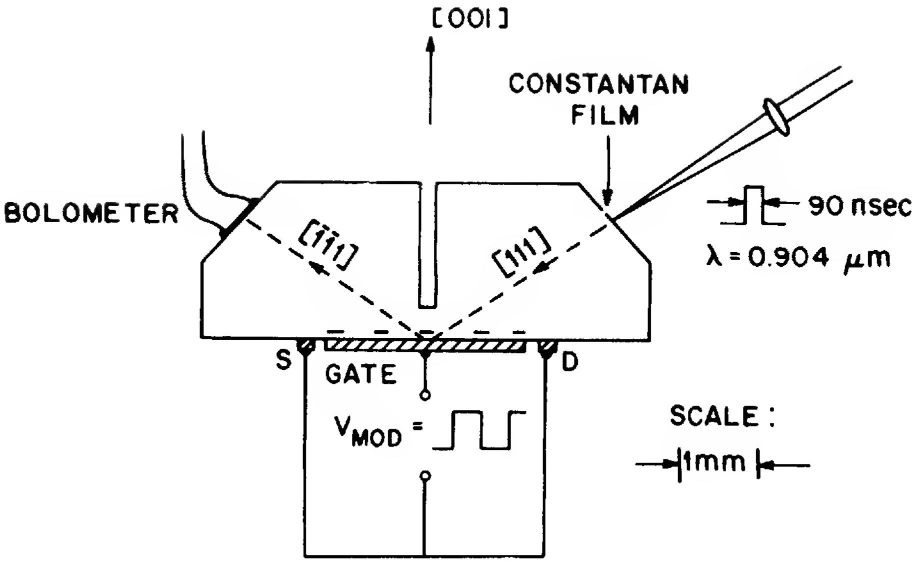

Fig 10: Measurement of phonon absorption by a 2DEG in a Si MOSFET at 2.15K [18]. The cut in the substrate prevents direct transmission between generator and bolometer.

experimental results are shown in fig 11(b).

The most striking feature is the apparent size of the absorption. The fractional fall in signal reached 2% and this is an order of magnitude larger than that predicted by the theoretical expressions given above. There is inevitably some uncertainty in the heat pulse spectrum through uncertainty in T_h as this is not measured directly but calculated from the power input to the constantan film. However this cannot account for the large discrepancy observed and this was explained later by Hensel et al [19]. They pointed out that phonons would not only be reflected at the Si-SiO$_2$ interface but also at the 2DEG as well. Reflection occurs whenever there is a change in acoustic impedance v_s, and, inside the Si, v_s is changed in the 2DEG by the presence of the electron gas. To see this, we recall that the wave equation relates the response of a system $\rho\ddot{\underline{u}}$ to a driving force. In the absence of conduction electrons, this force is caused by the strain because of the elastic modulus of the lattice. When electrons are present however there is an additional force on them due to the deformation potential caused by the strain. So the electrons not only

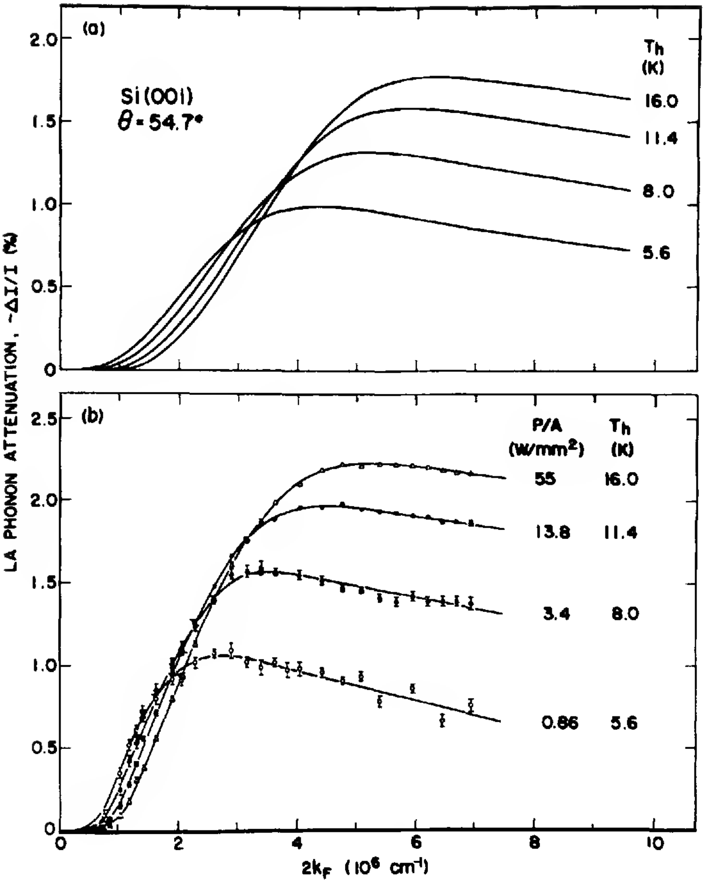

Fig (11): Phonon loss caused by a 2DEG in a Si MOSFET [19] as a function of $2k_F$. T_h is the phonon temperature calculated from P. (a) Theoretical calculations allowing for interference effects between the 2 reflected beams. (b) Experimental data from [18].

cause dissipation but also change the sound velocity and so the acoustic impedance. (The situation is not dissimilar to that of electromagnetic waves propagating in a conductor which can of course be described by a complex refractive index. Just as in the present case that leads to both absorption and to reflection at an interface).

Hensel et al first explained the effect of this additional reflection by using a simplified model in which the 2DEG is considered to be vanishingly thin and situated at a distance h from the $Si-SiO_2$

interface. A reflected LA signal can now arise from both 'interfaces' and interference occurs because of the phase difference $2q_z h$ between them. (The situation is actually more complicated than this because a reflected LA signal can also arise through processes involving mode conversion at both interfaces : LA $\longrightarrow$ TA$\longrightarrow$ LA). For the appropriate value of h, the phase differences $2q_z h$ for the q_z's of interest are restricted to a range from about 0 to 2π ($q_z = q_{\parallel}$ cot 55 and the reflection becomes small for $q_{\parallel} > 2k_F$). So the interference effect does not in fact average out for the broad frequency distribution used as might have been expected and it is large because the two reflected signals are of comparable amplitudes. This is partly because reflection at the Si-SiO_2 interface is rather weak since the incident angle happens to lie close to the Brewster angle. But another important feature is that the phonons transmitted into the amorphous SiO_2 are strongly scattered so that there is no reflected pulse arriving ballistically from its further face. Fig 11(a) shows the decrease in signal $\Delta I/I$ calculated allowing for these effects and is in convincing agreement with the experimental results shown in 11(b). The deformation potential parameters used to describe the electron-phonon interaction are those given previously so this agreement suggests that the interaction in 2D is similar in strength to that in 3D. (No allowance was made for screening).

The first experiments on field dependent absorption at high frequencies were by Eisenstein et al [20]. The 2DEG sample was in a GaAs/AlGaAs heterostructure ($N_s = 1.5 \times 10^{11}\,cm^{-2}$, $\mu = 4 \times 10^5\,cm^2 V^{-1} s^{-1}$) connected in Corbino geometry and the incident heat pulse was filtered by transmission through 1.3mm of liquid ^4He at <0.2K to obtain spectroscopic information on the absorption. Under these conditions, ^4He has the useful property, arising from the curvature of its dispersion curve, that it will transmit ballistically phonons with $\nu > \nu_0 = 200$ GHz but down-convert phonons of $\nu < \nu_0$ to $\lesssim 20$ GHz. ν_0 can be reduced by applying hydrostatic pressure (20 bar for $\nu_c = 0$) so reducing the intensity of down-converted phonons. For the fields and heat pulse temperatures used, the phonon energies $\ll \hbar\omega_c$ so absorption would be due to intra-Landau level transitions, which in these high mobility samples, can only affect low frequency, i.e. down-converted phonons. Eisenstein et al used the conductivity σ_{xx} of the 2DEG as a sensitive detector of phonon absorption and demonstrated that the absorption (i.e. $\Delta\sigma_{xx}/\sigma_{xx}$) decreased with pressure at all fields which seems consistent with this discussion. The decrease in pressure effect with field would seem to imply that the absorption increases with N, the index of the Landau level responsible for the absorption. The results are shown in fig.12.

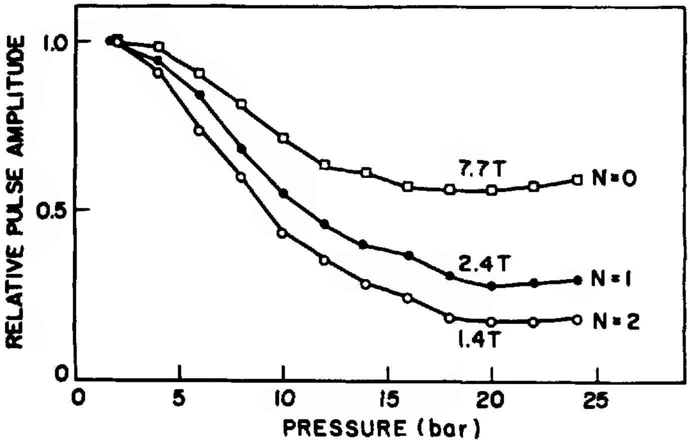

Fig 12 : The heat pulse amplitude detected as a result of absorption by a 2DEG in a GaAs/AlGaAs heterostructure [20]. The phonons passed through a ^{4}He filter tuned by hydrostatic pressure. Curves are shown at 3 magnetic fields and N shows the highest occupied Landau level.

Magnetic field dependent phonon absorption by a 2DEG has also recently been reported in heat pulse experiments on a 2DEG in a (100) Si MOSFET by the Nottingham group [21]. Measurements are being made using a similar geometrical arrangement to that used by Hensel et al but most of the work so far has been done at close to normal incidence, with the arrangement shown in fig 13.

CdS bolometers were used, as in the emission experiments, and these are mounted on top of the gate as shown. Heat pulses are generated by applying a voltage pulse to an Au film on the opposite face. The substrate is 5mm thick, the bolometer 3x3mm² and the heater 1x1mm² so that most of the phonons are incident on the 2DEG at angles between 0 and 20° or so. The detected signal falls detectably as N_s is increased to 4×10^{12}cm^{2} and this is presently being studied as a

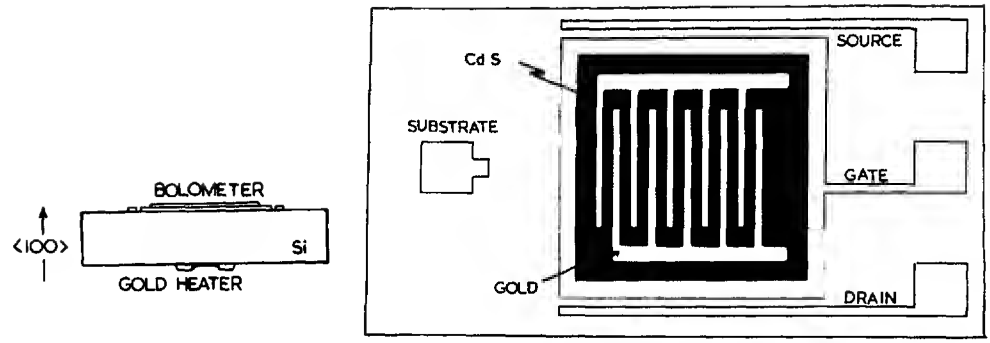

(a) (b)

Fig 13 : The experimental arrangement being used to measure the absorption of phonons by a cold 2DEG in a Si MOSFET in fields up to 7T [21]. (a) The general arrangement. (b) The bolometer showing the Au electrodes used to measure the resistance of the CdS film.

function of field up to 7T. Preliminary results of this work have been reported [21] and it is being continued to higher values of N_s, etc. The reduction in signal should again be partly due to absorption and partly due to reflection from the 2DEG but preliminary estimates suggest that the interference effects should now be rather weak so it is hoped that the analysis may be simpler.

Field dependent phonon absorption by a 2DEG in a GaAs/AlGaAs heterostructure has also been observed by Wixforth et al [22]. GaAs is piezoelectric and these experiments were carried out at 70 MHz using surface acoustic waves (SAW) generated and detected with interdigital transducers. At these frequencies, the acoustic wavelength, ∿40μm, is large compared with the thickness of the 2DEG and the other lengths in the problem (k_F^{-1}, and 1, the electron mean free path) so a description in terms of macroscopic variables is appropriate. The attenuation can be attributed to the dissipation of currents set up by the piezoelectric fields and Wixforth et al show that a good description can be obtained with the relaxation-type expressions

$$\Gamma = \alpha q(\sigma_{xx}/\sigma_m)/[1 + (\sigma_{xx}/\sigma_m)^2]$$

$$\Delta v_s/v_s = \alpha/[1 + (\sigma_{xx}/\sigma_m)^2]$$

where the values of σ_{xx} are taken from measurements made on a sample from the same wafer and α and σ_m are adjusted to obtain the fits shown by the dotted lines in fig 14. σ_{xx} varies rapidly with field as the Landau levels move through the Fermi level (Shubnikov-de Haas effect).

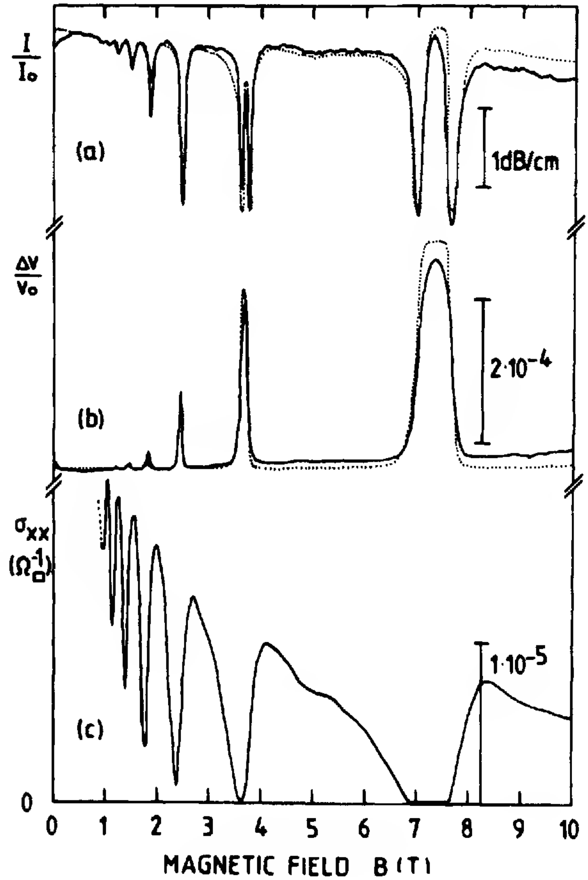

Fig 14: Magnetic field dependence of (a) the detected SAW intensity I/I_o, (b) the velocity $\Delta v_s/v_s$ and (c) the conductivity σ_{xx}. The dotted lines are a theoretical fit to the relaxation expression [22].

The expression for the attenuation Γ, shows that it reaches its maximum value at $\sigma_{xx} = \sigma_m$ and at the deepest minima, σ_{xx} passes through σ_m twice: once as it falls and once as it rises. So each of these minima gives rise to two minima in I. The overall agreement of this relaxation expression with experiment is clearly satisfactory. It is not quite perfect however and, for example, the two minima that we have discussed should evidently be of the same depth and not of slightly different depths. It would clearly be of considerable interest to extend this work to higher frequencies where ql>1.

4. Conclusion

There is still a great deal more to be learned about the details of the electron-phonon interaction in 2DEG systems. Some of this may emerge from more experimental and theoretical work on electrical transport particularly in high magnetic fields and thermoelectric power seems likely to be a worthwhile area of investigation for some time to come. It is also clear that phonon work by a variety of techniques has very considerable potential in this area and in principle can provide detailed information about the interaction with specific phonon modes which is not possible to obtain in any other way. The suggestion that cyclotron phonon emission from a hot 2DEG might be a useful tuneable source of 'monochromatic' phonons has still to be explored experimentally.

5. Acknowledgements

We are very grateful to all our collaborators in Nottingham, particularly Drs A.J. Kent and V.W. Rampton for many valuable discussions on the electron-phonon problem and to the Science and Engineering Research Council for their support of this work.

6. References

[1]. T. Ando, A.B. Fowler and F. Stern : Rev. Mod. Phys. 54, 437, 1982. This review is a valuable source of information on 2D systems. See also B.K. Ridley: J.Phys.C : 15, 5899, 1982 and refs. therein and in magnetic fields, M. Prasad and M. Singh: Phys. Rev. B29, 4803, 1984.

[2]. F.F. Fang and A.B. Fowler : J. Appl. Phys. 41, 1825, 1970; E. Gornik and D.C. Tsui Solid State Electron 21, 139, 1978. T. Neugebauer and G. Landwehr, Phys. Rev. B. 21, 702, 1980; W. Hönlein and G. Landwehr, Surf. Sci. 113, 260, 1982; S. Kawaji and Y. Kawaguchi; Proc. Int. Conf. on The Application of High Magnetic Fields in Semiconductor Physics, Grenoble 1982, ed G. Landwehr (Springer, Berlin), Lecture Notes in Physics, Vol 177, p53, 1983; R.A. Höpfel, E. Vass and E. Gornik : Solid State Commun, 49, 501, 1984; R.A. Höpfel and G. Weimann: Appl. Phys. Lett, 46, 291, 1985.

[3]. e.g. N.V. Zavaritsky and V.N. Zavaritsky, Zh. Eksp. Teor. Fiz. 83, 1182, 1982, (Engl Trans : Sov Phys.JETP 56, 674, 1982); N.V. Zavaritsky and Z.D. Kvon, Pis'ma v Eksp. Teor. Fiz. (Engl Trans: JETP Letts, 39, 61, 1984). The work of this group is reviewed by N.V.Zavaritsky, Physica 126B, 369, 1984.

[4]. R.J. Nicholas, T.M.H. Vuong, M.A. Brummell, J.C. Portal and M.A. Razeghi, Proc 17th Int. Conf. on Physics of Semiconductors, San Francisco, 1984, eds J.D. Chadi and W.A. Harrison (Springer, Berlin) p389, 1985.

[5]. R. Fletcher, J.C. Maan, K. Ploog and G. Weimann, Phys. Rev. B33, 7122, 1986.

[6]. B.L. Gallagher, C.J. Gibbings, M.Pepper and D.G. Cantrell, Proc. 18th Int. Conf. on Physics of Semiconductors, Stockholm, 1986, ed. O. Engström, (World Scientific, Singapore) in press.

[7]. R.J. Nicholas, J. Phys C18, L695, 1985.

[8]. D.G. Cantrell & P.N. Butcher, J. Phys. C19, L429, 1986.

[9] G.A. Toombs, F.W. Sheard, L.J. Challis & D. Neilson. Institute of Physics, Solid State Physics Conference, Imperial College, London, 1986 (unpublished) submitted to Solid St.Comm.G.W.Slater & A.M.S. Tremblay, Proc. 4th Int. Conf. on Phonon Scattering in Condensed Matter, Stuttgart, 1983, eds. W. Eisenmenger, K. Lassmann & S. Döttinger (Springer, Berlin), p49, 1984. Phys. Rev. B29, 2289, 1984; G.W. Slater : J.Phys.C 18, 2483 1985; L.J. Challis and V.W. Rampton: SERC grant application GR/C/96400, 1983 (unpublished); G.W. Slater, Ph.D. Thesis, University of Sherbrooke, 1984 (unpublished).

[10]. M. Rothenfusser, L. Köster and W. Dietsche: Phys. Rev. B34, 5518, 1986.

[11]. H. Ezawa, S. Kawaji and K. Nakamura : JPn. J. Appl. Phys. 13, 126, 1974, 14, 921 (E) 1975.

[12]. Y.Shinba, K. Nakamura, M. Fikuchi and M. Sakata. J. Phys. Soc. Japan, 51, 157, 1982; M.C. Payne, R.A. Davies, J.C. Inkson and M. Pepper, J. Phys. C. 16, L291, 1983; Weaker temperatures were calculated for example by T. Neugebauer and G. Landwehr, Phys. Rev. B21, 702, 1980 and E. Vass, Solid State Commun. 55, 847, 1985.

[13]. W. Dietsche, Proc. 5th Int. Conf. on Phonon Scattering in Condensed Matter, Urbana, 1986, eds. A.C. Anderson and J.P. Wolfe (Springer, Berlin) p366 and private communication.

[14]. A.J. Kent, M.I. Newton, G.A. Hardy, P.A. Russell, V.W. Rampton and L.J. Challis, Institute of Physics, Solid State Physics Conference, Imperial College, London, 1986 (unpublished), submitted to J.Phys.C.

[15]. M.A. Chin, V. Narayanamurti, H.L. Störmer and J.C.M. Hwang, Proc. 4th Int. Conf. on Phonon Scattering in Condensed Matter, Stuttgart, 1983, eds W.Eisenmenger, K.Lassmann & S.Döttinger (Springer, Berlin), p328, 1984. An alternative interpretation has been given by N.M. Guseinov & Y.B. Levinson:Solid State Comm. 45, 371, 1983.

[16] M.A. Chin, V.Narayanamurti, H.L. Störmer and A.C.Gossard,

Proc. 17th Int. Conf. on Physics of Semiconductors, San Francisco, 1984, eds J.D. Chadi & W.A. Harrison (Springer, Berlin)p,333, 1985.

[17]. This expression was previously used in P.S.S. Guimaraes, L. Eaves, F.W. Sheard, J.C. Portal and G. Hill : Physica 134B, 147, 1985. An equivalent but somewhat different form is given by J.R. Barker: J. Phys, C. 5, 1657, 1972.

[18]. J.C. Hensel, R.C. Dynes and D.C. Tsui : Phys. Rev B28, 1124, 1983.

[19]. J.C. Hensel, B.I. Halperin and R.C. Dynes : Phys. Rev Letts 51, 2302, 1983.

[20]. J.P. Eisenstein, V. Narayanamurti, H.L. Störmer, A.Y. Cho and J.C.M. Hwang, Proc. 5th Int. Conf. on Phonon Scattering in Condensed Matter, Urbana, 1986, eds A.C. Anderson & J.P. Wolfe (Springer, Berlin)p401, 1986.

[21]. M.I. Newton, A.J. Kent, G.A. Hardy, P.A. Russell, V.W. Rampton & L.J. Challis: Institute of Physics, Solid State Physics Conference, Imperial College, London, 1986 (unpublished) to be submitted to J.Phys.C.

[22]. A. Wixforth, J.P. Kotthaus and G.Weimann, Phys. Rev. Letts. 56, 2104, 1986.

ELECTRON-PHONON RELAXATION MECHANISMS AND KINETIC EFFECTS IN TWO-DIMENSIONAL CONDUCTING SYSTEMS

R.N. Gurzhi, A.I. Kopeliovich, S.B. Rutkevich
Institute for Low Temperature Physics and Engineering
Academy of Sciences of the Ukrainian SSR
Kharkov, 310164 USSR

The two-dimensional degenerate Fermi gas of electrons interacting with phonons is considered. The basic mechanisms of momentum relaxation in such a system, associated with electron-phonon, phonon-phonon and electron-electron collisions, are shown to be qualitatively different from similar mechanisms of the ordinary three-dimensional metal. The physical reason of the difference is that the two-dimensional system of interacting electrons and phonons breaks down into almost isolated groups between which the momentum transfer occurs through very slow, staged superdiffusion (mixing) processes. In this paper, the authors propose an efficient method for deriving superdiffusion equations, based on the detailed balancing conditions in the electron-phonon system. As has been found, the electric and thermal conductivity coefficients under certain conditions may be anomalously high, showing behaviour qualitatively different from that in three-dimensional metals. The effect of specifically two-dimensional relaxation mechanisms upon sound absorption and electric conductivity of thin samples is analyzed. The possibility of observing such effects experimentally in layered metal compounds of intercalated graphite type is discussed.

1. Introduction

Two-dimensional conductive structures have been intensively studied for a long time primarily owing to the qualitatively new physical phenomena they show, as localization of impurity-scattered electrons, Peierls instability and related effects, etc. The main result of this paper is that conventional mechanisms of electron relaxation in two-dimensional metal systems are also essentially different from similar mechanisms in three- and one-dimensional systems. Therefore, the kinetic properties of normal two-dimensional metals can be expected to be characterized at low temperatures by a range of new physical regularities which are not consistent with the traditional theory. The low temperature electric conductivity of a pure two-dimensional metal, in particular, cannot be described by the Bloch-Peierls theory. These differences are not due to any special properties of the electron-phonon interaction; they arise at the level of relaxation processes.

By two-dimensional we mean metals in which the electron energy depends only upon two components of the quasimomentum, while the phonon spectrum is generally three-dimensional. A model like this is a good approximation to many layered compounds, among which graphite and dichalcogenides of the transient group metals are best studied. The layered structures, including intercalated compounds, make up a family of numerous materials with a wide variety of properties [1].

2. The Diffusion Approximation

First, we are going to demonstrate that the conventional electron-phonon relaxation mechanism, that is mainly responsible for the electric resistivity (and other kinetic properties) of pure metals, cannot work in two-dimensional systems. As is known, the phonons excited in metals at low temperatures are mainly long wave phonons with the characteristic thermal momentum $q \simeq T/s \ll p_F$ (where s is the sound velocity and p_F the Fermi momentum). An absorption (or emission) of such phonons does not appreciably affect the electron momentum, which just slightly moves on the Fermi surface (FS). Since the collisions are of random nature, then it is clear from the physical considerations that the low-temperature electron-phonon scattering results in a diffusion of electrons on the FS, characterized by steps of the order of q, the phonon thermal momentum. The description of the relaxation in terms of diffusion may be rigorously justified, proceeding from the set of kinetio equations for the system of interacting electrons and phonons in an external electric field. By expanding the set in powers of the parameter q/p_F, we arrive at the following equation [2]:

$$\mathrm{div}\,\hat{D}_{\vec{p}}\,(\nabla f_{\vec{p}} - \vec{a}) = e\vec{E}\vec{n} - I^U \qquad (1)$$

Here $f_{\vec{p}}\, df_o/d\mathcal{E}$ is a nonequilibrium addition to the electron distribution function ($f_o(\mathcal{E})$ being the Fermi distribution), div and ∇ two-dimensional differential operators in the plane tangential to the FS, $\vec{n} = \vec{v}_{\vec{p}}/|\vec{v}_{\vec{p}}|$ the unit vector of the electron velocity, $\vec{E}$ the electric field intensity, and the term I^U gives the electron-phonon collisions attended by Umklapp processes. The diffusion tensor $\hat{D}_{\vec{p}}$ is proportional to the square of the electron-phonon interaction constant and varies with temperature as T^5. Its order of magnitude is $D \simeq q^2/t_1$, where $t_1 \sim T^{-3}$ is the electron mean free time for a single electron-phonon collision. Finally, $\vec{a}\{\nabla f\}$ is the linear integral functional

$$\vec{a} = \int dS_{\vec{p}'}\, \hat{A}_{\vec{p}\vec{p}'}\, \nabla f_{\vec{p}'} \qquad (2)$$

Integration is here over the whole FS.

Note that Eq. (1) is not quite a conventional diffusion equation, for the density of the electron flow on the FS in the momentum space contains, along with the familiar term proportional to the concentration gradient $\hat{D}\,\nabla f$, the integral term $\hat{D}\vec{a}$. Thus, the flow magnitude at a given point $\vec{p}$ is determined by the electron distribution over the whole FS. This nonlocal dependence results from the nonequilibrium of the phonons (phonon drag by electrons). The effect of phonon emission by some electron is twofold. Firstly, this electron is displaced to a distance about q, and secondly the momentum of another electron on the FS, which has absorbed the emitted phonon, also changes. Note that there would be no phonon drag only if there were a more efficient interaction of the phonons with some objects other than electrons, which is unrealistic for good conductors at sufficiently low temperatures.

Equation (1) describes steady-state diffusion of electrons continuously "created" by the electric field on one half of the FS (where $e\vec{E}\vec{n} < 0$) and "annihilating" on the other half (where $e\vec{E}\vec{n} > 0$). Under certain conditions [3] the equation yields Bloch temperature dependence of the electric resistivity of the metal $\rho_B \sim T^5$.

The situation is entirely different for the two-dimensional metal.

As can be rigorously proved, this is the only case where the integro-differential equation (1) is insoluble ([4], Appendix 2). With a two-dimensional FS, the kernel $\hat{A}_{\vec p \vec p'}$ has singularities at the points where $\vec n(\vec p) = \pm \vec n(\vec p')$, being equal to zero for other values of the momenta. In the particular case of a singly-connected convex FS, when there are only two such points ($\vec p' = \pm \vec p$), the left-hand side of Eq. (1) is

$$\frac{1}{2}\mathrm{div}\,\hat{D}_{\vec p}(\nabla f|_{\vec p} - \nabla f|_{-\vec p}) \tag{3}$$

with $\nabla f|_{-\vec p}$ denoting the magnitude of ∇f taken at $-\vec p$. The expression is identically zero, because $f_{\vec p}$ is an odd function of the quasi-momentum. Thus, the diffusion of electrons on the FS does not lead to relaxation.

Let us explain the physical meaning of this result important for the whole work. Owing to the energy and momentum conservation laws, a phonon can interact only with those electrons whose velocity vectors are nearly perpendicular to that of the phonon momentum, $\vec q$ (in the approximation corresponding to the diffusion equation (1) the vectors are strictly perpendicular to each other, $\vec q\,\vec n = 0$). For a metal with a cylindrical FS, this implies that phonon exchange is allowed solely for the electrons whose velocity vectors are parallel or antiparallel to each other (Fig. 1). The electrons with a certain velocity direction, $\pm \vec n$, and the phonons interacting with them make up an isolated subsystem that cannot transfer its momentum to another similar subsystem characterized by a different velocity direction, $\vec n'$. On the other hand, the diffusion flow of electrons at any

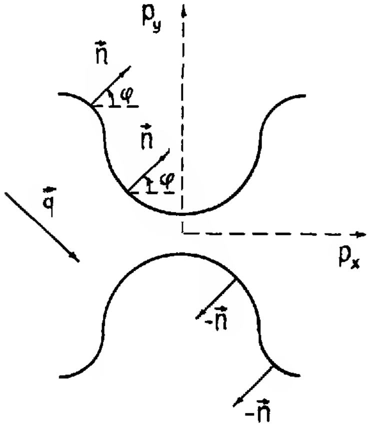

Fig. 1 Electron-phonon subsystem on a nonconvex (open) FS.

point of the FS should have some fixed direction, and thus, phonons of that direction should be permanently absorbed (or phonons of the opposite direction should be emitted). As the result, the subsystem will be depleted of such phonons and the diffusion process will stop at each point of the FS. In other words, after emission of a phonon, the electron shifts on the FS, however then it is returned to the initial state, since the emitted phonon is absorbed by "the same" electron. Thus, each electron is tied, as though with a spring, to a certain point of the FS. The case is different with ordinary three-dimensional metals, where any two electrons can exchange a phonon (its momentum is along the vector product of the two electron velocities) and therefore the momentum is mixed within the entire FS.

Note that despite its clearness, the concept of isolated subsystems is not quite a precise description of the physics involved and can cause misunderstanding. (E.g., one may think of bound states of electrons and phonons within a subsystem.) It is clear that each individual electron is as free to wander on a two-dimensional FS as in a three-dimensional case. Thus, actually the subsystem involves non-equilibrium electron states, not electrons. It is still more adequate to say that in the two-dimensional case there are difficulties in the relaxation of the electron distribution, specifically odd in momentum. An even distribution relaxes as easily in a two-dimensional system as in a three-dimensional metal (this can be seen from expression (3) which is now nonzero).

3. Superdiffusion Mechanisms

The idea of the electron-phonon system of a metal being broken up into isolated groups is only an approximation. On one hand, the phonon energy and momentum are thought to be vanishingly small. Besides, we considered only electron-phonon collisions, disregarding other types of quasiparticle interaction. The account of the above inaccuracies leads to three groups of relaxation mechanisms [5].

(1) The scattering of electrons by finite momentum phonons obviously violates the mutual isolation of the subsystems. However in a two-dimensional metal with a singly-connected convex FS, taking account of the phonon momentum finiteness does not result in relaxation. Indeed, consider an arbitrary pair of points $\vec{p}$ and $\vec{k}$ on the

FS, assuming for definiteness that the $\vec{p} \rightarrow \vec{k}$ transition occurs more frequently than the reverse one. Then the momentum of the preferrably created phonons is $\vec{q} = \vec{p} - \vec{k}$ (accordingly, that of the annihilating phonons is $-\vec{q}$). A process like this cannot be stationary, since it involves unlimited accumulation of the $\vec{q}$-phonons, i.e. unlimited increase in the phonon nonequilibrium. Ultimately, the probability of the reverse transition, i.e. $\vec{k} \rightarrow \vec{p}$ (with absorption of the $\vec{q}$-phonons) would increase to suppress the $\vec{p} \rightarrow \vec{k}$ channel. Note that we have essentially used the idea of each phonon being coupled to a single pair of electron states on the FS. Although actually there always exists a symmetrical pair of the points $-\vec{k}$, $-\vec{p}$ between which there also can occur a transition with the creation of $\vec{q}$-phonons, this does not affect our conclusion. Indeed, if, e.g., $f_{\vec{p}} > f_{\vec{k}}$, then $f_{-p} < f_{-k}$, (owing to the oddness of $f_{\vec{p}}$), and therefore, the channel $-\vec{k} \rightarrow -\vec{p}$ accumulates phonons of the same direction as the channel $\vec{p} \rightarrow \vec{k}$. Thus, relaxation of any electron distribution, save the central-symmetrical, proves impossible for all orders in q/p. Note, however, that the said conclusion is true only in the elastic collision approximation. Inasmuch as the phonon energy is finite, relaxation is possible, since the electron state pairs bound by a given phonon are not centrally-symmetric (see Fig. 2).

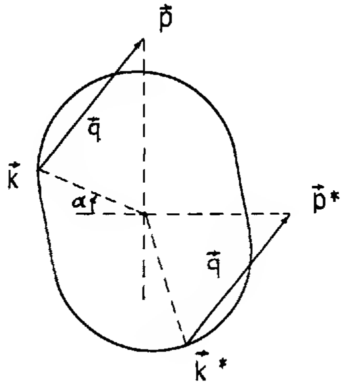

Fig. 2 States with which a phonon with the momentum $\vec{q}$ can interact, rigorously, are not centrally symmetric: $\vec{p}^* \neq -\vec{k}$, $\vec{k}^* \neq -\vec{p}$; the characteristic angle of deviation is $\alpha \simeq s/v$.

The above considerations result in the following general conclusion: relaxation is due to "multichannel" processes in which the phonon interacts with several pairs of electron states. In the elastic collision approximation, this requires that there should be at least two points with a particular direction $\vec{n}$ of the normal within the FS (nonconvex or multiply connected FS; see Fig. 1).

If the curvature radii are different at points with parallel normals, the momentum will be slowly (for small q) mixing over the whole FS. A nonzero result is only the case in the 6-th order of expansion in terms of the small parameter q/p_F (recall that the "ordinary" diffusion equation (1) corresponds to the second approximation in this parameter). This relaxation mechanism (we call it the "q/p superdiffusion") is given by a local differential equation, which however contains at a time all the states with the prescribed direction of the normal $\vec{n}(\varphi)$:

$$(1 + \frac{d^2}{d\varphi^2})\, D(\varphi)\, (1 + \frac{d^2}{d\varphi^2})\, \tilde{f}(\varphi) = G(\varphi) \qquad (4)$$

Here φ is the angle characterizing the direction of the normal to the FS; $\tilde{f}(\varphi) = \sigma R^{-1}\, df/d\varphi$, where σ and $R(\varphi)$ are the sign and the radius of curvature of the FS; the inhomogeneous term $G(\varphi)$ is proportional to the external electric field; $D(\varphi) \sim T^9$ is rather cumbersome. Note that R and f are different for points with parallel normals, whereas the function $\tilde{f}$ depends only on the variable φ. The corresponding relaxation time contains an additional large factor $(\theta/T)^4$, i.e. $t \simeq t_B(\theta/T)^4$, where $t_B \simeq t_1(\theta/T)^2 \sim T^{-5}$ is the time of "normal" electron diffusion by a distance of roughly p_F, appearing in the Bloch law, $\rho_B \sim t_B^{-1} \sim T^5$, $\theta = sp_F$.

Equations of superdiffusion are rather difficult to derive. Direct expansion of kinetic equations for electrons and phonons involves boundless calculations even in the quadratic approximation in the parameter q/p_F, corresponding to the diffusion equation (1). We used a method based on the variation principle which is that solving a system of kinetic equations is equivalent to finding nonequilibrium distribution functions of electrons $f_{\vec{p}}$ and phonons $g_{\vec{q}}$ minimizing the functional

$$F = \frac{\int d^3p\, d^3k\, d^3q\, K(\vec{p},\vec{k},\vec{q})\, (f_{\vec{p}} - f_{\vec{k}} - g_{\vec{q}})^2}{\left[\int d^3p\, \frac{df_o}{d\varepsilon}\, f_{\vec{p}}\, e\vec{E}\vec{v}\right]^2} \qquad (5)$$

with the kernel $K(\vec{p}, \vec{k}, \vec{q}) \geqslant 0$.

The variational problem is as difficult to exactly solve as kinetic equations. The structure of the functional however suggests possibility of approximate solution. Since the kernel K is positive, F can be essentially decreased only by compensation of the terms in the expression $(f_{\vec{p}} - f_{\vec{k}} - g_{\vec{q}})$ with the best possible aocuracy. To see how small the parenthesis can be, let us solve the set of equations

$$f_{\vec{p}} - f_{\vec{k}} - g_{\vec{q}} = 0, \quad \varepsilon_{\vec{p}} - \varepsilon_{\vec{k}} = \hbar \omega_{\vec{q}}, \quad \vec{p} - \vec{k} = \vec{q}$$

in the first, second, etc. orders in the small parameters q/p_F and s/v, till we arrive at an unsolvable equation. Thereby, it is possible, first, to substantially decrease the class of the functions to be varied and, second, to simplify the functional F with the accuracy required [5]. Variation of the simplified functional leads to a superdiffusion equation. Note that in contrast to conventional calculations using trial functions which are chosen more or less arbitrarily, our method is rigorous.

(2) The relaxation mechanisms of the second group are associated with finiteness of the phonon energy. As has been said, the isolation of the subsystems is enhanced in the measure of dissymmetry of the electron states which can exchange phonons. The relaxation has two stages. At the first stage, the energy dependence of the distribution function becomes such that there is no more mixing of the momentum, both in the linear and in the quadratic approximation in the parameter s/v (we call this state the "local drift"). The local drift relaxation, for any structure of the FS, may be provided by two mechanisms of a different nature.

One of them is the nonlocal mechanism associated with electron scattering by phonons whose momenta are nearly parallel to the FS generatrix (with the angular deviation of the order of s/v). It is readily seen from the energy and momentum conservation in the collision, that electron states bound by such phonons are by far not symmetric. Thus, exchange of such phonons may occur between any two electron states, as in the three-dimensional case. The relaxation time is here $t \simeq t_B\ (v/s)^3$.

The other is the local superdiffusion mechanism in which the relaxation results from phonon exchange between close electron states within the thermal layer. The multiplicity of channels is here due to the fact that each phonon may be responsible for many electron transitions in the region where the Fermi distribution is smeared (see Fig. 3). The relaxation time is here $t \simeq t_B \cdot (\mu/T)^2$, where μ is the chemical potential.

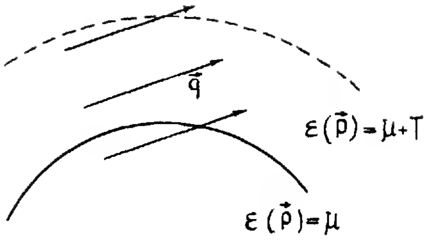

Fig. 3 A phonon with the momentum $\vec{q}$ can interact with various electrons in the FS thermal layer.

(3) Of the mechanisms of the third group, the role of the relatively rare phonon-phonon collisions is the most simple to understand. They provide means for momentum exchange between far apart (along the direction of the velocity $\vec{n}$) subsystems. Obviously, this non-local mechanism should be describable by an integro-differential equation like Eq. (1), in which the diffusion tensor $\hat{D}$ is proportional to the phonon-phonon collision frequency. The relaxation time here $t \sim (\theta/T)^9$. Note that this result is valid when phonons collide with electrons more frequently than with other phonons. In the opposite limiting case, there is momenta mixing inside the phonon system, and therefore $t \simeq t_B$, as in a three-dimensional metal.

Electron-electron collision in two-dimensional metals may also be inefficient. Indeed, in the case of the convex FS, the energy and momentum conservation laws suggest that the initial states $\vec{p}_1$ and $\vec{p}_2$ of colliding electrons are, to within the order of magnitude of T/μ the same as the final states $\vec{p}_3$ and $\vec{p}_4$: $\vec{p}_1 - \vec{p}_3 = \vec{p}_4 - \vec{p}_2 = \vec{K}$, $K \simeq p_F\, T/\mu$ (see Fig. 4).

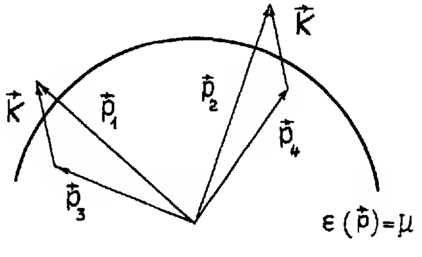

Fig. 4 In a two-dimensional metal with a convex FS, the initial states of colliding electrons are close to the final states.

Relaxation appears in the highest-order terms with respect to T/μ ; the corresponding time is $t \simeq t_0(\mu/T)^2$, where $t_0 \sim T^{-2}$ is the Landau-Pomeranchuk electron-electron collision time, characteristic of three-dimensional metals.

The electron scattering by impurities manifests itself unusually in two-dimensional systems. It goes without saying that the above mechanisms are fully valid for highly pure specimens, where the electron-impurity collision time t_i is much longer than the other transport times of relaxation. However, because of the staged character of the superdiffusion mechanisms, the time t_i can compete with the much shorter times of partial equilibration (e.g. the local drift time). This gives rise to specific interference mechanisms, with the "impure limit" ($t \simeq t_i$) reached only for $t_i \lesssim t_B$, as in the three-dimensional metal [5].

In reality, there always are some minor deviations of the FS from the strictly two-dimensional shape, due to electron tunneling between conducting layers. There are two possible cases. If the FS is within the Brillouin zone close to a strictly cylindrical surface, then the relaxation time is $t \simeq t_B \beta^{-2}$, where $\beta \ll 1$ is the angle characterizing the FS corrugation. If, on the contrary, a prolate FS, being locally nearly two-dimensional ($\beta \ll 1$), is not close to a cylindrical surface (such a geometry is characteristic, e.g., of nonintercalated graphite), then $t \simeq t_B$, as in a three-dimensional metal.

As we have seen, the specific character of the kinetics of two-dimensional metals is associated with an infinite number of approximate quasi-momentum conservation laws, one for each electron-phonon subsystems. However, irrespective of the dimension of the space, there is the problem of conservation of the total quasi-momentum. If there are no Umklapp processes, then in formula (5) the expression $(f_{\vec{p}} - f_{\vec{k}} - g_{\vec{q}})$ and also the functional F and the electric resistivity go to zero because of the drift distribution $f_{\vec{p}} = \vec{u}\vec{p}$ and $g_{\vec{q}} = \vec{u}\vec{q}$. Therefore, our results formally refer to metals with open FS's, where the drift is forbidden by the condition of periodicity of the function $f_{\vec{p}}$ in the $\vec{p}$ space. In the case of metals with closed FS's and unequal number of electrons and holes, the Umklapp processes must be taken into account. Nevertheless, in three-dimensional metals with closed FS's the electric conductivity is usually determined by the diffusion time t_B of electrons on the FS. The reason is that the Umklapp processes procede relatively easily down to quite low temperatures, and thus the diffusion is really the "bottleneck" of the relaxation [3]. It might seem that this should be still more true for two-dimensional metals, in which the diffusion time is much larger than t_B. However, in the two-dimensional case, electron-phonon collisions with Umklapp processes can play quite a different role. Since these give rise to more channels of phonon scattering, they can alter the superdiffusion mechanisms over the entire FS or in some part of it.

4. Sound Propagation

As we have seen, the electron-phonon relaxation time in a two-dimensional metal increases very rapidly as temperature decreases. For this reason, observation of the above asymptotic dependences of the electric conductivity $\rho^{-1} \sim t(T)$ (and under some conditions, of the thermal conductivity too [6]) is difficult, since at low temperatures the principal role is played by another type of oollisions. Besides, the effects considered do not manifest themselves in the electric conductivity of metals with small (as compared with the reciprocal lattice vector) dimensions of the FS, when Umklapp processes are impossible.

These difficulties are less severe in effects accompanying sound propagation in a two-dimensional metal [7]. Deformation interaction with a sound wave does not change the total quasi-momentum of the electron system at each point of the wave (the interaction is even in the momentum); therefore, Umklapp processes are not needed. Then, resonant sound absorption, i.e. when $kl \gg 1$, depends, as is known, on electrons of a narrow region ("belt") of the width $\delta p \simeq p_F(kl)^{-1}$ near the line $\vec{k}\vec{v} = \omega$ on the FS ($\vec{k}$ is the sound wave vector and ω the sound frequency). In such conditions, the relaxation consists in electron displacement in the momentum space by a distance δp small as against p_F. As the belt width decreases, the electron-phonon relaxation times clearly decrease substantially (e.g., in case of the q/p-superdiffusion, by a factor of $(kl)^6$), and these processes become more important than the electron-impurity or electron-electron scattering. Thus, it becomes possible to control the contributions of various relaxation processes by varying the sound wavelength.

Let us consider sound propagating in the plane of two-dimensional layers. Start with extremely long waves for which the space and time inhomogeneities are unimportant and sound absorption is subject to a viscous limit. In this case, the electron distribution function is even in momentum (due to evenness of the deformation potential), and the Bloch diffusion is not forbidden and can be an efficient mechanism of absorption which is qualitatively the same as in a three-dimensional metal: $W \simeq \omega^2 t_B$.

However, even for comparatively long sound waves, the effects of space and time dispersion become significant, which distinguish the two-dimensional system from three-dimensional. Electrons coming from areas with a different sound wave phase are responsible at each point of the space for the odd part of the nonequilibrium correction, whose relaxation is difficult. Thus, there arise in the problem two essentially different times: the even relaxation time $t_s \simeq \simeq t_B (kl)^{-2}$, and the odd relaxation time t_a (the latter being particularly due to the superdiffusion), where $t_s \ll t_a$. Absorption in this region essentially differs from the Landau collision-free absorption $W_L \simeq \omega s/v$, characteristic of the resonance situation in three-dimensional metals:

$$W \simeq W_L \left[\frac{t_a^{-1} + \omega}{t_s^{-1}} \right]^{1/2} \tag{6}$$

This absorption is sensitive to relaxation processes, depends on temperature and is featured by time dispersion. Still more important anomalies arise in the renormalization of the sound velocity [7].

5. Hydrodynamic Effects

The hydrodynamic mechanism of electric conductivity is that frequent normal collisions induce drift of the system of quasi-particles, whose velocity $\vec{u}(\vec{r})$ is determined by collisions with loss of the quasi-momentum in the bulk sample or on the sample surface. The electric conductivity order of magnitude [8] is

$$\rho^{-1} = \frac{ne^2}{p_F} l_{tr}, \quad l_{tr}^{-1} = \left(\frac{d^2}{l_N}\right)^{-1} + l_V^{-1} \tag{7}$$

Here l_N and l_V are the electron mean free paths with respect to normal collisions and collisions with loss of the quasi-momentum, respectively; d is the sample thickness, and l_V, $d \gg l_N$. The temperature dependence of the resistivity contains a minimum, because in the region determined by the inequalities,

$$l_N \ll d \ll (l_N\, l_V)^{1/2} \qquad (8)$$

where the dissipation is determined by the quasi-particle collision with the sample walls, $d\rho/dT < 0$.

The conditions (8) are difficult to fulfill in the case of three-dimensional non-compensated metals, because, owing to the large size of the FS, the electron-phonon Umklapp processes, contributing to the quantity l_V^{-1}, proceed there relatively easily, down to very low temperatures (still, the resistivity minimum, probably of hydrodynamic nature, has recently been observed in potassium [9]). In this respect, favourable materials to observe hydrodynamic effects are acceptor compounds of graphite, in which the electron-phonon U-processes at low temperatures may be neglected. These materials are characterized with small FS's ($p_F \leqslant b/10$, $\vec{b}$ being the reciprocal lattice vector) and very high anisotropy of the conductivity (10^6 or more).

Let us consider the electric conductivity of a plate, with the conductive layers perpendicular to the surface and the electric field applied along the layers and parallel to the plate surface. The drift distribution in a two-dimensional metal is established within the time t_N determined by the superdiffusion, the normal electron-electron collisions and other processes retaining the quasi-momentum (the local drift establishment is attended by very weak hydrodynamic effects which can be neglected). Therefore, when $d \gg l_N$, one naturally deals with the ordinary hydrodynamic situation (7). However, when $d \ll l_N$ there may arise special types of hydrodynamic effects in the two-dimensional case, associated with stopping of the Bloch diffusion for the momentum-odd part of the distribution function [10]. The nature of these effects can be explained by the following simple considerations. An electron moving at a small angle ϑ to the sample surface, emitting phonons, leaves the range of angles of the order of ϑ within the time $t(\vartheta) \simeq t_B\, \vartheta^2 + t_1$ and relaxes on the surface (recall that electric conductivity of a thin plate is determined by grazing electrons). But the phonons emitted are absorbed by an electron of the opposite momentum (the two-dimensional situation offers no alternatives) and also bring it out of the range of small angles. The result of these processes, i.e. that the electron vanishes in the small angle range and simultaneously a hole of the opposite momentum appears, is in a sense similar to the Andreev reflection effect in a superconductor. The hole moves in the opposite direction, but, having a positive charge, it takes energy from the field, as the electron does. Subsequent collisions again convert the hole into an electron having the same velocity as that of the initial. Thus, the effective mean free path length of an electron with respect to collisions with the sample surface is essentially increased as a result of collisions with phonons. It may be determined as the length of the trajectory of a particle involved in one-dimensional Brownian motion with the step $\vartheta l(\vartheta)$ (projected on the normal to the sample surface) and the step time $t(\vartheta)$ before its relaxation on the surface:

$$l_{tr} \simeq \frac{d^2}{\vartheta^2 l(\vartheta)}, \quad l(\vartheta) \simeq v_F\, t(\vartheta) \tag{9}$$

The increase of l_{tr} for small ϑ is restricted by scattering from impurities and any type of volume collisions disturbing the isolation of electron-phonon groups. So unusual hydrodynamics involving grazing electrons may be also the case for thin samples with $d \ll \min(l_B, l_i)$, where the three-diemnsional transport length of the free path is of the order of d. This effect can occur in relatively impure samples (it is only necessary that $l_i \gg l_1$), is almost insensitive to the sample cross section shape and generally is responsible for the minimum in the resistance as a function of temperature.

Note in conclusion that the experimental data for $C_{16}FeCl_3$ and some other intercalated graphite compounds may be described in terms of the ordinary hydrodynamic mechanism, but in conditions unusual for a three-dimensional metal. Namely, the retardation of joint drift is assumed to be determined in a wide temperature range by phonon-impurity rather than electron-impurity scattering. The large value of the thermo-emf $S \simeq e^{-1}$ points to the full mutual drag of electrons and quasi-two-dimensional phonons connected with the electrons. The same approach can account for the characteristically smooth temperature dependence of electric resistivity of these materials. Thus, it seems that even the now available intercalated graphite compound samples offer conditions to observe size effects of the hydrodynamic nature, including the minimum of resistivity as a function of temperature. The minimum due to specific two-dimensional effects must appear in these materials at $T < \Theta$, $d \gtrsim l_1 T \Theta^{-1}$.

References

1. Third Intl. Conference, 1983 - 3$^{\grave{e}me}$ Conférence Intérnationale sur les composés à insertion de graphite, Pont-à-Mousson, 23-25 mai, Sec. C-I. In: Synthetic Metals, 8, No 3-4
2. R.N. Gurzhi and A.I. Kopeliovich, Zh. Eksp. Teor. Fiz. 61, 2514 (1971) Sov. Phys. JETP 34, 1345 (1972)
3. R.N. Gurzhi and A.I. Kopeliovich, Zh. Eksp. Teor. Fiz. 64, 380 (1973) Sov. Phys. JETP 37, 195 (1973)
4. R.N. Gurzhi and A.I. Kopeliovich, Usp. Fiz. Nauk 133, 33 (1981) Sov. Phys. Usp. 24, 17 (1981)
5. R.N. Gurzhi, A.I. Kopeliovich and S.B. Rutkevich, Zh. Eksp. Teor. Fiz., 83, 290 (1982) Sov. Phys. JETP, 56, 159 (1982)
6. R.N. Gurzhi and S.B. Rutkevich, Fiz. Nizk. Temp. 9, 590 (1983) Sov. J. of Low Temp. Phys. 9, 298 (1983)
7. Yu.A. Klimenko and A.I. Kopeliovich, Fiz. Nizk. Temp. 11, 1062 (1985) Sov. J. of Low Temp. 11, 585 (1985)
8. R.N. Gurzhi, Usp. Fiz. Nauk 94, 689 (1968) Sov. Phys. Usp. 11, 255 (1968)
9. Z.-Z. Yu, M. Haerle, J.W. Zwart, J. Bass, W.P. Pratt, Jr., and P.A.Schroeder, Phys. Rev. Lett. 52, 368 (1984)
10. R.N. Gurzhi, A.N. Kalinenko, A.I. Kopeliovich and S.B. Rutkevich, Zh. Eksp. Teor. Fiz. 91, 686 (1986)

ELECTRON-PHONON INTERACTION IN SYSTEMS WITH STRONG ELECTRON CORRELATIONS

D.I. Khomskii
P.N. Lebedev Physical Institute of the Academy of Sciences, Moscow, USSR

1. Introduction

Lattice properties and effects of electron-phonon (EP) interaction in narrow-band systems have a number of specific features. They are connected mainly with the fact that in this case the energy scales of EP interaction (EP coupling constant g and so called polaron energy shift $E_B \sim g^2/\omega$, where ω is a characteristic phonon frequency) can be comparable and even much larger than the bandwidth W. In this case one cannot treat EP interaction as a small perturbation, as is usually done for standard wide band metals and semiconductors, and the properties of the system may change qualitatively. Presumably the best known phenomenon in such a situation is self-trapping of electrons and the formation of small polarons. There exist also other consequences of this interaction different in various specific cases.

In this lecture we will discuss certain topics related to the EP interaction in systems with strongly correlated electrons. It is of course impossible to cover in short lecture all aspects of this wide field. Instead, we shall discuss certain specific problems which will give you an impression of the typical effects of EP interaction in these systems.

We shall discuss below different situations starting from the simplest case of nondegenerate narrow bands (Hubbard model, Sect.2) and then making it successively more complicated, taking into account certain factors important in real substances. to this end we include orbital degeneracy (Sect.3), and we concentrate our attention on the specific phenomena connected with Jahn-Teller effect. Then, besides narrow band, we add also wide bands; the most interesting phenomena occuring in this case are connected with the possibility of valence fluctuations (mixed valence, heavy fermions etc. - Sect.4).

2. Nondegenerate narrow bands (Hubbard model)

The simplest model describing the strongly correlated electrons is the Hubbard model. Including also the electron-phonon interaction one can write down the corresponding Hamiltonian in the form

$$H = \sum_{<ij>,\sigma} t a^{+}_{i\sigma} a_{j\sigma} + U \sum_{i} n_{i\uparrow} n_{i\downarrow} + \sum_{iq\sigma} g_{qi} n_{i\sigma} (b^{+}_{q} + b_{-q}) + \sum_{q} \omega_{q} b^{+}_{q} b_{q} \quad . \qquad (1)$$

Here we take into account the interaction with phonons which bring about the shift of the electron energy levels, e.g. with breathing-type oscillations of ligands around transition metal ions. There exists, in principle, also another type of EP interaction due to a modulation of transfer integral t with the lattice spacing. It would give the terms of the type $g a^{+}_{i} a_{j} (b^{+}_{q} + b_{-q})$ and in momentum representation both these kinds of EP interaction can be written in the form $g_{pq} a^{+}_{p} a_{q+p} (b^{+}_{q} + b_{-q})$ with different g_{pq}. The EP interaction in the Hubbard model may have different consequences. We shall treat three different topics below.

2.1. Polaronic canonical transformation and band narrowing

The most straightforward way to treat EP interaction is the familiar polaronic canonical transformation [1]

$$H \to \tilde{H} = e^{-R} H e^{R} \quad , \qquad R = - \sum_{iq\sigma} (g_{qi}/\omega_{q}) n_{i\sigma} (b^{+}_{q} - b_{-q}) , \qquad (2)$$

or an equivalent shift of phonon operators $b_{q} \to b_{q} - \sum_{i,\sigma} (g^{2}_{qi}/\omega_{q}) n_{i\sigma}$. The transformed Hamiltonian takes the form

$$\tilde{H} = t \sum_{<ij>,\sigma} e^{-R} a^{+}_{i\sigma} a_{j\sigma} e^{R} - E_{B} \sum_{i,\sigma} a^{+}_{i\sigma} a_{i\sigma} + (U - 2E_{B}) \sum_{i} n_{i\uparrow} n_{i\downarrow} + \sum_{i \neq j} V_{ij} n_{i\sigma} n_{j\sigma'} + \sum_{q} \omega_{q} b^{+}_{q} b_{q} , \qquad (3)$$

where

$$E_{B} = \sum_{q} (g^{2}_{q}/\omega_{q}) \; , \qquad V_{ij} = \sum_{q} (g^{2}_{q}/\omega_{q}) e^{i\vec{q}(\vec{r}_{i} - \vec{r}_{j})} \; , \quad g_{qi} = g_{q} e^{i\vec{q}\vec{r}_{i}} \qquad (4)$$

It is readily seen that the transformation of one-site terms amounts to a level shift and to a decrease of Coulomb interaction. Besides this there appears phonon-induced interaction of electrons on different sites. And finally the bandwidth is renormalized:

$$t \to \tilde{t} = t \exp(-E_{B}/\omega) = t \exp(-g^{2}/\omega^{2}) \; . \qquad (5)$$

This is the well known polaronic band narrowing.

It is important to realize the criteria of applicability of such an approach. Polaronic band narrowing has a simple interpretation. Due to EP interaction the lattice around electron at a site i is deformed and the total wave function takes the form $|\Psi_i\rangle = |\psi_i\phi_i\rangle$ where ψ_i is an electron wave function and ϕ_i is the wave function describing the state of a lattice relaxed around electron. The bandwidth is determined by the matrix element $\langle\Psi_i|ta^+_{i\sigma}a_{j\sigma}|\Psi_j\rangle = \langle\psi_i|ta^+_{i\sigma}a_{j\sigma}|\psi_j\rangle\langle\phi_i|\phi_j\rangle = t\langle\phi_i|\phi_j\rangle$, and the scalar product $\langle\phi_i|\phi_j\rangle$ gives the reduction factor in Eq.(5). However, to apply these arguments it is necessary that the phonon cloud around the electron have enough time to be formed. The electron stays at a site for a time $\tau_{el} \sim \hbar/\tilde{t}$, and in order for it to be longer than the phonon time $\tau_{ph} \sim \hbar/\omega$ it is necessary to have $\omega > \tilde{t}$ or $\omega/t > \exp(-g^2/\omega^2)$. The sufficient condition would be $\omega/\tilde{t} > 1$, but at large enough $g^2/\omega^2 = E_B/\omega$ it becomes much less stringent.

2.2. Possible influence of polaronic effects on the exchange interaction

In case of strong interaction $U \gg t$ and half-filled bands $n = N_{el}/N_{at} = 1$ the Hubbard model describes Mott-Hubbard insulator with the localized electrons (see e.g. the review paper [2]). The only freedom left is that of spin orientation. Spin degeneracy is lifted in the second order in t/U and we get an antiferromagnetic exchange

$$H = J \sum_{\langle ij\rangle} \vec{S}_i\vec{S}_j \quad , \qquad J = 2t^2/U \quad . \tag{7}$$

The origin of this exchange is quite transparent. It is due to a virtual transfer of electrons to nearby sites, Fig.1. One sees that such virtual transitions which decrease the kinetic energy, $\Delta E < 0$, are possible for antiparallel spins and are forbidden due to a Pauli principle for parallel ones so that the antiferromagnetic state becomes favourable.

The question arises: how does EP interaction influence this exchange? It seems at first sight that in accordance with Eqs.(3)-(5) the exchange integral will be given by the same expression (7) but with $t \rightarrow \tilde{t}$ and $U \rightarrow U - 2E_B$. However, the detailed treatment shows that in most cases it is not true. In fact, one would obtain such a result if the system lives in all states, including a virtual state with transferred electron, long enough for lattice relaxation to occur. However, the electron stays in an intermediate state with an energy U only for a time $\tau_{virt} \sim \hbar/U$ which for typical cases with $U \gg \omega$ is much less than τ_{ph}. Thus, polaronic effects do not have time to develop and the exchange integral (7) remains unrenormalized [1,3].

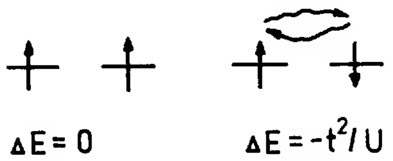

Fig. 1

2.3. "Negative U" and superconductivity of local pairs

Let us now study the effects due to the change of the interaction terms in Eq.

(3). The intersite interaction V_{ij} can bring about spatial correlations in electron positions (at $n \neq 1$); it is equivalent to a charge density wave (CDW) formation. The change of one-site interaction $U \rightarrow \tilde{U} = U - 2E_B$ may have more nontrivial consequences. For a strong enough EP interaction, U may in principle become negative, i.e. it will correspond not to a repulsion but to an attraction between electrons - the so called "negative U" model [4]. As a results, if $U < 0$ and $|U| > t$, all the electrons in the ground state will be bound in singlet pairs [5] which can be called bipolarons [6]. (Actually, it is not due to an EP interaction but rather due to an exchange interaction that such pairs can be formed [7]). Such local pairs have a binding energy $\Delta \cong |U|$ and in general their number is less than the number of sites.

These pairs may have different "fate". They can form a spatially ordered structure due to the interaction V_{ij} and to the second-order terms $\sim t^2/|U|$. Such a state is again equivalent to CDW or, in other words, these pairs will be localized in x-space, in the same way as usual valence pairs in chemistry. Such a state would be insulating.

However, a different kind of ground state is possible here. These pairs, which are similar to Cooper pairs in superconductors, may undergo Bose-condensation in k-space. The resulting state will be a superconducting one. It will be analogous not to a usual BCS state but rather to an old picture of superconductivity due to Schafroth, Butler, and Blatt [8].

It is convenient to describe such a state in the pseudospin representation [9], using the correspondence $\tau_i^z = n_{i\uparrow} + n_{i\downarrow} - 1$, $\tau_i^+ = a_{i\uparrow}^+ a_{i\downarrow}^+$, $\tau_i^- = a_{i\downarrow} a_{i\uparrow}$. Here $\tau_i^z = 1$ describes the state with an electron pair and an $\tau_i^z = -1$ - an empty site.

Using this representation, we can transform the Hubbard Hamiltonian with negative U and $|U| \gg t$ to an effective pseudospin Hamiltonian similar to (7):

$$H_{eff} = \frac{2t^2}{|U|} \sum_{<ij>} \vec{\tau}_i \vec{\tau}_j - \mu \sum_i \tau_i^z \quad , \tag{8}$$

where we have also introduced a term with the chemical potential μ which permits us to account for a fixed number of electrons in our system $n = \sum_i (1 + \tau_i^z)$.

The Hamiltonian (8) describes "isotropic antiferromagnet" in an external field. Antiferromagnetic ordering in τ^z, $<\tau_{2i}^z> = - <\tau_{2i+1}^z>$, would describe the structure with alternating occupied and empty sites, i.e. the CDW state. However, we know that in an isotropic antiferromagnet the spins orient perpendicular to the field. That is, not the averages $<\tau_i^z>$, but $<\tau_i^x>$ or $<\tau_i^+> = <a_{i\uparrow}^+ a_{i\downarrow}^+>$ are nonzero - and these are just the superconducting anomalous averages! So the superconducting ordering is quite probable here.

One can analyse different properties of such a superconductor with local pairs [9]. In contrast to the usual BCS state in which the radius of a Cooper pair is equal to the coherence length $\xi = \hbar v_F/T_c$ ($T_c \cong \Delta$ where Δ is an energy gap), here the binding energy of a pair is large, $\Delta \cong |U|$ - much larger than $T_c \cong t^2/|U|$. Correspondingly, the radius of a pair is of the order of interatomic distance d - much smaller than $\hbar v_F/T_c$. All the other properties of this state also differ markedly from those of the BCS state. Thus, the upper critical magnetic field $H_{c2} \sim \phi_0/d^2$ [9] is very high. The most important thing here is an interaction between "bosons" - the fact ignored in Ref. [10], which led the authors of this work to erroneous conclusions.

It seems that up to now there exist no real superconductor in which the strong inequality $|U| >> t$ holds. However, it is possible that some systems (e.g. heavy fermion superconductors or newly discovered high T_c superconductors of the oxide type (like $La_{2-x}(Ba,Sr)_xCuO_4$ [11]) approach this limit or at least are "on a way" to it. In any case, this model describes the opposite limiting case of extremely strong coupling wrt BCS (weak, coupling, $|U| << t$) and investigation of this case may be useful also for a qualitative understanding of the most interesting and delicate intermediate situation $|U| \sim t$.

3. Degenerate Hubbard model and cooperative Jahn-Teller effect

The first important aspect which we have to take into account when applying Hubbard model to transition metals and rare earth compounds is the orbital degeneracy of d and f-levels (see e.g. [12]). Such a degeneracy does often occur in actual cases; for instance such ions as Cu^{2+}, Cr^{2+} and Mn^{3+} have a doubly degenerate state in cubic crystalline field. The most interesting phenomena in this case are related to Jahn - Teller theorem which states that any degeneracy except the Kramers one, brings about instability of the system and (in a static case) results in the reduction of the symmetry and the lift of the degeneracy.

The interaction responsible for Jahn-Teller (JT) effect is the interaction of degenerate electronic states with the phonon modes lifting the degeneracy:

$$H_{JT} = \sum_{iq\sigma} g_{qi}(n_{i1\sigma} - n_{i2\sigma})(b_q^+ + b_{-q}) \quad . \tag{9}$$

Here the index σ describes degenerate orbitals and, say for Cu^{2+}, takes the values $\sigma=1,2$. More specifically, the ion Cu^{2+} in the oxygen or fluorine octahedron has a configuration $3d^9$ with one d-hole in a doubly-degenerate e_g-level. This degeneracy is lifted if we elongate or compress the octahedron (Fig.2), which stabilizes respectively the (hole) orbitals of $d_{x^2-y^2}$ or d_{z^2} type (there also exists another vibrational mode which additionally lifts this degeneracy).

If we exclude phonons in the usual way, we get, similar to the term with V_{ij} in Eq.(3), the interaction between degenerate orbitals on different centres:

$$H_{JT} = \sum_{ij\sigma\sigma'} V_{ij}(n_{i1\sigma} - n_{i2\sigma})(n_{j1\sigma'} - n_{j2\sigma'}) \ . \tag{10}$$

This interaction brings about the cooperative orbital ordering in a crystal (coopera-

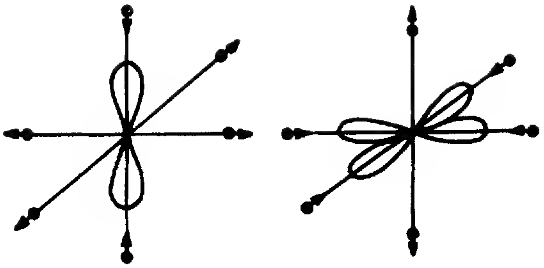

Fig. 2

tive in Jahn-Teller effect). As can be seen in Fig.2, the occupation of certain specific orbital is equivalent to the appearence of a quadrupolar moment so that this ordering is simultaneously a quadrupolar one. It is also evident that it is accompanied by the lattice distortion and yields the structural phase transition. Thus, in contrast to the more of other types of such transitions, cooperative Jahn-Teller ordering is nothing but just a type of structural phase transitions whose microscopic origin is certain.

The structures which arise as a result of such transitions may be fairly complicated. This is e.g. the case in a layered perovskite K_2CuF_4 with a basic structure of K_2NiF_4 - type and with Jahn-Teller ions Cu^{2+}. The orbital and crystalline ordering in it predicted theoretically [13], and later confirmed experimentally, is shown in Fig. 3. It consists of the elongated octahedrons CuF_6, with long axes alternating along the x and y axes in a basal plane, providing overall orthorombic symmetry. The same mechanism may, in principle, be operative in systems based on La_2CuO_4. One can even think that strong JT interaction between degenerate orbitals on Cu^{2+} ions and the corresponding vibrations of sorrounding O_6 octahedrons may be responsible for the high superconducting transition temperatures obtained in this class of materials.

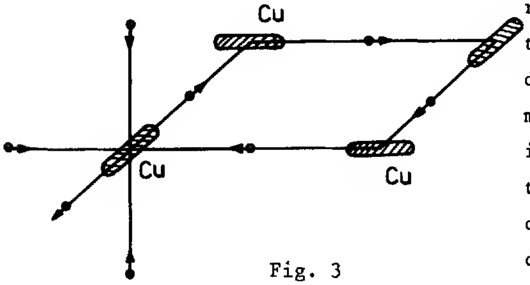

Fig. 3

It is also worth noting that besides the EP interaction (9) the orbital ordering may be caused by the usual superexchange interaction of the type (7) itself [12]. In this case for doubly-degenerate orbitals and with only a "diagonal" electron transfer $t_{11}=t_{22}=t$, $t_{12}=0$ we get instead of Fig.1 the situations shown in Fig.4. The corresponding energy gains are indicated below. Besides of the direct Coulomb interaction U we included also interatomic exchange interaction $- J_H \sum_i S_{i1}S_{i2}$ responsible for Hund rule which gives parallel orientation of electron spins in the atom.

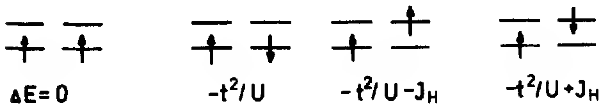

Fig. 4

Fig.4 shows that the lowest energy here has the state which is "antiferromagnetic" in orbitals and ferromagnetic in spins..Thus the very exchange interaction provides here the mechanism for both spin and orbital orderings. We may say that we have here "Jahn-Teller ordering without Jahn-Teller (i.e. electron-lattice) interaction".

The actual form of the resulting exchange Hamiltonian and the character of resulting orbital and magnetic structures depend on the specific form of the orbitals, the type of crystal structure etc., and may in general, be rather complicated but the qualitative ideas exposed above provide a general understanding of the problem EP interaction in systems with orbital degeneracy may have some extra consequences, e.g. strong temperature dependence of the effective exchange integrals [3]; we shall not discuss these problems here.

4. Electron-lattice interaction and valence fluctuations

Valence fluctuations, mixed valence (MV), and heavy fermions (HF) arise in compounds containing unfilled 4f- or 5f-shells when the corresponding (upper-most) f-levels E_f cross the conduction band and lie in the vicinity of the Fermi-level ε_F (see [14]). The usual description of these systems is based on the periodic Anderson model (Anderson lattice)

$$H = \sum_{k,\sigma} \varepsilon_k a^+_{k\sigma} a_{k\sigma} + \sum_{i,\sigma} E_f f^+_{i\sigma} f_{i\sigma} + U \sum_i n_{fi\uparrow} n_{fi\downarrow} + \sum_{i,k,\sigma} (V_{ik} f^+_{i\sigma} a_{k\sigma} + \text{h.c.}). \qquad (11)$$

In the simplest approach which is presumably valid for MV compounds, the f-level itself lies at ε_F. Due to f-d hybridization, V, it acquires a finite width $\Gamma = \pi\rho V^2$ (ρ is the density of states of the conduction band) and becomes a resonance. Γ plays a role of the bandwidth of "f-band" and corresponds to a width of a peak in the total density of states $\rho_f(\varepsilon)$ near ε_F. The usual scale of Γ in MV compounds is $\Gamma \sim 10^{-2}$eV $\sim$ $\sim 10^2$K; in HF compounds the width of corresponding peak near ε_F is even smaller, $\Gamma \sim$ $\sim 1 \div 10$ K (the nature of this peak in HF compounds may be more complicated, see below). It is important that here we have not impurities, but a concentrated system with such f-centres in each cell, i.e. the number of states in such a peak in ρ_f is $\sim$ 1 per cell ($\sim 10^{22}$ cm^{-3}).

As $\rho_F \sim 1/\Gamma$, the density of states at the Fermi-level in these systems is huge, $10^2 \div 10^3$ times larger than in ordinary metals like Cu or Al. Correspondingly large is, for instance, the electronic specific heat $c = \gamma T, \gamma \sim \rho_f(0) \sim 1/\Gamma$. Thus if, say, in Cu $\gamma = 0.7$ mJ/mole$\cdot$K^2, in UBe$_{13}$ $\gamma = 1000$ and for CeAl$_3$ $\gamma = 1620$ mJ/mole$\cdot$K^2. Similarly, the magnetic susceptibility is also large, $\chi(0) \sim \rho_f(0)$. If we recall that in the usual approach $\rho \sim p_F m^*$, we may say that high values of ρ_f mean large effective masses of electrons $m^* \sim 10^2 \div 10^3\, m_0$. These are just the "heavy fermions" [15].

Now, let us discuss the manifestation of EP interaction in valence-fluctuating compounds.

4.1. Electronic phase transitions

The position of f-level vs. Fermi-level may be effectively changed in these systems by the external pressure, composition, and sometimes the temperature. Thus, if we compress the substance, the f-level shifts upwards and may cross the Fermi-level. If $E_f < \varepsilon_F$, f-level is occupied e.g. by one f-electron (for simplicity we ignore here f-d hybridization). If however E_f becomes larger than ε_F, then part of f-electrons "spills over" into a conduction band. This leads to the decrease of the number of f-electrons, n_f, i.e. the valence of f-ions increases. Such a phenomenon is actually observed in many systems, for instance in SmS or in Ce. This transformation occurs usually as a first order phase transition sometimes ending at a critical point. Under this transition the volume of the crystal changes up to 20% but the lattice symmetry remains the same. From the large volume change and from the fact that such a transition is induced by the pressure, one can conclude that the electron-lattice interaction plays here an important role. It is connected with the fact that the ionic radius changes drastically during the valence change $(r(f^{n-1}) < r(f^n))$.

The simplest way to describe this effect is by taking into account the dependence of the f-level position E_f on a specific volume v: the distance between the f-level and the Fermi-level may be written as [14,16]

$$E_g = \varepsilon_F - E_f = E_{go} + a(v - v_o) \quad . \tag{12}$$

It is clear that this dependence yields the tendency to a first order phase transition induced by the pressure. If we compress our system, $\delta v = v - v_o < 0$, then the f-level shift upwards and it becomes easier to excite extra f-electrons from it to the conduction band across the "gap" E_g. But such excitation leads to a further decrease of v due to a formation of "small" ions with a configuration f^{n-1}. In turn this decrease about an extra rise of the f-level and a further decrease of E_g etc. At certain moment this process becomes avalanche-like and brings about the first order phase transition.

One can formalize the above arguments by writing down the total energy of the system as a function of volume and of a number of electrons excited into the band $\nu = 1 - n_f$:

$$E(\nu,v) = E_g\nu + \frac{B}{2}(\delta v)^2 = (E_{go} + a\delta v)\nu + \frac{B}{2}(\delta v)^2 \quad . \tag{13}$$

After minimization of the expression (13) in v we obtain $(\nu) = E_{go}\nu - (a^2/2B)\nu^2$. So we see that when for a deep f-level (large E_{go}) the minimum is reached at $\nu=0$, i.e. the f-level is occupied, for an f-level which is high enough (small E_{go}) the minimum jumps over to $\nu=1$ (empty f-level). Thus a first order phase transition occurs at which n_f jumps from 1 to 0.

There exist certain factors (see [16]) which stop this transition a "halfway" and stabilize the MV phase; due to space limitations we shall not discuss this question here.

Let us mention one extra point. The same mechanism of electron-lattice coupling which is responsible for phase transition influences significantly also the elastic properties of MV compounds. Thus the compressibility of these substances is usually anomalously high. But the most spectacular result was obtained in a study of phonon spectra of MV phase of SmS (with Y addition) [17]. It was found that in this crystal which resembles typical ionic substance (crystal structure of NaCl-type) longitudinal optical phonons lie below the transverse ones in the entire Brillouin zone! The same is also true for acoustic phonons in a large part of Brillouin zone. Presumably this is a unique situation in solid state physics. It is due to the factors discussed above: MV ions are very soft relative to breathing-type deformations and these deformations contribute strongly to the longitudinal modes and only weakly to transverse ones.

4.2. Polaronic narrowing of f-level

Similarly as in the case of Hubbard model (Sect.2), the EP interaction may lead to a substantial renormalization not only of a position but also of a width of f-level. As the lattice deformation around the sites with $n_f=1$ and $n_f=0$ is different, the respective matrix element for the transitions between these states V decreases: $V\to\tilde{V}=V\exp(-g^2/\omega^2)$. Correspondingly, the width of f-peak in the density of states will be narrowed, $\Gamma\to\tilde{\Gamma}=\pi\rho\tilde{v}^2$. Again for this narrowing to occur rather stringent conditions should be met. This question is discussed in detail in ref. [18].

Apparently, a more important effect may arise not due to the lattice relaxation during f-d transition but due to the relaxation of electrons themselves [19]. The electron density oscillations have different energies (from 0 to ε_F), and the question of time scales for them is not so critical as for phonons: there are always oscillations rapid enough to bring about the screening. For this mechanism, one obtains the renormalization of f-level width:

$$\Gamma \to \tilde{\Gamma} = \Gamma \exp\left\{-\lambda \int_{\tilde{\Gamma}}^{\varepsilon_F} \frac{\alpha(\omega)}{\omega}\, d\omega \right\} . \tag{14}$$

Here λ is a dimensionless coupling constant and $\alpha(\omega)$ is a spectral density of relevant oscillations. For phonons $\alpha(\omega)\to 0$ as $\omega\to 0$. But for electron-hole pairs (density oscillations in an electron gas) this is not the case: $\alpha(\omega)|_{\omega\to 0}\to\text{const}$. As a result, the integral in Eq.(14) diverges, and this would give $\tilde{\Gamma}\to 0$ which would correspond to orthogonality of electron states before and after f-d transition (Anderson orthogonality catastrophe [20]). In fact, in our case density oscillations not fast enough (with inverse frequencies longer than the lifetime of f-electron at a site $\tau\sim\hbar/\tilde{\Gamma}$, i.e. with energies $<\tilde{\Gamma}$) do not contribute to a relaxation so the integral in Eq.(14) has nonzero lower limit. The solution of a resulting equation gives the expression

$$\tilde{\Gamma} = \Gamma\left(\Gamma/\varepsilon_F\right)^{\frac{1}{1-\lambda}} , \qquad (15)$$

similar to that found in the X-Ray problem [21], which describes the strong narrowing of f-level due to a relaxation of the Fermi-sea of conduction electrons in the course of f-d transition.

One may also put forth the arguments that this effect becomes even stronger if we take into account the relaxation of the electrons of internal atomic shells [22]. All these factors together may presumably explain very small values of Γ and large m* in HF compounds.

4.3. Kondo-volume collapse

The last problem which we shall discuss here concerns a more sophisticated approach to the origin of heavy fermions and to an explanation of electronic phase transitions of the type of γ-α transition in Ce. In this concept the genesis of heavy fermions is sought in collective effects and is ascribed to a Kondo-effect. In this model it is supposed that the f-level lies, although not very deep, but still below ε_F and is occupied by a nearly integral number of electrons. In this case, the same as in Hubbard model with $U \gg t$ and n=1, one pass from the Anderson Hamiltonian (11) to an effective spin Hamiltonian which describes f-d exchange - the famous Kondo Hamiltonian

$$H_K = J \sum_i \vec{S}_i \vec{\sigma} \qquad , \qquad J = \frac{V^2}{\varepsilon_F - E_f} \quad . \qquad (16)$$

In this approach the peak in $\rho_f(\varepsilon)$ at ε_F arises due to a Kondo effect and its width is $\Gamma \sim T_k \simeq \varepsilon_F \exp(-1/J\rho)$. The EP interaction here enters the game through the dependence of E_f, V and consequently J and T_k on a volume v. This dependence may be rather strong and may lead to a first order phase transition with a simultaneous jumps of V, T_k and Γ. In this model, in contrast to the approach presented in Sect.4.1, it is the change of width and not of position of the peak in $\rho_f(\varepsilon)$ that is essential. This kind of approach was applied to discuss the γ-α transition in Ce [23]. Actually similar ideas were also used to describe the origin of superconductivity in HF compounds - the very interesting question which however in beyond the scope of this lecture.

* * *

Summarizing we say that the role of electron-phonon interaction in systems with narrow bands and strong electron correlations differs in many respects from that in the usual wide-band systems. It has many important consequences which should be taken into account in any realistic theory of corresponding phenomena.

References

1 P.M. Chaikin, A.F.Garito, A.J. Heeger, J.Chem.Phys.58,2336(1973)

2 D.I. Khomskii, Fiz.Metallov i Metallovedenie 29,31(1970)

3 K.I. Kugel, D.I. Khomskii, Sov.Phys. JETP, 52,501(1980)

4 P.W. Anderson, Phys.Rev.Lett.34,953(1975)

5 I.O. Kulik, A.G. Pedan, Sov.Phys. JETP 52,742(1980)

6 A. Alexandrov, J. Ranninger, Phys.Rev.B24,1164(1981)

7 P.W. Anderson, Mater.Res.Bull.8,153(1973)

8 M. Schafroth, S. Butler, J. Blatt, Helv.Phys.Acta, 30,93(1957)

9 L.N. Bulaevskii, A.A. Sobyanin, D.I. Khomskii, Zh.Exp.Teor.Fiz. 87,1490(1984) (Sov.Phys. JETP 60,856(1984))

10 A.S. Alexandrov, J. Ranninger, S. Robaszkiewicz, Phys.Rev.B33,4526(1986)

11 J.G. Bednorz, K.A. Müller, Zs.Phys.B64,189(1986)

12 K.I. Kugel, D.I. Khomskii, Sov.Phys. Uspekhi 25,231(1982)

13 D.I. Khomskii, K.I. Kugel, Solid State Commun.13,763(1973)

14 D.I. Khomskii, Sov.Phys. Uspekhi 22,879(1979)

15 G.R. Stewart, Rev.Mod.Phys.56,755(1984)

16 D.I. Khomskii, in Quantum Theory of Solids, Ed. I.M. Lifshits, Moscow, MIR Publ. 1982, p.70

17 H.A. Mook, R.M. Nicklow, T. Penney, F. Holtzberg, M.W. Shafer, Phys.Rev.B18, 2925(1978)

18 A.C. Hewson, D.M. Newns, J.Phys.C13,4477(1980)

19 Yu. Kagan, N.V. Prokofyev, Zh.Exp.Teor.Fiz.90,2176(1986)

20 P.W. Anderson, Phys.Rev.Lett.18,1049(1967)

21 P. Nozieres, C.T. DeDominics, Phys.Rev.178,1097(1969)

22 K.A. Kikoin, D.I. Khomskii, Abstracts of 24th Soviet conference on low temperatures, Tbilisi 1986, v.2, p.5; Pis'ma v Zh.Exp.Teor.Fiz.45,396(1982)

23 M. Lavagna, C. Lacroix, M. Cyrot, Phys.Lett.90A,210(1982)

DENSITY OF STATES OF A 2-D ELECTRON GAS IN A MAGNETIC FIELD

A. L. Efros
A. F. Ioffe Physico-Technical Institute,
194021 Leningrad, USSR

1 Introduction

The quasi-two-dimensional electron gas appears in the inversion layers near the interface of the MOS structure or in heterojunctions. The electron gas is confined in the narrow potential well in one direction (z-axis), so that the quantization of their motion in this direction leads to a set of discrete levels. The electron gas can be considered as two-dimentional if the energy separations between these levels are larger than any other energy of importance. An interest in the 2-D electron gas has increased during the last decade due to the wide technical applications of the structures with inversion layers and the discovery of the quantum Hall effect. In the magnetic field which is normal to the inversion layer, the energy spectrum of electrons becomes absolutely discrete due to the quantization of orbital motion in the plane of the layer. It has the form:

$$E_N = \hbar\Omega(N + 1/2) \;, \qquad (1)$$

where $\Omega = eH/mc$, H is the strength of the magnetic field, m is the effective mass of an electron, the quantum number N is an integer (or zero). The density of states (DOS) consists of a sharp δ-function peak at the energy $E = E_N$. The degeneracy of the levels (Landau levels-LL) in a unit area is $n_o = 1/2\pi\lambda^2$, where $\lambda^2 = \hbar c/eH$. Elastic scattering leads to a broadening of levels. For short range scatteres and strong magnetic fields the form of the peaks is known only for N=0. However the form of the wings of these peaks can be found at any N. Namely the density of states $G_n(E)$ is

$$G_N(E) \sim \exp\,(E - E_N)^2/\Gamma_N^2, \qquad (2)$$

where Γ_N is the LL width given by

$$\Gamma_N^2 = h\Omega \frac{\hbar}{\tau} f(N), \tag{3}$$

τ is the elastic scattering time, $f(N)$ is a dimensionless function, decreasing with increasing N as $\ln N/N$. Recent experiments on the activation energy [1,2], capacitance [3], and specific heat [4] show that the DOS inbetween the LLs is much larger than that given by eq.(2) with Γ_N(3). Moreover recent experiments on photoluminescence and some other experiments show that the DOS depends essentially on the filling factor $\nu = n/n_0$of LL. Here n is the surface concentration of electrons. The width of the level has a minimum at $\nu = q + 1/2$, where q is an integer and has maximum at $\nu = q$. So the width of the levels oscillates with the filling of the LLs. Its maximum value, as obtained from luminescence data, is of the order of $\hbar\Omega$ [5]. Then one should write the DOS $G(E,\nu)$ as depending on two arguments and when analyzing the data on the energy dependence of the DOS one must know whether they are obtained at fixed ν or not. From the above experiments only the luminescence can give the DOS at fixed ν. All others give $G(E_F)$, which is the DOS at the Fermi energy E_F as a function of E_F at different ν. For magnetocapacitance measurements [3]:

$$G(E_F) = \frac{dn}{dE_F}, \tag{4}$$

and this is an exact relation. I think that activation energy analysis [1,2] gives nearly the same DOS when E_F, refered from the nearest LL, is larger than the correlation energy of the electrons which occupy this level.

The occupation dependece reveals the many-electron nature of the DOS. Ando [7] put forward the idea that oscillation of the LL width in a strong magnetic field may appear due to the oscillation of electron screening. Shklovskii and Efros [8] follow this idea and propose a theory (see sect.2) which explains the large value of the DOS between LLs at integer ν. The theory uses the concept of long-range fluctuations of the concentration of charged impurities and nonlinear screening worked out by Shklovskii and Efros [9] for 3D electrons and by Gergel and Suris [10] for 2D electrons. In sect.3 the influence of separate centers is considered which provides an asymmetric energy dependence of the DOS.

2 Long-range fluctuations

Consider the plane z=0 with a 2-D electron gas and suppose that there are randomly distributed charge centers in the volume at z>0, with concentration N_i. These centers are impurities in the case of the GaAs-GaAlAs heterojunction or build-up charge of oxide in the case of the MOS structure. Our main points are:

i) Charge centers create a random potential which leads to the broadening of the LLs.

ii) The 2-D electrons screen the potential, however in the strong magntic field electrons of the filled levels do not take part in the screening.

iii) This leads to the oscillation of the random potential with the filling factor.

The broadening is maximal at integer ν and minimal at ν= integer + 1/2.

To find the random potential we devide the plane with the electron gas into squares L * L and build cubes L*L*L with these squares as bases. We consider now the random potential with characteristic length of the order of L. The mean number of charge centers within one cube is $N_i L^3$ and typical fluctuations of this number are $\sqrt{N_i L^3}$. So a typical value of the random potential with size L is of the order

$$\gamma(L) = \frac{e^2}{\varkappa L} (N_i L^3)^{1/2} \qquad (5)$$

(we neglected numerical factors here), $\varkappa$ is the dielectric constant. The $\gamma(L)$ tends to infinity as L tends to infinity which is a well known property of random Coulomb centers [9]. The 2-D electrons screen the long range potential. To find the screening radius we propose that all electrons of unfilled LL leave the squares with potential humps for the squares with potential wells. Their surface concentration in the well becomes twice as large but is still of the order of $\delta n=|n - N_0 n_0|$, where N_0 is the number of filled levels. The electron produce potential difference between the squares of the order of

$$\phi = \frac{e^2}{\varkappa}\delta n\, L \quad , \tag{6}$$

which smoothes the random potential. One can see that if $L \gg L_c$ where

$$L_c = \frac{N_i}{(\delta n)^2} \quad . \tag{7}$$

Then $\phi \gg \gamma$, which means that a small amount of electrons should pass from one square to another to screen the potential. However for $L \ll L_c$ we have $\phi \ll \gamma$ and this means that electrons cannot screen such harmonics of the random potential at all. So the length L_c is a nonlinear screening radius. The most important random potential harmonics has size L_c and amplitude

$$\gamma(L_c) = \frac{e^2}{\varkappa}\frac{N_i}{\delta n} \quad . \tag{8}$$

Fluctuations with larger L are screened by electrons while fluctuations with smaller L produce a smaller potential.
The lenght of L_c is much larger than the magnetic length λ so the random potential we have found can be considered as a smooth bending of all LLs (Fig.1). If $\delta n \ll n_0$, electrons are at the deepest wells and E_F as infered from the average LL position is of the order of $\gamma(L_c)$:

$$E_F = -\alpha \frac{e^2}{\varkappa}\frac{N_i}{\delta n} \quad , \tag{9}$$

where α is an unknown numerical factor. Using eq.(4) one obtains for the DOS

$$G(E_F) = \frac{d\delta n}{dE_F} = \alpha \frac{e^2}{\varkappa}\frac{N_i}{E_F^2} \quad . \tag{10}$$

Thus, we obtained a power law instead of an exponential law (eq.2). The activation energy is the difference between the percolation energy and the Fermi energy (Fig.1). For the 2-D symmetrical random potential the percolation level E_p coincides with the average value and is independent of δn. When analysing the activation energy data, the DOS

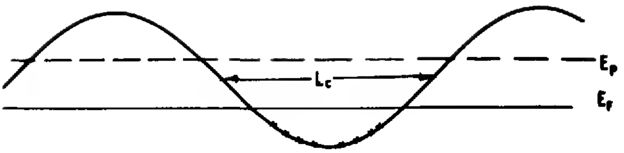

Fig.1. The full curve is the LL bended by the random potential. The straight line is the Fermi level and the dashed line is the percolation level. Crosses show the occupied electronic states.

G is defined by the relation

$$G^{-1}(E_A) = -\frac{dE_A}{d\delta n} \quad . \qquad (11)$$

Since $E_A = E_p - E_F(\delta n)$, one can use eq.(10) for the DOS obtained by activation energy analysis. Note that the energy dependence obtained in [1] is similar to an E_F^{-2} law. Eq.(10) can also be used for analysis of magnetocapacitance data.

So far we proposed that $\gamma(L_c) \ll \hbar\Omega$. When δn decreases the Fermi level goes down and at certain points in the plane the next filled LL, which is bended like the previous one, intersects the Fermi level. Holes then appear at this level (Fig.2) which take part in the screening. Hence the further decrease in the concentration of electrons decreases $\gamma(L_c)$ due to the screening of the random potential by the holes and electrons of the next LL.

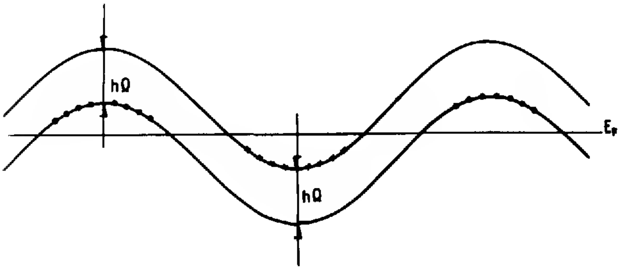

Fig.2. Electrons (crosses) and holes (circles) in the two LL bended by the random potential.

This means that the maximum width of the LL is of the order of $\hbar\Omega/2$. It occurs at the integer values of the filling factor. At these points the DOS is minimal and equals

$$G(E_F) = \alpha\,\frac{e^2}{\varkappa}\,\frac{4N_i}{(\hbar\Omega)^2} \quad . \qquad (12)$$

The above theory is applicable if $N_i L_c^3 \gg 1$ which means that

$$(\delta n)^{1/2} \ll N_i^{1/3} \ , \tag{13}$$

i.e. the average distance between electrons at the unfilled level is larger than the distace between the centers. It is also proposed that L_c is larger than the width of the region with charge centers (for example the oxide width in the MOS structures). Otherwise the DOS would be exponential.

3 The influence of the separate centers

In previous section we considered the fluctuations of charge concentration in volume containing large numbers of centers. We now show that the separate centers can produce a comparable effect when they are close to the interface. Consider the centers which are in a thin layer from z to z+dz. Their number per unit area is $N_i dz$. Suppose they are positive. If $z \gg \lambda$, each center lowers the LL in the nearest point in the plane $z=0$ by the energy $E=-e^2/\varkappa z$. The DOS can be calculated in a simple way

$$G(E) = N_i \frac{dz}{dE} = \frac{N_i e^2}{\varkappa E^2} \ . \tag{14}$$

If $\delta n \ll n_0$ all electrons lie in such wells, so that E_F can be found as follows:

$$\delta n = \int_{-\infty}^{E_F} G(E) dE = \frac{N_i e^2}{\varkappa E_F} \ . \tag{15}$$

By comparing eq.(15) with eq.(9) one can see that the separate centers produce a shift in the Fermi level of the same order as do the long-range fluctuations. The DOS however has in this case an asymmetrical form (Fig.3). For positive centers the tails of the LLs appear at low-energy edges and for negative centers they appear at high-energy edges. The DOS which is due to the long-range fluctuations is dependent of the sign of centers and symmetrical. The above consideration is valid if the average distance between electrons $(\delta n)^{-1/2}$ is much larger than the typical distance z from centers to

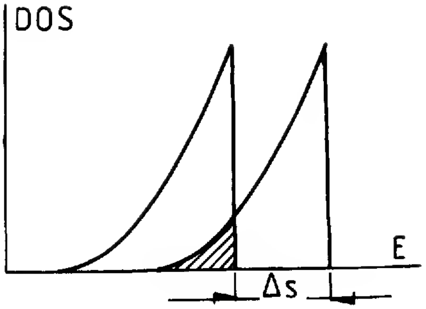

Fig.3. The DOS for two overlapping spin levels caused by separate positive centers

the plane. This distance is of the order of $e^2/\varkappa E_F$. We then see that the theory is valid if eq.(13) is fulfilled. Suppose now that a LL is filled. If the magnetic field is so strong that $e^2/\varkappa\lambda \ll \hbar\Omega$ the distribution of electrons in the plane is uniform and the potential of centers is unscreened. So, the occupation of the next LL goes through these stages which involve the same potential wells, created by the same separate centers, as was the case for the previous level.

For silicon however an opposite condition $e^2/\varkappa\lambda \gg \hbar\Omega$ is usually fulfilled. The situation with separate centers is more difficult . The potential wells formed by those centers which are very close to the plane do not change their occupation under the influence of a magnetic field. But, for remote centers whose potential $e^2/\varkappa\lambda \lesssim \hbar\Omega$, the magnetic field is strong and occupation of corresponding wells behaves as in the case of a strong field. Such centers create the DOS described by eq.(14) under each LL if its filling factor is small.

In general to calculate the DOS one must take into account both the long-range fluctuations and the separate centers. If however, the concentration of the centers is non-uniform one of these two mechanisms may prevail. If the concentration decreases with z, the separate centers are more important. If it increases they are less important. For example one should not take them into account if the structure has a spacer with length of the order of the average distance between the centers.

The assymmetrical DOS can explain the shift of the quantum Hall plateaus corresponding to the filled spin levels in Si MOS structures with increase in the Na^+concentration in the oxide, which has been observed by Furneaux and Reinecke [11]. The electron concentration corresponding to the centers of plateaus increases with the Na^+concentration N_i. The explanation proposed by the authors [11] is shown in Fig.3. Suppose that the DOS of different LL do not overlap but for the same levels the DOS of different spin levels do overlap.

One can see that to fill the lower spin level it is necessary to fill the shaded part of the higher spin level. The integral over the shaded region gives the shift. We can calculate it using the DOS eq.(14):

$$\Delta n = \int_{-\infty}^{\Delta s} \frac{N_i e^2}{\varkappa E^2}\, dE = N_{ox} \frac{e^2}{\varkappa d \Delta s} , \qquad (16)$$

where Δn is the shift, $N_{ox}=N_i d$, d is the oxide thickness, Δs is the spin splitting. The result satisfactorily fits the experimental data. The symmetrical part of the DOS provided by the long-range fluctuations does not contribute to the shift.

It should be noted finally that the charge centers play an important role in the formation of the DOS of the 2-D electron gas in a magnetic field at least when the filling factor is nearly integer.

REFERENCES

1. E.Stahl, D.Weiss, G.Weinmann, K. von Klitzing and K.Ploog, J.Phys.C 18, L783,(1985)
2. M.G.Gavrilov and I.V.Kukushkin, Pis'ma Zh.Exp.Teor.Fiz. 43 , 79, (1986)
3. T.P.Smith III, W.I.Wang, P.J.Stiles, Phys.Rev.B 34, 2995,(1986)
4. E.Gornik, R.Lassing, G.Strasser, H.L.Stoermer, A.C.Gossard, W.Weigmann, Phys.Rev.Let., 54, 1820,(1985)
5. I.V.Kukushkin,V.B.Timofeev, Pis'ma Zh. Exp.Teor. Fiz.43, 387, (1986)
6. S.G.Semenchinskii, Pis'ma Zh. Exp. Teor. Fiz. 41, 497, (1985)
7. T.Ando, J.Phys.Soc.Japan 43, 1616,(1977)
8. B.I.Shklovskii, A.L.Efros, Pis'ma Zh. Exp.Teor.Fiz. 44, 520, (1986)
9. B.I.Shklovskii, A.L.Efros, Electronic properties of doped semiconductors, Springer-Verlag (1984)
10. V.A.Gergel, R.A.Suris, Zh. Exp.Teor. Fiz. 84, 719, (1983)
11. J.E.Furneaux, T.L.Reinecke Phys.Rev. 33, 6897, (1986)

GENERATION AND PROPAGATION OF PHONONS IN CRYSTALLINE AND AMORPHOUS SILICON UNDER OPTICAL EXCITATION

T.I.Galkina
Lebedev Physical Institute Academy of Sciences
Moscow,USSR

1 Introduction

The heat pulse technique [1] is widely applied for the investigation of nonequilibrium phonons, but up to date it provides only the semiquantitative information on phonon propagation regime. This is caused by the lack of information about spectral distribution of initially generated phonons, the scarcity of experimental data about the values of phonon scattering rates due to the anharmonic interactions and isotopic impurities, τ^{-1} and $\tau^{*^{-1}}$, respectively and because of the mathematical difficulties with solution of the equation describing the nonequilibrium phonon propagation [2]. Neverthteles the first attempts based on Monte-Carlo computer simulation were undertaken to predict the spectrum of optically excited phonons [3].

An attempt of quantitative account for the shape of the heat pulse for various modes of propagation of optically excited phonons is presented in Sect.2.

The heat pulse technique also provides the information about thermalization of the spectrum of equilibrium phonons in a-Si:H film, which is discussed in Sect.3.

2 Quasidiffusion

Absorption by semiconductor crystal of laser light with $\hbar\nu > E_g$ results in generation of hot charge carriers near the illuminated sample surface. Losing its energy the carrier produces a train of high-frequency phonons: the optical and the acoustic ones. The optical phonons decay into phonons of acoustic branch. The two major types of interaction which the emitted acoustic phonons take part in, are: scattering by lattice imperfections (mainly isotopes) and three phonon anharmonic processes, i.e. decay and coalescence.

The rates of all the processes involved depend dramatically on the phonon frequency. With the frequency belonging to the linear part of the dispersion curve, the probabilities of the isotopic scattering ${\tau^*}^{-1}$, and anharmonic decay τ^{-1} are given by the well-known relations:

$$ {\tau^*}^{-1} = \eta\omega_D(\omega/\omega_D)^4 , \tag{1} $$

$$ \tau^{-1} = \gamma\omega_D(\omega/\omega_D)^5 . \tag{2} $$

Here ω_D is the Debye frequency, η and γ are material-defined constants [4].

If the defect scattering dominates, i.e. $\tau^* \ll \tau$, then the ω-frequency phonon during its lifetime τ will undergo multiple elastic collisions separated in time by τ^*. This results in diffusive propagation with frequency-dependent diffusion coefficient. Such a propagation mode, proposed in [5], was called "quasidiffusion". After the lapse of time equal to τ a phonon will be separated from the initial point by a mean distance l:

$$ l \sim \sqrt{D\tau} , \tag{3} $$

where D is the diffusion coefficient, $D = \frac{1}{3}s^2\tau^*$, and s is the sound velocity. The phonon mean free path with respect to elastic scattering will be:

$$ l^* = s\tau^* . \tag{4} $$

In the opposite case ($\tau \ll \tau^*$) the "quasiballistic" mode is expected to be settled, that is the phonons will propagate along the crystal decaying on the phonons of lower frequencies. For example, it was shown theoretically [6] that for Si the decay LA ⇒ TA + TA is the most probable one. In order to get the rough idea of the type of phonon propagation mode which is realized in our experimental conditions several estimations were done(cf. eqs.(1)-(4)). The calculated values of τ, τ^*, l_{LA*}, l_{TA*} and l/l_{LA*} for several successive phonon generations are given in the Table 1. The values of s_{LA}, s_{TA}, γ and η used for the calculations were taken from [6]. In fact, for $\nu \sim \omega_D/2\pi$, our estimates have only the illustrative purpose because the relations(1),(2)are valid only in the linear region of the dispersion curve.

Table 1

Parameters characterizing the nonequilibrium phonon kinetics in silicon.

ν [THz]	τ [s]	τ^*[s]	l_{LA}[cm]	l_{LA*}[cm]	l_{TA*}[cm]	l/l_{LA*}
8	$2.5*10^{-10}$	$1.0*10^{-10}$	$5.3*10^{-5}$	$9.0*10^{-5}$	$5.4*10^{-5}$	0.59
4	$7.9*10^{-9}$	$1.6*10^{-9}$	$1.2*10^{-3}$	$1.4*10^{-3}$	$8.7*10^{-4}$	0.83
2	$2.5*10^{-7}$	$2.6*10^{-8}$	$2.7*10^{-2}$	$2.7*10^{-2}$	$1.4*10^{-2}$	1.2
1	$8.1*10^{-6}$	$4.1*10^{-7}$	$6.2*10^{-1}$	$3.7*10^{-1}$	$2.2*10^{-1}$	1.7
0.5	$2.6*10^{-4}$	$6.6*10^{-6}$	13.9	5.9	3.6	2.4

$s_{LA}= 9*10^5$cm/s, $s_{TA}= 5.4*10^5$cm/s, $\gamma = 6.3*10^{-4}$, $\eta = 9.3*10^{-4}$

ν – frequency of phonons, τ –inverse scattering rate due to spontaneous decay, τ^*– inverse scattering rate related to the isotopic scattering, $l_{LA}*$, $l_{TA}*$- mean free paths of longitudinal and transverse phonons, limited by isotopic scattering, l – distance which phonons of a given generation pass during the lapse of time of order of τ ("diffusion length"), l/l^*– characterizes the "quality" of diffusion during the lifetime τ of a given phonon generation (phonons are in the diffusive regime if the inequality $l/l^* \gg 1$ holds). The data were calculated for 5 succesive phonon generations, the frequency of each next generation is 1/2 of the frequency of the previous one. The first generation arises after the decay of optical phonons with $k = 0$ into acoustic ones.

According to the Orbach model [7] one can expect the first generation of acoustic phonons to have the frequency $\omega_1 = \omega_{LO}/2$, where ω_{LO} is the frequency of a long-wave optical phonon. But only the phonons with $l \approx l^* \sim 1$cm can reach the detector. These phonons have frequency ≤ 1THz and can appear only after three successive decay events, i.e. in the fourth generation. It will take a time $t \sim \tau(\omega_1)+\tau(\omega_2)+\tau(\omega_3) \approx \tau(\omega_3)$, for our data $t \sim 0.3\mu s$ (cf. Table 1).

As we said the diffusive propagation of phonons take place if $l/l_{LA}* \gg 1$. Let us check this condition. It can be seen from the Table 1 that for the phonons of fourth generation $l/l_{LA}* \approx 1.7$. It means that even phonons of this generation do not move diffusively. Hence, the mode of nonequilibrium phonon propagation caused by the optical excitation of the crystal is nearly quasiballistic but not quasidiffusive one [8].

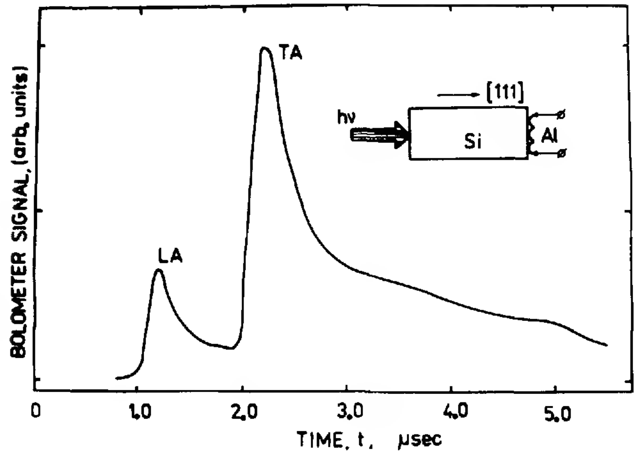

Fig.1. Heat (phonon) pulses arising after optical excitation of crystalline silicon.

We have measured the ratio (β) of amplitudes of LA- to TA-phonon peaks. in the wide range of excitation levels (from $10^{-1}\mu J/cm^2$ to $10^4\mu J/cm^2$). The basic geometry of our measurements is the conventional phonon "transmission" scheme [9], (see insert in the Fig.1). The 6mm in dia and of 10 mm length, cylinder-shaped Si sample was immersed in the LHe bath at the temperature 1.6K to 2K and was illuminated by $\lambda = 0.34\mu m$ radiation of pulsed nitrogen laser. The laser pulse energy was attenuated by the neutral filters, in the range 10^{-2} to $3\mu J$. The size of the laser spot at the sample was changed by the axial displacement of the lense and was in the range from $3*10^{-5}cm^2$ to $3*10^{-1}cm^2$. The duration of the laser pulse was $\sim$ 10ns. The granular Al thin film, evaporated onto sample surface, served as a phonon detector [10].

One can believe that with the density of incident energy less than $10^4 J/cm^2$ the occupation numbers remain small ($n < 1$) during the whole period of the time-evolution of nonequilibrium phonon distribution. That means that the process of three-phonon coalescence [11] can be disregarded.

Having taken into account the phonon focusing in [111] direction, the absorption of the phonons in the bulk of bolometer material (Al) and the acoustic mismatch of the media, we have estimated the value of β to be 0.6 - 0.7 in the whole range of the used incident energy densities [12]. One can conclude that in our experimental conditions the appreciable amount of heat propagates ballistically, or to be more precise, quasiballistically. The quasiballistic phonon propagation mode by contrast to quasidiffusive or diffusive one, do not smear the

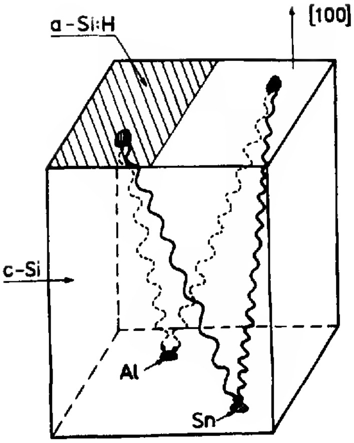

Fig. 2. Phonon generator -detector crystal geometry with electrically heated generators of phonons. Weavy lines show the propagation paths of fast TA-phonons. The detectors were located with the account of focusing of STA-phonons in [100] crystal direction.

phonon focusing pattern [13], so we believe, the ratio β does not differ essentially from the estimated value.

On the basis of the above speculations we can depict qualitatively the heat pulse shape: The beginning of the pulse leading edge is not delayed with respect to arrival time of ballistic phonons of given polarization and frequency but the pulse rise time is determined by the total of lifetimes of all preceding generations (here the three) which results with the time of $\sim 0.25\mu s$ in our case. The signal peak is followed by the flat decrease. Its time of decay is limited by the lifetime of the IV generation (Table 1 gives $\tau(\omega_4) \sim 8\mu s$), cf. Fig. 1.

3 Nonequilibrium phonons in amorphous films of a-Si:H

It is a well known fact that the anomalous thermal properties of the glasses (the temperature dependence of specific heat, plateau of the thermal conductivity, ultrasound absorption etc.) can be explained on the basis of two-level systems (TLS), the physical nature of which being not yet understood well. In spite of this, a number of models exist, suggesting several types of phonon interactions: Namely the resonant, elastic and inelastic and also the fracton model [14].

The data given in [15,16] resulted in contradictory conclusions, in particular in [15] it was asserted that the inelastic scattering process arises not in the amorphous film, but on the boundary of amorphous film/crystal.

The experimental procedure, widely used now, is the measurement scheme similar to the double-beam method in optics, that is two phonon beams are compared and on the path of one of them the amorphous film is situated. The substrate serves both for comparison and for the elongation of the phonon propagation time.

We have carried out two experiments with the a-Si:H films. The first series of experiments was performed in collaboration with W.Eisenmenger, K.Lassman and O.Koblinger (the Stuttgart University, FRG). The nonequilibrium phonons were injected into the Si sample by means of thin layered metallic heater.

It is worthwile to emphasize that in it was noticed already [17,18] that the shape of the heat pulse arising after optical excitation differs strongly from those generated by the metal film evaporated onto the surface of the sample (the case of "Planckian" generator). One can draw the conclusion that, as in the case of optical excitation, the phonon spectrum is enriched in the high-frequency region, and due to strong dependence of τ and τ^* on frequency (cf.(1),(2)), the heat pulse propagation modes in this two cases can be different and the thermalization processes of both the phonon spectra can be different too.

In our early work [9] we have observed the narrowing of the phonon pulses (as compared to the case of excitation of crystalline Si), generated under optical excitation of a-Si:H film. We have interpreted it in terms of phonon thermalization process in amorphous material. In [9] the existence of TLS was suggested. Two level states provide the phonon thermalization in a-Si:H. Later on similar data were obtained by Strom et al [18]. The measurements of the specific heat and thermal condutcivity at 0.1-5K [19] supported this idea.

In our experiments a layer of a-Si:H of thickness of 1.5μm was sputtered in Ar + H_2 atmosphere (H ~ 12%) onto the half of the upper surface of the c-Si sample. Next a thin-film metal heaters were evaporated (of the area of 1 mm^2) on this layer and on the free surface of the sample . The heaters were heated by electrical current pulses. Phonons emitted by the heaters penetrated into the sample (propagation direction nearly parallel to [100]) and were detected by two detectors, Fig.2.

The alignment of the generator and the detector was adjusted in such a way, that the crystallographic directions of phonon propagation from a-Si:H and c-Si towards the detectors were the same (in purpose

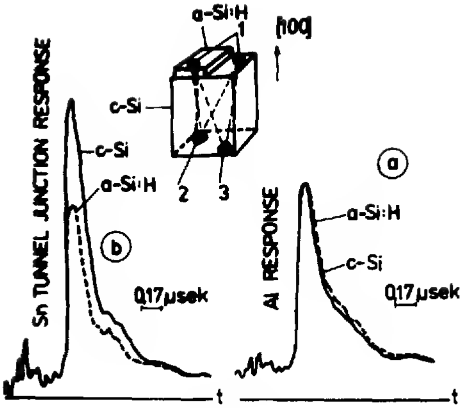

Fig.3. Experimental data with electrically heated generators of phonons.

a. Phonon signals from a-Si:H and c-Si : Response of a broadband detector (Al).

b. Phonon signals from a-Si:H and c-Si: Response of Sn - STJ superconducting tunnel junction (a frquency-threshold detector)

to eliminate the focusing effects [13]) and the distances of propagation of both beams of phonons were equal.

The first detector acted as a broadband phonon detector (Al) but the second one - superconducting tunnel junction (Sn-I-Sn) had the threshold frequency ∽ 290 GHz. Therefore the former (Al) detected all the phonons, and the latter (Sn) - mainly the phonons with the frequency greater than 290 GHz.

While using the Al detector both the signals from a-Si:H and c-Si were practically equal (cf. Fig.3a). Any changes of the initial phonon spectrum occuring in the a-Si:H layer could not influence the response of the detector. On the contrary, in the case of Sn-detector the signal coming from the a-Si:H was of 40% less, Fig.3b. That means the initial "Planckian" phonon spectrum after phonons have been crossing the a-Si:H layer is rearranged in such a manner, that nearly half of

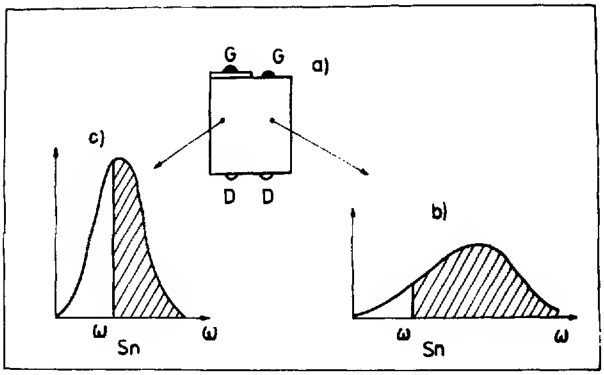

Fig.4. Schematic drawing of nonequilibrium phonon spectrum thermalization in a-Si:H layer.

a. Sample

b. Phonon spectrum in c-Si

c. Phonon spectrum in c-Si after phonons have been traversing the a-Si:H layer first.

ω_{th} - threshold frequency of STJ, (STJ is sensitive to the shaded part of the spectrum only).

it is shifted towards the frequency range less than 290 GHz. The qualitative explanation of the observed effect is given schematically in Fig.4.

Analogous experiment was carried out under optical excitation of phonons. The arrangement of the upper face of the sample (with the a-Si:H) was analogous as in the first case. On the opposite side of the sample the structure Sn-SnO-Sn was evaporated. One of the Sn films acted as a bolometer while the structure as a whole formed the superconducting tunnel junction. The threshold frequency was ≈ 290 GHz as previously. The measurements were carried out at the temperature ∼ 1.28 K, for the bolometer working point shifting ($T_C^{B=0}$=3.7K) the superconducting solenoid was used. The nitrogen laser beam was focused (λ = 0.34μm) at two points at the sample surface, Fig.5.

The ratio of phonon signal integrals from a-Si:H and c-Si was measured. It should be pointed out that in the case of a broadband registration (bolometer) the integral of phonon signal from a-Si:H was larger than from c-Si. We have noted this fact earlier in [9]. It is interesting, that in the case of metal film heating these signals were equal, see Fig.3a. We have no clear explanation of this phenomenon yet. One can suggest this is connected with the different quantum efficiency of a-Si:H and c-Si. Therefore not the amplitudes but the integrals of the signals were compared. That is we compared the quantities of energy registered by the detector.

It was found out that in the case of bolometer registration the ratio of signal integrals from a-Si:H and c-Si was about 1.5. In the

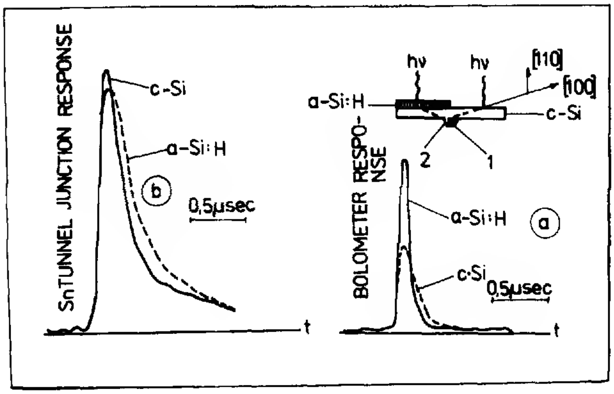

Fig.5. Experimental data with optical excitation phonons.
a. Phonon signals from a-Si:H and c-Si : Response of broadband detector (Al).
b. Phonon signals from a-Si:H and c-Si: Response of frquency -threshold detector (Sn-STJ).
Insert: Experimental geometry.
1. Sn-bolometer.
1-2. Sn STJ.

case of frequency-threshold registration this ratio decreases down to 0.9, Fig.5. In other words the a-Si:H layer thermalizes the nonequiibrium spectrum, shifting it to the region of frequencies less than 290 GHz.

These results were obtained in cooperation with M.M.Bonch-Osmolowskii, A.J.Blinov, and Ju.Ju.Pokrovskii.

REFERENCES

1. R.J.von Gutfeld, in "Physical Acoustics", ed.by W.Mason, Acad. Press, London v.5,(1968).
2. D.V.Kazakovtsev, Y.B.Levinson, Phys.st.sol.(b),96, 117,(1979).
3. J.P.Wolfe, G.A.Northrop, in : Proc.of the fourth Int.Conf.on Phonon Scattering in Cond.Mat.,Stuttgart, 1983, ed.by W.Eisenmenger, K.Lassmann, S.Dottinger, Springer-Verlag, Berlin, p.100,(1984).
4. J.W.Tucker, V.W.Rampton, Microwave ultrsonics in solid state physics, North-Holland, Amsterdam (1972).
5. D.V.Kzakovtsev, Y.B.Levinson, Pis'ma Zh.Exp.Teor.Fiz.27,194,(1978).
6. Sh.Tamura, Phys.Rev.B 31, 2574, (1985)
7. R.Orbach,Phys.Rev.Lett., 16, 15,(1966).
8. A.S.Alekseev, M.M.Bonch-Osmolovskii, T.I.Galkina, Proc.of the second Int.Conf.on Phonon Physics, ed.by J.Kollar,N.Kroo, N.Menyahard, World Scientific, (1985) p.445,.
9. A.S.Alekseev, M.M.Bonch-Osmolovskii, T.I.Galkina, J.B.Levinson, D.P.Utkin-Edin, Pis'ma Zh.Exp.Teor.Fiz. 37, 490, (1980)
10. A.S.Alekseev, A.Yu.Blinov, M.M.Bonch-Osmolovskii, T.I.Galkina, Kr.Soobshch.po fizikie FIAN, N11, 12, (1984).
11. D.V.Kzakovtsev, Y.B.Levinson, Zh.Exp.Teor.Fiz. 88, 2228,(1985).
12. A.S.Alekseev, M.M.Bonch-Osmolovskii, J.Ju.Verkialis, T.I.Galkina, D.P.Utkin-Edin, Fiz.Tverd.Tela (Leningrad), 29, 393, (1987).
13. H.J.Maris, Journ.Acoust.Soc.Am., 50,part 2, 812, (1971).
14. S.Hunklinger, W.Arnold, in "Physical Acoustics", ed.by W.Mason, R.N.Thurston, Acad.Press, London v.12, p.155, (1976).
S.Alexander,R.Orbach,J.Phys.-Lettres, 43, L625, (1982).
15. J.Wolter, R.Horstman, Sol.St.Comm., 37, 171, (1981).
16. W.Dietsche, H.Kinder,Phys.Rev.Lett., 47, 1413, (1979).
17. V.S.Bagaev, G.Bielska-Lewandowska, M.M.Bonch-Osmolovskii, T.I.Galkina, S.J.Lewandowski, G.N.Mikhailova, A.G.Poyarkov, G.Jung, Zh.Exp.Teor.Fiz. 77, 2117, (1979).
18. U.Strom, J.C.Culberston, P.B.Klein, S.A.Worf, ref.6, p.338.
19. J.E.Graubner, B.Golding, L.C.Allen, J.P.Knights, D.K.Biegelsen, Phys.Rev.B 29, 3744, (1984).

BOUND QUASIPARTICLES SCATTERING BY POINT IMPURITIES IN ONE-DIMENSIONAL SYSTEMS AS A SOLITON PROBLEM

A.M. Kosevich , Yu.S. Kivshar and O.A. Chubykalo

Institute for Low Temperature Physics and Engineering
47 Lenin Avenue, Kharkov-164, 310164, USSR

Contents

1. Introduction
2. Scattering of nonlinear Schrödinger soliton
   2.1. Soliton-type excitations of nonlinear Schrödinger equation
   2.2. Evolution of soliton parameters
   2.3. Emission from fast soliton
   2.4. Two point impurities. Resonant soliton scattering
   2.5. Scattering of soliton by random impurities
3. Scattering of small-amplitude sine-Gordon breather
   3.1. Localized impurity."Relativistic" case
   3.2. Correlation between sine-Gordon breather and nonlinear Schrödinger soliton

1. Introduction

Many kinetic characteristics of crystals are determined by the nature of the quasiparticle excitation scattering (e.g., phonons, spin waves etc.) by impurities. Intensive external perturbations in crystals can arise quasiparticle fluxes of high density, when the interaction between scattering quasiparticles becomes essential. Accounting of this interaction seems to be particularly important when it is attractive and can form the bound state of quasiparticles. If the collisions of the quasiparticles with impurities occur rather seldom, the quasiparticles manage to form the bound state between collisions. Then they scatter by an impurity not separately, but as a cluster. Naturally, a question arises in what way the scattering intensity of a single cluster consisting of N quasiparticles relates to the total scattering intensity of N free quasiparticles. To answer this question, it is necessary to examine the role of quasiparticles interaction in scattering. This analysis is the simplest in one-dimensional case when many problems of particles interaction are exactly solvable.

Dynamics of a system of interacting quasiparticles in the mean field approximation is described by a nonlinear equation (e.g., nonlinear Schrödinger or sine-Gordon equation). Consider a point center in such nonlinear one-dimensional system which is able to scatter elementary excitations. Let the incident flux of quasiparticles be dense enough to form their bound state before scattering. The bound state of a large number of quasiparticles in a nonlinear system is equivalent to a dynamical soliton, its amplitude being proportional to the number of bound quasiparticles [1 - 4]. We shall calculate the intensity of the "N-particle" soliton scattering and compare it with the total intensity of free N-particle scattering.

In Section 2 scattering of a soliton by a point impurity is considered in terms of the nonlinear Schrödinger (NLS) equation. The NLS equation is known to describe the nonlinear dynamics of quasiparticles in many problems of solid state physics. For example, excitations of weakly non-ideal Bose gas in self-consistent approximation can be described by this equation (see [1 - 3]). Consideration of the nonlinear magnetization wave dynamics in a ferromagnet of the easy-axis type anisotropy [4] , as well as the problem of the soliton motion along the quasi-one-dimensional moleoular chain, reduce to the analysis of the soliton-type solutions of the NLS equation. And, finally, the NLS equation describes both the dynamics of the envelope of phonon excitations under intensive pulsed action on a crystal [5,6] and the propagation of the surface nonlinear waves in dielectrics or semiconductors [7] . In the Section scattering of a soliton by localized point impurity, by a pair of impurities, and by a random system consisting of a large number of impurities is considered.

Section 3 deals with the scattering of a small-amplitude, two-parameter soliton (breather) of the sine-Gordon (SG) equation by an isolated impurity. The SG equation is usually employed when describing the magnetization wave motion in a ferromagnet with the easy-plane anisotropy [4] , nonlinear excitations of magnetic flux in long Josephson junctions [8] and in case of localized optical oscillation in anharmonic chains [9] .

2. Scattering of Nonlinear Schrödinger Soliton

2.1. Soliton-Type Excitations of Nonlinear Schrödinger Equation

Let us consider weakly non-ideal gas of quasiparticles with the following dispersion law

$$\omega = \omega_0 + k^2 . \tag{1}$$

In the mean field approximation the states of the gas are described by the wave function $\Psi(x,t)$ which, in absenoe of the scattering centres, obeys the equation (see, e.g., [1 - 3]):

$$i\Psi_t - \omega_0\Psi + \Psi_{xx} + 2g|\Psi|^2\Psi = 0 , \tag{2}$$

where g characterizes the potential of binary interaction ($g > 0$).

Consider the case of an impurity in the matrix which locally changes the characteristic frequency ω_0 of the system. Then the additional singular term should be introduced to the right-hand side of the Eq.(2) :

$$i\Psi_t - \omega_0\Psi + \Psi_{xx} + 2g|\Psi|^2\Psi = \varepsilon\,\delta(x)\Psi , \tag{3}$$

where ε is the local perturbation intensity. The solution of the Eq.(3) being presented in the form

$$\Psi(x,t) = g^{-1/2}\, u(x,t)\, \exp(-i\omega_0 t)$$

the following equation takes place for the function $u(x,t)$:

$$iu_t + u_{xx} + 2|u|^2 u = \varepsilon\,\delta(x)\, u , \tag{4}$$

here the parameter ε will be treated as small ($\varepsilon^2 \ll 1$).

Equation (4) for any value of real parameter ε has the following integral of motion

$$N = \int_{-\infty}^{\infty} |u|^2\, dx \tag{5}$$

which corresponds to the total number of quasiparticles.

In the linear limit ($u \ll 1$) when one can neglect the third (nonlinear) term in the left-hand side (4), this equation would describe scattering of the wave excitation with the dispersion law $\omega = k^2$ by a point impurity. This scattering is characterized by the single value - reflection coefficient R_0 ,

$$R_0 = \varepsilon^2/(\varepsilon^2 + 4k^2) , \tag{6}$$

where k is the wave number of the incident wave. The transmission coefficient T_0 is defined as

$$T_0 = 1 - R_0 = 4k^2/(\mathcal{E}^2 + 4k^2). \tag{7}$$

When scattering N equivalent free quasiparticles by an impurity, R_0N of them reflect while T_0N transmit.

If interaction between quasiparticles is taken into account, i.e. if the nonlinear term in Eq.(4) is considered, the result becomes more complicated because scattering in this case depends on greater set of parameters. It should be noted at first that in homogeneous nonlinear system, i.e. at $\mathcal{E} = 0$, a bound state of quasiparticles exists which is described by an exact solution of the NLS equation in the form of two-parameter dynamical soliton (we use designations accepted in the Ref. 10)

$$u_s(x,t) = 2i\eta \frac{\exp\left[-2i\xi x - i\Delta(t)\right]}{\cosh\left[2\eta(x - x_0(t))\right]}, \tag{8}$$

$$\Delta(t) = 4(\xi^2 - \eta^2)t, \qquad x_0(t) = -4\xi t, \tag{9}$$

where 2η is the soliton amplitude describing the number of bound in it quasiparticles :

$$N = 4\eta, \tag{10}$$

the soliton velocity in the designations being $V = -4\xi$. The soliton energy then equals to

$$E_s = 4\eta\omega_0 + 16(\xi^2\eta - \tfrac{1}{3}\eta^3) \tag{11}$$

and represent the sum of free quasiparticle energies $4\eta\omega_0 + 16\xi^2\eta = N(\omega_0 + 4\xi^2) = N(\omega_0 + V^2/4)$ and their interaction energies (attraction) :

$$E_{int} = -\frac{16}{3}\eta^3 = -\frac{1}{12}N^3. \tag{12}$$

The form of the attraction energy (12) corresponds to the well known property of weakly non-ideal Bose gas with attraction, namely collapse occurs in the system at $N \to \infty$. This unnatural behaviour of the real system can be avoided, e.g., by accounting for weak three-particle repulsion between the quasiparticles (see Ref. 3).

Using Eq.(12) one can easily obtain the binding energy of a quasiparticle in the soliton as a minimum work required to remove one particle from the soliton and to convert it into a free particle. The binding energy takes the form

$$|\partial E_{int}/\partial N| = \tfrac{1}{4}N^2 = 4\eta^2. \tag{13}$$

At $\eta \to 0$ the soliton (8) delocalizes and corresponds to a linear wave (quasiparticle) with the wave number k , where $k^2 = 4\xi^2$.

2.2. Evolution of Soliton Parameters

It is well known that the slow variations of the soliton parameters due to the perturbation (a local inhomogeneity in our case) can be obtained in adiabatic approximation. The latter is based on an assumption that the form of a soliton is still described by Eq.(8), however its parameters ξ , x_0 , η and Δ are, in addition, dependent on "slow" time εt . The simplest method for derivation of adiabatic equations which determine the time dependence of the soliton parameters is as follows. The Hamiltonian of the perturbed system (4) takes the form

$$H = \int_{-\infty}^{\infty} dx \, (|u_x|^2 - |u|^4 + \varepsilon \delta(x) |u|^2) . \tag{14}$$

Then the function $u(x,t)$ is taken in the form (8) with indefinite parameters. Symple calculations yield the result

$$H = 16 (\xi^2 \eta - \tfrac{1}{3} \eta^3) + 4\varepsilon \eta^2 \operatorname{sech}^2(2\eta x_0) . \tag{15}$$

Now suppose that relations between canonically conjugated variables (which correspond to a soliton in the unperturbed NLS system) remain the same after the perturbation is "switched on". The mentioned canonical variables can be naturally introduced in terms of the inverse scattering transform (see Ref. 10):

$$p_1 = - 4\xi , \quad p_2 = 4\eta , \quad z_1 = 2\eta x_0 , \quad z_2 = \Delta . \tag{16}$$

The Hamiltonian (15) being presented as a function of the variables (16) and the Hamiltonian equations being written for the variables, i.e. $dp_n/dt = - \partial H/ \partial z_n$, $dz_n/dt = \partial H/ \partial p_n$ (where $n = 1,2$), the following equations are obtained for the soliton parameters :

$$dx_0/dt = - 4\xi , \tag{17}$$

$$d\xi/dt = - 2\eta^2 \varepsilon \tanh(2\eta x_0) \operatorname{sech}^2(2\eta x_0) , \tag{18}$$

$$d\eta/dt = 0 , \tag{19}$$

$$d\Delta/dt = 4 (\xi^2 - \eta^2) + 2\eta \varepsilon \operatorname{sech}^2(2\eta x_0) . \tag{20}$$

If no restrictions are imposed on the perturbation amplitude , the Eqs.(17)-(20) can be treated as a consequence of variational principle based on the perturbed Hamiltonian (15). However it should be noted that these equations are the first step in the consistent perturbation theory for solitons by Karpman and Maslov [11,12].

As follows from (19) the soliton amplitude in the adiabatic approximation does not change, i.e. $\eta = \eta_0$ = const. Eqs.(17) and (18) uncouple from the Eq.(20) and reduce to the equation of classical mechanics

$$\frac{d^2x_0}{dt^2} = -\frac{\partial}{\partial x_0} U(2\eta x_0), \quad U(Z) = \frac{2\varepsilon\eta}{\cosh^2 Z} \qquad (21)$$

which describes the motion of a particle of unit mass with coordinate x_0 in the effective potential $U(2\eta x_0)$. Note that the intensity of the effective potential and the width of its localization (see (21)) depend considerably on the soliton amplitude.

It is easy to obtain a solution of the equation (21) describing adiabatic behaviour of the soliton parameter x_0 (the coordinate of the effective particle) when scattering of a soliton by an impurity:

a) in case $4\xi^2 < \eta\varepsilon$ at $\varepsilon > 0$ (reflection of a soliton from an impurity)

$$x_0(t) = -\frac{1}{2\eta}\mathrm{Arsh}\left\{\left[(\varepsilon\eta/4\xi_0^2) - 1\right]^{1/2}\cosh(8\eta\xi_0 t)\right\}; \qquad (22)$$

b) in case $4\xi^2 > \varepsilon\eta$ at $\varepsilon > 0$ and arbitrary ξ^2 at $\varepsilon < 0$ (passing of a soliton over the impurity)

$$x_0(t) = -\frac{1}{2\eta}\mathrm{Arsh}\left\{\left[1 - (\varepsilon\eta/4\xi_0^2)\right]^{1/2}\sinh(8\eta\xi_0 t)\right\}, \qquad (23)$$

where $\xi_0 \equiv \xi(t = -\infty)$. The soliton velocity $V = -4\xi(t)$ and its phase $\Delta(t)$ for a given dependence $x_0(t)$ is determined by the relations (17) and (20).

For $\varepsilon < 0$ oscillatory motion of a soliton is possible near the attractive inhomogeneity (the bound state of a soliton with an impurity is equivalent in linear limit to the so-called local oscillations, see Ref. 13). However solutions of this type will not be considered here because we are interested in the scattering processes only.

2.3. Emission from Fast Soliton

The unperturbed NLS equation is well known to be exactly integrable by the inverse scattering technique [10]. Thus, it is naturally to study the scattering process at small ε in terms of the theory of perturbations based on the inverse scattering transform (e.g., [11,12]).

Consider at first scattering of a rather fast soliton by an impurity (this process is schematically illustrated in the Fig. 1 ; it corresponds to $\xi_0 > 0$). The term "rather fast" would mean the soliton whose velocity variations during its interaction with an impurity are small. The corresponding condition has the following form :

$$\xi_0^2 \gg |\varepsilon| \eta \ . \tag{24}$$

This condition allows to neglect the velocity variations in scattering.

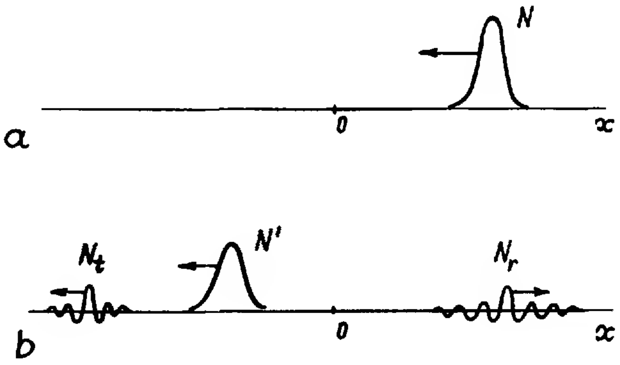

Fig.1. Scattering of a fast soliton (the impurity is located in the point $x = 0$): a) before scattering, b) after scattering; N_t and N_r being the numbers of quasiparticles radiated in forward and backward directions, N' being the number of bound quasiparticles after the scattering

The spectral density of quasiparticles $n(\lambda)$ emitted by the scattering soliton can be obtained using the well-known relation of the inverse scattering transform [10] (see also Refs. 13)

$$n(\lambda) = \pi^{-1} |b(\lambda)|^2 , \tag{25}$$

where $b(\lambda)$ is the scattering coefficient (the so-called Jost coefficient) used in the inverse scattering technique (in the framework of perturbation theory one can takes $|b(\lambda)|^2 \ll 1$), λ is the real spectral parameter related with the wave number $k(\lambda)$ and frequency $\omega(\lambda)$ of the emitted linear waves (quasiparticles), i.e. $\omega(\lambda) = k^2(\lambda) = 4\lambda^2$. Evolution of the Jost coefficient $b(\lambda)$ in the presence of perturbations is determined by the equation (see, e.g., [11-13])

$$\frac{\partial b(\lambda,t)}{\partial t} = 4i\lambda^2 b(\lambda,t) + \varepsilon\int_{-\infty}^{\infty} dx\, P[u]\,\varphi_1(x,t;\lambda)\,\psi_2^*(x,t;\lambda) - $$
$$- \varepsilon^*\int_{-\infty}^{\infty} dx\, P^*[u]\,\varphi_2(x,t;\lambda)\,\psi_1^*(x,t;\lambda)\,, \qquad (26)$$

where $\varphi_{1,2}(x,t;\lambda)$ and $\psi_{1,2}(x,t;\lambda)$ are the components of one-soliton Jost functions [10], $\varepsilon P[u]$ is the right-hand side of Eq.(4), i.e. in the considered case it is of the form $\varepsilon P[u] = \varepsilon\delta(x)u$.

The Jost functions for the soliton (8) take the form [11,12]

$$\psi(x,t;\lambda) = \begin{pmatrix}\psi_1(x,t;\lambda)\\ \psi_2(x,t;\lambda)\end{pmatrix} = \frac{e^{i\lambda x}}{(\lambda-\xi+i\eta)}\begin{pmatrix}\lambda-\xi+i\eta\tanh Z\\ i\eta\,\mathrm{sech}\,Z\;\; e^{-2i\xi x - i\Delta}\end{pmatrix}, \qquad (27)$$

$$\varphi(x,t;\lambda) = \begin{pmatrix}\varphi_1(x,t;\lambda)\\ \varphi_2(x,t;\lambda)\end{pmatrix} = \frac{e^{-i\lambda x}}{(\lambda-\xi+i\eta)}\begin{pmatrix}i\eta\,\mathrm{sech}\,Z\;\; e^{2i\xi x + i\Delta}\\ \lambda-\xi-i\eta\tanh Z\end{pmatrix}, \qquad (28)$$

where $Z = 2\eta(x - x_0)$ (see Eq.(8)), $\Delta \equiv \Delta(t)$ and $x_0 \equiv x_0(t)$ in absence of external perturbations change in time according to (9).

Until scattering ($t \to -\infty$) all quasiparticles are considered to form a bound state. That means the initial condition for Eq.(26) should be taken in the form $b(\lambda, t=-\infty) = 0$. Then the total quasiparticle density $n_{rad}(\lambda)$ emitted by the soliton during the scattering is determined by the value (25) at $t=+\infty$ and is equal to

$$n_{rad}(\lambda) = \pi^{-1}\left|b(\lambda, t=+\infty)\right|^2 . \qquad (29)$$

Since the parameter ε is small, calculation of a radiation generated by a soliton can be carried out in terms of the perturbation theory for solitons. According to the evolution equation (26) and (27),(28) one can obtain the following expression for $|b(\lambda, t=+\infty)|$:

$$\left|b(\lambda, t=+\infty)\right| = 2\eta\left|\varepsilon\int_{-\infty}^{\infty} dt\,\frac{\exp(-4i\lambda^2 t + i\Delta(t))}{\cosh(2\eta x_0(t))}\right.$$
$$\left.\left[1 + 2\eta\,\frac{i(\lambda-\xi(t)) - \eta\tanh(2\eta x_0(t))}{[(\lambda-\xi(t))^2+\eta^2]}\tanh(2\eta x_0(t))\right]\right|. \qquad (30)$$

Instead of $x_0(t)$, $\xi(t)$ and $\Delta(t)$ the perturbation-induced time dependence of these parameters should be used which were obtained in adiabatio approximation. For a fast soliton when Eq.(24) is valid the relations $x_0(t) = -4\xi_0 t$, $\xi = \xi_0 = \mathrm{const}$ take place. The latter means that the variations of the soliton velocity could be neglected (this approach is the so-called Born approximation in the scattering theory).

In this case the expression for $n_{rad}(\lambda)$ takes the form :

$$n_{rad}(\lambda) = \frac{\pi\varepsilon^2}{4(2\xi)^6}\,\frac{[(\lambda-\xi)^2+\eta^2]^2}{\cosh^2[\pi(\lambda^2-\xi^2+\eta^2)/4\eta\xi]} \,. \tag{31}$$

The spectral density of emitted quasiparticles $n_{rad}(\lambda)$ is given in Fig. 2.

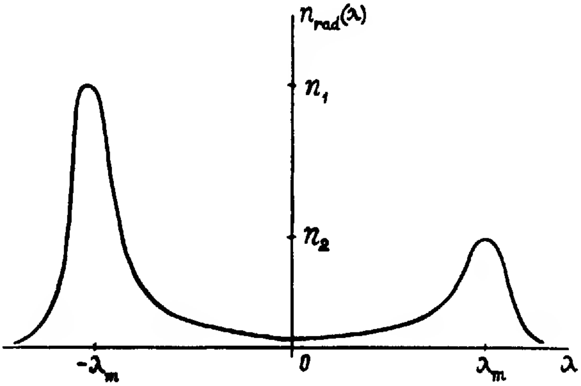

Fig. 2. Spectral density of quasiparticles radiated by a fast soliton ($\eta \ll \xi$)

As it follows from Eq. (31) at $\eta \ll \xi$ the spectral density $n_{rad}(\lambda)$ has two distinguished maxima (which width is of order in η) in the points $\lambda = \pm\lambda_m$, where $\lambda_m = (\xi^2-\eta^2)^{1/2} \sim \xi$. Estimates of maximum density values have the form ($\eta \ll \xi$): $n_1 \equiv n_{rad}(-\lambda_m) \sim \varepsilon^2/\xi^2$, $n_2 \equiv n_{rad}(\lambda_m) \sim \varepsilon^2\eta^4/\xi^6 \ll n_1$. When $\lambda = 0$, as it follows from (31), $n_{rad}(0) \ll n_{1,2}$. Far from the vicinity of the points $\lambda = \pm\lambda_m$ the function $n_{rad}(\lambda)$ exponentially decreases.

The number of quasiparticles emitted by a soliton in forward (N_t) and backward (N_r) directions (see Fig. 1) can be obtained by integrating the density (31) with respect to the corresponding region of the spectral parameter, namely

$$N_t = \int_0^{\infty} n_{rad}(\lambda)\, d\lambda \,, \qquad N_r = \int_{-\infty}^{0} n_{rad}(\lambda)\, d\lambda \,. \tag{32}$$

Because N is the integral of motion (see Eq. (5)) the number of quasiparticles which remain in the bound state equals to $N' = N - N_r - N_t$.

We define the reflection coefficient of a soliton as a ratio of the number of reflected quasiparticles N_r to the total number of quasiparticles $N = 4\eta$. One can obtain from Eqs.(31),(32)

$$R = N_r/N = \frac{\pi \varepsilon^2}{2^{10} \alpha \xi^2} \int_0^\infty dx \frac{[(x+1)^2 + \alpha^2]^2}{\cosh^2[\pi(x^2+\alpha^2-1)/4\alpha]} \, , \quad \alpha = \eta/\xi . \qquad (33)$$

Let us compare the expression (33) with the reflection coefficient of linear waves (i.e. free quasiparticles) (6). Since the inequality (24) was used when deriving Eq.(33), it is necessary to simplify Eq.(6) taking $R_0 \approx \varepsilon^2/16\xi^2$. In the case $\eta \ll \xi$ (the so-called "light" soliton) the following expansion takes place from Eq.(33) :

$$R = R_0 (1 + 2\eta^4/15\xi^4) . \qquad (34)$$

It illustrates that the reflection coefficient of a soliton exceeds that of a free quasiparticle. In the opposite case, i.e. $\eta \gg \xi$, ("heavy" soliton) we obtain considerably smaller value as compared with R_0, i.e.

$$R = (\pi/16\sqrt{2}) R_0 \alpha^{7/2} \exp(-\pi\alpha/2), \quad \xi/\varepsilon \gg \alpha \gg 1 . \qquad (35)$$

The general behaviour of the function defined in (33) is shown in Fig. 3 . A characteristic feature of this non-monotonous dependence consists in rapid deorease of the reflection coefficient with the parameter η/ξ grouth, i.e. when increasing the relative number of quasiparticles or their binding energy in the soliton. At $\alpha \to 0$ the reflection coefficient tends, as naturally could be expected, to its "linear" value R_0 (6).

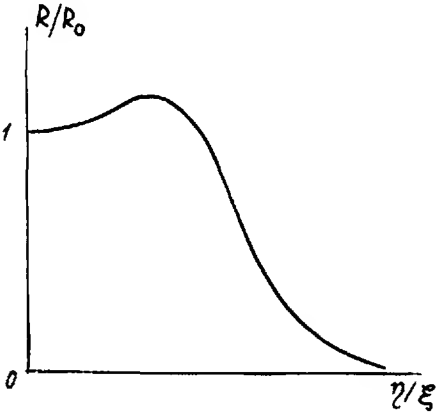

Fig.3. Dependence of the soliton reflection coefficient on the parameter η/ξ at $|\varepsilon|\eta \ll \xi^2$; the case $\eta/\xi \to 0$ corresponds to the scattering of a free quasiparticle

Let us calculate now the number of quasiparticles emitted by a soliton in forward direction. We denote by D their relative number:

$$D = N_t/N \, . \tag{36}$$

As can be easily seen this magnitude is described by Eq.(33) in which $(x+1)^2$ scould be replaced by $(x-1)^2$ in the integrand. A qualitative dependence of the radiation coefficient D is presented in Fig.4. At $\alpha \ll 1$ the number of forward emitted quasiparticles is very small :

$$D = \varepsilon^2 \eta^4 / 120\, \xi^6 \, . \tag{37}$$

At large value of the parameter α asymptotics of the function $D(\alpha)$ coincides with that of the function $R(\alpha)$ and takes the form (35).

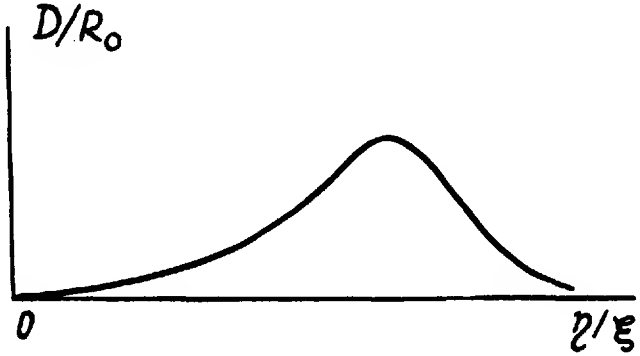

Fig.4. Dependence of the relative number of quasiparticles radiated by the soliton in forward direction on the parameter η/ξ

Now let us discuss briefly the presented results. At first in the case $\alpha \ll 1$ when the NLS soliton is close to a free quasiparticle (i.e. "light" soliton) we have the following situation. In the main approximation (up to the terms of order in α^2) the backward emission from a fast soliton dominates (cf. Eq.(34) and Eq.(37)). That means the quasiparticles passed the impurity to remain in the bound state. Thus only the soliton corresponds to the transmitted wave.

Exponentially small emission intensity (as well as the coefficients R and D) is typical for scattering of a "heavy" soliton (when $\eta \gg \xi$). This result can easily be interpreted in terms of simple physical considerations: in the studied case binding energy of quasiparticles in the soliton ($\sim \eta^2$) considerably exceeds its kinetic energy ($\sim \xi^2$), therefore for $\eta \gg \xi$ it is more difficult to "tear out" a quasiparticle off the soliton than in the opposite case. This feature manifest itself in decrease of the scattering coefficients R and D .

2.4. Two Point Impurities. Resonant Soliton Scattering

Consider now the scattering of a soliton by a number of scattering centres. We start with two point impurities, distance between them being a. The analysis of the resonant soliton scattering is of special interest when the amplitudes of the impurities are equal. We restrict our consideration with the case of fast soliton scattering (in the Born approximation) when variations of its velocity during scattering could be neglected.

The scattering of a linear wave (i.e. free quasiparticle) by two equivalent point impurities is known to be resonant, namely, the reflection coefficient by a pair of them $R_0^{(2)}$ oscillates depending on the parameter $d = ak$, where k is the wavenumber of the incident wave. In the Born approximation for our designations we have

$$R_0^{(2)} = 4\,R_0^{(1)} \cos^2 d \ , \quad d = 2a\xi \ , \tag{38}$$

where $R_0^{(1)} \approx \varepsilon^2/16\xi^2$ is the reflection coefficient by a single impurity in the same approximation (see (6)). The reflection coefficient $R_0^{(2)}$ turns to zero at $d_n^{(0)} = \pi/2 + \pi n$ ($n = 0,1,\dots$). The latter condition corresponds to the coincidence of the incident quasiparticle energy $k^2 = 4\xi^2$ with that of the resonant state between two delta-type potentials. The maximum values of the reflection coefficient ($4\,R_0^{(1)}$) relate to the quasiparticle reflection from a single impurity of binary intensity, i.e. when $\varepsilon \to 2\varepsilon$.

The scattering process of a soliton is treated in accordance to the procedure described in the previous subsection. Substitution of the perturbation in the form $\varepsilon\, P[u] = \varepsilon\left[\delta(x) + \delta(x-a)\right]u$ into Eq.(26) yields in the Born approximation the following expression for the spectral density of the scattered quasiparticles

$$n_{\rm rad}^{(2)}(\lambda) = 4\, n_{\rm rad}^{(1)}(\lambda)\ \cos^2\left\{\frac{a}{2\xi}\left[(\lambda-\xi)^2 + \eta^2\right]\right\} . \tag{39}$$

where $n_{\rm rad}^{(1)}(\lambda)$ is the quasiparticles density (31) emitted by a soliton scattered by a single impurity. The reflection coefficient of a soliton by the pair of impurities $R^{(2)}$ we obtain in a similar way (see (33)) :

$$R^{(2)} = \frac{\pi\varepsilon^2}{2^8\alpha\xi^2}\int_0^\infty dx\ \frac{\left[(x+1)^2+\alpha^2\right]^2}{\cosh^2\left[\pi(x^2+\alpha^2-1)/4\alpha\right]}\cos^2\left\{\frac{d}{4}\left[(x+1)^2+\alpha^2\right]\right\}. \tag{40}$$

Let us analyse the dependence of the reflection coefficient (40) on the parameter d for small nonlinearity parameter ($\alpha \ll 1$). In the main approximation in α one can write

$$R^{(2)} \cong \frac{\pi\mathcal{E}^2}{2^8\alpha\xi^2}\int_0^\infty dx\,\frac{(x+1)^4\cos^2[d(x+1)^2/4]}{\cosh^2[\pi(x^2+\alpha^2-1)/4\alpha]} \quad . \tag{41}$$

Introduce the variable $z=\pi(x^2+\alpha^2-1)/4\alpha$ and note that if $\alpha \ll 1$ the region $\delta z \sim 1$ gives the main contribution to the integral (41). Thus for $\alpha^2 d \ll 1$ one can write

$$R^{(2)} \cong \frac{\mathcal{E}^2}{8\xi^2}\int_{-\infty}^{\infty} dz\,\cos^2[d(1+4\alpha z/\pi)]\,\mathrm{sech}^2 z \quad . \tag{42}$$

Simple manipulations give the following result

$$R^{(2)} = 2R_0^{(1)}\left(1+\frac{2\alpha d}{\sinh(2\alpha d)}\cos 2d\right) \tag{43}$$

which in the case $\alpha \ll 1$ can be used at any values of d .

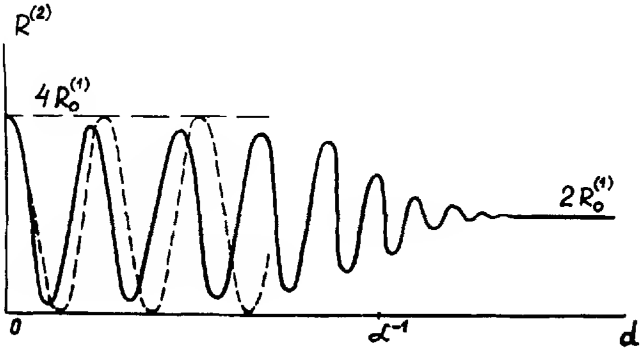

Fig.5. The reflection coefficient of a soliton scattering by two identical impurities as a function of $d=2a\xi$ for $\alpha \ll 1$; $R_0^{(1)}$ being the reflection coefficient of the free quasiparticle by a single impurity (6)(in the born approximation)

The reflection coefficient $R^{(2)}$ dependence on the parameter d for small is schematically shown in Fig.5. The width of the soliton ($\sim \eta^{-1}$) exceeding considerably the distance a between the point impurities (this corresponds to the condition $a\eta = \alpha d \ll 1$), distinguished interference phenomena are seen which manifest themselves in oscillations of $R^{(2)}$ with the parameter d growth. Apart from the linear approximation $R^{(2)}$ does not turn into zero because $x < \sinh x$ for $x \neq 0$, however when $d = d_{min} = (1 - 2\alpha^2/3)\,d_n^{(0)}$ the reflection coefficient has the minimum values

$$R^{(2)}_{\min} = \frac{2}{3}(\alpha d_{\min})^2 \simeq \frac{2}{3}(\alpha d^{(0)}_n)^2 = \frac{2}{3}\alpha^2\left(\frac{\pi}{2}+\pi n\right)^2$$

vanishing under the condition $\alpha d \ll 1$. The maximum values $R^{(2)}_{\max}$ correspondingly decrease, the latter taking place for $d = d_{\max} = (1 - 2\alpha^2/3)(\pi n)$, namely $R^{(2)}_{\max} \cong 4R^{(1)}_0(1-(\alpha\pi n)^2/3)$.

When the soliton width becomes comparable with the distance a ($\alpha d \sim 1$) the interference drops and the scattering coefficient exponentially (with the parameter αd growth) approaches the value $2R^{(1)}_0$. This result can be interpreted in a simple way. The soliton width being considerably less than the distance between the impurities ($\alpha d \sim a\eta \gg 1$), the scattering by each impurity occurs independently and $R^{(2)} \cong 2R^{(1)}$. Thus the interaction between quasiparticles causes a qualitative change in their resonant scattering.

2.5. Scattering of Soliton by Random Impurities

Natural generalization of the above problem leads to the study of the soliton scattering by a system of a large number of impurities. We restrict ourselves with the case of random spatial distribution of the impurities. The initial system is then described by the stochastic NLS equation

$$i u_t + u_{xx} + 2|u|^2 u = \varepsilon \sigma(x) u \ , \tag{44}$$

$\sigma(x)$ being a random function attributed to the disordered set of a large number M ($M \gg 1$) point impurities (see for details Ref. 15). For the sake of convenience the mean value $\langle \sigma(x) \rangle$ will be included in the renormalization of characteristic frequency ω_0 in Eqs.(2) and (3), so in future we shall only consider fluctuations of the random function $\sigma(x)$ taking $\langle \sigma(x) \rangle = 0$ (the previous designation will be used for fluctuations). As is known (see, e.g., Ref. 15) in the case $M \to \infty$ the function $\sigma(x)$ becomes Gaussian and its binary correlator can be given in the form

$$\langle \sigma(x)\, \sigma(x') \rangle = l^{-1}\, \delta(x - x') \tag{45}$$

where parameter l means the mean distance between the impurities while the angle brackets imply averaging with respect to all realizations of the random function. Suppose the region occupied by the impurities to be of finite length, i.e. the random function $\sigma(x)$ is defined within the interval $-L/2 \leq x \leq L/2$ and turns into zero throughout of it.

It is of interest to examine the averaged spectral density of the emitted quasiparticles with respect to all realizations of the random function. This value can be obtainen in terms of the soliton perturbation theory if $\varepsilon^2 \ll 1$. Calculations using Eq.(29) together with Eq.(30) leads to the general result

$$n_{rad}(\lambda) = n^{(1)}_{rad}(\lambda) \int_{-L/2}^{L/2} dx \int_{-L/2}^{L/2} dx' \, \sigma(x) \, \sigma(x') \exp[ic(\lambda)(x - x')], \quad (46)$$

here $c(\lambda) = ((\lambda - \xi)^2 + \eta^2)/\xi$, and $n^{(1)}_{rad}(\lambda)$ is the function (31) characterizing the soliton scattering by a single point impurity. If $\sigma(x)$ is a random function then averaging the result (46) in accordance with (45) we obtain

$$\langle n_{rad}(\lambda) \rangle = (L/l) \, n^{(1)}_{rad}(\lambda) = M \, n^{(1)}_{rad}(\lambda). \quad (47)$$

The mean reflection coefficient is determined as follows (see subsection 2.3):

$$\langle R \rangle = N^{-1} \int_{-\infty}^{0} d\lambda \, \langle n_{rad}(\lambda) \rangle = M R^{(1)}(\alpha), \quad (48)$$

$R^{(1)}(\alpha)$ being the reflection coefficient of the soliton by a single point impurity (33).

The result (48) (together with (47)) shows that the soliton scattering by the random system of point centres is non-resonance (see end of the subsection 2.4), i.e. the average scattering of a soliton by each point impurity of the system occurs independently.

3. Scattering of Small-Amplitude Sine-Gordon Breather

3.1. Localized Impurity. "Relativistic" Case

As another example we consider scattering of the sine-Gordon breather by an impurity. Relations between the breather of classical SG system and the bound state of elementary excitations in quantum SG model have been discussed in literature (see, e.g., [16 - 18]), thus we shall pay no attention to the problem. Note only that the number of quasiparticles bound in a breather is determined in quasiclassical approximation by direct quantization (by Bohr-Zommerfeld) of the breather-type excitation. The most surprising is the coincidence of the quasiclassical result with the exact one at any number of bound quasiparticles. It can be probably attributed to the exact integrability of the systems.

We shall analyse scattering of the small-amplitude SG breather by a single point impurity in terms of the SG equation of the form

$$u_{tt} - u_{xx} + \sin u = \mathcal{E}\,\delta(x)\,\sin u\,, \tag{49}$$

where dimensionless variables have been introduced. The parameter characterizes the impurity amplitude. Equation (49) takes place, e.g., when describing nonlinear dynamics of magnetic flux in long Josephson junction with inhomogeneous critical bias current (see, e.g., [8,19]).

In absence of the impurity ($\mathcal{E} = 0$) Eq.(49) has an exact solution of the breather type describing the bound state of quasiparticles [10]. When the amplitude μ of the excitation is small it takes the form :

$$u_{br}(x,t) \approx 4\mu \sin\left[\gamma(1-\mu^2/2)(t-Vx)\right] \operatorname{sech}\left[\mu\gamma(x-Vt)\right]\,, \tag{50}$$

V being the velocity of the breather mass centre ($V^2 \leqslant 1$), and $\gamma = (1-V^2)^{-1/2}$.

The problem of the breather (50) scattering by an impurity (this problem was solved by the authors with collaboration Dr. B.A. Malomed) is considered in terms of the soliton perturbation theory developed for the SG equation in papers [20,21] . The most interesting is the reflection coefficient as in the above case of NLS soliton. To obtain this function one should note that in the nonlinear system another definition of the reflection coefficient is possible which differs from that considered in the subsection 2.3. Namely, one can determine the reflection coefficient as the ratio of energy emitted by the soliton in the backward direction (with respect to its motion) to that of the incident soliton, i.e. total energy. (In the linear case both definitions coincide). Herefore, let us start studying the energy emitted by the SG small-amplitude breather scattering by an impurity.

The spectral energy density emitted by the breather can be calculated using the result of inverse scattering transform for the SG equation (see, e.g., [10])

$$e_{rad}(\lambda) = \pi^{-1}\,(4 + 1/\lambda^2)\,\left|B(\lambda,\ t = +\infty)\right|^2, \tag{51}$$

λ being the positive spectral parameter of the inverse scattering problem for SG system which determines the radiation wavenumber K :

$$\lambda \equiv \lambda(K) = \tfrac{1}{2}\,(K + \sqrt{1+K^2}\,)\,. \tag{52}$$

The Jost coefficient B(λ, t) obeys the evolution equation similar to (26) which in the explicit form is given, e.g., in [20,21] . As follows from (51),(52), the spectral energy density as a function of the wavenumber K takes the form :

$$e_{rad}(K) = \left[e_{rad}(\lambda)\,(d\lambda/dK)\right]_{\lambda=\lambda(K)} = (4/\pi)\left|B(\lambda(K),\ t=+\infty)\right|^2 \tag{53}$$

where $\lambda(K)$ is presented by Eq.(52).

We shall not consider in details the calculations of the emitted energy (they are more complicated than in the case of NLS soliton), are present here the final result :

$$e_{rad}(K) = \frac{\pi\varepsilon^2(1-V^2)\left[A+B(1+C^2)\right]^2}{V^2\left[(K+V\omega)^2+\mu^2(1-V^2)\right]^2}\ \mathrm{sech}^2(\pi C/2) \tag{54}$$

where

$$A = (K+V\omega)^2 - \mu^2(1-V^2) - 2(\sqrt{1-V^2}/V)(K+V\omega)\left[\sqrt{1-\mu^2} - \omega\sqrt{1-V^2}\right],$$

$$B = (\mu^2/4)\,(\omega+KV)\left[3(\omega+KV) + \sqrt{1-V^2}\right],$$

$$C = \left(\sqrt{1-\mu^2} - \omega\sqrt{1-V^2}\right)/\mu V,$$

and $\omega \equiv \omega(K) = \sqrt{1+K^2}$ is the dispersion law of the linear SG excitations.

The energy carried back (E_r) and forward (E_t) is determined by integration with respect to the corresponding region of the wavenumber variation (cf. (32))

$$E_r = \int_{-\infty}^{0} dK\ e_{rad}(K)\ , \qquad E_t = \int_{0}^{\infty} dK\ e_{rad}(K)\ . \tag{55}$$

Note that $e_{rad}(K)$ is asymmetrical in K, therefore E_r and E_t, strictly speaking, differ from each other.

Let us analyse at first the case $V^2 \ll 1$ accounting for $V^2 \sim \mu^2$. Analysis of Eq.(54) shows that in this case the main contribution into the integrals is provided by $K \sim V \sim \mu \ll 1$, i.e. one can write $\omega \approx 1 + K^2/2$ and Eq.(54) simplifies. In particular $C \approx (V^2 - \mu^2 - K^2)/2\mu V$.

Retaining the main terms in V and carrying out some simplifications we obtain for $|B(K,\ t=+\infty)|$ the result (30) in which the following changes should be done

$$\xi = -V\ , \qquad \eta = \mu\ . \tag{56}$$

Having determined the reflection coefficient R as the ratio of the "reflected" energy E_r (i.e., energy radiated by the breather in backward direction) to the energy of the incident breather $E_{br} \approx 16\mu/\sqrt{1-V^2}$ (see Ref. 10) we obtain the result which is four times more than (33) where $\alpha = -\mu/V$. Thus, a characteristic feature of the slow breather scattering (i.e. $V^2 \ll 1$) is a dominate back scattering of quasiparticles which was noted in subsection 2.3.

In the opposite case when the incident breather is "relativistic", i.e. $1-V^2 \ll 1$ (but $\mu^2 \ll 1$) we obtain more complicated spectral distribution of the emitted energy. Its maxima are located near the points $K = \pm K_m$ where $K_m \sim \nu \equiv (1-V^2)^{-1/2} \gg 1$, the spectral energy density being still asymmetrical. Rather cumbersome calculations result in the following expansion for the considered case:

$$E_r = 4\,\varepsilon^2 \mu\, \nu^{-1}(1 - 9\mu^2/2)\,. \tag{57}$$

The reflection coefficient takes the form :

$$R = (\,\varepsilon^2/4\,\nu^2)\,(\,1 - 9\mu^2/2\,)\,. \tag{58}$$

For the forward emitted energy we have

$$E_t = 4\,\varepsilon^2 \mu\, \nu^{-1}(\,1 + O(\mu^2)\,)\,. \tag{59}$$

The following result should be noted, in spite of the spectral density $e_{rad}(K)$ is asymmetrical with respect to K , the integrated characteristics of the radiation in the limit $\mu \to 0$ coincided (compare Eqs.(59) and (57)). It is noteworth that in the "ralativistic" case non-monotonous dependence of the reflection coefficient on the amplitude of nonlinear excitation vanishes and the reflection coefficient R of the breather in this case is always less than that R_0 of the free quasiparticle ($R_0 \approx \varepsilon^2/4\,\nu^2$ at $\nu \gg 1$).

3.2. Correlation between Sine-Gordon Breather and Nonlinear Schrödinger Soliton

In the final subsection we discuss in detail coincidence of the results for the scattering of the small-amplitude SG breather and NLS soliton by an impurity. Such effect is caused by the correspondance of the small-amplitude (but "non-relativistic") breather of the SG equation and the NLS soliton (see, e.g., Ref. 22).

Really, for $u \ll 1$ Eq.(4) is simplified: $u_{tt} - u_{xx} + u - (1/6)u^3 = \varepsilon\,\delta(x)\,u$. Let a solution of this equation is presented in the form: $u = U \exp(-it) + U^{*}\exp(\,it\,)$. Now we separate the coefficients multiplying high frequency terms. In the lowest approximation one can obtain

$$U_{tt} - 2iU_t - U_{xx} - \tfrac{1}{2}|U|^2 U = \varepsilon\,\delta(x)\,U\,. \tag{60}$$

If we put in Eq.(60) $U_{tt} \ll U_t$ (that corresponds to the "non-relativistic" case when $V^2 \ll 1$) and change variables

$$x' = x/2\quad,\quad t' = t/8\quad, \tag{61}$$

then the following equation is obtained (the primes being omitted)

$$iU_t + U_{xx} + 2|U|^2 U = -2\varepsilon\delta(x) U ,$$

which coincides with Eq.(4) if in the latter -2ε is replaced by ε. With this the change of variables (61) converts the breather (50) into the solution

$$u_{br} = u_s(x',t')\, e^{-it} + u_s^{*}(x',t')\, e^{it}$$

where $u_s(x,t)$ has the form (8),(9), the parameters ξ and η expressing in terms of those of the breather in according to the relations (56).

It is the equivalence of the "non-relativistic" small-amplitude SG breather and the NLS soliton (taking into account exchange of ε) that causes the coincidence of the reflection coefficients. Of course, the coincidence does not take place for arbitrary breather's velocity V , moreover in this case the results are essentially different from those of the NLS soliton (cf. (58) and (34)).

References

1. J.B. McGuire : J.Math. Phys. 5 , 622 (1964).
2. F. Calogero and A. Degasperis : Phys. Rev. 11 A , 265 (1975).
3. A.S. Kovalev and A.M. Kosevich : Fiz. Nizk. Temp. 2 , 913 (1976).
4. A.M. Kosevich , B.A. Ivanov and A.S. Kovalev : Nonlinear Magnetization Waves. Dynamical and Topological Solitons (Naukova Dumka, Kiev, 1983) (in Russian).
5. V. Narayanamurti and C.M. Varma : Phys. Rev. Lett. 25 , 1105 (1970).
6. F.D. Tappert and C.M. Varma : Phys. Rev. Lett. 25 , 1108 (1970).
7. T. Sakuma and Y. Kawanami : Phys. Rev. 29 B , 869, 880 (1984).
8. K.K. Likharev : Introduction in Dynamics of Josephson Junctions (Nauka, Moscow, 1985) (in Russian).
9. A.M. Kosevich and A.S. Kovalev : Zh. Eksp. Teor. Fiz. 67, 1793 (1974).
10. V.E. Zakharov , S.V. Manakov , S.P. Novikov and L.P. Pitaevskii : Theory of Solitons (Nauka, Moscow, 1980).
11. V.I. Karpman and E.M. Maslov : Zh. Eksp. Teor. Fiz. 73 , 537 (1977).
12. V.I. Karpman : Physica Scripta 20 , 462 (1979).
13. A.M. Kosevich : Foundations of Crystal Lattice Mechanics (Nauka, Moscow, 1972) (in Russian).
14. Yu.S. Kivshar and B.A.Malomed : Phys. Letters 115 A , 377 (1986); J. Phys. 19 A , L967 (1986); Physica 24 D , in press (1986).
15. I.M. Lifshitz , S.A. Gredeskul and L.A. Pastur : Introduction in Theory of Random Systems (Nauka , Moscow, 1982) (in Russian).
16. T.H.R. Skyrme : Proc. R. Soc. 247 A , 260 (1958); 262 A , 233 (1961).
17. L.D. Faddeev and V.E. Korepin : Phys. Reports 42 C , 1 (1978) .
18. R. Rajaraman : Solitons and Instantons (North-Holland Publishing Company, Amsterdam et al, 1982).
19. D.W. McLaughlin and A.C. Scott : Phys. Rev. 18 A , 1652 (1978).
20. D.J. Kaup and A.C. Newell : Proc. R. Soc. 361 A , 413 (1978).
21. Yu.S. Kivshar : On the Perturbation Theory for Sine-Gordon Equation Solitons (ILTP preprint No. 24-84 , Kharkov, 1984)(in Russian).
22. A.C. Newell : J. Math. Phys. 19 , 1126 (1978).

PHONON SCATTERING ON DISLOCATIONS AND RECOVERY PROCESSES IN PLASTICALLY DEFORMED ^{4}He CRYSTALS

A. A. Levchenko, L. P. Mezhov-Deglin
Institute of Solid State Physics,
Chernogolovka, USSR

1. Introduction

Solid helium is an ideal material for studying the role of various energy transfer mechanisms in dielectric solid [1]. Its large compressibility at small pressures enables the characteristic properties of the crystals (Debye temperatúre, molar volume) to be changed significantly from experiment in one and the same apparatus, by varying the solidification pressure. Helium crystals can easily be obtained with a high degree of perfection: the effective phonon mean free path is of the order of 1cm at the concentration of impurities $<10^{-6}$%. The study of the thermal conductivity of perfect ^{4}He crystals leads to the discovery of a new hydrodynamic heat conductivity mechanism in solids [2,3]. These studies stimulated the appearance of a whole series of investigations devoted to the study of kinetic phenomena in solid helium. The oscillations of atoms of helium crystals are so large that they are highly anharmonic and, as the pressure at which they are grown decreases, the quantum effects become important [4]. Recently the properties of defects in quantum crystals have attracted a considerable interest. For example the diffusion of ^{3}He atoms in solid ^{4}He has been carefully investigated and the existence of quantum mechanism of the diffusion of impurities at low concentration and the phenomenon of the localization of impurities at large concentration has been discovered. The information about the properties of dislocations has been obtained practically only from ultrasound investigations [5]. Therefore it is interesting to investigate the interaction of phonons with dislocations in helium crystals. One of the methods of investigation of this interaction is the study of the effect of plastic deformation on the thermal conductivity.

2. Experimental aspects

The helium crystals were grown from purified ^{4}He, containing 10^{-5}%. of ^{3}He impurity atoms and mixtures containing 0.005%, 0.05%, 0.5% and 5% ^{3}He impurity atoms in ^{4}He. The containers were a thin-walled metal capillaries of the internal diameters of 1mm and 1 - 8 mm. The capillaries were initially bent on a 7cm diameter template. The container was soldered to the bath with liquid ^{3}He. The upper end of the container could be moved vertically over the distance up to 2cm by means of the drawstring. The extent of the deformation of helium crystal in the container, calculated from change in the radius of curvature of the capillary was $\simeq$1%

We used the following method of experimental investigation of the thermal conductivity of the deformed specimens. The thermal conductivity of the initial specimen K_i was first measured over the temperature range 0.4-1.3K. The specimen was then deformed at temperatures $\leqslant$ 0.4 K and the thermal conductivity was measured first with the increase and then with the decrease in the temperature. The annealing of the specimen is observed with the increase of the temperature after deformation. Only the results obtained with the decrease of the temperature are reproducible. In this way we established the temperature dependence of the specimen thermal conductivity.

The method of studying the annealing kinetics was as follows. First the thermal conductivity of the initial specimen was measured, then the specimen was deformed at $T \ll 0.4$ K and the thermal conductivity of the specimen was measured at a given temperature T_o. The temperature of the specimen was then raised at the rate of $\approx$ 1K/min to a given temperature T_{ann}, and held at this temperature during a certain period of time t, then the temperature was again lowered to T_o and the measurement of K was repeated. The dependence of the additional thermal resistivity W_d at T_o on annealing time at a given T_{ann} was determined in this way. Here, $W_d = K_d^{-1} - K_i^{-1}$ where K_d is the thermal conductivity of a deformed specimen. The annealing temperature was changed in 0.05 K steps in the range of 0.45 - 1.1K. The time of annealing at a given T_{ann} between the consecutive measurements was varied from 1 to 30 min.

3. Results

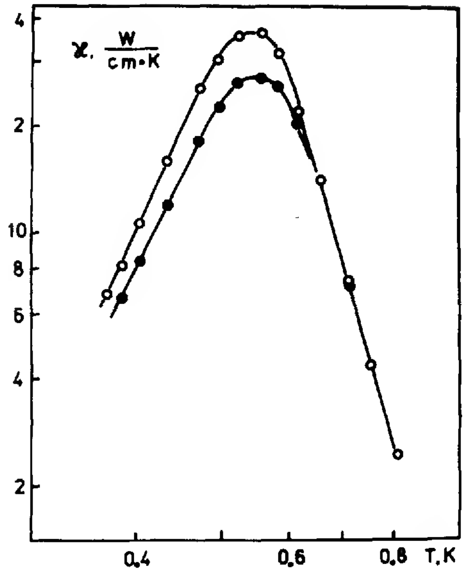

Fig. 1a

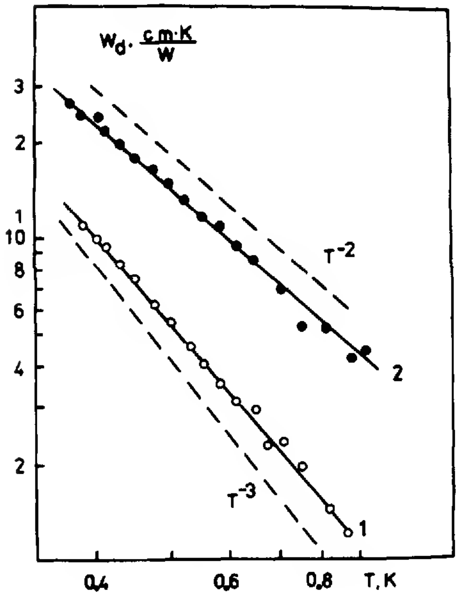

Fig. 1b

The deformation of helium crystals at T ≤ 0.4K leads to a reduction of the thermal conductivity. An example of the change in the conductivity of specimen grown at 26atm in the container of an internal diameter 1.8 mm after 1% deformation (capillary bent and bent back at T ≤ 0.4K) is shown in Fig.1a. Curve 1 represents the thermal conductivity of the initial specimen, curve 2 represents the thermal conductivity of the deformed specimen after annealing for 1h at 0.7 K, measured with the decrease of the temperature. The dependence of the additional thermal resistivity $W_d(T)$ is close to T^{-3}. This dependence is observed in all the specimens of ^{4}He grown at the pressures ranging from 26 up to 84 atm and at the concentration of ^{3}He atoms up to 0,5%. When the concentration of impurities increases up to 5% the temperature dependence of the additional thermal resistivity changes significantly, and $W_d(T) \sim T^{-2}$, but the value of W_d at T_0 increases. Fig.1b shows the temperature dependence of the additional thermal conductivity in deformed crystals grown from mixtures ^{4}He + ^{3}He at a constant pres-

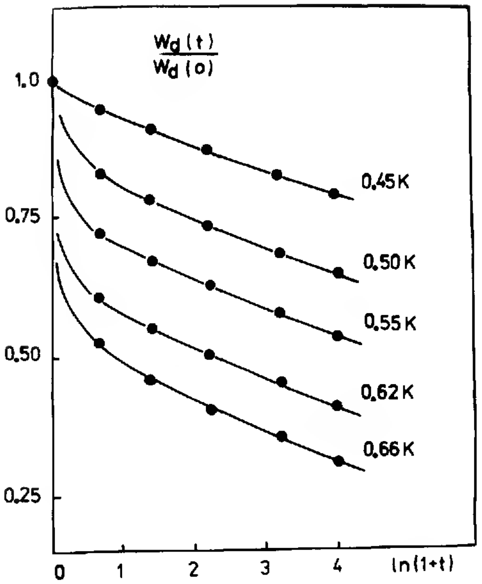

Fig. 2

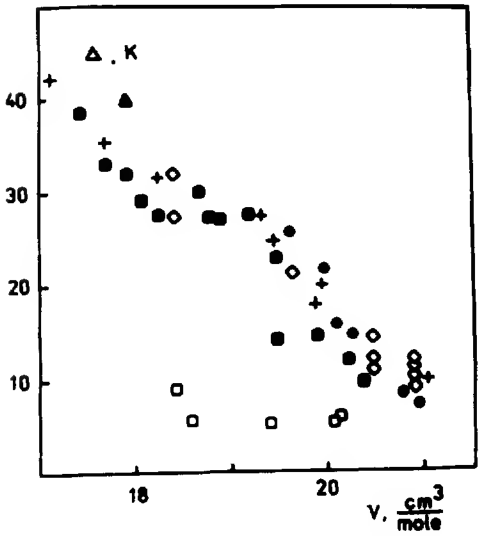

Fig. 3

sure 84 atm. Curve 1 corresponds to the mixture ^{4}He + 0.5% ^{3}He, and curve 2 to the mixture ^{4}He+5% ^{3}He.

An example of the recovery kinetics in a deformed specimen, grown at 26 atm is shown in Fig.2. Here $W_d(0)$ is the initial additional thermal resistivity at T=0.384 K. $W_d(T)$ is the additional thermal resistivity after annealing at the temperature T_{ann}. The curves are labeled with the annealing temperatures. It turnes out that the recovery kinetics is described by an expression of the form

$$W_d(t)/W_d(t) =$$
$$= 1 - A\ln(1 + t/\tau),$$

where A is a constant coefficient, τ is the characteristic relaxation time which dependends on the temperature

$$\tau \sim \exp\ (\Delta/T), \qquad (1)$$

where Δ is effective activation energy of the recovery process. It turns out that Δ is practically the same as the effective activation energy for the diffusion of point defects in ^{4}He crystals with the same molar volume [6]. The values of Δ for purified ^{4}He are shown in Fig.3 by rhombs. An increase of the concentration of ^{3}He in ^{4}He up to 0,5% leads to a systematic lowering of the thermal conductivity of crystals but it affects the values of the activation energy only insignificantly. The activation energy falls more then twice when the concentration of ^{3}He in ^{4}He increases up to 5% (■ in Fig. 3). The remaining symbols corespond to the activation energy of point defects. It turns out that the values of A and Δ practically do not change with an increase in the degree of deformation. The coefficient A is temperature independent in specimens containing up to 0.5% ^{3}He atoms, however for ^{4}He + 5% ^{3}He mixtures the value of A is proportional to temperature, A ~T.

4. Discussion

Bending of helium crystals grown from pure ^{4}He and the mixtures containing up to 0.5% impurity atoms ^{3}He in ^{4}He at pressures 26, 31, 50 and 84 atm leads to a considerable decrease of the coefficient of thermal conductivity. The measurements [7] indicate that the additional thermal resistivity W_d of deformed specimens is primarily due to the scattering of phonons by newly introduced dislocations, since to change the value of $W_d(0)$ in such extent the concentration ~ 50% of point defects is required. Obviously this value is not resonable for our specimens. The crossection of the phonon-dislocation scattering, calculated from $W_d(0)$ at T = 0.4 K and for the estimated density of dislocations (~ 10^7 cm^{-2}) exceeds 10^2 times the known theoretical values for the scattering on the static dislocations. Furthermore, the experimentally observed dependence

$$W_d(T) \sim T^{-n} \qquad (n \simeq 3)$$

differs strongly from the quadratic one, which is characteristic for the scattering on static dislocations. Thus, we conclude that in deformed crystals the scattering of phonons by freely vibrating dislocations plays the dominant role. Introduction of 5% ^{3}He into ^{4}He apparently does not lead to pinning of dislocations, since the value of W_d should decrease in this case. In our experiment the value $W_d(0)$ increases with increasing concentration ^{3}He from 0.5% to 5% for all pressures of solidification.

In the process of recovery, the decrease of the magnitute of W_d may be related to the annihilation of dislocations of different sign in the bulk, on surfaces and as a result of rearrangement of the dislocations at defects, grain boundaries and due to mutual intersections. Since the kinetics of recovery processes in specimens containing up to 0.5% ^{3}He impurity atoms does not depend on the degree of deformation and on the concentration of impurity atoms, we can assume that the recovery processes are due neither to the pinning of dislocations by impurities nor to the classical thermally activated diffusion across the barrier. We can therefore, assume that the movement of dislocations due to their interactions with point defects plays the main role in the recovery processes. This movement can be achieved by the transport of atoms to dislocations or out from them, caused by the migration of vacancies. It may be supposed so, that the inverse of τ in eq.(1) is the frequency of atom jumps on an atomic distance d. Thus, we can estimate the diffusion coefficient of atoms near dislocations as $D \sim d^2/\tau$. The dependence of D on the temperature agrees with the behaviour of the diffusion coefficient of point defects in the region of thermally activated diffusion. This fact confirms our assumptions. Since D is proportional to the concentration of vacancies we can estimate it at low temperatures. The concentration of vacancies at the melting point is ~0.2% for crystals grown at 31 atm.[8]. We obtain that for $T \leqslant 0,45$ K ths vacancy concentration does not exceed $2 * 10^{-10}\%$.

The drop of the activation energy of recovery processes indicates that for the specimens of ^{4}He + 5% ^{3}He mixtures the other mechanism of recovery acts. This fact may be related to the phenomenon of localization of impurity atoms at such concentration [9].

References

1. R. Berman, Thermal Conduction in Solids, Clarendon Press, Oxford, 1976.
2. L.P. Mezhov-Deglin,.Zh. Eksp. Teor. Fiz .49,66, 1965; 52,866,1967.
3. R.N. Gurzhi, Usp. Fiz. Nauk 94, 689,1968.
4. A.F. Andreev, I.M. Lifshitz, Zh. Eksp.Teor. Fiz. 56, 2057,1969.
5. R. Wanner, I.Iwasa, S.Walles, Solid State Comm. 18, 853,1976.
6. A.A.Levchenko, L.P.Mezhov-Deglin, Zh. Eksp. Teor. Fiz. 86, 2123, 1984.
7. A.A.Levchenko, L.P.Mezhov-Deglin, Fiz. Nizk. Temp. 10,1110, 1984.
8. B.A. Fraass, S.M.Held, R.O.Simmons, Proceedings of International Quahtum Crystals Conf. Colorado 1977, p.73.
9. V.A. Mikheev, N.P.Mikhin, V.A. Maidanov, Fiz. Nizk Temp. 9, 901, 1983.

INELASTIC PHONON SCATTERING IN AN AMORPHOUS SUBSURFACE LAYER AND THE ESTABILISHMENT OF A TEMPERATURE BELOW 1K

Y.B.Levinson
Institute of Problems of Microelectronics Technology
and Superpure Materials, USSR Academy of Sciences,
142432 Chernogolovka,Moscow District,USSR

There are many experiments [1-5] that yield the evidence of inelastic phonon scattering near a crystal surface or interface. In most cases the crystal surface is damaged as a result of the methods used to estabilish it. In the subsurface layer the atoms are not at regular lattice positions and the material in this layer is to some extent in an amorphous state. Moreover two-level systems (TLS) can be present in such a layer, and the TLS can interact with phonons and are a source of phonon inelastic scattering [6]. In what follows we discuss how the TLS help to estabilish a nonequilibrium phonon temperature T which differ from the bath temperature T_0. We restrict ourselves to temperatures below 1K.

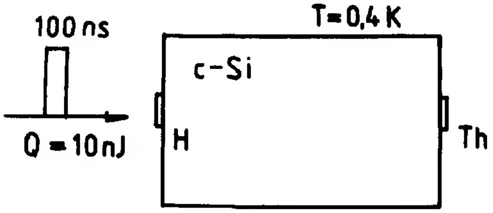

Fig.1. Typical experimental arrangement

A typical experimental arrangement is shown in Fig.1. The sample is a high-purity Si crystal at the bath temperature T_0=0.4K. The heater H on the left side of the crystal is an evaporated metallic film, and the thermometer Th on the right side is a carbon film. Energy Q=10nJ is imparted to the heater from a current pulse of 100ns duration, and the heater temperature rises to $T>T_0$. The resistivity of the carbon film is measured, and from the temperature dependence of that resistivity the thermometer themperature $T_0+\Delta T$ can be calculated. Eventually the temperature of the crystal is raised by $\Delta T=Q/C$, where C is the heat capacity of the sample. The time required to estabilish this new temperature can be obtained through time resolved thermometer measurements.

In Fig.2. the time dependence $\Delta T(t)$ is depicted from the results of Knaak and Meissner [7]. The measured saturation value of $\Delta T(t>1ms)$ is equal to the calculated $\Delta T=Q/C$. This is a proof that at time $t>1ms$ a new equilibrium is estabilished, and that the thermometer temperature is equal to the crystal temperature, which is, in fact, the phonon temperature. For lapses of time smaller than 1ms no temperature exists in the crystal and the thermometer temperature reflects only the number of phonons which are absorbed in the carbon film at a given moment. This temperature has nothing to do with the phonon distribution in regions of the crystal distant from the thermometer.

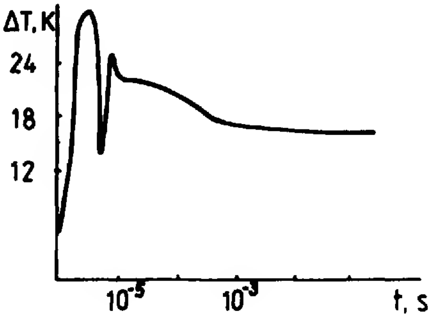

Fig.2. The time dependence of the thermometer temperature increase (after W.Knaak and M.Meissner)

When a new crystal temperature is estabilished, two things happen:

i) The phonons injected from the heater are uniformly distributed over the crystal,

ii) The frequency distribution of all the phonons in the crystal is the Planck distribution with the temperature $T_o+\Delta T$, i.e. the phonon occupation numbers are

$$n(\omega) = n_{T_o+\Delta T}(\omega) \ , \tag{1}$$

where

$$n_T(\omega)=(e^{\hbar\omega/kT}-1)^{-1}. \tag{2}$$

To understand how the temperature in the crystal is estabilished, we have to consider the scattering of phonons. In pure crystals with no free electrons there are two mechanisms of bulk scattering:

1) Elastic scattering by isotopic atoms. The corresponding scattering rate is:

$$1/\tau^*(\omega) = (\Delta M/M)^2 c\omega_D(\omega/\omega_D)^4 \ , \tag{3}$$

where M is the atomic mass, ΔM is the mass defect, c the concentration of isotopic atoms, ω_D the Debye frequency.

2) Inelastic phonon-phonon scattering (phonon decay and coalescence). The corresponding scattering rate is given by:

$$1/\tau(\omega) \simeq \gamma\omega_D(\omega/\omega_D)^5, \qquad (4)$$

where γ is the adiabatic parameter

$$\gamma = \hbar\omega_D/Ms^2 \simeq 10^{-3}$$

and s is the sound velocity. Taking $\omega_D \simeq 10^{14}s^{-1} \simeq 400$ K, $\Delta M/M \simeq 0.1$, and $c \simeq 0.5$ for phonons of frequency $\omega \simeq 0.4$K we obtain $\tau^* \simeq 1$s and $\tau \simeq 10^4$s.

The time necessary for a phonon to travel across the crystal is L/s, where L is the crystal dimension. For $L \simeq 1$cm and $s=5*10^5$cm/s on obtains $L/s \simeq 10^{-5}$s. So if heater temperature T is not very high ($T \leq 10T_0$) an injected phonon will cross the crystal many times during the average time between succesive scattering events.

After a few reflections from the crystal boundaries the injected phonons spread uniformly over the sample. The time necessary to estabilish a phonon distribution homogeneous in space is of the order of L/s. In average during this time no phonon scattering occurs, and the injected phonons do not interact with the bath phonons nor do they interact among themselves. Then, if the surface reflections are elastic, as it is usually assumed, the phonon frequency distribution does not change during the lapse of time in which the phonons fill the available volume. Therefore at $t \geq L/s$ the phonon distribution function is (see Fig.3):

$$n(\omega) = n_{T_0}(\omega) + n'(\omega) \quad , \qquad (5)$$

where the first term is the distribution of the thermal bath phonons and the second is the distribution of the injected phonons. The center of the first distribution is near $\hbar\omega = kT_0$ and that of the second distribution near $\hbar\omega = kT > kT_0$. Eventually distribution (5) is transformed to Planck distribution (1) with the temperature $T_0+\Delta T$, which is inbetween T_0 and T. This transformation proceeds due to the scattering of injected phonons by thermal phonons. As a result the frequencies of injected phonons diminish and the frequencies of thermal phonons grow. The time t_T necessary to estabilish the distribution (1) is called the thermalization time t_T. It can be estimated from the phonon-phonon scattering time (4) (see [8]):

$$t_T \simeq \tau(\omega)|_{\omega\simeq T_o+\Delta T} \tag{6}$$

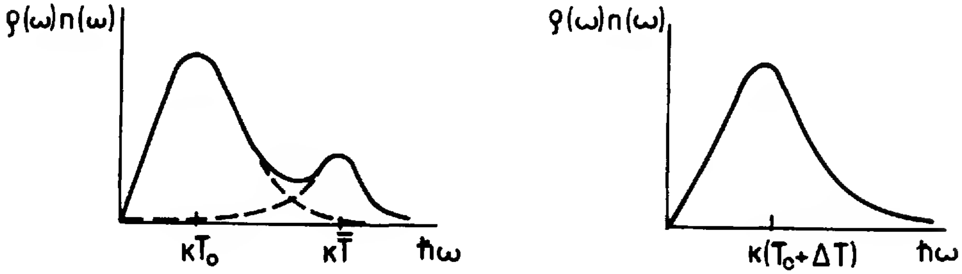

Fig.3. Phonon energy distribution.

a) For time $L/s \le t \le t_T$. The low energy peak is the distribution of thermal bath phonons , the high energy one is the distribution of the injected phonons.

b) For time $t \ge t_T$. All the phonons belong to a single Planck distribution.

For $T_o = 0.4$K and $\Delta T \le T_o$ one obtains $t_T \simeq 10^4$s, which is much longer than the experimental value $t_T \simeq 10^{-3}$s. In what follows we attempt to show that the fast thermalization time is due to phonon inelastic scattering by two level systems (TLS) which exist in damaged subsurface layer.

A TLS [9,10] is described by two quantities; namely the splitting ε between the upper and the lower level and the lifetime τ_1 of the upper level against the transition to the lower one accompanied by the phonon emission. The suitable transition rate is

$$1/\tau_1 \simeq \alpha\varepsilon, \qquad \alpha \simeq \frac{\Xi^2}{Ms^2}\, a_o^3 \rho(\omega)|_{\omega=\varepsilon} , \tag{7}$$

where Ξ is the deformation potential constant, $\rho(\omega)$ the phonon density of states, a_o^3 the volume of the unit cell. For $\omega \simeq 0.4$K the small parameter $\alpha \simeq 10^{-4}$ and the lifetime $\tau_1 \simeq 10^{-6}$s.

A very important point is that there exist TLS with any splitting ε. Threfore a phonon with an arbitrary frequency ω can be resonantly absorbed to excite a TLS. The corresponding phonon lifetime is

$$1/\tau_R \simeq \eta\omega , \quad \eta = \frac{\Xi_3^2}{Ms^2}\, a_o g , \tag{8}$$

where g is the TLS density of states. For glasses the small parameter $\eta \simeq 10^{-3}$, so for a phonon of frequency $\omega \simeq 0.4K$ the lifetime $\tau_R \simeq 10^{-7}s$.

When a phonon of energy $\hbar\omega$ is absorbed TLS with $\varepsilon = \hbar\omega$ is excited. The fastest way to relax is to emit a phonon of the same energy $\hbar\omega$. The phonon absorption and emision is equivalent to elastic scattering and does not change the phonon frequency distribution. But there is another way of the TLS deexcitation, namely to emit two phonons such that $\hbar\omega_1 + \hbar\omega_2 = \varepsilon$. The lifetime of the upper level due to two-phonon emission is

$$1/\tau_2 \simeq \alpha^2 \varepsilon \ . \tag{9}$$

We consider two-stage processes in which the phonon ω is absorbed and then two phonons ω_1 and ω_2 (with $\omega_1 + \omega_2 = \omega$) are emitted. This two-stage process is equivalent to the decay of a phonon ω into two phonons ω_1 and ω_2. If the two-stage process occurs in the bulk (as in the case for a glassy sample) the bottleneck is the second stage, since it is a second-order process.

The lifetime of a phonon ω against the TLS assisted decay is $\tau_2|_{\varepsilon=\hbar\omega}$. In order to compare it with the lifetime (4) against anharmonic decay we shall write the parameter α of the expression (7) in the form $\alpha \simeq \gamma^{-1}(\varepsilon/h\omega_D)^2$. Then from (9) we obtain:

$$1/\tau_2|_{\varepsilon=\hbar\omega} = \gamma^{-2}\omega_D\left(\frac{\omega}{\omega_D}\right)^5 \ . \tag{10}$$

Now we can see that the TLS-assisted phonon decay is faster by a factor $\gamma^{-3} \simeq 10^5$ in comparison with anharmonic phonon decay. Anharmonicity in an insulator arises due to polarization of atomic shells, whose excitation energies are of the order of the atomic energy $Ms^2 \simeq \Xi \simeq 5eV$. The excitation energies of the TLS are much lower, typically 5meV, and this is the reason , why the TLS-assisted phonon decay is faster than the anharmonic one.

The situation changes if TLS exist only in the subsurface layer of thickness $d \simeq 10^{-4}cm$. The time of fly across this layer $d/s \sim 10^{-10}s$ is much shorter than the absorption time $\tau_R \simeq 10^{-7}s$. That means a phonon will be absorbed after crossing the crystal $\tau_R/(d/s)$ times. In other words, the effective adsorption time is $(L/s)*\tau_R/(d/s) = \tau_R(L/d)$. Therefore the effective phonon decay time is:

$$\hat{\tau} \simeq \tau_R(L/d) + \tau_2 \ , \tag{11}$$

instead of that which follows from expression of (10). In the case of thin damaged layers and/or low TLS densities the first term in (11) may be important. If we take as an estimate the values noted above then $\hat{\tau}\simeq\tau_2\simeq 10^{-2}$s, compared to the measured thermalization time $t_T\simeq 10^{-3}$s.

The other possible mechanism for inelastic phonon scattering is the Raman scattering. The lifetime of a phonon against Raman scattering by a TLS also can be estimated. The scattering rate is

$$1/\tau_S \simeq \eta\alpha\omega \ . \qquad (12)$$

Under the conditions of phonon trapping [10], when $\eta\gg\alpha$, we have $\tau_S\ll\tau_2$. However, under these conditions the probability for a phonon to be scattered inelastically during the lapse of time of the order of τ_R is $\tau_R/\tau_S\simeq\alpha$. For this reason, inelastic scattering will occur only after α^{-1} events of the phonon reabsorption, i.e. after the lapse of time $\alpha^{-1}\tau_1\simeq\tau_2$. In other words, the effective time of inelastic phonon scattering by TLS is the same as the effective time of TLS-assisted phonon decay.

Acknowledgements:

The author acknowledges Drs. W.Knaak and M.Meissner for making available their experimental results prior to publication.

REFERENCES:

1. J.K.Wigmore, J.Appl.Phys.41 (1970) 1996; Phys.Lett.A37 (1971) 293
2. H.J.Trumpp, W.Eisenmenger, Z.Phys.B28 (1977) 159
3. R.G.Ulbrich, V.Narayanamurti, M.A.Chin, J.Phys.(Paris) 42 C6 (1981) 226
4. L.J.Challis, A.A.Ghazi, M.N.Wybourne, J.Phys.(Paris) 42 C6 (1981) 229; Phys.Rev.Lett.48 (1982) 759
5. R.Soltis, J.Trivisonno, Phys.Rev.B30 (1984) 6191
6. Y.B.Levinson, JETP Lett.37 (1983) 190
7. W.Knaak, M.Meissner, private information
8. Y.B.Levinson,in Nonequilibrium Phonon in Nonmetallic Crystals, ed.by W.Eisenmenger and A.A.Kaplyanskii, North-Holland,1986 p.91
9. P.W.Anderson, B.I.Halperin, C.M.Varma, Phil.Mag.25 (1972) 1
10. W.E.Bron, Rep.Progr.Phys.43 (1980) 301

PROPAGATION AND RELAXATION OF NONEQUILIBRIUM PHONONS IN THIN MONOCRYSTAL PLATES

A.A. Maksimov and I.I. Tartakovskii

Institute of Solid State Physics, Academy of Sciences of the USSR
142432 Chernogolovka, USSR

A phonon spectrometer with high spatial and temporal resolution has been used to study the propagation and relaxation of nonequilibrium acoustic phonons in thin anthracene crystals.

Optical methods are widely used to generate and detect short-wave acoustic phonons with frequencies $10^{11}-10^{12}$ Hz . During the photoexcitation of crystals, the nonequilibrium phonons, which are generated as a result of fast ($\lesssim 10^{-10}$ s) radiationless relaxation processes of electron excitation, begin to propagate out of the excitation region into the unexcited parts of the crystal. The propagation of these phonons is accompanied by processes of spontaneous decay or coalescence of phonons. These processes in turn play an important role in establishing the phonon propagation conditions [1,2]. In the present investigation we have used a new method of phonon detection with frequency selectivity and high spatial and temporal resolution to follow the relaxation and establishment of the propagation regime for nonequilibrium phonons in thin crystal plates [3,4] starting immediately after the excitation of these phonons. The generation and propagation peculiarities of deformation waves excited in thin crystals by laser pulses of nanosecond duration have been studied as well.

The experiments were performed using thin ($d=2-20\mu$) single crystal anthracene plates with a developed [001] surface. The measurements were carried out in a helium optical thermostat, the bath temperature was kept at $T_0=4.5$ K . Short-wave phonons and deformation waves were produced by exciting the crystal surface with pulses from a nitrogen laser ($\lambda=3371$ Å , pulse duration $\tau_p=4.5$ ns , repetition frequency 25 Hz ,and optical pumping intensity $P=10-200$ kW/cm^2) . The nitrogen laser radiation was absorbed in a thin surface layer $\sim 0.5\mu$.

The appearance of nonequilibrium phonons in the bulk of the crystal under study was detected from the change in the absorption coefficient $\Delta\kappa=\kappa(\omega)-\kappa_0(\omega)$, in the frequency region near the bottom of the lowest exciton b-band ($\omega_T=25096$ cm^{-1}). The difference $\Delta\kappa$ was measured at various times after the nitrogen laser pumping pulses, by means of a tunable dye laser ($\tau_p=3$ ns , lasing bandwidth $\lesssim 1$ cm^{-1} , light polarization $E\parallel b$ axis). The tunable laser pulses were delayed with respect to the nitrogen laser pumping pulses by an amount $t_D=0-150$ ns by means of an optical delay line.

The operating principle of the method of phonon detection is as follows. The polariton group velocity V_g in anthracene crystals for the lower polariton branch at frequencies $\omega \gtrsim \omega_T$ [5,6] is lower than the sound velocity u, so that one-phonon transitions involving the absorption of high-frequency acoustic phonons from polariton states below the bottom of the exciton band into the region $\omega \gtrsim \omega_T$, are allowed. According to experimental data [7] and calculations, in the frequency region $\omega \sim \omega_T$ there is a comparatively narrow ($\sim 3\ \mathrm{cm}^{-1}$) peak in the polariton state density. It is easy to see that in this case the anti-Stokes scattering of polaritons with frequency ω (which are excited by the tunable laser pulses) is dominated by one-phonon transitions involving short-wave acoustic phonons of frequency $\Omega_a \simeq \omega_T - \omega$. Consequently, the increase in the absorption coefficient, $\Delta\kappa$, can be said quite accurately to be proportional to the change in the occupation numbers of phonons of frequency $\Omega_a \simeq \omega_T - = \Delta$. Accordingly, one can determine the change in the occupation numbers (Δn) for non-equilibrium phonons of different frequencies at various times after the pumping pulse by varying the ω_{exc} value by means of a tunable dye laser and the delay time t_D. The net result is the development of a phonon spectrometer with a frequency resolution $\sim 3\ \mathrm{cm}^{-1}$ and time resolution ($\sim$ 3 ns) , determined by the laser pulse duration. This method has a good spatial ($\sim$ 10μ) resolution, and because of high intensity of the tunable laser radiation, there is no need to use photoelectric recording method with high time resolution and sensitivity, which greatly simplifies the experiment.

The presence of strain (tension or compression) in the crystal results also in the changes of light transmission in the frequency region near by the bottom of the exciton band. These changes are determined by the frequency shift of the exciton band bottom ω_T under the influence of deformation [8]. Correspondingly, tension or compression results in the frequency ω_T increasing or decreasing. Consequently, at a fixed frequency ω_{exc} at the absorption edge one can observe the decrease or, on the contrary, increase of the transmission

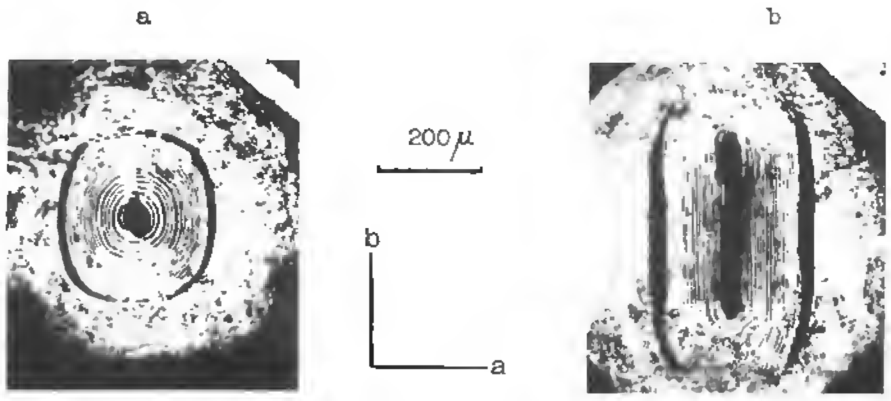

Fig. 1. The patterns of tunable laser radiation transmitted through the anthracene crystal at different shape of the excitation spot. T=4.5K, t_D=68 ns , d=7μ.

light intensity in the deformed regions of the crystal.

The fundamental absorption edge of anthracene crystals is in the visible (violet) spectral region, so the propagation patterns on nonequilibrium phonons and deformation waves proved to be visualized. The microphotographs represented in Fig. 1, a and b, show the transmission patterns of tunable laser radiation through the anthracene crystal at different shape of the excitation spot.

The quantitative measurements of the spatial distribution of the tunable laser radiation passed through the crystal plate were obtained by means of a photoelectrical recording system as follows. The pumping spot on the crystal surface was formed in the shape of a narrow strip with a width of $a \lesssim 20\mu$ and a length of ~ 2mm, oriented along the b axis. The light from the tunable laser transmitted through the crystal plate was detected by an optical system from a fixed region in the form of a narrow strip with a transverse dimension $\sim 10\mu$, oriented parallel to the excitation region. The spatial distribution of the transmitted light measured by scanning the excitation spot over the crystal surface along the a axis (i.e. by smoothly changing the distance between the regions at which the phonons are excited and detected) at various times t_D. The results of such measurements, obtained in the crystal with a thickness $d=18\ \mu$, is shown in Fig. 2.

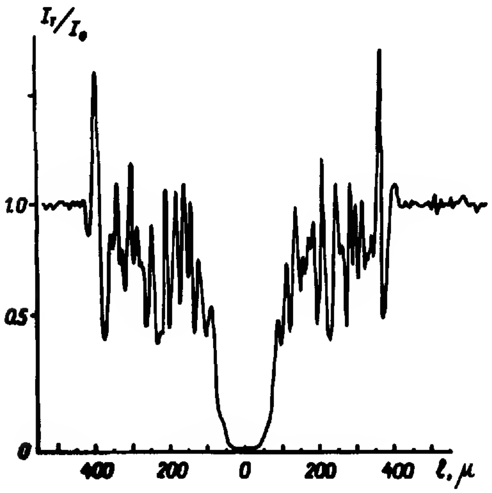

Fig. 2. Spatial distribution of the tunable laser radiation transmitted through the crystal. Pumping level $P=200\ \mathrm{kW/cm^2}$, $d=18\mu$, $T=4.5$ K, $t_D=144$ ns, $\Delta=20\mathrm{cm^{-1}}$.

The light transmission pattern in the frequency region near the exciton resonance essentially depends on the pumping level. Fig. 3 shows typical dependence of spatial transmission pattern of the tunable laser light on the pumping level.

The light transmission pattern is apparently sensitive to transverse dimensions of the excitation spot (Fig. 4). We note, that with the increase of the transverse dimension a together with a strong decrease of light transmission in the central region ($\lesssim 100\ \mu$) a shift of the position of distant sharp peculiarities in the transmission pattern takes place being exactly equal to the variation of a.

The measurements performed at various values of time delay t_D lead to the following: i) linear dimensions of the domain where variations of light transmission are

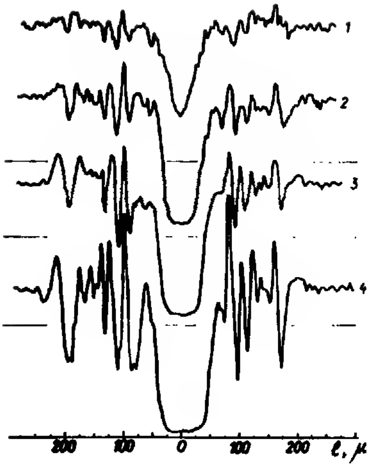

Fig. 3. The same as in Fig.2 at different pumping levels P: 1 - 20, 2 - 40, 3 - 8, 4 - 160kW/cm^2. Here T=4.5K, t_D=67 ns , Δ=16cm^{-1}.

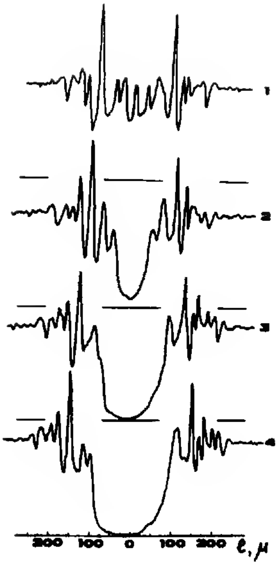

Fig. 4. the same as in Fig. 2 at different transverse dimensions of the exciting strip a: 1 - 20, 2 - 50, 3 - 100, 4 - 135 μ . The pumping level is 160kW/cm^2 and T=1.9K, t_D=67 ns , Δ=9cm^{-1}.

observed increase proportionally to t_D; ii) the propagation velocity of the most distant peculiarities and its anisotropy are in a good agreement with that calculated for quasilongitudinal sound propagation in the [001] plane; iii) the transmission pattern has a complicated structure of different domains with increasing or, on the contrary, decreasing crystal transmission. Analysing these data one can conclude, that the distant domains of the transmission pattern correspond to deformed (by tension or compression) parts of the crystal, initially created at the edges of the excited region and propagating afterwards with the sound velocity. Our estimations show that the frequency shift of the exciton band bottom ω_T by ~1 - 2cm^{-1} [9] can yield the observed changes in the light transmission. One can obtain the same value for this frequency shift estimating thermal strains of the crystal created by the initial excitation (under assumption of the equilibrium heating) and corresponding shifts of ω_T [8]. The complicated structure of maxima and minima in the light transmission pattern probably results from the interaction of normal modes, propagating in an elastic waveguide, such as a thin anthracene crystal plate [10].

An essential increase of the optical density is observed in the vicinity of the excited domain. This increase is due to nonequilibrium high frequency phonons. The spatial distribution of changes in absorption coefficient $\Delta\kappa \sim \Delta n$ depends both on the value of $\Delta = \omega_T - \omega$ and delay time t_D. It can be seen from Fig.5 that there are nonequilibrium phonons of essentially all frequences at

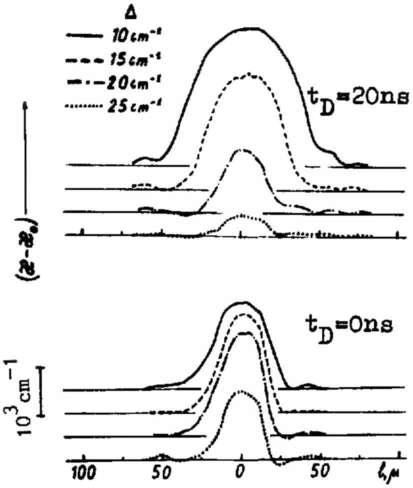

Fig. 5. Spatial change in the absorption coefficient during the pump pulse and 20 ns later at the different frequencies and T=4.5 K.

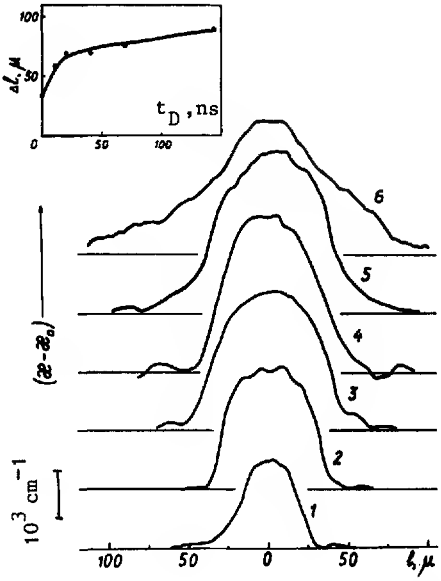

Fig. 6. Spatial change in the absorption coefficient (Δ=10cm^{-1}) for various delay times t_D: 1 - 0; 2 - 10; 3 - 20; 4 - 40; 5 - 68; 6 - 144 ns. d=10μ, P=30kW/cm^2.

the initial time in the excitation region (in anthracene crystals, $\Omega_0 \simeq 30$ cm^{-1} is the limiting frequency of the acoustic phonons). After the pump pulse, we observe a decrease in the occupation numbers of phonons with fequency Ω_a=20-25cm^{-1}. Their degradation is accompanied by an increase in the occupation numbers of phonons of lower energy and by a propagation of the latter into the cold regions of the crystal. According to the measurements carried out at time delays t_D=0-40 ns, phonons of frequency Ω_a=20-25cm^{-1} are essentially trapped in the excitation region. This trapping is apparently due to two factors: the short lifetime with respect to decay and scattering and the low group velocity of phonons of frequency $\Omega_a \simeq \Omega_0$.

Figure 6 shows data on the spatial distribution of nonequilibrium phonons of frequency $\Omega_a \simeq 10$ cm^{-1} at various times after the pump pulse. It follows from these results that the "spreading" of the phonon packet initially (t_D=20 ns) occurs at a velocity $\simeq 10^5$cm/s, close to the sound velocity in anthracene crystals (u=(1-4)×10^{5}cm/s, depending on the polarization and propagation direction [11,12]), i.e., the phonons propagate in a quasiballistic regime over a distance L≃20μ. At later times, the propagation of phonons slows down markedly (see the insert in Fig.6; Δ is the width at half-maximum of the spatial distribution of phonons of frequency $\Omega_a \simeq 10$cm^{-1}), demonstrating a decrease in the mean free path of the phonons at $t_D > 20$ ns, at least to

$l_u < L \simeq 20\mu$. An estimate of the mean free path of the phonons with respect to phonon-phonon scattering with nonconservation of quasi-momentum, involving thermal (equilibrium) phonons, at a crystal temperature $T_o = 4.5\,K$, $l_u^o = l_o \exp(\Omega_o/T)$, where [1] $l_o \simeq 0.01\mu$, yields $l_u^o \simeq 140\mu$. A significant decrease in the mean free path, $l_u \ll l_u^o$, could be caused only by an increase in the occupation numbers of phonons with energies near the Debye energy $(\Omega_a \simeq \Omega_o)$ in the volume of the crystal occupied by nonequilibrium phonons. As follows from the data in Fig.5, phonons of frequency $\Omega_a \simeq \Omega_o$, which arise in the crystal during the pump pulse, are localized in the excitation region. Consequently, an increase in the occupation numbers of phonons with energies near Debye energy in parts of the crystal far from the excitation region can be achieved only as a result of the coalescence of lower-frequency nonequilibrium phonons. An increase in the occupation numbers on the high-frequency tail of the phonon distribution, with the result that there is a change in the propagation regime for nonequilibrium phonons, would naturally be linked with the establishment of a temperature $T > T_o$ in the crystal. Estimates show that under these experimental conditions the temperature can reach $T \simeq 9\,K$; at this temperature we would have $l_u \simeq 1\mu$. The observed transport of energy from the excitation region into the cold regions of the crystal is reminiscent of the mechanism of nonlocal thermal conductivity proposed in Ref. 13.

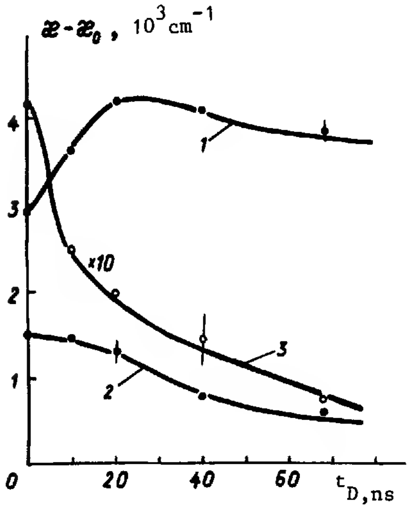

Fig. 7. Time evolution of the absorption coefficient at different frequencies Δ: 1 - 10; 2 - 15; 3 - 20cm⁻¹ (uniform excitation of the crystal surface at $P = 8\,kW/cm^2$, $d = 12\mu$).

In the case of uniform excitation of the entire crystal surface, the conditions for a plane experimental geometry [1] hold, so that the propagation of phonons along the surface of the sample can be ignored. It follows from the data in Fig. 7 that just after the excitation (at $t_D < 20$ ns) the changes in the occupation numbers of the phonons of different frequencies are quite different. For example, the occupation numbers of high-frequency phonons with $\Omega_a \simeq 20\,cm^{-1}$ decrease sharply, because of their fast spontaneous decay. For lower-frequency phonons with $\Omega_a \simeq \Omega_o/3 \simeq 10\,cm^{-1}$,the occupation numbers increase because the decay of the phonons of a given frequency is slower than the rate at which they are generated by the decay of high-energy phonons. For phonons of intermediate frequency, $\Omega_a \simeq 15\,cm^{-1}$, the occupation numbers stabilize, demonstrating that the excitation and spontaneous decay of phonons of a given frequency do not cancel out at $t_D \lesssim 20\,\text{ns}$. Later (at $t_D \gtrsim 40\,\text{ns}$), the occupation numbers of phonons with $\Omega_a=10\text{–}20\,\text{ns}$ fall off smoothly, and they tend toward their equilibrium values as the temperature $T > T_o$ is established. The complex nature of the kinetics may also be due to the existence of different spontaneous-decay time for phonons of the quasilongitudinal and quasitransverse branches.

We wish to thank D.V. Kazakovtsev and I.B. Levinson for useful discussions.

References

1. V.L. Broude, N.A. Vidmont, D.V. Kazakovtsev, V.V. Korshunov, I.B. Levinson, A.A. Maksimov, I.I. Tartakovskii and V.P. Yashnikov, Zh.Eksp.Teor.Fiz. 74 314(1978)
2. D.V. Kazakovtsev and I.B. Levinson, Pis'ma Zh.Eksp.Teor.Fiz.27,194(1978)
3. A.A. Maksimov and I.I. Tartakovskii, Pis'ma Zh.Eksp.Teor.Fiz.42,458(1985)
4. A.A. Maksimov and I.I. Tartakovskii, Pis'ma Zh.Tech.Fiz.12,112(1986)
5. M.D. Galanin, Sh.D. Khan-Magometova and E.N. Myasnikov, Mol.Cryst.Liq.Cryst. 57,119(1980)
6. N.A. Vidmont, A.A. Maksimov and I.I. Tartakovskii, Pis'ma Zh.Eksp.Teor.Fiz. 37,578(1983)
7. N.A. Vidmont, A.A. Maksimov and I.I. Tartakovskii, Fiz.Tverd.Tela 24,1384(1982)
8. R. Sonnenschein, K. Syassen and A. Otto, J.Chem.Phys.74,4315(1981)
9. N.A. Vidmont, A.A. Maksimov and I.I. Tartakovskii, Izv. AN SSSR, Ser.fiz.47, 1296(1983)
10. T.R. Meeker and A.H. Meitzler in Physical Acoustic (ed. W.P. Mason) v.1A, Academic Press, New York - London (1964)
11. U. Lutz, Gitterdynamik von Anthrazen, Diss.,Technischen Hochschule, Zürich,(1970)
12. D.V. Kazakovtsev, I.B. Levinson and V.P. Yashnikov, Zh.Eksp.Teor.Fiz.74, 328(1978)
13. I.B. Levinson, Zh.Eksp.Teor.Fiz.79,1384(1980)
14. J.W. Tucker and V.W. Rampton, Microwave Ultrasonics in Solid State Physics, North-Holland, Amsterdam (1972)

MOLECULAR DYNAMICS STUDY OF A MODEL WITH INCOMMENSURATE PHASES

K.Parlinski
Institute of Nuclear Physics
ul.Radzikowskiego 152, 31-342 Cracow, Poland

Abstract. The mechanism of the change of the characteristic wavevector of the modulation in the incommensurate crystal relies in the nucleation of striplles. The striplle is a finite object constructed from discommensuration planes. The nucleation and growth of the striplle is demonstrated by the molecular dynamics simulation of a two-dimensional model. The influence of point defects on striplle growth are discussed.

1. Introduction

Recently a number of crystals has been discovered[1] which show in some temperature interval a long range modulation of some degree of freedoms with a period being incommensurate with the underlying lattice, i.e. the wavelenght of the modulation is not an integral multiple of the unit cell edge. Such phases of a crystal are called incommensurate in contrary to the commensurate ones for which the wavevector is an integral multipler of the lattice constant of high temperature unit cell. The modulation can propagate in one, two or three-dimensions but below we shall concentrate on the one dimensional modulations only.

The modulated degree of freedom of the incommensurate phase can be either of displacive or occupational type, in full analogy to the distorted degree of freedoms which form the low symmetry phase after structural phase transition. The averaged atomic arragement in the one-dimensional incommensurate phase of displacive type relies in static displacements of some atoms from the positions in which they were residing in the high symmetry phase. The displacements form a periodic static wave propagating in one direction. No two atoms along the direction of the modulation are displaced by the same distance. The displacement in the plane perpendicular to this direction are the same in each unit cell. In real crystals the pattern of atomic distorsions is usually complicated but the displacements can be combined to few static modes, which specify the incommensurate modulation.

The incommensurate modulation can be directly observed by the X-ray and neutron diffraction method. In the incommensurate phase the usual Bragg reflections are accompanied by satellite reflections located in some distance from the main Bragg spots. The position of a satellite with regard to the main reflection defines the wavevector of the incommensurate modulation.

The incommensurate phase usually arrises from a commensurate high symmetry phase below some critical transition temperature T_c. The phase transition to incommensurate phase can be well described by a generalization of the soft mode theory of structural phase transitions. According to this concept, in the high symmetry phase of the crystal exists a mode, which softens under temperature lowering. At the phase transition to the incommensurate phase the soft mode reaches the zero energy at the critical wavevector q. Below T_c, the diffraction satellite appears at position q and the soft mode converts into the phason and amplitudon modes. The amplitudon mode is an optic-like mode and its energy increases under temperature lowering.

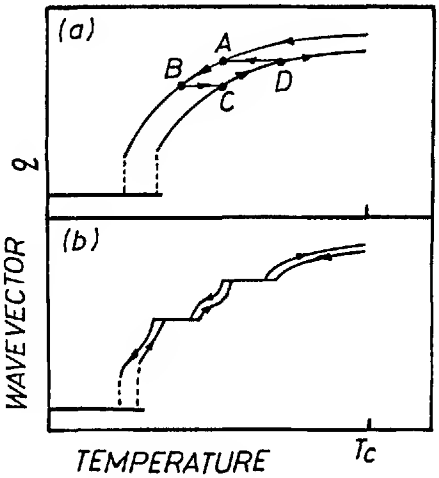

Fig.1 - Temperature dependence of the characteristic incommensurate wavevector of (a) a contineous type and (b) devil's staircase type. The cooling and heating runs define the global histeresis. The path ABCDA specifies a local histeresis. Steps in (b) correspond to lock-in phases.

The phason mode corresponds to oscillations of the phase ε of the displacement wave. In the continuum limit it is acoustic-like and gapless as it takes zero energy to slide whole condensed modulation throughout the crystal. The sliding mode comes from the fact that in the incommensurate phase the phase ε of the modulation is not fixed in space by any potential. If, however, the characteristic wavevector of the modulation is close to a commensurate value $q \approx n/m$, where n and m are small integers, then the crystal might gain energy if it forms a commensurate structure. Such a commensurate phases are called lock-in. In the lock-in phase the phase ε of the modulation is fixed and the phason is no longer an acoustic-like mode but exhibits a finite energy gap between the minimum of its dispersion curve and zero energy.

The incommensurate modulation characterized by a wavevector being close but not equal to a commensurate value n/m, consists not of sinusoidal configuration of particles but of pieces of commensurate regions which are separated by intermediate configurations called discommensurations. The density of discommensurations tends to zero when the wavevector q of the modulation approaches the lock-in commensurate value n/m. The discommensuration forms a plane perpendicular to the direction of the modulation. From the structural point of view a discomensuration is equivalent to a domain wall. However, in equilibrium, the domain wall increases the crystal energy while the discommensuration decreases it.

As a rule the characteristic wavevector q of the incommensurate modulation changes as a function of temperature, pressure or external field. Experimentally this variation can be continuous, Fig.1a, or discontinuous, Fig.1b. Each plateaux in Fig.1b corresponds to a lock-in phase. The curve like in Fig.1b carries the name Devil's staircase.

The cooling and heating curves of temperature dependence of the wavevector q usually do not coincide, Fig.1. The two curves form a loop called global histeresis. The separation between the cooling and heating curves is usually not large, but it may become considerable in vicinity of wide lock-in phases or in a crystal which contains defects.

The local histeresis is described by a loop ABCDA denoted in Fig.1a. The wavelenght of the incommensurate modulation may change in three-dimensional crystal by inserting into it (or removing) some number of discommensuration planes. There are topological restrictions, which define the complete set of discommensuration planes which must be simultaneously inserted or removed. A small object constructed from such set of discommensurations and bordered by so called deperiodization[2] or dislocation lines[3] at which all the additional discommensuration planes meet, is called stripple. The deperiodization line forms a closed loop which might terminate at the surface of the crystal only. A stripple plays an analogous role to the nuclei in the first order phase transition. The additional discommensuration planes change the value of the characteristic wavevector q of the modulation.

2. Experiment and theory

The way the incommensurate crystal changes the characteristic wavevector has been studied in charge density-wave material 2H-TaSe$_2$ using the superlattice dark-field electron microscopy[4,5]. The 2H-TaSe$_2$ has hexagonal structure and below 112 K goes over to an incommensurate phase. This incommensurate phase exhibits on a microscopic scale a one-dimensional modulation called also stripe phase. The incommensurate - commensurate phase transition occurs at 84 K on cooling and 92 K on warming. On warming a single domain of commensurate phase transforms to a single stripe phase. On cooling the incommensurate phase is found to be build up of domains of stripe phases which on larger scale retain a hexagonal symmetry. Many images showing the pattern of discommensuration lines have been obtained. They indicate clearly that the distance between discommensuration planes changes by the nucleation and growth of stripples.

Some macroscopic data also indicate that the striplle mechanism is common in the incommensurate phases. For example, the phase transition from incommensurate to look-in phase is always accompanied by a large histeresis with often estonishing slow kinetics. Such effects have been observed in Rb$_2$ZnCl$_4$[6,7,8], thoiurea[9] and barium sodium niobate[10,11]. The two first crystals show remarkable global and local histeresis over the whole range of incommensurate phases. The experiments confirm that the presence of defects widen the global histeresis[9]. Interesting observation has been made for barium sodium niobate[11]. The line shape of the satellite reflection narrowed and its intensity increased with characteristic time of several hours when the crystal was kept at constant temperature after heating from the low temperature lock-in phase to the incommensurate one.

A number of theoretical studies has been undertaken to describe the nucleation mechanism by striplles. Janovec[2] has proposed the group-theoretical method to find the topological structure of the striplle which appear in vicinity of a given lock-in phase. The analysis is based on the possible set of domains[13] of the lock-in phase which can arrise from a single domain of high symmetry phase of the crystal. Such analysis is usually straightforward for one-dimensional incommensurate modulation but needs this mathematical method in two and higher dimensional cases[14].

Another approach was initiated by Kawasaki[15]. Starting from the Landau type free energy the kinetic equation of motion for discommensuration lines have been derived[3]. Solving them numerically[16,17] it was possible to demonstrate the growth of already nucleated striplle, or half-striplle, and to reproduce the head-on collision of two deperiodization lines and a passing of a deperiodization line through the curved discommensuration line.

Starting from the Landau free energy description Prevlovsek and Rice[18] have examined the homogeneous nucleation process of a striplle for 2H-TaSe$_2$. The estimated energy barrier was somewhat too high to account for the homogeneous nucleation rate.

Below, using the molecular dynamics simulation we demonstrate the microscopic mechanism, which leads to the nucleation and propagation of striplles and to the appearence of global and local histeresis. The influence of substitutional defects will also be discussed.

3. The model and the molecular dynamics method

The model system used in the simulation[19] was defined as a two-dimensional rectangular lattice with one particle per unit cell. Each particle can move out of the system plane and its displacement was z_n. The particles interact via the following potential energy

$$V = \frac{1}{2} [\sum_n \sum_j A_j z_n z_{n+j} + G \sum_n z_n^4] \qquad (2.1)$$

where $n=(n_x, n_y)$ denotes the unit cell, and j runs over the neighbours. Four neighbours in y, two in x and one in diagonal directions have been taken into account. The numerical values of the parameters were found due to the following procedure. The quadratic form of Eq. (2.1) can be transformed by

$$z_n = \sum_k Q(k) \exp[2\pi i(k_x n_x + k_y n_y) \qquad (2.2)$$

into a diagonal form

$$\sum_k \Omega^2(k) \; |Q(k)|^2 \qquad (2.3)$$

We intend to consider a one-dimensional incommensurate modulation along the y-direction, so we choose the set of potential parameters such that the minimum of $\Omega^2(k)$ occurs along the [0,1] direction, at a desired wavevector $k=k_p$.

A model doped with 2% of substitutional point defects has also been studied. The defects have been defined by much deeper local double minimum potential $A_0 z^2 + G z^4$. Due to the high barrier between the minima, the defects were almost always remaining in one of the local minima

Below we shall study processes which occur as a function of k_p. Thus, the ground state energy at T=0 for the one-dimensional modulation in y-direction reaches minimum for the wavevector km being not necesserly equal to k_p. The relation $k_m = f(k_p)$ between the two wavevectors at the minimum of the potential energy are called Devil's staircase of the ground state and for our choise of the model parameters it is shown in Fig.4. The curve consists entirely from lock-in phases.

The two-dimensional system used in the simulation consisted of 97x97 particles. Free boundary conditions were used and that has allowed the extended defects to flow out of the system. The Newton equations of motions were iteratively solved by the simple difference scheme. The temperature was described by kinetic energy. The system could be cooled or heated by delicate changes of particle velocities in each iteration step. Moreover, by contineous changing the potential parameters the minimum of $\Omega^2(k)$ at k_p could be altered.

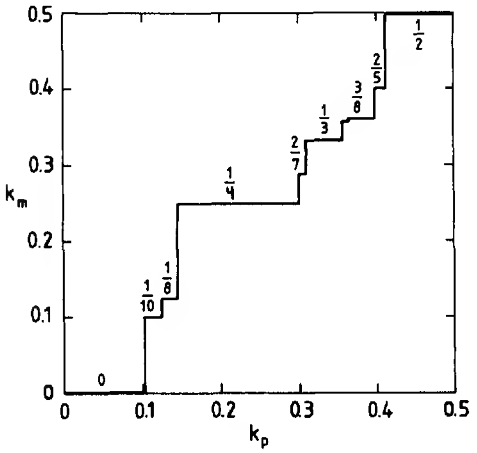

Fig.2 -The ground state Devil's staircase curve of the model.

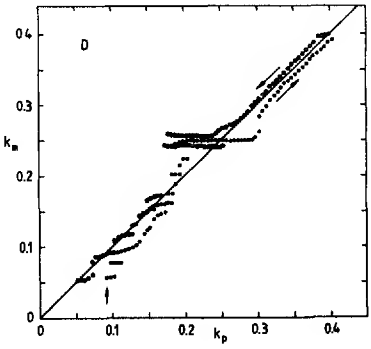

Fig.3 - The position of the diffraction satellites detected by the diffuse scattering function F(k) as a function of the wavevector k_p for a constant rate dk_p/dt. Closed and open points correspond to 0 -> 0.4 and 0.4 -> 0 runs, respectively.

The simulation confirmed that at relatively high temperature the system with fixed k_p shows properties of a normal crystal. The satellite reflections calculated by the diffuse scattering function appear under cooling below a critical temperature T_c. For k_p being far from commensurate values 0 and 1/4 the phase remained incommensurate till the lowest temperature, while in the case of k_p close to 0 or 1/4 the system transformed under cooling to few domains of lock-in phases 0 or 1/4, respectively.

4. Kinetic behaviour of the incommensurate modulation.

In real incommensurate crystals the minimum of k_p of the soft mode $\Omega^2(k)$ often shifts as a function of temperature, because of its renormalization by fluctuations of other modes. So, in experiment one may influence the position of the minimum at k_p only by varing the temperature , pressure or external field applied to the sample. In computer simulation in order to study the mentioned effects the following procedure was used. Ths position of the minimum at kp of the dispersion curve $\Omega^2(k)$ was shifted in time with a constant rate dk_p/dt by appropriate change of the potential energy parameters A_j. Two runs in opposite directions were studied, an increasing one from $k_p=0$ to 0.4 and a decreasing one from $k_p=0.4$ to 0. During that process the diffuse scattering function F(k) was calculated. The F(k) contained satellite reflections. Its position as a function of the wavevector k_p for the increasing and decreasing runs are shown in Fig.3. The points in Fig.3 characterize the configurations which, except the initial ones, correspond not necesserly to the equilibrium state and therefore, they define the non-equilibrium Devil's staircase. The relaxation towards equilibrium in the range of $k_p=0.27-0.40$, was so fast that the satellite position chnges in a continuous way. In the vicinity of $k_p=0.25$ the modulation locks-in to the commensurate phase 1/4. The observed splitting of the satellite is due to the domain structure of the phase 1/4. Below $k_p<0.18$ an irregular variation of the satellite position with sometimes two or three peak structure occurs. That indicates that the incommensurate structure is far from being perfect. Global hysteresis between increasing and decreasing runs, and especialy around the lock-in phase 1/4, is clearly seen. The histeresis manifests the necessity of nucleation and growth of striplle. Besides the lock-in phases 0 and 1/4 no other commensurate phases have been detected, because the lock-in energies of these not observed commensurate phases were too small, the temperature of the runs too high and the rate dk_p/dt too fast to allow good equilibration.

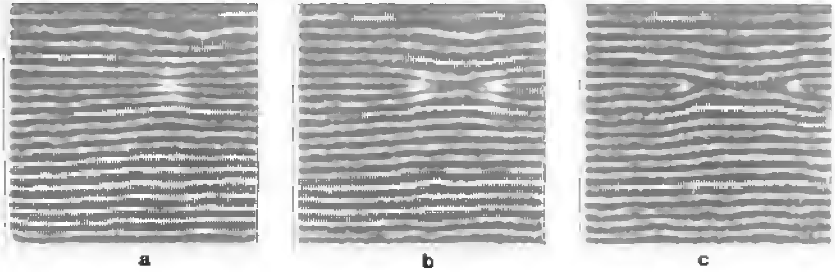

Fig. 4 - Example of homogeneous nucleation and growth of the striplle of the incommensurate modulation. The maps a, b, c, correspond to k_p=0.375, 0.385, 0.395, respectively.

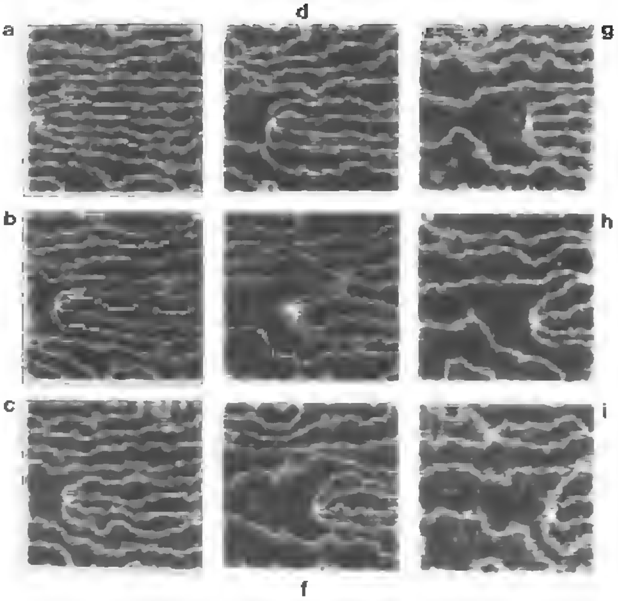

Fig. 5 - Subsequent configuration maps in the process where kp changes from 0.2744 (map a) to 0.2616 (map i).

The analysis of many pictures of particle configurations allowed to conclude that the mechanism of the change of the incommensurate wavevector relies in homogeneous nucleation of a stripple within the crystallite and afterwards in the growth of it. The striplle is a nucleus formed from additional discommensuration planes which fit to the surrounding incommensurate modulation and which meet along one closed line called the deperiodization line. In Fig. 4 three stages of this process are given. The stripes on the maps correspond to the discommensuration lines. The striplle arrises as a result of accidental concentration of energy fluctuation and can be noticed in Fig. 4a. Later it grows to the left and to the right, Figs 4b, 4c, by motion of the deperiodization line.

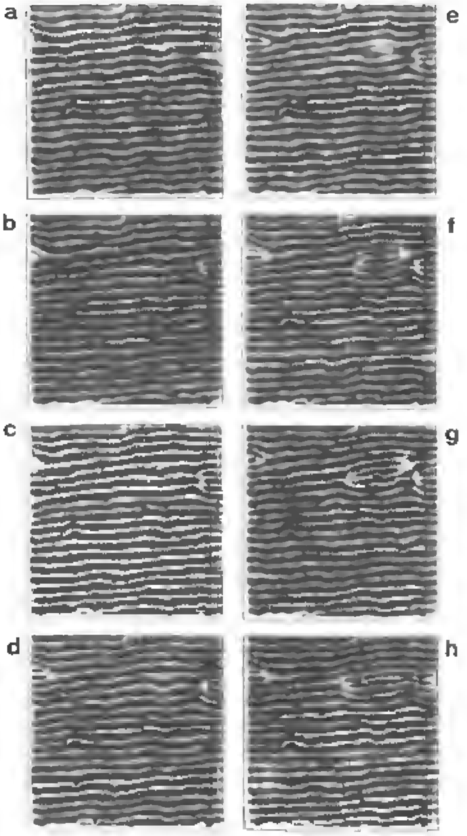

Fig. 6 – Propagation of the striplles in the system containing 2% of point defects. The wavevector in maps from a to h changes from 0.3672 to 0.3792.

An example of a more complicated mechanism is presented in Fig. 5. The maps show the subsequent configurations in the process of decreasing the wavevector k_p and close to the commensurate phase 1/4. The stripes on the map (a) are discommensuration lines between regions of commensurate phase 1/4. The striplle, related with the commensurate phase, consists of at least four discommensuration planes which confine regions belonging to three different domains of phase 1/4. Indeed, if the surrounding commensurate domain is characterized by the phase $\varepsilon(\frac{1}{4})=\pi/4$ then the domains within the striplle must form a sequence of domains with phases $\varepsilon(\frac{1}{4})=3\pi/4$, $5\pi/4$

and 7π/4. Other sequence would cost too much energy. In the map (b) a half-striplle, seen as a bundle of four discommensuration lines which meet in the deperiodization point, splits out from the left middle edge of the crystallite and on the (c) to (i) maps it moves towards the right edge leaving behind a large region of commensurate phase 1/4.

The defects hinder the propagation of the deperiodization line. Fig.6 illustrates such a process. At the edge on right upper part of map 6a, a nucleus is seen. The nucleus, map (b), tries to enter the crystallite but a group of five defects does not let it through. This strained state lasts for some time, maps (c,d) and then a new nucleus inside the system appears close to previous one, map(e). The new nucleus grows, map (f-h), through the whole crystallite. The modulation wavevector k_p of the system, as detected by the diffuse scattering function, stays constant for some range of the k_p variation, because the propagation of the deperiodization line is hindered by the energy barriers introduced by the defects.

References

1. R.Blinc and A.P Levanyuk, "Incommensurate Phases in Dielectrics", Modern Problems in Condensed Matter Sciences 14 (1986).
2. V.Janovec, Phys.Lett. 99a, 384 (1983)
3. K.Kawasaki, Physica, 124B, 156 (1984).
4. K.K.Fung, S.McKernan, J.W.Steeds and J.A.Wilson, J.Phys.C: Solid State Phys.,14, 5417 (1981).
5. C.H.Chen, J.M.Gibson and R.M.Fleming, Phys.Rev., B26, 184 (1982).
6. H.Mashiyama, S.Tanisaki and K.Hamano, J.Phys.Soc.Jpn 50, 2139 (1981).
7. H.Mashiyama, S.Tanisaki and K.Hamano, J.Phys.Soc.Jpn 51, 2538 (1982).
8. H.G.Unruh, J.Phys.C:Solid State Phys., 16,3245 (1983).
9. B.Andre, D.Durand, F.Denoyer, R,Currat and F.Moussa, Phys.Rev., B, to be published.
10. E.Errandonea, J.C.Toledano, A.Litzler, H.Savary, J.Schneck and J.Aubree, J.Physique Lett., 45 L329 (1984).
11. J.Schenck, G,Calvarin and J.M.Kiat, Phys.Rev., B29, 1476 (1984).
12. J.M.Kiat, G.Calvarin and J.Schenck, J.Phys.Soc.Jpn, 24 Supplement 24-2, 832 (1985).
13. V.Janovec, Ferroelectrics 35, 105 (1981)
14. V.Janovec and V.Dvorak, Ferroelectrics, 66, 169 (1986).
15. K.Kawasaki, J.Phys.C: Solid State Phys., 16, 6911 (1983).
16. K.Kawasaki and S.Iwamoto, Physica, 133B, 76 (1985).
17. K.Kawasaki and S.Yamanaka, Phys.Rev., B34, 7986 (1986).
18. P.Prelovsek and T.M.Rice, J.Phys.C: Solid State Phys., 16, 6513 (1983).
19. K.Parlinski, Phys.Rev., B, to be published.

ANISOTROPY OF RELAXATION OF ACOUSTIC PHONONS SCATTERED BY ISOTOPIC IMPURITIES

Zygmunt K. Petru
Joint Institute for Nuclear Research, Dubna, SU
and
Institute of Theoretical Physics, University of Wrocław
50-205 Wrocław, ul.Cybulskiego 36, Poland

Exact solutions of the phonon Boltzmann equation describing relaxation of acoustic phonons scattered by isotopic impurities are found for the case of spatially homogeneous systems. The solutions depend on the symmetry of the system. If the symmetry of a crystal or the symmetry of the disturbed phonon distribution function is lower than cubic, the effective relaxation time is elongated as compared to the value obtained within the relaxation-time approximation. This new relaxation time is strongly direction-dependent.

1. Introduction

The phonon Boltzmann equation (PBE) has, in general, the form of a nonlinear integro-differential equation [1] and usually does not allow an exact treatment. The number of solvable models is very limited, and they are based on rather drastic assumptions about the collision integral. We mention the instructive Claro-Wannier model describing relaxation of acoustic phonons towards equilibrium due to anharmonic interactions [2]. In this lecture we shall consider another mechanism of relaxation which provides the solvable PBE, namely, the relaxation due to the scattering of acoustic phonons by isotopic impurities. This idea comes from recent experiments on the ballistic phonon propagation in monocrystals at low temperatures. The samples used were so large and so chemically and structurally perfect that phonons felt isotopic impurities as main scatterers [3]. Then, it seems quite reasonable to consider the model in which phonons in their relaxation process are scattered only by isotopic impurities (strictly speaking, only by mass differences) [4,5].

2. The model

The object under consideration is a phonon gas in an anisotropic homogeneous elastic continuum. Now phonons are equivalent to sound wave quanta of frequencies $\omega(\vec{k}j)=|\vec{k}|c(\hat{\vec{k}}j)$, with sound velocities $c(\hat{\vec{k}}j)$ depending, in general, on a wave-vector direction given by the unit vector $\hat{\vec{k}} = \vec{k}/|\vec{k}|$, and on the phonon branch index j. We shall consider two kinds of the disturbances of the phonon distribution: one which retains symmetry of the system and the other one which lowers it. In both cases the space homogeneity is assumed. The relaxation of phonon distribution function $N(\vec{k}j;t)$ is governed by PBE of the form

$$\frac{\partial}{\partial t} N(\vec{k}j;t) = \frac{\nu}{(2\pi)^3} \sum_{j'} \int d\vec{k}' w(\vec{k}j;\vec{k}'j')\cdot\delta(\omega(\vec{k}j) - \omega(\vec{k}'j'))\cdot[N(\vec{k}'j';t) - N(\vec{k}j;t)] \tag{1}$$

where ν is the volume of a unit cell. The probability per unit time, w, that phonon is scattered elastically from a $\vec{k}j$-state into a $\vec{k}'j'$-state for the sample with randomly distributed isotopic impurities of small concentration was calculated by Klemens [6] (see also [5])

$$w(\vec{k}j,\vec{k}'j') = \frac{\pi}{2}\cdot g\cdot \omega(\vec{k}j)\cdot\omega(\vec{k}'j')\cdot|\vec{e}(\vec{k}j)\cdot\vec{e}(\vec{k}'j')|^2, \tag{2}$$

where $\vec{e}$ is the normalized polarization vector ($|\vec{e}(\vec{k}j)|^2=1$). Here $g=\sum_i f_i(1-m_i/m)^2$ where f_i is a fraction of unit cells with the mass m_i, and m is the averaged mass of the unit cell, $m=\sum_i f_i m_i$. Let us note that in the case of low-energy phonons the formula (2) is valid also for multiatomic crystals. Here we would like to stress that scattering of high-energy phonons allows only the numerical treatment [4,5].

In the system described by (1) the total energy as well as the total number of phonons are conserved. Moreover, the energy of an individual phonon scattered elastically by a mass defect is conserved, i.e. $\omega(\vec{k}j)=\omega(\vec{k}'j')\equiv\omega$. Thus the number of phonons with given energy $\hbar\omega$ is also constant. We can then label the long-wave phonon by its frequency ω, wave-vector direction $\hat{\vec{k}}$, and branch j to which it belongs, i.e. $\{\vec{k},j\}=\{\omega,\hat{\vec{k}},j\}$. So, the integration over the wave vector $\vec{k}'$ in collision integral is reduced merely to the integration over the solid angle $\Omega'\equiv\Omega(\hat{\vec{k}}')$.

Let us now define the averaged value of the distribution function according to the formula

$$\langle N(\omega;t)\rangle \equiv \frac{1}{3}\sum_j \int\frac{d\Omega}{4\pi}\left(c_D/c(\hat{\vec{k}}j)\right)^3 N(\omega\hat{\vec{k}}j;t) , \tag{3}$$

where c_D is the Debye velocity given as usual by

$$c_D^{-3} = \frac{1}{3}\sum_j \int\frac{d\Omega}{4\pi} c^{-3}(\hat{\vec{k}}j) . \tag{4}$$

From the fact just mentioned that the number of phonons with a given energy $\hbar\omega$ is conserved it follows that (3) is constant in time

$$\langle N(\omega;t)\rangle = \langle N(\omega;t=0)\rangle \equiv \bar{N}(\omega) = \text{constant}. \tag{5}$$

It means that all phonons of energy $\hbar\omega$ relax towards their average value $\bar{N}(\omega)$, and so we are looking for a deviation from $\bar{N}(\omega)$ defined as

$$n(\omega\hat{\vec{k}}j;t) = N(\omega\hat{\vec{k}}j;t) - \bar{N}(\omega). \tag{6}$$

Since the phonon frequency is a constant of motion and appears only as a fixed parameter, it will be omitted thereafter.

3. Symmetry of the collision integral

As we have already mentioned, the analytical solution of PBE depends on the symmetry of a system because the form of the collision integral is symmetry-dependent. To see this, let us first consider the collision-out term of PBE. The factor in front on $N(\hat{\vec{k}}j;t)$ on the right-hand side of Eq.(1), usually called the collision rate or the reciprocal of the collision time, can be written for long-wave phonons as follows

$$\nu(\hat{\vec{k}}j) = \frac{\nu}{4}\frac{g}{\pi}\,\omega^4 \sum_{j'} \int \frac{d\Omega'}{4\pi}\, c^{-3}(\hat{\vec{k}}'j')\cdot(\vec{e}(\hat{\vec{k}}j)\cdot\vec{e}(\hat{\vec{k}}'j'))^2 \quad . \tag{7}$$

Spatial anisotropy of the collision rate is due to its dependence on polarization vectors. The right-hand side of Eq.(3) contains the following tensor

$$f_{\alpha\beta} = \frac{1}{3}\sum_{j'} \int \frac{d\Omega'}{4\pi} \left(c_D/c(\hat{\vec{k}}'j')\right)^3 e_\alpha(\hat{\vec{k}}'j')e_\beta(\hat{\vec{k}}'j') \quad , \tag{8}$$

whose trace is normalized to unity. A similar tensor appears in the collision-out term of (1) but now it includes the distribution function

$$F_{\alpha\beta}(t) = \frac{1}{3}\sum_{j'} \int \frac{d\Omega'}{4\pi} \left(c_D/c(\hat{\vec{k}}'j')\right)^3 e_\alpha(\hat{\vec{k}}'j')e_\beta(\hat{\vec{k}}'j')n(\hat{\vec{k}}'j';t) \quad . \tag{9}$$

The tensor (9) is traceless due to (6). The number of nonvanishing tensor components of $f_{\alpha\beta}$ and $F_{\alpha\beta}$ depends on the symmetry of the phonon system.

3.1. Cubic symmetry

For the elastic continuum having the cubic symmetry the tensor (8) is proportional to the unit matrix and the tensor (9) simply vanishes

$$f_{\alpha\beta} = \frac{1}{3}\,\delta_{\alpha\beta} \qquad ; \qquad F_{\alpha\beta}(t) = 0 \quad . \tag{10}$$

By inserting the first of Eqs.(10) into (7) we find only one collision rate common for all directions $\hat{\vec{k}}$ and branches j, given by [5]

$$\nu(\hat{\vec{k}}j) = \frac{\nu\cdot g}{4\pi}\,\frac{\omega^4}{c_D^3} \equiv \nu_c \tag{11}$$

Thus we come to the conclusion that the spatial isotropy characterizes the scattering of acoustic long-wavelength phonons by mass defects in cubic crystals.

3.2. Tetragonal symmetry

In this case the matrix (8) is diagonal with three nonvanishing elements $f_{xx}=f_{yy}$ and f_{zz}, where we have taken the fourfold axis along the z-axis. Because, in general, $f_{xx}\neq f_{zz}$ we should, in addition to the Debye velocity, introduce another constant, say f_{zz}. Having noticed that $f_{xx}=f_{yy}=(1-f_{zz})/2$ we can rewrite the collision rate (7) in a more convenient form [7]

$$\nu(\hat{\vec{k}}j) = \nu_c \frac{3}{\Gamma+2} [1 + (\Gamma-1)e_z^2(\hat{\vec{k}}j)] , \tag{12}$$

where we have introduced the anisotropy parameter Γ defined as

$$\Gamma \equiv \frac{f_{zz}}{f_{xx}} \quad . \tag{13}$$

It means that for a symmetry lower than cubic the collision rate is spatially anisotropic. The anisotropy comes from the dependence of the z-component of the polarization vector on the direction $\hat{\vec{k}}$ and is different for different modes j. For crystals with the cubic symmetry as well as for isotropic media $f_{xx}=f_{zz}$ and $\Gamma=1$, so we return to the result (11) as it should be.

A more important consequence of the lowering of a symmetry is that the tensor $F_{\alpha\beta}$ has non-zero components. For the elastic continuum of tetragonal symmetry the nonvanishing components (i.e. $F_{xx}=F_{yy}$ and F_{zz}) are connected with each other for the tensor is traceless. So we may choose of the components, say F_{zz}, and denote it, for brevity, by F

$$F(t) = F_{zz}(t) = - F_{xx}(t) = - F_{yy}(t) \neq 0. \tag{14}$$

As a result of (14), the PBE for a phonon system with tetragonal symmetry preserves its form of integro-differential equation.

3.3. Hexagonal symmetry

All results of the previous section are also valid for the anisotropic continuum of hexagonal symmetry. But here additional simplifications take place. The z-component of the polarization vector of pure transverse phonons, j=T, vanishes for any $\hat{\vec{k}}$ by definition (see [8]). As a result, equation (12) for this mode is reduced to [7]

$$\nu_T = \frac{3}{2+\Gamma} \nu_C \tag{15}$$

It means that ν_T is isotropic and differs from the cubic case (11) only by a factor which tends to unity when Γ approaches 1. For quasilongitudinal and quasitransverse modes the formula (12) is still valid but now with e_z depending only on $\hat{k}_z$ and j [7].

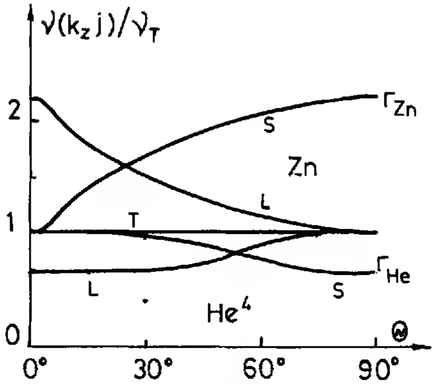

Fig.1. Relative value of the phonon scattering rate of two hcp crystals: ^4He ($\Gamma<1$) and Zn ($\Gamma>1$) versus the angle between wave-vector direction and sixfold axis. L, T, and S are quasilongitudinal, pure transverse, and quasitransverse modes, respectively.

Simplifications just mentioned appear as a result of the symmetry. Namely, the anisotropic continuum of hexagonal symmetry is transversally isotropic [8]. Having this we are able to calculate the anisotropy parameter Γ for all hexagonal crystals for which elastic constants are known (Table I). It is also easy to analyse the spatial anisotropy of the scattering rate (12). In Fig.1. two cases are presented: hcp helium-4 crystal for which $\Gamma<1$ and hcp zinc with $\Gamma>1$. For further analysis it is important to note that for $j \neq T$ the scattering rate changes monotonically with $\hat{k}_z$ and reaches extremum at $\hat{k}_z=0$.

4. Exact solutions of the phonon Boltzmann equation

As we have just shown, the symmetry of the system determines the final form of PBE. Now we are able to show how the solution of PBE depends both on a symmetry of a crystal itself and on a symmetry of a disturbance.

4.1. Relaxation in crystals of cubic symmetry

Let us first consider such a disturbance of the phonon distribution which does not lower its cubic symmetry. For this case the tensor (9) vanishes, $F_{\alpha\beta}(t)=0$. This essentially simplifies the collision integral, and PBE is reduced to [9]

$$(\partial/\partial t + \nu_c)n(\hat{\vec{k}}j;t) = 0. \tag{16}$$

Thus, in this case the exact solution of PBE is

$$n(\hat{\vec{k}}j;t) = n(\hat{\vec{k}}j;t=0)\exp(-t\nu_c). \tag{17}$$

In the general case equation of the form (16) is assumed in the relaxation time approximation (RTA) [6], where the collision integral is change to $\nu_c \cdot n(\hat{\vec{k}}j;t)$.

As a next example let us consider a crystal of cubic symmetry with such a disturbance of the phonon distribution function which lowers its symmetry to tetragonal. It can be realized by generation of homogeneous flows of phonons propagating in parallel with one of a fourfold axis (say, z-axis). The tensor $F_{\alpha\beta}$ containing such disturbed distribution function should reflect the tetragonal symmetry (see Eq.(14)). It means, that PBE preserves now the form of integro-differential equation

$$(\partial/\partial t + \nu_c)n(\hat{\vec{k}}j;t) = \frac{3}{2}\cdot \nu_c\cdot(3e_z^2(\hat{\vec{k}}j) - 1)\cdot F(t). \tag{18}$$

Multiplying both sides of (18) by $e_z^2(\hat{\vec{k}}j)$ and averaging them according to the definition (9) we obtain the equation determining the integral term

$$(\partial/\partial t + (1-\alpha)\cdot\nu_c)(F(t) = 0 \tag{19}$$

Its solution decays exponentially

$$F(t) = F(0)\ \exp\{-t\nu_c(1 - \alpha)\}. \tag{20}$$

The parameter α will be defined later on.
Substitution of (20) into (18) gives us the final result in the form

$$n(\hat{\vec{k}}j;t) = n(\hat{\vec{k}}j;t{=}0)e^{-t\nu_c} + \frac{3}{2}\cdot\frac{F(t{=}0)}{\alpha}\ (3e_z^2(\hat{\vec{k}}j) - 1)(e^{-t(1-\alpha)\nu_c} - e^{-t\nu_c}). \tag{21}$$

The first term on the right hand side of (21) is nothing but the result usually obtained from RTA. The second term comes out as a consequence of the exact treatment of the collision - in part of the collision integral. Let us first note that this part of the solution vanishes for some directions in the k-space, namely, for those which fulfil the condition $e_z^2(\hat{\vec{k}}j)=1/3$. For any other phonons the time evolution of the distribution function is described by two relaxation times. In addition to $\tau_c \equiv 1/\nu_c$ a new relaxation time appears

$$\tau_*^{-1} \equiv \nu_* \equiv (1 - \alpha)\nu_c\ . \tag{22}$$

with the parameter α given by

$$\alpha \equiv \frac{3}{2}\ (3f_{zzzz} - f_{zz}). \tag{23}$$

The symmetric tensor of the fourth rank, $f_{\alpha\beta\gamma\delta}$ is defined in the same way as (8) but with four polarization-vector components instead of two. It follows from the definition of α, that for the crystals of cubic symmetry $1/9 < f_{zzzz} < 1/3$ or, equivalently, $0<\alpha<1$. The inequality $\alpha<1$ guarantees the stability of the solutions (20) and (21). Positivity of α leads to the following inequality

$$\tau_* > \tau_c \ . \tag{24}$$

We can conclude from (21) and (24) that the disturbance lowering the symmetry of the phonon distribution leads to elongation of the asymptotic relaxation time.

It is worth to consider, as an example, such a disturbance which does not change the distribution of some phonons whereas the symmetry of the distribution functions of any other phonons is lowered from, say, cubic to tetragonal. In other words, the initial condition for these undisturbed phonons is given by $n(\vec{k}j;t=0) = 0$. Such phonons cannot be described in the framework of the relaxation time approximation. However, within our description their distribution function is given by the second term on the right-hand side of (21). As a function of time it starts to grow from zero, reaches its extremum at $t_{ex}=-(\tau_c/\alpha)\ln(1-\alpha)$ which is of an order of τ_c, and its asymptotical behaviour is determined by the (longer) relaxation time τ_*.

Let us finally notice that the results just obtained remain also valid for an isotropic elastic medium (instead of the cubic one) with the initial distribution function of the axial symmetry. In this simplest case using only symmetry arguments we get $f_{zzzz} = 1/5$ so that $\alpha = 2/5$ and $\tau_* = (5/3)\tau_c$.

4.2. Relaxation in crystals of tetragonal symmetry

As we have shown in Section 3.2. in a crystal of a symmetry lower than cubic the collision rate is anisotropic. If we disturb the phonon distribution in such a crystal we shall obtain that $F(t) \not\equiv 0$. So, in the case of elastic continuum of tetragonal symmetry the relaxation of the disturbance which does not lower the initial symmetry is governed by PBE having the form

$$(\partial/\partial t + \nu(\hat{\vec{k}}j))n(\hat{\vec{k}}j;t) = \frac{3}{2}\,\nu_c(3e_z^2(\hat{\vec{k}}j) - 1)F(t) \ . \tag{25}$$

The integro-differential equation (25) can also be treated exactly. The discussion can be made more simple by transforming (25) into a double-integral equation of the form

$$n(\hat{\vec{k}}j;t) = n(\hat{\vec{k}}j;t=0)e^{-t\nu(\hat{\vec{k}}j)} + \frac{3}{2}\,\nu_c(3e_z^2(\hat{\vec{k}}j) - 1)\int_0^t e^{-(t-t')\nu(\hat{\vec{k}}j)}F(t')dt' . \tag{26}$$

Now we should find an equation determining the unknown integral F(t). As in the previous section, we can get it easily by substituting (26) into the definition (9). We have

$$F(t) = \rho(t) + \int_0^t K(t-t')F(t')dt' \tag{27}$$

where, for brevity, we have denoted the new integral kernel by

$$K(t) \equiv \frac{\nu_c}{2} \sum_j \int \frac{d\Omega}{4\pi} \left(\frac{c_D}{c(\hat{\vec{k}}j)}\right)^3 e_z^2(\hat{\vec{k}}j)(3e_z^2(\hat{\vec{k}}j) - 1)e^{-t\nu(\hat{\vec{k}}j)} , \tag{28}$$

and the inhomogeneous term by

$$\rho(t) \equiv \frac{1}{3} \sum_j \int \frac{d\Omega}{4\pi} \left(\frac{c_D}{c(\hat{\vec{k}}j)}\right)^3 e_z^2(\hat{\vec{k}}j)n(\hat{\vec{k}}j;0)e^{-t\nu(\hat{\vec{k}}j)} \tag{29}$$

In this way we have reduced the PBE to a set of two inhomogeneous Volterra integral equations of the second kind with kernels depending only on the difference of arguments. Thus, equation (27) is simply an integral equation of the convolution type. The solution of (27) can be put in the standard form [10]

$$F(t) = \rho(t) + \int_0^t R(t-t')\rho(t')dt' , \tag{30}$$

with the resolvent R(t) given as the inverse Laplace transform

$$R(t) = \int_{\varepsilon-i\infty}^{\varepsilon+i\infty} \frac{dz}{2\pi i} \frac{\tilde{K}(z)}{1-\tilde{K}(z)} \cdot e^{zt} \quad . \tag{31}$$

Here $\tilde{K}(z)$ is the Laplace transform of the kernel K(t). Moreover, let us note that z/(1-z) as a function of the complex variable is analytic in the neighbourhood of zero including the point z=0 at which it vanishes. The last two statements in accordance with the theorem presented in [11] guarantee the existence of the inverse Laplace transform (31). Equations (26)-(31) give the general solution of PBE (25). We note that the resolvent (31) depends only on analytical properties of the Laplace transform of the kernel $\tilde{K}(z)$ and not on initial conditions. The slow relaxation time is given by this value of z at which $\tilde{K}(z)=1$. The last condition is fully determined by internal phonon characteristics of a given crystal sample: sound velocities, polarization vectors, and collision rates.

Let us note that the general solution (26)-(31) has exactly the same form also for a hexagonal symmetry and therefore we shall present a detailed discussion of (26)-(31) in the next section.

4.3. Relaxation in crystals of hexagonal symmetry

The elastic continuum of hexagonal symmetry is the only anisotropic medium for which the Christoffel equation can be solved analytically, and formulae for sound velocities and polarization vectors can be written down in an explicit form [8,7]. Hence, we can determine the value of the anisotropy parameter Γ (13) and the behaviour of relaxation rates (12) and (15) as functions of the wave vector and branch index. Having these we can study analytic properties of the Laplace transform of the resolvent (31). The singularities of it in the complex z-plane are the following:

(a) A cut along the spectrum of collision rate, $z = -\nu(\hat{k}_z, j)$, i.e., from $z = -\nu_T$ to $z = -\Gamma\nu_T$, due to the integral of the Cauchy-type in $\tilde{K}(z)$;

(b) An isolated pole located at a point $z = -\nu_*$ at which $\tilde{K}(z) = 1$. It is important to underline that $0 < \nu_* < \nu_T$ for $\Gamma > 1$ or $0 < \nu_* < \Gamma\nu_T$ for $\Gamma < 1$. To see this, let us recall that $\nu(\hat{k}_z, j)$ is a monotonic function of k_z for $j \neq T$ (see Fig.1) and so $\tilde{K}(z)$ is also monotonic for $z = x > \max\{-\nu_T, -\Gamma\nu_T\}$. Next, we should check that for $\Gamma > 1$ the following inequalities take place: $\tilde{K}(0) < 1$ and $\tilde{K}(-\nu_T) > 1$ (for $\Gamma < 1$ instead of the latter inequality we have $\tilde{K}(-\Gamma\nu_T) = +\infty$).

As a consequence of the above set of singularities R(t) consists of two contributions: the first contribution comes from the integral along the cut and the second one originates from the pole at $z = -\nu_*$

$$R(t) = a_* e^{-t\nu_*} + \frac{\nu_c}{2} \sum_j \int \frac{d\Omega}{4\pi} \left(\frac{c_D}{c(\hat{k}_z, j)} \right)^3 e_z^2(\hat{k}_z\, j)\, (3e_z^2(\hat{k}_z\, j) - 1)$$

$$|\tilde{K}(-\nu(\hat{k}_z, j) + i0|^{-2}\, e^{-t\nu(\hat{k}_z\, j)} \qquad (32)$$

where

$$a_* = \lim_{z \to -\nu_*} (z + \nu_*) / (1 - \tilde{K}(z)).$$

We get the solution of PBE (25) by substituting the resolvent (32) into (30) and then F(t) into (26). The final solution for the phonon distribution function consists, in general, of three terms: (i) a RTA - like term proportional to $\exp\{-t\nu(\hat{k}_z, j)\}$, (ii) the integral along the cut leading to exponential decay with the effective decay time being between $1/\nu_T$ and $1/\Gamma \cdot \nu_T$, i.e. within the spectrum of $\tau(\hat{k}_z\, j) = 1/\nu(\hat{k}_z\, j)$; and (iii) a qualitatively new term decaying exponentially with a new relaxation time $\tau_* = 1/\nu_* > 1/\nu_T$ for $\Gamma > 1$ or $\tau_* > 1/\Gamma \cdot \nu_T$ for $\Gamma < 1$. Numerical values presented in Table 1 show that τ_* is a few times as large as τ_T. For $t \gg \tau_T$ relaxation is dominated by the term (iii) which has the form

$$\frac{1}{2} \nu_c a_* (3e_z^2(\hat{k}_z\, j) - 1) \sum_{j'} \int \frac{d\Omega'}{4\pi} \left(\frac{c_D}{c(\hat{k}'_z j')} \right)^3 \frac{e_z^2(\hat{k}'_z j')\, n(\hat{k}'_z j'; 0)}{\nu_* - \nu(\hat{k}'_z j')} \times$$

$$\times \left(\frac{e^{-t\nu_*} - e^{-t\nu(\hat{k}_z j)}}{\nu_* - \nu(\hat{k}_z j)} + \frac{e^{-t\nu(\hat{k}'_z j')} - e^{-t\nu(\hat{k}_z j)}}{\nu(\hat{k}_z j) - \nu(\hat{k}'_z j')} \right) . \qquad (33)$$

Table I. Anisotropy parameter Γ and the ratio of the relaxation time τ_* to τ_T for crystals of hexagonal symmetry

	Be	C	Cd	Hf	He^4	H_2	Mg
Γ	0.847	51.46	2.117	0.920	0.647	0.821	0.945
τ_* / τ_T	2.8	11.1	2.6	3.3	5.3	6.7	3.57

	Re	Ti	Tl	Y	Zn	Zr
Γ	0.924	0.849	0.385	0.965	2.215	0.997
τ_* / τ_T	4.2	3.7	6.2	3.6	2.1	3.8

Let us note that the new relaxation time τ_* is the same for all $\hat{k}$ and j. The only exceptions are those wave vectors which fulfil the condition $3e_z^2(\hat{k}_z, j) = 1$. With the last condition the terms (ii) and (iii) vanish (see (26)). The corresponding modes decay exponentially with a decaying time exactly equal to τ_c (Eq. (11) but with c_D taken for crystals of hexagonal symmetry). For the case of hexagonal symmetry the wave vectors of these modes form two cones, one for a longitudinal mode, the other for a slow transverse mode. Let us add that for some crystals the cone for the latter mode intersects the surface of constant energy almost at the same points as the cone of collinear points does. For example, for hcp ^4He the corresponding angles are equal 44° and 48°, respectively, and for hcp Zn 37° and 36°, respectively.

References

[1] R.E. Peierls, Quantum Theory of Solids (Oxford, Clarendon Press, 1955).
[2] F.H. Claro and C.H. Wannier, J.Math.Phys.12,92(1971).
[3] R.G. Ulbrich, V. Narayanamurti and M.A. Chin, Phys.Rev.Lett.45,1432(1980)
[4] M. Lax, V. Narayanamurti, P. Hu and W. Weber, J.Phys.(Paris), Colloq.42,C6-161 (1981).
[5] S. Tamura, Phys.Rev.B27,858(1983), B30,849(1984).
[6] P.G. Klemens, in Solid State Physics, F.Seitz and D.Turnbull, eds.(Academic Press, New York, 1958), vol.7.
[7] Z.K. Petru, in Proc. 2nd Int.Conf. on Phonon Physics, J.Kollár, N.Croo, N.Menyhárd and T.Siklós, eds. (World Scientific, Singapore, 1985).
[8] F.I. Fedorov, Theory of Elastic Waves in Crystals (Plenum, New York, 1968).
[9] Z.K. Petru, Communication of JINR, No. E17-86-632 (1986).
[10] E.C. Titchmarsh, Introduction to the Theory of Fourier Integrals (Oxford, Clarendon Press, 1948), G. Doetsch, Anleitung zum Praktischen Gebrauch der Laplace-Transformation and Z-Transformation (Oldenbourg, Munchen, 1967).
[11] G. Doetsch, Handbuch der Laplace-Transformation (Verlag Birkhauser, Basel,1950) vol. 1, Chapt.8.

SELECTED TOPICS ON POLARON

Michael A.Smondyrev
Joint Institute for Nuclear Research, Dubna
P.O.Box 79, Head Post Office, 101000 Moscow, USSR

Intensive theoretical and experimental investigations in condensed matter physics of recent years stimulated the revival of attention to various polaron models described by the well-known Fröhlich Hamiltonian. We discuss exact results known for such polaron characteristics as the ground-state energy,average number of phonons, and effective mass. The weak-coupling expansion can be constructed within a special diagrammatic technique developed in our paper [1]. Diagrams for the ground-state energy of a moving polaron are of the φ^3-type, but there exist some distinctions between them and conventional ones. In addition to the ordinary strongly connected diagrams we have also the disconnected ones. On the other hand, there are no weakly connected diagrams which can be separated into two parts by cutting an electron propagator. Furthemore, together with the electron-phonon vertices there exists another type of vertices whose role is to change the powers of the corresponding electron propagator. The latter depends on the number of phonons in a given virtual state and we have no integration over energies of virtual phonons. For more details we refer to paper [1]. This technique can be easily generalized to different kinds of polarons in arbitrary spatial dimensions [2] and allows us to obtain a perturbation series for the ground-state energy and effective mass. For example, the perturbation series in powers of the coupling constant α for the energy of a bulk 3-dimensional optical polaron is as follows:

$$E(\alpha) = -\alpha - 1.591362\cdot10^{-2}\alpha^2 - 0.806\cdot10^{-3}\alpha^3 + O(\alpha^4) \qquad (1)$$

In the strong-coupling regime we have the expansion in inverse powers of α (see [3]):

$$E(\alpha) = -0.108513\,\alpha^2 - 2.836 + O(1/\alpha^2), \qquad (2)$$

Analogous expansions for the average number of phonons can be obtained from the relation derived in [1]. For a motionless polaron it takes the form:

$$N(\alpha) = E(\alpha) - \frac{3}{2}\alpha E'(\alpha) \tag{3}$$

Discussing the optical polaron some physicists conjectured that if the electron-phonon coupling α increases, then at a certain critial value α_c there occurs a phase transition and the polaron gets localized. As one supposes, the ground-state energy $E(\alpha)$ is not analytic at that point, and other characteristics (e.g. $N(\alpha)$) have jumps. We dare say, there are no physical reasons for the electron being self-trapped in this theory which does not include the structure of the lattice. To prove the smoothness of the function $E(\alpha)$, we use two-point nondiagonal Padé approximants

$$E(n,n-1) = -\alpha \frac{1 + a_1\alpha + \ldots + a_n\alpha^n}{1 + b_1\alpha + \ldots + b_{n-1}\alpha^{n-1}}, \tag{4}$$

where the coefficients a_k, b_k can be defined by comparing Eq.(4) with Eqs.(1),(2). Using the information abcut weak- and strong- coupling expansions equivalently leads us tc two alternative cases: to obtain n equations for a_k, b_k from Eq.(1) and (n-1) equations from Eq.(2) or vice versa. These alternatives yield upper and lower bounds for the polaron energy and other quantities.

We demonstrate the power of the method by an example of the Feynman polaron where we calculated a rather large number of coefficients in expansions (1) and (2). For the actual polaron energy exact results are exhausted with Eqs.(1), (2), so we can construct only lower bounds E(2,1) and E(3,2) and upper bound E(2,1), the discrepancy between which does not exceed 10% in the intermediate coupling regime. The exact solution lies between two smooth functions which have no poles at $\alpha \geqslant 0$. The investigation of $N(\alpha)$ by the same technique excludes the phase transition with jumps $\Delta N \sim 10$ which has been declared in some papers. Thus, we do not see any hints of the phase transition and it seems almost incredible that it occurs at all.

References

1. M.A.Smondyrev. Teor. i Mat. Fiz. 68, 29(1986) (in Russian).
2. O.V.Seljugin, M.A.Smondyrev. JINR preprint E17-86-428, Dubna, 1986 (to be published in Physica A).
3. S.Miyake. J. Phys. Soc. Jap. 38, 181(1975); 41, 747(1976).

PHONON DETECTION BY MEANS OF TSEE

T.L.Hałaczek*, B.Sujak**
* Institute for Low Temperature and Structure Research , Polish Academy of Science, Wrocław,Poland
**Institute of Experimental Physics,Wrocław University, Depertment of Experimental Physics, Wrocław, Poland

For many purposes in phonon spectroscopy it is of great interest to have a sensitive phonon detector of high spatial resolution. Recently some attempts have been done [1,2] with superconducting tunnel junctions (STJ). We would like to propose quite different phonon detector which idea is in exploiting of the thermally stimulated emission of electrons (TSEE) [3,4]. Such an emission is observed from energetically excited surface of a sample covered with a thin layer of oxide or adsorbed gases. The surface layer should be excited i.e. loaded with electrons of energy of the order of 100 eV, which are trapped inside the layer during the excitation process. And then each change of the state of the layer acts in emerge of the electrons which are detected by means of typical electron sensitive devices e.g. electron multiplier working in a pulse regime. Similar effect of emission is caused by heating the sample (TSEE). The lowest temperature of existence of TSEE peak, about 3K, was evidenced in the case of cryocondensed layer of hydrogen. Such an emission peak from solidified thin layer of hydrogen is observed for different substrata e.g.Al, Al_2O_3, Si [6]. The peak positions at the emission intensity versus temperature characteristics (i.e. thermal spectrum of TSEE) should not depend on the pretreatment of a substrate surface. The temperature at which the emission starts can be regarded as a measure of the detector threshold energy. In our case it is within the range of some meV which is comparable with energy threshold of STJ. In other hand the electron emission is accompanied by gas desorption from the sample surface. An advantage of this type of detector is in good spatial resolution, because the electrons could be detected with the spatial resolution as high as some μm [7], when electron focusing lenses are used. Unfortunately at the moment the stimulation probability of electron by a phonon is not known, therefore we cannot predict neither the efficiency of emission process nor the demanded intensity of the phonon beam. In the present state of the theory of TSEE this problem can be solved inan experimental way only.

It seems to be obtainable, by proposed technique, the phonon focusing pattern without scanning of the sample surface, when one use the channel plate [8].

Acknowledgements

One of us, (TLH), is very indebted to Professors H.Kinder and J.M.Worlock for fruitful discussions and to Professors L.J.Challis, W.E.Bron and Y.B.Levinson for their remarks on the possibility of performing the TSEE-phonon experiment.

REFERENCES

1. H.Kinder in: Nonequilibrium Phonon Dynamics, ed.by W.E.Bron, NATO-ASI series 124, Plenum (1985).
2. L.J.Challis in: Physics of Phonons, ed.T.Paszkiewicz, Springer Verlag, Berlin (1987)
3. A.Scharmann in: Proc.4th Intern.Symp.EEE and Dosimetry,Liblice (1973),p.12.
4. B.Sujak, Jap.J.Appl.Phys.,24, (1985), Suppl.24-2,p.11.
5. B.Sujak, F.Gołek in: Proc.6th Intern.Symp.on Exoelectron Emission and Applications, Ahreshoop (1979),p.108.
6. F.Gołek, private communication.
7. A.Scharmann in: Proc. 6th Intern. Symp. on Exoelectron Emission and Applications, Ahreshoop (1979), p.28.
8. P.Braunlich in: Proc.4th Intern.Symp.EEE and Dosimetry,Liblice (1973),p.30.

LIST OF PARTICIPANTS

BIALYNICKI-BIRULA I.	Theoretical Physics Group,Institute of Physics,Polish Acad. Sci. Al.Lotnikow 32/46, 02-668 Warszawa,Poland,tel.470-920, tx. 812468
BEBEN J.	Institute of Experimental Physics,University of Wroclaw, Cybulskiego 36,50-205 Wroclaw,Poland,tel.223-365, tx:712791 uwr pl
BODZENTA K.	Instytut Fizyki Politechniki Slaskiej w Gliwicach,Krzywoustego 2, 44-100 Gliwice, Poland, tel.318-671, tx:36304 posl pl
BRON W.	University of California, Department of Physics, Irvine, California 92717, USA
BULL M.	Department of Theoretical Physics,University Oxford ,1 Keble Road, Oxford OX1 3NP, UK,tx.83295 NUCLOX G
CHALLIS L.J.	Department of Physics, The University of Nottingham,University Park, Nottingham NG7 2RD, UK,tel.(0602) 506101,tx:37346 UNINOT G
CHANCEY C.C.	Department of Theoretical Physics,University Oxford ,1 Keble Road, Oxford OX1 3NP, UK,tx.83295 NUCLOX G
CIEPIELEWSKI P.	Institute of Physics,Polish Acad.Sci. , Al.Lotnikow 32/46, 02-668 Warszawa,Poland, tel.437-001,tx. 812468
CISLO J.	Institute of Theoretical Physics,University of Wroclaw, 50-205 Wroclaw, Cybulskiego 36, Poland, tel.222363, tx: 712791 uwr pl
CWIKILEWICZ J.	Instytut Badan Jadrowych, ul.Radzikowskiego 152, 31-342 Krakow, Poland,tx. 0322461 ifj pl,tel.370222,ext 286,570
CZACHOR A.	Institute of Physics,Polish Acad.Sci. , Al.Lotnikow 32/46, 02-668 Warszawa,Poland,tel.437-001, tx. 812468
DJAFARI ROUHANI B.	Universite de Haute-Alsace,Faculte des Sciences et Techniques, Institute des Sciences Exactes et Appliques, 4 Rue des Freres Lumiere, F-68093 Mulhouse Cedex,France,tx.IRPMULH 881302 F
DURCZEWSKI K.	Institute of Low Temperature and Structural Research , Pl . Katedralny 1, P.O. Box 937, 50-329 Wroclaw, Poland, tel .221071, tx:0712-777 int
EFIMOV V.B.	Solid State Physics Institute, Acad. Sci. USSR, 142432 Chernogolovka,USSR
EFROS A.L.	Ioffe Physico-Technical Institute of Acad.Sci.USSR, 194021 Leningrad, Politechnicheskaya St.26,Leningrad K-21 USSR
ESCHRIG H.	Akademie der Wissenschaften der DDR,Zentralinstitut fur Festkorperphysik und Werkstofforschung,8027 Dresden, Helmholtzstrasse 20 ,DDR, tel.46590,tx:2131 zfw dd

FEHSKE H.	Karl Marx University, Sektion Physik, 7010 Leipzig, Linnestrasse 5, DDR,tel.68580,tx:051350
GALASIEWICZ Z.M.	Institute of Theoretical Physics,University of Wroclaw, 50-205 Wroclaw, Cybulskiego 36, Poland, tel.222363, tx: 712791 uwr pl
GALKINA T.I.	P.N.Lebedev Physical Institute of Acad.Sci USSR, Leninsky prosp. 53, 117924 Moscow , USSR, tel. 135-22-50, Cables B-333 FIAN
GOLEK F.	Institute of Experimental Physics,University of Wroclaw, Cybulskiego 36,50-205 Wroclaw,Poland,tel.223-365, tx:712791 uwr pl
GORSKI A.	Instytut Badan Jadrowych, ul.Radzikowskiego 152 ,31-342 Krakow, Poland,tx. 0322461 ifj pl,tel.370222,ext 283
GULACSI M.	Institute of Isotopic and Molecular Technology ,3400 Cluj-Napoca 5, P.O. Box 700 , Romania , tel. 84037 ext. 231
GULACSI Zs.	Institute of Isotopic and Molecular Technology ,3400 Cluj-Napoca 5, P.O. Box 700 , Romania , tel. 84037 ext. 231
GURZI R.N.	Physico-Technical Institute of Low Temperatures Acad.Sci. Ucrainian SSR,310-164 Kharkov 86,Lenin Ave.47,USSR,tel.321223
HALACZEK T.	Institute of Low Temperature and Structural Research , Pl . Katedralny 1, P.O. Box 937, 50-329 Wroclaw, Poland, tel .221071, tx:0712-777 int
HORTON G.K.	The State University of New Jersey, Department of Physics and Astronomy, P.O.Box 849,Piscatway,N.J. 08 8554, USA,tx:703528
IHLE D.	Karl Marx University, Sektion Physik, 7010 Leipzig, Karl-Marx-Platz, DDR,tel.7192586
JAHNE E.	Zentralinstitut fur Elektronenphysik,1086 Berlin, Hausvogteiplatz 5-7, DDR
JACAK L.	Technical University of Wroclaw,Institue of Physics,Wybrzeze Wyspianskiego 27, 50-370 Wroclaw, Poland,tel.229-696,209-395 tx:034254 polit.pl
JEDRZEJEWSKI J.	Institute of Theoretical Physics,University of Wroclaw, 50-205 Wroclaw, Cybulskiego 36, Poland, tel.222363, tx: 712791 uwr pl
JURCZYSZYN L.	Institute of Experimental Physics,University of Wroclaw, Cybulskiego 36,50-205 Wroclaw,Poland,tel.223-365, tx:712791 uwr pl
KAGANOV M.I.	Institute of Physical Problems Acad.Sci.USSR, 117 331 Moscow, Kosygin St.,USSR
KAMBA S.	Institut of Physics,CSAV,Na Slovance 2,180-40 Prague 8, Czechoslovakia, tx.122018 atom c,tel.842241
KASNER M.	Karl Marx University, Sektion Physik, 7010 Leipzig, Karl-Marx-Platz, DDR,tel.7192586

KAZAKOVCEV D.V.	Solid State Physics Institute, Acad. Sci. USSR, 142432 Chernogolovka,USSR
KECHRAKOS D.	Department of Theoretical Physics,University Oxford, 1 Keble Road, Oxford OX1 3NP, UK,tel.865-53281,tx.83295 NUCLOX G,
KHOMSKII D.I.	P.N.Lebedev Physical Institute of Acad.Sci USSR, Leninsky prosp. 53, 117924 Moscow , USSR, tel. 135-22-50, Cables B-333 FIAN
KINDER H.	Physik Department der Technischen Universitat Munchen, Insitut fur Festkorperphysik, 8046 Garching b. Munchen, James - Franck Strasse, BRD, tel. (089) 3209-2401 ,tx: 522 854 tu mue d
KOMODA A.	Institute of Theoretical Physics,University of Wroclaw, 50-205 Wroclaw, Cybulskiego 36, Poland, tel.222363, tx: 712791 uwr pl
KONWENT H.	Instytut Fizyki WSP,ul.Rejtana 16a,35-310 Rzeszow,Poland
KRUKOWSKI S.	Zaklad Wysokich Cisnien PAN "Unipress",ul.Sokolowska 29, 01-142 Warszawa, Poland,tx:817618 zuc pl,tel.321635
KRZYSZTON T.	Institute of Low Temperature and Structural Research , Pl . Katedralny 1, P.O. Box 937, 50-329 Wroclaw, Poland, tel .221071, tx:0712-777 int
KUHNEL A.	Karl Marx University, Sektion Physik, 7010 Leipzig, Linnestrasse 5, DDR,tel.68580,tx:051350
KUPKA M.	Institute of Experimental Physics,Slovak Academy of Science, Solovjevova 47, 04353 Kosice,Czechoslovakia ,tel.004295-28158, tx:773 48 SAV-c
KURZYNSKI M.	Uniwersytet im. A.Mickiewicza, Instytut Fizyki, Zaklad Teorii Ciala Stalego, ul.Matejki 48/49 , 60-769 Poznan , Poland, tel.62487, tx:0413260 uam pl
LEFEBVRE J.	Laboratoire de Dynamique des Cristaux Moleculaires Lille I, Universite des Sciences et Technique de Lille 59655 Villeneuve d'Ascq Cedex, France
LEVCHENKO A.A.	Solid State Physics Institute, Acad. Sci. USSR, 142432 Chernogolovka,USSR
LEVINSON Y.B.	Institute of Microelectronics, Acad. Sci. USSR, 142432 Chernogolovka,USSR
LORENC J.	Institute of Theoretical Physics,University of Wroclaw, 50-205 Wroclaw, Cybulskiego 36, Poland, tel.222363, tx: 712791 uwr pl
LORENZ B.	Central Institute for Physics of the Earth, Acad.Sci GDR, 15 Potsdam,Telegrafenberg,DDR,tel.4551, tx:015305
LULEK T.	Uniwersytet im. A.Mickiewicza, Instytut Fizyki, Zaklad Teorii Ciala Stalego, ul.Matejki 48/49 , 60-769 Poznan , Poland, tel.62487, tx:0413260 uam pl
LATKA M.	Technical University of Wroclaw,Institue of Physics,Wybrzeze Wyspianskiego 27, 50-370 Wroclaw, Poland,tel.229-696,209-395 tx:034254 polit.pl

LUCZKA J.	Instytut Fizyki, Uniwersytet Slaski, ul.Uniwersytecka 4 40-007 Katowice, Poland,tel.543-647
LUSAKOWSKI A.	Institute of Physics,Polish Acad.Sci. , Al.Lotnikow 32/46, 02-668 Warszawa,Poland,tel.437-001 ext.535 , tx. 812468
MARADUDIN A.A.	Department of Physics, University of California at Irvine, Irvine, California 92717, USA,
MEZHOV-DEGLIN L.P.	Solid State Physics Institute, Acad. Sci. USSR, 142432 Chernogolovka,USSR
MIRJANIC D.	Faculty of Technology, University of Banja Luka, Danka Mitrova 63 b, YU-78000 Banja Luka, Yugoslavia, tel. 038-78-46-081
MISIAK P.	Instytut Chemii Organicznej i Fizycznej ,Politechnika Wroclawska, Wybrzeze Wyspianskiego 27,50-370 Wroclaw,Poland,tel.202894, tx:034254 polit. pl
MORAWIEC P.	Institute of Theoretical Physics,University of Wroclaw, 50-205 Wroclaw, Cybulskiego 36, Poland, tel.222363, tx: 712791 uwr pl
MULLER R.	Karl Marx University, Sektion Physik, 7010 Leipzig, Linnestrasse 5, DDR,tel.68580,tx:051350
NAWROCKA W.	Institute of Theoretical Physics,University of Wroclaw, 50-205 Wroclaw, Cybulskiego 36, Poland, tel.222363, tx: 712791 uwr pl
NEUGEBAUER A.	Uniwersytet im. A.Mickiewicza, Instytut Fizyki, Zaklad Teorii Ciala Stalego, ul.Matejki 48/49 , 60-769 Poznan , Poland, tel.62487, tx:0413260 uam pl
OLEKSY Cz.	Institute of Theoretical Physics,University of Wroclaw, 50-205 Wroclaw, Cybulskiego 36, Poland, tel.222363, tx: 712791 uwr pl
PARLINSKI K.	Instytut Badan Jadrowych, ul.Radzikowskiego 152, 31-342 Krakow, Poland,tx. 0322461 ifj pl,tel.370222,ext 209
PASZKIEWICZ T.	Institute of Theoretical Physics,University of Wroclaw, 50-205 Wroclaw, Cybulskiego 36, Poland, tel.222363, tx: 712791 uwr pl
PAWELEK A.	Instytut Przerobki Plastycznej i Metaloznawstwa,AGH, Al.Mickiewicza 30, 30-059 Krakow,Poland,tel.338000 ext.26-65
PETRU Z.K.	Institute of Theoretical Physics,University of Wroclaw, 50-205 Wroclaw, Cybulskiego 36, Poland, tel.222363, tx: 712791 uwr pl
PLAKIDA N.M.	Joint Institute for Nuclear Research,Laboratory of Theoretical Physics,Dubna,Head Post Office P.O.Box 79,Moscow 101000, USSR
PODOLSKA - STRYCHARSKA A.	Institute of Theoretical Physics,University of Wroclaw, 50-205 Wroclaw, Cybulskiego 36, Poland, tel.222363, tx: 712791 uwr pl
POPKO E.	Technical University of Wroclaw,Institue of Physics,Wybrzeze Wyspianskiego 27, 50-370 Wroclaw, Poland,tel.229-696,209-395 tx:034254 polit.pl
PUSZKARSKI H.	Uniwersytet im.A.Mickiewicza, Instytut Fizyki,Zaklad Fizyki Powierzchni,ul.Grunwaldzka 6,60-780 Poznan,Poland, tel.699181, tx:0413260 uam pl

RADNY M.	Institute of Experimental Physics,University of Wroclaw, Cybulskiego 36,50-205 Wroclaw,Poland,tel.223-365, tx:712791 uwr pl
RIEDEL M.	Central Institute for Physics of the Earth, Acad.Sci GDR, 15 Potsdam,Telegrafenberg,DDR,tel.4551, tx:015305
SCHMIDT W.	Instytut Fizyki Molekularnej PAN,ul.Smoluchowskiego 17/19, 60-179 Poznan,Poland,tel.674071, tx:0415647 ifm pl
SCHOBER H.	Institute fur Festkorperfoschung der Kernforschung-slage, Julich GmbH , Postfach 1913, D-5170 Julich, BRD ,tel. (02461) 614222, tx:833556-10 kf d
SCHREIBER J.	Technische Universitat Dresden, Sektion Physik, 8027 Dresden, Mommsenstr 13, DDR,tel.4633855,tx.02278
SETRAJCIC J.	Institute of Physics , Faculty of Sciences, University of Novi Sad, Dr Ilije Djuricica 4 , YU - 21000 Novi Sad , Yugoslavia, tel.021-55-318
SKRAJNA D.	Institute of Theoretical Physics,University of Wroclaw, 50-205 Wroclaw, Cybulskiego 36, Poland, tel.222363, tx: 712791 uwr pl
SLOMIAN M.	Uniwersytet im. A.Mickiewicza, Instytut Fizyki, Zaklad Teorii Ciala Stalego, ul.Matejki 48/49 , 60-769 Poznan , Poland, tel.62487, tx:0413260 uam pl
SMONDYREV M.A.	Joint Institute for Nuclear Research, Lab. of Theor. Physics, Dubna, Moscow 10100, P.O.Box 79,USSR
SOCZKIEWICZ E.	Instytut Fizyki Politechniki Slaskiej w Gliwicach, Krzywoustego 2, 44-100 Gliwice, Poland, tel.318-671, tx:36304 posl pl
STACHOWIAK H.	Institute of Low Temperature and Structural Research , Pl . Katedralny 1, P.O. Box 937, 50-329 Wroclaw, Poland, tel .221071, tx:0712-777 int
STRYCHARSKI Z.	Institute of Theoretical Physics,University of Wroclaw, 50-205 Wroclaw, Cybulskiego 36, Poland, tel.222363, tx: 712791 uwr pl
SUJAK-CYRUL B.	Technical University of Wroclaw,Institue of Physics,Wybrzeze Wyspianskiego 27, 50-370 Wroclaw, Poland,tel.229-696,209-395 tx:034254 polit.pl
SZAJEK K.	Instytut Fizyki Molekularnej PAN,ul.Smoluchowskiego 17/19, 60-179 Poznan,Poland,tel.674071, tx:0413617 ifm pl
TARTAKOVSKII I.I.	Solid State Physics Institute, Acad. Sci. USSR, 142432 Chernogolovka,USSR
TEKIEL P.	Institute of Low Temperature and Structural Research , Pl . Katedralny 1, P.O. Box 937, 50-329 Wroclaw, Poland, tel .221071, tx:0712-777 int
THELLUNG A.	Insitut fur Theoretische Physik der Universitat Zurich Schonberggasse 9, CH-8001 Zurich, Switzerland,tel.01/2572946, tx:54864 uni zh ch

THOMAS M.	Uniwersytet im. A.Mickiewicza, Instytut Fizyki, Zaklad Teorii Ciala Stalego, ul.Matejki 48/49 , 60-769 Poznan , Poland, tel.62487, tx:0413260 uam pl
TSOI V.S.	Solid State Physics Institute, Acad. Sci. USSR, 142432 Chernogolovka,USSR
VISWANATHAN K.S.	Department of Physics, University Centre,Karyavattom-695 581, Trivandrum,INDIA,tel.Off 8420,Res 8415,tx:884 295 ate in
WANG Yi-ming	Dept. of Electronic Engineering , The Beijing Polytechnic University, Eastern Suburbs , Beijing , China , tel. 78-4631 ext 430 , 432 , tx: d 712791
WEIS O.	Universitat Ulm , Abteilung fur Festkorperphysik , Oberer Eselsberg, Postfach 4066, D-7900 ULM, BRD, tel. (0731) 176-2046
WELLER W.	Karl Marx University, Sektion Physik, 7010 Leipzig, Linnestrasse 5, DDR,tel.68580,tx:051350
WOJCIECHOWSKI R.	Uniwersytet im. A.Mickiewicza, Instytut Fizyki, Zaklad Teorii Ciala Stalego, ul.Matejki 48/49 , 60-769 Poznan , Poland, tel.62487, tx:0413260 uam pl
WORLOCK J.N.	Bell Communications Research, Inc. 331 Newman Springs Road, Box 7020 , Red Bank, New Jersey 07701-7020, Room 3X-283, USA, tx :275318 bell ur
WOSICKI P.	Instytut Fizyki Molekularnej PAN,ul.Smoluchowskiego 17/19, 60-179 Poznan,Poland,tel.674071, tx:0413617 ifm pl
WROBEL P.	Institute of Low Temperature and Structural Research , Pl . Katedralny 1, P.O. Box 937, 50-329 Wroclaw, Poland, tel .221071, tx:0712-777 int
WYSOKINSKI K.I.	Instytut Fizyki, UMCS, 20-031 Lublin, Nowotki 10,Poland, tel.382-41, tx. 0643223a umcs pl
ZALUZNY M.	Instytut Fizyki, UMCS, 20-031 Lublin, Nowotki 10,Poland, tel.382-41, tx. 0643223a umcs pl
ZENG Ling-zhi	Dept. of Applied Physics, The Beijing Polytechnic University, Eastern Suburbs, Beijing , China,tel.78-4631 ext 460,tx:d 712791
ZIPPER E.	Instytut Fizyki, Uniwersytet Slaski, ul.Uniwersytecka 4 40-007 Katowice, Poland,tel.543-647
ZOSSEL R.	Institute of Low Temperature and Structural Research , Pl . Katedralny 1, P.O. Box 937, 50-329 Wroclaw, Poland, tel .221071, tx:0712-777 int